# A methodology to investigate the cause of quenching in once-through tower type power plant boilers


Gary de Klerk
DKLGAR002

Thesis Presented for the Degree of
DOCTOR OF PHILOSOPHY
Department of Mechanical Engineering
UNIVERSITY OF CAPE TOWN
**February 2020**



Supervisor:
Prof Pieter Rousseau
Co-supervisor:
Prof Louis Jestin

**Key Words:** Boilers, Process modelling, Quenching, Superheater

# *Abstract*

Due to the penetration of variable renewable energy (VRE) sources, conventional coal fired power plants need to operate with greater flexibility via two-shifting or low load operation whilst remaining reliable and conserving the lifetime of components. Thick sectioned components are prone to thermal fatigue cracking as a result of through-wall temperature gradients during start up and shutdown. These temperature gradients can be significantly amplified during quenching when components at high temperature are unintentionally exposed to colder liquid or steam. Such quench events are known to occur during two-shift operation of a large once-through coal fired tower type boiler, which is the subject of this study.

The purpose of this study is to develop and demonstrate a methodology to determine the root cause of quenching in a once-through tower type boiler and provide information that can be used to predict the impact on thick-walled components by estimating the through-wall temperature gradients.

The first modelling element in the methodology is a simplified transient heat transfer model for investigating condensation of steam in the superheater. The model is presented and verified by comparison with real plant data.

The second element is a liquid tracking model that approximates the liquid level in the superheater as a function of time to predict the location and magnitude of through-wall temperature gradients. The complex geometry of the superheater was divided into a number of control volumes and a dynamic thermo-fluid process model was developed to solve the transient conservation of mass and energy equations for each volume using a semi-implicit time wise integration scheme. The liquid tracking model was verified by comparison with a similar model constructed in Flownex and also by comparison with plant data. Varying levels of discretisation were applied to a particular quench event and the results are presented.

The third modelling element is a two-dimensional transient pipe wall conduction model that is used at selected localities to evaluate the temperature gradients within the pipe wall. The temperature gradients and internal heat flux were verified by temperature measurements from the outer surface of a main steam pipe undergoing quenching. The stresses associated with the temperature gradients were also briefly considered.

The real plant quenching problem is analysed in detail and found to be caused by liquid overflow from the separators. A particular plant configuration creates a previously unidentified siphon of water from the separating and collecting vessel system into the superheater. This situation is not recognised by plant operators and thus persists for some time and causes flooding of the superheater.

Analysis of the resultant through-wall temperature gradients show that quenching causes significant stresses which can be avoided. By understanding the causes and preventing the occurrence of quenching, the life of thick-walled high temperature components can be conserved.

# *Declaration*

I, Gary Brett de Klerk, hereby declare the work contained in this thesis to be my own. All information which has been gained from various journal articles, text books or other sources has been referenced accordingly. I have not allowed, and will not allow, anyone to copy my work with the intention of passing it off as their own work or part thereof.

Signed by candidate

Gary Brett de Klerk

05 / 10 / 2020

Date

# *Acknowledgements*

Firstly, I thank God, in whom I trust, for the wisdom, the ability and the favour afforded to me to complete this work.

Then to my wife, Libby and to my daughters, Piper and Bailie, I thank you for all your love, support and faith in me. You have made sacrifices and shown great patience for which I am truly grateful.

To my family, thank you for the support and encouragement.

To my supervisor, Prof Pieter Rousseau, thank you for your knowledge, guidance and wisdom. Your detailed reviews and constructive commentary were invaluable.

To my co-supervisor, Prof Louis Jestin, and my industrial mentors, Dr Mark Newby of Eskom RT&D and Dr Michael Hindley, formerly of Eskom RT&D, thank you for the ideas and guidance. Special thanks to Dr Mark Newby for providing the equipment and facilities for the experimental work.

To my managers, Peter Magner and Kapil Sukhnandan, thank you for the opportunity and the support for the project. Without your support, this work would not have been possible.

To my colleagues, Laurence Greyvenstein, Andre Roussouw, Thokozani Ntuli, Craig Fath, Rohit Bhagwandas, Priyesh Gosai and many others, thank you for the interest in my project and always being willing to help me to obtain the data and information that I required.

The project was sponsored by Eskom through the Eskom Power Plant Engineering Institute (EPPEI).

# *Table of Contents*

# List of Figures

# List of Tables

# List of Nomenclature

## General symbols

| | |
|---|---|
| a | Absorption coefficient |
| A | Area [$m^2$] |
| Bi | Biot number |
| $c_p$ | Specific heat capacity [J/kg K] at constant pressure |
| C | Constant used in radiation heat transfer involving gasses, Capacitance [$kJ/m^3$ K], Heat capacity [J/K] |
| $C_{nb}$, $C_{max}$, $C_{min}$ | Constants used in pool boiling correlations |
| d,D,$d_m$ | Diameter [m], Mean diameter |
| E | Elastic modulus, Energy [kJ] |
| $f$ | Darcy friction factor |
| $\mathcal{F}_{12}$ | Radiation transfer factor from surface 1 to surface 2 |
| g | Gravitational constant [$m/s^2$] |
| Gr, Gz | Grasshof number, Graetz number |
| h | Enthalpy [kJ/kg K], Heat transfer coefficient [$W/m^2$ K], Height [m] |
| $h_0$, $h_{fg}$ | Total enthalpy [kJ/kg K], Latent heat of vaporisation [kJ/kg K] |
| $h_c$, $h_r$ | Convective, Equivalent radiative heat transfer coefficient [$W/m^2$ K] |
| Ja | Jacob number |
| k | Conductivity [W/m K], Radiation extinction coefficient |
| $k_f$ | Stress concentration factor, Fluid conductivity [W/m K] |
| K | Head loss coefficient |
| L,$l$ | Length [m], Liquid level [m] |
| $L_c$ | Equivalent length for nucleate boiling correlation [m] |
| m,M | Mass [kg] |
| $\dot{m}$ | Mass flow [kg/s] |
| n | Number of, Manning resistance coefficient |
| $\overline{Nu_D}$ | Average Nusselt number |
| $\overline{Nu_D}^{10+}$ | Average Nusselt number for 10 rows of tubes or more |
| P,p | Pressure [Pa] |
| $P_0$ | Total pressure |
| Pr, $P_w$ | Prandtl number, Wall parameter |
| q,$\dot{Q}$ | Heat flux [$W/m^2$], Heat transfer rate [kW] |
| r, $r_1$, $r_2$ | Volumetric fraction, radius [m], pipe inside radius $r_1$ [m], pipe outside radius $r_2$ [m] |
| Re | Reynolds number |
| $R_h$ | Hydraulic radius |

| | |
|---|---|
| s | Wall thickness [m], Geometric mean beam length [m] |
| $S_0$ | Slope |
| $s_1$, $s_T$ | Transverse tube pitch i.e. perpendicular to the gas flow direction in a tube bundle [m] |
| $s_2$, $s_L$ | Longitudinal tube pitch i.e. parallel to the gas flow direction in a tube bundle [m] |
| t | Time [s], Thickness [m] |
| T | Temperature [$^oC$ or K] |
| $\bar{T}$ | Mean temperature [$^oC$ or K] |
| u, $u_0$ | Internal energy [kJ/kg], Total internal energy [kJ/kg] |
| V | Volume [$m^3$], Velocity [m/s] |
| $V_T$ | Rate of temperature change [K/s] |
| x | Steam quality |
| z | Elevation [m] |

# Greek symbols

| | |
|---|---|
| $\alpha$ | Void fraction, Thermal diffusivity [$m^2/s$] |
| $\alpha_c$ | Euler integration factor |
| $\beta$ | Coefficient of thermal expansion [1/K] |
| Δt, ΔT, ΔP | Time step, Temperature difference, Pressure drop |
| ε | Emissivity, Effectiveness, Pipe roughness |
| μ | Mass concentration, Dynamic viscosity [Pa s] |
| σ | Stress, Surface tension or Stefan-Boltzmann constant ($5.67 \times 10^{-8}$ $W/m^2 K^4$) |
| θ | Angle [rad] |
| ρ | Density [$kg/m^3$] |
| φ | Heat flux [$W/m^2$] |
| φ | Arrangement factor for a tube bank |
| $\psi$ | Tube bundle void fraction |
| ν | Poisson's ratio, Kinematic viscosity [$m^2/s$], Velocity [m/s], Specific volume [$m^3/kg$] |

# Subscripts

| | |
|---|---|
| 1,2 | Initial state, final state |
| a | Ash |
| Eq | Equivalent |
| e,w,n,s | Position of the element boundary to the east, west, north and south of the point under consideration |
| E,W,N,S,P | Designation of the element to the East, West, North and South of the element P under consideration |
| f | Fluid |

| | |
|---|---|
| g,G | Gas, Gas phase |
| H, C | Hot, Cold |
| in | Inner |
| i,e | Inlet, Exit |
| L,$l$ | Liquid |
| m | Metal, Mid |
| min, max | Minimum, Maximum |
| o,out | Outer, outlet |
| s | Steam |
| sat | Saturation |
| v | Vapour |
| w | Wall |
| x,y | Co-ordinates that define a physical location |

# Acronyms and Abbreviations

| | |
|---|---|
| ANSYS | ANSYS Mechanical Enterprise is software that uses finite element analysis (FEA) for structural analysis of mechanical components and systems. |
| APROS | Apros is software for modelling and dynamic simulation of power plants, energy systems and industrial processes. |
| CFD | Computational fluid dynamics |
| DCS | Distributed control system |
| Flownex | Flownex SE (Simulation Environment) is software that performs one dimensional thermo-fluid network solving. |
| HP | High Pressure |
| LTM | Liquid tracking model |
| LMTD | Log mean temperature difference |
| NPSH | Net pump suction head |
| NTU | Number of transfer units |
| Scilab | Scilab is free and open source software for numerical computation. It is a high level programming language with access to advanced data structures and 3D graphical functions. |
| SH | Superheater |
| TC | Thermocouple |

# 1. Introduction

Coal is likely to continue as a significant power source at least until 2040 with global installed capacity remaining almost constant over the time period. However, global market share of coal fired power generation is predicted to decline from 40% to 25% against increasing renewable power production. Nuclear is expected to retain a global market share of 10%. [1]

Due to the penetration of variable renewable energy (VRE) and more stringent emission levels, coal fired plants will need to be more flexible and operate at lower loads. [1]

Both Nuclear and renewable power plants have defined load priority: Nuclear is regulated to generate at constant load (although new Nuclear plants are being designed for load following capability [2]) whilst renewable is 'must run' capacity (preference to generate when available) owing to the objective of reducing overall emissions. This, coupled with the inherently variable production of most renewable power plants, results in rapid load variation required from coal fired plants.

Unless the problems associated with carbon capture and storage (CCS) are resolved, which does not seem likely even in the long term (20 years), the role of the future coal fired plant will be mid-merit capacity. This means that both existing plants and new coal fired plants will need to use innovative methods to rapidly change load, operate at lower loads or even perform two shift operation whilst remaining reliable and conserving the lifetime of their components. Two shift operation requires that a boiler-turbine unit is shut down after evening peak, kept warm overnight and then restarted again in the morning.

A risk that affects a plant that has been temporarily shut down but is still hot is that of quenching. Quenching is a term borrowed from materials science and metallurgy where it is a useful process for hardening steel by immersing a hot work piece in water or oil to rapidly cool it. In the context of this work, quenching refers to an undesired process where components at their operating temperature are exposed to colder liquid or steam and this causes a rapid decrease in temperature of the component with associated thermally induced deformation and stresses.

Typically, quenching occurs when water flows by gravity into hot thick-walled components. The water causes rapid cooling of the internal surface of the component. The remainder of the wall thickness of the component cools more gradually as heat diffuses through the material. This results in significant temperature differences through the wall of the component. The temperature differences cause thermal stress as a result of differential thermal expansion of the material.

This type of quenching causes damage to the components. The damage can be immediate, as in the case of the development and growth of an internal surface crack and it can also be longer-term accumulation of damage in the form of fatigue.

## 1.1 Power Station A

This study was initiated as a result of observations at Power Station A. A brief description of the station and the observations are provided in this chapter.

All six units of Power Station A were commissioned between 1996 and 2001. The once-through pulverised fuel (PF) boilers are rated at 2077 t/h each with final steam parameters of 540°C and 17.4 MPa.

*Figure 1. Power Station A*

Intermittent two-shift operation was implemented at the power station from when the plant was commissioned until approximately 2011. At the end of 2013, the number of actual operating hours accumulated by the units ranged from 74 000 hours to 81 000 hours. The plant experienced the most cycling of all the plants in the Eskom fleet.

As part of Eskom's life assessment and risk management plan for creep exposed components [3], metallographic replicas are taken at specific locations of the main steam piping, hot reheat piping, boiler headers, turbine inlet loop pipes and other locations. The replicas are analysed for material degradation and classified according to the following scale [3]:

- Class 4: >100 000 hours remaining life, inspect in 6 years.
- Class 3: 60 000 hours to 100 000 hours remaining life, inspect in 3 years.
- Class 2: 30 000 hours to 60 000 hours remaining life, replace within 3 years.
- Class 1: <30 000 hours remaining life, replace immediately.

At Power Station A, a number of main steam piping components such as bends and welds have had to be replaced as a result of the damage found. Figure 2 shows that these components had been in

service for less than 80 000 hours when the damage was found. The root cause of this damage is suspected creep-fatigue interaction as well as poor original material properties [4]. Certainly, the damage is premature considering the design life of 200 000 hours.

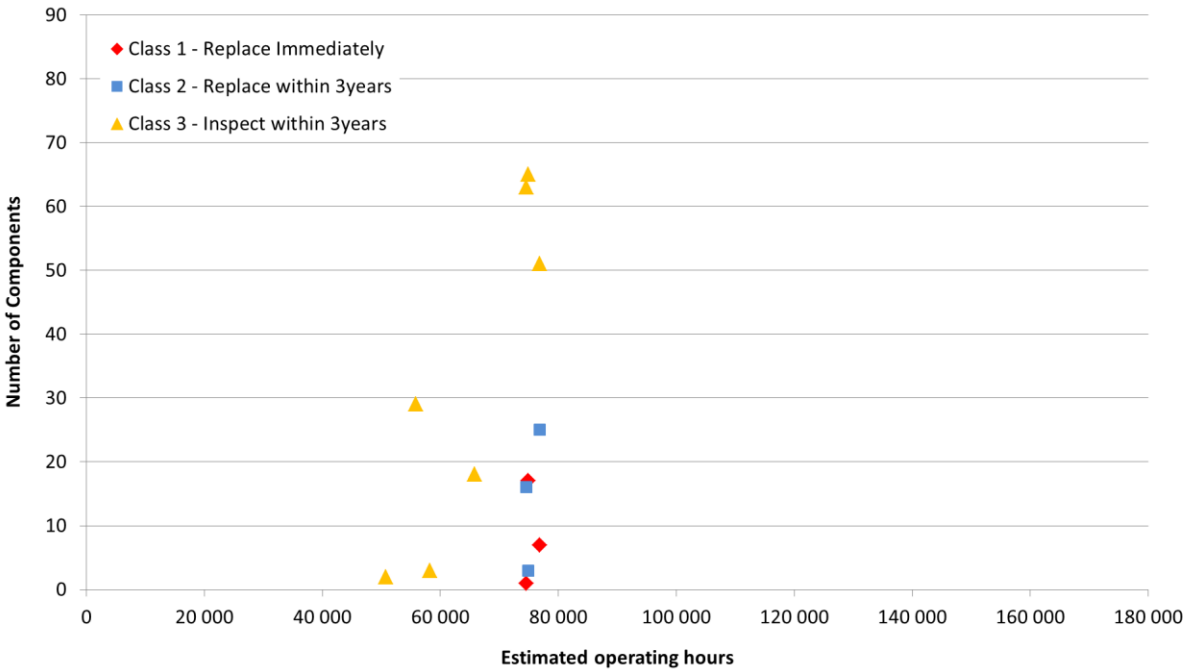


*Figure 2.History of damaged components found up to end 2013 at Power Station A*

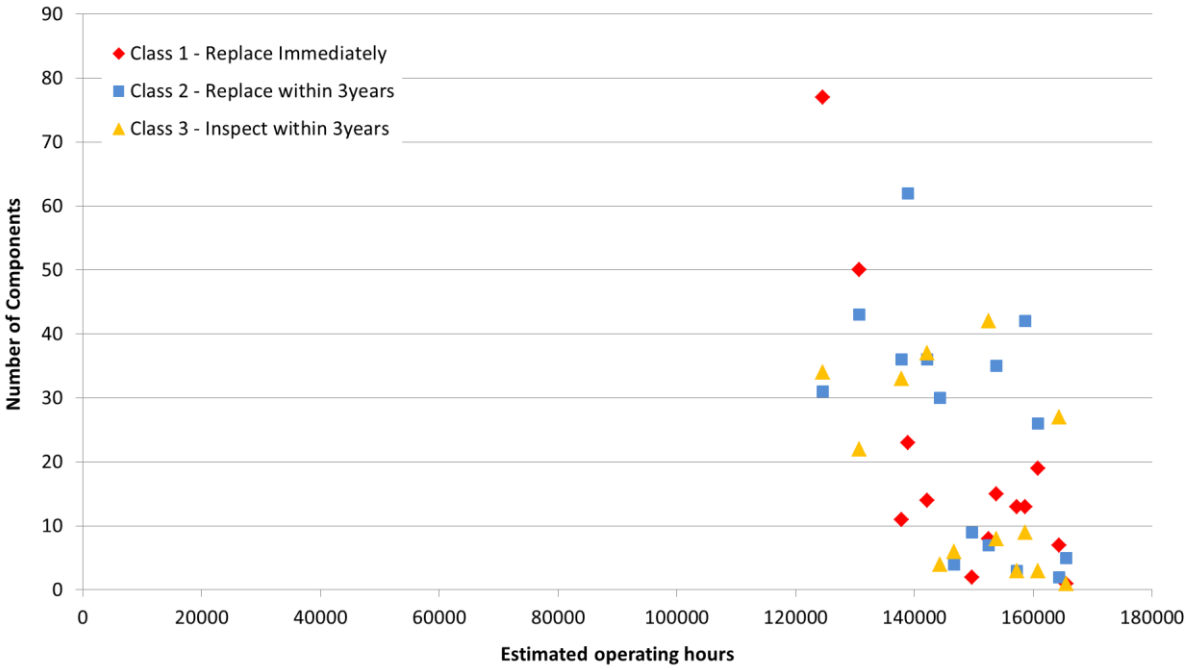


*Figure 3. History of damaged components found up to end 2013 at Power Station B*

As a comparison, similar information for another power station is provided in Figure 3. In this case, a significant amount of damaged components also occurred prior to the design life of 200 000 hours; however, the biggest contributors to early creep exhaustion were found to be operating the unit above design temperature and poor original material properties [4].

In addition to the apparent creep-fatigue damage at Power Station A, there have also been a number of turbine quench incidents that have occurred (Refer Table 1). The high pressure turbine was mainly affected and the consequences ranged from moderate to severe. Normally the turbine would be on barring when these quench events occurred. A quench is considered to be severe when the barring gear trips and the turbine shaft seizes. This is due to differential thermal expansion of different parts of the turbine which result in interference of the moving and stationary parts. Eventually after the turbine has had some time for temperature differences to dissipate, the shaft becomes free and barring can continue. Turbine rotors that have experienced such an event often sustain a permanent bend or deformation. If they are able to be returned to service, they run with high vibration.

The data in table 1 is manually captured each time the turbine inlet metal temperatures experience a high differential temperature. A total of 77 events were recorded over the time period from 2006 to November 2018 and of these, 21 events resulted in turbine damage.

Similar data for the boiler is not available. However, it should be noted that the number of superheater and main steam piping quench incidents is at least equal to the number of turbine quenches, but most likely even more.

Potentially turbine quenching at Power Station A is related to the premature creep-fatigue damage found in the boiler and main steam piping components (Figure 2).

*Table 1. Summary of recorded turbine quench events (November 2018) [5]*

| | Number of events recorded | Number of severe events that led to turbine shaft seizure | Date of latest incident |
|---|---|---|---|
| Unit 1 | 20 | 5 | 2016/08/08 |
| Unit 2 | 18 | 7 | 2017/03/30 |
| Unit 3 | 9 | 3 | 2017/10/29 |
| Unit 4 | 8 | 3 | 2016/02/28 |
| Unit 5 | 14 | 1 | 2018/08/19 |
| Unit 6 | 8 | 2 | 2018/10/08 |
| Total | 77 | 21 | |

## 1.2 Quenching at Power Station A

The boilers are once-through tower type boilers (Figure 4). In operation, pulverised coal and air are introduced into the furnace or combustion chamber via the burners (Item D in Figure 4). Combustion takes place and the hot combustion products then flow upwards through the various convective heat exchangers before leaving the boiler at the top. The convective heat exchangers consist of superheater stages and reheater stages that transfer heat from the hot gasses to steam. The superheaters produce main steam to drive the high pressure turbine and the reheaters produce intermediate pressure steam for the intermediate pressure turbine.

The furnace is lined with spiralling tubes of the evaporator that absorb heat mainly by radiation from the combustion process. Prior to the evaporation of the water into steam in the tubes that line the walls of the boiler, the feed water is preheated in the economiser. The water steam path is shown in Figure 5. After the economiser, the pre-heated water travels to the bottom of the boiler where it enters the evaporator. The water flows upwards through the evaporator and absorbs heat which results in a phase change from liquid to steam. At the evaporator outlet at the top of the boiler, water and steam are separated in the separator vessels (Item F in Figure 4). The water is collected in a collecting vessel (Item G in Figure 4) and recirculated by a pump (Item H in Figure 4) back to the economiser inlet. This recirculation occurs during start up. If the boiler load is above the Benson load (approximately 40% of the nominal load), then the outlet of the evaporator is dry and there is no water recirculation. Thus, above the Benson load, the circulation pump is off and the flow path is direct from feed water to steam.

The steam from the evaporator exits at the top of the separator vessels and then flows though the superheater stages before achieving final temperature at the boiler outlet. The superheated steam is directed from the boiler outlet to the high pressure turbine (Item N in Figure 4) via the main steam piping system.

After the steam has expanded in the high pressure turbine, it returns via the cold reheat piping system to the boiler to be reheated. The reheater typically consists of two stages (refer items O and P in Figure 4) and heats the intermediate pressure steam to the hot reheat outlet temperature. The steam then flows via the hot reheat piping system to the intermediate pressure turbine.

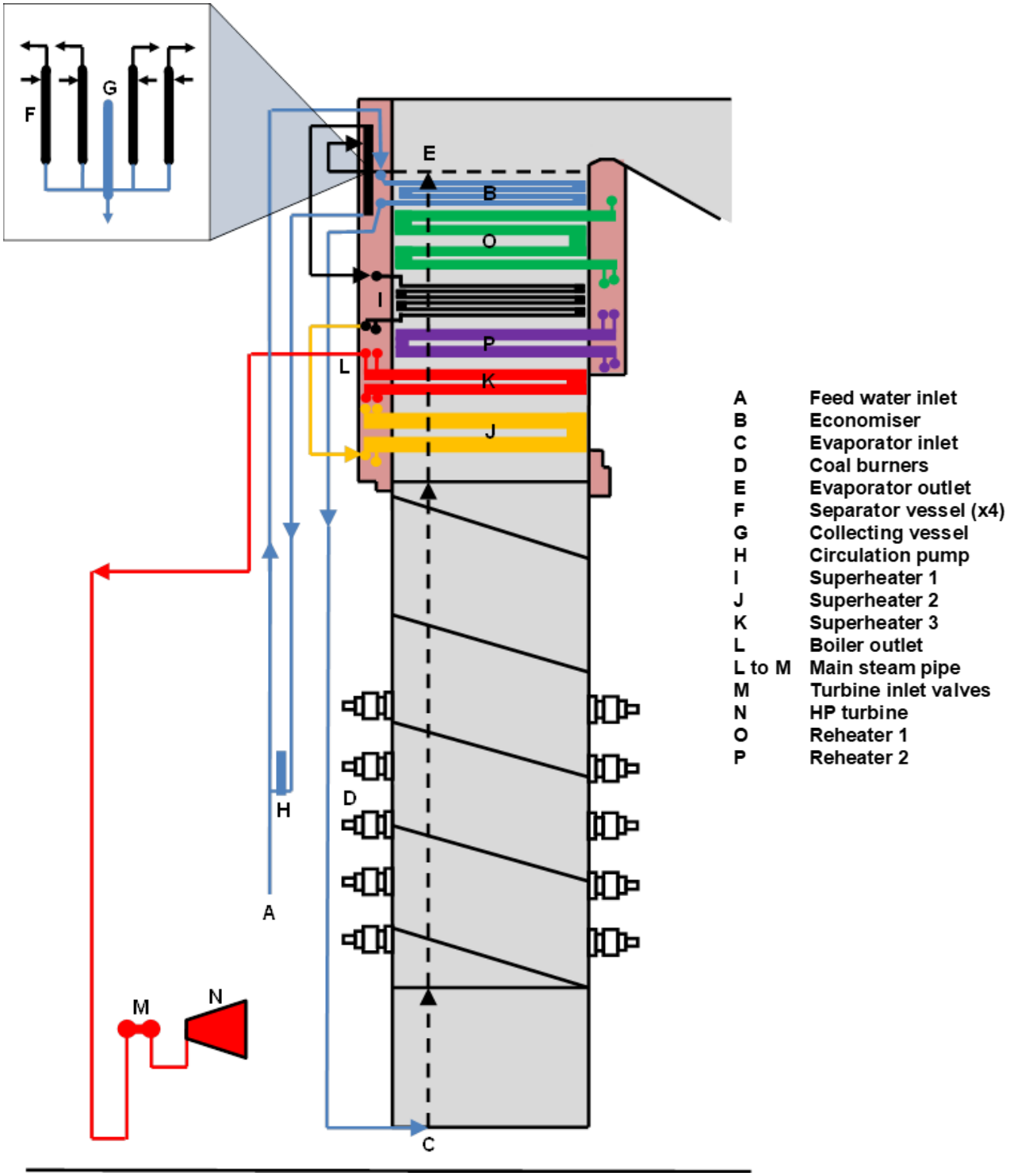


*Figure 4. Schematic of a once-through tower type pulverized fuel boiler*

Quenching typically occurs after trip or shut down of the boiler. Fires are out. The boiler is isolated on the steam side and ready for a hot restart. Steam temperature and pressure are retained as far as possible; however it is necessary to perform a purge of flue gas from the boiler which results in some cooling.

The purge is performed by the boiler fans which are used to drive air flow through the boiler and ensure any residual fuel and/or carbon monoxide is expelled. The purge is performed according to the requirements of the Fossil Fuel Firing Regulation (FFFR) [6].

Since the saturation temperature of the steam at the associated pressure is usually higher than the purge air temperature, heat is transferred away from the steam and can result in condensation. If not drained, the condensate can accumulate and flow by gravity to other parts of the system which are still close to operating temperature and this causes quenching.

Another known cause of quenching is overflow of the separating vessels. This occurs when the level in the circulation system rises to the point where the separating and collecting vessels are completely filled with water and these overflow by gravity into the superheater.

The cause of such separator overflow can often be linked to malfunction of the feed water system or the collecting vessel drains system. In the case of the feed water system, if an excessive amount of water is fed to the boiler, then the separating vessels fill up and overflow into the superheater.

The collecting vessel level is normally controlled by the circulation pump, however the level can also be managed by the quick drain valves when the level gets too high. The quick drain valves are susceptible to malfunction and often get stuck in position. Thus, at times they fail to manage the high collecting vessel level, especially when it rises sharply and this causes the separator vessels to fill and overflow into the superheater.

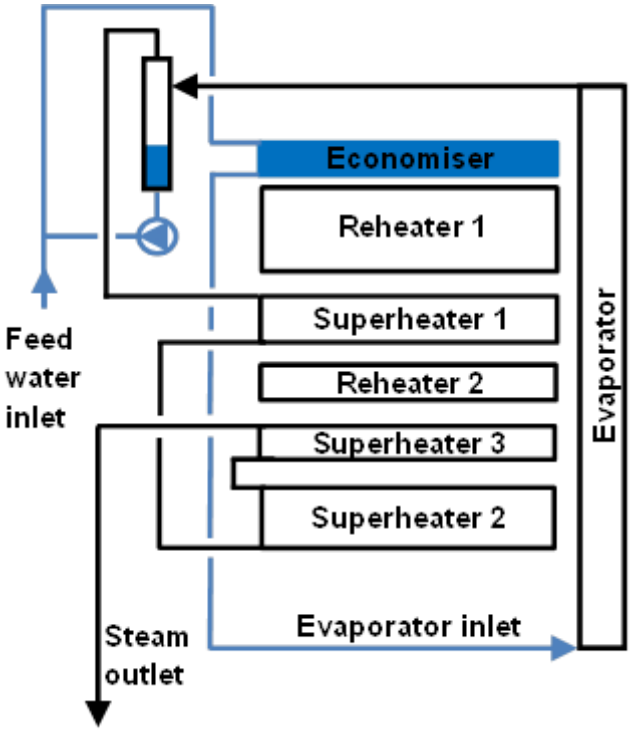


*Figure 5. Schematic showing the water and steam path through the boiler*

## 1.3 Pipe temperature measurements

Due to concerns arising from the creep-fatigue damage that was found during inspections and also due to a buckled pipe hanger on the main steam system of Unit 1 at Power Station A, a project was initiated to install strain gauges on the hanger as well as thermocouples on the outer surface of the main steam pipe. The thermocouples were installed as shown in Figure 6 on the top and bottom of the pipe at three locations. The plant code for this section of pipe is LBA13.

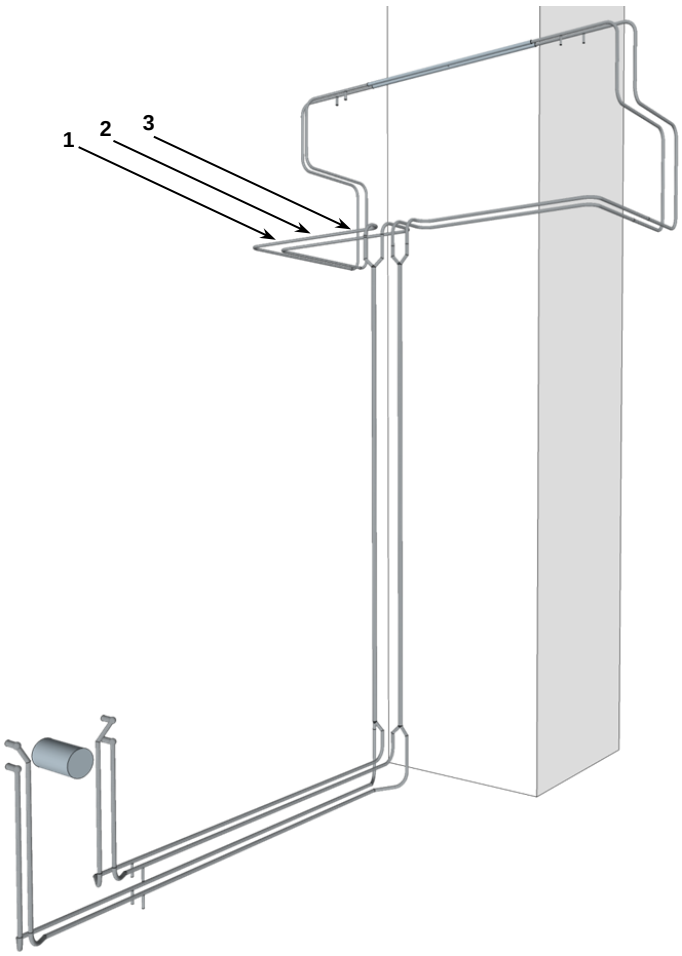


*Figure 6. Boiler outline showing main steam piping system and location of thermocouples*

After the installation, the pipe was re-insulated and this included the area where the thermocouples were located. Unfortunately, during installation the bottom thermocouple at position 1 was damaged.

The pipe outer metal temperatures were monitored from 2013 to 2015 and on a number of occasions, a significant differential temperature between the top and bottom of the pipe was observed. The highest differential temperature measured was 120$^{o}$C (Figure 7).

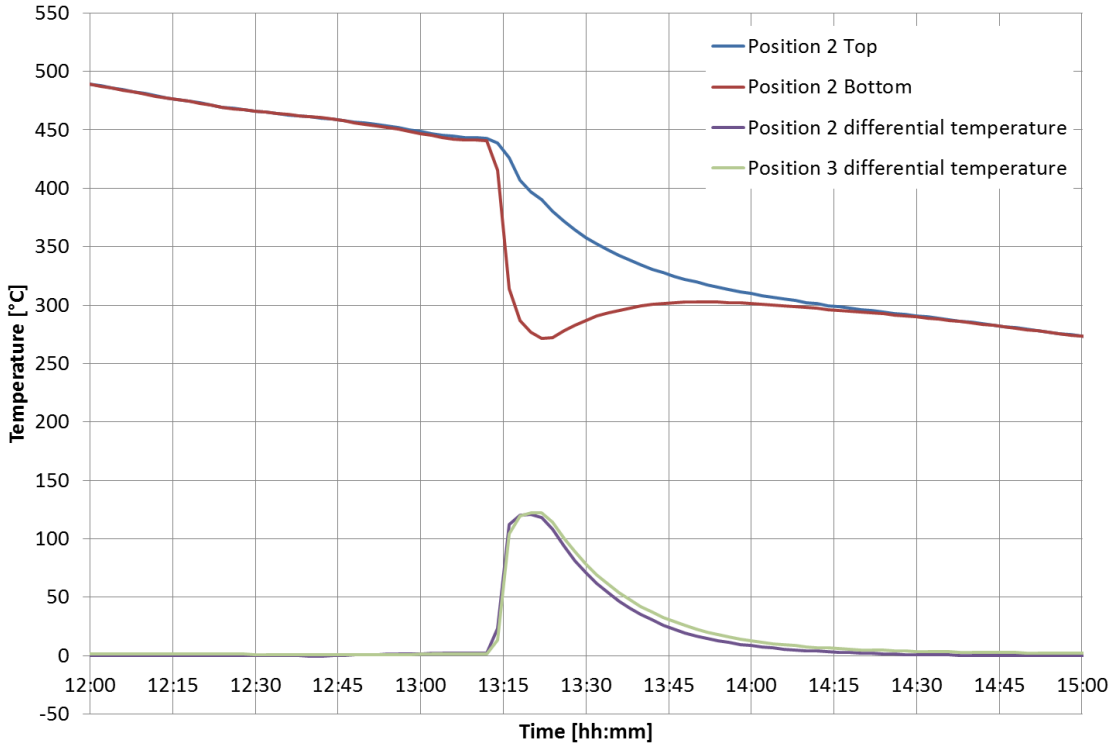


*Figure 7. Main steam pipe outer metal temperatures – Unit 1 (17/04/2015)*

The incidents of differential temperature measured on the outer surface of the pipe were correlated with data from the plant instruments as recorded in the plant data historian. It was observed that the boiler outlet steam temperatures measured on the plant had dropped close to the saturation temperature each time a differential temperature was recorded between the top and bottom of the pipe. When the boiler steam outlet temperature drops to the saturation temperature, it indicates that a two-phase mixture of steam and water exists in the system at the location of the temperature measurement point.

The data presented in Figure 8 shows a 7-day period in 2013 during which there had been a number of failed starts of Unit 1. The peaks in differential temperature shown at the bottom of the graph generally align with the boiler outlet temperature dropping to the saturation temperature at the particular point in time. Each instance of this occurring is highlighted by a black arrow on the graph.

When a steam measurement drops to saturation it does not necessarily mean that there is liquid phase present. The steam may be saturated but still dry. Saturated dry steam is not capable of selectively cooling a pipe in a way that would cause a top to bottom differential temperature. However, separated wet steam consisting of gas at the top of the pipe and liquid at the bottom of the pipe would be able to create significant differential temperatures due to the higher heat transfer that occurs to the liquid phase compared to the gas phase.

Besides liquid phase inside the pipe, only single phase flow stratification could potentially cause a differential temperature between the top and bottom of the pipe. Stratification of steam at the significantly different temperatures needed to create the measured outer temperature profiles is unlikely to exist in practice.

Thus, the evidence indicates that the differential temperature between the top and bottom of the pipe was caused by liquid inside the pipe.

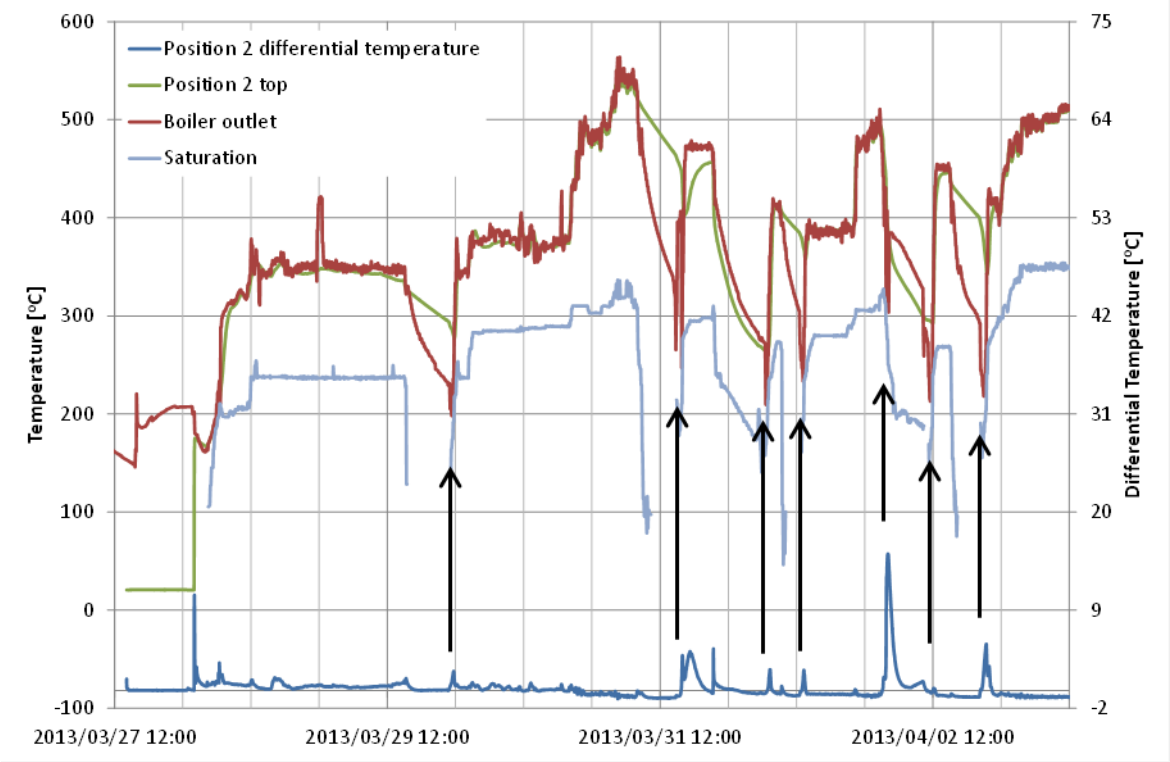


*Figure 8. Plant data and measured main steam pipe outer metal temperatures – Unit 1*

## 1.4 Problem statement

The premature creep-fatigue damage, the recorded HP turbine quench incidents and the measured pipe outer top to bottom differential temperatures, prove that quenching at Power Station A is a significant problem. In order to solve the problem, it is necessary to determine where the liquid phase in the main steam pipes originates from. Once the root cause of quenching is known, the progression of liquid in the superheater system can be determined.

The extent of damage caused by quenching is not well understood. The liquid flows through the superheater system and quenches thick-walled components such as headers and interconnecting piping which accumulate fatigue damage. Knowledge of the extent of the through-wall temperature gradients in these components will enable evaluation of the thermally induced stresses.

## 1.5 Hypothesis

A methodology can be established to determine the root cause of quenching in a once-through tower type boiler and provide information that can be used to predict the impact on thick-walled components by estimating the through-wall temperature gradients.

## 1.6 Scope of the project

This work is intended to identify the root cause of quenching at Power Station A and from that experience to develop a generic methodology for evaluating other similar plants.

A general principle to be applied is that of simplified modelling using the available, but often limited, plant information. Reduced detail and complexity that still provide useful information are preferred over detailed models that require excessive computational resources.

This project focuses on thermo-fluid process modelling and does not include the interpretation of stresses and the damage models necessary to evaluate the effects of quenching on the life of the component.

# 2. Literature Review

## 2.1 Damage caused by quenching

Plants that had quenching incidents of main steam piping have suffered damage such as wall cracks, permanent distortions, severe damage to hangers and supports, and loss of material structural properties [7]. Often quenching damage causes cracks and surface indications that require premature replacement of components [8]. Repeated cycles of thermal shock leads to permanent distortion such as excessive bending and sagging, especially if the pipe supports are not functioning correctly [9]. In general, failure of high temperature components can be attributed to creep, fatigue, creep-fatigue and thermal fatigue [10].

Creep damage occurs due to exposure to high temperatures and stress and it leads to deformation that causes dimensional changes of components. Localised deformation can cause swelling and eventual leaks in headers, steam pipes and superheater tubes. The failures are related to intergranular cavitation and crack growth over time [10].

Generally, creep related damage appears at welds before it affects the original material. Thus, the welds are used as an indicator of the condition of the overall component and non-destructive testing is focused on welds [10].

Fatigue is weakening of a material by microscopic cracks that occur due to the repeated application of loads above a certain threshold value. Cracks begin to form at stress concentrations and grow with each load cycle. Eventually the crack will reach a critical value and rapid brittle fracture of the component will occur. The fatigue life of a component is affected when the component is exposed to simultaneous creep loading. The combined damage mechanism is referred to as creep-fatigue.

Thermal shock failure typically refers to sudden failure as a result of a rapid change in temperature. When the exterior of a component is exposed to a temperature change, then during the transient, parts of the component are at different temperatures. This causes thermally induced stresses due to the change in volume of the material which is a function of its temperature. The volume of the material is related to the temperature by the coefficient of thermal expansion. The differences in volume cause thermal stress and if this stress exceeds the strength of the material, then the component will crack.

Thermal fatigue refers to repeated application of thermal loads that cause damage in the material by microstructural cracking and accumulation of those cracks. Thermal fatigue arises from temperature gradients such as those typically observed during start up, shut down and load changes of a power plant. The principal components at risk are any thick-walled sections such as boiler

superheater headers, steam pipework, valves, turbine stop valves, governor valves, loop pipes and turbine inlet belts [11] [12] [13]. High pressure feed water heaters and economiser inlet headers are also frequently exposed to similar effects due to rapid cooling by cold feed water. Thin walled sections such as boiler tubes and reheater headers are less prone to the problem [12].

Water quench thermal fatigue damage in pipes and headers is often characterised by internal longitudinal cracks [14]. This arises from the significant tensile stresses at the inner surface of a hot component undergoing quenching by water.

A steam pipe might not crack from fatigue damage caused by quenching, but the residual stresses in the pipe may result in a reduction in the creep rupture life of the pipe material [7]. This occurred in the case of Philadelphia Electric's Eddystone Unit No.1 power plant in March 1983, where significant cracks were found in the main steam pipes. A sample of the failed pipe is shown in Figure 9. In this case, the cause of the cracks was found to be creep rupture; however, the creep rupture occurred prematurely at 130 000 hours of operation and the pipes had not swelled as would be expected in the case of normal creep rupture failure. It was determined that the failure occurred because of residual stresses induced in the piping by repeated thermal 'down-shock' [15]. The paper does not explain the details of how the repeated 'down-shock' or quenching had occurred, but the cracks only occurred in piping upstream of the boiler stop valves, indicating that the quenching had happened when the valves were closed.

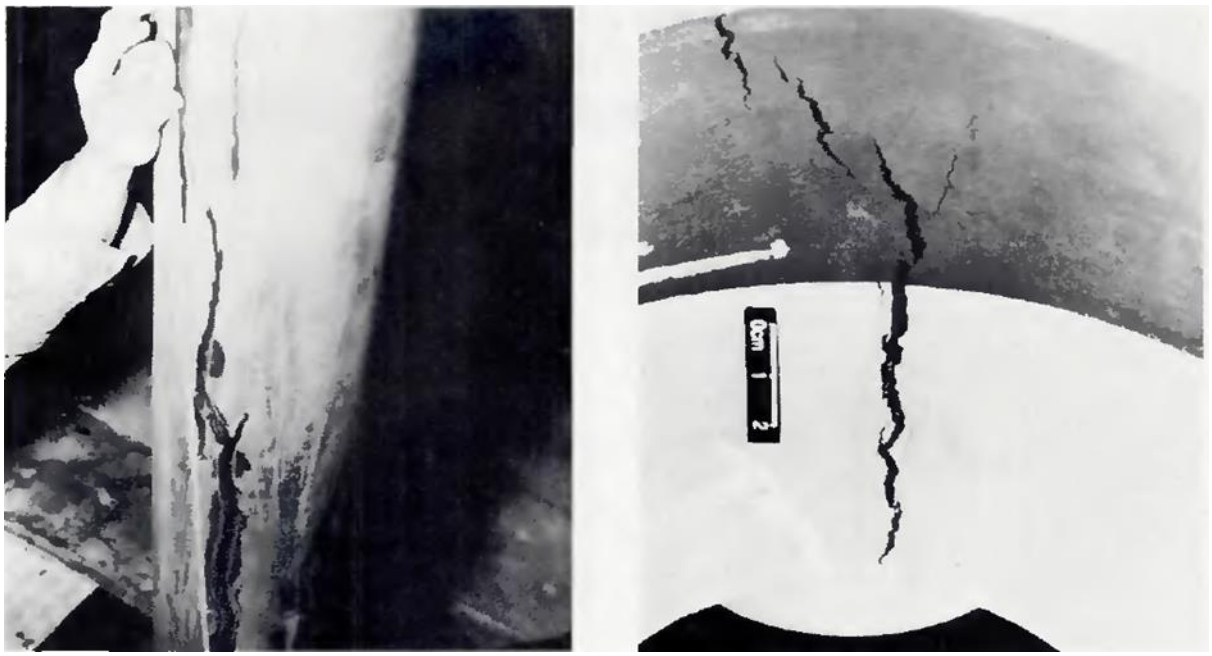


*Figure 9. Near through wall longitudinal cracks in 316 Stainless steel main steam pipe (Eddystone power plant) [15].*

Sudden change of temperature of metal components has been studied by various authors [16]. When quenching occurs in a metal component, there is a sudden contraction of the material at the surface which results in tensile stresses. As diffusion of heat occurs through the material, the stresses are reduced and almost disappear when a steady state is again reached. The high stresses, particularly over a number of stress cycles, lead to thermal shock cracking on the surface of the component.

Price [16] published results of testing of carbon steel specimens that were repeatedly quenched in a test rig. From the results, guidelines are provided for the avoidance of crack initiation and also the assessment of existing cracks. Price notes that there are four stages to failure as a result of thermal shock fatigue combined with a primary stress. These are:

1. Initial crack growth due to the local stress exceeding the tensile strength of the material. This region of crack growth is termed the High Strain Fatigue (HSF) region.
2. Corrosion dominated crack growth region.
3. Paris growth region (linear elastic fracture mechanics) where corrosion is limited because of access into the crack. In this region, the crack is often arrested.
4. Plastic collapse: Final failure occurs in carbon steels when the crack fails to slow down and arrest before there is plastic collapse of the remaining material.

To avoid crack initiation, Price recommends that the temperature gradients are controlled to maintain stresses below the maximum allowable stress of the material. The following equation is used to determine the maximum theoretical thermal stress ($\sigma_{max}$):

$$\sigma_{max} = \frac{E\beta\Delta T_m}{2(1-\nu)} k_f \quad (1)$$

E is the elastic modulus of the material, $\beta$ is the coefficient of thermal expansion, $\Delta T_m$ is the maximum temperature difference that occurs at the surface, $\nu$ is Poisson's ratio and $k_f$ is the stress concentration factor due to geometric discontinuities. The maximum temperature difference can be taken as the difference in maximum and minimum fluid temperature that occurs. This assumes infinite heat transfer at the surface of the material and is reasonable for quenching situations with boiling heat transfer.

Taler et al. [17] studied the allowable heating and cooling rates of a superheater header and note that during heating the compressive stress caused by temperature change on the inside of the pipe is compensated by tensile pressure stresses. Thus, the total circumferential stress is greater at the outside of the pipe which becomes the limiting factor for heating of the header. During cooling, both pressure and thermal stress at the inside of the pipe are tensile and thus the strength of the inside of the pipe wall becomes the limiting factor. For the outlet header of a final superheater, Taler et al. calculated allowable heating and cooling rates of 4.45K/min and 5.4K/min [17].

Taler et al. [17] provide formulae for quasi steady state evaluation of stress in cylindrical components undergoing a constant rate of heating or cooling. By superposition of stress, we have that the combined stress, $\sigma_\varphi$, is the sum of the hoop stress due to pressure, $\sigma_p$, and the thermal stress, $\sigma_T$:

$$\sigma_\varphi = \sigma_p + \sigma_T \tag{2}$$

The stress due to pressure can be evaluated from:

$$\sigma_p = \frac{pd_m}{2s} \tag{3}$$

Where *p* is the pressure, $d_m$ is the mean diameter and *s* is the wall thickness. Then the thermal stress can be evaluated using the quasi steady state formula as follows:

$$\sigma_T = \phi_{cyl} \frac{V_T s^2}{\alpha} \frac{E\beta}{1-\upsilon} \tag{4}$$

$$\phi_{cyl} = \frac{(u^2-1)(3u^2-1)-4u^2 \ln u}{8(u^2-1)(u-1)^2} \tag{5}$$

$$u = \frac{r_2}{r_1} \tag{6}$$

where $\phi_{cyl}$ is the shape factor for a cylindrical vessel, $V_T$ is the constant rate of temperature change, α is the thermal diffusivity, $r_2$ is the outer radius and $r_1$ is the inner radius of the pipe or component.

Thermal stratification has been studied in nuclear plants where failures have occurred. Three failures in unisolable portions of piping systems attached to the reactor coolant loop were caused by thermal stratification as a result of valve leakage and subsequent thermal cycling caused by turbulence penetration [18]. Subsequent monitoring at another plant indicated top to bottom thermal gradients of 215°F (102°C), with cycling having a 2-20 minute period.

Schuler and Herter [19] discuss the stresses associated with thermal stratification and thermal shock loading. For a fluid stratification temperature difference of 100°C and small interface layer, stresses of 300MPa are produced in the pipe wall [19]. Thermal shock loading refers to the sudden change of temperature passing a point in the piping system. The whole inner surface of the pipe experiences a sudden change in temperature.

Da Silva et al. [20] measured temperatures and strains on the external surface of a section of 304L stainless steel piping with an external diameter of 141mm and a wall thickness of 9.5mm. They found that temperature changes of 160°C produced maximum principle stresses of 80MPa on the outer surface of the pipe during heating. Stresses were measured at the bottom of the pipe for heating and cooling cycles. Stress reduced during cooling cycles. This is to be expected for the outside surface of the pipe. The inner surface most likely experienced high tensile stress during the cooling cycle but those strains were not measured directly.

It is clear that quenching can be very costly since the resulting high stresses, particularly over a number of cycles, can lead to thermal shock cracking on the surface of the component, permanent distortion, severe damage to hangers and supports, and loss of material structural properties that result in premature replacement of components.

### 2.1.1 Design for Fatigue

Historically, the design codes assumed that the effects of fatigue were contained within the conservatism of the design stresses. This was an adequate assumption for base load plants but it is now recognized that fatigue, especially in conjunction with creep-degraded material, is a significant concern [11]. Modern design codes include creep-fatigue interaction as a design criterion [21] [22] [23]. An example of applying the ASME calculation procedure for creep-fatigue design of a superheater tube is given by Stoppato et al [24] and Mirandola et al [25].

When designing a power plant, the expected number of load cycles is specified by the purchaser - typically the number of cold starts, warm starts and hot starts that the power plant is expected to endure. The designer determines the stress cycle that the component will experience based on process conditions and uses the stress cycle to determine the fatigue life fraction consumed per event. Each transient event can be considered to consume life of the power plant components.

The European Norm (EN12952-3) suggests that a cold start is 20 times more damaging than a warm start and the stress range for a hot start is typically below the fatigue limit and does not contribute to total fatigue damage [26]. The total life before crack initiation is determined from the creep-fatigue limit curve for a particular material [27]. Figure 10 below shows an example of the creep-fatigue limit curve and illustrates the possible damage paths that may be followed by a particular power station component. The potential reduction in life fraction due to transient operation can be seen.

The allowable rate of temperature change for cold starts for thick-walled components (90mm) is around 2$^{o}$C per minute and can be up to 9$^{o}$C per minute for 2000 cycles fatigue life [26]. The allowable rate can be chosen based on a fatigue life calculation or the stress limits for protection of the inner magnetite layer. To prevent cracking of the internal magnetite layer, overall stress limits are minus 600MPa to plus 200MPa.

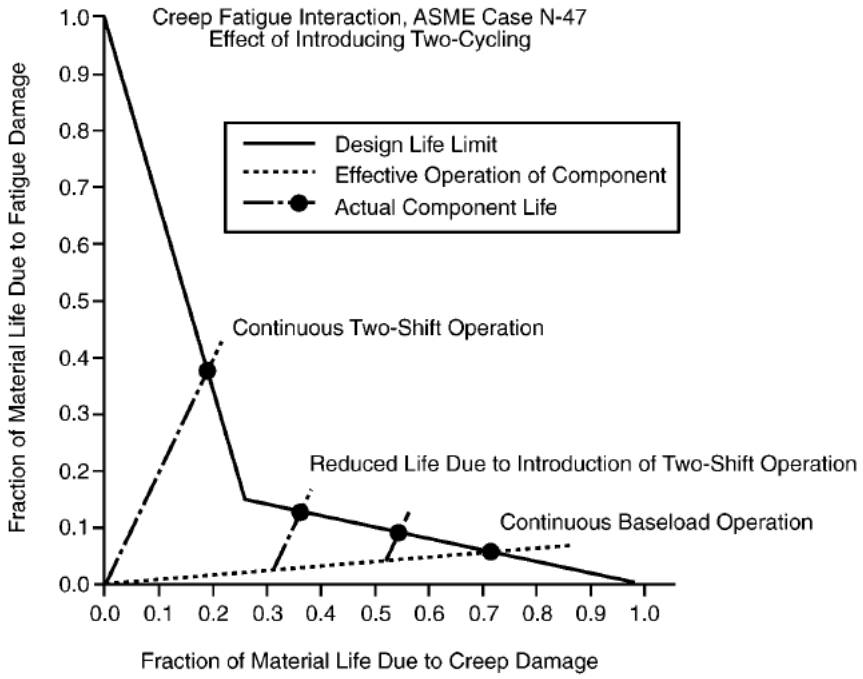


*Figure 10. Interaction and consequences of creep and fatigue (Based on ASME N-47) for a typical power plant steel (2.25Cr1Mo) [11].*

High temperature superheater headers operate in the creep range and are subjected to the combined effects of creep and thermal fatigue related to cycling and load following operation (not quenching). Problems include: Internal bore hole and ligament cracking and external weld cracking at tube stubs, nozzles and hanger plates [28]. There is limited access for repair inside the header and generally if damage occurs, the header will need to be replaced. Kwon et al. [29] demonstrate how repeated temperature fluctuations of greater than 30°C are the biggest contributor to crack growth in a superheater outlet header, highlighting the need to better understand and manage the problem.

The EN standard ignores superheater quenching which occurs due to the presence of condensate inside the still-hot superheater during gas purging. This quickly cools some parts of the component relative to others, and induces low cycle fatigue in the overall warm start-up cycle. Although the phenomenon is damaging, it is very difficult to take account of because of its empirical nature. Good engineering practice must prevail in the form of an effective drainage system [26].

The above discussion applies to known operating scenarios that can be taken into account at the design stage. Quenching is not considered to be normal operation and is thus not considered in the design.

### 2.1.2 Creep and fatigue monitoring

Thermocouples are installed on the plant to monitor metal temperatures. This is done based on experience and for thick-walled components in highly stressed areas [12]. The measurement may be outer surface temperature or even through-wall measurements [2] [17]. Using outer surface temperature measurements only, it is not possible to determine the stresses when there are rapid changes in inner fluid temperature [17].

It is possible to estimate the thermal gradient experienced by the component from the temperature data. Using finite element analysis methods, the temperature gradients can be translated into stresses. Based on the stress cycle for the full transient event, the life consumption can be calculated [27]. These principles are used by the commercially available creep and fatigue monitoring tools. The tools however don't relate the measured temperatures to the process conditions which induced them. They simply measure the damage a component accumulates in order to predict the time when replacement will be necessary.

Thermal stresses in thick-walled components are commonly measured by installing two thermocouples at a selected location on a component. The thermocouples are located at differing depths, such as one thermocouple located close to the inside surface to give an inner surface temperature, and the other thermocouple located at half the wall thickness to provide a mid-wall temperature measurement (Figure 11). Some boiler manufacturers make use of three thermocouples located at different depths to improve the accuracy because the estimated stresses using only two measurements are understated [17].

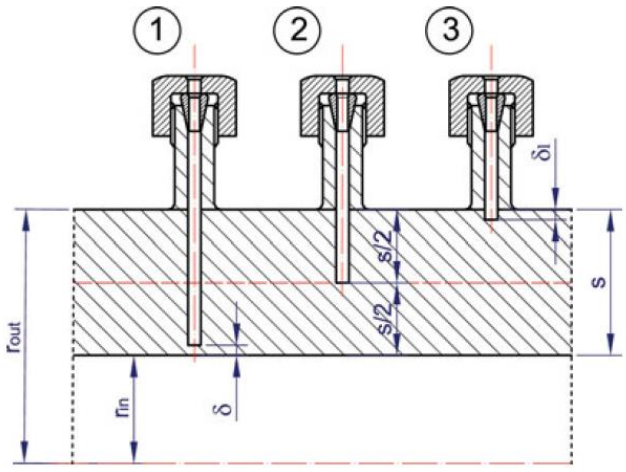


*Figure 11. Mid-wall temperature measurements by thermocouples located at different depths [17]*

With an inner thermocouple and one at the midwall, the thermal stress at the inside surface of the wall can be determined by the following formula:

$$\sigma_{in} = \frac{E\beta}{1-\nu}\left(T_m - T|_{r=r_1}\right) \tag{7}$$

This formula assumes a quasi-steady state and is appropriate when temperature changes are not too fast [17]. Thus the method is not applicable during quenching. The mean temperature is given by:

$$T_m = \frac{2}{r_o^2 - r_{in}^2}\int_{r_{in}}^{r_o} rT(r,t)\, dr \tag{8}$$

Which can be approximated using the trapezoidal rule:

$$T_m = \frac{1}{r_0^2 - r_{in}^2}\sum_{i=2}^{N}(r_{i-1}T_{i-1} + r_i T_i)\,\Delta r \tag{9}$$

The mean temperature may in some cases be insufficient. Therefore another method of temperature determination is provided by fitting a second order polynomial to the measured temperature history to obtain the temperature distribution through the wall [30]:

$$T(r,t) = a(t) + b(t)r + c(t)r^2 \tag{10}$$

Assuming that the outer surface is adiabatic, then the gradient of the temperature function at the outer wall, $r_{out}$, must be equal to zero. It is not necessary to make this assumption if a third temperature measurement on the outer surface is installed.

Now using the two measured temperatures, $T_1$ at $r_{in}$ and $T_2$ at $r_m$ respectively, the following polynomial coefficients are obtained:

$$a = T_{in} - \frac{r_{in}(T_{in}-T_m)(2r_{out}-r_{in})}{(r_m^2 - r_{in}^2) - 2r_{out}(r_m - r_{in})} \tag{11}$$

$$b = \frac{2r_{out}(T_{in}-T_{out})}{(r_m^2 - r_{in}^2) - 2r_{out}(r_m - r_{in})} \tag{12}$$

$$c = \frac{T_{out}-T_{in}}{(r_m^2 - r_{in}^2) - 2r_{out}(r_m - r_{in})} \tag{13}$$

Thus, by measuring the temperature at the inner surface and at the midwall of a component, the local temperature gradient and thus the local thermal stress can be calculated using the above equations. This calculation can be performed online and thus the thermal stress cycles experienced by the component can be monitored.

## 2.2 Sources of water

The water or condensate that causes quenching of hot components in the boiler superheater and piping systems can originate from various potential sources. Rosario [8] discusses spray attemperation systems and how they are known to cause localised quenching damage due to spray pattern, poor atomisation of water droplets and control logic problems that result in over-spraying under certain operating conditions.

King [9] explains that the water can originate from reverse flow from drains or sample lines or by condensation of steam. In particular, King mentions that horizontal superheater elements are prone to condensation of steam in the tube bundle and subsequent flow of the liquid by gravity into headers and piping that are still at a higher temperature. This causes quenching of the hot components.

Mandke et al. [7] also list back flow from drains as a potential source of water as well as failure of spray attemperation systems and boiler main steam stop valves getting stuck. Even if boiler stop valves are closed, superheater headers are still at risk [7].

EPRI [31] performed a case study of shutdown management of a once-through subcritical plant and found that in that case, quenching was caused by condensation in the superheaters, faulty drain valves and collecting vessel overflow. In their study, they also considered reverse flow, excess attemperator spray and inadequate drain capacity.

Cooling of the superheaters by unfired gas flow through the furnace occurs when the boiler purge is performed. This is done by running the fans and expelling the gas from the boiler. The unfired air flow enters the furnace after being heated by the air heater where it attains a temperature of around 250°C. The furnace section of the boiler does not contribute significantly to increasing the temperature of the air flow and thus the air flow into the convection pass is at a temperature below the temperature of the superheater. If the heat exchanger contains superheated steam, then the steam and metal temperatures in the heat exchanger will be reduced. If the temperature of the steam is already reduced to the saturation temperature, then further heat transfer away from the steam at constant pressure results in condensation of the steam to water. Figure 12 shows the condensing process from point b to c on temperature vs entropy axes for steam at constant pressure. The volume of condensate produced is dependent on the magnitude and duration of heat transfer.

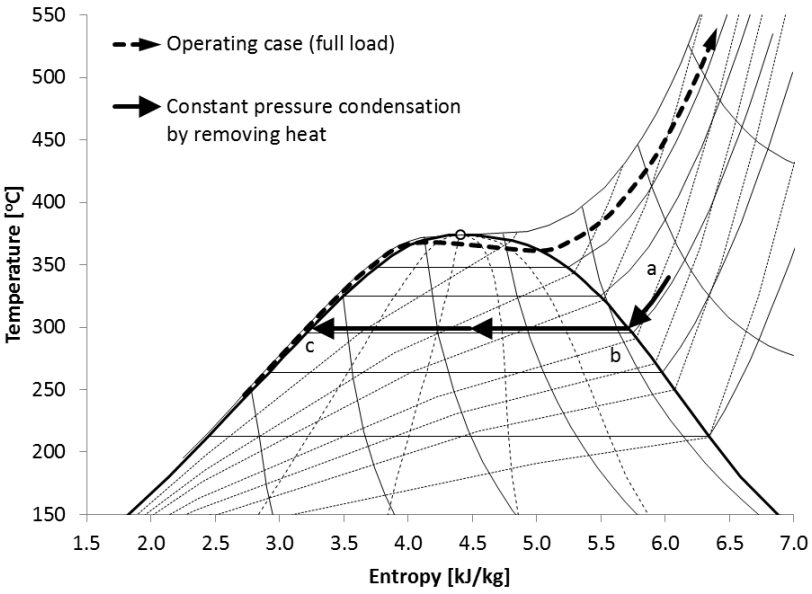


*Figure 12. Constant pressure condensation by removal of heat (T-s diagram)*

The design of most large coal fired boilers allows for drainage by sloping the headers, pipes and tubes of the heat exchangers towards the drainage points. The drains are opened if the measured temperature at the low point drops below a set value, such as the saturation temperature plus 30°C [32]. Some condensation of steam in the heat exchangers is inevitable under shutdown conditions. However, the volumes of condensate produced are usually small and are controlled by drainage measures.

In cases where the drains fail to open or the drains have insufficient capacity to deal with the volume of water or condensate that is present, this liquid can accumulate and flow by gravity to other parts of the system [33]. If this occurs when a boiler has recently been shut down, parts of the boiler and main steam piping system are still hot and experience a rapid temperature transient or quenching event.

One solution for avoiding condensation is to depressurize the boiler at each shutdown or trip. This method is typically employed in combined cycle gas turbine (CCGT) plants to avoid quenching [32]. The downside of this is that pressure part temperatures are cycled and it requires significantly more time to restart the plant, thus pressurized hot restarts are preferred.

Cooling down the boiler for emergency repairs can result in quenching [7]. The boiler fans are used to force cool the boiler and when the superheater tube metal temperature drops below the saturation temperature then steam condenses within the superheater section. The condensation of steam significantly reduces the specific volume and the subsequent reduction in pressure in the system allows water at the evaporator to flash into steam and travel into the superheater. The phenomenon is known as a thermal siphon [7]. In pendant type superheaters, water from

condensation flows down into the bottom of the u-tubes and blocks the tubes. This halts the thermal siphon effect. Such blocking of the flow path is generally not possible in horizontal type superheater heat exchangers.

Although pendant type superheaters are less prone to the thermal siphon effect, there is a significant disadvantage of short term overheating of tubes due to the blocked steam flow path when the boiler is fired again [34]. Another disadvantage associated with undrained low points is that, during start-up, the water can be blown out of the tube into already hot downstream components. This was the case for a certain design of superheater outlet header where water trapped in a spacer tube of a pendant superheater was repeatedly blown out during startup [14]. The water was blown out of the spacer tube by pressure difference and the water quenched the outlet header.

The second major mechanism of quenching listed by EPRI [31] is overflow of the separator vessels (Refer Figure 4, item F). The process is shown from point d to point e in Figure 13. Liquid is added to the closed system which increases the mass inside. If the added liquid is close-to or above the saturation temperature, then this results in a pressure increase as well as condensation of the steam. If the added liquid is sufficiently subcooled, then the steam is condensed with a decrease in pressure.

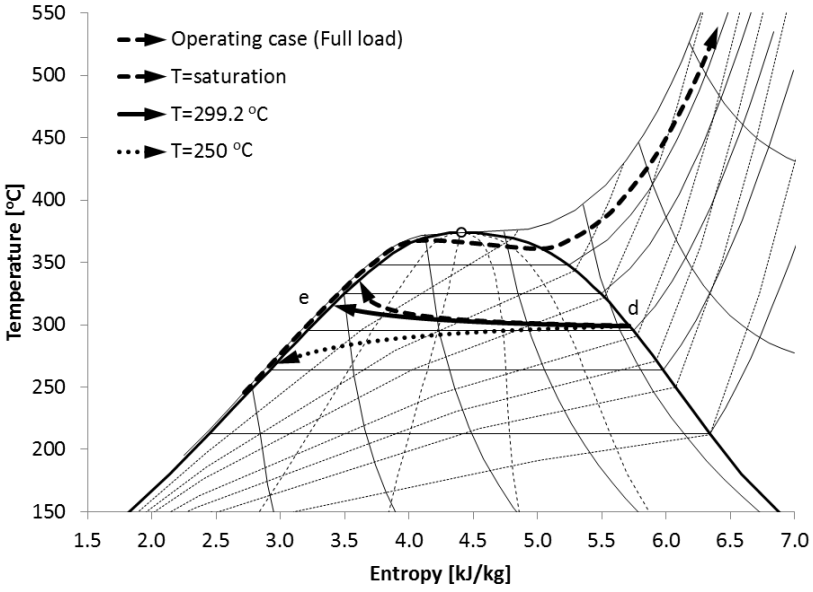


*Figure 13. Condensation by adding liquid (T-s diagram)*

In once-through boilers, the start-up or collecting vessel has a relatively small volume compared to the drum of a drum boiler. This makes it more difficult to control the level during circulation or start-up operation of a once-through boiler.

The start-up system for subcritical or supercritical boiler designs includes separators with tangential steam/water inlet nozzles and a water storage tank or collecting vessel [35]. At the design phase of a boiler, the selection of a minimum once-through flow determines the Benson point and depends on such factors as mode of operation, circuit stability, and tube materials. For boilers that are primarily base loaded, the once-through minimum load should be selected as high as possible. This results in the lowest pressure drop in the waterwalls at full load. Steam generators that are required to cycle must be designed for a lower Benson point so that once-through operation is extended to the lowest load practical [35].

Traengbaek [36] discusses control strategies for maintaining the collecting vessel level of a once-through boiler at low load operation when operating on load with recirculation is necessary. Load increases are considered. The control is constrained to avoid exposing the separators and collecting vessels to temperature gradients exceeding 0.1K/s. The flow through the recirculation pump is used to control the collecting vessel level. However, non-minimum phase behaviour is noted when the collecting vessel level rises and the controls increase the recirculation flow, but the recirculation flow is much hotter than the feed water and causes a further increase in the collecting vessel level due to the reduced density of the hotter fluid in the recirculation loop.

Boje [37] proposes an economiser bypass system for improving the control of the circulation system on a once-through boiler. The bypass is chiefly aimed at reducing temperature fluctuation but Boje notes that it will also reduce oscillations of the collecting vessel level control.

Eitelberg and Boye [38] studied the control of collecting vessel level and proposed a simple condition for circulation control loop design, namely that the collecting vessel level control bandwidth should be less than the feed water control bandwidth. Practically this means that the circulation control system performance depends on the response times of the pumping equipment.

Control of the collecting vessel level during start up is a problem in large once-through boilers. Present literature proposes improved control philosophies and there are dynamic thermo-fluid models available to analyse the circulating system as described later in this chapter. The factors that may cause excessive collecting vessel level and the consequences of collecting vessel overflow into the superheater are not presently available.

In general there is a lack of specific analysis related to the quenching of the superheater by condensation or by overflow of the collecting vessel system. There is also no methodology available for identifying the sources of liquid that cause quenching.

## 2.3 Thermo-fluid modelling

Modelling of the steam and water processes that lead to and exist during quenching is necessary to understand the cause and define the problem. It is expected that the heat transfer is transient and thus a simulation of the overall behaviour is required. A review of applicable thermo-fluid modelling is given in this section.

### 2.3.1 Lumped parameter heat exchanger methods

A mass and energy balance across each stage of the boiler superheater has been shown to be a useful tool for analysing the performance from measured plant data [39]. The steam inlet and outlet temperatures are measured and together with the pressure this is used to find the inlet and outlet enthalpy. The measured steam flow can then be used to obtain the overall quantity of heat transferred to the steam. The mass and energy balance can be applied to the streams crossing the boundary of any control volume and in this case it provides the overall resultant heat transfer of a superheater stage. The method does not enable calculation of the actual heat transfer process.

The heat transfer process in heat exchangers is commonly analysed using the logarithmic mean temperature difference (LMTD) or the effectiveness number of transfer units (ε-NTU) method [40]. Both methods provide similar results when applied correctly. The LMTD method is useful when the inlet and outlet temperatures are known but it requires iteration if the outlet temperatures are sought. The LMTD method is used by Hajebzadeh et al. [41] to model the heat exchangers of a 320MW boiler in steady state. Radiation and convection heat transfer are considered. Plant data for loads from 240MW to 290MW are compared to simulated values with a maximum relative error of 8.72%.

The ε-NTU method solves for outlet temperature in one step if the heat exchanger characteristics are known. It is used by many to predict the heat exchanger outlet temperatures when modelling superheaters and reheaters of large coal fired boilers [42] [43] [44]. The ε-NTU method requires that the flow configuration of the particular heat exchanger is characterised by a relationship of effectiveness versus number of transfer units. The simplest case is for a single stream heat exchanger as follows:

$$\varepsilon = 1 - e^{-NTU} \tag{14}$$

$$NTU = \frac{UA}{C_{min}} = \frac{UA}{(\dot{m}c_p)_{min}} \tag{15}$$

$$\varepsilon = \frac{C_H(T_{H,in} - T_{H,out})}{C_{min}(T_{H,in} - T_{C,in})} = \frac{C_C(T_{C,out} - T_{C,in})}{C_{min}(T_{H,in} - T_{C,in})} \tag{16}$$

Where $U$ is the overall heat transfer coefficient, $A$ is the total area of the heat exchanger, $C_{min}$ is minimum heat capacity of the two streams, $\dot{m}$ is the mass flow rate of the stream, $c_p$ is the specific heat capacity of the fluid at constant pressure and $T$ refers to temperature of the hot, subscript H, and cold, subscript C, fluid temperatures respectively.

A block simulation method is demonstrated by Kim et al. [45] and applied to analyse a pilot scale circulating fluidized bed boiler. In the convective pass, the heat exchangers are considered as well mixed tanks or blocks. Thus, there is only a single temperature for each block, and it is equal to the average of the inlet and outlet temperature of the flow. A mass and energy balance of the gas block and of the steam block is carried out. Heat transfer is calculated based on the temperature difference between the blocks. This simplification removes the need for using the LMTD or ε-NTU method.

Use of lumped heat exchanger methods for simplified calculation of steady state heat transfer in large boiler superheaters is common. Application of these methods to analyse quenching has not been considered. In the superheater quenching situations discussed in this document, the steam flow is much lower than design values. The flow rate is also unknown and transient. These are significant differences that require new application of the lumped parameter approach to enable useful simplified models for superheater quenching to be developed.

### 2.3.2 Systems Modelling of Thermo-Fluids

Thermal-fluid dynamic component or system models that are properly constructed consist of the following elements [46]:

1. The three fundamental conservation laws of mass, energy and momentum.
2. Closure relations that describe the relevant fluid property relationships.
3. Closure relations that describe the relevant component specific characteristics.
4. Initial and boundary values.

In system modelling, the conservation equations are typically integrated between the inlet and outlet of a complete component or various increments of a larger component in a simplified one dimensional approach [46].

In general, a simplifying assumption is made that the fluid is homogeneous. A two-phase flow can be considered as homogeneous provided that the velocities of the liquid and the gas can be considered to be the same throughout the volume. The assumption of thermal equilibrium implies that the phases all have the same temperature.

The review paper by Alobaid et al. [47] describes the progress in dynamic modelling of coal fired plants. Existing dynamic plant models have been developed for response to disturbances; start-up procedure evaluation and flexibility increase. Generally, these models are extensive and have successfully predicted the integrated response of the whole plant for the cases considered. For specific application to once-through coal fired power plants, transient process models for load changes have been considered and are presented by Starkloff et al. [48], Kuronen et al. [49] and Sarda et al. [50] amongst others.

More recently, a dynamic model of a 600 MW supercritical plant was developed in APROS and used for studying start-up from ignition to 30% load [51]. This model included the economiser, evaporator, separator, water circulation pump and the superheaters. The separator and water tank (collecting vessel) were modelled as a single cylindrical volume wherein the level was calculated. The evaporator part of the model considered the two phases separately in a six equation formulation. When steam was being generated in the evaporator, the “false water level phenomenon” in the separator would appear. This caused the separator / collecting vessel level to rise rapidly and require a particular control strategy utilising quick drain valves and circulation flow to manage the level. The authors demonstrate that the level could be controlled [51].

Tang et al. [52] demonstrate the application of steady state modelling of the water walls of the evaporator of a circulating fluidized bed boiler. Their approach is to utilise the axis of symmetry down the centre of the boiler and discretise half the evaporator into 68 flow loops connected in series and parallel. The loops each consist of multiple pipes in parallel. Each loop is discretised into a number of smaller elements in the flow direction. The gas side and water/steam side heat transfer coefficients are calculated for each element. The model calculates the flow distribution in the tubes based on the pressure drop characteristic. The method is used to design the heat transfer surface for the load range from 100% load and down to 25% load. The flow distribution in the loops and the metal temperature distribution were found to be acceptable for the design of the boiler.

Zima [53] describes a generic modelling process applied to a 910MW supercritical pulverised coal boiler with the aim of calculating the required boiler pressure setpoint curve. The curve, known as the ‘modified sliding pressure’ curve determines the amount of throttling that is necessary at the turbine inlet valves to enable a rapid load increase when the valves are opened fully. The response from opening the valves is transient because the boiler pressure decays unless additional heat is added from the firing system to maintain the higher steam mass flow. The model was programmed in Fortran and solves the one dimensional equations of conservation of mass, momentum and energy for a homogeneous fluid. Transient heat conduction in the tube walls is also considered. Detailed results of a load increase from 50 to 55% are provided.

For subcritical drum type boilers, Adam and Marchetti [54], Lazaroiu [55], Walter [56], Taler et al. [57] and Sunil et al. [58] have presented methods to model the boiler and especially the evaporator and steam drum. Sunil et al. [58] make use of a lumped drum model that solves the equations of mass and energy balance to find the pressure and the level in the drum.

Mertens et al. [59] present the dynamic simulation of a drum type triple pressure heat recovery steam generator for a combined cycle plant in APROS. The transient behaviour of the heat exchangers is studied for the start-up and shut down and the results are compared with measured plant data. Detailed measurements for the hot start-up and shutdown of the plant are presented. Drum level increase during start up is mentioned, but it is stated that the level could be controlled by feed water flow manipulation. No mention of quick drain valves was made.

Various software tools have implemented dynamic systems modelling using the assumption of a homogeneous fluid in thermal equilibrium. Examples of such software tools are:

1. APROS as used by Alobaid et al. [60] , [61] and Starkloff et al. [48]
2. Matlab Simulink as used by Benato et al. [62] and Ray et al. [63]
3. Dymola based on the Modelica language as used by Benato et al. [62]
4. Aspen Plus Dynamics as used by Alobaid et al. [60] and Sarda et al. [50]
5. Flownex as used by Botha and Hindley [64] and Rousseau and Gwebu [65]

A quench situation where colder water enters a steam system probably cannot be considered to be a homogeneous fluid in thermal equilibrium. Extensive work has been done on modelling with two-phase steam and water flows [66]. Software tools dealing with non-homogeneous and non-equilibrium conditions are less common. The RELAP5–3D code is based on a model for two-phase systems that is solved by a fast, partially implicit numerical scheme and has traditionally been used in the simulation of operational and accidental transients in fission nuclear plants [67]. The NEPTUNE software platform is aimed at advanced two-phase flow thermal hydraulics covering three modelling scales, namely system scale which utilises the CATHARE code, CFD in porous mediums and CFD in open mediums [68].

The level of detail required in the results affects the modelling approach. The one dimensional approach can be applied in a discretized manner as demonstrated by Rousseau and Gwebu [65] to achieve more detailed results.

Pierobon et al. [69] discuss a methodology for the preliminary design of power generation systems that consider fulfilling dynamic requirements. A case study of modelling an organic Rankine cycle is presented. The authors show that simplifying assumptions, such as ignoring the heat transfer coefficient on the inside of a heat exchanger tube, still provides reasonable accuracy when

considering overall dynamic behaviour of the plant. It is not clear if these simplifications would be possible when investigating transient component temperatures.

Benato et al. [62] compare a Matlab/Simulink model with a Dymola Modelica model for evaluating load change induced transients of a single pressure heat recovery steam generator. They conclude that the geometry detail implemented in the Dymola model provides better information about the trend of temperature gradients along the wall thickness of the components and is better suited to evaluating thermo-mechanical fatigue effects.

Alobaid et al. [60] simulate the behaviour of a heat recovery steam generator during a start-up and compare the simulated results to plant data. The simulated results show steam generation and superheat sooner than the real plant. This is attributed to lower mass and hence inertia in the model and Alobaid et al. [60] suggest including all sub-systems such as vent and draining circuits in the model to improve the accuracy.

Ray et al. [63] model a superheater attemperator system and compare the results to plant data for a single transient case. The paper proposes a control strategy for the attemperator stages to minimise exergy destruction during transients and highlights the need for control systems to be modelled in order to achieve realistic transient results in a wider plant model.

Terdalkar et al. [70] evaluated the transient operation of a solar steam generator in APROS and noted that the six equation model can allow for rising steam and simultaneous falling condensate in the evaporator system. The superheater is kept pressurized overnight to keep it hot. Fatigue damage of bottom headers is mentioned due to quenching by cold condensate that runs down during night preservation or cloud events. No evidence is provided that these were looked at in great detail. The model was used to optimize start-up and shutdowns, cloud events and failure scenarios.

There is a large body of information published on one dimensional dynamic systems modelling of boilers and superheaters. The modelling method is applied to analyse plant performance over the operating load range. The level of detail can be customised to suit the application and the accuracy of the results required. This type of modelling has not been applied to quenching before and a methodology specifically for analysing quenching does not exist. Such a methodology should describe the level of detail necessary for useful results, which is also not discussed in present literature.

### 2.3.3 3D Computational Fluid Dynamics (CFD)

The use of three dimensional computational fluid dynamics (3D CFD) may also be considered such as the work presented by [44] [71] [72] and [73].

The model used by Angerer et al. [73], makes use of a transient 3D CFD simulation for the analysis of an innovative thermal buffer storage for combined cycle plants. The application considers single phase flow with Reynolds number greater than 100 and heat transfer to a discretized solid wall that enables detailed temperature prediction in the wall for estimating the storage capacity.

Although 3D CFD would provide detailed information, it requires a large effort to execute on such large systems. Trojan [74], presents a 3D CFD calculation of a single tube row of a superheater which required a mesh size of $7.8 \times 10^6$ elements. Expanding this to 40 or 80 rows and considering multiple stages of the superheater would be impractical. A simplified approach is to make use of a porous media method to represent the heat exchangers.

The porous media method enables the heat exchangers of the convection pass to be included in detailed CFD models of the boiler gas side. The heat exchangers are divided into cells along the length of the tubes. For each cell, a sink is included in the energy balance equation and a pressure drop is included in the momentum equation. This energy sink term and the pressure drop term is calculated at each time step from correlations that consider the detailed characteristics of the heat exchanger and the gas flow over it.

A method of modelling the superheater for the purposes of calculating the effects of gas flow and temperature maldistribution as well as ash fouling or tube inner scale fouling is presented in [43]. An example of discretization of a single superheater element into multiple control volumes is provided. Each control volume can be considered as a cross flow heat exchanger. Some measured temperatures of a real boiler with ash fouling occurring over time are provided. The thermal resistance of the outer ash layer on the superheater is measured to be 0.02425K/W. The paper concludes that the method is useful for modelling flow or temperature maldistribution. Scaling on inner and/or outer surfaces leads to steam temperature reduction and specifically scaling on the inner surface leads to an increase of the tube metal temperature which could lead to damage. A higher flue gas temperature over part of the superheater leads to higher temperature steam in those tubes but also higher pressure drop which reduces the flow in the tube. This can lead to overheating of the tube.

Drosatos et al. [44], produced a CFD model of the convection pass of a tower boiler using a porous media method and noted that it was possible to predict temperatures and heat flux distribution throughout the convective section. The boundaries of the model were the steam inlet and outlet of

each heat exchanger and the gas inlet and outlet of the convection pass. A full load comparison of the simulated results with operating data from Meliti Power Plant (330 MWe) in Florina, Greece, showed good agreement. It was noted that the inlet velocity and temperature profile (i.e. at the furnace exit) is required to obtain accurate results.

Coupling of one dimensional system analysis with CFD is common where process conditions are required as input to the more detailed CFD models. In the case of Schuhbauer et al. [71], a one dimensional process calculation is performed in APROS on the steam side of the heat exchanger tubes and this is coupled to the porous media method within a CFD calculation implemented in ANSYS Fluent. The tube inner surface temperature was chosen as the interface point between the APROS model and the CFD model. The APROS would calculate the tube inner metal temperature. The tube inner metal temperature at inlet and outlet of the heat exchanger was linearly interpolated for each cell. A tube heat conduction model was then used to calculate a tube outer temperature based on a heat flow from the previous time step. The storage term for the transient heat conduction through the tube wall is not described so it is assumed that the method was only applied to steady state scenarios. The tube outer temperature was then used to calculate the heat transfer from the gas (i.e. the sink term in the energy equation). The heat transfer relies on the heat transfer coefficient that was made up of a convective term and a radiative term. Radiation from the gas ($H_2O$, $CO_2$) was considered, as well as radiation from the ash particles. The methods of calculating the heat transfer coefficient are provided, but actual values for some of the input variables are not given, such as the mean efficiency for absorption and the fraction of backscatter for the ash particles. Good agreement with the Alstom design case at 100% load was achieved after a uniform ash layer was included on all the heating surfaces. (Ash conductivity of 1W/m K and a thickness of 2.64mm – thermal resistance estimated to be 0.0184K/W). Part load cases down to 40% are also modelled.

A CFD model integrated with a systems model was considered by Kruger and du Toit [75]. A complex flow field of the combustion chamber of a boiler was modelled with CFD and this was coupled to a one-dimensional systems model of the riser tubes in the furnace walls. The advantage of the coupling of these two types of models was that more detail and accuracy could be obtained.

Coupling of a lumped heat exchanger method is also possible such as the coupling of an LMTD method with CFD in [76].

Condensation of steam in a pipe is tested experimentally and modelled by He et al. [77]. A theoretical calculation and a 3D CFD model are both compared to experimental results. The 3D CFD provides a more accurate calculated result but the error compared to the experimental data is still more than 20% for the stable operation case.

3D CFD is generally applied to the gas side of large coal fired boilers and especially in the furnace zone. Simplifications are made for including the convective pass, but the methodology for detailed 3D CFD of the convection pass is also available [74].

Large scale 3D CFD computation of the steam side of the superheater heat exchangers as would be required for quenching investigation was not found in literature.

### 2.3.4 Fluid Structure Interaction (FSI)

The temperature of the fluid inside a component has a direct impact on the stresses experienced by the structure of the component. Botha and Hindley [64] demonstrate a one-way FSI coupling between a 1D and 3D domain to solve for the stresses in a large boiler tube assembly. A one dimensional thermo-fluid system model of the set of individual boiler tubes and the interconnections is solved to match a set of input conditions and measured metal temperature data. This technique is effective because it eliminates the need to accurately estimate the gas side heat transfer and distribution.

As stated by Botha and Hindley [64], work is ongoing in the bio-medical research field to establish correlations between flow dynamics and arterial diseases where 1D arterial flow is coupled to 3D CFD simulations. Areas of interest, where the blood vessel pressure distribution is required, are solved by using 3D CFD. The remainder of the arterial tree is solved using system modelling. The continuity at the coupling interface between the 1D system node and a 2D inlet area to the 3D mesh is maintained. A similar approach may be effective for estimating temperature distributions in power plant components.

Zhang and Lu [78] demonstrate a coupled CFD and finite element method (FEM) analysis of a T piece undergoing fatigue damage as a result of turbulent mixing and wall temperature fluctuations. The coupling is one way from the CFD to the FEM and the accumulation of fatigue damage can be analysed per position along the mixing length of the T-piece. This fluid-structure interaction could be considered for analysing the quenching phenomena and the stresses it causes.

Modelling of quenching by fluid structure interaction methods has not been considered. It is not practical to model the large superheater at the level of detail that would be required; however the local quenching process that takes place at component level could certainly be modelled using this technique. In the case of a horizontal pipe undergoing quenching, one way coupling of the temperature field to the finite element analysis would be required and this would provide the transient stress distribution within a pipe wall. The tools to perform such a calculation exist in literature but the specific application to quenching does not.

## 2.4 Metal temperature measurement

In order to obtain metal temperature measurements for detailed stress monitoring or model verification, the practical aspect of installing temperature measurements on a plant must be considered. Plant modification for thermowell installation and direct metal temperature measurement is difficult. Surface temperature measurement on the outside of a component is simpler to install and cost effective.

Rudolph et al [2] describe a pipe temperature measurement device specifically for nuclear application. The aim of the device is to measure thermal stratification. For horizontal pipes, seven or more equally spaced thermocouples are mounted on a thin tape the length of the pipe circumference. The tape can be rapidly installed on the plant by wrapping it around the pipe. It is covered by a protective shell before it is covered with the normal pipe insulation. Correction factors are applied specific to the measurement section to account for the capacitive effect of the device. The device is a commercially available tool.

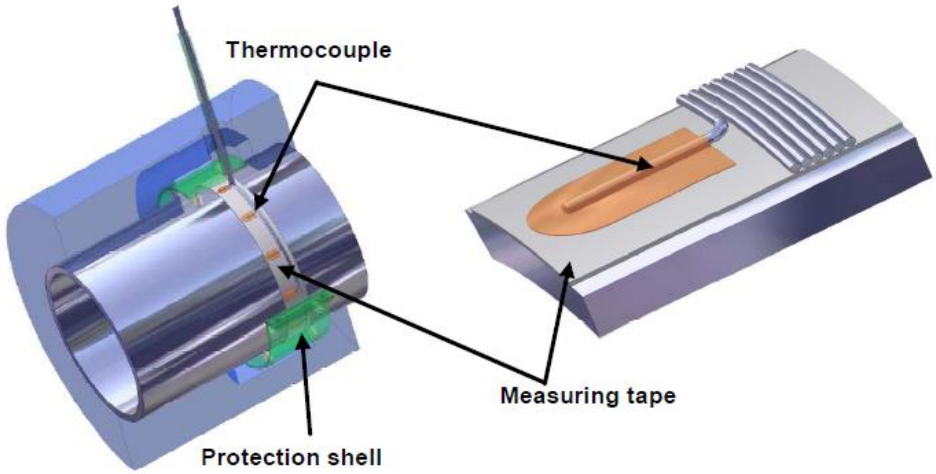


*Figure 14. Pipe outer temperature measurement device [2]*

Resistance Temperature Detectors (RTDs) are also possible instruments for outer surface temperature measurement, but are more expensive and limited in temperature range to a maximum of about 430$^{o}$C [79].

Surface mounted thermocouples are routinely installed on power plant components as stand-alone systems for particular investigations. The tip of the thermocouple must make good contact with the outer surface of the pipe. An example of such an installation can be seen on an experimental steam header in Figure 15.

*Figure 15. Installation of surface thermocouples for outer metal temperature measurement [80]*

Using outer surface thermocouple measurements, temperature gradients due to quenching of 33.3°C/min at the bottom of a pipe are reported [7] with top to bottom differential temperature of up to 277°C.

The problem of measuring outside temperatures to predict the inner surface temperature during quenching is that the transient heat transfer must be calculated. The change in temperature of the fluid inside the pipe over time, causes a transient temperature gradient through the pipe wall and causes the thermal stresses that we are interested in. Steady state methods of calculating the heat transfer through the pipe wall are thus inadequate because they assume that thermal equilibrium has been reached. At thermal equilibrium through the pipe wall, there may still be stresses as a result of steady temperature differences, the thermal coefficient of expansion of the material and the annular shape of the pipe wall. Such stresses in the case of a heat exchanger are calculated in [81].

In the case of quenching, a transient inverse heat conduction calculation is required. Methods of estimating the through-wall temperature distribution by solving the inverse heat conduction problem using the outside wall temperature are available [2] [46] [82]. Taler and Duda describe a numerical-analytical method for solving one dimensional heat conduction problems with constant material properties [83]. They also explain the step marching method used in one dimension for solving non-linear inverse heat conduction when the material properties are variable and described by third order polynomials.

Taler et al. [84] explain that an added advantage of the inverse method is that the inner heat transfer coefficient between the fluid and the wall is not required for calculating the through wall

temperature gradients. If the heat conduction problem is solved in the forward direction, then a measured value of fluid temperature is used without any metal temperature measurements, but the results are affected by the heat transfer coefficient which would need to be derived from correlations or estimated.

The inverse heat conduction problem can be solved by the space marching method in multi-dimensions as described by Duda et al. [85] and Taler et al. [82]. The method is designed to reconstruct the transient temperature distribution in a component based on measured temperatures taken at selected points on the outer surface of the component. The method was applied to experimental data and shown to produce reasonable temperature profiles through the solid.

The inverse heat conduction problem solved by the space marching method is also applied to fluid temperature measurement by Jaremkiewicz [86]. A low inertia thermometer coupled with the space marching method enable fluid temperature transients to be measured in high pressure steam lines. The inverse method is used to predict the temperature on the outside of a thermowell by using the inner measured temperature.

Argaud et al [87] employ an impulse response and data assimilation technique to reconstruct the through wall temperature profile from outer surface measurements. The method achieved an accuracy of better than 0.4%, with a maximum error of 3$^{o}$C on values of the order of 80$^{o}$C to 240$^{o}$C. The transient heat conduction through the pipe wall is calculated using Code Aster thermo-mechanical reference solver and the ADAO module within the SALOME framework. The approach demonstrated that a simple 1D calculation at each measurement point around the circumference of the pipe gave an incorrect answer for a stratified flow case and that a 2D method is required to account for the influence of thermal diffusion in the pipe wall.

Another approach to solving the inverse heat conduction problem is to iterate the direct heat transfer calculation until a solution is found. Lu et al. [88] use this method and apply a conjugate gradient method solver to determine the inner wall temperatures in three dimensions of a pipe elbow based on outer temperature measurements.

The partial differential equation that describes the transient heat diffusion through the solid can be solved by an explicit finite difference method, however, the maximum time step size for stability is limited by the fineness of the mesh size and the rate of diffusion. The time step size necessary for stability and convergence can be found by ensuring the Courant, Friedrichs and Lewy (CFL) [89] number is less than unity. The CFL number relates the rate that information travels over a timestep to the distance between the discrete points of the calculation. The calculation becomes unstable when the time step is too large or the distance between the spatial points is too small. Stability in

this context of using outer wall temperature measurements to determine through-wall temperature profiles is not discussed in literature, except for cases where additional measured outer temperature data points were created to improve stability [82].

For analysis of outer pipe temperature measurements, methods for solving the inverse heat transfer problem and obtaining an estimate of through wall temperature gradients exist. However; specific application to quenching is not published.

## 2.5 Summary of literature

As evident from the literature review, there is a large body of knowledge available for designing, operating and monitoring transient plant operation as well as management of creep, thermal fatigue and creep-fatigue damage. The existing knowledge considers temperature gradients that occur in normal operation.

Quenching is not normal operation and thus it is not considered in design. However, quenching results in significant temperature gradients and stress in thick-walled components. Quenching should be avoided as far as possible by drainage of condensate, operation of the plant within the design envelope and adequate maintenance. Repeated quenching causes damage in the form of cracks or voids in the material that are classified as thermal fatigue cracks or creep-fatigue damage. Damaged components require costly replacement.

The causes of quenching are described in literature, but little is published on how to analyse the causes. The causes are broadly classified as valve related issues, drainage problems, condensation by heat transfer in the superheater and collecting vessel overflow. Mostly the causes of quenching, such as valve failures, do not require further analysis. However, two potential causes of quenching, namely condensation in the superheater and overflow of the collecting vessel, are potentially difficult to identify in practice and lend themselves to further thermo-fluid modelling and study.

Work on modelling of the overall steam and water processes during quenching of a boiler superheater was not found in literature. Thus, the particular application has not been considered before.

One dimensional transient models, often referred to in literature as dynamic models, have been used by many authors and they offer a good balance between computational resource requirements and detail and accuracy of results. Although 3D CFD modelling or one-way coupled FSI would be possible with present knowledge, the computational effort required would not be justified.

Thermo-fluid modelling of the steam and water processes involved in quenching have not been considered before on the scale necessary to understand the cause, especially when aimed at providing the order of magnitude of the process variables using a minimum amount of information.

One dimensional transient plant models have not been developed before for coal fired boilers in a shut down state with almost zero flow. Existing models of the superheater have a known overall flow rate of steam on the inside of the tubes, although they may consider flow maldistribution between tubes. In existing work, the flow rate is often used as a boundary condition. For quenching of a superheater that is isolated on the steam side, the steam flow is unknown. Hence the model needs to solve for the flow rate between different heat exchanger sections in the superheater. This type of modelling has not been published before, other than one peer-reviewed conference paper [90] and one journal paper [91] that were produced in the course of this project.

A simplified model that enables relatively fast assessment of potential causes of quenching would be a useful tool. The model must be part of a methodology that aims to identify the cause of quenching. The literature survey did not reveal a method for analysis of quenching and neither did it provide a process for identification of the root cause of the problem. Given the costly consequences of quenching, there is a clear need for a methodology that can be employed to identify the causes of quenching as well as to quantify its contribution to stresses that can cause component damage.

# 3. Methodology

The purpose of this study is to develop and demonstrate a methodology to determine the root cause of quenching in a once-through tower type boiler and provide information that can be used to predict the impact on thick-walled components by estimating the through-wall temperature gradients.

A quenching incident is one where any thick-walled component experiences a significant temperature drop in a short period of time that cools the component at a rate that exceeds the allowable temperature decrease rate determined by the design of the component. Although quenching by saturated steam is possible, it is not the primary concern of this work. This work is concerned with quenching by water or condensate.

Water quenching can be recognised by a sudden drop of temperature as measured by the plant instrumentation. The temperature reading drops to saturation temperature as water reaches the location of the measurement point. For a typical steam temperature measurement point, the temperature decrease rate is of the order of 100$^{o}$C per minute or more.

Quenching can be identified by scanning plant data for steep temperature decrease rates. When a chosen threshold is exceeded, then further investigation is warranted. Typically, in this study, the plant was shut down with the fires out and the superheater isolated but still pressurised when quenching occurred, but this need not be the case.

If quenching occurs without the water passing a temperature measurement point, then it will not be possible to detect quenching using temperature measurements. In this case, quenching would probably go undetected until a plant failure occurred. If during failure investigation quenching is suspected, then this methodology can be applied.

The methodology is executed in a given order. However, the order can be adjusted and some steps omitted as required for the particular problem under investigation. Typically, once-off incidents will not require all the steps to be completed but repeat incidents require more in-depth analysis and evaluation of long-term plant health.

The proposed methodology for investigating suspected quenching incidents is summarized in Figure 16 and the details of each activity are provided in the subsequent chapters.

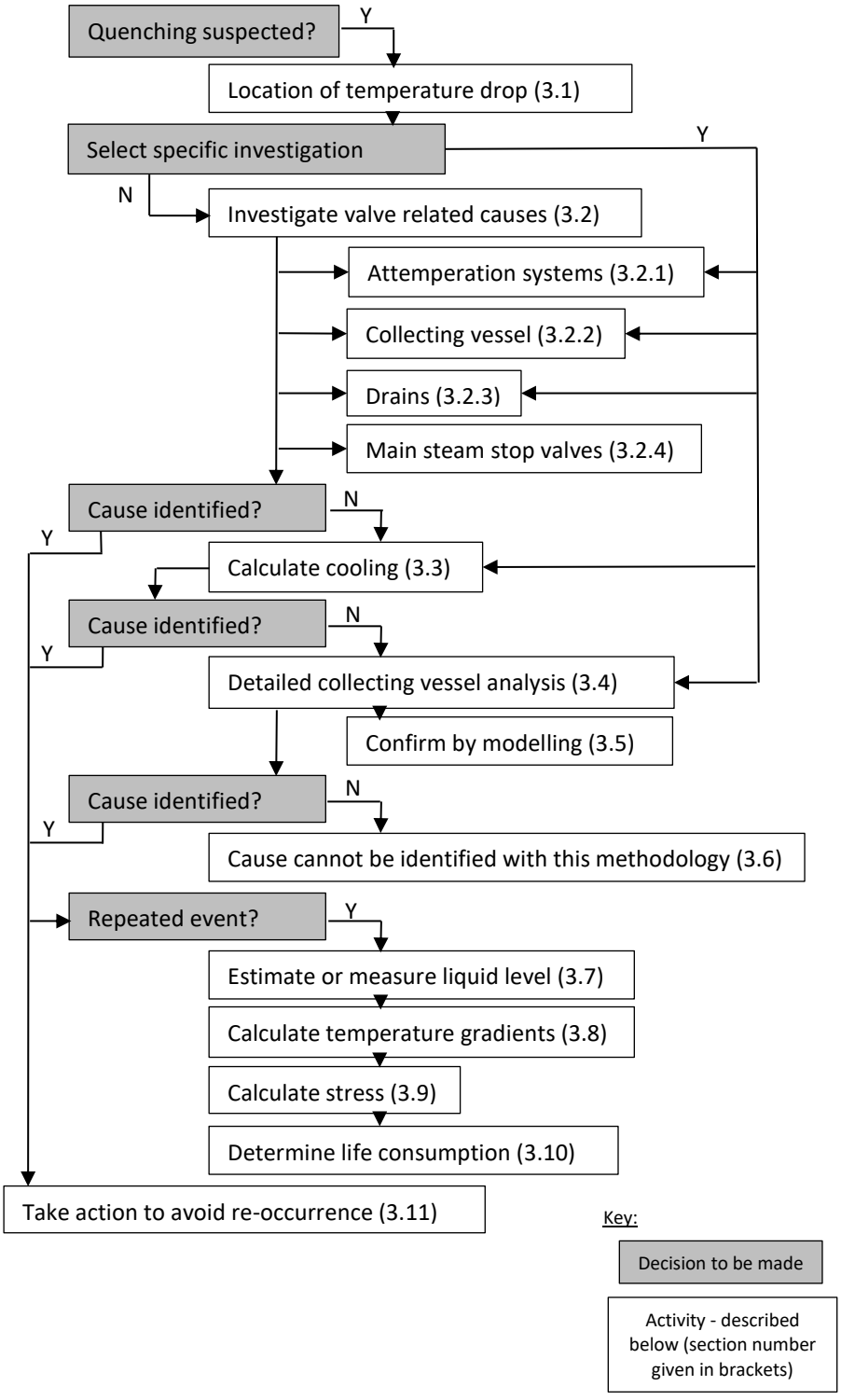


*Figure 16. Methodology to determine root cause of quenching showing sequence of execution*

## 3.1 Location of temperature drop

The first activity in the methodology is to understand the evidence that led to the initiation of the investigation. The exact number and location of measurement points that were quenched must be identified. The extent of quenching is also useful - some points may have been cooled to below the saturation temperature indicating the presence of subcooled liquid.

The potential sources of liquid closest to the location of the measurement points that were first quenched, should be the first to be investigated. In some cases, the source of water and the cause of quenching is obvious and thus a specific investigation can be selected. Alternatively, the order of the investigations that will be undertaken should be prioritised.

## 3.2 Investigate valve related causes

Following a water quenching incident, a systematic approach of checking for sources of water should be followed. All potential sources of water, as listed in Table 2, should be investigated by confirming valve positions from the plant data system.

These causes of quenching can be a root cause or only a contributor to the extent of the quenching that took place. The causes are discussed further in the sections below.

*Table 2. Valve related causes of quenching*

| **Valve related cause** | **Issue** | **Root cause?** | **Indicators** |
|---|---|---|---|
| Spray attemperation system | Spray water valve leaks water into superheater | Yes | Valve positions, Temperatures, Spray water flow measurement |
| Collecting vessel level | Quick drain valve fails to control level | Yes | Collecting vessel level, Valve position |
| | Feed water control valve causes over-feeding | Yes | Collecting vessel level, Valve position |
| Drains | Drain fail to open | No | Valve position, Drain temperature |
| | Drain reverse flow | Yes | Valve position, Temperatures |
| Main steam stop valves | Valve open | No | Valve position |

### 3.2.1 Spray attemperation systems

Spray attemperation systems are used for temperature control of the steam in a superheater. Typically attemperators are installed between each stage of the superheater. The attemperator sprays are incorporated into the headers and interconnecting piping. When on load, a controlled amount of water is sprayed into the steam flow to maintain the required outlet temperature of the subsequent superheater stage. A spray water valve controls the flow to each attemperator according to the control logic.

When the boiler is on load, poor atomisation of the water at the spray nozzle or over-spraying can lead to water droplet impingement on the downstream piping. Generally, this cannot be identified from the steam temperature measurements, but it causes localised damage and eventually failure. The failure will be confined to a portion of piping downstream of the attemperator and thus the root cause should be easily identifiable.

If the spray valve malfunctions or leaks and fails to isolate the water when the boiler is shut down, then the valve causes quenching. Initially the spray water will quench the piping in the immediate vicinity of the attemperator spray. The water will then flow by gravity and cause quenching of the hot components that it comes into contact with.

Attemperator spray valve malfunction can be identified by checking the behaviour of the upstream and downstream temperature measurements and comparing that with the other legs in the superheater. Typically, failures only affect one valve at a time, thus when the temperatures in a single leg at the attemperator show a decline on shut down and a drop to saturation temperature, it is an indication of excessive water being added to the superheater and the state of the spray valve should be investigated further.

Often the spray system is equipped with flow meters on each spray water line and these can also be used to identify spray flow that continues after shut down of the boiler. In such cases, it should be noted that the accuracy of the flow measurement at low flow is poor and that it may indicate a flow when in reality there is none.

### 3.2.2 Collecting vessel level

The collecting vessel level measurement data should be evaluated to determine if an overflow occurred. A high level in the collecting vessel, particularly when the level exceeds the range of the measuring instrument, indicates that potentially water overflowed into the superheater.

The recirculation pump and the quick drain valves control the collecting vessel level. Typically, the pump is a fixed speed pump with a control valve on the discharge line to control the flow. If this

valve malfunctions, then it may lead to loss of control of the collecting vessel level. When the collecting vessel level is high, the quick drain valves open to dump water from the system. If the quick drain valves fail to open fully when required, then it is likely that the collecting vessel will overflow.

The quick drain valves are important for establishing the recirculation flow. When the boiler trips or is shut down, there is a transition from superheated steam at the evaporator outlet to saturated steam and eventually to only water when fires are out. The collecting vessel level suddenly rises and it is difficult to put the recirculation pump into service until a stable level is achieved.

The rate of increase of the circulation flow is also limited to avoid thermal fatigue of the thick walled components in the economiser and evaporator. Rapid introduction of a high circulation flow would cause a slug of hot water in the circulation loop and expose the components in the loop to a sudden temperature change. Thus, a gradual increase of circulation flow is required to mix the circulation flow with the incoming feed water and create a uniform temperature in the loop. The quick drain valves are required to manage the level in the collecting vessel until the recirculation pump can take over.

The combination of collecting vessel level and quick drain valve position should be investigated to evaluate if this was the cause of quenching. If the quick drain valves failed to open or became stuck in position, then they are most likely the root cause of quenching that resulted in overflow of the collecting vessel. However, if the quick drain valves functioned correctly, but the collecting vessel level went high, then other causes should be investigated.

In some cases, a malfunction of the feed water system can occur and result in over-feeding the boiler to the extent that the quick drain valves are unable to evacuate the amount of water needed to keep the collecting vessel in control. Typically, the feed water regulating station consists of valves for controlling feed water flow when the boiler is in circulation mode (start-up valves) and a main valve in parallel to operate the boiler normally. If the main valve is open during start up, the boiler feed pumps will deliver excessive amounts of water and ‘flood’ the boiler. A similar situation could occur if the start-up valve(s) are stuck in an open position. Over-feeding can also be caused by malfunction of control logic.

Thus, if the quick drain valves are found to be fully open but unable to control the collecting vessel level, then the feed water regulating valve positions and the feed water control actions should be investigated to determine if they were the root cause of quenching.

### 3.2.3 Drains

Superheaters and main steam systems are equipped with drains to allow any accumulated condensate to be discharged. The condensate typically arises from starting up and shutting down the boiler. When starting up, particularly a cold start, there is a large amount of metal to be heated. Until the metal reaches the saturation temperature of the steam, the steam condenses on the cold surfaces and this condensate flows by gravity to the low points and is removed by the drains.

On shut down, as the boiler cools, condensation occurs in the superheater. Again, the drains allow this condensate to be removed. If the drain valves fail to open, this can cause condensate to accumulate and flow to other parts of the superheater which are still hot and thus cause quenching. By confirming drain valve positions, it can be determined if the drains played a role in causing quenching. The failure of a drain valve to open is not a root cause of quenching but rather a contributor to the extent of the quench. Another mechanism needs to be present to provide the water for quenching, such as an open attemperator valve or condensation of the steam in the superheater by cooling.

Another potential problem with the drains is that the design of the drainage system may be prone to reverse flow. In this case, a drain valve may open but the effect is to introduce water or colder steam into the superheater rather than removing the condensate. Such reverse flow of drains generally points to a design error and can occur when drains are interconnected and the capacity of the downstream system is insufficient. Reverse flow of water through drains into the superheater is a root cause of quenching.

Reverse flow can also occur directly from the drainage system, but this is generally only possible if the boiler is depressurised and the elevation of the drain point is lower than the drain tank. Reverse flow from a drain point can be identified by the behaviour of temperature measurement points near the drain when the valve opens.

### 3.2.4 Main steam stop valves

The main steam stop valves are not a root cause of quenching. However, the valves can be used to isolate the boiler from the main steam piping system and thus limit the extent of quenching that takes place.

If the boiler is equipped with main steam stop valves, the position of the valves at the time of the quench should be investigated. If the stop valves were closed, then quenching of the main steam system is highly unlikely. However, this can be confirmed from temperature measurements in the

main steam system. The superheater system is not protected from quenching when the main steam stop valves are closed and thus further investigation is still required.

## 3.3 Calculate cooling

Once the valve related causes have been investigated and the cause of quenching has still not been determined, the potential for condensation in the superheater should be evaluated. The evaluation is by calculation of heat transfer in the boiler. Owing to the uncertainty of boundary conditions and heat transfer under low flow conditions, simplifying assumptions are made. The results of the calculation provide an estimated time taken to initiate condensation in the superheater and the subsequent condensation rate. Details of the calculation are provided in chapter 4. This heat transfer calculation is the first modelling element of the methodology.

As liquid moves through the superheater, it can cause a particular progression of temperature drops. The exact order in which the thermocouple temperatures dropped can give information about the direction of travel of the water. If the temperature drops are in the normal direction of flow (See Figure 17) and assuming the Superheater 1 is at a higher elevation than Superheater 2, then a collecting vessel overflow is likely. However, if the temperature drops at the lowest point first and then proceeds to drop in the order of elevation of the measurement points, then potentially the superheater was filling up due to undrained condensate collecting in the superheater.

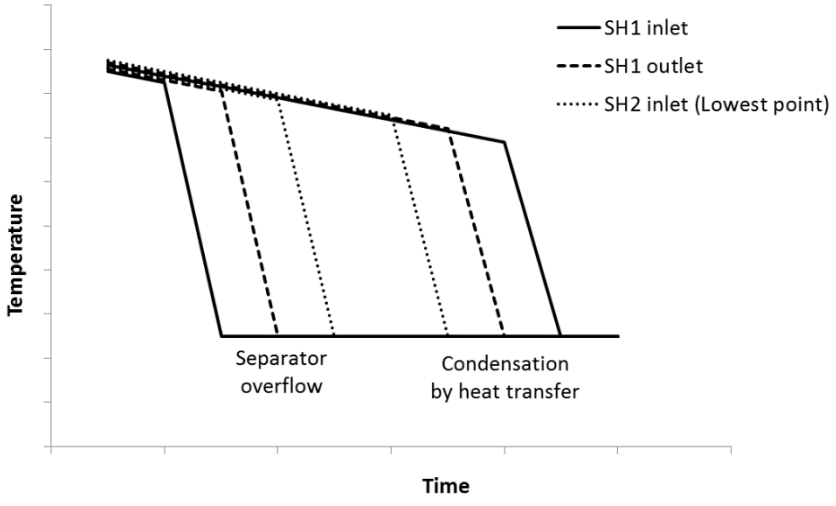


*Figure 17. Superheater steam temperature behaviour for different quenching causes*

## 3.4 Detailed collecting vessel level analysis

In the event that valve related causes and condensation by heat transfer fail to explain the quenching observed, then further detailed analysis of the collecting vessel and separator vessel system is warranted. This aspect is addressed in chapter 5.

If the collecting vessel level remained relatively in control, but a separator overflow is suspected, then either the collecting vessel level measurement was faulty, or the water diverted from the separator vessel into the superheater without filling the collecting vessel.

If the level measurement was faulty, it could report a lower level than was actually the case. This may result in the separating and collecting vessel system overflowing into the superheater without the operator knowing about it. Furthermore, the control logic based on level measurement would not react. A detailed investigation of the level measurement should be carried out to verify that the level measurement can be trusted. An example of such an investigation is described in Appendix A.

Once the validity of the collecting vessel level measurement is confirmed and a separator overflow is still suspected, then potentially the water is not reaching the collecting vessel and instead diverting from the separators into the superheater. Detailed analysis of the actual plant geometry is required in order to determine if such an occurrence is possible. This is discussed in chapter 5.

## 3.5 Confirm by modelling

Modelling the superheater can provide insight into the causes of quenching. Thus, if the analysis above provides uncertain results, then modelling can be used to assist in narrowing down the causes or confirm whether a particular cause is valid. This type of modelling is considered to be the second modelling element of the methodology and is addressed in chapter 6.

A simplified modelling approach was developed for this purpose. It was not the intention to create an accurate heat transfer model, but rather to use the lowest level of detail possible and make use of plant measurements to adjust the model and obtain the correct overall behaviour that can be correlated with phenomena on the real plant.

Three separate approaches were used to model the superheater: A simplified model was created in Microsoft Excel (refer section 6.2), a model was created in Flownex (refer section 6.3) and another separate model, named the “Liquid Tracking Model” or LTM, was programmed in Scilab (refer chapter 7). The aim of the LTM was to track the progression of liquid through the superheater. Either the simplified model, the Flownex model or the LTM can be applied to model the separator overflow and confirm the cause of quenching.

## 3.6 Cause cannot be identified with this methodology

In the event that the above activities have failed to identify the root cause of quenching, then the cause is potentially a new issue that has not been identified before. It is recommended that the previous steps above be revisited to check that a known cause has not been overlooked.

## 3.7 Estimate or measure liquid level

In cases where repeat quench events have occurred, it is important to evaluate the damage that has taken place and what the impact on component life is. This is done by calculating the thermal stresses from the temperature gradients in the walls of the components. In order to calculate the temperature gradients, it is necessary to estimate the liquid level in the superheater over time. A Liquid Tracking Model is proposed in chapter 7 to address this.

Once the source of water that caused quenching has been determined, it is possible to determine the path of the water and the direction of travel through the superheater. The path of water flow is determined by inspection. The water flow is classified as gravity driven flow. From the point of entry, the water will flow to the lowest point in the superheater without completely filling the tubes and headers. This is termed a “flow-through” quenching situation. If not drained from the lowest point, then the water will accumulate and fill the superheater. This type of quenching is known as “flooding”.

For vertical pipe runs that are affected by flow-through quenching, determining the extent of inner pipe surface wetted by water is not trivial. A conservative approximation can be made that the wetted / un-wetted interface remains stationary during the event which gives the greatest temperature gradients in the pipe wall.

For horizontal pipe runs, open channel flow analysis is appropriate. The slope of the horizontal pipes and headers are required for the calculation and these can be obtained from drawings or a typical value can be assumed. An example of a transient level estimation for a point in a horizontal pipe is given in Section 7.8.2.2.

## 3.8 Calculate metal temperature gradients

At selected locations, it is possible to calculate the temperature gradients in the walls of the components. In order to do this, a transient conduction model of the heat transfer in the pipe wall is required. This model is the third modelling element of the methodology.

For complex geometries, a one dimensional analysis could be used to evaluate the evolution of temperatures through the wall of the component as it is quenched. Liquid level as a function of time

would not be required in this case. For pipe components, a simplified two dimensional transient conduction model can be applied as demonstrated in Section 8.4. The liquid level as a function of time causes a transient two dimensional temperature distribution.

In order to apply the transient conduction model, the heat transfer in the gas and liquid space at the inside surface of the pipe is required. The heat transfer can be estimated by a convective heat transfer coefficient and the difference in temperature between the inside surface of the pipe and the saturation temperature of the steam.

The heat transfer coefficients were measured by processing the data from an experimental test rig and from thermocouples installed on the outside of a pipe in a plant that underwent quenching. By processing these outer wall temperature measurements with an inverse heat transfer calculation, an estimate of the inner heat transfer and the temperature distribution through the pipe wall was determined (Refer section 8.3.3).

There is significant measurement uncertainty associated with the measured heat transfer coefficients. However, the values can be used to obtain an estimate of the temperature distribution in the pipe wall.

## 3.9 Calculate thermal stresses

The temperature distribution in a two dimensional section can be used in a finite element analysis calculation to determine the stresses in the pipe wall. This is briefly discussed in Section 9. The transient thermal stresses can then be superimposed over the other loads on the pipe, such as the internal pressure, to determine the overall stress.

## 3.10 Determine life consumption

This step is not included in this document since it is outside the scope of this project. However, it is acknowledged that techniques exist in the area of physical metallurgy to interpret a stress cycle and the impact on fatigue life of a component. Further work, such as that in [92], is required to determine what damage would occur over repeated quench cycles and what the impact on the life of the component would be.

## 3.11 Take action to avoid re-occurrence

Irrespective of whether or not the quenching is a repeat event or if the damage and life consumption due to quenching has been calculated, it is necessary to take action to prevent it from re-occurring. The root cause of the quench should be addressed by improving control logic, replacing defective

equipment, increasing maintenance, updating operating procedures and/or modifying the plant. The plant should also be monitored to ensure that the measures put in place are effective.

## 3.12 Summary

This chapter describes the methodology to investigate and determine the root cause of quenching as well as the steps required in order to calculate the life consumption of repeated quench events. In the subsequent chapters, parts of the methodology are described in detail and are applied to the quenching events studied at Power Station A.

In chapter 4, a heat transfer model for calculating condensation in the superheater is developed to support the "Calculate Cooling" activity of the methodology. The heat transfer model is subsequently developed further in chapters 6 and 7 to enable the effects of a separator overflow to be calculated. Prior to modelling the separator overflow, it is necessary to fully describe the details and root cause of the quenching events at Power Station A. This is done in chapter 5 that describes the detailed collecting vessel level analysis and serves to justify the features and level of detail used in the separator overflow models.

The remaining chapters discuss the measurement and calculation of through-wall temperature gradients for the purposes of determining stresses. Chapter 7.8 considers how liquid levels could be determined while chapter 8 looks at how the liquid level would be used to calculate the temperature distribution in a pipe wall. Lastly, chapter 9 briefly describes the calculation of stresses due to the temperature gradients.

# 4. Calculation of cooling and condensation in the superheater

This chapter describes a calculation procedure to estimate the rate of cooling of the superheater after the boiler is shut down. This is in support of activity 3.3 of the proposed methodology, as shown in Figure 18.

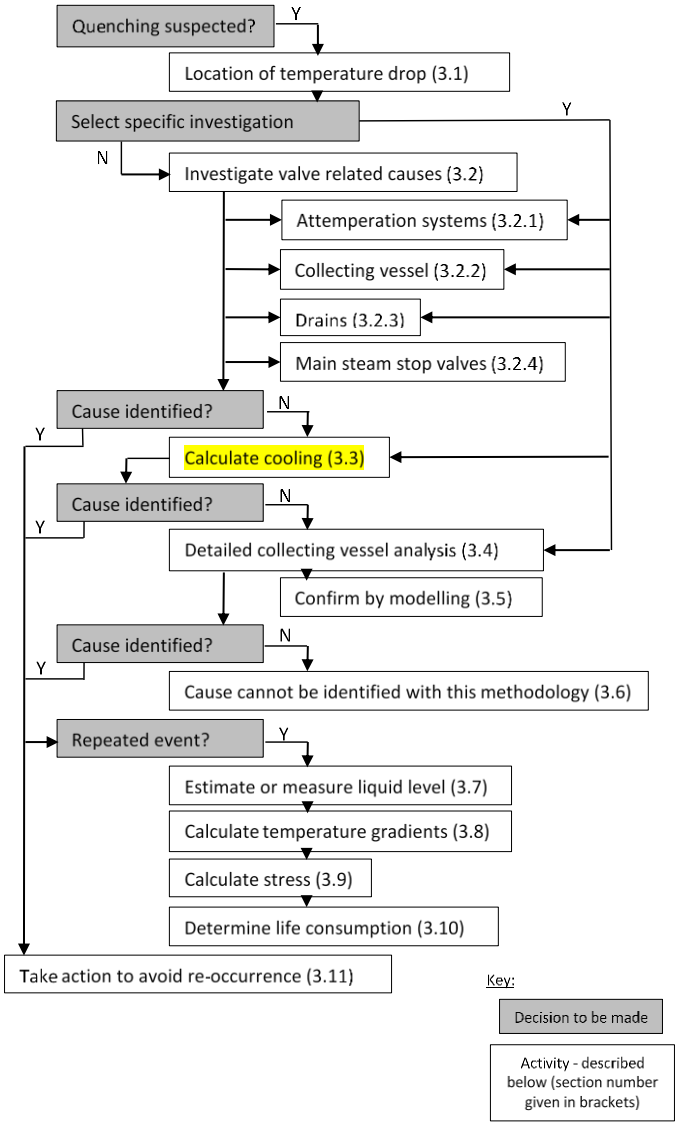


*Figure 18. Activity 3.3. in the methodology*

After shut down of the boiler, the superheater remains pressurised on the steam side and the fans are in operation. Heat transfer on the gas side of the superheater tubes cools the superheater to the extent that the steam on the inside of the tubes condenses.

The intention of the calculation is primarily to investigate the time taken to reach saturation temperature and the subsequent rate of condensate production. In situations where drains malfunctioned, it enables the quantity of undrained condensate to be estimated and hence the extent of quenching to be determined.

## 4.1 Heat transfer model

Consider the superheater as a single control volume, $V_s$ as shown in Figure 19. The steam volume is defined by a height equal to the height between the lowest tubes in the superheater and the header at the top of the heat exchanger, multiplied by an equivalent plan view area, so that the steam volume is equal to the actual internal volume of the superheater. Typically, the initial steam pressure is 8MPa and the control volume is at a uniform temperature of 400°C (this would correspond to the average temperature of steam in the superheater).

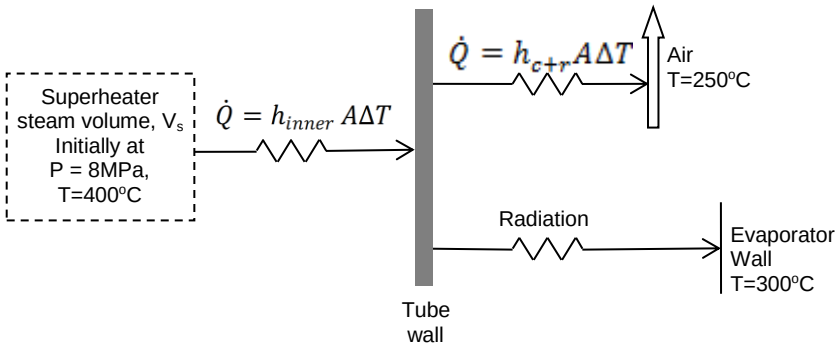


*Figure 19. Simplified lumped parameter model to estimate cooling rate*

Heat transfer occurs from the steam through the tube walls to the gas flow. On the inside of the tube bundles, there is convection heat transfer which is dependent on the average heat transfer coefficient, $h_{inner}$, the applicable surface area, $A$, and the applicable temperature difference, $\Delta T$, which in this case is the temperature difference between the steam and the inner surface of the tubes.

On the outside of the superheater tubes, the heat transfer occurs to the gas/air flow by means of convection and radiation. The radiation is considered by calculating an equivalent radiation heat transfer coefficient and adding it to the convective heat transfer coefficient to give a combined average heat transfer coefficient, $h_{c+r}$. This is multiplied by the applicable surface area and temperature difference to get the magnitude of the heat transfer rate, $\dot{Q}$.

There is also radiation from the outside of the superheater tube bundle to the surrounding evaporator tubes which are at a lower temperature. This radiation heat transfer is included in the calculation, although the magnitude is significantly smaller than the other heat loss from the superheater to the air flow. Each heat transfer mechanism is discussed further below.

The calculation procedure is shown schematically in Figure 20. The relevant section where each step is described in detail is given in brackets.

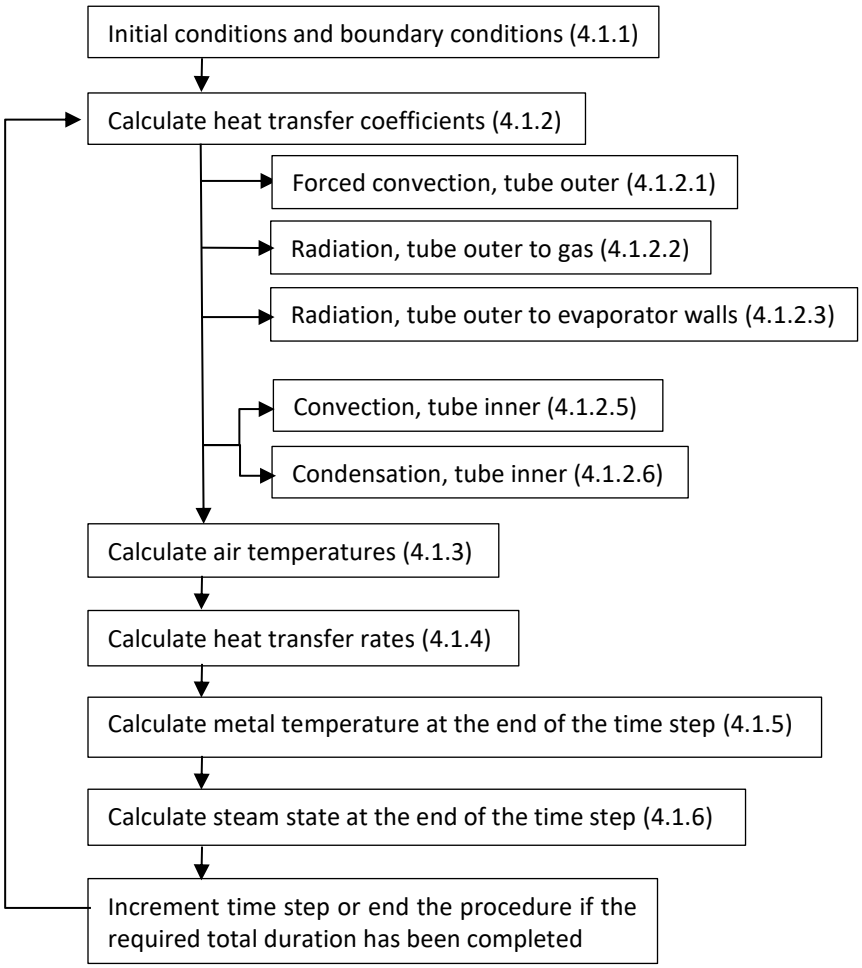


*Figure 20. Heat transfer calculation procedure*

## 4.1.1 Initial conditions and boundary conditions

The initial steam temperature and pressure in the superheater are specified at the beginning of the first time step. The heat transfer of each stage of the superheater is considered separately and thus each stage has an associated initial tube bundle metal temperature that must be specified.

The boundary conditions necessary for the calculation are the air mass flow rate through the superheater, the inlet temperature of the air and the temperature of the evaporator walls surrounding the superheater. A simplification for cases where the evaporator wall temperature is

not available is to assume that the temperature of the evaporator walls is equal to the saturation temperature at the superheater pressure.

## 4.1.2 Calculate heat transfer coefficients

Based on the temperatures at the beginning of the time step, the correlations described below can be applied to find the relevant heat transfer coefficients. The heat transfer coefficient is assumed to be constant for the duration of the time step.

#### 4.1.2.1 Forced convection, tube outer

The rate of heat transfer by forced convection is characterised by a convective heat transfer coefficient, $h_c$, which is obtained from correlations that have generally been derived from empirical data. The correlations are presented in dimensionless form using Nusselt number, $Nu_D$, Reynolds number,$Re_D$, and Prandtl number, $Pr$:

$$Nu_D = \frac{h_c D}{k_f} \tag{17}$$

$$Re_D = \frac{\rho V D}{\mu} \tag{18}$$

$$Pr = \frac{\mu c_p}{k_f} \tag{19}$$

Where $k_f$ is the thermal conductivity of the fluid, $\rho$ is the fluid density, $V$ is the free stream fluid velocity, $\mu$ is the fluid dynamic viscosity, $c_p$ is the fluid specific heat capacity at constant pressure and $D$ is the diameter of the tube. In general, the fluid properties are evaluated at the film temperature which is approximated by the average of the fluid and wall temperature.

The correlations for a single tube in cross flow have been summarised by Rossouw [93]. The range of Reynold's numbers expected in the superheater when the boiler is shut down and being purged with air varies from 500 to 1500 depending on the air mass flow rate.

The Hilpert correlation [94] for the applicable Reynold's number range is given by (40<Re<4000):

$$Nu = 0.683 Re^{0.466} Pr^{0.33} \tag{20}$$

The Prandtl number of air at 250°C is approximately 0.67 which gives a Nusselt number range of 10 to 18. This translates to a heat transfer coefficient in the range of 11 to 19W/m$^2$ K.

The Hilpert correlation was improved by other researchers [95] who reworked the data using improved fluid properties to get:

$$Nu = 0.583 Re^{0.471} Pr^{0.33} \tag{21}$$

Using the updated correlation gives heat transfer coefficients in the range of 10 to 17W/m$^2$ K.

The Žkauskas correlation [96] has a similar form to the correlations above, but includes a Prandtl number ratio as follows (0.7<Pr<10, 40<Re<1000):

$$Nu = 0.52Re^{0.5}Pr^{0.37}\left(\frac{Pr}{Pr_w}\right)^{0.25} \tag{22}$$

Where $Pr_w$ refers to the Prandtl number of the fluid evaluated at the wall temperature. This correlation gives similar results to the Hilpert correlation for the range of input values expected. The correlation was used by Cantrell and Idem [42] in their on-line performance model of the boiler heat exchangers.

The Churchill and Bernstein correlation [97] is applicable across a wide range of Reynold's numbers and Prandtl numbers and is given by ($Re_D$ Pr > 0.2):

$$\overline{Nu_D} = 0.3 + \frac{0.62Re_D^{\frac{1}{2}}Pr^{\frac{1}{3}}}{\left[1+\left(\frac{0.4}{Pr}\right)^{\frac{2}{3}}\right]^{\frac{1}{4}}}\left[1+\left(\frac{Re_D}{282\,000}\right)^{\frac{5}{8}}\right]^{\frac{4}{5}} \tag{23}$$

For Reynold's number less than 10 000, the following simplification is recommended:

$$\overline{Nu_D} = 0.3 + \frac{0.62Re_D^{\frac{1}{2}}Pr^{\frac{1}{3}}}{\left[1+\left(\frac{0.4}{Pr}\right)^{\frac{2}{3}}\right]^{\frac{1}{4}}} \tag{24}$$

Applying the Churchill and Bernstein correlation to the expected values for the superheater gives a heat transfer coefficient in the range of 12 to 20W/m$^2$ K. These values are greater than the values predicted by the other correlations above. Considering that greater heat transfer coefficient will result in a faster cooling rate of the superheater, the Churchill and Bernstein correlation is preferred for this project because it will result in a more conservative estimate of the minimum time to condense steam in the superheater.

The above heat transfer correlations are only applicable to a single tube in cross flow. The superheater consists of multiple tubes and thus the average heat transfer coefficient must be adjusted to account for the effect that the tubes have on each other.

The configuration of tubes in a superheater is in-line as shown in Figure 21. The characteristic velocity in the Reynolds number formulation is replaced by the average velocity in the void between the tubes in the row. The void fraction, $\psi$, is given by:

$$\psi = 1 - \frac{\pi D}{4S_T} \; for \; \frac{S_L}{D} \geq 1 \tag{25}$$

$$\psi = 1 - \frac{\pi D^2}{4S_T S_L} \; for \; \frac{S_L}{D} < 1 \tag{26}$$

Where $S_T$ is the transverse pitch of the tube bundle and $S_L$ is the longitudinal pitch. The Reynolds number is now defined as:

$$Re_\psi = \frac{\rho V l}{\psi \mu} = \frac{\rho V \frac{\pi}{2} D}{\psi \mu} \tag{27}$$

Where $l$ is the length of the flow path over a single tube.

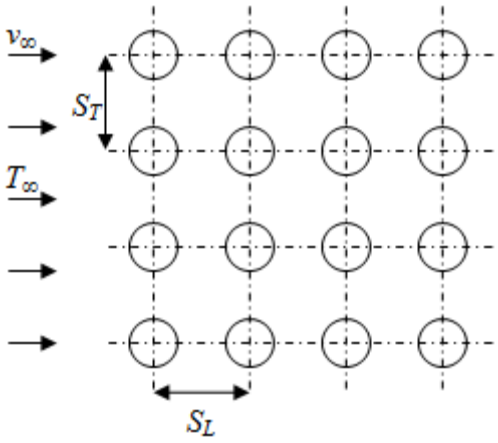


*Figure 21. Aligned tube heat exchanger configuration*

The convection coefficient can also be calculated using the Gnielinski correlation [98] applied to a bank of tubes as done by [71]. A laminar and a turbulent Nusselt number are combined to give an average Nusselt number for a single row of tubes as follows:

$$Nu_{row} = 0.3 + \sqrt{Nu_{l,lam}^2 + Nu_{l,turb}^2} \tag{28}$$

$$Nu_{l,lam} = 0.664\sqrt{Re_\psi}\sqrt[3]{Pr} \tag{29}$$

$$Nu_{l,turb} = \frac{0.037 Re_\psi^{0.8} Pr}{1 + 2.443 Re_\psi^{-0.1}(Pr^{\frac{2}{3}} - 1)} \tag{30}$$

$$Nu_{row} = \frac{h_c \frac{\pi}{2} D}{k_f} \tag{31}$$

Applying the Gnielinski correlation to the expected values for the superheater gives a heat transfer coefficient in the range of 10 to 17W/m$^2$ K. Again, the Churchill and Bernstein correlation gives higher values and is thus preferred for this study.

Gnielinski [98] accounts for multiple rows in the tube bundle by modifying the single row Nusselt number using the arrangement factor for the tube bundle, $f_{A,in-line}$ :

$$Nu_{bundle} = f_{A,in-line} Nu_{row} \tag{32}$$

This relationship is only valid for calculating the average Nusselt number for more than 10 rows. Fewer than 10 rows require that the equation is further modified to account for the entrance effects.

The bundle arrangement factor is given by:

$$f_{A,in-line} = 1 + \frac{0.7\left(\frac{S_L}{S_T} - 0.3\right)}{\psi^{1.5}\left(\frac{S_L}{S_T} + 0.7\right)^2} \quad (33)$$

Mills [40] demonstrates the application of the Churchill and Bernstein correlation [97] to a tube bundle. The single tube correlation is applied using the modified Reynolds number and then this is translated to an average bundle Nusselt number using the tube bundle arrangement factor. This method is applied to calculate the tube outer forced convection heat transfer coefficients for the superheater in this work.

Trojan and Taler [43] use the following correlation from [99] for in-line tubes in their work:

$$Nu = C_s C_z Re^{0.65} Pr^{0.33} \quad (34)$$

Where $C_s$ and $C_z$ are correction factors for the tube arrangement and the effect of the number of tubes rows in the bundle respectively. This correlation was not investigated further.

#### 4.1.2.2 Radiation, tube outer to gas

Radiation from the tube outer surface occurs to the gas passing through the heat exchanger owing to the ash in the gas flow and any participating species in the gas flow. Under normal operating conditions, the radiation can be considered by the sum of grey gases model [100].

A simplified formulation for calculating the radiation heat transfer from a gas containing ash particles is given by Taler and Taler [101]. Their method was shown to be within +/-12.5% of CFD results. The method is applicable for platen superheaters as well as convection heat exchanger bundles. For convective heat exchangers, a radiation heat transfer coefficient is added to the convective heat transfer coefficient as follows:

$$h_{cr} = h_c + h_r \quad (35)$$

$$\dot{Q}_{cr} = h_{cr} A\left(T_w - T_g\right) \quad (36)$$

Where $\dot{Q}_{cr}$is the heat transfer rate from the tubes to the gas flow, $A$ is the tube bundle outer area, $T_w$ is the outer wall temperature of the tubes and $T_g$ is the fluid temperature of the gas flowing through the tube bundle.

The simplified expression from [101] for the radiation heat transfer coefficient is given as follows:

$$h_r = \frac{\sigma \varepsilon_{eq} as}{as + \varepsilon_{eq}} \frac{\left(\bar{T}_g^4 - T_w^4\right)}{\left(\bar{T}_g - T_w\right)} \quad (37)$$

$$\varepsilon_{eq} = \frac{2\varepsilon_w}{2-\varepsilon_w} \quad (38)$$

Where $\sigma$ is the Stefan-Boltzmann constant ($\sigma = 5.67 \times 10^{-8} W/(m^2K^4)$), $\varepsilon_w$ is the tube wall emissivity, $a$ is the absorption coefficient and $s$ is the geometric mean beam length. The wall emissivity is assumed to be 0.8 as recommended by others [101] [102].

The beam length for in-line and staggered tube bundles is given by:

$$s = C\frac{D}{4}\left(\frac{4}{\pi}\frac{s_T s_L}{D^2} - 1\right) \quad (39)$$

Where the constant $C$ is selected based on the product $as$ and can range from 3.4 to 3.8. If $as > 0.1$ then a $C$ of 3.4 should be used. For the superheater geometry under consideration, the product of $as$ is often less than 0.1 and thus $C$ is chosen to be 3.6. For Power Station A, the values of mean beam length vary from 0.2m to 1.6m.

The equivalent emissivity of the gas mixture and the absorptivity are related as follows:

$$\varepsilon_g = 1 - e^{-as} \quad (40)$$

$$a = -\frac{ln(1-\varepsilon_g)}{s} \quad (41)$$

The absorption coefficient, $a$, can also be expressed in terms of an extinction coefficient, $k$, which for a mixture of gas and ash particles, is given by:

$$a = kp \quad (42)$$

$$k = k_g r_n + k_a \mu_a \quad (43)$$

Where $p$ is the total pressure of the gas, $k_g$ is the extinction coefficient of the gas, $k_a$ is the extinction coefficient of the ash particles, $r_n$ is the volume fraction of triatomic gases and $\mu_a$ is the fly ash concentration.

For gasses, an expression from [101] can be used:

$$k_g p = \left(0.78 + 1.6 r_{H_2O} - 0.1\sqrt{p_{sum}s}\right)\left(1 - 0.37\frac{T_g}{1000}\right)\sqrt{p_{sum}s} \quad (44)$$

Where $r_{H_2O}$ is the volume fraction of water vapour, $p_{sum}$ is the sum of partial pressures of the triatomic gases and $T_g$ is the gas temperature in Kelvin. This equation is valid for a gas composition that includes carbon and sulphur dioxide and water vapour which is typical of the participating gas species present in flue gas under normal operation. With fires out, the concentration of triatomic gases decreases until only the gases present in the intake air are available for radiation heat transfer. The volume fractions of the gases are unknown but assumed to be small a few minutes after fires out. Thus the contribution of triatomic gases is considered to be negligible.

Gwebu [103] uses the Gurvich boiler thermal calculation model [102] which is based on the former Soviet Union's standards. An expression for the extinction coefficient of ash and the ash concentration is provided as follows:

$$k_a = \frac{4300\rho_g}{\sqrt[3]{T_g^2 d_a^2}} * 10^{-5} \quad (45)$$

$$\mu_a = \frac{\%FA\, x_{ash}}{G_g} \quad (46)$$

Where $\rho_g$ is the gas density, $d_a$ is the diameter of the ash particles, $\%FA$ is the percentage fly ash compared to coarse ash (typically 90%), $x_{ash}$ is the fuel ash content in mass percentage and $G_g$ is the flue gas mass excluding ash which can be calculated from stoichiometric combustion and an excess air assumption. This relationship is intended for a boiler in operation with a continuous stream of fly ash. In the case of a boiler with fires out, the fly ash concentration in the gas stream is unknown. Even after shutdown, there is a substantial quantity of ash in the superheater and this ash is not necessarily transported by the gas stream which is much reduced compared to normal operating flow. Thus, the amount of ash present in the superheater cannot be assumed to be negligible.

Gwebu [103] calculates a typical fly ash concentration in operation to be 0.035$kg_{ash}/kg_{gas}$. This value is assumed to be valid even after fires out when the air density is approximately half the density of the flue gas in operation. Hence the ash loading on a volumetric basis for the gas path with fans running and fires out is actually assumed to be half the loading during normal operation.

Using a tube diameter of 0.045m, a gas temperature of 573K and an average ash particle diameter of 14µm, gives an extinction coefficient of the ash, $k_a$ of 6.6 x $10^{-5}$/mPa. Using the ash concentration of 0.035$kg_{ash}/kg_{gas}$ and atmospheric pressure of 85 x $10^3$ Pa gives an absorption coefficient, $a$, of 0.196. This translates to an emissivity of between 0.04 and 0.28 for the mean beam lengths under consideration.

Brummel [104] provides methods for estimating the emissivity of an ash particle cloud. The particle load has the highest impact on the emissivity and for pulverised fuel boilers a simple model that ignores radiation scattering by the particles can be used with good accuracy. By using the data from studies by Biermann and Vortmeyer [105] on various fly ash samples, a nomogram was created for determining the emissivity of dispersed ash particles. Using typical values for the ash properties as provided in the example by Brummel [104], and looking up the product of ash loading and mean beam lengths given above, results in a dispersed particle emissivity of 0.05 to 0.38. These values are similar to the above calculation and thus provide verification of the numbers.

By considering a wall temperature of 400°C, the radiative heat transfer coefficient, $h_r$, is calculated for the above parameters and found to vary from 2.3 to 14.5W/$m^2$ K.

Owing to the number of assumptions necessary for this evaluation, it was decided to use a constant emissivity of 0.1 for the ash particles. This assumption gives a value of heat transfer coefficient, $h_r$, of 5.5W/m$^2$ K for the above example.

#### 4.1.2.3 Radiation, tube outer to evaporator walls

Radiation heat transfer also occurs from the superheater tube bundle to the evaporator tubes that line the walls of the convection pass. The evaporator tubes are at a lower temperature than the superheater tubes and thus have the potential to contribute to the cooling of the superheater.

Radiation heat transfer between two surfaces can be defined in terms of a radiation transfer factor, $\mathcal{F}_{12}$, as follows [40] :

$$\dot{Q}_{12} = A_1 \mathcal{F}_{12} (\sigma T_1^4 - \sigma T_2^4) \tag{47}$$

Where $\dot{Q}_{12}$ denotes heat transfer from surface one to surface two, $A_1$ is the area of surface one, $\sigma$ is the Stefan-Boltzmann constant ($\sigma = 5.67 \times 10^{-8} W/(m^2 K^4)$), and $T_1$ and $T_2$ are the surface temperatures in Kelvin.

The radiation transfer factor is available for various configurations. The simplest is the case of a small object of area $A_1$ in large nearly black surrounds. In this case, $\mathcal{F}_{12} = \varepsilon_1$ where $\varepsilon_1$ is the emissivity of the object. This simplified approach is conservative and was adopted for the heat transfer model in this work.

Another approach is to consider the radiation heat transfer as though the superheater and the evaporator walls were two parallel flat plates. The radiation transfer factor for two flat plates is given by:

$$\mathcal{F}_{12} = \frac{1}{\frac{1}{\varepsilon_1} + \frac{1}{\varepsilon_2} - 1} \tag{48}$$

If both surfaces have the same emissivity of 0.8, then this transfer factor is 0.67.

When considering the radiation heat transfer from surface to surface, the ash layer coating the surfaces is important. The total emissivity of ash deposits varies from approximately 0.8 at 400K ash temperature down to 0.4 at 1200K. The total absorptivity of the ash deposit is both a function of the gas temperature and the ash temperature with values ranging from around 0.6 at a gas temperature of 600K and ash temperature of 975K down to 0.3 at a gas temperature of 1800K with an ash temperature of 975K [106]. In this work, the effect of the ash layer is ignored.

#### 4.1.2.4 Conduction

Heat conduction occurs through the walls of the metal tubes of the superheater. Steady state conduction heat transfer is given by [40]:

$$\dot{Q} = \frac{2\pi kL(T_1 - T_2)}{\ln\left(\frac{r_2}{r_1}\right)} \quad (49)$$

The length of the tube or pipe is given by $L$ and the radius of the inner surface and outer surface are given by $r_1$ and $r_2$ respectively. The rate of heat conduction is also proportional to the conductivity of the material, $k$, and the temperature difference between the inner and outer surface, $T_1 - T_2$.

The calculation of heat conduction through the pipe wall can also consider layers of fouling or ash on the surfaces of the pipe by applying the above equation to layers of different thermal conductivity. The thermal conductivity of ash is of the order of 0.01W/m K to 2W/m K, depending on the temperature of the deposit, but more importantly on the microstructure with sintered deposits at high temperatures having higher values and less dense deposits having lower values [106]. The conductivity can also be influenced by the composition of the deposit with components such as iron oxide increasing the thermal conductivity. The effect of an ash layer on the outside of the tubes is not considered in the calculation. In reality the ash with its lower conductivity reduces heat transfer and thus increases the time taken for the temperatures to be reduced to saturation.

As described below, the steady state heat conduction through a cylindrical shell is not used in this simplified heat transfer calculation. Rather, a lumped parameter assumption is used to represent the thermal capacity of the pipe walls and conduction effects are ignored.

#### 4.1.2.5 Convection, Tube inner

Soon after shutdown of the boiler, the superheater is isolated and steam flow is much reduced. The pressure and temperature of the steam is retained but convection between the steam and the inside of the tubes takes place.

Typically for turbulent forced convection inside smooth tubes and pipes, the heat transfer coefficient can be calculated using the Dittus-Boelter correlation [107]. The correlation is given by:

$$Nu_D = 0.023 Re_D^{0.8} Pr^n \quad (50)$$

Where $Nu_D$ is the average Nusselt number based on the pipe inner diameter or the hydraulic diameter, $Re_D$ is the corresponding Reynolds number, $Pr$ is the Prandtl number of the fluid and $n$ is an exponent equal to 0.4 for the heating the fluid and 0.3 for cooling the fluid respectively. The fluid properties are evaluated at the film temperature which is the average of the wall and fluid temperatures.

The correlation is valid for smooth tubes with Reynolds number >10 000, Prandtl numbers from 0.6 to 160 and pipe length to diameter ratio greater than 10. The correlation is less accurate for rough tubes, especially when the difference between the bulk fluid temperature and the wall temperature is large.

The Gnielinski correlation [108] for turbulent flow in tubes and pipes is more accurate, but more complex, and considers the roughness of the pipe internal surface:

$$Nu_D = \frac{\frac{f}{8}(Re_D - 1000)Pr}{1+12.7\left(\frac{f}{8}\right)^{\frac{1}{2}}\left(Pr^{\frac{2}{3}}-1\right)} \tag{51}$$

Where $f$ is the Darcy friction factor which is conveniently calculated by the explicit Churchill equation [109] using the pipe roughness, $\epsilon$:

$$\frac{1}{\sqrt{f}} = -2\log\left(\frac{0.27\epsilon}{D} + \left(\frac{7}{Re}\right)^{0.9}\right) \tag{52}$$

The Gnielinski correlation is valid for Reynolds numbers from 3000 to 5 x $10^6$ and for Prandtl numbers from 0.5 to 2000 [108].

Considering the boundary conditions for the above correlations for forced convection heat transfer inside tubes, it is evident that they are not valid for static or low flow conditions. Static or low flow conditions occur on the steam side of a boiler that is isolated. The tubes are filled with superheated steam and the steam is cooled by the tube inner surfaces by natural convection.

A correlation for free convection inside a circular conduit is not readily available. Thus, the heat transfer coefficient is approximated using a correlation by Morcos and Bergles [110] for combined free and forced convection of laminar flow inside a tube:

$$Nu_D = \left(4.36^2 + \left(0.055\left(\frac{GrPr^{1.35}}{Pw^{0.25}}\right)^{0.4}\right)^2\right)^{\frac{1}{2}} \tag{53}$$

$$Gr = \frac{g\beta\rho^2 D^3(\overline{T_w} - T_f)}{\mu^2} \tag{54}$$

$$Pw = \frac{hD^2}{k_w t} \tag{55}$$

Where $Gr$ is the Grasshof number and $Pw$ is a tube wall parameter that accounts for the effect of tube wall conduction on the internal heat transfer, $g$ is the gravitational acceleration, $\beta$ is the isobaric thermal expansion coefficient of the fluid, $\rho$ is the density of the fluid, $D$ is the pipe inner diameter, $\overline{T_W}$ is the average wall temperature, $T_f$ is the fluid temperature, $\mu$ is the dynamic viscosity of the fluid, $h$ is the average heat transfer coefficient, $k_w$ is the thermal conductivity of the wall and $t$ is the wall thickness. The fluid properties are evaluated at the film temperature which is the average of the wall and fluid temperature.

Note that the heat transfer coefficient, $h$, appears in both the Nusselt number, $Nu_D$, and the wall parameter, $Pw$, thus iteration is required in order to solve for $h$.

The correlation is expected to be valid for:

$$3 \times 10^4 < GrPr < 10^6 \quad (56)$$

$$4 < Pr < 175 \quad (57)$$

$$2 < Pw < 66 \quad (58)$$

The experiments for determining the correlation were performed with water and ethylene glycol and hence the Prandtl number range does not include steam. However, the correlation is convenient because it does not require the flowrate, flow velocity or Reynolds number of the flow.

Other correlations for laminar flow forced convection can be considered since pure laminar flow convection rarely occurs because natural convection effects are always present [111]. Note that laminar flow is considered to apply for Reynolds number less than 2100. Several empirical laminar flow correlations do exist and they are based on the Graetz number:

$$Gz = RePr\frac{D}{L} \quad (59)$$

Where $L$ is the length of the tube. For long tubes, where the Graetz number is less than 4, there is a limiting value of Nusselt number of 3.66 for a constant wall temperature and 4.36 for a constant heat flux [111].

If we consider typical values for the boiler superheater, it is possible to calculate limiting velocities and mass flows for individual tubes. Assuming that D=0.033m, and with the kinematic viscosity of the steam of the order of $8 \times 10^{-7}$ m$^2$/s, the velocity in the tubes must be less than 0.05m/s for the flow to be laminar. That equates to a flowrate of the order of 0.001kg/s in a single tube. Considering that the tube bundles consist of between 400 and 1000 tubes, for uniformly distributed flow, flowrates of between 1 and 0.4kg/s will result in transitional flow where laminar flow correlations are no longer valid.

Going back to the Dittus-Boelter correlation for turbulent flow, and using the minimum Reynolds number of 10 000, and a Prandtl number of 1 gives a Nusselt number of 36.4. Considering a tube diameter of D=0.033m and a fluid conductivity of 0.064W/m K, gives a heat transfer coefficient, $h_c$ of 70.7W/m$^2$ K. This heat transfer coefficient would be achieved at a flow rate of approximately 0.005kg/s per tube or between 2 and 5kg/s for the whole tube bundle.

The Gnielinski correlation is valid at a minimum Reynolds number of 3000. Using the correlation and assuming a surface roughness of 50µm and a Darcy friction factor of 0.042, gives a Nusselt number of 10.6 which equates to a heat transfer coefficient of 20.5W/m$^2$ K. Again, this heat transfer

coefficient would be achieved when there is flow in the tube of at least 0.0015kg/s or between 0.6 and 1.5kg/s in the whole tube bundle.

Owing to the lack of flow rate information for this simplified heat transfer model, the Morcos and Bergles [110] correlation was used.

#### 4.1.2.6 Condensation, Tube inner

Once the superheater tubes have cooled sufficiently, it is possible for the steam to condense inside the tubes. The tube wall temperatures must be lower than the steam temperature for this condensation to occur.

Internal condensation in horizontal tubes is dependent on the flow profile. Chato [112] studied internal condensation where the flow profile is stratified consisting of a film of liquid that runs down the walls and a pool that exists at the bottom of the pipe. The fluid flow is driven by gravity and not by external pressure. Later researchers modified Chato's work to account for a varying pool depth that is consistent with pressure driven flows [113].

Chato developed the following correlation applicable to high void fraction situations:

$$Nu_D = 0.555\left(\frac{D}{k_f}\right)\left(\frac{g\rho_f(\rho_f-\rho_g)k_f^3 h'_{fg}}{\mu_f D\Delta T}\right)^{\frac{1}{4}} \quad (60)$$

$$h'_{fg} = h_{fg} + \frac{3}{8}c_{pf}\Delta T \quad (61)$$

The correlation is valid for vapour phase Reynolds numbers less than 35 000. At higher Reynolds numbers, the flow profile changes to wavy or spray flow and requires a different approach to determining the heat transfer coefficient.

Traviss et al. [114] provide the following similar formulation which omits the modified enthalpy of vaporisation, but includes the steam quality, x:

$$Nu = 0.728K\left(\frac{g\rho_L(\rho_L-\rho_G)D^3 h_{fg}}{\mu_L k_L(T_{sat}-T_w)}\right)^{\frac{1}{4}} \quad (62)$$

Where

$$K = \left(1-\frac{1-x}{x}\left(\frac{\rho_G}{\rho_L}\right)^{\frac{2}{3}}\right)^{-\frac{3}{4}} \quad (63)$$

In this work, when in-tube condensation occurs, it is anticipated to occur without significant vapour velocity and thus Chato's correlation or that of Traviss et al. is deemed to be sufficient. The Travis et al. [114] correlation was used in the simplified heat transfer model in this work.

#### 4.1.2.7 Fluid properties

The fluid properties of steam were obtained from steam tables based on the IAPWS IFC-97 formulation [115]. The gas properties were assumed to be those of air at one atmosphere of pressure and at the appropriate temperatures. The average air temperature between the inlet and outlet of each stage of the superheater was used to determine the fluid properties.

Air property data was obtained from [116] and verified by comparison with values from [40]. Curves were fitted to provide air property relationships. The relationships are valid for a pressure of 101.3kPa and a temperature, *T*, in the range from 230°C to 480°C:

$$\rho = (-0.31743 \ln T + 2.427) \text{ kg/m}^3 \quad (64)$$

$$c_p = (8.3571(10)^{-5}T^2 + 0.17256T + 985.88) \text{ J/kg K} \quad (65)$$

$$k = (-2.1643(10)^{-8}T^2 + 7.3916(10)^{-5}T + 0.02476) \text{ W/m K} \quad (66)$$

$$\mu = (-1.4357(10)^{-11}T^2 + 4.2503(10)^{-8}T + 1.7807(10)^{-5}) \text{Pa.s} \quad (67)$$

$$\nu = \frac{\mu}{\rho} \text{ m}^2/\text{s} \quad (68)$$

$$Pr = \frac{c_p \mu}{k} \quad (69)$$

## 4.1.3 Calculate air temperatures

The temperature of the air flow at the outlet of each stage of the superheater is calculated using the effectiveness, ε, and number of transfer units, NTU, method (Refer section 2.3.1).

Typically the ε – NTU method is applied to steady state conditions for two streams passing through a heat exchanger and the appropriate ε – NTU relationship would be selected for the particular configuration. In this case, the one stream is air flowing through the heat exchanger, but the other "stream" is the hot metal surface of the tubes. Thus, the ε – NTU relationship for a single stream heat exchanger is used:

$$\varepsilon = 1 - e^{-NTU} \quad (70)$$

The number of transfer units are defined in terms of the combined convective and radiative heat transfer coefficient, the outer area of the tubes (A), the air mass flow rate ($\dot{m}$) and the specific heat capacity of the air:

$$NTU = \frac{h_{c+r}A}{\dot{m}c_p} \quad (71)$$

Once the effectiveness is determined, the gas outlet temperature, $T_{g\,out}$, can be calculated from:

$$T_{g\,out} = \varepsilon\left(T_m - T_{g\,in}\right) + T_{g\,in} \quad (72)$$

Where $T_m$ is the metal temperature of the tube bundle, and $T_{g\,in}$ is the gas inlet temperature to the superheater stage. The superheater stages are calculated in order of gas flow. Where reheater stages exist between the superheater stages, the gas side heat transfer for these must also be calculated in order to obtain the inlet air temperatures for all of the superheater stages.

### 4.1.4 Calculate heat transfer rates

The heat transfer rates, assumed constant for the time step, can now be calculated. For each stage of the superheater, the outlet gas temperature was calculated in the previous step. The heat transfer to the gas per stage can now be quantified using an energy balance of the gas stream as follows:

$$\dot{Q} = \dot{m} c_p \left(T_{g\,out} - T_{g\,in}\right) \tag{73}$$

Where $\dot{m}$ is the mass flow rate of gas passing through the tube bundle and $c_p$ is the specific heat capacity of the gas at constant pressure.

The component of radiation to the walls surrounding the superheater heat exchangers is calculated using equation 47. The radiation transfer factor, $\mathcal{F}_{12}$, is evaluated by assuming the superheater to be a body enclosed by a nearly black surface using an emissivity of 0.8 which is a common value used for boiler tubes. The effective outer area, *A*, is then assumed to be the sum of the projected area of the front, back and side views of the tube bundle. This avoids calculating a specific shape factor for the radiation from the tube bundle to the walls, which would require a detailed evaluation of the geometry.

The heat transfer inside the superheater tubes and headers is calculated using:

$$\dot{Q} = h_{inner} A (T_s - T_m) \tag{74}$$

Where $h_{inner}$ refers to the heat transfer coefficient for combined free and forced convection of laminar flow or the heat transfer coefficient for condensation, *A* is the internal surface area of the tubes, $T_s$ is the steam temperature inside the tubes and $T_m$ is the tube metal temperature.

### 4.1.5 Calculate metal temperature at the end of the time step

The superheater steam volume is connected to a metal volume that represents the tubes, via a thermal resistance that emulates the internal convective heat transfer coefficient between the steam and the metal. The metal volume is defined by a metal slab with thickness equal to the average heat exchanger tube wall thickness, and an area equal to the total wetted surface area of all the tubes. Both the heat transfer to the tubes and the thermal mass of the tubes are therefore accounted for.

The metal temperatures are approximated by the lumped parameter model i.e. temperature gradients within the metal are ignored and the whole mass of metal is lumped together with one representative average temperature. This assumption is reasonable when the diffusion of heat within the metal occurs more rapidly than the convective heat transfer from the surfaces.

The lumped parameter assumption for the temperature distribution in the metal is considered valid if the Biot number is less than 0.1. At a Biot number of 0.1, the heat transfer error as a result of the lumped parameter assumption is within 5%.

$$Bi = \frac{Lh_c}{k} \tag{75}$$

Where L is taken as the thickness of the tube and k is the conductivity of the material.

There is a substantial increase in heat transfer when the type of heat transfer changes from convection to condensation. The Biot number criterion for the lumped parameter assumption is no longer valid when condensation starts. This was ignored for the purposes of the calculation because it increases the cooling rate which makes the calculation more conservative.

By rearranging an energy balance for a mass of metal, m, undergoing heat transfer, an expression for the rate of change of temperature can be defined. The rate of change of the metal temperature is proportional to the cooling rate ($\dot{Q}_{net}$) and inversely proportional to the mass, *m*, and specific heat capacity, *c*, of the metal:

$$\frac{dT}{dt} = \frac{\dot{Q}_{net}}{mc} \tag{76}$$

The above equation is approximated by Euler integration over the time step, t, to give:

$$T = T_0 + \left((1 - \alpha_c)\dot{Q}_{net,0} + \alpha_c \dot{Q}_{net}\right)\frac{t}{mc} \tag{77}$$

Where $\alpha_c$ is a weighting factor of the source terms evaluated at the previous time step and the new time step respectively. In this model, an explicit formulation was applied ($\alpha_c = 0$) and found to be stable for the parameters encountered in the superheater and a time step size of one second.

If $\alpha_c$ = 0, (forward Euler) then the formulation is explicit which enables direct solution without iteration to find a result but can also lead to instability if the time step is too large. If $\alpha_c$ = 1, (backward Euler) then the solution is implicit and unconditionally stable but can be inaccurate if large time steps are used. When 0<$\alpha_c$<1, the formulation is said to be semi-implicit. When $\alpha_c$=0.5, this is termed the Crank-Nicholson solution, which can also be unstable, but permits larger time steps while still maintaining accuracy. It is found that $\alpha_c$=0.7 provides a good balance of stability and accuracy [65].

As cooling of the superheater tube bundles occurs, some steam will flow depending on which part of the tube bundle is affected more by the cooling. It is assumed that this flow of steam will pass

through the headers and interconnecting piping and cool them. Thus, heat transfer from the headers is calculated using the same principles as the inside of the tubes, i.e. combined forced and natural convection but ignoring condensation. Condensation is ignored because the headers are insulated externally and thus cannot be cooled other than by the steam on the inside. Hence the headers remain hotter than the steam and cannot condense any steam on their inside surfaces.

The heat transfer rate from the headers is included in the calculation of net heat loss from the steam control volume and it is also used to calculate the rate of change of header metal temperature. Again a lumped parameter assumption is used for the header metal temperatures.

### 4.1.6 Calculate steam state at the end of the time step

In order to complete the condensation calculation, the state of the steam in the control volume must be calculated. The cooling of the steam reduces the internal energy, *u*, such that by conservation of energy:

$$\frac{du}{dt} = -\frac{\dot{Q}_{loss}}{M} \tag{78}$$

The rate of change of specific internal energy, *u*, is equal to the net loss of heat, $\dot{Q}_{loss}$, divided by the total mass of fluid in the superheater, *M*. When considering heat transfer only, the total mass is assumed to remain constant. This means there is no mass flow in or out of the superheater. Again the Euler integration method can be applied to give:

$$u = u_0 - \left( (1 - \alpha_c) \frac{\dot{Q}_{loss,0}}{M_0} + \alpha_c \frac{\dot{Q}_{loss}}{M} \right) t \tag{79}$$

This equation is solved using an explicit solution ($\alpha_c$= 0).

To facilitate working with steam tables, it is convenient to convert the internal energy to enthalpy:

$$h = u + \frac{p}{\rho} \tag{80}$$

Where, for constant mass:

$$\rho = \frac{M}{V} \tag{81}$$

Using the enthalpy, *h*, and density, *ρ*, at each time step, it is possible to use steam tables to determine the pressure, *p*, of the steam in the control volume. Once the pressure is known, the temperature can be found using pressure and enthalpy. Then the steam quality, *x*, is found by comparing the new enthalpy to the saturated values at the new pressure:

$$p = f(h, \rho) \tag{82}$$

$$T = f(p, h) \tag{83}$$

$$x = \frac{h - h_L}{h_G - h_L} \quad (84)$$

This procedure enables the state of the steam or steam/liquid mixture in the superheater to be determined at the end of the time step. Once this is completed, all the values at the end of the current time step have been determined and the calculation can proceed to the next time step.

## 4.2 Application of the model

The above calculation procedure was implemented in a Microsoft excel spreadsheet. The calculations were based on the geometry and material properties of Power Station A as given in Table 3 below. In addition to the calculation procedure discussed above, there were specific calculation details relevant to Power Station A which are discussed below.

In the case of the Superheater 2, the bottom of the tube bundle radiates downwards because the tubes are exposed to the combustion chamber below them which is lined with evaporator tubes. The spacing of the tubes is wide apart (960mm pitch with a 44mm diameter tube) and thus it does not make sense to take the plan view area as the effective area for radiation. Instead the view factors for a column of tubes were estimated and summed to obtain an estimate of the overall radiation normal to the tube surface that would escape the tube bundle in a downwards direction. Hence the larger effective area for radiation of the Superheater 2 tube bundle to the evaporator walls in Table 3.

The sling tubes that support the weight of the heat exchangers pass through the tube bundles. These sling tubes are part of the evaporator circuit and are thus at the temperature of the liquid flowing in the evaporator. The exposed area of these tubes within the heat exchanger bundles was added to the effective area of each superheater stage for radiation heat transfer to the evaporator walls.

The sling tubes are physically attached to the heat exchangers by means of brackets on which the horizontal superheater tubes rest. Thus, conduction heat transfer directly from the tube bundle to the sling tubes occurs. The narrowest area, *A*, of the bracket perpendicular to heat flow is approximately 40mm x 8mm. As a conservative estimate, the heat flow is calculated across a 20mm distance, L, from a point where the superheater tube temperature applies to a point on the sling tube where the evaporator temperature applies. The resultant heat flow is 500W for a single bracket when the material conductivity, *k*, is 42W/m K and the temperature difference is 200$^{o}$C. In reality a complex three dimensional temperature field would exist at the connection of the two tubes. There is also a contact resistance between the superheater tube and the bracket that would need to be taken into account. However, as a conservative estimate, the conductance across the brackets was calculated using the total number of brackets, *n*, the dimensions above and the actual temperature difference between the superheater tube, $T_m$, and the evaporator, $T_w$, at the time:

$$\dot{Q} = n\frac{kA}{L}(T_m - T_w) \quad (85)$$

The sum of conduction heat transfer across all the brackets calculated using equation 85 amounts to 3MW for all the superheater tubes at an initial temperature of 400°C and an evaporator temperature of 300°C. This magnitude of heat transfer is non-negligible in determining the rate of cooling of the superheater.

*Table 3. Main parameters of the boiler*

| | **Volumes** | **Estimated Volume** | **Equivalent Diameter** | **Equivalent Height** | **Base elevation** |
|---|---|---|---|---|---|
| 1 | Superheater | 126m$^3$ | 2.98m | 18.1m | 69.1m |
| 2 | Evaporator | 279m$^3$ | 1.95m | 93.4m | 4.5m |
| 3 | Main steam | 35m$^3$ | 0.78m | 73.4m | -1.6m |

| | **Heat Exchangers** | **Outer convective surface area** | **Wall Thickness** | **Specific heat capacity** | **Conductivity** | **Mass of the tube bundle** |
|---|---|---|---|---|---|---|
| 4 | Superheater 1 | 10 522m$^2$ | 5.1mm | 0.56kJ/kg K | 42W/m K | 366 840kg |
| 5 | Superheater 2 | 2 330m$^2$ | 5.5mm | 0.58kJ/kg K | 35W/m K | 87 730kg |
| 6 | Superheater 3 | 3 235m$^2$ | 5.2mm | 0.58kJ/kg K | 25W/m K | 116 090kg |
| 7 | Reheater 2 | 5 601m$^2$ | 5.2mm | 0.57kJ/kg K | 35W/m K | 211 390kg |
| 8 | Evaporator | 3 182m$^2$ | 5.4mm | kJ/kg K | 45W/m K | 628 570kg |

| | **Headers, piping and unheated tube length** | **Inner diameter** | **Inner convective surface area** | **Wall Thickness** | **Specific heat capacity** | **Conductivity** | **Mass** |
|---|---|---|---|---|---|---|---|
| 9 | Superheater 1 | 37.4mm | 639m$^2$ | 7.1mm | 0.58kJ/kg K | 42W/m K | 52 560kg |
| 10 | Superheater 2 | 46.5mm | 178m$^2$ | 12.3mm | 0.58kJ/kg K | 34W/m K | 27 080kg |
| 11 | Superheater 3 | 41.7mm | 163m$^2$ | 12mm | 0.58kJ/kg K | 25W/m K | 19 550kg |
| 12 | Main steam | 303mm | 643m$^2$ | 32.1mm | 0.6kJ/kg K | 25W/m K | 144 540kg |

| | **Parameters for gas side of heat exchangers** | **Tube diameter** | **Transverse pitch** | **Longitudinal pitch** | **Area for radiation to walls** |
|---|---|---|---|---|---|
| 13 | Superheater 1 | 44.5mm | 120mm | 85mm | 478m$^2$ |
| 14 | Superheater 2 | 44.5mm | 960mm | 70mm | 546m$^2$ |
| 15 | Superheater 3 | 44.5mm | 480mm | 70mm | 347m$^2$ |
| 16 | Reheater 2 | 57mm | 240mm | 110mm | Not considered |

## 4.2.1 Verification of the heat transfer model

The model was verified by comparing the calculated cooling rate to plant data from Power Station A. The criteria used to select a suitable case from the plant data is given below. Both controlled shutdown events and trips were considered. Unfortunately, plant data for a case when condensation occurred in the tubes was not available.

- Fires out.
- Boiler remains pressurised above 5MPa.
- Fans in operation.
- HP bypass valves, superheater drain valves, main steam leg drain valves and collecting vessel quick drain valves all remain closed.
- No collecting vessel level to avoid possibility of separator overflow affecting the results.

U1 trip on 11 September 2018 fulfilled the above criteria from 04h25 for a period of 48minutes. The plant data was used to determine the weighted average temperature of the superheater. Firstly the inlet and outlet steam temperature of each stage was averaged to get a representative temperature for that stage. Then the volume of each stage was used to weight the stage temperatures and determine an overall weighted average. The initial overall weighted average temperature was 435.9$^{o}$C and this was used as the initial steam and metal temperatures in the calculation. The trip had occurred five minutes prior to the start of the data selected for the calculation and thus it was assumed the local steam and metal temperatures in the superheater had equalised by that time.

The air temperature at the outlet of the air heater and the measured total air flow were used as boundary values in the calculation. Initially the fans were off and thus the airflow was zero until 25 minutes as shown in Figure 22. The fans also ramp up for the purge at approximately 43 minutes.

An average of the evaporator steam temperatures was used for the wall temperature. The average was made up of measurements at approximately the level where the lowest superheater tubes are located and the evaporator outlet at the top of the boiler.

#### 4.2.1.1 Results

As shown in Figure 22, the rate of decrease of measured pressure is greater than the rate of decrease of simulated pressure. The behaviour when the fans ramp up for the purge is also different with the measured pressure flattening while the rate of decrease of simulated pressure increases. Considering that the measured pressure drops faster than the simulated pressure, it implies that the real cooling rate is greater than the simulated one, however this is not the case when comparing the temperatures.

The weighted average measured temperature and the simulated steam temperature are plotted in colour in Figure 23. The simulated steam temperature decreases faster than the average measured temperature. This may be as a result of the model overestimating the cooling that occurs, which is not totally unexpected since conservative estimates were adopted throughout. Or, it could be due to the steam temperature measurements not measuring the actual temperature in the tube bundle.

The measured steam temperatures at all locations in the superheater are plotted as a background in greyscale in Figure 23. This image gives perspective of the real spread of steam temperatures that occur when the boiler is shut down. All these steam temperature measurements are located on headers and interconnecting piping and thus do not measure the steam temperature in the tube bundle. However, in Figure 23, some of the measured steam temperatures show the same behaviour as the simulated temperature. The measured temperatures may have been influenced by some steam flow that occurred in the superheater and exposed the measurement points to steam from the tube bundle.

On the plant, there are tube metal temperature measurements on the outlet end of twelve tubes of the Superheater 2 and 3. These were compared to the simulated metal temperatures in Figure 24.

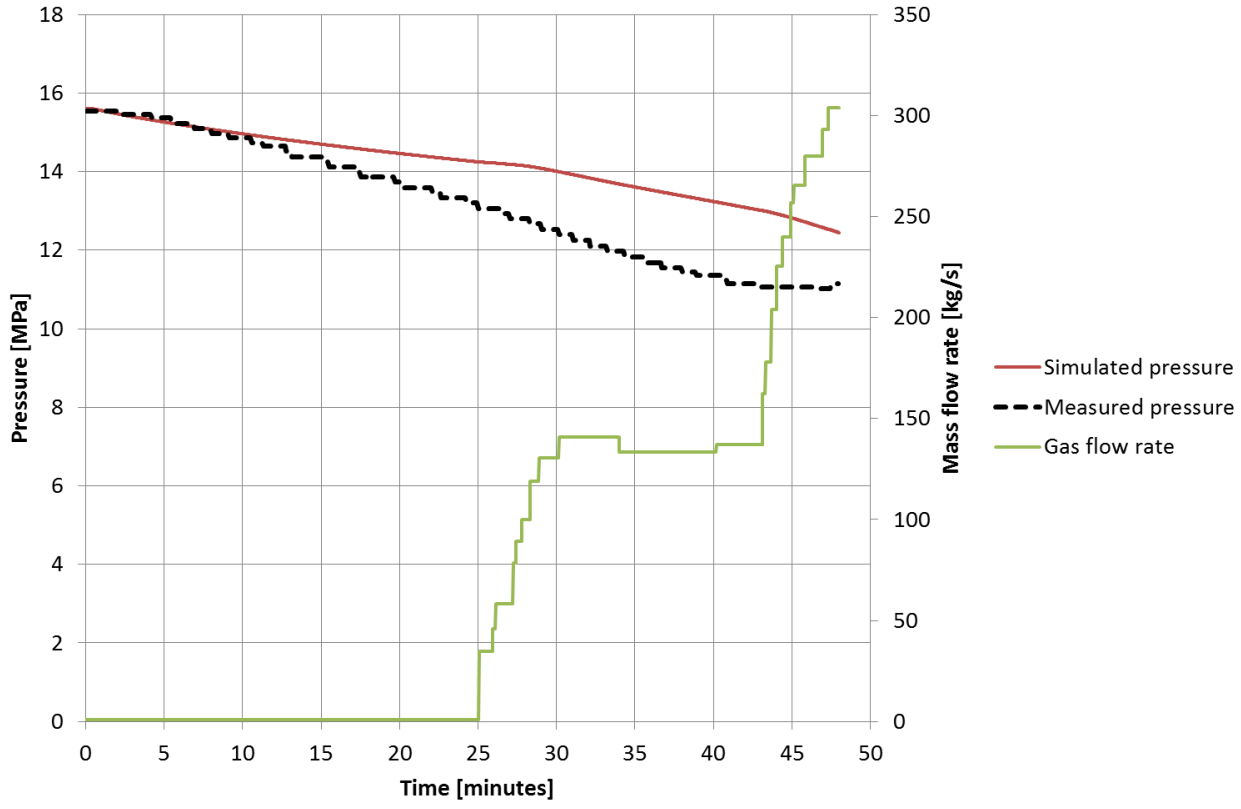


*Figure 22. Verification of the heat transfer model – superheater pressure*

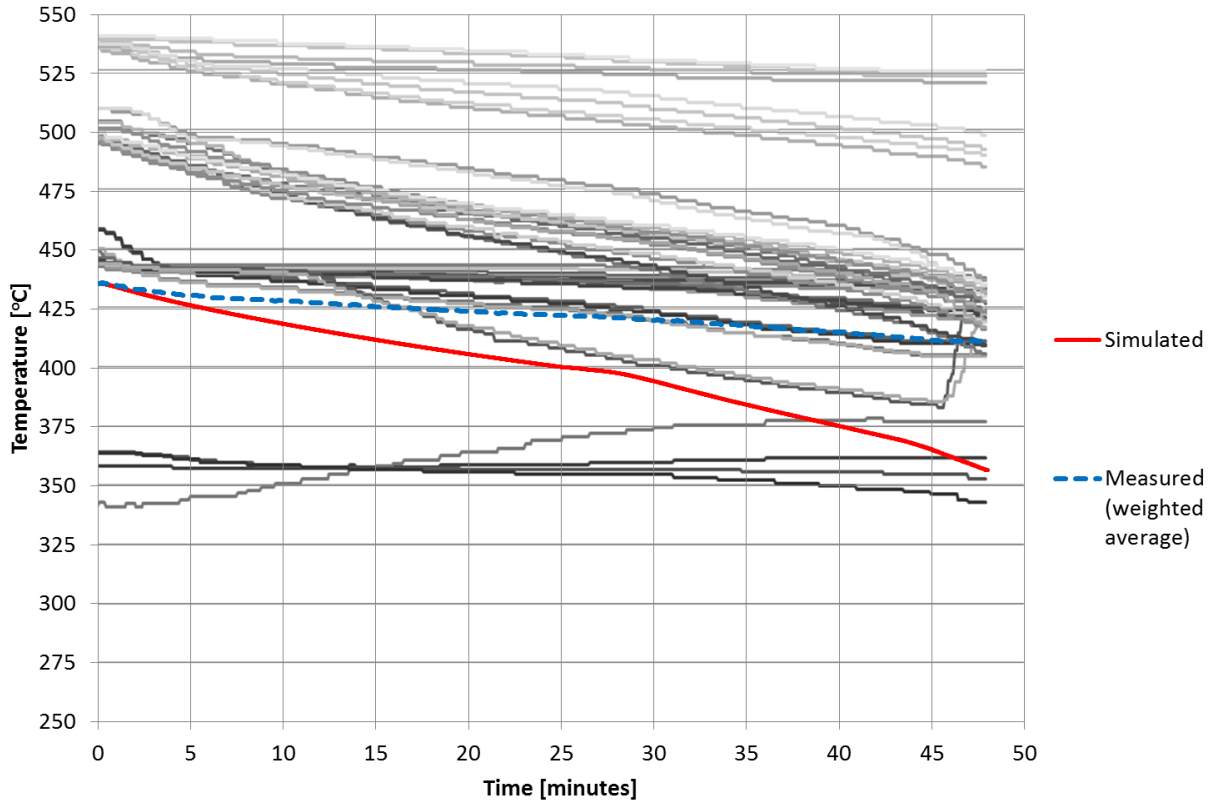


*Figure 23. Verification of the heat transfer model – Steam temperatures (All measured temperatures in grey scale)*

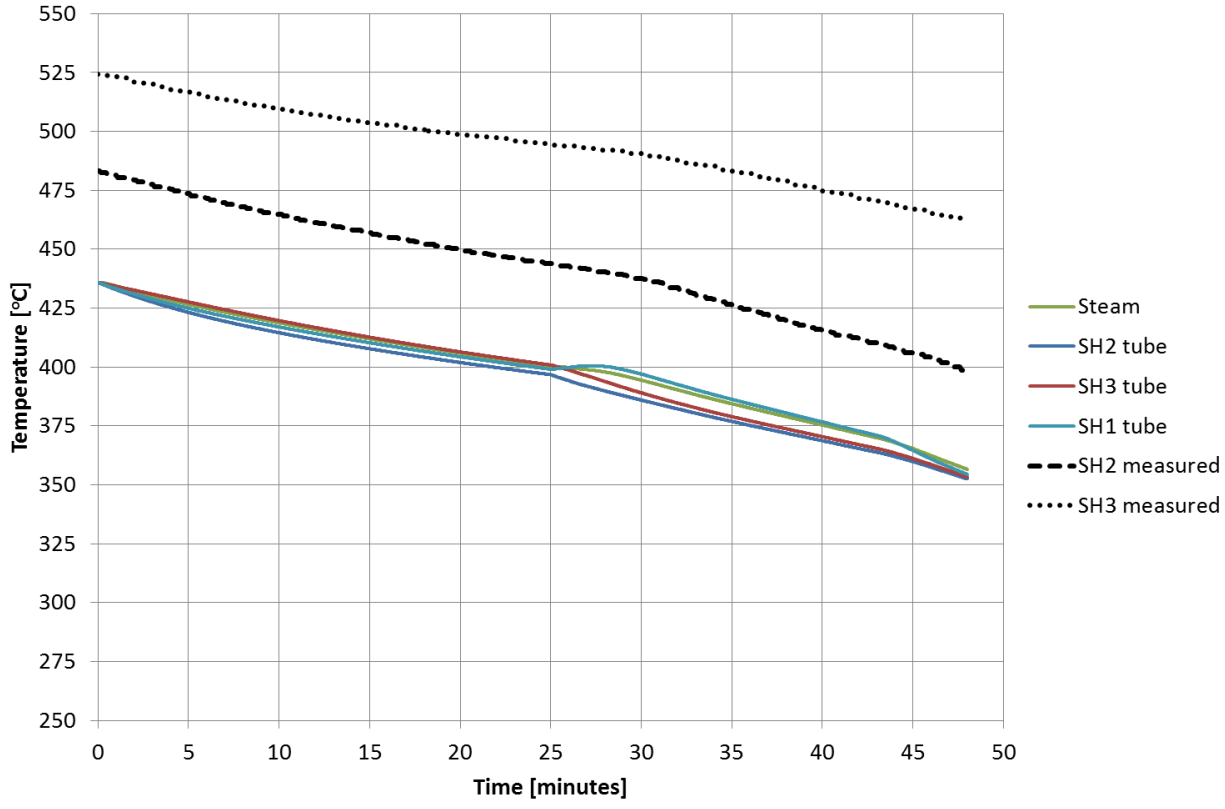


*Figure 24. Verification of the heat transfer model – tube metal temperatures*

By visual inspection, the slope or cooling rate of the measured temperatures is the same as that of the simulated temperatures. This correlation of the cooling rates provide verification that the model is producing the correct magnitude of heat transfer. The offset of measured temperatures compared to the simulated ones is due to the actual locations of the measured temperatures which are at the outlets of Superheater 2 and Superheater 3.

The more rapid drop in measured pressure compared to simulated pressure is an anomaly. Potentially it can be explained by leakage rather than cooling. From the plant data, there was evidence of leakage at two of the main steam leg drains where high temperature in the drain lines indicated flow of hot steam even though the valve limit switch reported that the drain valves were closed.

In Figure 25, the measured and simulated Superheater 1 gas outlet temperatures show reasonable agreement. For the first 25mins under free convection conditions, the simulation model was run with a value of 1kg/s to enable it to solve. In reality there was most likely a natural convection flow that occurred on the gas side of the superheater. During that time, the properties of the gas were unlikely to be that of air. Due to the boiler trip and fans running down about a minute thereafter, the boiler was still filled with unburnt fuel and combustion products. Only after the fans had restarted and displaced the volume of the boiler would the gas properties have started to approach that of air.

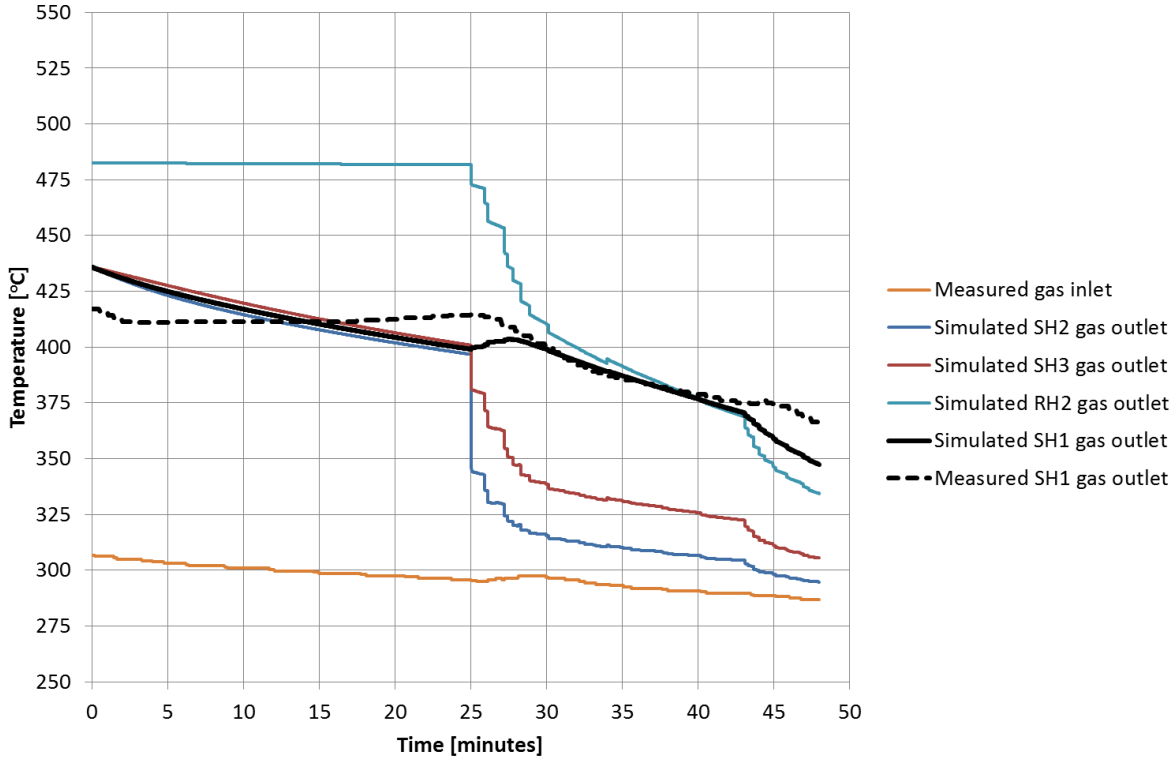


*Figure 25. Verification of heat transfer model - Gas side temperatures*

A further omission from the model is the fouling in the boiler. The tubes of the superheater are coated with ash. The ash is an additional thermal resistance and reduces the outer temperature of the tubes, which reduces the convection and radiation heat transfer from the tube bank. The ash also affects the emissivity of the tubes. The problem with including ash fouling in the model is that the thickness of the ash layer as well as the ash properties are unknown. Thus it was decided not to introduce ash fouling in the model.

In summary, the accuracy of the model is considered to be sufficient to provide useful information about cooling of the boiler after shutdown. Based on the steam temperature drop in Figure 23, the model is considered to be conservative and thus suitable for finding minimum times for condensation in the superheater to occur.

## 4.3 Results of condensation at Power Station A

The heat transfer model was used to simulate a general case at Power Station A to determine the potential for condensate production by cooling of the superheater. The results are shown in Figure 26, Figure 27, Figure 28 and Figure 29. The air flowrate was kept constant at 390kg/s for the duration of the simulation. The air inlet temperature was reduced by 0.36°C per minute to align with typical plant data.

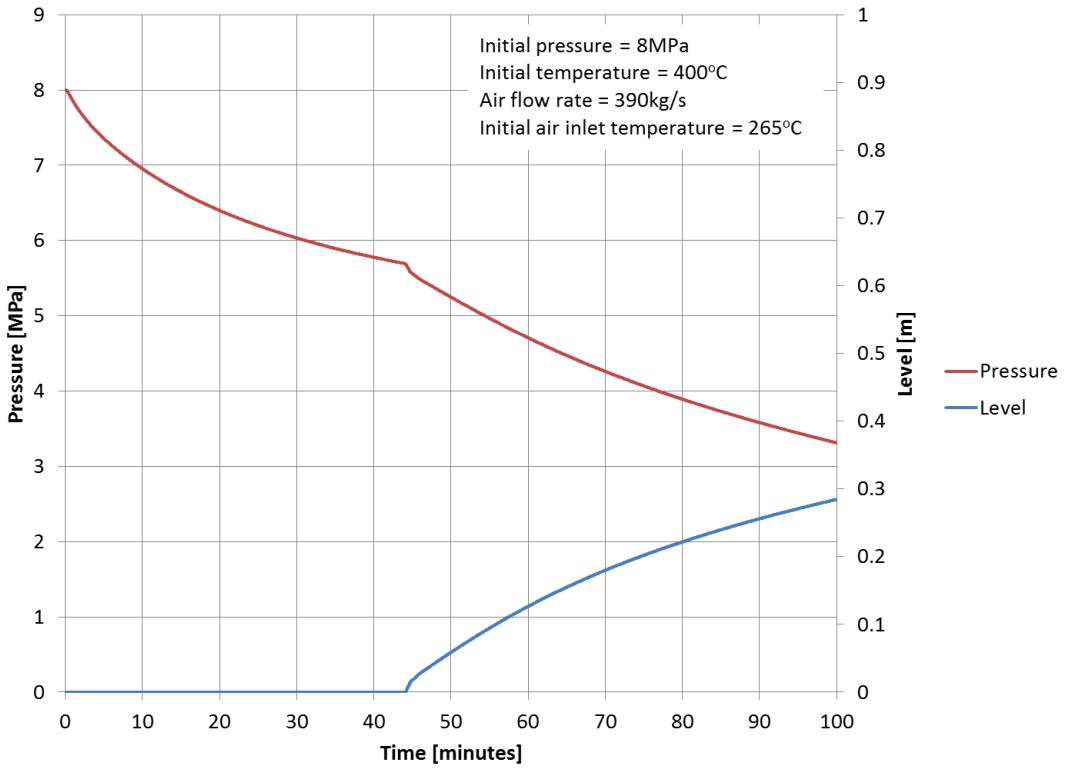


*Figure 26. Power Station A condensation by heat transfer calculation results: Superheater pressure and condensate level*

The simplified heat transfer calculation predicted that the superheater would be cooled sufficiently for condensation to commence after 44 minutes. In that time, the superheater pressure would decrease significantly as the steam was cooled to saturation temperature.

In Figure 26, the predicted height of the liquid level generated by condensation is shown in blue. The overall height of the superheater volume is 18.1m. Thus, the liquid level fraction is less than 2% after 100minutes.

The air flow rate of 390kg/s is the maximum purge flow rate used at Power Station A. Typically a purge lasts no longer than 15minutes. Thus, the results show that condensation by cooling of the superheater under these conditions is unlikely.

The temperatures in the superheater tend towards the saturation temperature of the steam (Figure 27 and Figure 28). The tendency of the metal temperatures to closely match the steam temperature is not realistic. The model assumes the steam in the superheater is well mixed and all at the same temperature because the model simplifies the steam space to a single homogeneous control volume. In reality, limited mixing will occur and each superheater stage will approximately retain its own steam temperature. Thus in reality, there will be less dispersion of heat between the superheater stages.

As the steam cools, its specific volume reduces. This causes flow in the superheater to occur from hotter areas to colder ones. Thus, a flow of steam from the superheater stages in the hotter air flow is likely to occur to those stages that are exposed to colder air flow. In this case, flow from Superheater 1 is likely to occur to Superheater 2. Similarly flow will also occur from Superheater 3 to Superheater 2.

The real situation will retain more stored energy in Superheater 1 and Superheater 3. Steam will be transferred to Superheater 2 and condensed there without having to cool all the metal of the Superheater 1 and Superheater 3 tube bundle to below the saturation temperature.

The air temperatures shown in Figure 29 tend towards the inlet air temperature. The inlet air temperature provides the driving temperature difference for heat transfer. Thus, the results are dependent on the assumption of air inlet temperature used. A reduction of the initial air inlet temperature of 10$^{o}$C from 265$^{o}$C to 255$^{o}$C results in the start of condensation occurring almost 7 minutes earlier. In reality, the inlet air temperature is determined by the rotary regenerative air heater which transfers heat from the gas leaving the boiler to the incoming air. Thus the inlet air temperature is a function of the air temperature leaving the boiler. It is possible to calculate the inlet air temperature by modelling the remainder of the convection pass of the boiler and the regenerative air heater. This would require additional detail and was not pursued further for this simplified heat transfer model.

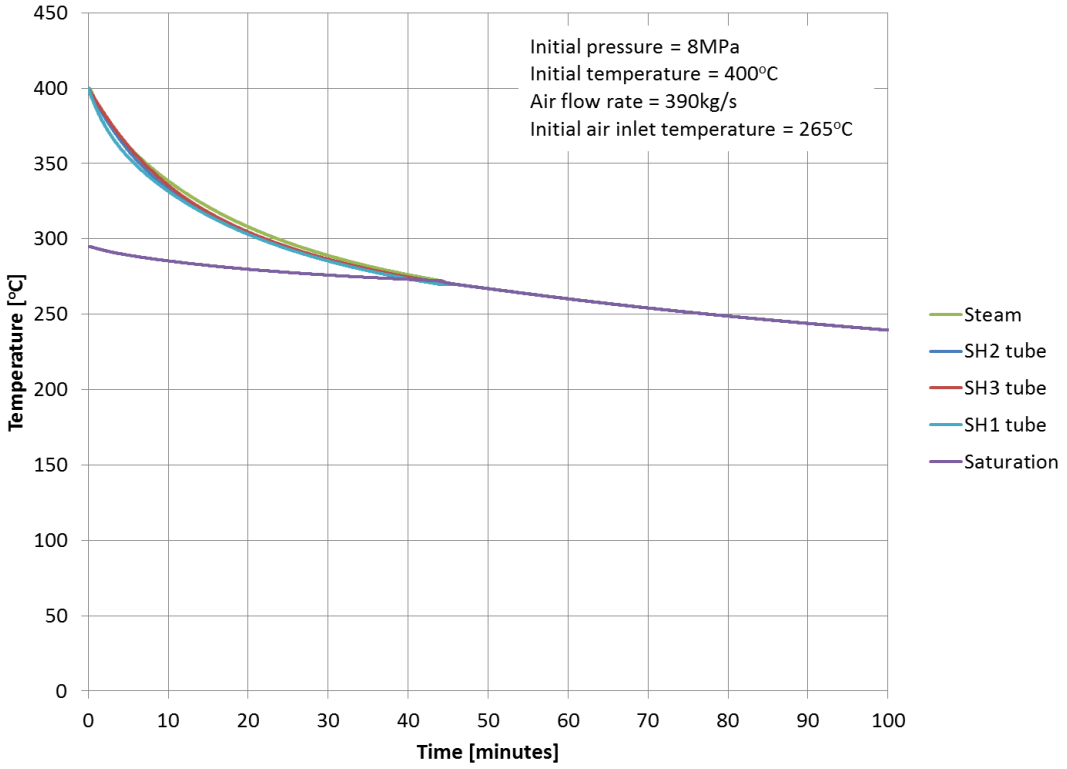


*Figure 27. Power Station A condensation by heat transfer calculation results: Tube bundle and steam temperature*

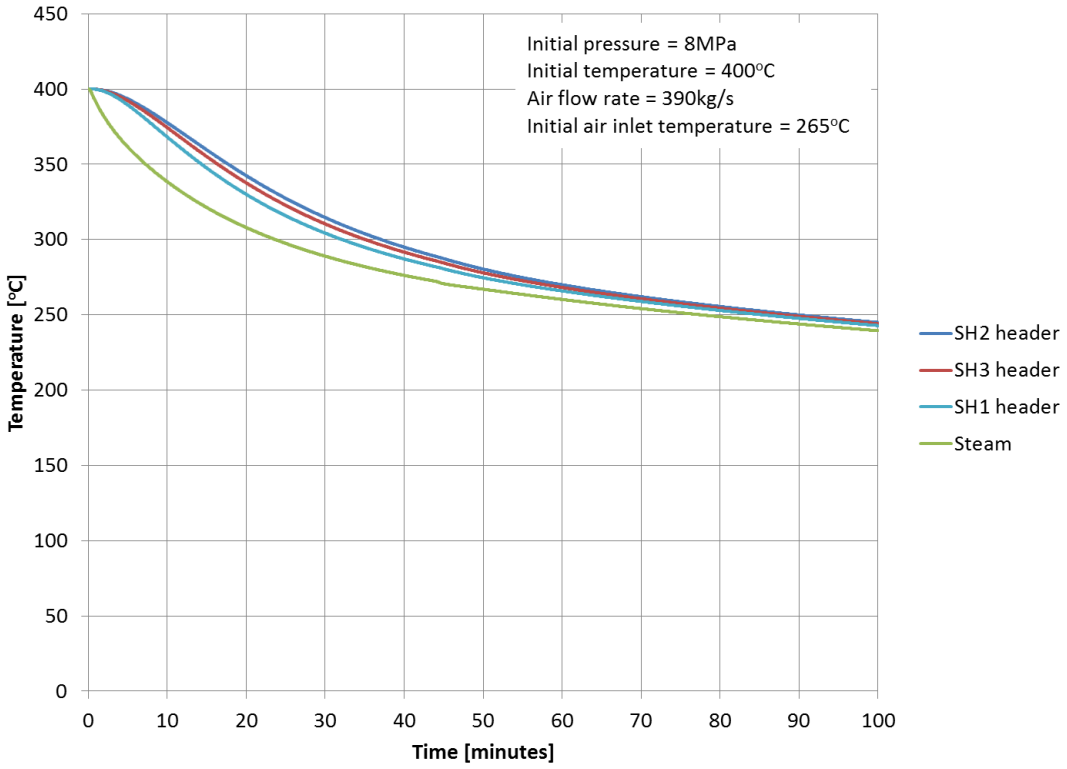


*Figure 28. Power Station A condensation by heat transfer calculation results: Header temperatures*

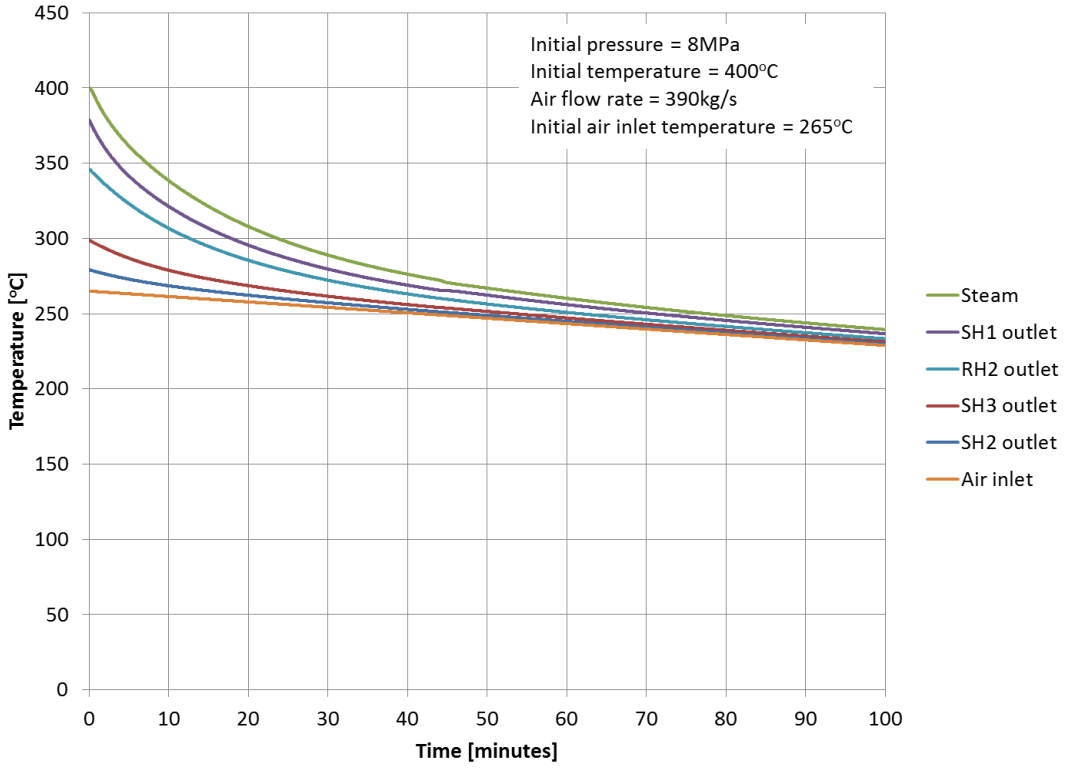


*Figure 29. Power Station A condensation by heat transfer calculation results: Air temperatures*

The above scenario is a normal situation after fires out; however abnormal situations also exist. Abnormal post shutdown temperatures occur when the boiler trips during a start-up. Such failed starts can result in colder superheater metal temperatures. Thus the condensation calculation was also performed for a range of initial conditions and constant gas flow rates. It was found that the time taken to start condensation was influenced by the initial superheat available in the superheater. The initial condition has a significant effect on the time to start condensing (Refer Figure 30). The higher initial temperatures require more cooling than the lower initial temperatures before they reach the saturation temperature of the steam. This is expected because the initial temperature determines the amount of energy stored in the metal. The time to start condensing was also influenced by gas flow rate, with higher flow rates accelerating cooling and thus reducing the time to start condensation.

In Figure 31, the effect of initial pressure is shown. The higher the initial pressure, the sooner condensation starts. Practically this means it is better to reduce the superheater pressure to a lower value when shutting down the boiler to avoid condensation. At the extreme, if the boiler pressure was continually reduced to the saturation pressure corresponding to the incoming air temperature, then no condensation would be possible. Realistically, the boiler must still be kept hot and pressurised and thus the pressure cannot be continually reduced.

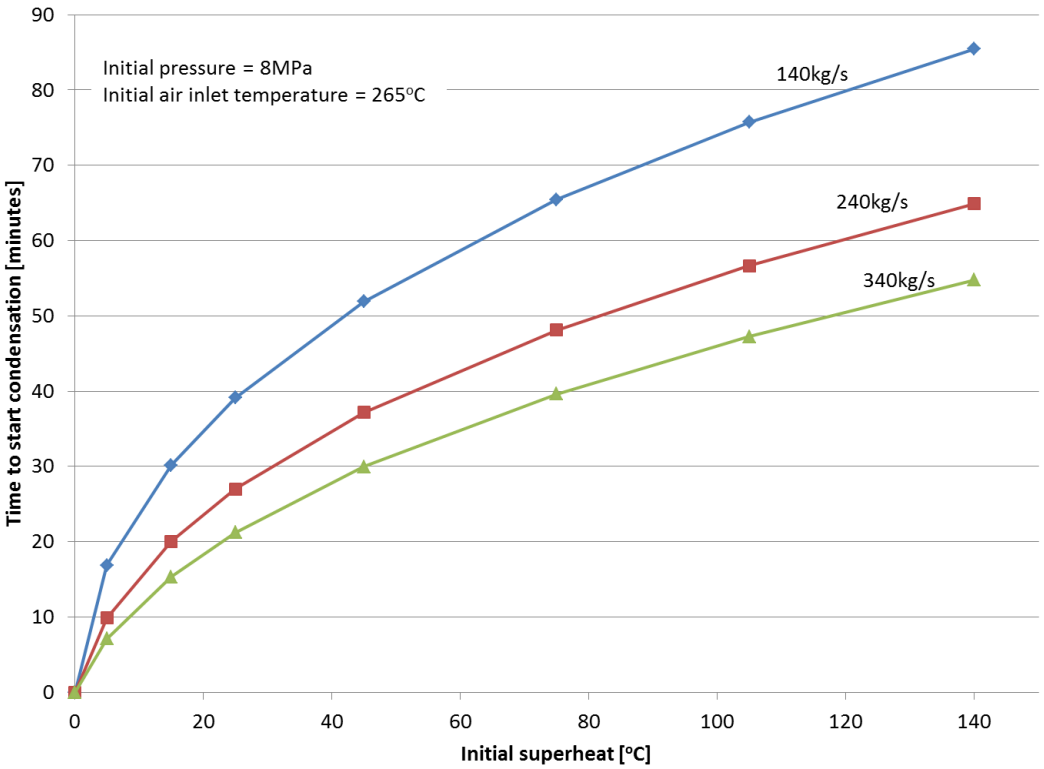


*Figure 30. Time to start condensation by heat transfer at Power Station A: Variation with air flow*

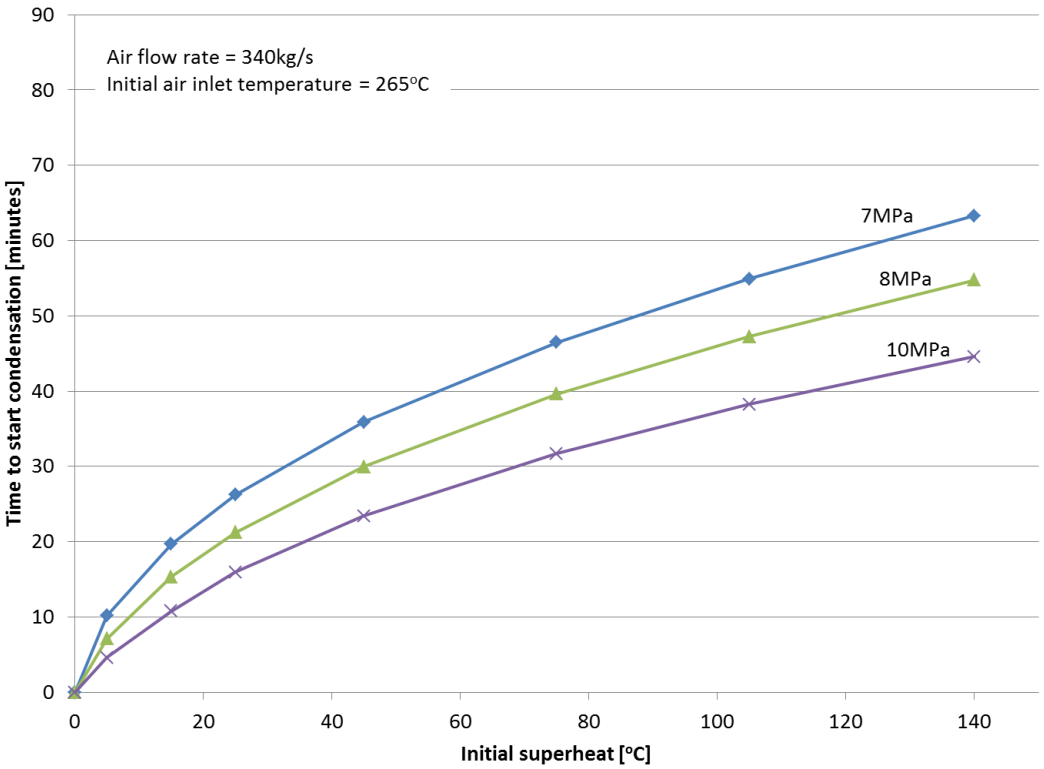


*Figure 31. Time to start condensation by heat transfer at Power Station A: Variation with initial pressure*

The change in specific volume of the steam as it cools and condenses causes a reduction of pressure owing to the fixed volume of the superheater. At the superheater inlet or evaporator outlet, there exists a steam / water interface in the separator vessels. If the water in the vessels is at saturation temperature, then a reduction in pressure at the interface causes evaporation of liquid to the gas phase. The steam so generated flows into the superheater to balance the pressure throughout the system. In this way, a thermal siphon can be created as discussed in section 2.2.

A thermal siphon is caused by a reduction in superheater pressure that flashes liquid off in the separating vessels. The steam produced travels into the superheater towards the low pressure regions. The low pressure regions are where the highest cooling rates occur and where condensation takes place. The liquid is thus transferred out of the separator and into the superheater. This mechanism could potentially transfer large amounts of water into the superheater.

However, if the liquid in the separating vessels is subcooled, then the thermal siphon is not applicable because the liquid in the separating vessel cannot flash to steam. Conversely there is condensation of steam at the steam/liquid interface. This results in a flow of steam from the superheater towards the separating vessels. This phenomenon is considered further in Section 6.1.

For the range of cases considered, the maximum rate of condensation amounted to 5kg/s. This occurred with an initial superheater pressure of 10MPa. It is more common for the superheater pressure to be around 8MPa, in which case the maximum rate of condensation amounted to 2.8kg/s. Although not the purpose of the calculation, these values could be used for capacity analysis of the superheater drains system.

## 4.4 Summary

This chapter describes a heat transfer model that can be used to calculate the cooling of a superheater and determine if condensation by heat transfer caused quenching. The heat transfer model is relatively easy to implement and is an activity in the overall methodology for finding the root cause of quenching as described in section 3.3.

The model was verified by comparison with plant data which was difficult to reconcile and provide conclusive evidence that the model represented reality. However, the measured metal cooling rates of the superheater tubes were shown to match the calculated values. Overall, the model is thought to be conservative and predict higher cooling rates than would be found in reality.

The model was applied to Power Station A and it was found that condensation by heat transfer during the gas purge of the boiler was unlikely to result in quenching. A range of parameters were investigated and, besides the significant period of time required to initiate condensation inside the

tubes, the maximum condensation rate amounted to 5kg/s which is well within the capability of the superheater drains system. However, Power Station A has suffered many quenching events. The next chapter discusses the detailed collecting vessel analysis activity applied to Power Station A with the aim of finding the root cause of quenching.

# 5. Detailed collecting vessel analysis

This chapter addresses the detailed separator and collecting vessel level analysis in support of activity 3.4 of the proposed methodology, as shown in Figure 32. Besides uncovering the underlying problem at Power Station A, this chapter also provides an example of the investigation required when the cause of quenching is not a well-known failure.

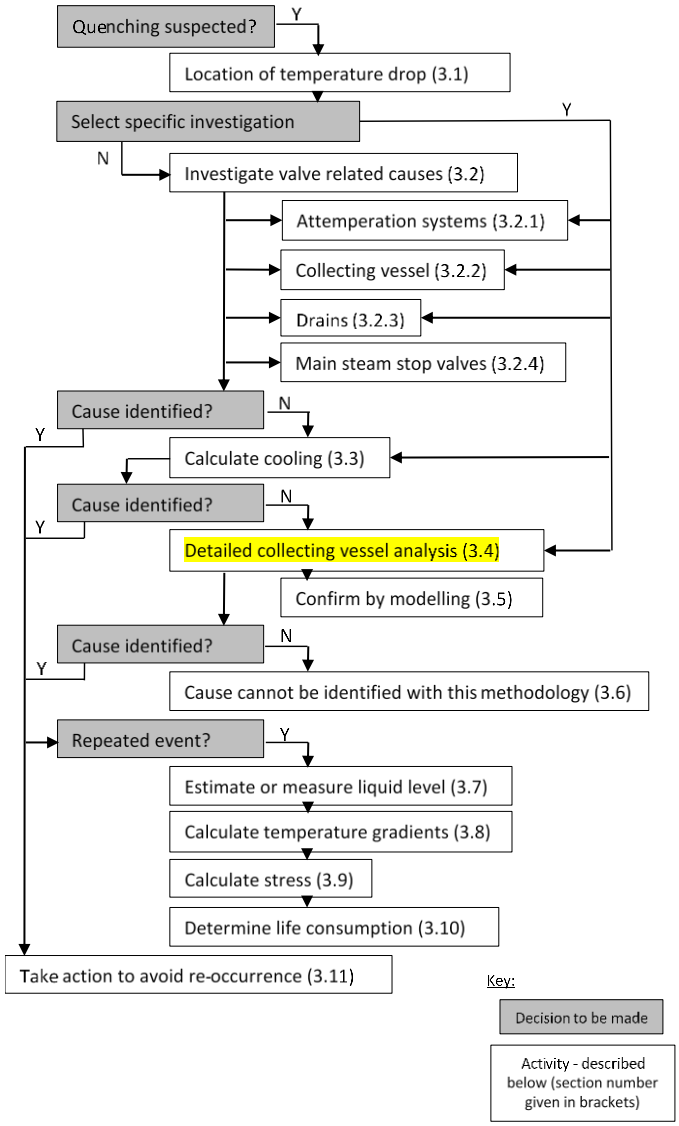


*Figure 32. Activity 3.4 in the methodology*

Originally, the quenching experienced at Power Station A was thought to be caused by cooling and condensation in the superheater. However, as proven in chapter 4, the time taken to start condensation and the quantity of water produced does not match the real events at the plant.

By analysing plant data from various quench events at Power Station A (essentially performing item 3.1 of the methodology), it became evident that the quench initiated at the separator vessels. However, after executing activity 3.2.2, it was found that the collecting vessel level remained in control. Thus, the detailed collecting vessel level analysis, activity 3.4, was carried out. Section 5.1 below describes the detailed evaluation of the separator and collecting vessel system and section 5.2 describes the modelling of the system.

In section 5.3, the analysis of four quench cases is presented and from these cases it emerges that the root cause of the quenching is a siphon which is described in section 5.4. The design at Power Station A is compared to other similar boilers in section 5.5 to show that other configurations are less prone to the siphon and quenching by separator overflow.

## 5.1 Evaluation of the separator and collecting vessel system

The configuration of the separator and collecting vessel system is shown in Figure 33. The diagram shows the vertical evaporator tubes at the outlet of the evaporator where they connect to the wall headers. The outlet from the evaporator is connected to a ring header at the top of the boiler. Note that the pipes that connect the top wall headers to the outer ring header are not shown. The flow in the ring header travels around the left and right sides and then into the front wall part of the ring header. After connection of the front wall evaporator collection header tubes and the outer sling tubes, the left and right flows meet in the centre of the front wall header.

Sixteen separate distribution pipes are connected at the centre location of the outer ring header and these distribute the flow to the four separator vessels, four distribution pipes per vessel. The distribution pipes enter the separator vessels tangentially at the top of the separator vessels and are angled downwards. This introduces a downward spiralling flow pattern in the separator vessel. Owing to the density differences of the liquid and gas phases of the incoming fluid, the liquid phase is driven to the outside of the spiral or cyclone. The liquid phase then runs down the walls of the separator to the liquid level at the bottom of the vessel. The less dense gas phase swirls around the middle of the vessel before travelling up the inner core of the cyclone and exiting the vessel at the top towards the superheater.

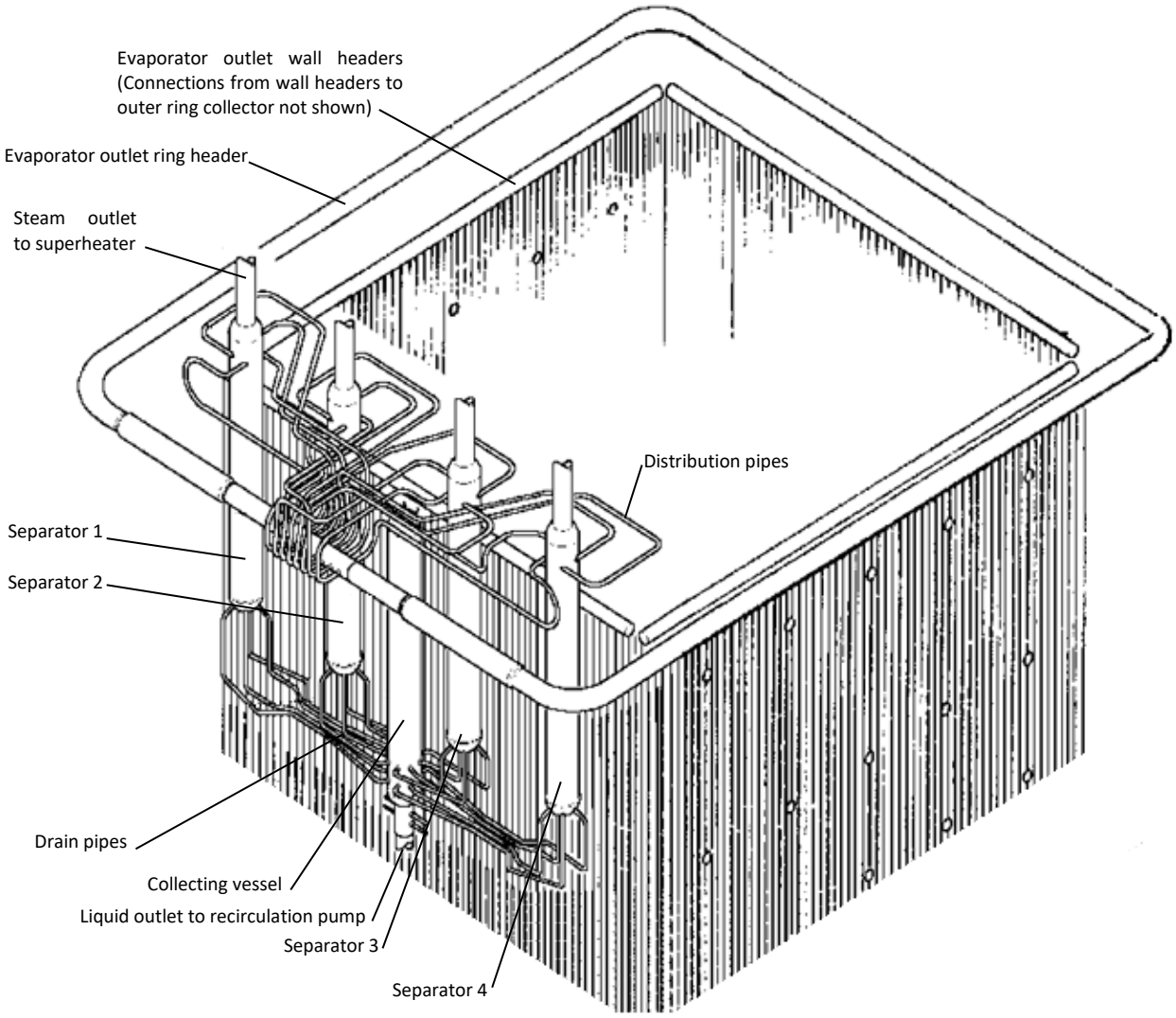


*Figure 33. Separator vessels, collecting vessel and their interconnections*

The separator vessels are equipped with an internal deflector plate (see Figure 39) that reduces the influence of the steam on the water level and limits re-entrainment of water droplets in the steam flow. The separators are 8m in length. The top of the horizontal deflector plate is 1750mm below the steam inlets at the top of the vessel. There is a 70mm gap between the circular deflector plate and the vessel shell to allow the water to pass. The vertical supports of the deflector plate assist in straightening the water flow.

In Benson mode, the steam entering the separator vessel is dry and there is no liquid phase to be driven outwards to the walls by centrifugal force. The steam merely cyclones inside the vessel and then leaves at the top of the vessel.

In circulation mode without fires in, there is only liquid phase or water entering the separator vessel. The water enters at much lower velocity than steam does and thus the cyclone velocity is lower.

The water falls by gravity to the bottom of the separator vessels and drains out. The steam space above the water may be filled with stagnant saturated steam or even air in the case of a cold start-up of the boiler.

The liquid phase collects at the lower part of the separator vessel and then drains via four separate liquid drain pipes to the lower part of the collecting vessel. The collecting vessel has 16 nozzles arranged in two bands around the lower circumference to accept the drains from the four separator vessels. The water fills up the collecting vessel to a level. The collecting vessel level is measured and is controlled by the outlet water flow rate. Water leaving the bottom of the collecting vessel can either be recirculated by the circulation pump or dumped to the boiler blow down vessel.

The collecting vessel has four vent or pressure balancing connections at the top of the vessel. The other end of each pressure balance line is connected to one of the separator vessels. The pressure balance lines ensure that the collecting vessel is at the same pressure as the separating vessels by allowing gas to flow between the vessels.

In Benson mode, there is no liquid level in the collecting vessel. To ensure that the vessel remains warm and ready for service in the event of a trip or a shutdown, there is a connection at the bottom of the collecting vessel that leads to the superheater system. This line is controlled by a motorised isolation valve and should only be open when the boiler is in Benson mode. When the valve is opened, the pressure difference between the separating vessels and the superheater causes a small steam flow from each separator vessel through the drain and vent lines to the collecting vessel and to the superheater system. The steam is introduced into each of the attemperator sprays between Superheater 2 and Superheater 3. A diagram of the spray arrangement is shown in Figure 34 (refer to “Injection water for hot standby system”).

When the boiler is filling or in recirculation mode, the level of liquid or water in the collecting vessel is controlled. The recirculation pump takes suction from a line that leads off from the bottom of the collecting vessel. The circulation pump discharges via a control valve into the feed water line that leads to the economiser inlet. The control valve is used to control the circulation flow such that when the collecting vessel level is at 2.5m, the valve starts to open. Under steady state conditions, the valve then opens linearly with increasing level. At 5.5m collecting vessel level, the flow is set to 280kg/s. Maximum circulation pump flow is 310kg/s.

Besides the evaporator outlet flow, additional water is provided to the collecting vessel to protect the pump. A connection at the bottom of the collecting vessel injects colder water from the spray water system which in turn is supplied from the feed water system. This additional water improves the net pump suction head available to the pump and is only added to the collecting vessel when the circulation pump is running.

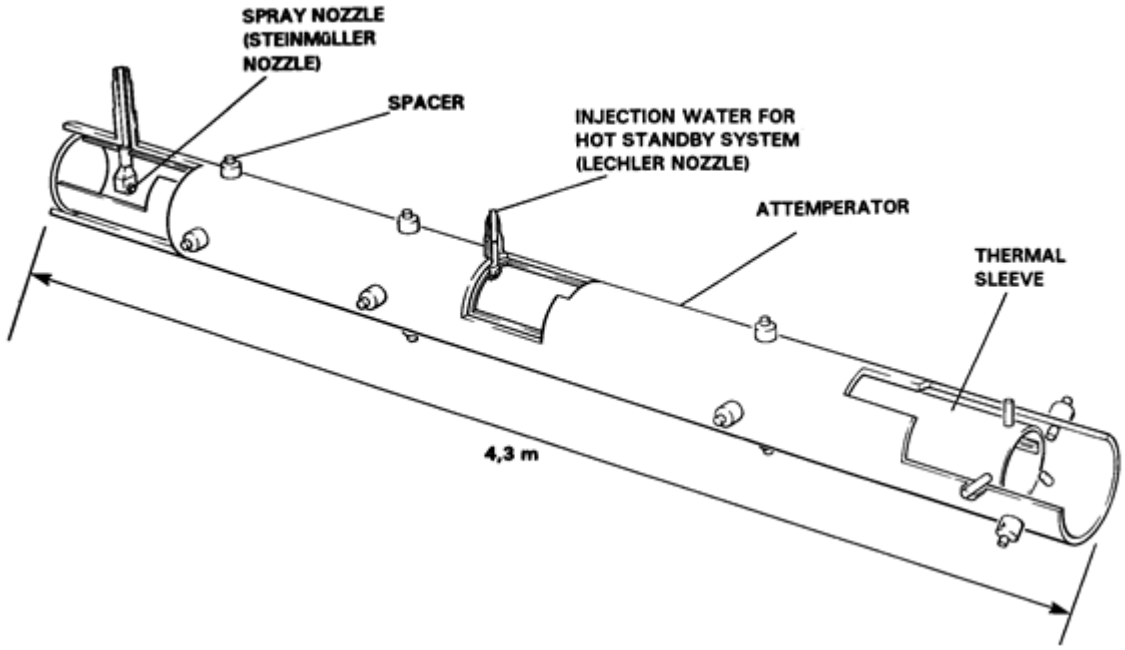


*Figure 34. Arrangement of superheater attemperator between SH2 and SH3*

When there is low forward flow through the pump, a recirculation line is used to maintain minimum flow. A valve opens when low flow is measured and allows flow from the pump discharge to recirculate back to the bottom of the collecting vessel.

When the collecting vessel level is not adequately controlled by the recirculation pump, such as before the pump is able to establish flow or if the level rises beyond the pump's capability, then a pair of quick drain valves act to reduce the level. The quick drains are connected at the circulation pump suction and discharge to the boiler blowdown vessel. Each valve has a capacity of 60kg/s of water. The first valve starts opening at a collecting vessel level of 5.7m, while the second valve opens from a level of 6.5m.

### 5.1.1 Collecting vessel level measurement

The detailed evaluation of the collecting vessel level measurement is discussed in Appendix A. It was found that the method of correcting for the density of the steam and water at operating conditions causes up to a 250mm lower reading compared to the true level. The arrangement of the impulse piping also introduces an error of up to 250mm. Thus, the true level can exceed the indicated level by up to 500mm. This delays the reaction of the controls to a rising high level in the collecting vessel.

### 5.1.2 Typical operation of the separating and collecting system

Following a boiler trip from Benson load, the fires are immediately extinguished by cutting off the fuel flow. The evaporator is partially filled with water and steam and this settles down to form a liquid level. Some evaporation of water in the evaporator continues while the metal walls are cooling but this subsides within a few minutes.

The evaporator is now refilled with water by adding feed water at a rate of approximately 60kg/s. The feed water is pumped by the boiler feed pumps through the economiser, down to the bottom of the evaporator and then fills the evaporator from the bottom upwards.

The inlet feed water is colder than the metal surfaces and gets heated as it travels through the system. However, the heat capacity of the liquid is higher than that of the metal and the temperature available in the metal for evaporating the water is soon dissipated. Thus significant volumes of steam are not produced.

As the water fills the evaporator, the steam in the tubes is displaced. During this filling process, initially superheated steam is pushed out of the evaporator and as cooling progresses, the steam becomes saturated. The steam travels upwards to the evaporator outlet and via the separators into the superheater. The steam pressure is relieved by the HP bypass system which controls superheater pressure. When the steam at the evaporator outlet becomes wet, the liquid phase starts to collect and flow down the walls of the separators and into the collecting vessel.

Once a level of 2m is registered in the collecting vessel, the circulation pump starts with the discharge valve closed and the recirculation line open. The NPSH line is opened to feed colder water into the collecting vessel. The introduction of the circulation flow is delayed with a slow ramp up over ten minutes. This is necessary to smooth the temperature variation of the feed water flow at the economiser inlet. If the recirculation flow suddenly increased, it would cause a slug of hot water which would circulate through the economiser and evaporator. The hot water slug would cause significant temperature gradients and lead to damage of the economiser headers and parts of the evaporator.

If the collecting vessel level goes high while the circulation flow is ramping up, then the quick drain valves are required to open and control the level. Once the ramp up limiter has concluded, the circulation flow is released and the recirculation control valve controls forward flow of the pump based on a proportional set point derived from the collecting vessel level. With the circulation pump on, the economiser flow set point is 260kg/s. This causes the feed water system to increase flow to meet the economiser minimum flow requirement.

At this point, the economiser/evaporator circuit is largely filled with incompressible liquid, hence the increase in flow causes an immediate increase in filling rate of the evaporator. At the evaporator outlet, the steam quality decreases rapidly. The liquid level then gets to the evaporator outlet and the separators.

The separator drains to the collecting vessel have a large capacity to pass the required flow; however, they need a liquid level in the separator to do so. Thus, a level builds up in the separator vessels and this ensures a drain flow to the collecting vessel. The collecting vessel level rises rapidly and this can be managed by the quick drain valves until the circulation pump has sufficient forward flow to reduce and maintain the level. Typically the level stabilises and the quick drain valves can be closed.

During a controlled shutdown, a similar sequence occurs, but the circulation pump is brought into service earlier while fires are still in because the controlled reduction in load allows the evaporator outlet to become saturated while still on load.

### 5.1.3 Feed water control

The feed water control receives an economiser inlet flow set point that is calculated as a function of boiler load, with influence from boiler pressure control and boiler enthalpy control. The economiser inlet flow is measured. The feed water control thus varies the speed of the boiler feed pumps to obtain the required economiser inlet flow.

At start up and low load, the start-up feed regulating valves are used to provide the required back pressure on the boiler feed pump to keep the pump within its operating envelope. Once boiler load is above 50%, a main feed water valve opens fully as there is sufficient pressure in the boiler to keep the pump(s) within the operating limits.

The minimum economiser inlet flow set point is 50kg/s, however, this is increased to 260kg/s when the circulation pump is on or the fires are in. The economiser inlet flow is made up of the feed water flow as well as the recirculation flow. The recirculation flow is independently controlled and thus when the circulation pump is running, the feed water flow only makes up the difference between the recirculation flow and the required economiser inlet flow. In the case of low level in the collecting vessel, the circulation flow is less than the required minimum economiser inlet flow and the feed water system adds feed water to achieve the required flow.

## 5.2 Modelling the separator and collecting vessel system

In order to confirm that the separator and collecting vessel system functions as per the design, a one dimensional thermo-fluid model of the system was created in Flownex. Flownex is a

commercially available software package for one dimensional thermo-fluid modelling of physical processes (Refer to section 6.3.1 for more details about Flownex). An input specification for the model is given in Appendix B.

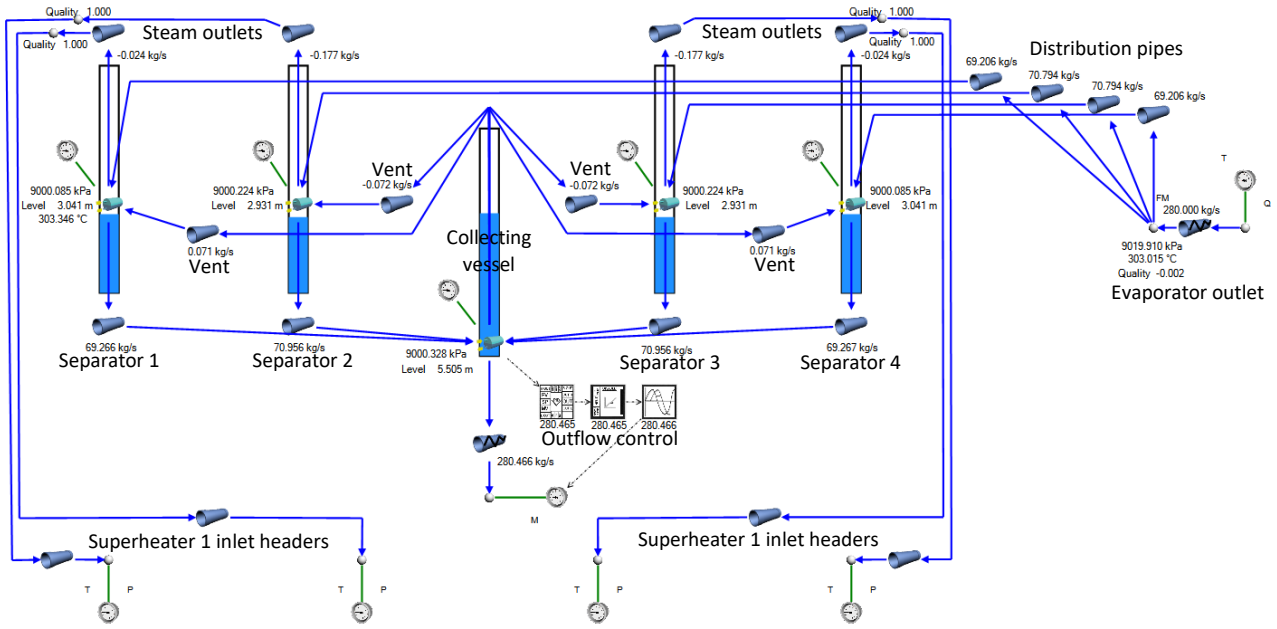


*Figure 35. Flownex model of the separator and collecting vessel system*

The fluid enters the model on the right from the evaporator outlet. The temperature and quality of the inlet boundary condition can be set. This enables both saturated or subcooled inlet conditions to be considered. The inlet flow rate boundary condition is specified by a fixed mass flow at the flow resistance element.

The flow then splits into the four sets of four distribution pipes, which are modelled using four pipes with four parallel legs each. The distribution pipes connect to the separating vessels. Each separating vessel is modelled by a two-phase tank component with a corresponding track bar to visually represent the level in the vessel during a run. The elevation of the bases of the tanks, the height of the tanks and the height fraction of connections are set to match the real plant values.

The two-phase tanks in the model are each initiated by a boundary condition that specifies the starting level in the tank. These boundary conditions are also required to enable a steady state solution to be found. When solving in transient, the tank boundary conditions are removed at the second time step to allow the tank level and pressures to vary during the run.

The separating vessels drain via four sets of four pipes to the collecting vessel. The collecting vessel elevation is lower than the separating vessels and the collecting vessel is vented to each of the separating vessels.

A controller manages the outflow boundary condition at the bottom of the collecting vessel. The controller is configured similar to the behaviour seen in plant measurements. It uses a proportional control of collecting vessel level to determine outlet flow rate. There is also a rate limiter and a time delay to mimic the response of the real plant.

The steam outlets of the separating vessels connect to a node, each at the highest point of the piping system which matches the elevation of the pipes in the real plant. From there, the pipes drop 18m down to the Superheater 1 inlet headers. The pipe diameter and length are set to the same values as the real plant.

Lastly the superheater boundary conditions are used to set the pressure in the superheater system. It is assumed that each superheater 1 inlet header can have a different pressure and thus four separate boundary conditions are used. A temperature boundary condition is also provided to ensure that any reverse flow into the model has a specified temperature.

### 5.2.1 Steady state results

The Flownex model described above was used to investigate the working levels for various constant inlet liquid flow rates. The model was run in transient with constant inlet and outlet conditions until the values throughout the model had stabilised. The results are shown in Figure 36.

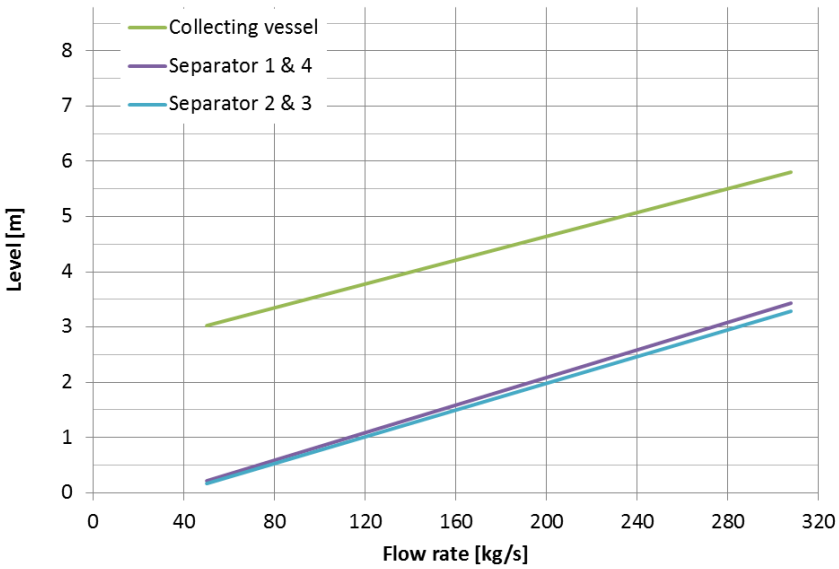


*Figure 36. Steady levels of the separator and collecting vessel system for various inlet flow rates*

The steady state collecting vessel level compared to outlet flow is linear as expected because of the proportional controller. The separator vessel levels are also effectively linear because the flow related pressure drop in the drain pipes from the separator vessels to the collecting vessel is small.

At normal operation of the circulation system at up to 280kg/s, it can be seen that the separating vessels operate with substantial level in them. Thus the separating vessels actually contribute to the volume of the collecting vessel.

In steady state, there is no significant difference between the levels in Separator 1 and Separator 4 compared to Separator 2 and Separator 3, but Separator 1 and Separator 4 do have a higher level because of the pressure losses in the drain pipes which are higher for the vessels further away from the collecting vessels. The steady state operating levels of the separator and collecting vessel system are well below any of the outlet connections and thus do not cause any problems for normal functioning of the system.

### 5.2.2 Transient results

In order to investigate the transient performance of the separator and collector system, the input mass flow rate from the evaporator was manipulated by introducing a step change and then the resulting level behaviour as a function of time was observed.

The effect of inlet quality was investigated by running cases with different values. It was found that qualities greater than zero produce less liquid phase in the separators and thus result in lower liquid flows and lower levels in the vessels. Thus, only the case with inlet quality equal to zero (i.e. saturated liquid) is presented here because it is the most likely to result in a separator overflow.

The results in Figure 37 show the response to an increase in the evaporator outlet flow from 50kg/s to 280kg/s. The flow was increased at a rate of 30kg/s/s. This rate of change was estimated from the highest rate of change of economiser flow measurement value seen in plant data.

The reason for the step change of the inlet flow is due to the economiser flow rate set point that changes. When this set point changes, the feed water pumps react to meet the new set point. The feed water thus provides the additional water to the system to increase the collecting vessel level and thereby increase the circulation flow until the flow meets the economiser flow set point.

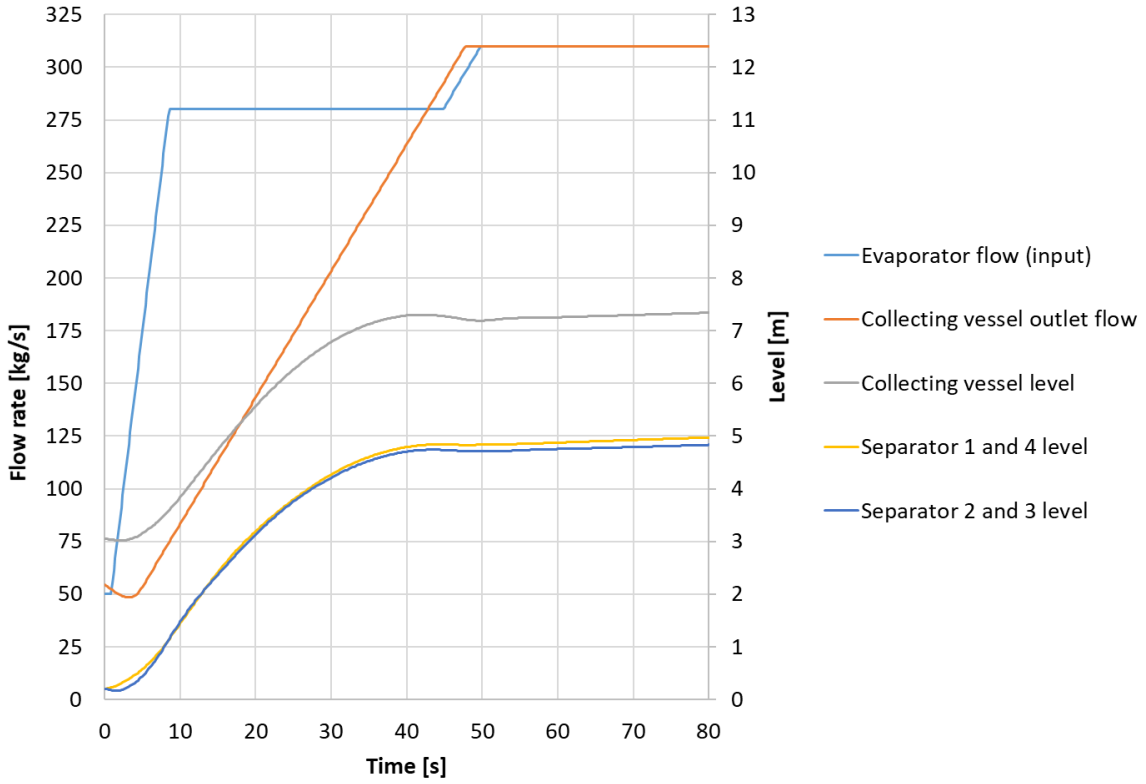


*Figure 37. Transient separator and collecting system results (Inlet quality = 0, flow ramp from 50kg/s to 280kg/s at 30kg/s/s)*

The sudden increase in flow coming into the separator and collecting vessel system first starts increasing the separator vessel levels which in turn increases the collecting vessel level. The maximum collecting vessel level of 7.3m occurred at 41s after the transient started. The maximum separator vessel during the event is 5m, which is below the height of the connection of the vent to the separator and would not cause flooding of the vent.

It can be seen that the collecting vessel outlet flow lags behind the inlet flow to the model. This is mainly because the proportional controller requires the collecting vessel level to increase before it reacts and the rate limiter imposes a delay on the ramp up time of the circulation flow. The collecting vessel outlet flow increases with rising level in the vessel until the maximum limit of the circulation system is reached (310kg/s). This exceeds the inlet flow of 280kg/s.

Now if we consider that the circulation system is a closed loop, then it is not possible for the outlet flow of the circulation pump to exceed the inlet flow coming from the evaporator when the circulation loop is filled with water. Thus, in the model, the inlet flow is increased to match the outlet flow with a two second delay when the outlet flow exceeds the inlet flow. It is interesting to note that the levels after this transient are about 1.5m higher than the steady state levels shown in Figure 36.

Under normal circumstances, the real plant is equipped with drain valves that would open to prevent the collecting vessel level from reaching 7m. The drain valves are not included in the model. These results show that, provided the circulation pump is able to respond within 40seconds, the system without drain valves is capable of managing a step change in economiser inlet flow without overfilling the separators and causing an overflow to the superheater.

### 5.2.3 Collecting vessel vent

The vent at the top of the collecting vessel, that connects to the side wall of each separator vessel, is an important feature for proper functioning of the system. The vents are necessary to ensure that a bubble of incondensable gas or even saturated steam does not prevent the collecting vessel level from rising when the liquid flow increases.

The Flownex model was used to investigate the system response to the same transient described above but with the vents removed. Without a collecting vessel vent, the pressure in the collecting vessel increases due to the saturated steam trapped in the vessel. This prevents the collecting vessel from filling and without a level increase, the liquid drain flow control does not increase the outlet flow. The result is that the separator vessels fill up and overflow.

The case modelled with no collecting vessel vent is extreme and does not match plant data that shows the collecting vessel increasing. Thus it is unlikely that the vents are not functioning at all. If the vents were partially blocked, it may cause delayed filling of the collecting vessel which could resemble the real plant behaviour. All four vents would need to be affected simultaneously.

There is a possibility that the vents are impeded by a water curtain in the separator vessels as depicted in Figure 38 (Refer item E which is the collecting vessel vent connection). The liquid phase in the separator vessel tends to flow down the wall of the vessel. This is due to the four distribution pipes tangentially entering the vessel at the top which causes a downward spiralling flow of water along the wall that passes the gap between the shell and the deflector plate.

The size of the annular gap between the deflector plate and the shell is approximately 70mm. The only available details of the deflector plates are shown in Figure 39. The deflector plate is supported by a section of pipe which is supported by four vertical gusset plates between the pipe and the walls of the separator vessel.

The collecting vessel vent is connected just below the deflector plate. There is likely to be some interaction between the falling water flow and the vent flow at that point. During periods of low vent flow, the vent may be impeded. If the vent flow is negative, which occurs when the collecting vessel level is falling, then water may be drawn into the vent.

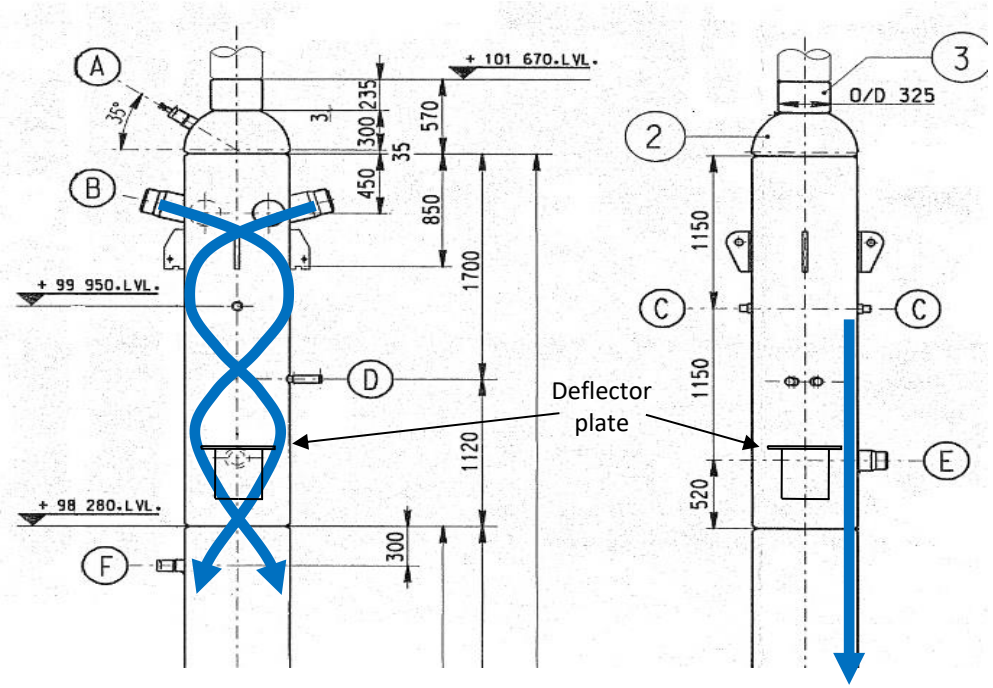


*Figure 38. Separator vessel showing expected liquid flow*

The maximum positive vent flow predicted by the Flownex model for the transient case above was 1.25kg/s, which equates to a velocity in the vent line of 11m/s. This flow has the potential to interfere with the liquid draining past the defector plate. However, the density of the liquid is much greater than the steam, so other than redirecting the liquid flow, the vent flow is unlikely to prevent the separator vessel from draining.

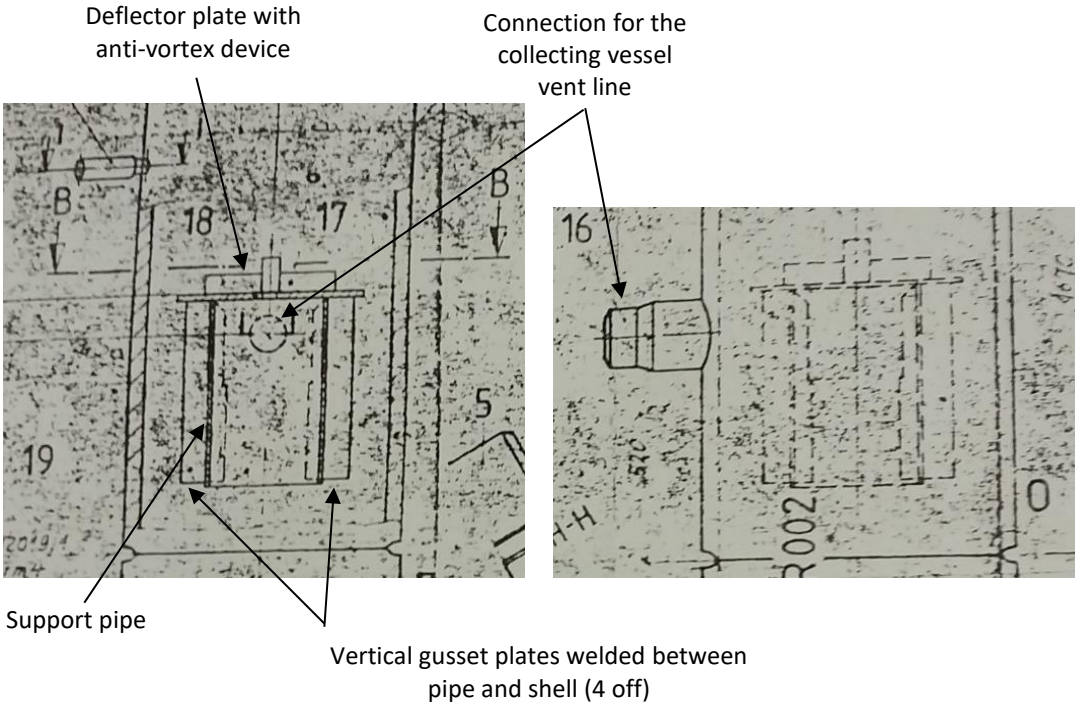


*Figure 39. Separator vessel deflector plate details and collecting vessel vent connection*

### 5.2.4 Influence of superheater pressure

The superheater pressure is controlled by the HP bypass system when the boiler fires are out but the boiler is still hot. Some steam is still generated by the hot metal surfaces and the dissipation of temperature gradients in the walls of the evaporator. Thus the HP bypasses relieve that steam at a controlled rate to maintain the required superheater pressure.

The superheater pressure influences the separators, collecting vessel and evaporator. Variations in pressure can cause changes in levels and disturbance of flow. Saturated liquid exposed to a drop in pressure leads to flashing whereby some liquid evaporates into steam. Conversely an increase in pressure leads to condensation of some steam into liquid.

Pressure changes were investigated by means of the Flownex model. The model was run at a fixed inlet flowrate of 280kg/s and an inlet quality of 0.05. The model was run until the values were steady. A step change in superheater pressure was introduced to all four boundary conditions at the same time and the response observed.

The step changes in superheater pressure caused a disturbance in the separating vessels pressure and levels and some oscillating pressure behaviour was observed. The oscillations are not uncommon in systems where flashing and condensation takes place, however in this case the oscillation is due to the response of the system to a step change in pressure. The steam in the pipes acts as a gas spring.

Superheater pressure step changes of +/-30kPa and +/-100kPa were tested. In all cases the oscillations damped out within 15s. The highest separator vessel level change was 264mm. Thus, sudden changes in superheater pressure are unlikely to disturb the system to an extent that a separator overflow occurs.

### 5.2.5 Unbalanced superheater pressure

The four separator vessels are independently connected to the superheater system which consists of four parts or legs. The superheater legs are interconnected at different places, but not in such a way that would guarantee uniform pressure at the four superheater inlets.

Pressure differences between the superheater legs can occur due to flow differences in the legs caused by non-uniform operation of downstream equipment such as unequal heat transfer, HP bypasses not all controlling equal flow, drain valves not all opening simultaneously, and spray valves stuck open.

Under steady conditions, a lower pressure at one of the superheater inlet headers may cause the associated separator vessel to overflow. By running the Flownex model to steady state with a

different constant superheater pressure boundary condition for the superheater inlet headers connected to Separator 1, the effect on separator levels could be observed.

The pressure change has a significant effect on the flow distribution from the evaporator to the separators. The separator with lower pressure receives significantly more flow and thus its level increases.

The change in level of the separators with increasing differential pressure is shown in Figure 40. The results for Separator 1 are extrapolated to determine the pressure difference required to increase the level above the overflow height (the top point of the steam outlet pipe). Overflow to the superheater would occur at a differential pressure of 36kPa.

Considering that the density of the liquid at 8MPa is approximately 700kg/m$^3$, the height difference induced by the pressure difference of 36kPa is approximately 5.2m. The remainder of the height necessary to overflow is as a result of the flow maldistribution that occurs. As the liquid drain flow from Separator 1 becomes larger it requires more head to drive the flow and overcome the flow related losses. The magnitude of this dynamic pressure drop of the liquid drain flow is identified in Figure 40.

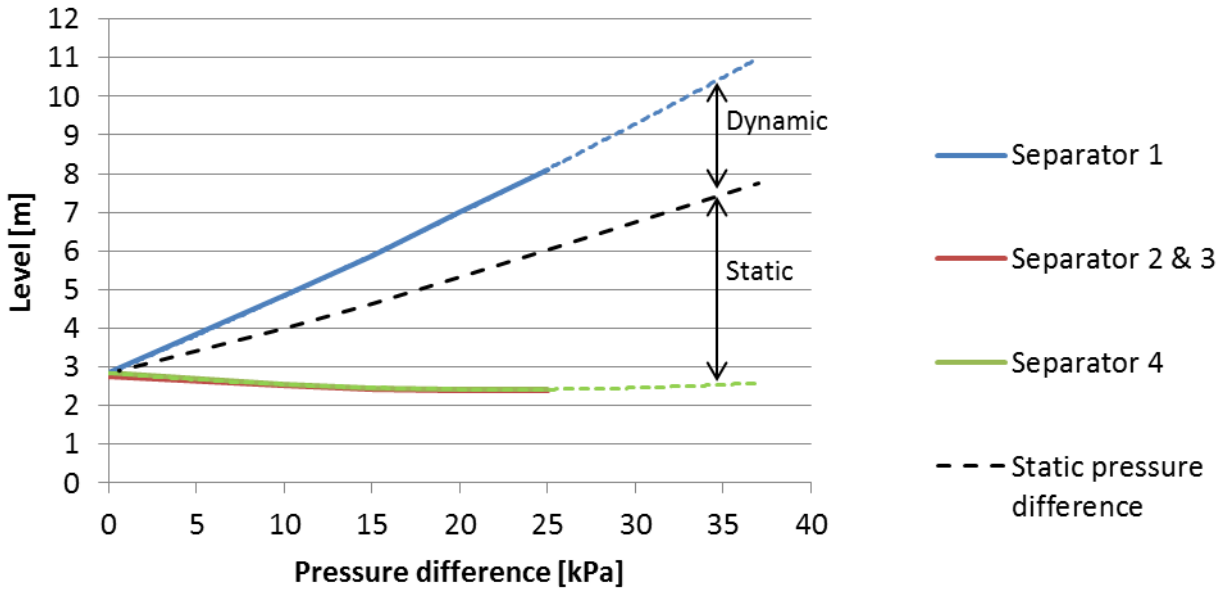


*Figure 40. Steady state separator levels with differential superheater pressure at separator 1 (Inlet flow 280kg/s)*

Thus, unbalanced superheater pressure provides an explanation of why the separator vessels do not necessarily have the same levels at all times. From plant data, experience suggests that separator vessels one and four are more likely to overflow. Separator vessels one and four most likely experience lower static pressure which increases their levels above the levels in Separator 2 and three. This pressure difference would need to be about 15kPa to create a 3m level difference

for Separator 1 and four to overflow, while the level in Separator 2 and three would not yet have reached the height of the inlet nozzles.

Although unbalanced pressure between the separator outlets can cause different levels between the separators, unbalanced pressure to the extent required for one of the separator vessels to overflow is unlikely. The headers and pipes are sized for much greater flow rates and thus pressure drops for the small flows that occur during quenching are almost negligible. In the case where the collecting vessel level goes high, all four separator vessels go high and unbalanced superheater pressure could determine which separator vessel overflows first.

## 5.3 Analysis of plant data

Plant data was analysed in an effort to find the root cause of quenching at Power Station A. Evaluation of all available plant measurements were carried out and details of Case A, Case B, Case C and Case D are provided in Appendix C, Appendix D, Appendix E and Appendix F respectively.

The problem is not unit specific with similar features noted across all four case studies, each of which took place at a different unit (Unit 3, Unit 5, Unit 6 and Unit 1 respectively). For Case A and Case D (Unit 3 and Unit 1 respectively), the collecting vessel level measurement went above the top tapping point for a period of time sufficient to fill the separators. The collecting vessel level measurement in Case B and Case C was high but did not actually saturate to confirm that the level went above the top tapping point. This potentially highlights some differences between the measurement systems of Units 1 to 3 compared to Units 5 to 6.

In each case, the collecting vessel level was high at times and outside of the normal control range. The initial high level in the collecting vessel was triggered by an increase in feed water flow and the quick drain valves not opening as required to reduce the level. The increase in feed flow was due to the control logic that increases the economiser inlet flow set point when the circulation pump starts and this coincides with subcooled liquid arriving at the evaporator outlet.

This subcooled liquid had been flowing in at the feed water inlet and made its way through the economiser and evaporator until it reached the evaporator outlet. It cooled the metal surfaces to the extent that the entire circuit is now filled with incompressible subcooled liquid. Thus, there existed a direct relationship between inlet flow and outlet flow of the economiser / evaporator circuit. If feed water is added to the circuit, it must be balanced by dump flow to prevent the separators from overflowing into the superheater. However, the quick drain valves do not perform as required and thus the collecting vessel and separating vessels fill and overflow into the superheater.

It is assumed that due to pressure differences at the separator outlets, the separators fill at different rates and overflow at different times. Either of Separator 1 or Separator 4 normally overflow first. In Case 2, there is some evidence of Separator 2 overflowing, but generally the centre two separators do not overflow. Overflow is evident from the separator outlet temperatures that become subcooled. The separator outlet temperatures follow a distinct pattern with generally one becoming subcooled and the others becoming superheated when the evaporator outlet becomes subcooled. Once a separator steam outlet temperature becomes subcooled, the collecting vessel level drops and appears to be in control.

The consequence of subcooled liquid overflowing from the separators is that the falling liquid column in the pipe that connects the separator to the superheater inlet header creates a siphon. The siphon rapidly decreases the pressure in the separator and causes water from the other separator vessels and the collecting vessel to flow towards the overflowing separator. This causes a physical reduction in collecting vessel level and a malfunction of the level control philosophy. The circulation system reduces flow because it appears that the collecting vessel level is under control. However, a portion of the water bypasses the collecting vessel and flows directly from the evaporator outlet to the superheater via the overflowing separator.

This situation causes a mismatch between circulation flow and economiser inlet flow. Hence, feed water is added to the boiler to make-up the economiser inlet flow rate set point. A significant amount of water is then added to the system because the philosophy of the controls is to add feed water to increase the collecting vessel level and thus increase circulation flow, however, the level does not increase due to the siphon that is active.

## 5.4 Siphon effect

### 5.4.1 Evidence of the siphon from plant data

The plant is equipped with thermocouples on eight out of the sixteen distribution pipes from the evaporator outlet to the separator vessels. The location of the thermocouples are shown in plan view in Figure 41. The four separator vessels can be seen along the top of the image with their associated tangential entry distribution pipes. The path of each distribution pipe can be traced in the reverse normal flow direction to the evaporator outlet header.

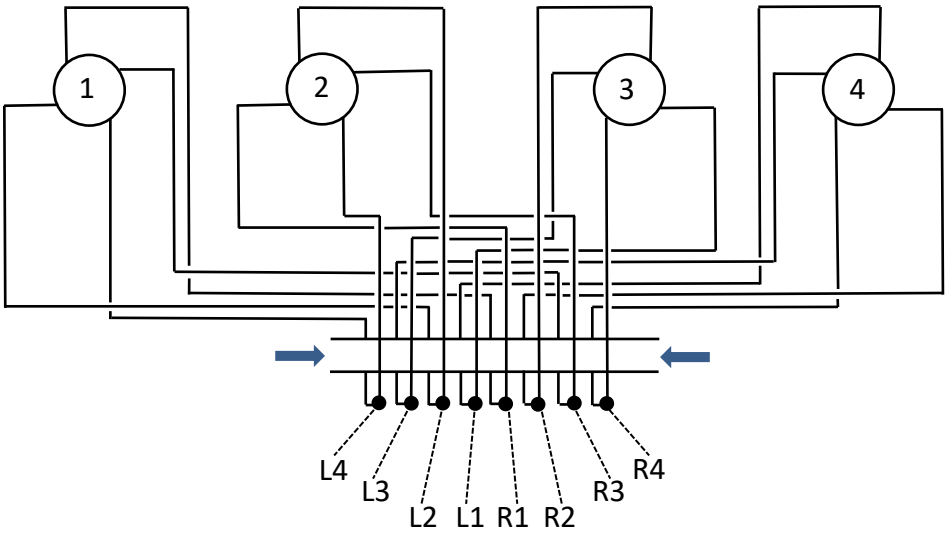


*Figure 41. Plan view of steam distribution lines showing thermocouple locations*

The evaporator outlet header can be seen at the bottom of the image with the thermocouples identified on the left side (L1 to L4) and on the right side (R1 to R4). The inner three thermocouples on each side are at a height of 2m above the centreline of the evaporator outlet header. The thermocouples labelled L4 and R4 are at a height of 900mm above the centreline of the evaporator outlet header.

The distribution lines in Figure 41 follow a specific pattern of connection to the separators. On the separator side of the evaporator outlet header, the distribution lines feed Separator 1 and Separator 4. The distribution lines on the opposite side of the evaporator header (bottom of the image) feed Separator 2 and Separator 3. Thus the thermocouples in the steam distribution lines only measure the temperature of the fluid in the distribution lines to Separator 2 and Separator 3. The inlet temperatures of Separator 1 and Separator 4 are not measured. This is unfortunate because it would be useful to be able to see the fluid tempertures in the lines to Separator 1 and Separator 4.

The evaporator outlet temperature measurement points are not shown in Figure 41, but they are located approximately at the blue arrows in the evaporator outlet header. The temperature measurements during a typical event are shown in Figure 42. The evaporator outlet temperature (green line) shows that liquid was flowing out of the evaporator from approximately 3:02. The purple lines showing the distribution pipe temperatures associated with Separator 3 (L1, L3, R2, R4) indicate that this liquid was in the lines to Separator 3 until approximately 03:11. Between 03:11 and 03:12, the measured temperatures associated with Separator 3 increased to above the saturation temperature. This indicates that flow from the evaporator outlet to Separator 3 stopped. After 03:12, the distribution pipes contained steam which flowed in reverse from the separator into the steam distribution pipes.

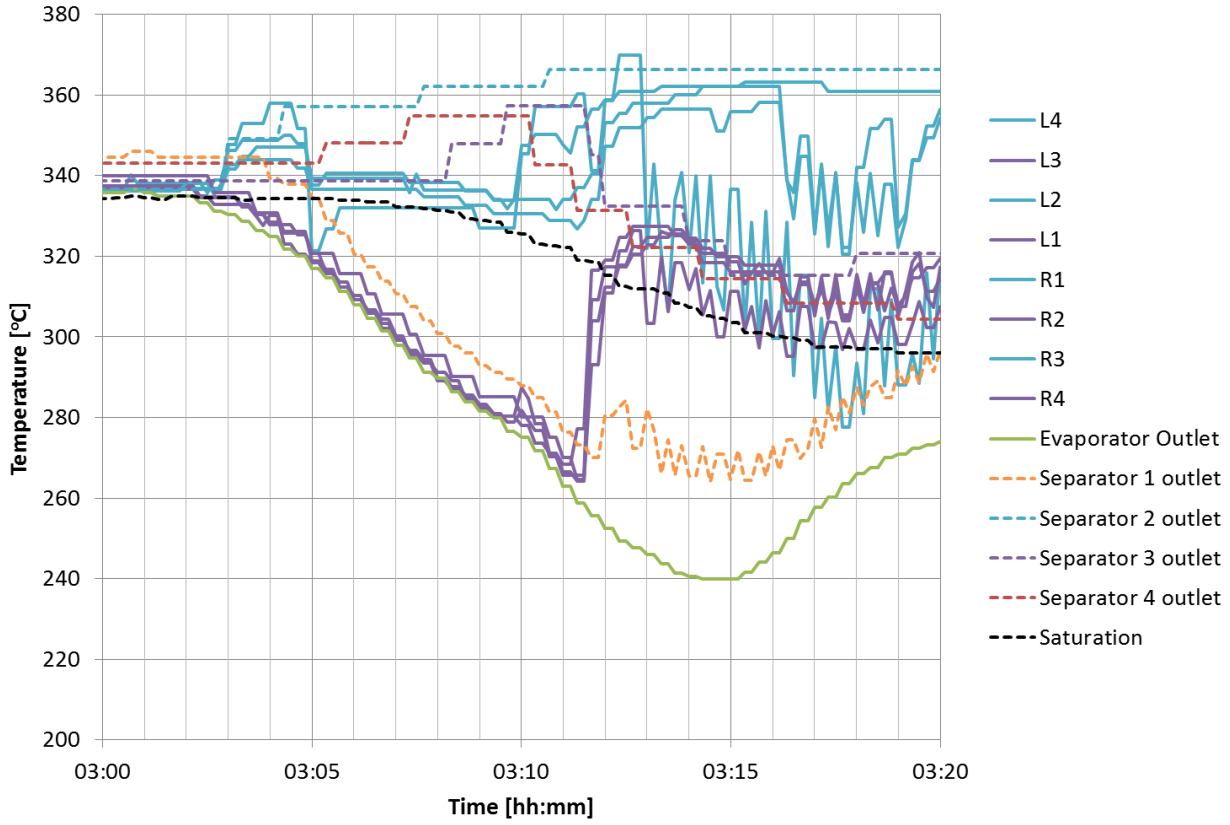


*Figure 42. Evaporator and separator steam temperature measurements (U6, 08-10-2018)*

The temperature measurements in the distribution lines to Separator 2 (L2, L3, R1 and R4) indicate that water did not flow in these lines from 3:03. Only L4 indicated subcooled temperatures at 3:05 and again after 3:16. Recall that L4 is located lower than the other thermocouples, thus it could have been affected by a changing liquid level in the distribution pipes and not necessarily by flow of liquid (Refer to thermocouple position d in Figure 51).

The separator steam outlet temperatures indicate that Separator 1 overflowed into the superheater system. Separators 2, 3 and 4 showed superheated temperature indicating reverse flow of steam from the superheater into those vessels. Prior to 03:02:30, all temperatures were saturated and it is not possible to identify which separators may have been overflowing.

It is interesting to note that the arrival of subcooled liquid at the evaporator outlet at 03:03 triggered the temperatures in the separator outlet and the distribution lines to Separator 2 to suddenly increase to superheated temperatures by 03:03. This indicates a sudden reverse flow of steam into the distribution lines.

Prior to subcooled water entering the system, Separator 1 may have already been overflowing but with saturated water. Saturated water would not be able to effectively create a siphon owing to the evaporation of some of the liquid as soon as the pressure drops. Thus, as a slug of liquid overflows into the separator outlet going down to the superheater inlet header, it reduces the upstream

pressure which causes gas bubbles to form in the liquid. The more the pressure reduces, the more gas phase is created. The gas phase has much increased specific volume and thus prevents the water slug from reducing the pressure further.

Once sufficiently subcooled liquid starts overflowing from the separator, the liquid evaporation due to pressure change stops. The siphon then becomes effective and suddenly reduces pressure in the separator system. Hence the sudden reverse flow of steam into the separating vessels and distribution pipes.

A similar event is shown in Figure 43. In this case the temperatures in the distribution pipes to the separators did not show significantly superheated conditions immediately after the arrival of subcooled liquid (15:02). In this case, Separator 4 overflowed into the superheater as seen by the drop to subcooled temperatures at the separator outlet starting at 15:02:30.

Liquid continued to exist in the distribution pipes to Separator 2 and three until 15:06. However, the flow in those lines may have stopped by 15:04 already when the temperatures deviated from the evaporator outlet temperature.

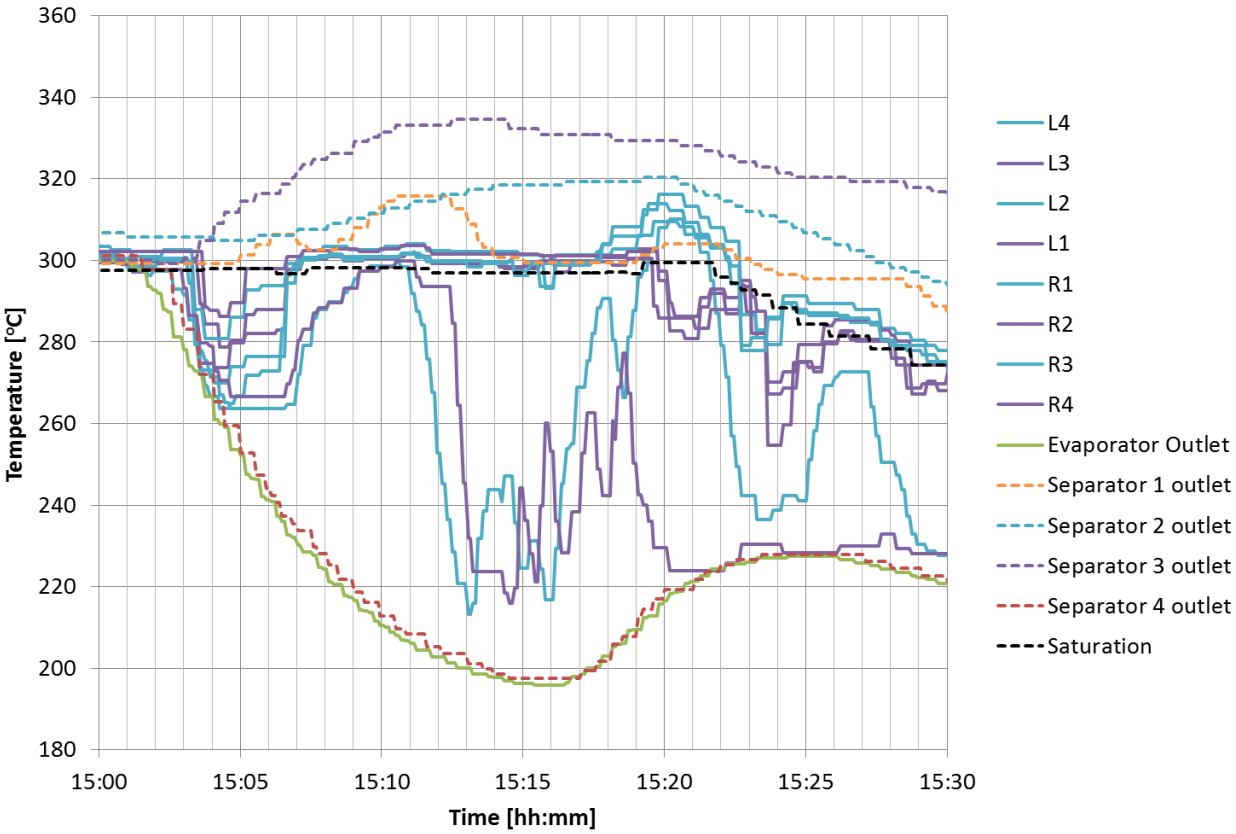


*Figure 43. Evaporator and separator steam temperature measurements (U1, 25-05-12)*

Besides L4 and R4, the temperatures in the distribution pipes become saturated from 15:07 to 15:18 thus indicating that there was no reverse flow of superheated steam from Separator 2 and three,

but there was also not any water flow coming directly from the evaporator outlet which was significantly subcooled. Again L4 and R4 which are at a lower elevation show variable temperatures lower than saturation but higher than the evaporator outlet temperature. This is an indication of the liquid level in the steam distribution pipes rather than actual flow in those pipes.

These examples from plant data support the hypothesis of the formation of a siphon from Separator 1 and Separator 4 in Figure 42 and Figure 43 respectively. The siphon reduces the pressure in the associated separating vessel to the extent that the flow in the steam distribution pipes to the other separating vessels stops or reverses.

### 5.4.2 Modelling the siphon

The initiation of the siphon was investigated using the model described in section 5.2. Once the separator levels are disturbed, and a vessel reaches a level that allows it to overflow into the superheater system some water goes over the highest point of the separator outlet steam line and downwards into the superheater. For the purpose of the model, assume that this occurs at the Separator 1 outlet.

Initially the economiser/evaporator circuit is completely filled and the separator vessels are overfilled (Figure 44 a). One of the separators starts overflowing first due to subtle differences in superheater pressure.

This water will quench the piping system and some steam will be generated. Note that the piping system is not at temperatures that are significantly superheated at this point. The evaporation of some water may cause an increase in pressure in that leg that has overflowed but the steam can flow into other parts of the superheater system without necessarily pressurising the overflowing separator leg.

Once a slug of water is formed in the pipe coming down from the top of the boiler to the Superheater 1 inlet header, the weight of the slug causes a reduction in pressure which draws more water from the separator. The falling slugs of water rapidly establish a siphon as shown in Figure 44 b. Owing to the large height difference between the separator outlet and the superheater 1 inlet (16m), the water flow in this pipe running full under the action of gravity can be considerable. This draw of water reduces the affected separator vessel pressure to an extent that all of the evaporator outlet flow directs towards the overflowing separator vessel.

The other separator vessels experience a drop in level and the flow of water from the evaporator to those vessels may cease. The water is also drawn away from the collecting vessel which suddenly shows a drop in level as the siphon is established.

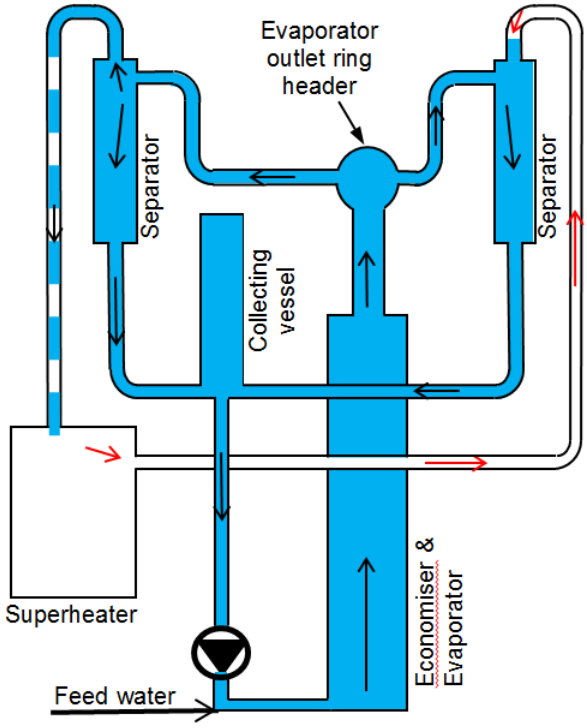


a)

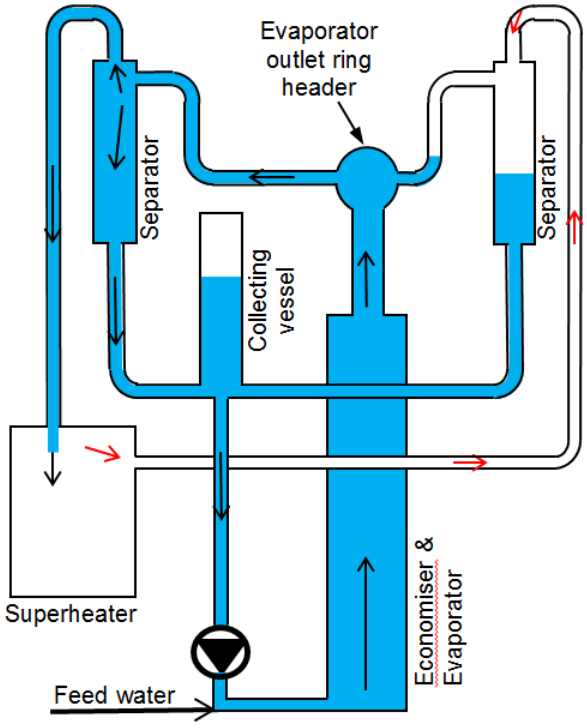


b)

*Figure 44. Separator overflow and subsequent liquid siphon a) Start of overflow b) Siphon established*

The results of a transient run of the Flownex model at a point in time in Figure 45 shows some typical values that may occur during the separator overflow once the pipe from Separator 1 to the superheater has filled and is now flowing with water. The Separator 1 liquid overflow of 344kg/s exceeds the evaporator flow of 280kg/s. The difference is made up by the levels in the other separators and the collecting vessel dropping as well as from reverse flow of steam from the superheater back to the non-overflowing separators.

It can be seen that the overflowing Separator 1 has a significantly lower pressure and is filled with subcooled liquid owing to the subcooled inlet at the evaporator. This lower pressure causes the evaporator outlet flow to distribute mainly to Separator 1. The distribution pipes to the other separator vessels have no flow or even reverse flow.

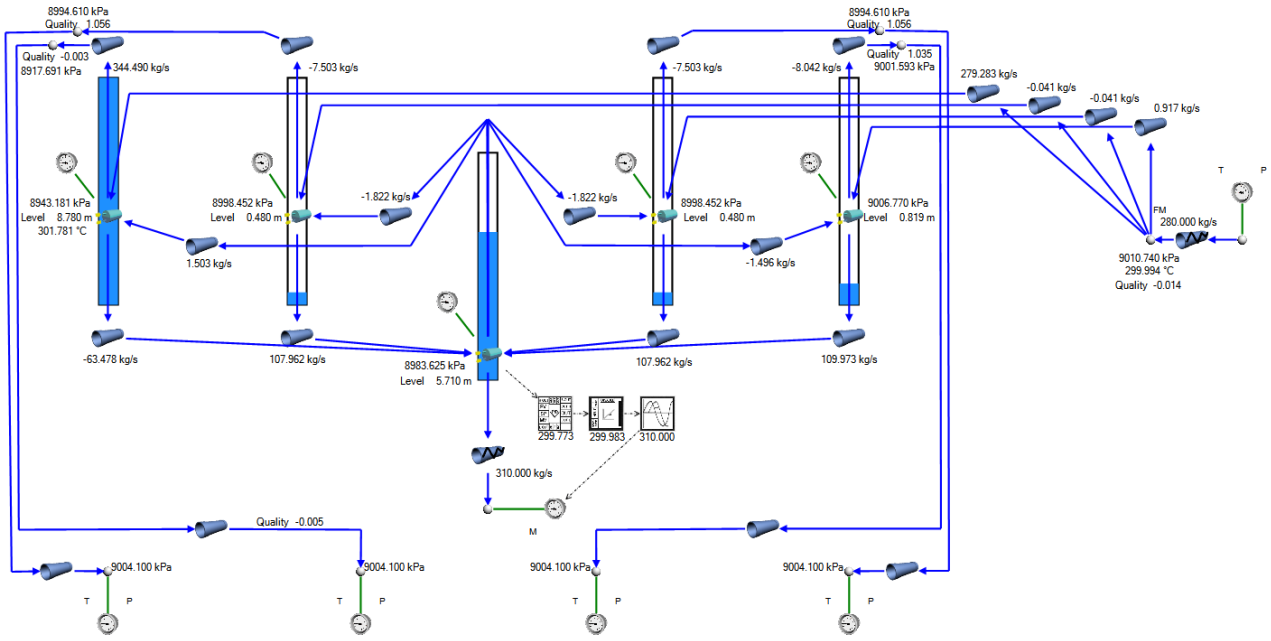


*Figure 45. Transient simulation at a point in time showing overflow from Separator 1 and siphon effect*

The simulated vessel levels during the transient are plotted in Figure 46. Initially the collecting vessel is full and the separating vessel are close to capacity with the level rising. Separator 1 is first to reach the top of the vessel and starts overflowing which initiates the siphon. The siphon then empties the other vessels, including the collecting vessel, with the siphon flow rate reaching 400kg/s (Figure 47). The separator 1 drain flow becomes negative and the distribution of the flow from the evaporator outlet swings almost entirely to Separator 1.

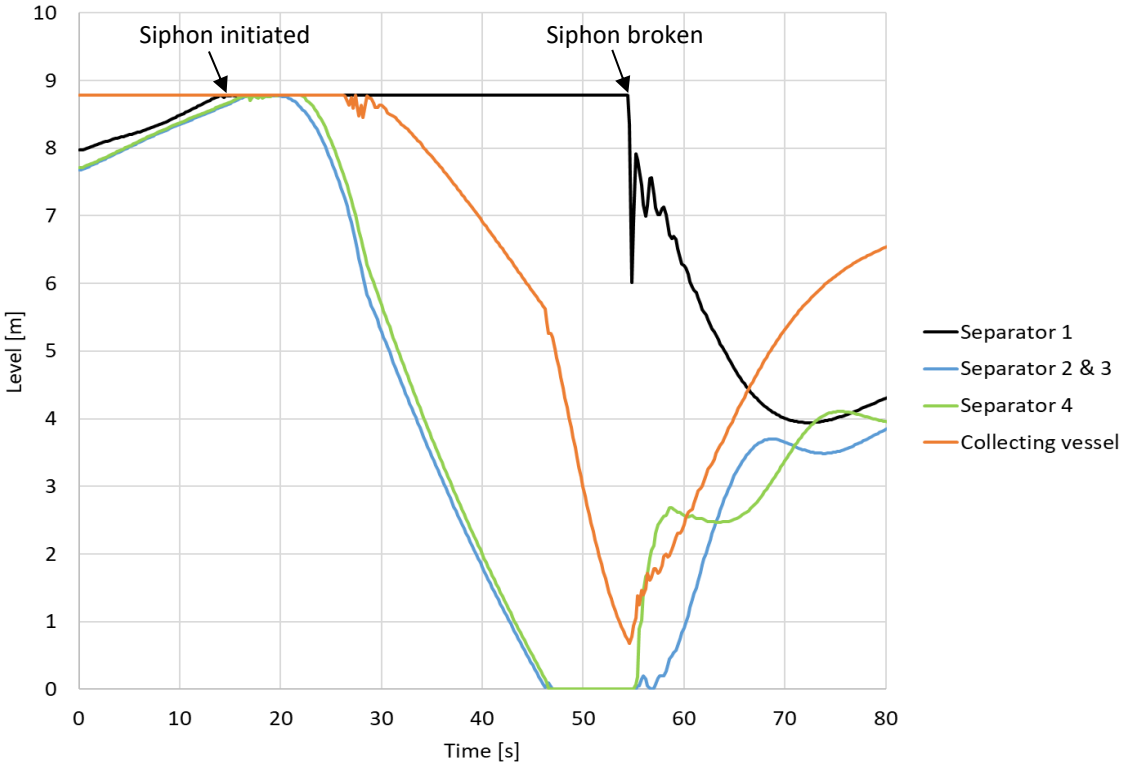


*Figure 46. Simulated vessel levels during a siphon event*

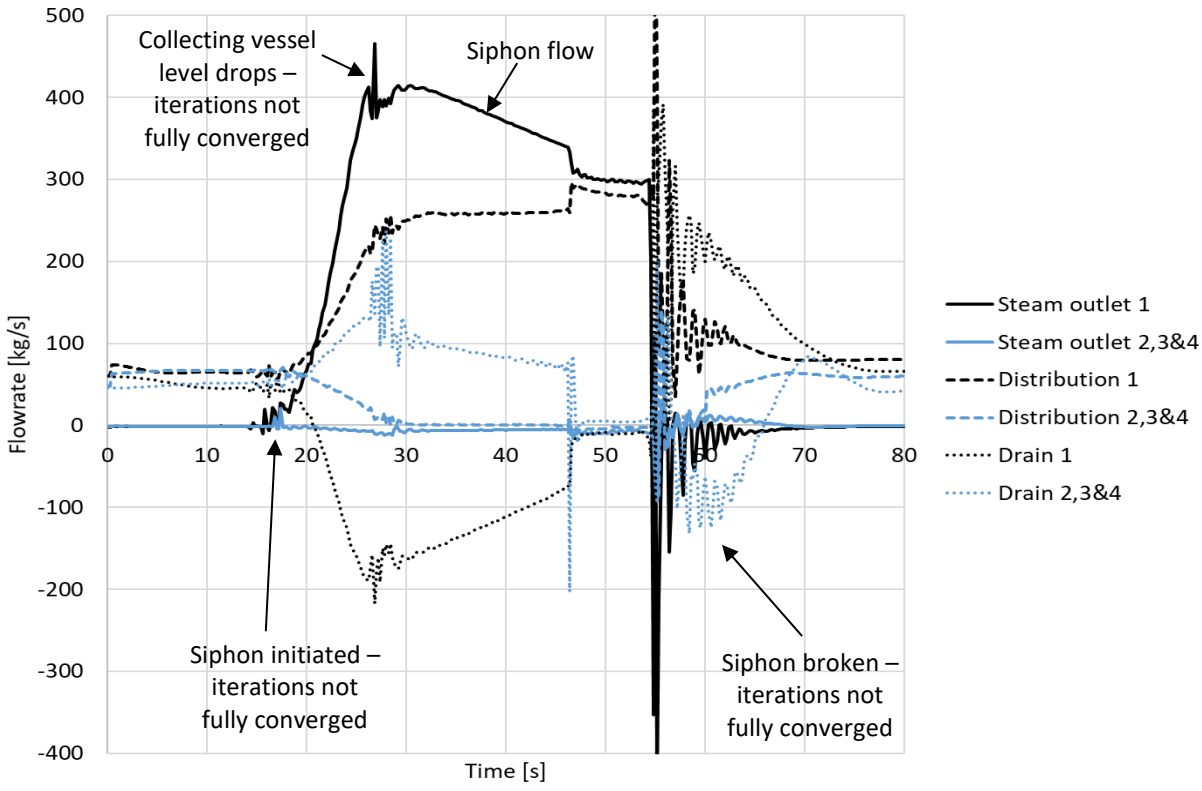


*Figure 47. Simulated flowrates during a siphon event*

At approximately 55seconds, the collecting vessel level drops below the height of the drain connection from Separator 1. This allows steam to be sucked into Separator 1 and the siphon is broken. The Flownex model iterations do not fully converge at this time and thus the rapid and severe oscillation in flow rates which is not a real effect.

The Flownex model does not fully converge each time a vessel exceeds full, drops from full, becomes empty or starts filling from empty. The results during non-convergence are not a real effect. However, once the model has stabilised, the results can again be trusted although the initial condition is now the first iteration where the model converged again. Thus, the exact level and flow modelled in the system during the event may not be accurate, but the overall behaviour demonstrates the siphon effect.

## 5.5 Comparison with other similar boilers

The configuration and equipment of the boilers under consideration are similar to other once-through tower type boilers. However, each boiler is unique and differs in exact layout of the systems and the dimensions of the various components. Other than physical differences, there are also differences in the way that the boilers are operated. The general principles of operation are the same, but the specific control philosophy and the exact set points vary from plant to plant.

The separator overflow and subsequent siphon problem discussed above may be a plant specific problem due to the particular combination of plant layout, equipment configuration and control practice employed. This was investigated by comparison of the boiler in this study to the boilers at two other similar plants. The similar plants do not have a history of significant and recurring turbine quench incidents although some incidents have occurred.

It was found that the separating vessels and collecting vessel configuration and piping layout is almost identical between the three plants. The dimensions of the vessels are smaller in the two comparison plants, but they are smaller boilers with lower design flowrates. The following relevant differences were observed:

- The boilers at Power Station A lack one set of vent pipes when compared to the other power stations. These additional vent pipes connect from the top of the collecting vessels to the steam outlet pipes of the separating vessels. The ‘missing’ pipes are shown in Figure 54. The existence of the smaller vent lines directly to the steam side of the separators at these other plants may improve the pressure balancing between the collecting vessel and the separating vessels. It also avoids the potential venting problems that may occur as a result of the interaction of the water and steam flows at the deflector plates in the separating vessels.

- The separator steam outlets of the comparison plants both connect to a single sling tube header that is approximately 4.6m below the highest point of the steam pipes. This distance is much less than the boiler of Power Station A considered in this study, which drops 18m from the highest point to the Superheater 1 inlet headers. Furthermore, the interconnection of the four separator outlet pipes at the sling tube inlet header avoids pressure differences occurring at the separator vessels which could lead to differences in levels.
- The controls of the circulation system of the comparison plants are similar to one another and do not automatically increase the economiser inlet flow set point when the circulation pump is in service. The feed water pumps fill the boiler at 50kg/s (or 100kg/s if hot) until there is collecting vessel level and the circulation pump can be started. The circulation flow is established and then the operator manually increases the economiser flow set point. This gradually increases the collecting vessel level and circulation flow. The operator ensures that the circulation flow is greater than the minimum economiser flow prior to ignition. On ignition, the automatic control becomes active to maintain the economiser inlet flow. Provided the operator has gradualy increased the flow prior to ignition, this avoids a sudden increase in the circulation flow.

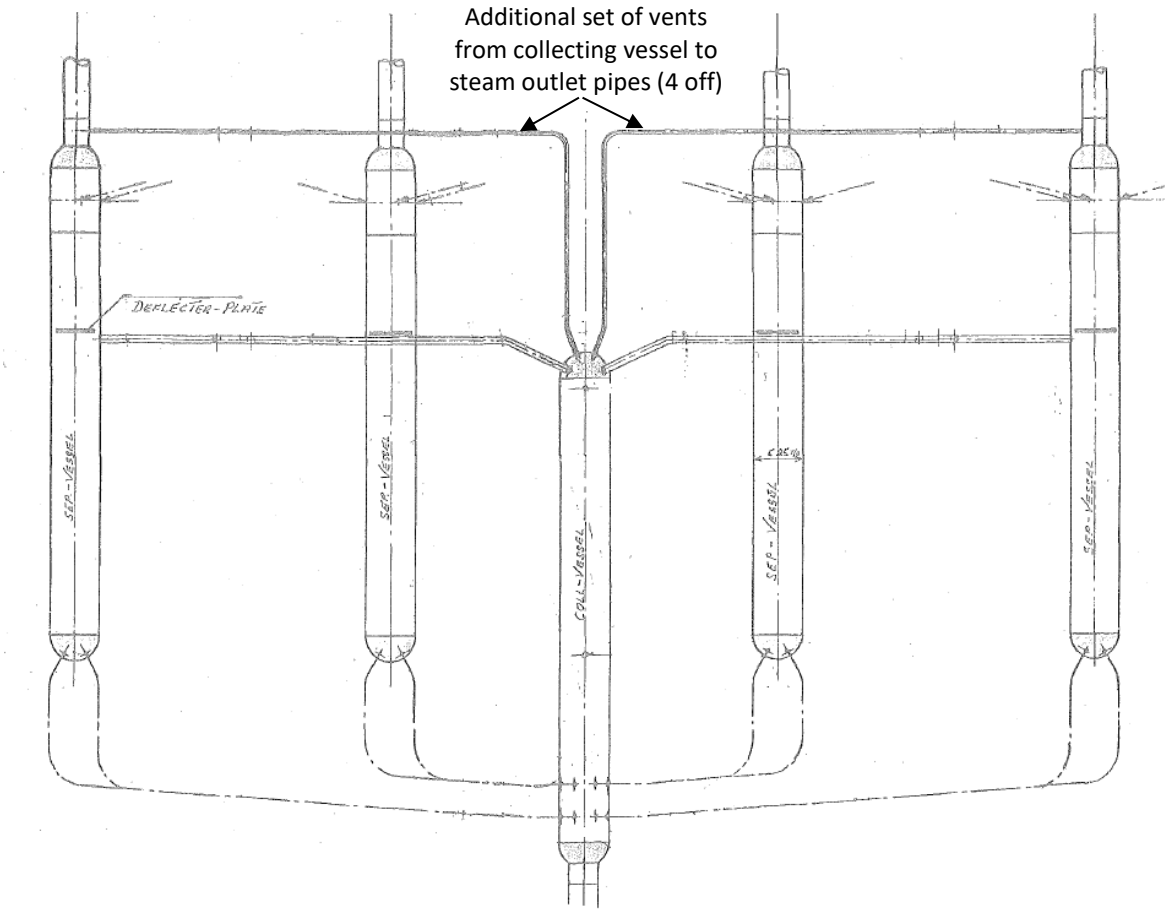


*Figure 48. Diagram of collecting vessel system of another plant showing additional vent pipes*

Thus, it would appear that the configuration and operation of the circulation system at the comparison plants are less prone to collecting vessel venting problems and to imbalances of separating vessel levels. They also avoid rapid level increases before circulation flow is properly established. This reduces the probability of an initial separator overflow.

In the event that the levels do go high and a separator overflow towards the superheater occurs, the probability for setting up a siphon, and the severity of the siphon will be much reduced compared to the boilers studied in this work. In order to quantify the siphon at the comparison plants, the Flownex model was modified to match the comparison plant configuration (Refer Figure 49). The Separator 1 steam outlet boundary condition was biased to create a separator overflow. A siphon did occur, however it was unable to empty the collecting vessel. The image in Figure 49 shows the model after it has run for some time to a near steady state condition.

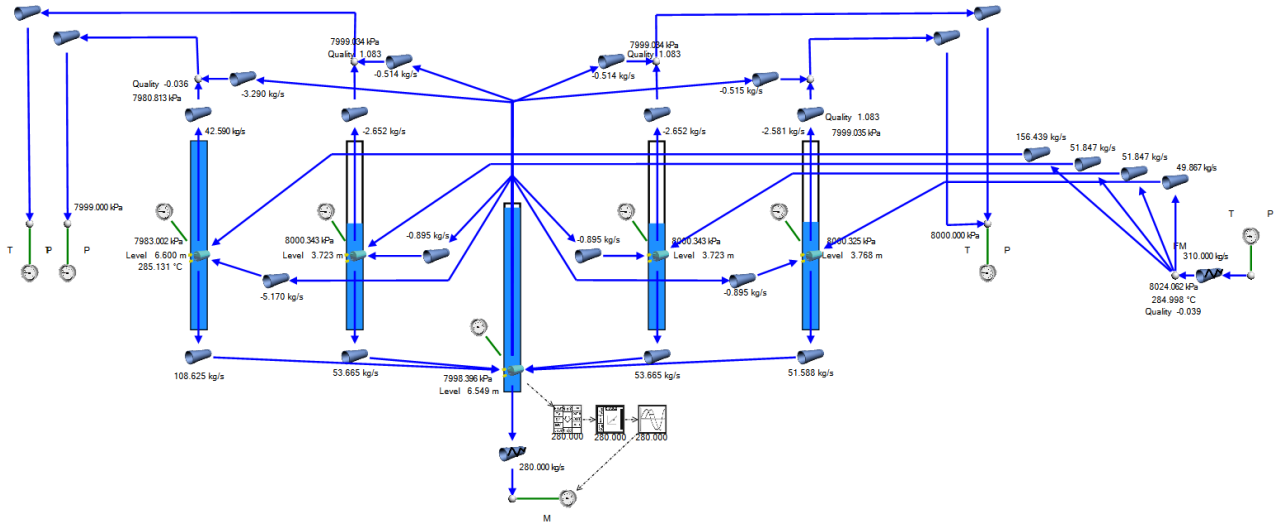


*Figure 49. Flownex model of the collecting vessel system of the comparison plants in separator overflow condition*

If the collecting vessel level remains high, then the plant controls and the operator will react by using the collecting vessel drain valves to reduce the level. From the condition shown in Figure 49, the outlet liquid flow was adjusted to simulate a valve opening. This caused the siphon flow to drop together with the levels in all the vessels. The siphon was broken and then all the levels returned to normal. Thus the comparison plants have the advantage that although a siphon can occur, it is not strong enough to continue once the collecting vessel level is in the normal working range.

In contrast, the boiler in this study has a significant height drop without interconnection of the separator outlet pipes, which causes a strong siphon. The siphon reduces collecting vessel level and thus avoids detection.

## 5.6 Root cause of quenching at Power Station A

The initial separator overflow in the cases considered above is caused by over-filling the economiser and evaporator circuit. The high level is observed in the collecting vessel, however the level measured deviates from the true level which gives less time to the control system to react. When the collecting vessel level is high, the control system uses the drain valves to reduce the level; however, the drain valves are unreliable and fail to open or get stuck which allows the collecting vessel level to rise above the top tapping point of the level measurement transmitters.

The situation is further worsened by the mismatch of economiser flow set point that automatically increases on starting of the circulation pump, and the limitation on the circulation pump which cannot quickly ramp up to full flow because of the thermal transients that it would induce in the economiser/evaporator circuit. This forces the feed water pumps to make up the difference in flow and overfill the evaporator when it is already full of water.

There is also some indication that the measured collecting vessel level does not increase as rapidly as the flow information suggests it should. This could either be related to the level indication not giving correct information i.e. the true level is increasing at a very fast rate but this is not picked up by the level measurement or the true level is delayed. The latter problem could only be related to the collecting vessel vent not functioning fully, causing delayed release of the gas phase above the liquid level in the collecting vessel.

Once the water level exceeds the height of the collecting vessel, it fills the vent pipes and it soon exceeds the height of the deflector plates in the separating vessels. This may cause carry over to the superheater if there is any residual steam flow occurring. It also allows pressure differences between the separators to occur.

The level in either Separator 1 or Separator 4 is first to overflow. This tends to occur while the evaporator outlet is still saturated. The saturated liquid starts flowing into the superheater, but some of it evaporates due to heat transfer and/or pressure drop and prevents it from forming a siphon.

When subcooled liquid arrives at the evaporator outlet, it flows into the overflowing separator and causes a siphon. The siphon acts over a substantial height difference and thus significantly reduces the pressure in the overflowing separator. This causes most of the flow from the evaporator to direct towards the overflowing separator and it causes the collecting vessel and the other separators to drain. With a reduced collecting vessel level, the control system and the operator are unaware that the separator is overflowing and thus the overflow can persist for some time.

The substantial height difference from the separator outlets to the superheater inlet headers without any interconnection at the steam side of the separators allows a strong siphon to form. This plant configuration is a design flaw and is the root cause of quenching at Power Station A.

In order to break the siphon, it is necessary to stop feeding water and allow the siphon to drain the collecting vessel to the point where steam is sucked into the siphon. The gas bubble then breaks the siphon and allows the levels in the vessels to equalise.

To prevent quenching, the collecting vessel level must be better managed and the siphon must be prevented from starting. This requires upgrades and improvements to the drain valves and improved logic to better manage the amount of water that needs to be drained.

The collecting vessel level measurement can be improved so that the plant controls will react sooner. The collecting vessel vents should be studied further to determine if they are causing problems.

To prevent the siphon from forming it will be necessary to install an interconnection of the steam outlets of the separators at the highest point. The diameter of the interconnection should be sized for maximum balancing steam flow when a siphon is active at either Separator 1 or Separator 4. This will eliminate pressure differences at the separators under all operating conditions, but, more importantly, it will prevent a siphon from forming.

## 5.7 Summary

The detailed collecting vessel level analysis was performed as per activity 3.4 of the methodology and the findings at Power Station A have been presented in this chapter. The analysis included a detailed description of the physical characteristics of the system and its operation. One-dimensional thermo-fluid modelling of the separating vessels, the collecting vessel and the interconnecting piping showed that the system was adequately sized and able to deal with transients.

Investigation of the level measurement system of the collecting vessel showed that the measured value could indicate a level up to 500mm lower than the true level and this was confirmed in the plant data. This measurement error delays the control actions to a rising level, but does not account for the separator overflow.

Analysis of plant data revealed that the cause of quenching at Power Station A is a siphon. The siphon initiates when subcooled conditions exist at the evaporator outlet and the collecting vessel level is high which results in liquid overflowing from the separator into the superheater. Owing to the effect of the siphon, the collecting vessel level drops and the plant controls continue to add feed water.

As shown by thermofluid modelling of other once-through boilers with a similar layout, the initiation of a siphon is possible at those plants but it cannot be sustained. At Power Station A, the height of the separator outlets above the superheater inlet headers and the lack of an interconnection of the separator steam outlets causes a strong siphon to develop. This design flaw is the root cause of quenching at Power Station A.

Besides the modelling described in this chapter, further modelling of the superheater was also undertaken. The modelling was concerned with the thermo-fluid effects of the separator overflow on the superheater. The following chapter 6 discusses the modelling which fulfils activity 3.5 of the methodology and confirms if a separator overflow did occur.

# 6. Modelling the separator overflow

In order to further investigate the liquid level over time, the separator overflow can be modelled in support of activity 3.5 of the methodology, as shown in Figure 50.

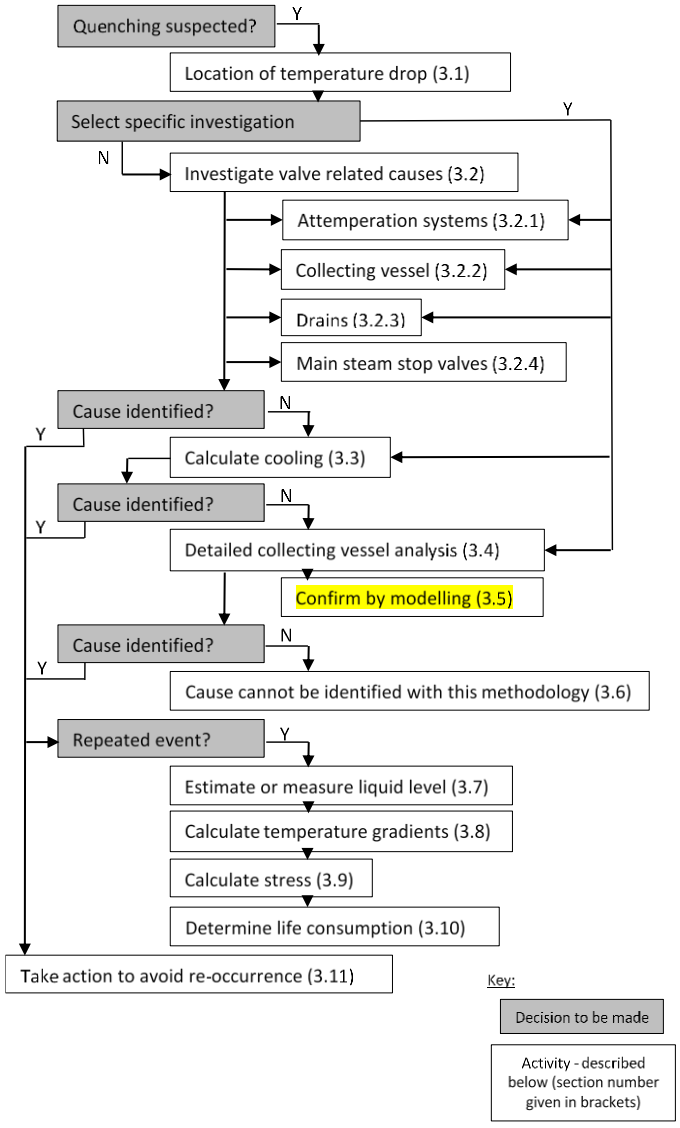


*Figure 50. Activity 3.5 in the methodology*

A simplified calculation is provided here in section 6.2, followed by more detailed calculations in section 6.3. Any of these modelling techniques can be used to confirm the separator overflow as proposed in the methodology in section 3.5. Before embarking on modelling, it is necessary to discuss the effect of the subcooled liquid interface because it must be considered in the model.

## 6.1 Subcooled liquid interface

The separator overflow introduces liquid into the superheater. The metal of the superheater is at a temperature above the water-steam saturation temperature. The differential between the initial liquid temperature and the metal surfaces can be as high as 200$^{o}$C. This causes rapid vaporization and boiling of the liquid.

In a closed system, the expansion of the liquid as it turns into steam results in a pressure increase. The pressure increase depends on the amount of steam generated which is dependent on the amount of energy that was released from the hot metal. The rate of pressure increase is directly related to the heat transfer rate.

Considering the case studied at Power Station A (Appendix C, Appendix D, Appendix E and Appendix F), the measured superheater pressure did not rise significantly. A separator overflow should have caused a pressure increase. If the steam was able to escape from the system, then the addition of water and its subsequent evaporation would not cause a pressure rise. The superheater was isolated thus, assuming no leaks; steam could only exit the superheater by reverse flow to the evaporator.

The liquid evaporates when it comes into contact with hot metal in the superheater and this causes a substantial increase in specific volume. This drives a flow into other parts of the superheater. The steam is able to flow via the common superheater headers into the opposite half of the superheater in reverse flow back to the separator vessels.

At the same time, the steam is exposed to a subcooled liquid interface at the separators which condenses steam at the interface. The specific volume of the steam is significantly reduced as it condenses and this draws more steam towards the interface (Refer red arrows and location of subcooled interface in Figure 51).

The rate of condensation of steam into the subcooled liquid at the interface has a direct impact on the steam pressure in the superheater. The condensation rate can be estimated from plant measurements or by calculation if the interface area and the effective heat transfer coefficient are known. However, the exact nature of the interface is unknown. It could occur in a separator with liquid flow that would provide good mixing and high heat transfer. It could also occur by steam flow through the vents and into the collecting vessel. Thus it is difficult to calculate the condensation rate and rather plant data is used to calculate the rate.

The hypothesis of condensation at the subcooled liquid interface was confirmed by evidence from plant data. During the separator overflow, there is a temperature rise in the subcooled liquid that exits the separator and collecting vessel. This is determined from thermocouples located in the

evaporator outlet header (Position a in Figure 51), located in the separator steam outlets (Positon b in Figure 51) and located at the circulation pump suction (Position c in Figure 51).

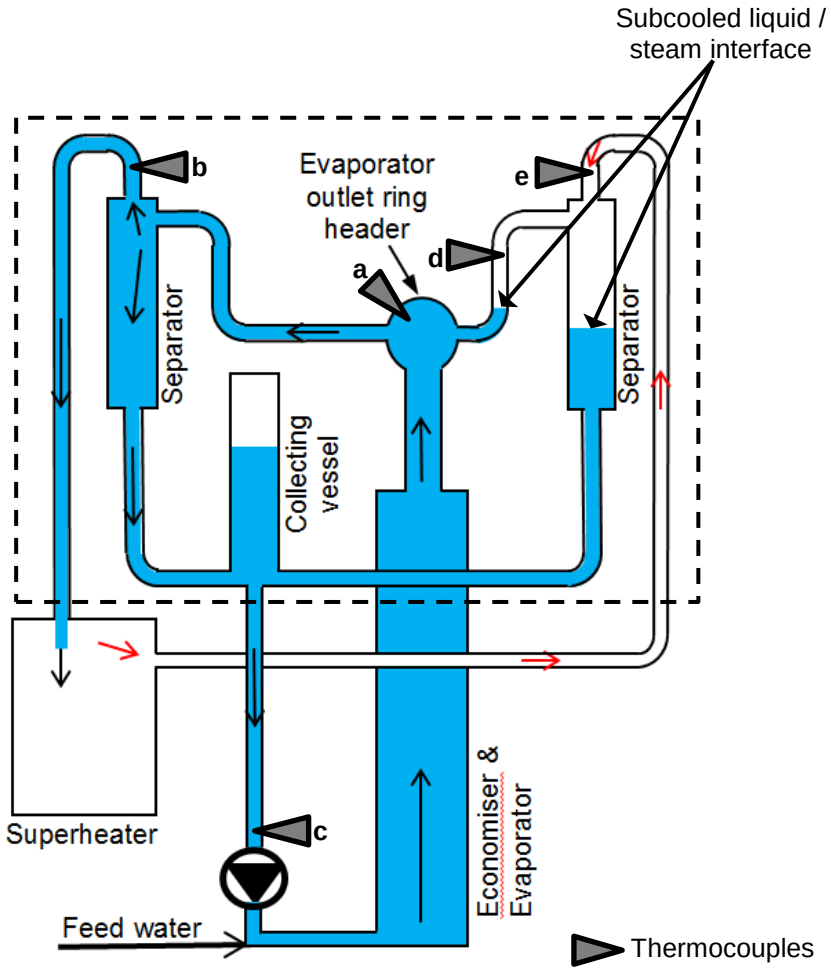


*Figure 51. Separator overflow – location of subcooled interface and plant thermocouples*

By an energy balance of the control boundary shown as a dashed line in Figure 51 above, the following expression for the steam flow into the control boundary can be derived:

$$\dot{m}_{steam} = \frac{\dot{m}_{evap} c_p (T_{b/c} - T_a)}{h_{steam\ at\ e} - h_{steam\ at\ b}} \quad (86)$$

It is assumed that the liquid leaving the control boundary is at the average temperature measured at the separator outlet (point b) and the circulation pump inlet (point c). The reason is that the flow splits with some quantity of overflow passing point b. So more accurately, a ratio of the two temperatures should be used but the flow ratio is unknown.

Another simplification is that the NPSH flow rate is ignored. This flow of approximately 10kg/s joins the circulation pump suction line at the collecting vessel. Thus the flow affects the temperature measured at point c. The NPSH flow rate is less than 10% of the circulation flow and this error is considered to be insignificant in the overall error of this calculation. Also, by ignoring the flow, we

assume the collecting vessel outlet temperature is lower than it actually is, which results in a lower estimate of the condensing steam flow rate.

The behaviour of the measured temperatures and the calculated steam flow during one of the separator overflow events is shown in Figure 52. From 03:05 until 03:15, the average steam flow to the subcooled liquid interface is 22.3kg/s. In other cases, the temperature rise at the separator outlet and circulation pump inlet is not as pronounced and thus the calculated steam flow is smaller in magnitude (Figure 53). It is assumed that in these cases, the dynamics of the flows inside the separating and collecting vessel system were different with reduced interface area and mixing.

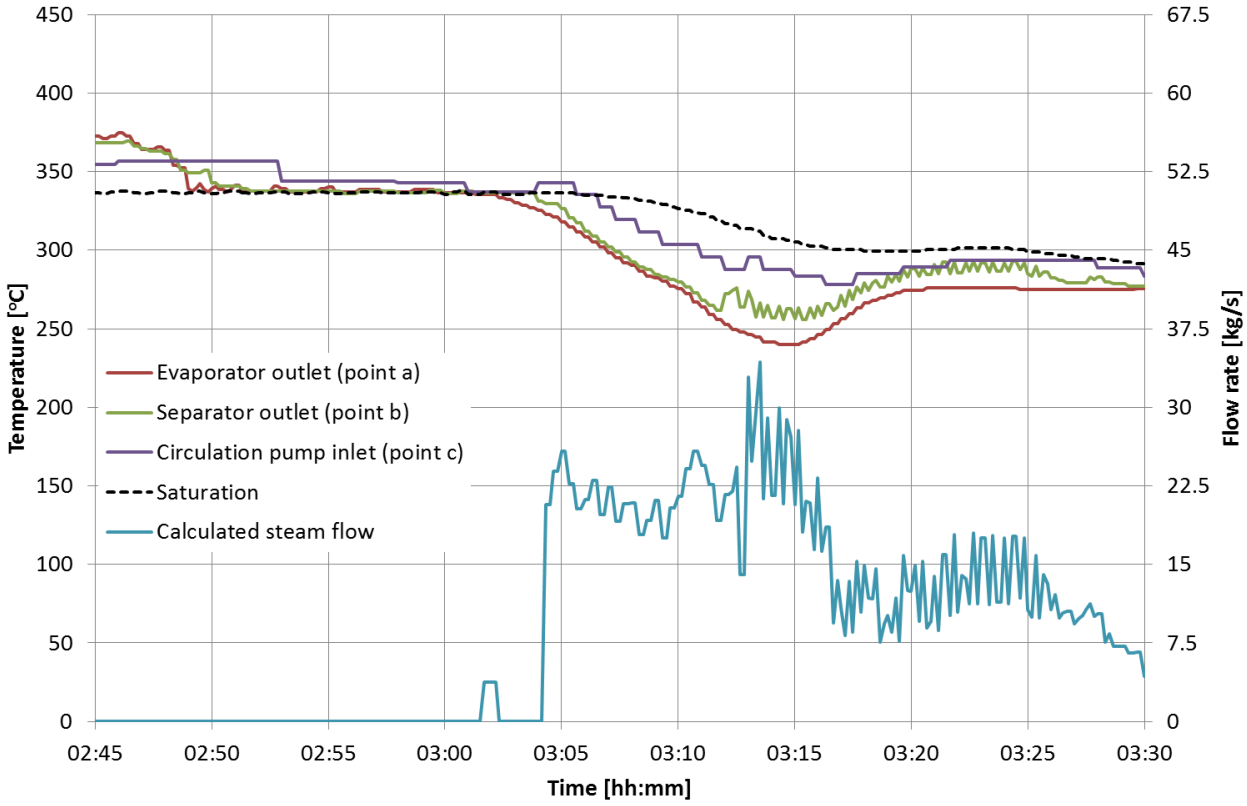


*Figure 52. Subcooled evaporator outlet temperature and calculated flow of steam condensing at the subcooled liquid interface (Case C U6 08/10/2018)*

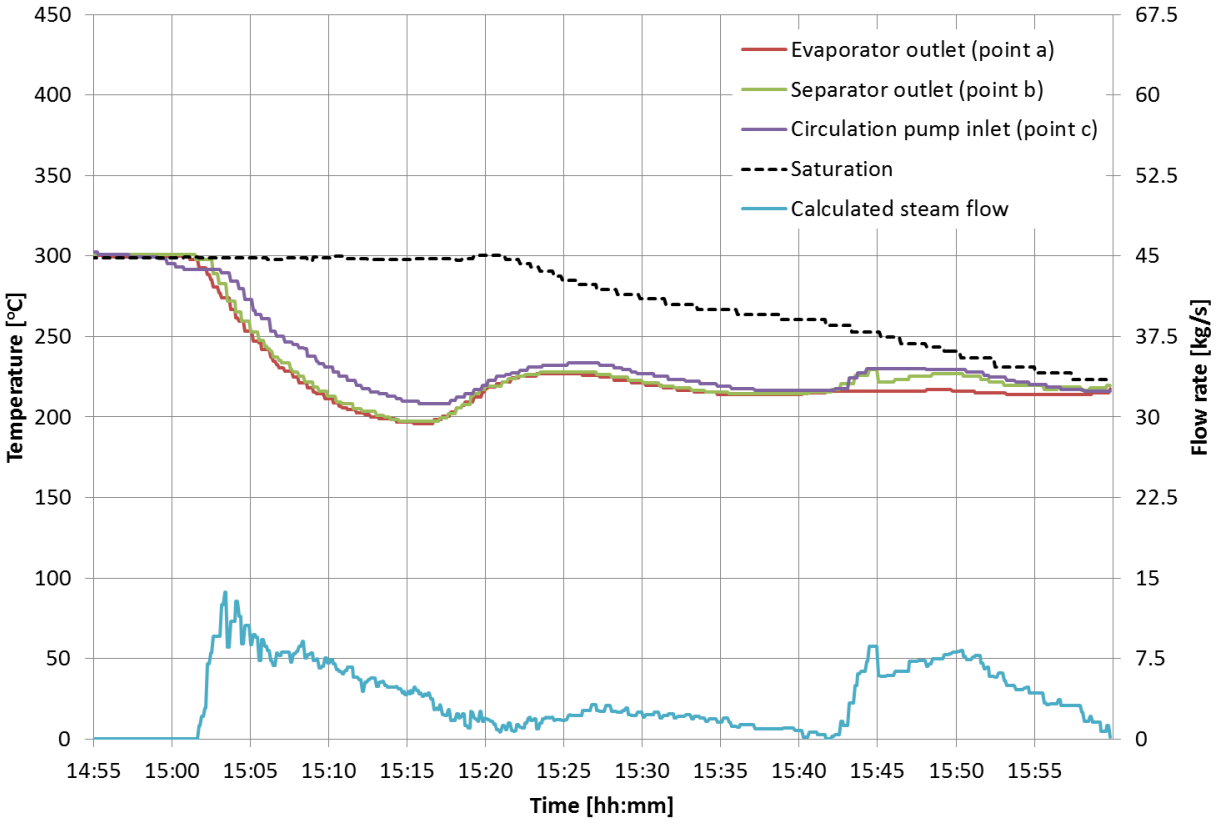


*Figure 53. Subcooled evaporator outlet temperature and calculated flow of steam condensing at the subcooled liquid interface (Case D U1 25/05/2012)*

The steam flow to the subcooled liquid interface is an important factor to consider when modelling the superheater. The flow affects the pressure of steam inside the superheater as further demonstrated below.

## 6.2 Simplified calculation of separator overflow

A simplified calculation of the effects of the separator overflow on the superheater control volume is presented here. The calculation determines the superheater pressure as a function of the separator liquid overflow rate. The intention is to introduce a methodology that can be developed further in the subsequent chapters. The simplified model is useful for providing an explanation of superheater pressure behaviour during a quench but it is not accurate enough for determining liquid level. For that purpose, the heat transfer rates and the flow of steam leaving the control volume to the subcooled liquid interface should be calculated in greater detail. This is addressed in later sections.

For the simplified model a similar control volume approach as used above in section 4.1 is applied as shown in Figure 54. The configuration of the metal volume is different to the previous approach

in that a single metal volume is attached to the steam control volume independently of the gas side heat transfer. The metal volume, $V_m$, connects to the steam volume via a thermal resistance that emulates the internal convective heat transfer coefficient between the steam and the metal. The heat transfer on the outside of the tubes is summed and included as a single heat transfer directly from the steam control volume.

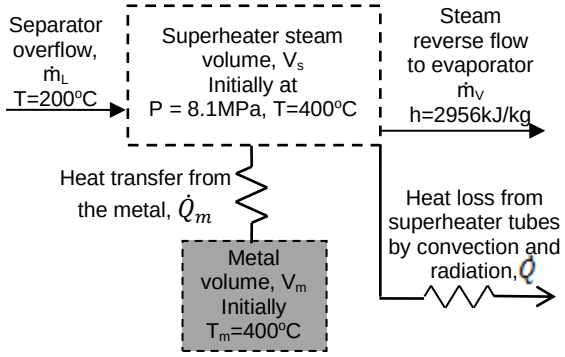


*Figure 54. Simplified separator overflow calculation*

The separator overflow is assumed to enter the control volume at a specified temperature and flow rate, $\dot{m}_L$. An allowance is made for the flow of steam leaving the control volume because it is being condensed at the subcooled liquid interface, $\dot{m}_V$, as discussed above.

By adding liquid to the steam space control volume via the separator liquid overflow, the temperature of the system can be reduced until it reaches the saturation temperature. By continuing to add more liquid, the steam volume can be filled up with liquid to a specified level.

The control volume is sized to have the same volume as the total internal volume of the real superheater. The superheater volume is approximated by a vertical cylinder of height equal to the difference between the highest and lowest point of the real superheater. An equivalent diameter is calculated for the superheater to satisfy the height and volume. The dimensions of the real superheater are a height of 18.1m and a total volume of 157m$^3$ which equates to an equivalent cylindrical volume with a diameter of 3.32m. If the superheater is flooded and filled with liquid, it overflows into the main steam system. Thus, when the liquid level inside the equivalent cylindrical volume reaches a level of 5.6m, the liquid overflows. The purpose of this simplified calculation is to determine how much liquid needs to be added to the equivalent cylindrical volume to achieve the 5.6m level and what the state of the system would be when that occurs.

The total mass of steam and water in the control volume depends on the amount of flow entering and leaving the control volume over the time period, t:

$$M_2 = M_1 + \dot{m}_L t - \dot{m}_V t \tag{87}$$

Where M represents the total mass of fluid in the control volume and t is the time step duration. At any point in time, the homogeneous density of the fluid is the total mass of fluid divided by the fixed internal volume of the superheater, V:

$$\rho = \frac{M}{V} \tag{88}$$

Consider an energy balance of the system starting from the initial quantity of energy in the control volume, $E_1$, and transitioning to the final quantity of energy, $E_2$, over a time period, t:

$$E_2 = E_1 + \dot{m}_L h_L t - \dot{m}_V h_V t - \dot{Q}t + \dot{Q}_m t \tag{89}$$

Allowance is made for the separator overflow rate, $\dot{m}_L$, and the flow of steam leaving the control volume, $\dot{m}_V$, as well as for heat transfer from the superheater tubes to the gas on the outside by convection and radiation, $\dot{Q}$, and also for heat transfer from the metal to the steam inside the tubes, $\dot{Q}_m$ (Refer Figure 54).

The total energy in the control volume can also be expressed as follows:

$$E = Mu \tag{90}$$

where M is the mass of fluid in the control volume and u is the specific internal energy for a homogeneous mixture of water and steam.

By substituting the above equations, an expression for the specific internal energy at the end of the time step can be determined:

$$u_2 = \frac{M_1 u_1 + \dot{m}_L h_L t - \dot{m}_V h_V t - \dot{Q}t + \dot{Q}_m t}{M_2} \tag{91}$$

This can be converted to an expression for enthalpy to facilitate finding the fluid properties from steam tables since:

$$h = u + \frac{p}{\rho} \tag{92}$$

An iterative process is required to find the new pressure:

$$h_2 = \frac{M_1 u_1 + \dot{m}_L h_L t - \dot{m}_V h_V t - \dot{Q}t + \dot{Q}_m t}{M_2} + \frac{p_2}{\rho_2} \tag{93}$$

The heat transfer from the outside of the tubes to the gas flow by convection and radiation, $\dot{Q}$, can be calculated using the methods described in Section 4. Note that the radiation from the outside of the tube bundle to the evaporator walls is ignored for this simplified calculation.

The estimated heat transfer coefficient would need to be updated at every time step. A simplified approach is to consider a constant total heat transfer based on a single calculation using the heat transfer correlations developed in Chapter 4 for the convection and radiation from the outside of the tubes.

The heat transfer is given by:

$$\dot{Q} = hA(T_m - T_g) \tag{94}$$

Where $h$ is the heat transfer coefficient, $A$ is the surface area, $T_m$ and $T_g$ are the metal and gas temperatures respectively. A single representative value of $\dot{Q}$ is assumed to apply for the duration of the calculation.

The heat transfer between the steam space and the metal is determined by:

$$\dot{Q}_m = hA(T_m - T_s) \tag{95}$$

The metal temperature at each time step can then be calculated by using the lumped parameter assumption as follows:

$$T_{m2} = T_{m1} - \frac{\dot{Q}_m t}{M_m c} \tag{96}$$

Where $T_{m1}$ and $T_{m2}$ are the lumped metal temperature at beginning and end of the time step respectively, $M_m$ is the total mass of metal in the tube bundle and $c$ is the average specific heat capacity of the metal.

Now using the fluid property relationships, it is possible find the state of the fluid in the control volume using the same method described in Section 4.1:

$$p = f(h, \rho) \tag{97}$$

$$T = f(p, h) \tag{98}$$

$$x = \frac{h - h_L}{h_G - h_L} \tag{99}$$

The fluid properties are assumed to be homogeneous, however, in the steam control volume, it is assumed that the liquid is all located at the bottom part and the gas or vapour phase is located at the top part, such that there is a liquid level. The level is related to the quality, x, of the fluid in the control volume:

$$L = \frac{\frac{(1-x)M}{\rho_L}}{V} \tag{100}$$

Where M is the total fluid mass, $\rho_L$ is the density of saturated liquid and V is the volume of the superheater.

The enthalpy of the separator overflow and the steam leaving the control volume are assumed to be constant. An overflow liquid enthalpy of 855kJ/kg was chosen based on a temperature of 200°C. The steam leaving the control volume, $\dot{m}_V$, is discussed in section 6.1 and for this calculation was assumed to have a flow rate of 15kg/s at an enthalpy of 2956kJ/kg. The heat loss from the superheater tubes, $\dot{Q}$, was assumed to be constant at 14MW which is an estimated average value

over the time period. The heat transfer between the steam volume and the metal volume was estimated by a convective heat transfer coefficient of 100W/m$^2$ K over an area 12 545m$^2$.

A Microsoft excel spreadsheet was set up to solve the above set of equations using a simple explicit finite difference scheme with a time step size of 0.2 seconds. The results of the above calculation show that over an assumed duration of 6minutes, a constant separator overflow of 112.9kg/s resulted in a final liquid level of 5.6m in the superheater control volume. This equates to a total overflow of 40.6 tons of water. The final temperature of the control volume was calculated to be 283.1$^o$C at a corresponding saturation pressure of 6.73MPa.

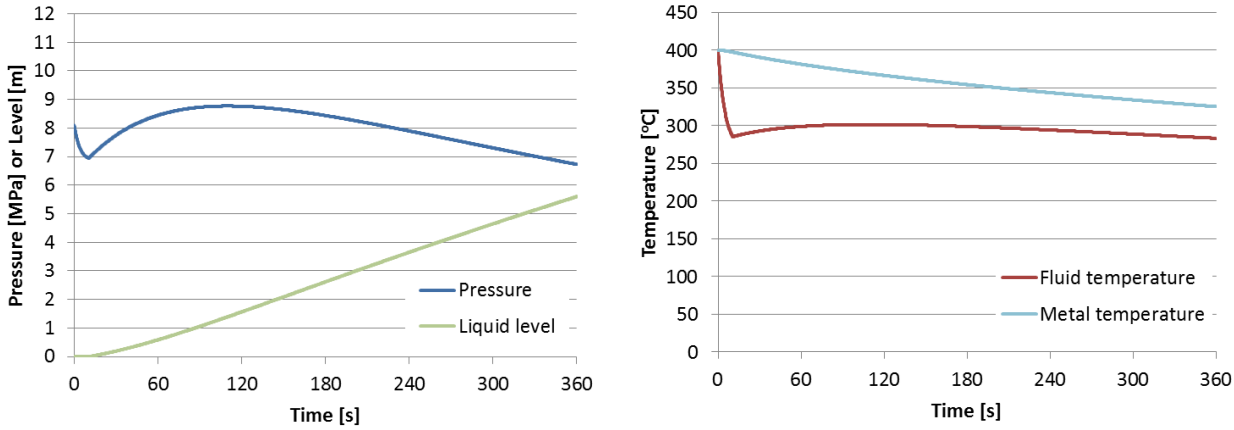


*Figure 55. Results of simplified separator overflow calculation*

In Figure 55, the results show that initially the pressure and temperature dropped sharply as the subcooled liquid was added to the steam control volume. The liquid cools the steam and reduces the overall specific volume, even though more mass is added to the control volume. After ten seconds, the control volume is saturated and a level starts to appear. At this point in time, the heat transfer from the metal to the steam is at a maximum because the highest differential temperature between the metal and the steam is reached.

In the next phase, the pressure rises as there is a net increase in internal energy arising from heat transfer from the metal and the addition of colder water. As time goes on, the amount of heat released from the metal decreases and thus the balance swings and the pressure starts to decrease. If the steam flow leaving the control volume to the subcooled liquid interface is assumed to be zero but all the other parameters are kept constant, then the results show increased pressure and a greater final liquid level (Figure 56). This is due to the increased energy and mass retained in the control volume.

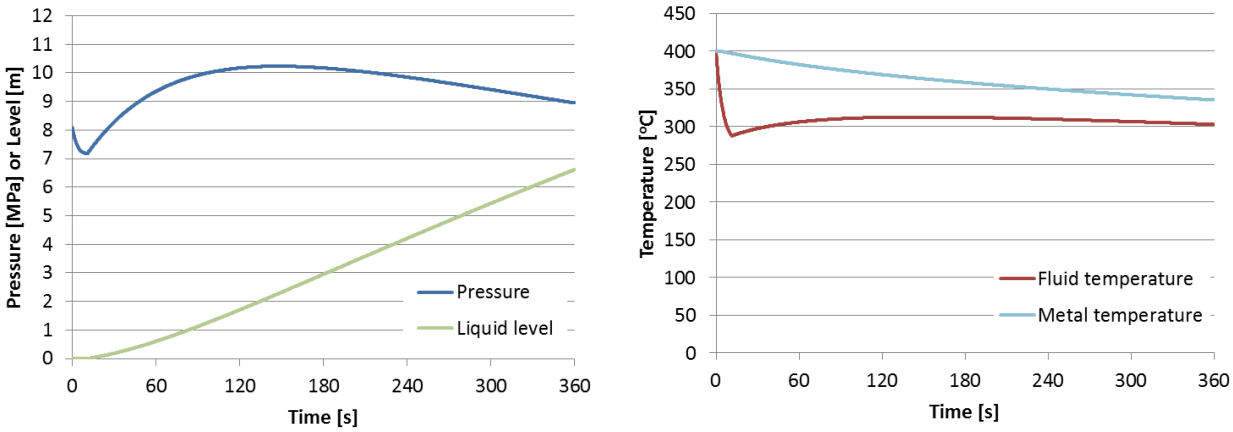


*Figure 56. Results of simplified separator overflow calculation, $\dot{m}_V = 0$*

This simplified model provides useful insight into the behaviour of the superheater during a separator overflow. The relationship between separator overflow and superheater pressure is evident; however, the accuracy of other parameters, such as the heat transfer rates and the flow of steam leaving the control volume to the subcooled liquid interface should be calculated in detail. Thus, the simplified model is useful for providing an explanation of superheater pressure behaviour during a quench but it is not accurate for determining liquid level.

## 6.3 Modelling the separator overflow in Flownex

The next level of detail considered in the development of methods to investigate the separator overflow and track the liquid level was to implement a model in Flownex. Flownex is commercially available software for one dimensional thermo-fluid modelling of physical processes.

### 6.3.1 Flownex Theory

Flownex uses the implicit pressure correction method to solve the transient one dimensional mass, energy and momentum conservation equations for a network consisting of nodes and interconnecting elements [117]. An element represents a physical component, such as a pipe or a pump, through which the fluid flows. The element has one inlet and one outlet. The inlet and outlet of the element are connected to separate nodes. The element has a flow characteristic and an energy characteristic associated with it. These component specific characteristics are defined by the user for each element and make up the necessary closure relationships to solve the main equations. An example of such relationship is the head loss and heat transfer of an uninsulated pipe: the friction factor provides the flow characteristic for the element, while the outer heat transfer coefficient and ambient temperature provide the energy characteristic. The fluid properties for any characteristic relationship for that element are assumed to be the average value between the inlet

and outlet. An element can also be divided into increments in which case, each increment is treated as a separate element with the intermediate nodes automatically included by the software.

The elements are considered to have zero volume. To account for the volume contained within the specific component, the volume is halved and added to each of the upstream and downstream nodes. Now the mass balance equation for the element is no longer transient. The mass entering the element is the same as the mass leaving the element at any point in time. The energy characteristic for the component can also be applied at any point in time to calculate the outlet enthalpy of the flow.

To obtain the flow through the element, the transient momentum equation must be solved for the element. This equation provides the mass flow in terms of the upstream and downstream pressures which are the node pressures.

The simplified partial differential form of the transient momentum conservation equation for one dimensional single phase incompressible flow is given by:

$$\frac{\partial \dot{m}}{\partial t} = \frac{A}{L}\left((p_{0i} - p_{0e}) + \rho g(z_i - z_e) + \Delta p_{0W} - \Delta p_{0L} + Lv\frac{\partial \rho}{\partial t}\right) \quad (101)$$

Where $\dot{m}$ is the mass flow of fluid in the element, $t$, is time, $A$ is the cross sectional flow area, $L$, is the length of the flow path, $\rho$ is the fluid density, $g$ is the gravitational constant and $z$ is the height of the inlet or outlet respectively. The pressures are expressed as total pressures, $p_0$, at inlet and outlet respectively in terms of the static pressure, p, and fluid velocity, $v$, as follows:

$$p_0 = p + \frac{1}{2}\rho v^2 \quad (102)$$

The component characteristics are used to determine the total pressure increase due to work, $\Delta p_{0W}$ and the pressure decrease due to losses $\Delta p_{0L}$. For pipe elements, the pressure loss term is expressed in the form of a loss coefficient, K as follows:

$$\Delta p_{0L} = K\frac{1}{2}\rho v^2 \quad (103)$$

The nodes are the connection points of the network and they may also represent a physical entity such as a tank. All the fluid volume and mass is assumed to be contained in the nodes. Multiple elements can connect to the same node, allowing for multiple inflows and outflows. It is assumed that the change in momentum between the various inlets and outlets at a node is negligible. Hence the conservation of momentum equation does not need to be solved at the nodes. The properties of the fluid within a node are assumed to be homogeneous and in thermal equilibrium.

The node pressures are determined by the transient mass and energy conservation equations coupled with the fluid property relationships. The one dimensional transient partial differential equations for the conservation of mass and energy are as follows:

$$\frac{\partial \rho}{\partial t} = \frac{1}{V}(\sum \dot{m}_i - \sum \dot{m}_e) \quad (104)$$

$$\frac{\partial h_0}{\partial t} = \frac{1}{\rho V}\left(\sum \dot{m}_{in}(h_{0in} - gz_{in}) - \sum \dot{m}_{out}(h_{0out} - gz_{out}) + \dot{Q} - \dot{W} + V\left(\frac{\partial p}{\partial t} - h_0 \frac{\partial \rho}{\partial t}\right)\right) \quad (105)$$

Where $V$ is the volume of the node and the total enthalpy, $h_0$, at inlet and outlet respectively is given by:

$$h_0 = h + \frac{1}{2}v^2 \quad (106)$$

The rate of heat transfer to the control volume, $\dot{Q}$, and the power output from the control volume, $\dot{W}$, are derived from the component characteristics.

The partial differential equations are solved by integrating over a discrete time step, Δt, using Euler integration. The terms on the right hand side of the partial differential equations for momentum, energy and mass conservation are known as the source terms, $S$, and these can be evaluated at a point in time. As discussed above in Section 4.1, a weighting factor, $\alpha_c$, is incorporated in the discrete integration of the source terms over the time step such that:

$$\rho = \rho^o + \left((1 - \alpha_c)S_c^o + \alpha_c S_c\right)\Delta t \quad (107)$$

$$h_0 = h_0^o + \left((1 - \alpha_e)S_e^o + \alpha_e S_e\right)\Delta t \quad (108)$$

$$\dot{m} = \dot{m}^o + \left((1 - \alpha_m)S_m^o + \alpha_m S_m\right)\Delta t \quad (109)$$

The software conveniently handles the time wise integration of the equations to provide the transient solution. The user can specify the time step size and the type of solution: explicit ($\alpha = 0$), implicit ($\alpha = 1$) or semi-implicit ($0 < \alpha < 1$).

For implicit and semi-implicit integration, the solution is iterative at each time step. The solution method is based on the following concept: From an initial set of pressures, a set of flow rates can be calculated in all the elements in the network by the momentum conservation equation. Then, mass and energy conservation can be applied at the nodes to find new values of density and enthalpy. The fluid property relationships can then be used to find new pressures at the nodes and the cycle can be repeated, as shown in Figure 58, until the pressures converge.

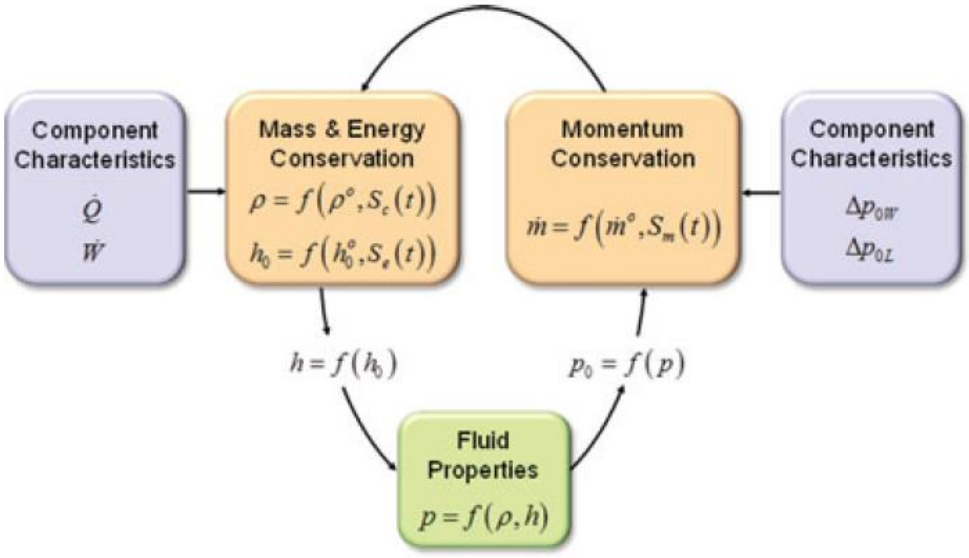


*Figure 57. Flownex transient network solution methodology [65]*

The numerical solution scheme applied in Flownex is an implicit pressure correction method [118]. The mass and momentum conservation equations are combined to obtain a total pressure correction matrix which is then solved to obtain pressure and density corrections in an iterative manner.

## 6.3.2 Application to separator overflow

For flow in pipes, Flownex uses a homogeneous two-phase fluid model in thermal equilibrium. This is an acceptable assumption for a number of flow situations but is not valid when stagnant conditions occur where the liquid phase settles out. This can be dealt with by using a two-phase tank component in Flownex that is actually a node that allows for separation of the phases. The software applies the same concept used above in Section 6.2: the liquid phase occupies the bottom part of the container and the gas phase the upper part such that there is a liquid level that can be defined.

The two-phase tank accepts homogeneous inflows into the tank, but outflows are taken as a single phase depending on the connection height of the outflow element and the level in the tank at the time. For outflows below the liquid level, saturated liquid is assumed to flow and for outflows above the liquid level, saturated steam is assumed to flow.

The two-phase tank methodology was used to model the superheater system. This assumption is reasonable considering that there is no significant flow in the system which would prevent the liquid from settling out. A similar approach was applied by Wang, et al. [119] who demonstrated a model for steam transport with continuous condensate removal as in the case of a steam pipeline with regularly spaced steam traps.

The effective density, ρ of the fluid in the control volume can be described in terms of the void fraction α and the liquid ($\rho_L$) and gas ($\rho_G$) densities as follows:

$$\rho = (1 - \alpha)\rho_L + \alpha\rho_G \tag{110}$$

The void fraction is related to the effective quality of the steam in the node, and in the case of a two-phase tank, also to the liquid level. Flownex thus provides dynamic level tracking and this can be used to monitor the progression of liquid in the superheater system.

Flownex iteratively solves for the effective density and total enthalpy at the nodes in the network as described above. Then, using fluid property relationships, the pressure at the node and void fraction are determined. The principle is the same as that used in the simplified calculation in Section 6.2 above. A schematic of the model used in this work is shown in Figure 58 while the layout of the model in Flownex is shown in Figure 59.

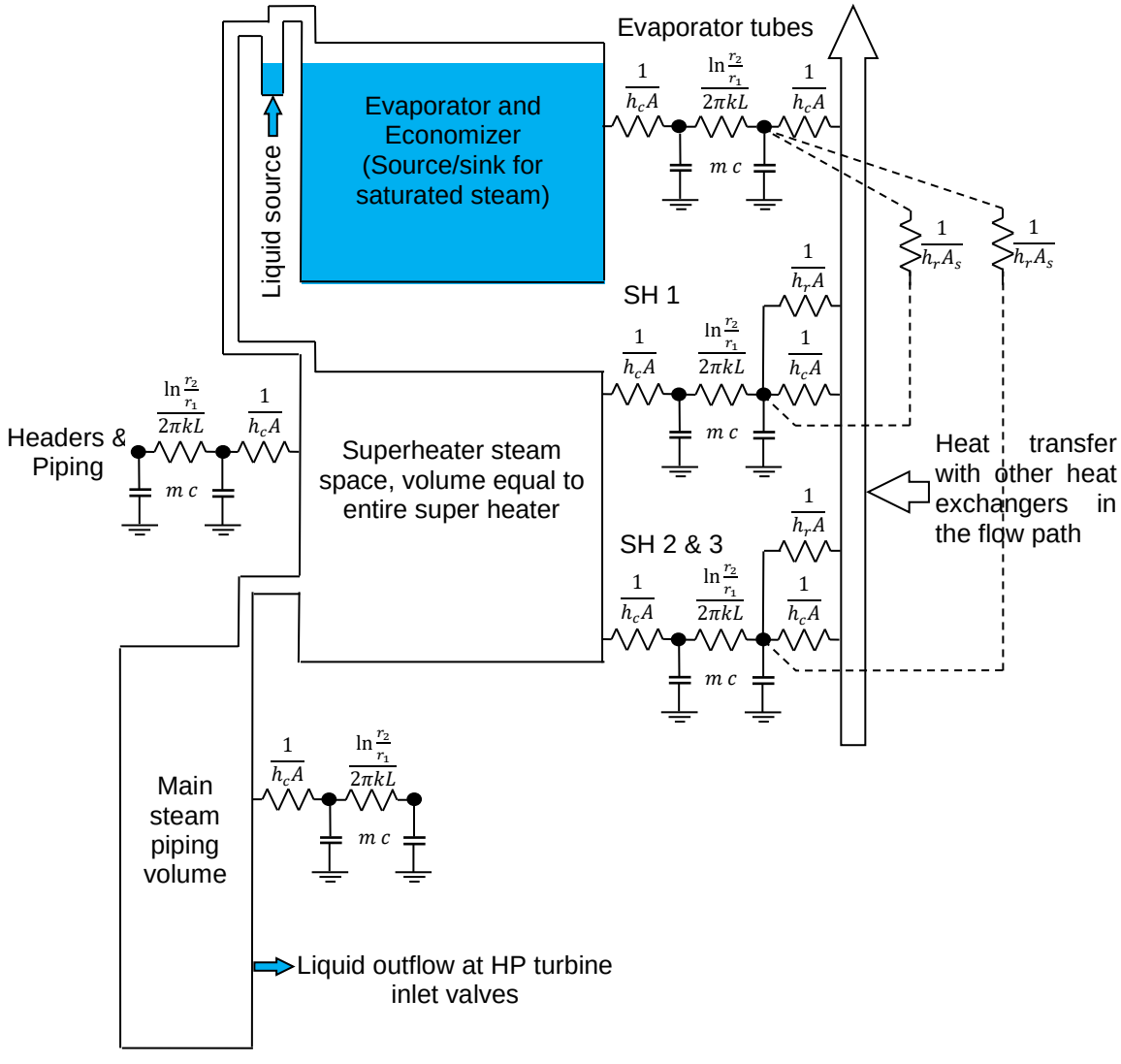


*Figure 58. Schematic of the transient superheater model*

The superheater is modelled as a two-phase tank, initially filled with superheated steam. The evaporator, economiser, collecting vessel and separators are modelled by another two-phase tank containing water and steam that are in thermal equilibrium at the saturation temperature. The tanks are connected by a pipe element connected to the top of the evaporator and the top of the superheater which allows flow of steam between the tanks. In the model, the evaporator is at saturation temperature and it is thus a source of steam to the superheater if there is a drop in pressure in the system. It is assumed that any condensate in the superheater is able to flow by gravity through the heat exchanger and collect in the lower part without significant pressure drop occurring.

The main steam system is represented by another separate two-phase tank connected to the superheater by a conduit. The conduit is made up of two elements as can be seen in Figure 59, that allow for simultaneous flow of steam in the one element and liquid in the other. The liquid conduit is connected to the superheater tank at the height of the outlet header of superheater 3 and on the other side to the top of the main steam tank. This allows liquid to flow downwards under gravity. The steam conduit connects to the top of the superheater tank and on the other side, to the top of the main steam tank to allow steam that is generated in the main steam system or displaced from the system to flow upwards towards the superheater.

At the bottom right of the model, an allowance is made for leakage out of the main steam system to simulate leakage at the high pressure turbine. This was known to have occurred during the particular event being studied.

The fluid properties in the superheater tank are considered on an average basis, while the heat transfers for each stage of heat exchangers and for the headers are calculated separately. The heat conduction and storage in the tube wall was considered using the average geometry and material properties of the tubes and headers. The convective heat transfer coefficients are calculated for each of the heat exchangers and the headers using the correlations provided above in section 4.1.

To obtain the temperature of the evaporator tube outer surface for completing the surface to surface radiation heat transfer, a part of the heat transfer from the flue gas flow to the evaporator was included in the model. In reality this temperature of the tubes of the real plant would be lower than the model because of the sub cooled liquid in the evaporator. The effect of this difference between model and reality is within the accuracy of the heat transfer calculations and was not considered further. Fixed convective heat transfer coefficients were used for the inside and outside of the evaporator tubes of 100W/$m^2$ K and 10W/$m^2$ K respectively. The heat conduction and storage in the tube wall was considered using the geometry and material properties of the tubes.

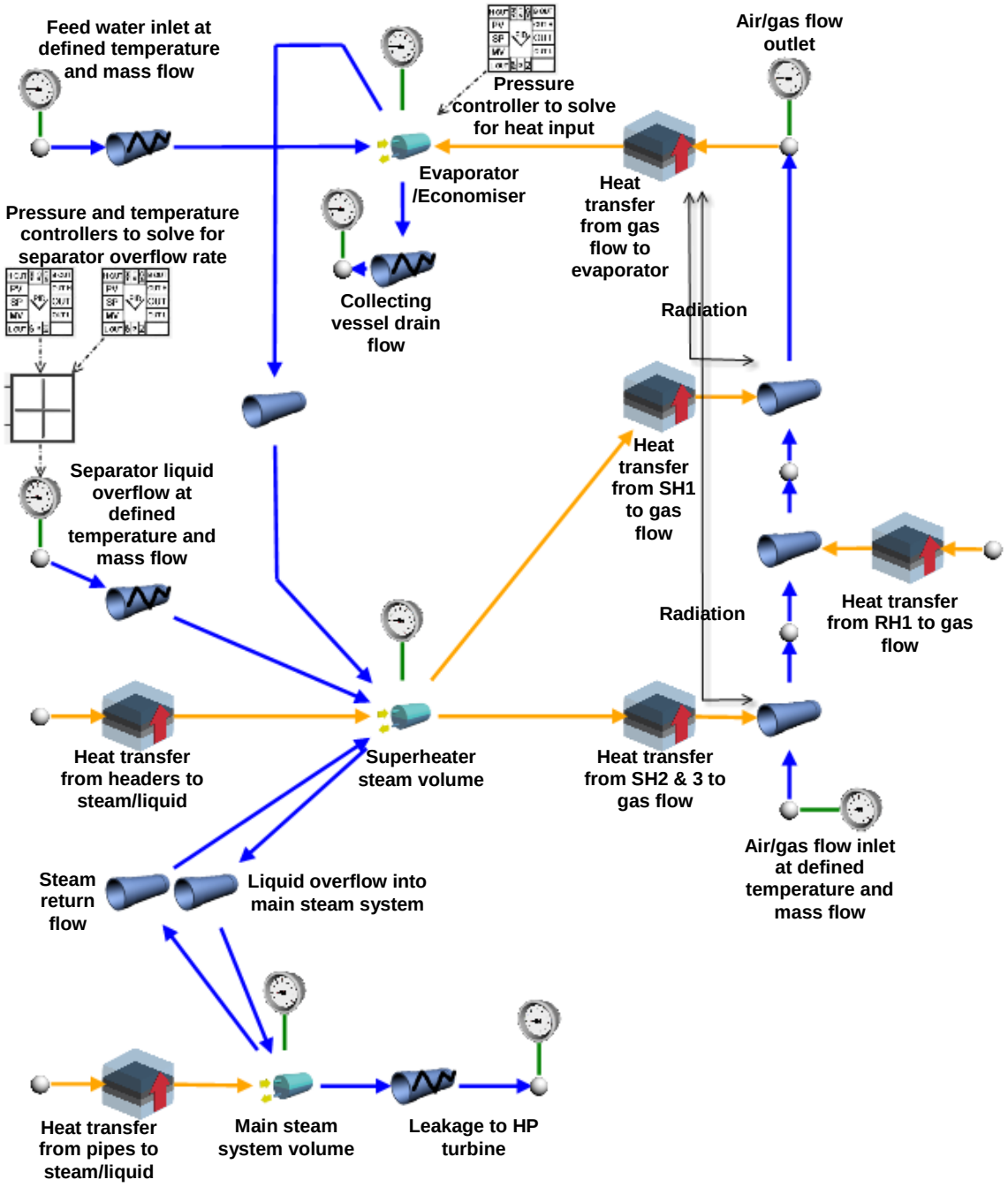


*Figure 59. Implementation of the model in Flownex*

The model includes a liquid source that emulates a potential separator overflow. The overflow is configured to admit water directly into the superheater and the temperature of the water is an adjustable boundary condition that can be set according to the relevant plant data.

The two-phase tanks were initialized by setting a pressure and temperature or quality boundary condition at the beginning of the simulation. Thereafter those boundary conditions were disabled and the parameters in the tanks were free to vary.

On the real plant, once the evaporator is full with subcooled liquid, it does not generate steam when heat is transferred to it and hence it does not affect the superheater. Thus heat transfer to the evaporator and economiser is not modelled except for the section of evaporator tubes discussed above. In the model, the evaporator and economiser are modelled as a two-phase tank and remain at saturated conditions. Thus, to better match reality, the pressure in the evaporator tank was controlled to the measured value by heat input to the tank (See top right of Figure 59).

The flow rate of steam leaving the superheater and flowing to the evaporator outlet where it was being condensed at the subcooled liquid interface was not calculated in Flownex. A separate calculation was performed to estimate the condensation rate over time as per the method in section 6.1. This flow rate was used as a boundary condition to set the flow in the pipe joining the evaporator and superheater tanks in the Flownex model. At times when there was potentially still steam flow coming from the evaporator into the superheater, a controller component was used to balance pressure in the superheater by the heat input to the evaporator. The difference between the measured superheater pressure and the simulated pressure was used as the sensor and the heat input to the evaporator was used as the actuator. When the simulated pressure dropped, an increase in heat input caused evaporation in the evaporator and a flow of steam in the pipe joining the evaporator to the superheater. This increased the mass of steam in the superheater and hence the pressure increased back to the measured value.

The boundary conditions acting on the air flow to the right of the model shown in Figure 59, continuously set the mass flow rate and inlet temperature of the air according to the measured values.

### 6.3.3 Heat transfer during quenching

The heat transfer that occurs inside the tubes and headers during quenching is a complex problem that is difficult to simplify to the level of detail that this work aims to make use of. Initially the approach was to use the correlation for free and forced convection of laminar flow inside a tube using Morcos and Bergles [110]. It was found that the coefficient becomes larger when the temperature difference between the wall and the fluid temperature in the superheater control volume increased. This aligns with the expectation of higher heat transfer that occurs during quenching, but it is not a valid correlation to use for the boiling that occurs. In reality the boiling heat transfer is localized and not applicable to the whole heat transfer area simultaneously. Thus further investigation of boiling heat transfer is warranted.

### 6.3.4 Tube inner, Boiling heat transfer

During quenching of a hot tube or header component, condensate or subcooled liquid, flows into the component by gravity. Thus the liquid comes into contact with the bottom inner surface of the component. Depending on the extent of the temperature difference between the liquid and the hot metal surface, boiling occurs. Energy is transferred from the metal to the liquid owing to the temperature difference and the liquid evaporates into steam.

Pool boiling is the boiling of a liquid in absence of bulk flow and the motion of the fluid is due to the density gradients in the liquid and buoyancy of the gas bubbles. As the temperature difference between the hot surface and the saturation temperature of the liquid increases the type of boiling changes as shown in Figure 60. At lower temperature differences, natural convection boiling occurs. Then with increasing temperature difference, bubbles start to form. This is known as nucleate boiling. With increasing temperature difference, there are more bubbles and they rise to the surface and enhance heat transfer up to a maximum value known as the peak or critical heat flux, $q_{max}$.

At a temperature difference beyond the peak heat flux, the liquid evaporates at a rate that releases sufficient vapour that the liquid cannot come into contact with the hot surface. The liquid becomes separated from the hot surface by the vapour. The layer of vapour acts as a thermally insulating film causing the liquid to evaporate much more slowly than if it remained in contact with the surface. This phenomenon is known as the Leidenfrost effect [120].

Further temperature increase now reduces the amount of heat transfer because of vapour pockets on the surface that interfere with nucleate boiling. As more vapour blankets the surface, less heat transfer to the fluid occurs until a stable film of vapour covers the whole surface. This is the Leidenfrost point or the minimum heat flux, $q_{min}$ and this type of boiling is known as film boiling. If the temperature difference is increased even further, the heat flux increases again due to additional temperature difference to drive film boiling.

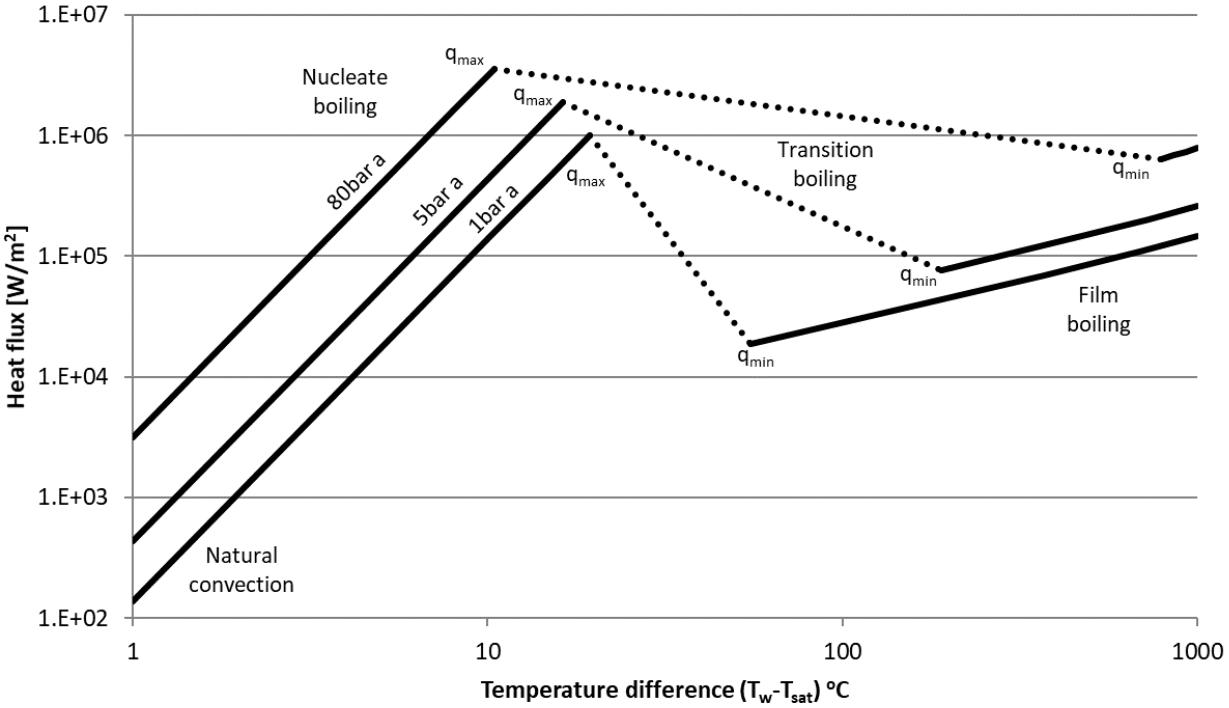


*Figure 60. Boiling heat transfer of water at constant pressure*

Nucleate boiling is commonly estimated by the Rohsenow correlation [121] which is described in terms of the average Nusselt number, *Nu*, in Mills [40] as follows:

$$Nu = \frac{Ja^2}{C_{nb}^3 Pr_l^m} \tag{111}$$

$$Ja = \frac{c_{pl}(T_w - T_{sat})}{h_{fg}} \tag{112}$$

Where *Ja* is the Jakob number, $Pr_l$ is the Prandtl number of the liquid, $c_{pl}$ is the isobaric specific heat capacity of the liquid, $T_w$ is the wall temperature, $T_{sat}$ is the saturation temperature and $h_{fg}$ is the enthalpy of vapourisation of the fluid. The constant $C_{nb}$ and the exponent, $m$ are surface and fluid specific and for the case of water in relatively smooth steel pipes we assume $C_{nb} = 0.013$ and $m = 2$. This correlation is not accurate and errors of up to 100% in $q$ can be expected [40].

In this case, the Nusselt number is defined in terms of a characteristic length, $L_c$ as follows:

$$Nu = \frac{hL_c}{k_l} \tag{113}$$

$$L_c = \left[\frac{\sigma}{(\rho_l - \rho_g)g}\right]^{\frac{1}{2}} \tag{114}$$

Where $h$ is the heat transfer coefficient, $k_l$ is the liquid conductivity, $\sigma$ is the surface tension between the gas and liquid phases, $\rho_g$ and $\rho_l$ are the gas and liquid densities respectively and $g$ is the gravitational constant.

The nucleate boiling peak heat flux is limited by the rate at which vapour can leave the wall. It can be calculated by the method of Kutateladze [122] and Zuber [123]:

$$q_{max} = C_{max} h_{fg} \left[\sigma \rho_g^2 (\rho_l - \rho_g) g\right]^{\frac{1}{4}} \quad (115)$$

The value of the constant $C_{max}$ is taken to be 0.12.

Beyond the peak heat flux, $q_{max}$, there is a region of transition boiling before the wall temperature is high enough to achieve film boiling. For film boiling, the average heat transfer coefficient, $\bar{h}$, can be estimated using the turbulent vapour flow formula developed by Frederking and Clark [124] :

$$\bar{h} = 0.15 \left[\frac{(\rho_l - \rho_g) g h'_{fg} k_g^2}{\upsilon_g (T_w - T_{sat})}\right]^{\frac{1}{3}} \quad (116)$$

$$h'_{fg} = h_{fg} + 0.5 c_{pg} (T_w - T_{sat}) \quad (117)$$

Where $k_g$ is the thermal conductivity of the gas, $v_g$ is the kinematic viscosity of the gas, $c_{pg}$ is the specific heat of the gas at constant pressure and $L$ is the length of the vapour film, taken as the internal diameter of the pipe. The correlation is valid for:

$$\frac{L^3 (\rho_l - \rho_g) g h'_{fg}}{k_g \upsilon_g (T_w - T_{sat})} > 5\text{x}10^7 \quad (118)$$

The minimum heat transfer rate can be estimated by assuming that the vapour film breaks down when the vapour generation rate is too low to sustain Taylor instability wave action [125] :

$$q_{min} = C_{min} \rho_g h_{fg} \left[\frac{\sigma g (\rho_l - \rho_g)}{(\rho_l + \rho_g)^2}\right]^{\frac{1}{4}} \quad (119)$$

Where $C_{min}$ is 0.09 for large horizontal surfaces.

Radiation influences film boiling by increasing the rate of vapour production and thus reducing the overall heat transfer [40]. This needs to be considered for temperatures above 600K. Considering the expected quenching conditions for this study, the initial temperature difference between the hot surfaces and the saturation temperature of the liquid are of the order of 200°C. Thus a point in a horizontal pipe being quenched by saturated liquid initially experiences film boiling heat transfer on the bottom internal surface.

As the surface temperature cools, the temperature difference between the wall and the fluid reduces until film boiling is no longer sustained. The liquid starts wetting the surface and a rapid increase in heat transfer is experienced. This point is known as the re-wetting front and it travels along the pipe at a certain velocity. Takrouri et al [126] measured the re-wetting front velocity on

the outside of horizontal tubes. Their diagram (Figure 61) of the boiling situation can be interpreted for flow inside horizontal pipes.

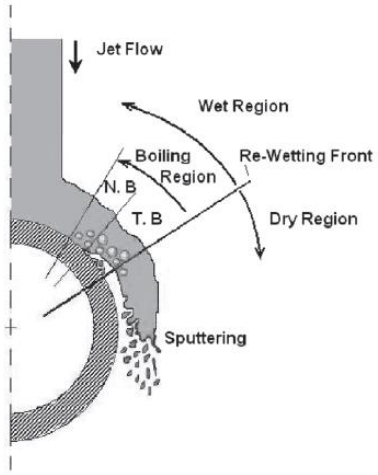


*Figure 61. Progression of boiling for a liquid quenching the outside of a horizontal pipe [126]*

The initial front of liquid passing a point in a horizontal pipe floats on a film of vapour. The inner surface of the pipe remains dry. As the surface temperature of the metal is cooled, the vapour film eventually starts to collapse when the re-wetting front passes the point in the pipe. The boiling regime then changes from film boiling to transition boiling and then nucleate boiling before boiling ceases when the metal temperature is at or below the saturation temperature.

Chill-down of pipes conveying cryogenic fluids have similarities to quenching of steam pipes. In [127] a model for the local heat transfer coefficient inside the pipe is presented, while in [128], an inverse heat transfer technique was devised for computation of local heat transfer coefficient and local heat flux.

For steam at 80bar, the maximum heat flux, $q_{max}$, is approximately 3.6MW/m$^2$ and it occurs at a difference between the wall temperature and the saturation temperature of 10.4K. This peak heat flux is short lived at the point in the pipe under consideration because the inner surface of the metal is rapidly quenched. Following the initial surface quenching, the heat flux is limited by the rate of conduction through the metal to the inner surface.

The local boiling heat transfer coefficient including the effects of conduction in the tube wall, for a single 18m long horizontal tube undergoing quenching was estimated (refer Figure 62). The heat transfer coefficient was related to average conditions for the control volume and not the local wall and fluid temperature conditions. The graph gives a snap shot of the conditions at 19 seconds after water entered the tube when the re-wetting front was at 2m along the length of the tube and it was moving from the left to the right. Nucleate boiling peak heat flux occurred at 1.7m.

The heat transfer coefficient ahead of the liquid is assumed to be forced convection by virtue of the steam flow generated by boiling and now travelling down the tube to the right (estimated using the Dittus Boelter correlation [107] ).

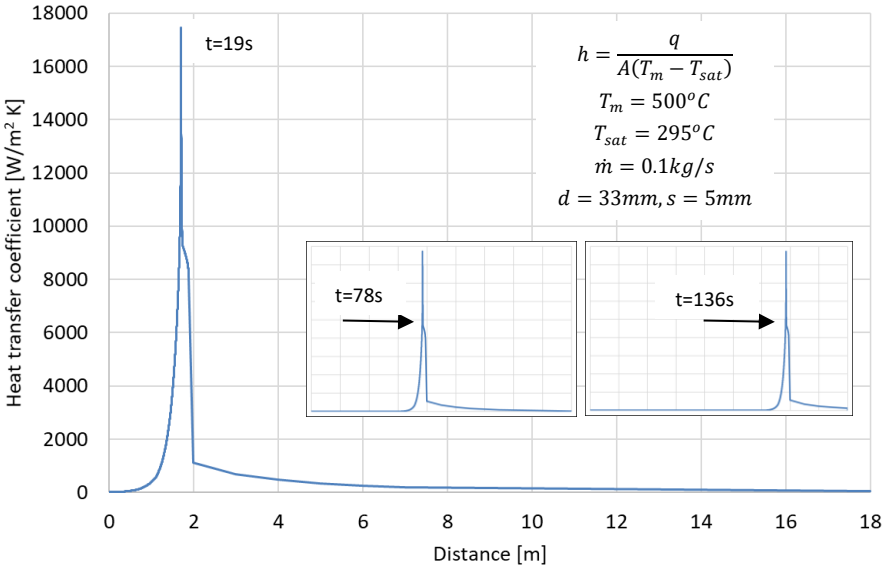


*Figure 62. Theoretical heat transfer coefficient for a single tube undergoing quenching*

The application of the boiling correlations were found to be problematic when applied to the simplified superheater models. The level of detail required in order to calculate the heat transfer that occurs is not available. The superheater is a large heat exchanger with detailed geometry and many tubes. Predicting the passage of liquid as it flows into the superheater and determining the position of the re-wetting front as a function of time would be a significant challenge and would not address the objectives of this work.

Practically for the purposes of the simplified modelling approach, each specified heat transfer in the model can only have a single value of heat transfer coefficient that relates the total surface area and temperature difference to the heat transfer rate. The significant variation in heat transfer coefficient seen in Figure 62 and the resulting temperature difference in the metal are impossible to reconcile back to a single heat transfer coefficient value.

Assuming the whole surface area to be at boiling conditions is not realistic because the liquid does not come into contact with the whole surface simultaneously. An area weighted approach is more reasonable but is still difficult to evaluate because the internal area of the superheater affected by boiling liquid is not known.

Hence the approach was to assume that the correlation for free and forced convection of laminar flow inside a tube using Morcos and Bergles [110] applies over 20% of the area and the remaining 80% of the internal area of the superheater was assumed to have a constant heat transfer

coefficient of 30W/m$^2$K. This combined average heat transfer coefficient was applied together with an upper limit of 300W/m$^2$K to give an approximation of the total inner heat transfer.

The correlation was programmed as a script in Flownex to calculate the area weighted internal heat transfer coefficient per stage. The results were then transferred to the relevant heat transfer element in model.

### 6.3.5 Inverse modelling methodology

Initially the approach was to iterate the input boundary conditions and vary them over time until suitable results were achieved. This time consuming trial and error process had limited capability. Thus, an inverse approach, discussed below, was devised to enable desired outcomes to be achieved by automatically manipulating the relevant input variables over time.

It was found that the measured superheater pressure is a global indicator of events occurring in the superheater during the transient. A Flownex controller component was used to infer what the separator overflow must have been in the real plant, to obtain the measured evolution of the system pressure. The mass flow of the separator overflow was controlled using the error between the simulated superheater pressure and the actual measured pressure. The parameters of the controller are given in Table 4.

*Table 4. Flownex settings for inverse method of finding separator overflow*

| **Description** | **Settings** |
|---|---|
| Pressure controller to solve for separator overflow rate as per the inverse method | Control error in kPa<br>Proportional gain: 5 |
| Temperature controller to solve for separator overflow rate | Control error in $^o$C<br>Proportional gain: 20 |
| Pressure controller to solve for evaporator heat input | Control error in kPa<br>Proportional gain: 1000<br>Integral gain: 100 |
| Solver | Time step size: 100ms<br>Default Euler integration and relaxation parameters, except pressure relaxation parameter which was set to 0.5.<br>Explicit pressure calculation option used for all 2 phase tanks |

As shown in Figure 13, the addition of liquid to the superheater can only result in a decrease in the pressure if the liquid is subcooled. Thus the pressure controller was only used when subcooled liquid was present at the evaporator outlet. To control the overflow prior to the separator outlet becoming subcooled, the superheater temperature in the model was compared to the average measured temperature. Again, a controller was used to adjust the separator overflow rate to obtain a match between the measured and simulated temperature.

### 6.3.6 Results and discussion

The model was configured with the dimensions given in Table 2 and applied to the quenching Case A (See Appendix C). Initially the model was used to investigate how much condensate could be produced by heat transfer only and with no separator overflow. It was found that after 60 minutes, the superheater temperatures had not yet reduced sufficiently to start condensation. This aligns with the findings in chapter 4 above.

A separator overflow was then simulated with the aid of the inverse method described above. The model was able to obtain a reasonable match between the calculated and measured system pressure as shown in Figure 63.

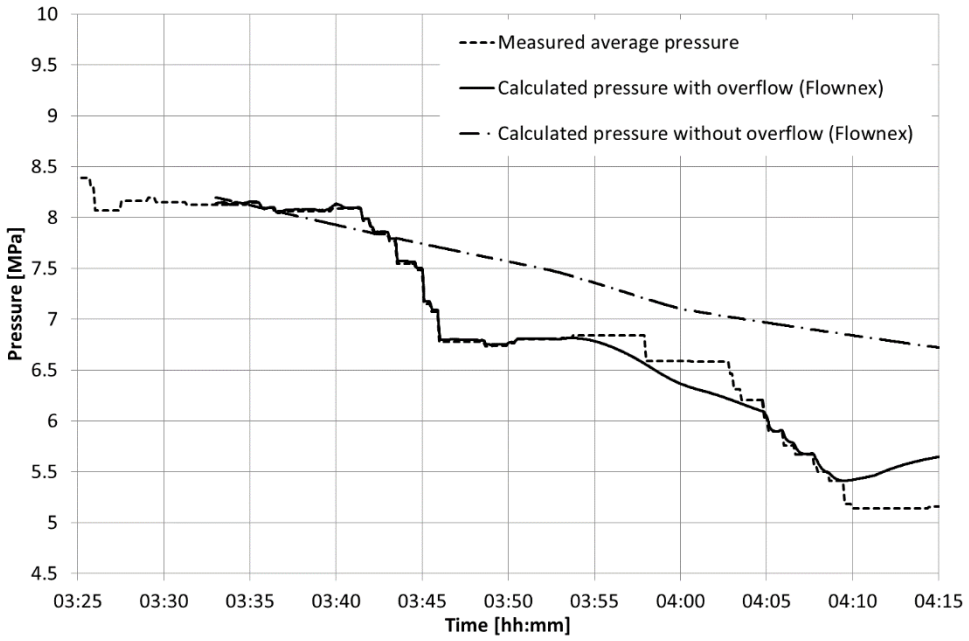


*Figure 63. Superheater steam pressure results*

In Figure 64 the calculated superheater temperature history is compared to the measured values for the whole superheater system, which is based on a weighted average of several measurements at discrete points. It can be seen that the initial cooling rate shows good agreement when the temperature controller for the separator overflow rate is active. The calculated temperature then rapidly drops to saturation once the pressure controller is switched on. This is due to the simplifications made in the model which cannot deal with liquid running down only one leg of the superheater at a time.

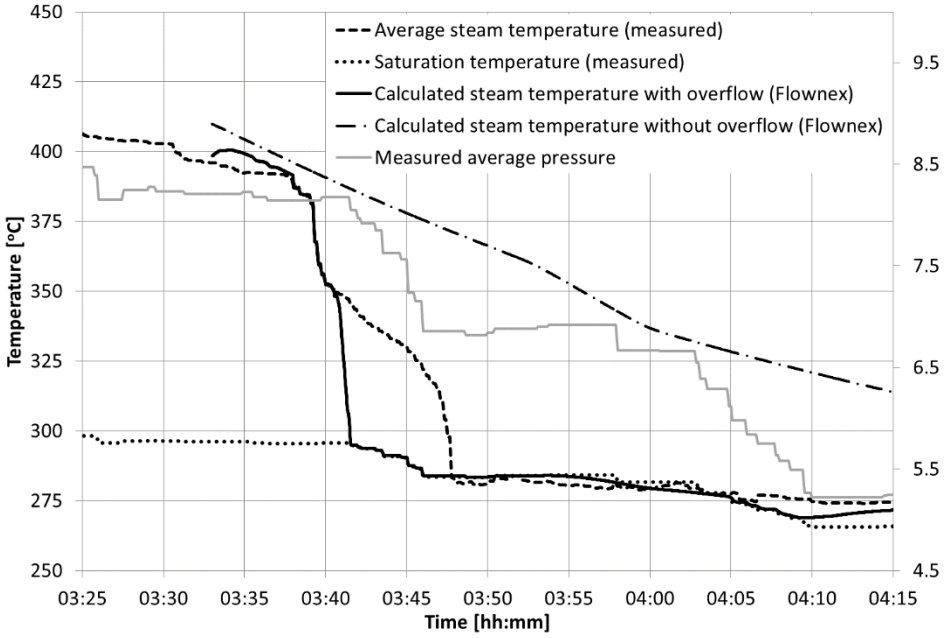


*Figure 64. Superheater steam temperature results*

The comparison of measured gas outlet temperature from the superheater compared to the calculated values is shown in Figure 65. The gas temperature measurements are corrected for radiation effects because the installed thermocouples do not have radiation shields.

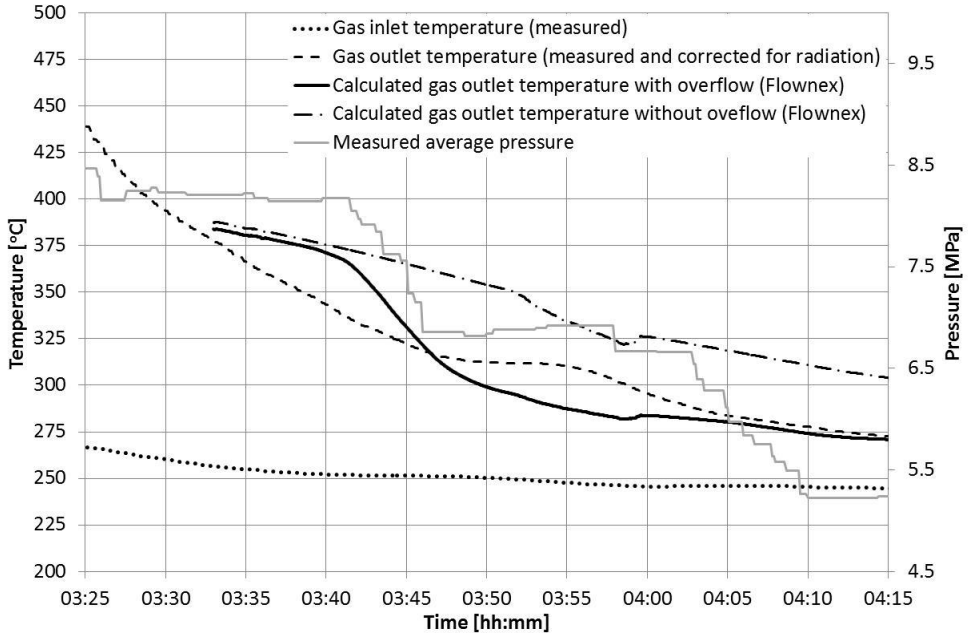


*Figure 65. Gas outlet temperature results*

The graph shows temperature differences of up to 30°C between the corrected measurements of gas temperature and the gas temperature calculated in Flownex. These differences were not investigated further, but are evidence that either the gas measurements were not reliable or the heat transfer model was not accurate enough. It's not unusual that the air and flue gas local temperature measurements in such large ducts as those encountered in large boilers, deviate from the average actual temperature by a few tens of degrees.

The calculated transient rate of overflow from the separator vessel is shown in Figure 67. The separator overflow estimated by the model can be compared to an estimated over-feeding of the boiler based on plant data.

It is assumed that the evaporator was full of liquid at 03:37 when the evaporator outlet temperatures dropped to subcooled. The evaporator volume is fixed, so any increase in the amount of liquid in the fixed volume must result in separator overflow. The system is shown in Figure 66. A mass balance of the system can be used to calculate the overflow rate. An allowance is also made for the change in density of the liquid in the evaporator based on average temperature as follows:

$$\dot{m}_{overflow} = \dot{m}_{feed\,water} - \dot{m}_{dump} + \dot{m}_{condensed} - \frac{\Delta\rho.V_{evaporator}}{\Delta t} \qquad (120)$$

The result for Case A indicates an average measured separator overflow rate of 63kg/s from 03:38 onwards which gives an accumulated overflow of 30 tons by 03:46. Note that this method ignores the effect of any siphon which could for periods of time extract greater flows from the separator.

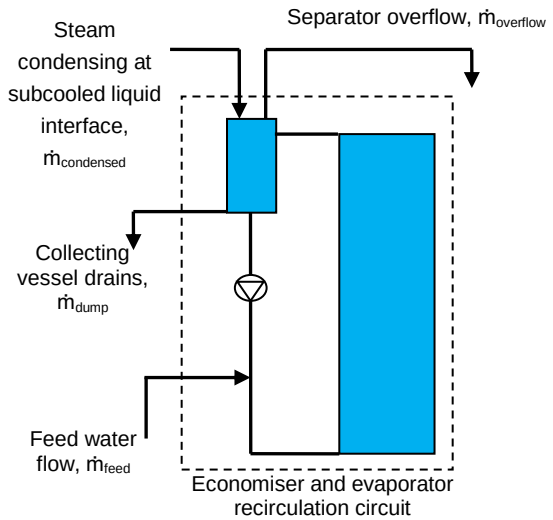


*Figure 66. Control boundary for estimating the separator overflow*

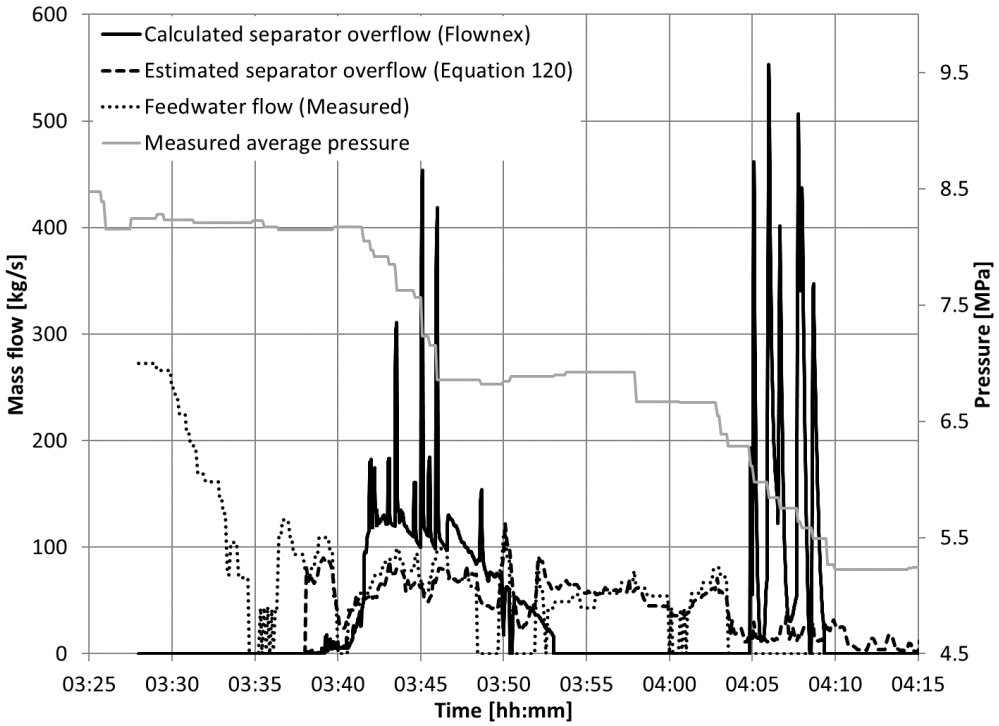


*Figure 67. Calculated separator vessel overflow rate*

The separator overflow rate results calculated by the Flownex model and plotted in Figure 67 show two main peaks of separator overflow corresponding to the two distinct drops in pressure (at 3:42 and 4:05 respectively.) The separator overflow calculated by the model is driven by the measured pressure changes and thus the predicted overflow occurs mainly when the pressure drops. The spikes in calculated separator overflow are caused by the unsmoothed measured pressure data which exhibits steps in value and this in turn causes high separator overflow at each step.

At 3:46, two of the superheater outlet temperatures drop to almost saturation (Figure 140) and this is assumed to coincide with the overflow of liquid from the superheater into the main steam piping system. This flow of liquid would have boiled on the hot metal and released the heat from the main steam pipes. The result was to sustain the pressure at almost constant value from 03:46 onwards (Refer Figure 63). By 03:58, the net effect of steam production from the heat in the main steam pipes and the addition of subcooled liquid to the superheater caused the pressure to start dropping again.

From 03:53 to 04:05, the model predicts zero overflow but the estimated overflow calculated by equation 120 indicates that the overflow should be non-zero during this time. The model is thought to react faster than the real plant does and hence requires more rapid overflow to achieve the desired pressures. Thus the model does not predict the instantaneous overflows accurately but is able to predict cumulative volume with better accuracy (Figure 68). The calculated result of

cumulative overflow obtained from the Flownex model is within 14% of the estimated value from equation 120.

Figure 68 shows the cumulative amount of water that overflowed from the separator. The cumulative feed water flow, derived by integrating the feed water flow measurement can also be compared to the result obtained from equation 120. The difference between these two values show how density changes and condensation contributed to additional liquid overflow from the separator.

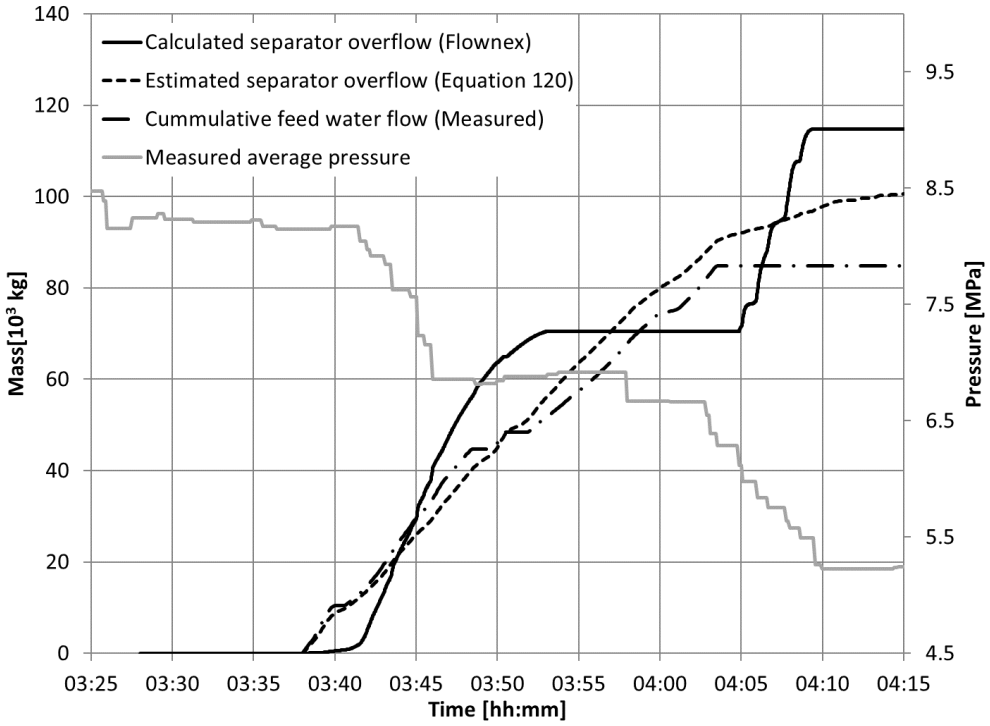


*Figure 68. Calculated total mass of separator overflow compared to feed water flow*

In summary, the Flownex model is capable of capturing the basic behaviour of the system and is able to predict results that match measured plant data. The model is an improvement on the simple model presented in section 6.2; however, it is not capable of investigating the behaviour of the four separate legs of the superheater. The Flownex model can only be configured with a single control volume to represent the entire superheater. The model did not solve when the superheater was discretized into more control volumes. The reason for this was not conclusively determined.

There are two limitations of representing the superheater by a single control volume. Firstly, the real flow of liquid and subsequent evaporation and reverse flow of vapour cannot be captured. Secondly, the heat transfer on the inner surfaces is calculated from one temperature difference that

is assumed to apply over the whole inner surface of the superheater. This causes high heat transfer rates and drop of metal temperatures. In order to compensate, the model must add high separator overflow rates that are not realistic.

The next chapter deals with tracking the liquid level in the superheater over time. A different approach is developed for solving multiple connected steam control volumes without the need for solving the momentum equation. By dividing the superheater into a number of control volumes, the accuracy of the model can be improved.

# 7. Liquid tracking model

The liquid tracking model (LTM) is intended to be a simplified modelling technique for tracking liquid level and superheater pressure in support of activity 3.7 in the proposed methodology, as shown in Figure 69.

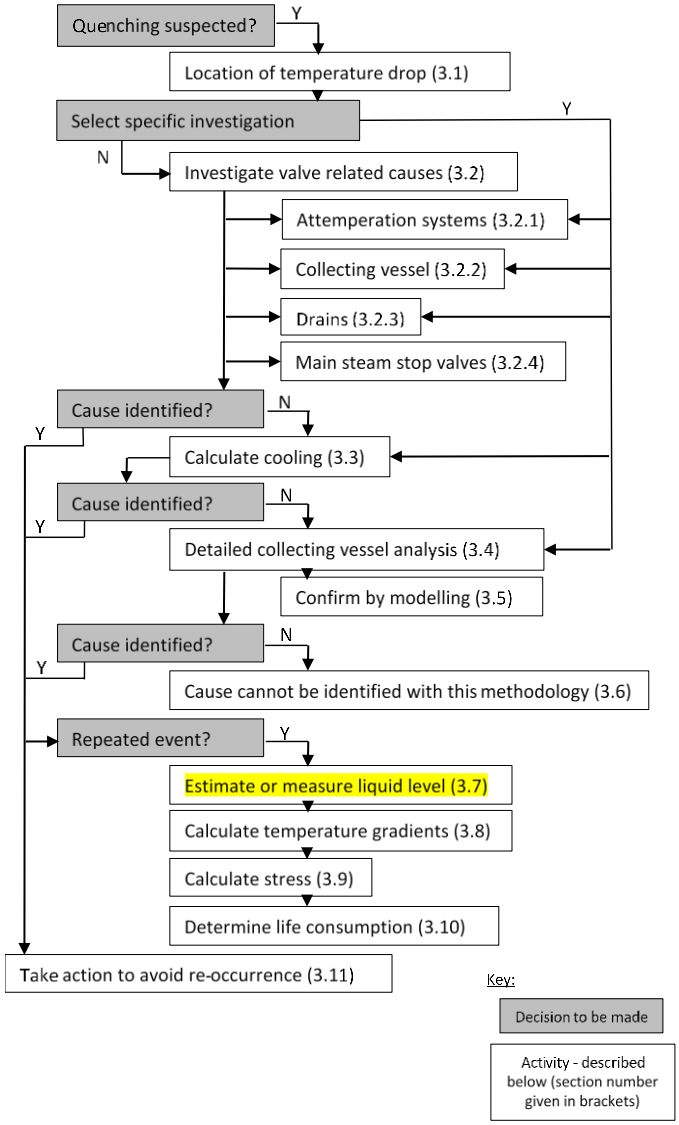


*Figure 69. Activity 3.7 in the methodology*

## 7.1 Basic element and governing equations

The LTM solves the mass and energy balance equations for a number of connected control volumes containing steam. The superheater steam space is divided into control volumes, each of which can represent a bundle of tubes located on a similar level across the width of the boiler. Each control volume has constant volume, V, which is equal to the internal volume of the tubes, headers and

interconnecting pipework that make up the superheater. The steam exchanges heat with the headers and tube bundle as shown in Figure 70.

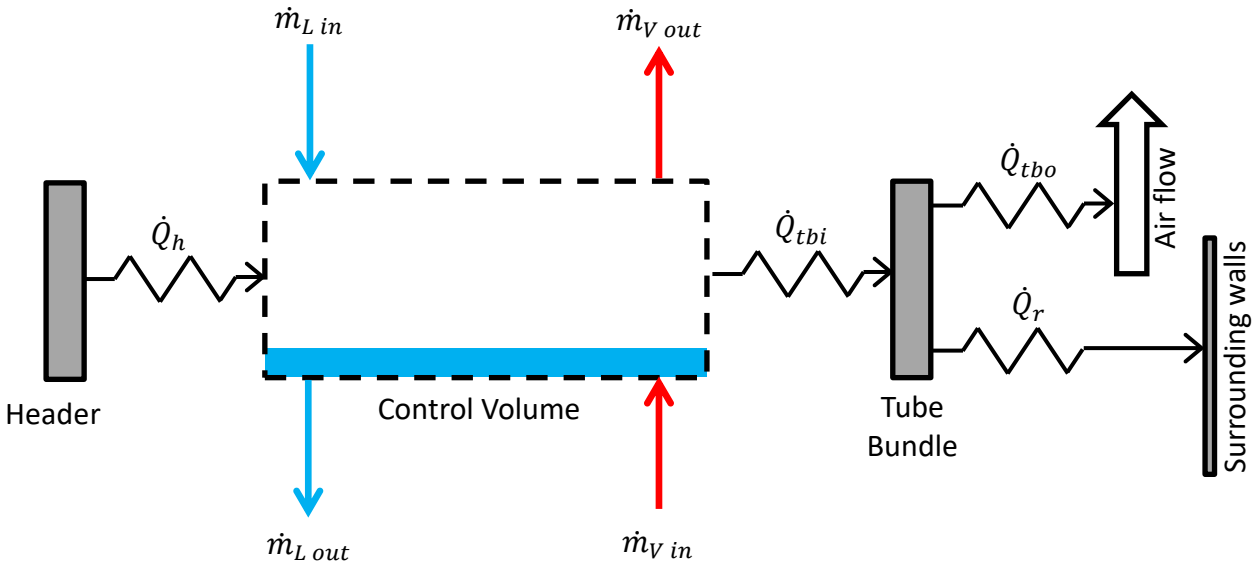


*Figure 70. Configuration of the basic element used in the liquid tracking model*

The control volume has constant volume, V, and it contains either superheated steam or saturated steam and liquid. In the case of saturated steam, the liquid and gas phase are assumed to be in thermal equilibrium, however the phases are separated. The liquid phase is assumed to occupy the bottom part of the control volume and the gas phase occupies the top part. The assumption of thermal equilibrium implies infinite heat transfer between the phases. The assumption prevents subcooled liquid or superheated steam from co-existing with the steam or liquid respectively in a single control volume.

The mass flows in and out of the control volume are each dealt with as single phase only. There is a liquid stream flowing in to the control volume ($\dot{m}_{L\,in}$ ) and a liquid stream flowing out of the control volume ($\dot{m}_{L\,out}$ ). Similarly there are vapour flows in and out of the control volume ($\dot{m}_{V\,in}$ and $\dot{m}_{V\,out}$ respectively).

The transient mass conservation equation for the control volume in one-dimensional form and spatially integrated is given as follows:

$$\frac{\partial \rho}{\partial t} = \frac{1}{V}[(\dot{m}_{L\,in} + \dot{m}_{V\,in}) - (\dot{m}_{L\,out} + \dot{m}_{V\,out})] \qquad (121)$$

Where $\rho$ is the total density of the liquid and vapour in the control volume and $t$ is time.

The steam in the control volume is subject to heat exchange with the pipes, tubes and headers that contains it. At the inner surfaces of headers, they exchange heat with the steam in the control

volume ($\dot{Q}_h$). The outer surfaces of the headers and interconnecting piping are insulated and are thus assumed to be adiabatic.

The tube bundles located in the boiler gas path exchange heat not only at their inner surfaces but also by convection and radiation from their outer surfaces. The heat transfer rate from the steam in the control volume to the tube bundle is denoted $\dot{Q}_{tbi}$ while the heat transfer rate from the outer surface of the tube bundle to the air flow is denoted $\dot{Q}_{tbo}$. The radiation from the outer surface of the tube bundle to the surrounding walls is denoted $\dot{Q}_r$.

The transient energy conservation equation for the control volume in one-dimensional form is given by:

$$\frac{\partial u}{\partial t} = \frac{1}{\rho V}\left(\sum \dot{m}_{in}(h_{0in} - gz_{in}) - \sum \dot{m}_{out}(h_{0out} - gz_{out}) + \dot{Q} - \dot{W}\right) \qquad (122)$$

Where $u$ is the specific internal energy of the liquid and vapour in the control volume, $h_0$, is the stagnation enthalpy, $g$ is the gravitational constant, $z$ is elevation, $\dot{W}$ is work and $\dot{Q}$ is net heat transfer to the control volume.

Height differences are important considering the gravity driven liquid flow, however in the context of the LTM control volumes, the amount of energy change due to height difference is small. Thus differences in height, $z$, are assumed to be negligible. It is also assumed that the velocity component of the total enthalpy, $h_0$, is negligible and there is no work, $\dot{W}$, done by or on the system. Hence equation above becomes:

$$\frac{\partial u}{\partial t} = \frac{1}{\rho V}\left((\dot{m}_{Lin}h_{Lin} + \dot{m}_{Vin}h_{Vin}) - (\dot{m}_{Lout}h_{Lout} + \dot{m}_{Vout}h_{Vout}) + \dot{Q}_h + \dot{Q}_{tbi}\right) \qquad (123)$$

The above equations describe the behaviour of the system. The timewise integration is carried out using semi-implicit Euler integration with a weighting factor of $\alpha_c$ =0.7. The time dependent equations for change of density and change of internal energy are solved using the same weighting factor:

$$\rho_1 = \rho_0 + \frac{t}{V}(\alpha_c[(\dot{m}_{L\,in} + \dot{m}_{V\,in}) - (\dot{m}_{L\,out} + \dot{m}_{V\,out})]_1 + (1-\alpha_c)[(\dot{m}_{L\,in} + \dot{m}_{V\,in}) - (\dot{m}_{L\,out} + \dot{m}_{V\,out})]_0) \qquad (124)$$

$$u_1 = u_0 + \frac{t}{\rho V}\Big(\alpha_c\big[(\dot{m}_{Lin}h_{Lin} + \dot{m}_{Vin}h_{Vin}) - (\dot{m}_{Lout}h_{Lout} + \dot{m}_{Vout}h_{Vout}) + \dot{Q}_h + \dot{Q}_{tbi}\big]_1 + (1-\alpha_c)\big[(\dot{m}_{Lin}h_{Lin} + \dot{m}_{Vin}h_{Vin}) - (\dot{m}_{Lout}h_{Lout} + \dot{m}_{Vout}h_{Vout}) + \dot{Q}_h + \dot{Q}_{tbi}\big]_0\Big) \qquad (125)$$

Where the subscript '1' refers to values evaluated at the end of the time step, t, and the subscript '0' refers to values from the beginning of the time step.

Once the internal energy of the control volume has been determined at the end of a time step, it can be converted to enthalpy:

$$h_1 = u_1 + \frac{p_1}{\rho_1} \quad (126)$$

The enthalpy is dependent on the final pressure in the control volume and thus the solution is an iterative process as described further below.

In order to obtain a solution for a single control volume at a particular time step, it is necessary to firstly obtain the heat transfer rates, the mass flow rates into and out of the control volume and the respective enthalpies of the flows. Then, integrating the mass and energy conservation equations over time enables the density and enthalpy of the steam in the control volume to be calculated. The property relationships for steam are then used to determine the pressure in the control volume.

## 7.2 Heat transfer and metal and gas temperatures

The heat transfer correlations used are the same as that in discussed in section 4.1.2 above and also in section 6.3.3. The heat transfer correlations are summarised in Table 5 below. The tube bundle and header internal heat transfer model used in the LTM deviates from the method used in the Flownex model in Section 6 as described below.

During quenching, the Morcos and Bergles correlation is not valid to use for the localized boiling that occurs. The large changes in heat transfer coefficient and wall temperature demonstrated in Figure 62 shows that a lumped approach for the header and tube metal temperature is unrealistic. The LTM makes use of a revised methodology for approximating the aggregate effect of local heat transfer and heat diffusion through the metal.

The tubes are discretized in two dimensions which are along the length of the tubes and through the thickness of the tube wall as shown in Figure 71. The tubes are not calculated individually but rather the conditions across all the tubes in parallel on a similar level are assumed to be the same.

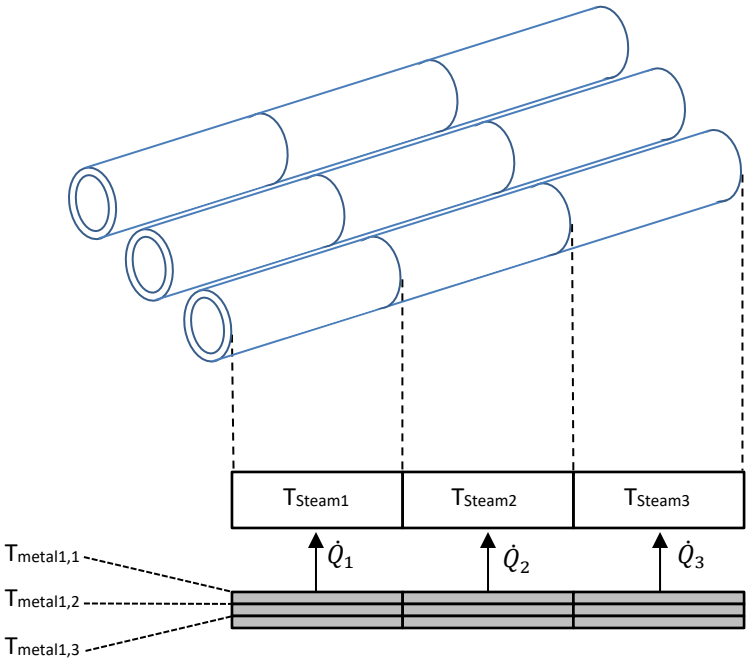


*Figure 71. Discretization of the metal tubes and headers*

A corresponding steam volume per metal volume is defined along the length of the tubes in order to calculate the steam temperature at each point ($T_{Steam1,2,3}$… in Figure 71). The sum of the smaller steam volumes add up to the total volume of the basic element from Figure 70.

The level in the larger control volume is used to find the point along the series of smaller steam volumes where the interface between the liquid and steam exists. Thus, it is assumed that there is a relationship between the level of liquid in the larger control volume and the amount of metal that has been quenched.

In reality, the tubes and headers are horizontal and they may either be exposed to liquid flowing through the tubes down to a lower level or they may be flooding by filling up from the bottom (See Figure 72).

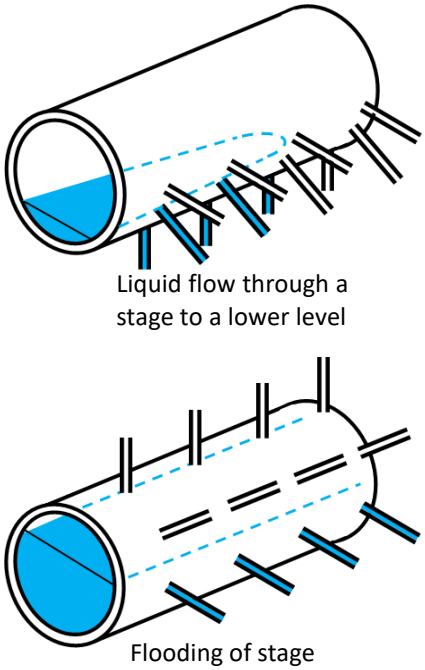


*Figure 72. Types of liquid flow that cause quenching*

The steam control volume in the model represents many tubes with the associated headers depending on the level of discretization applied. During quenching when water flows down to a lower level, water flows into the control volume, but the number of tubes affected by the water at any time is not known. Such details would only be available from detailed three-dimensional geometry and computational fluid dynamics of the open channel type liquid flow. In order to provide a basis for developing the model it is assumed that the tubes fill with liquid from the bottom.

The representation in Figure 71 is for illustrative purposes and in the case of the model, it is assumed that the liquid flows from left to right in a slug along all the tubes simultaneously. This could only truly happen in vertical tubes flooding from the bottom and thus the localized boiling model is drawn as a vertical stack of steam and metal control volumes in Figure 73.

The headers are treated the same as the tubes and although the header is discretized along the length and does not align with the direction of quenching, the intention is only to give an approximation of the amount of metal quenched and not to actually predict the metal temperature at any point. The headers are equally divided between the inlet and outlet of the tube bundle.

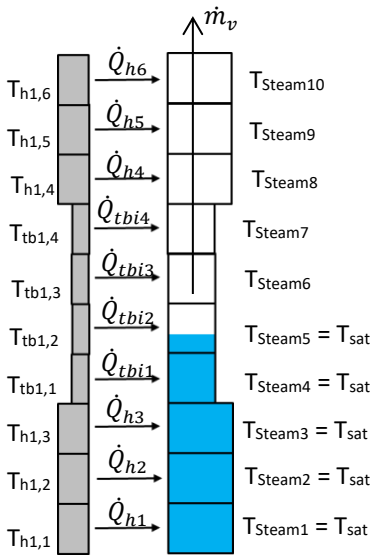


*Figure 73. Localised boiling model showing interaction of inner metal elements and steam*

At each point, the local tube and header internal heat transfer coefficients are calculated. The pool boiling methodology described above is applied to the 'wet' steam volumes based on the difference between the inner metal temperature and the saturation temperature.

In order to prevent instability in the metal temperature calculation, a limit is applied and the maximum boiling heat transfer coefficient is limited to:

$$h_{boiling} < 0.5 \frac{CV_{m\,x,y}}{A_{x,y}t} \tag{127}$$

The rate of change of the metal temperature of each discretized metal volume depends on C, the capacitance of the metal, which is assumed to be homogeneous, and $\dot{Q}_{m\,net}$, the net rate of heat transfer from the metal:

$$\frac{dT_{metal\,x,y}}{dt} = \frac{\dot{Q}_{m\,net\,x,y}}{CV_{m\,x,y}} \tag{128}$$

The net rate of heat transfer to the metal volumes includes terms for conduction in the solid in the radial and axial directions. In the radial direction, the formula for conduction through a cylindrical wall is used (Refer section 4.1.2.4).

The mass flow of steam in the dry steam volumes is due to the steam generated by boiling in the wet region. The value is provided by the main LTM calculation (see below). Using the mass flow of steam, the steam properties at the point and the cross sectional flow area based on the number of tubes and their diameter, the velocity and Reynolds number of the flow can be calculated.

The Reynolds number and Prandtl number are used in the Dittus Boelter correlation for forced convection to find the heat transfer coefficient. The heat transfer is then calculated using the

temperature difference and the internal surface area of the discrete metal element. The internal area is based on the number of tubes in the control volume and their internal diameter with a length equal to the total tube length divided by the number of elements along the tube.

A transient energy balance of the discrete steam volumes are calculated at each point. The calculation is iterative to solve for the steam temperatures, the metal temperatures and the heat transfer rates ($\dot{Q}_{hx}$ and $\dot{Q}_{tbix}$ refer Figure 73). Once the level and vapour flow boundary values are available from the LTM, the system of equations for the localised boiling model are solved independently of the LTM. The resulting heat transfer is then transferred back to the LTM.

The sum of heat transfer calculated between the discretized steam volumes and the inner metal elements is used in the calculation of the energy balance for the larger control volume of the LTM as depicted in Figure 74. The discrete steam volume and metal temperature calculation is a sub calculation of the main LTM calculation.

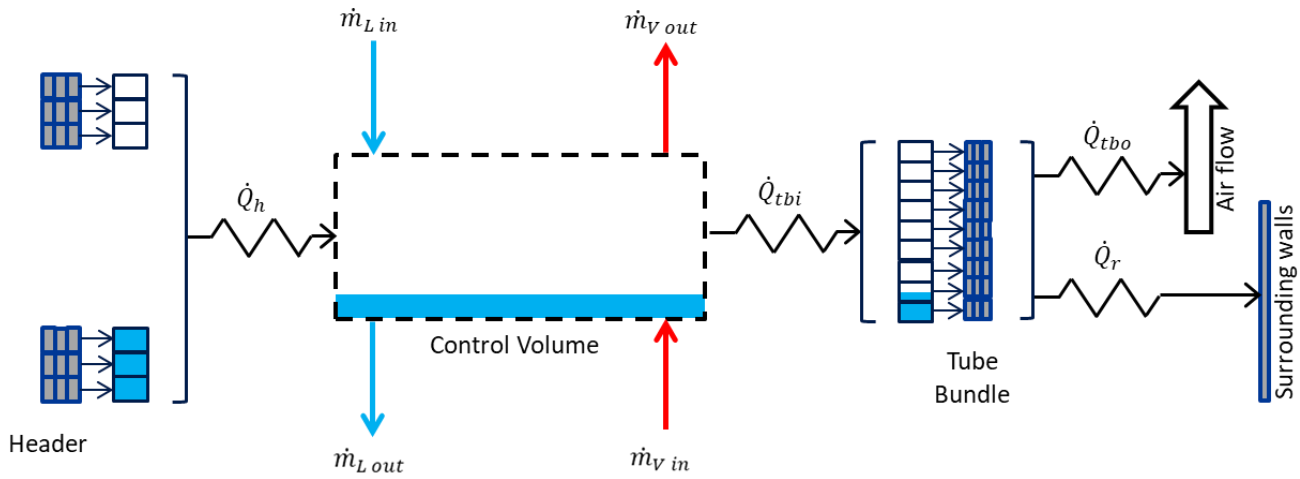


*Figure 74. Modified LTM configuration that includes local boiling effects*

The metal volumes on the outside of the tube bundle are exposed to convection and radiation from the gas stream. An assumption of uniform heat transfer is assumed for the discrete metal elements based on the calculation of a heat transfer rate using the average outside metal temperature of the tube bundle.

Table 5. Heat transfer considered in the LTM

| **Type** | **Method** |
|---|---|
| Headers internal, Dry, $\dot{Q}_h$<br>Tube bundle internal, Dry, $\dot{Q}_{tbi}$ | The greater of combined free and forced convection, Morcos and Bergles [110]:<br>$$Nu_D = \left(4.36^2 + \left(0.055\left(\frac{GrPr^{1.35}}{Pw^{0.25}}\right)^{0.4}\right)^2\right)^{\frac{1}{2}}$$<br>Or forced convection, Dittus Boelter correlation [107]:<br>$$Nu_D = 0.023Re_D^{0.8}Pr^n$$<br>with $n$ equal to 0.4 for the heating the fluid |
| Headers internal, Wet, $\dot{Q}_h$<br>Tube bundle internal, Wet, $\dot{Q}_{tbi}$ | Nucleate pool boiling, Rohsenow correlation [40] :<br>$$Nu = \frac{Ja^2}{C_{nb}^3 Pr_l^m}$$<br>With $C_{nb} = 0.013$ and $m = 2$.<br>Limited to a maximum heat flux calculated using Kutateladze [122] and Zuber [123]:<br>$$q_{max} = C_{max}h_{fg}\left[\sigma\rho_g^2(\rho_l - \rho_g)g\right]^{\frac{1}{4}}$$<br>Beyond the maximum, the transition heat flux is estimated by linearly interpolating down to the minimum film boiling heat flux [125] :<br>$$q_{min} = C_{min}\rho_g h_{fg}\left[\frac{\sigma g(\rho_l - \rho_g)}{(\rho_l + \rho_g)^2}\right]^{\frac{1}{4}}$$<br>Where $C_{min}$ = 0.09 for large horizontal surfaces. Beyond the minimum, film boiling is assumed by the Frederking and Clark correlation [124] :<br>$$\bar{h} = 0.15\left[\frac{(\rho_l - \rho_g)gh'_{fg}k_g^2}{\upsilon_g(T_w - T_{sat})}\right]^{\frac{1}{3}}$$ |
| Tube bundle external, $\dot{Q}_{tbo}$<br>$$h_{cr} = h_c + \varepsilon\sigma\frac{T_m^4 - \bar{T}_g^4}{T_m - \bar{T}_g}$$<br>$$\dot{Q}_{tbo} = h_{cr}A(T_w - T_g)$$ | Forced convection over tube bundle, Churchill and Bernstein [97]:<br>$$\overline{Nu_D} = 0.3 + \frac{0.62Re_D^{\frac{1}{2}}Pr^{\frac{1}{3}}}{\left[1 + \left(\frac{0.4}{Pr}\right)^{\frac{2}{3}}\right]^{\frac{1}{4}}}$$<br>$$\overline{Nu_D}^{10+} = \varphi\overline{Nu_D}$$<br>Radiation to ash in the gas flow – assumed emissivity, ε = 0.1. |

| | |
|---|---|
| Tube bundle radiation to walls, $\dot{Q}_r$<br>$\dot{Q}_r = A_1\mathcal{F}_{12}(\sigma T_1^4 - \sigma T_2^4)$ | Radiation to walls using projected area of the tube bundle and emissivity of 0.8:<br>$A_1\mathcal{F}_{12} = 0.8A_{projected}$ |

## 7.3 Mass flow rates and their respective enthalpies

### 7.3.1 Principles

The liquid mass flow rate from one control volume to the next is determined by the liquid level in the upstream control volume. If the level is below the height of the specified overflow, then the liquid flow rate is assumed to be zero. If the height is above the specified overflow height, then it is assumed that the volume of liquid above the overflow transfers to the downstream control volume (Refer Figure 75). In reality it would take a finite amount of time for the liquid to flow from one zone of the superheater to another; however this assumption avoids the details required for solving the momentum equation for the liquid flows. The liquid flow instantly transfers to the downstream control volume without any pressure losses or time delay.

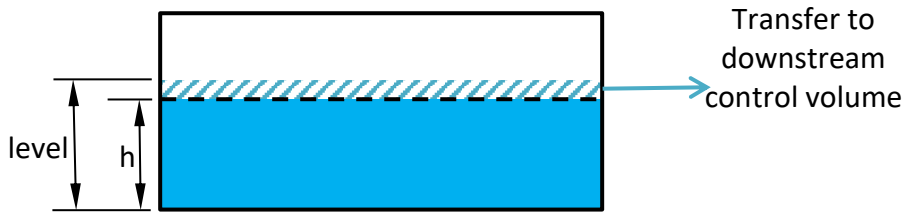


*Figure 75. Liquid flowrate to downstream control volume*

This method of calculating the liquid flows is based on the level in the control volume:

$$if\ level > h\ then\ \dot{m}_L = \frac{(level-h)V\rho_L}{t}\ else\ \dot{m}_L = 0 \qquad (129)$$

Where $level$ is the volume fraction of liquid in the control volume, $h$ is the specified overflow fraction, $V$ is the volume of the control volume, $\rho_L$ is the density of the liquid phase and $t$ is the time step size.

The level in the control volume from the previous time step is used as a starting point for the new time step. Once the new level has been calculated, the liquid overflow rate must be updated and the calculation iterated to obtain convergence.

The enthalpy of the liquid that overflows is assumed to be the enthalpy of saturated water at the new time step pressure. The boundary values at the separator are specified in terms of a mass flow rate of liquid and the temperature. This temperature must be saturated or subcooled for the overflow to be liquid. Hence the model assumes saturated liquid if the specified temperature boundary condition exceeds the saturation temperature at the pressure of the system at the time.

Another boundary value included in the model is the mass flow of vapour leaving the superheater at the separator. This allows for the reverse flow of steam that is being condensed at the sub cooled liquid interface in the separator vessels. The enthalpy of the vapour leaving the system is determined by the state of the fluid in the control volume/s connected to the separators. If the state is superheated, then the pressure and temperature in the control volume are used to determine the enthalpy from the steam tables. Otherwise, the state is saturated and only the pressure is required to determine the saturated vapour enthalpy.

The model solves for the vapour flow rates between the control volumes. The principle is that the pressure in all the control volumes should be equal. Thus after the heat transfer, liquid flow rates and boundary conditions have been taken into account, the solver finds the combination of vapour flows that give the same pressure in all the control volumes.

This assumption again negates the need for solving the momentum equation. Besides simplifying the model, another advantage is that even small vapour flows can be easily calculated. Typically with a large system at low flow rates, it is difficult to solve the momentum equation. The LTM avoids this problem.

The relative magnitude of the vapour flow compared to normal operating conditions is low. Thus, the pressure drops are likely to be small considering the relatively large cross sectional areas available for flow. Potentially the momentum equation could be used to calculate the vapour flows; however, even for the maximum flows observed, the pressure drop required to drive the vapour flows are insignificant.

The mechanism for solving the vapour flows is by a sub-routine or function that takes guess values of vapour flows as input and returns the pressure in each control volume as output. Thus the function can be called multiple times with updated guess values that converge on the solution.

Within the function, an enthalpy is assigned to each of the input vapour flows. The flows can be positive or negative and thus the direction of flow is considered when assigning the enthalpy. The gas enthalpy of the confirmed upstream control volume is used for each flow. The vapour flow may be superheated or saturated depending on the state of the upstream control volume.

### 7.3.2 Parallel flow paths

The above discussion is relatively easily implemented for control volumes aligned in series. However, in the real superheater, there is interconnection of the different legs at different points. Hence parallel control volumes are required with liquid and vapour flows that can cross over from one leg to another.

Considering liquid flows, calculation of the flow path by gravity as liquid overflows from one part of the superheater to another is complex and requires detailed knowledge of the internal shapes of the pipes and headers. Consider also that the hot condition of the boiler has a different shape to the cold condition and thus slopes of pipes do change between hot and cold positions. Hence accurate calculation of how the flow splits is not possible.

In order to proceed with modelling of parallel flow paths, the liquid flow split between two interconnected downstream control volumes in the LTM is specified by the user. The parameter is defined as a fraction per downstream control volume, the sum of which must equal one.

The vapour flows for parallel paths are calculated in the same way as they are for the series connection. However, additional unknowns are introduced because the vapour flow leaving a control volume splits into multiple streams. Each interconnection or split effectively becomes another node in the network. The interconnection nodes have no volume and thus a simple mass and energy balance can be used to solve for the flows and their enthalpies.

The mass balance is incorporated in the overall vapour flow and pressure solving routine. The mass balance at each interconnecting node is driven to zero. This occurs at the same time that the solving routing finds the set of vapour flows that result in equal pressure in all the control volumes.

Within the sub-routine or function, the energy balance of each interconnecting node is used to assign enthalpies to the vapour flows. This ensures that the correct vapour flow enthalpy is used in the calculations related to the control volumes.

## 7.4 Property relationships

Once the density and enthalpy of each control volume have been calculated, the state of the fluid within the control volume can be determined. The structure of steam tables does not allow direct determination of the state of the fluid from the density and the enthalpy. The steam tables require a search routine that iterates based on other properties, such as pressure and density to determine the values that match the required density and enthalpy.

An alternative is the rate based formulation of the equation of state [129]. The rate based formulation allows for the development of a time history of system pressure, which can then be

integrated for specific time steps to give the pressure value at discrete moments in time. The rate based formulation for a homogeneous two phase fluid in equilibrium is given as follows:

$$\frac{dp}{dt} = G_1(p,x)\frac{d\rho}{dt} + G_2(p,x)\frac{dh}{dt} \tag{130}$$

Where

$$G_1(p,x) = \frac{(h_g - h_f)[xv_g + (1-x)v_f]^2}{\left[x\frac{\partial h_g}{\partial p} + (1-x)\frac{\partial h_f}{\partial p}\right](v_g - v_f) - \left[x\frac{\partial v_g}{\partial p} + (1-x)\frac{\partial v_f}{\partial p}\right](h_g - h_f)} \tag{131}$$

$$G_2(p,x) = \frac{(v_g - v_f)}{\left[x\frac{\partial h_g}{\partial p} + (1-x)\frac{\partial h_f}{\partial p}\right](v_g - v_f) - \left[x\frac{\partial v_g}{\partial p} + (1-x)\frac{\partial v_f}{\partial p}\right](h_g - h_f)} \tag{132}$$

This equation provides the unknown rate of change of pressure in terms of the known rates of change of density and of enthalpy. The constants, $G_1(p,x)$ and $G_2(p,x)$ require iteration to determine since they depend on the pressure, p, and quality, x, of the fluid.

Fick [129], provides tables of approximate functions for all the quantities required to determine $G_1(p,x)$ and $G_2(p,x)$. The approximate functions all use pressure as the independent variable and are divided into ranges for accuracy. The functions include the gas and liquid enthalpies and specific volumes, $h_g$, $h_f$, $v_g$ and $v_f$respectively and the rates of change of those quantities with pressure ($\frac{\partial h_g}{\partial p}$, $\frac{\partial h_f}{\partial p}$, $\frac{\partial v_g}{\partial p}$, $\frac{\partial v_f}{\partial p}$). The accuracy of the approximate functions and the rate method is reported to be within 1%.

These approximate functions were coded to enable them to be used in the LTM. The functions were verified by comparing the error between the function and the steam table value with the error plots found in Fick [129].

The rate based method was implemented and used in the LTM for saturated conditions. This provided a faster method of determining the state of fluid from the density and enthalpy values compared to the steam table lookup. The rate based formulation also assisted with stability at the point where the fluid became saturated.

For superheated conditions, the steam tables were used to determine the state of the fluid. This was due to the work of Fick [129] not having extended the rate based method to superheated conditions.

## 7.5 Solution scheme

The solution procedure is shown schematically in Figure 76. The procedure is repeated for each time step. The first part of the procedure solves the localised boiling model. The values for the liquid level and vapour mass flow are sourced from the previous timestep of the main LTM. Thus the calculation is explicit in that respect.

The calculation starts by determining the discrete steam volume temperatures before calculating the heat transfer coefficients for the heat transfer from the metal to the steam. Using the heat transfer coefficients, the heat transfer rates are calculated. Next, the metal temperatures and gas temperatures at the end of the time step are determined. This process is repeated until the temperatures have converged to within the specified convergence tolerance.

The liquid level in each control volume is then considered to determine the liquid overflow rate (if any) from the control volumes. These are summed per control volume. The energy flow of each is also summed per control volume for ease of use in computing the mass and energy balance of the control volumes.

Next, the solving routine determines the vapour flows required to obtain equal pressures in all the control volumes. A set of guess values for the vapour flows is assigned and a set of non-linear equations is created that describe the pressure equality criteria. The set of equations are solved using a Newton-Raphson solver that utilises matrix algebra for finding the next set of values. The solver iterates until the change in vapour flows is less than the convergence criteria.

In the process of solving the pressures, the density and enthalpy in each control volume are found. This allows the quality and the level in each control volume to be determined.

The LTM was coded in Scilab and a copy of the program is available in Appendix G.

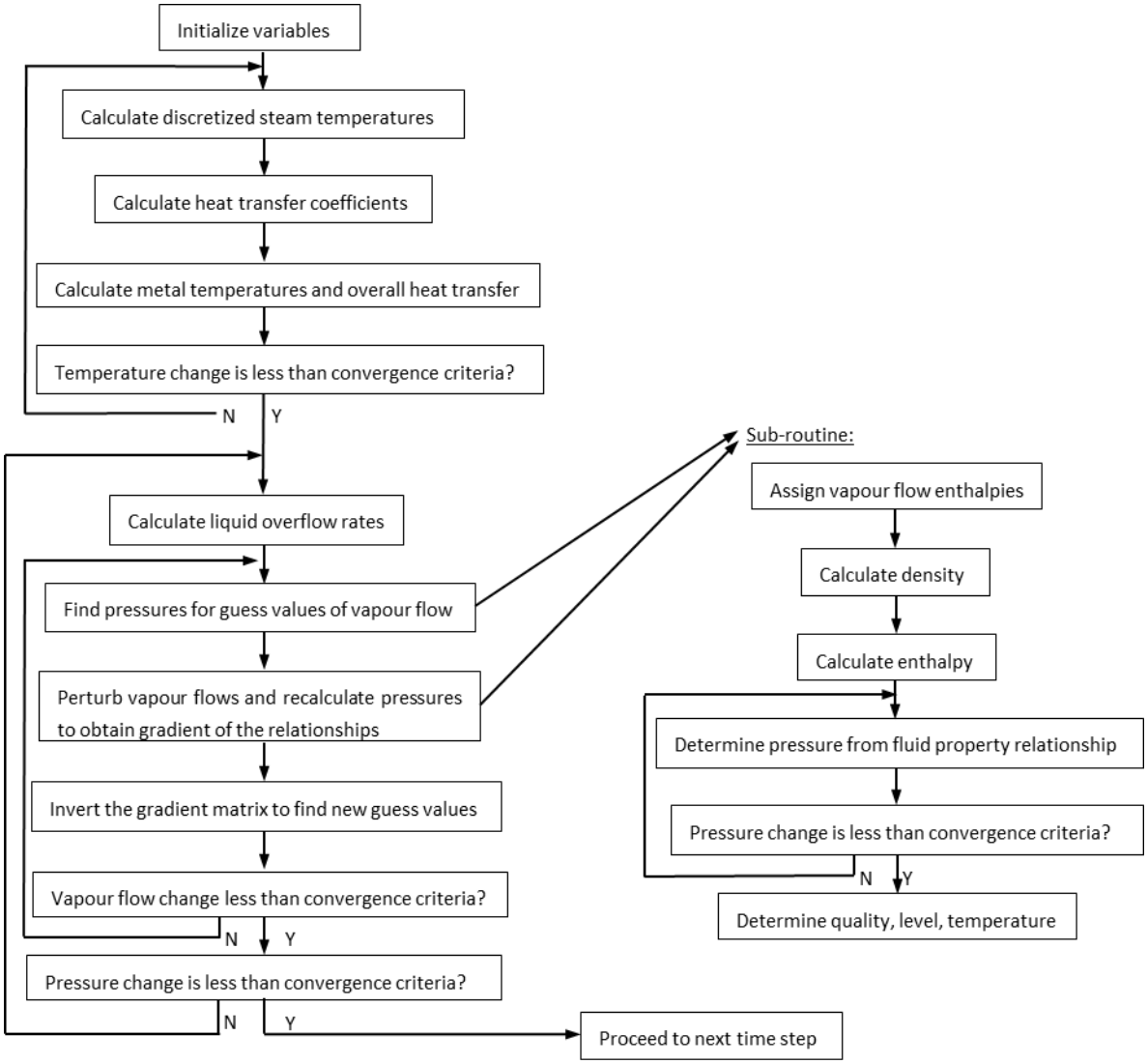


*Figure 76. Schematic of the solution procedure used in the LTM*

Besides the limitations imposed by the underlying theoretical assumptions, the model as implemented in SciLab is limited. Care is required in configuring the control volumes and the connections between them.

The minimum number of control volumes is two. The maximum liquid level in any control volume cannot equal or exceed a level fraction of one. There is no hard limit in the coding to prevent levels exceeding a fraction of one, but if it occurs then the results are no longer valid.

As a result of the liquid fraction being less than one in all cases, the program is unable to achieve subcooled conditions in any control volume. There is always a small fraction of steam in the control volume in thermal equilibrium with the liquid.

The liquid phase can only overflow in the direction specified. This means that reverse flow of liquid cannot occur in the LTM model. For cases where reverse flow was required, a specific routine had to be written and included in the code.

Where multiple control volumes are connected, the interconnection mass and energy balance must be specifically configured. The program cannot detect and define the matrices required. This implementation of the solving routine affects the maximum number of interconnections that can realistically be solved.

## 7.6 Verification

### 7.6.1 Mass and energy conservation

In order for the model to be valid, the total mass must be conserved. This was verified by using the model to perform a calculation and then comparing the change in total mass of fluid in the system to the amount of separator overflow specified and vapour outflow specified. This was done at each time step and the error was less than $10^{-12}$ kg.

Similarly, it was verified that the model conserves energy by comparing the change in total energy per time step to the amount of heat transfer that occurred as well as the energy gain and loss due to inflow and outflow. The error was less than $5 \times 10^{-5}$ kW.

### 7.6.2 Comparison with Flownex

After successful verification of the LTM compared to two basic Flownex cases (Refer Appendix H), the LTM was compared to the Flownex model used in section 6.3 above. The LTM was configured with only two control volumes, namely the superheater and the main steam control volume. For the purposes of verification, the heat transfer coefficient on the inside of the tubes and headers was set to 20W/m$^2$ K for both the LTM and the Flownex models. This avoided differences in calculation of the heat transfer coefficient in the two models due to different fluid properties and also the effects of different temperatures. The LTM uses a lumped parameter assumption for the metal temperatures whereas the Flownex model has discretised tube and header walls. In this case the minimum number of two elements were used in the Flownex model.

The Flownex model and inverse method (section 6.3.5) were applied to calculate a separator overflow profile to use as an input boundary condition for the LTM as shown in Figure 77 a). Similarly, Flownex was used to calculate the steam flow rate to the subcooled liquid interface in order to balance the pressure prior to the separator overflow occurring. Beyond 03:42:20, the steam flow was specified to be zero (Refer Figure 77 b).

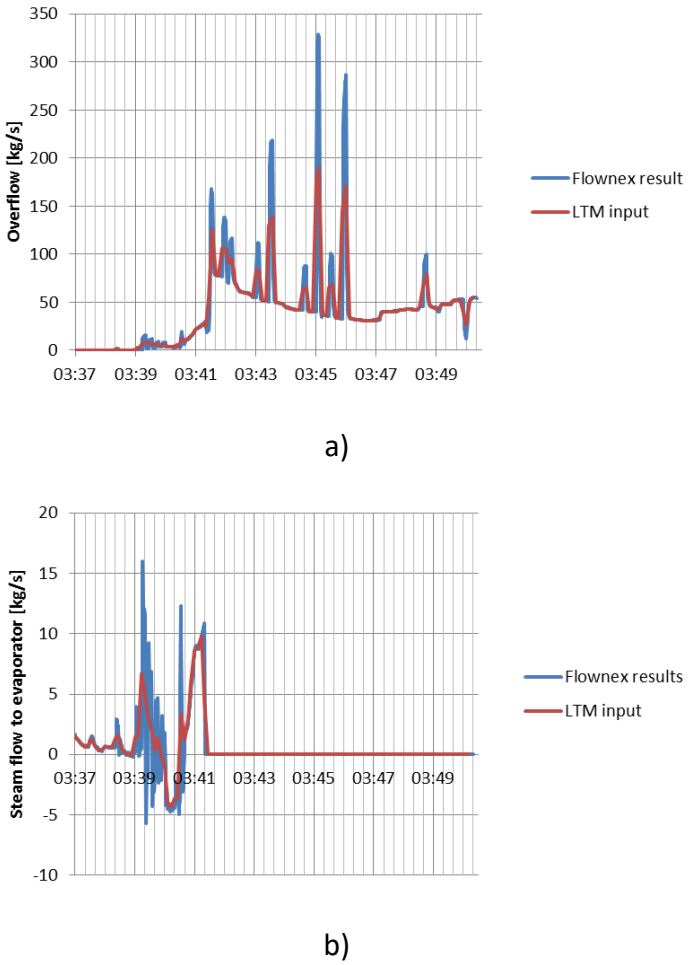


*Figure 77. Flownex results used as LTM input boundary conditions: a) Separator overflow b) Steam flow to subcooled liquid interface*

The results show that the LTM produced similar results to the Flownex model as seen in Figure 78 a) and b). Initially the LTM superheater control volume has a cooling phase which reduces the steam pressure and temperature. This had to be compensated by increasing the initial values so that the models were aligned at 03:38:40 when the comparison effectively starts.

The LTM superheater pressure deviates from the Flownex pressure at 03:43:40, 03:45:00 and 03:46:00. These deviations align with the peaks in separator overflow in the input data and indicate a difference in heat transfer on the inside of the tubes as discussed below.

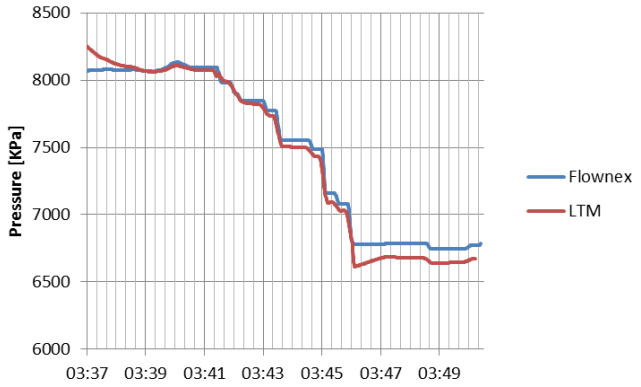


a)

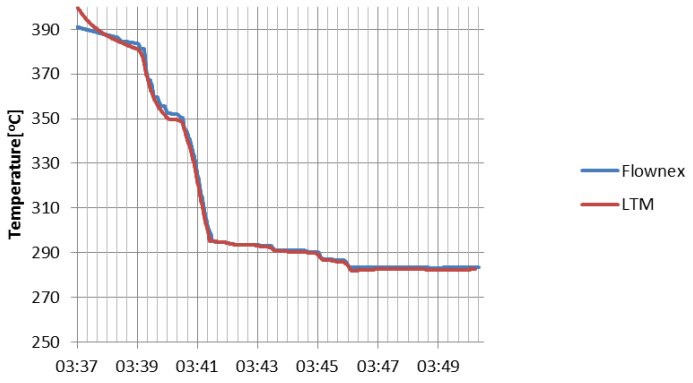


b)

*Figure 78. LTM results compared to Flownex results: a) Superheater pressure b) Superheater temperature*

In Figure 79 a) it can be seen that up until 03:41:20, the total internal heat transfer in the LTM matches the Flownex value. From 03:41:20 onwards, there is a deviation which affects the superheater pressure. Note that the control volume is saturated at that point and thus there is almost no effect on superheater temperature (Figure 78 b).

The difference in heat transfer is caused by different metal temperatures. The heat transfer per superheater stage is different between the models. The LTM only has one tube bundle heat transfer for the single superheater steam control volume whereas the Flownex model has a single control volume with two separate heat transfers for the superheater stages. This results in different metal temperatures used in the heat transfer calculations as shown in Figure 79 b).

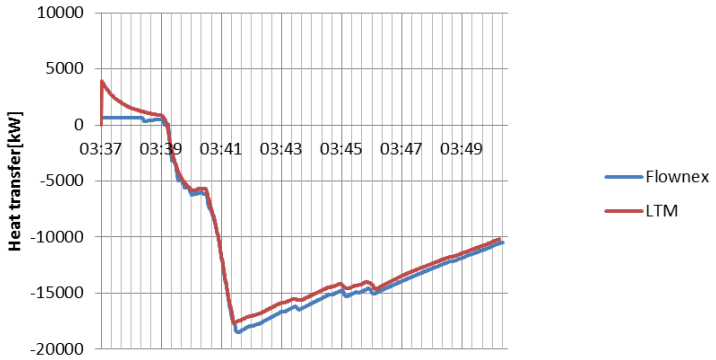


a)

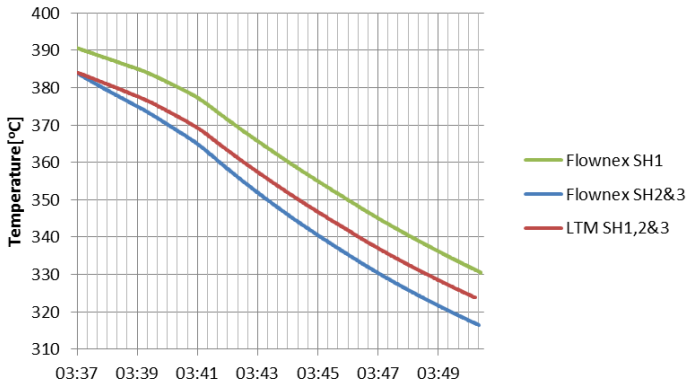


b)

*Figure 79. LTM results compared to Flownex results: a) Internal heat transfer to superheater b) Tube metal temperatures*

Besides the temperature differences, the overflow behaviour also affects the superheater pressure. In Figure 80 a) it can be seen that the levels in the LTM and Flownex are similar up until 03:46:00. At that point in time, the superheater overflows to the main steam control volume. The LTM overflow is immediate and maintains the superheater control volume at the overflow height. The Flownex model solves the momentum equation for the flow element that connects the superheater and the main steam control volumes. It thus requires a differential pressure or water level to drive the flow. This effect is amplified by the size of the flow element which is smaller than the pipe on the real plant to enable Flownex to solve for the flow more easily.

The effect of the differences in overflow behaviour of the LTM and Flownex are also evident in the main steam control volume temperature shown in Figure 80 b). The LTM methodology results in a large instantaneous overflow into the main steam system and immediately drops the steam temperature to saturation at 03:46:00. The Flownex model predicts a drop to saturation over two minutes.

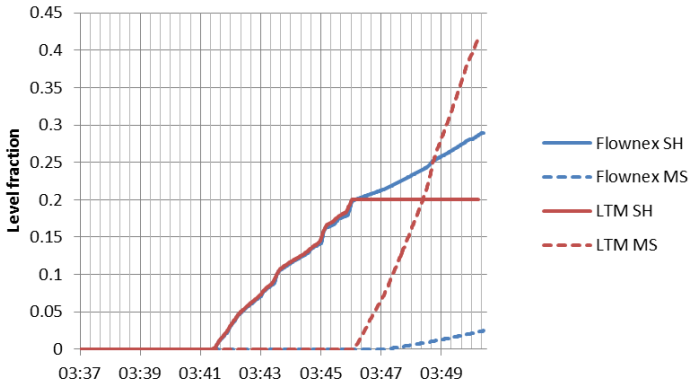


a)

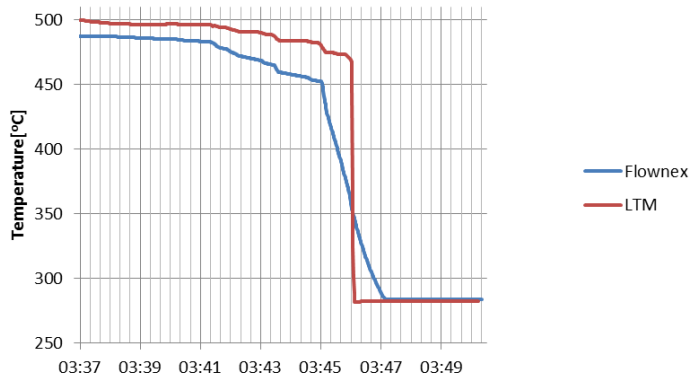


b)

*Figure 80. LTM results compared to Flownex results: a) Levels b) Main steam control volume temperatures*

In summary, the comparison of the LTM and Flownex highlight the different methods employed by the two approaches; however, the comparison also verifies that the LTM produces valid results for the simplified model of the superheater. Thus, the LTM is considered to be verified by comparison with the Flownex model.

## 7.7 Application

The LTM was applied to Case A of the plant data (Refer Appendix C). A different approach to the Flownex controllers discussed in section 6.3.5 was utilised for the application of the LTM to the case study (See Table 6). The LTM used the measured separator overflow calculated from the plant measurements as a boundary condition and calculated the required exit steam flow to balance the superheater pressure to the measured pressure. Thus the evaluation of the LTM results is performed by comparing the calculated exit steam flow to the 'measured' flow of steam condensing at the subcooled liquid interface.

*Table 6 : Comparison of the application of the LTM and the Flownex model*

| | **LTM** | **Flownex** |
|---|---|---|
| Separator liquid overflow | Boundary condition | Determined by the model (Calculated) |
| Steam flow rate leaving superheater towards evaporator | Determined by the model (Calculated) | Boundary condition |

### 7.7.1 Grid independence study

A comparison of the LTM analysis of three levels of discretisation of the superheater, namely, four, eight and sixteen control volumes, was performed and the results are given in Appendix I. It was found that the eight control volume model was the most appropriate for the level of detail available. The eight control volume model provided better results than the four control volume model and required less effort than the sixteen control volume model to configure and run. The increase in discretisation from eight to sixteen control volumes did not improve the results because the phenomenon of reverse flow of liquid in the superheater was already captured in the eight control volume model.

The interconnection of each leg and stage of the superheater as well as the gas path interaction is shown schematically in Figure 81. The grey blocks representing superheater tube bundles are numbered to show the control volume numbers in the sixteen control volume model. The blue headers can be seen at inlet and outlet of each stage. The separator vessels are numbered

separately at the top of the figure. It can be seen that the path from Separator 1 and Separator 4 connects to control volume 2 and 14 at stage 3. Similarly, the path from Separator 2 and Separator 3 connects to control volume 6 and control volume 10 at stage 3. These two paths do not interconnect and this is the reason why it is important to separate the superheater into at least eight control volumes to capture this detail. Using eight control volumes, the four superheater legs are grouped into two groups of two. The gas paths cannot be accurately represented with eight control volumes, but this did not cause significant errors.

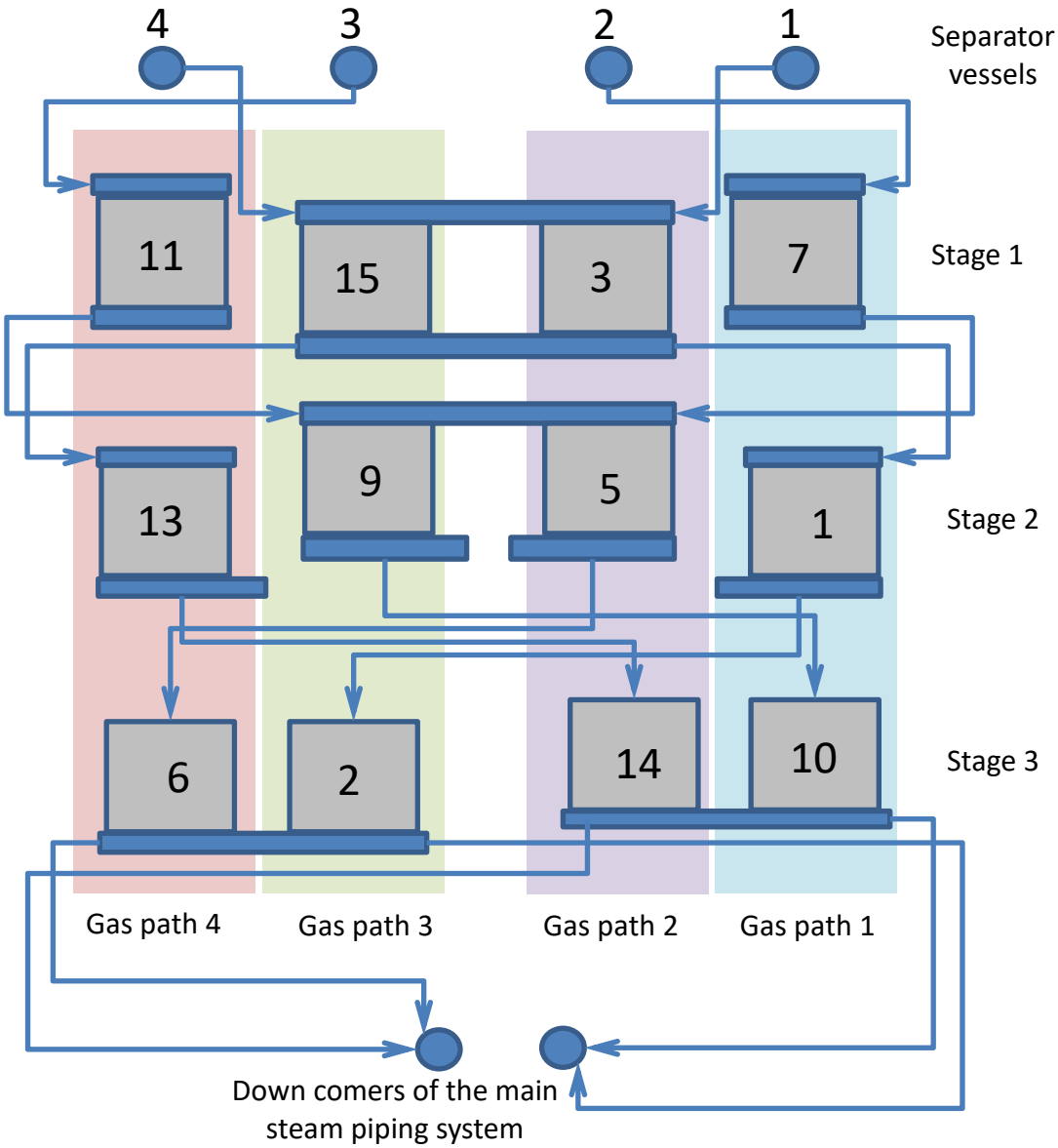


*Figure 81. Configuration of the superheater showing control volume numbers and gas path allocation*

## 7.7.2 LTM Results

The results presented in this section include the localised boiling model described in section 7.2. The complete model was applied to the same case study A using the eight control volume level of discretisation (Refer Figure 82). The assumed overflow heights, h, are shown on each applicable control volume in Figure 82 and the liquid overflow split ratios are given at the relevant blue arrows.

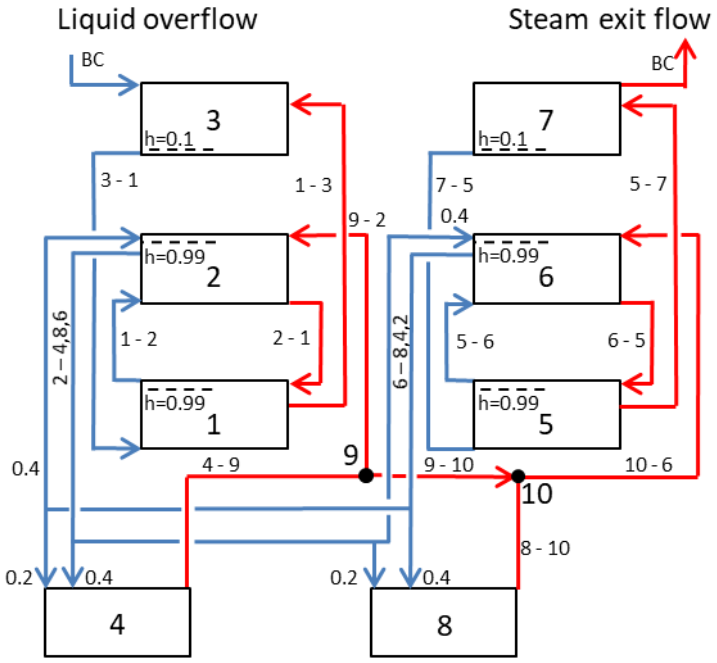


*Figure 82. Application of the LTM to an 8 control volume model of the superheater*

For the calculation of internal heat transfer, each tube bundle was discretized into 100 elements along the length of the tubes and three layers through the thickness of the tube wall. The headers for each control volume were similarly discretized into 20 elements along the length and six layers through the wall thickness.

The separator liquid overflow boundary condition was specified and the required steam exit flow was determined in order to match the calculated pressure to the measured pressure (Refer Figure 83). For comparison purposes, the results without the localised boiling model, calculated using the area weighted average Morcos and Bergles correlation and lumped metal temperatures, are also shown.

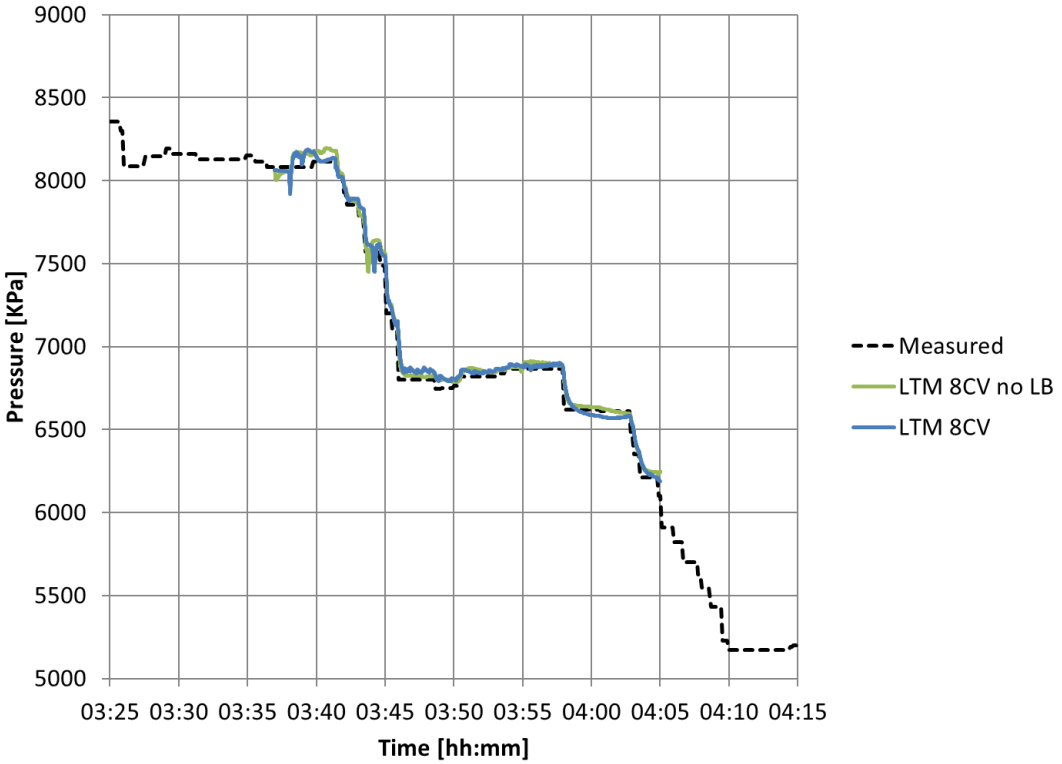


*Figure 83. Calculated superheater pressure with localised boiling model and without*

The calculated steam exit flow compared to the measured steam flow to the subcooled liquid interface shows good agreement until 04:00 (Figure 84 and Figure 85). At 04:00 the heat transfer to the steam is inadequate to sustain the steam exit flow and even causes the exit flow to become negative indicating that steam had to be supplied to sustain the pressure. Prior to 04:00, the steam exit flow was erratic but definitely followed the measured value.

While previously the peaks in exit flow were mainly caused by the steps in measured pressure, in this case the spikes are also caused by sudden increases in heat transfer. As the liquid level increases past the interface between metal elements it causes boiling heat transfer in the next element. This rapidly releases the heat in that element and leads to increases in superheater pressure and the erratic behaviour of the steam exit flow. Up until 04:00, the performance of the LTM with localised boiling was better than the model without.

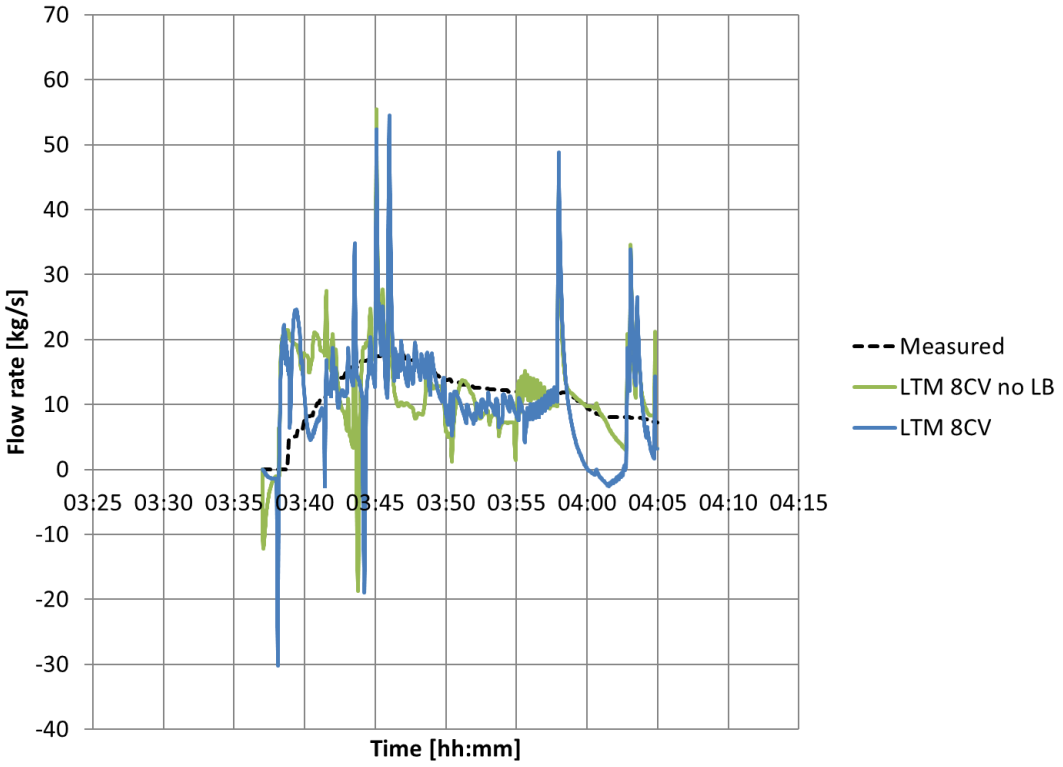


*Figure 84. Steam exit flow results – 8CV with localised boiling model and without*

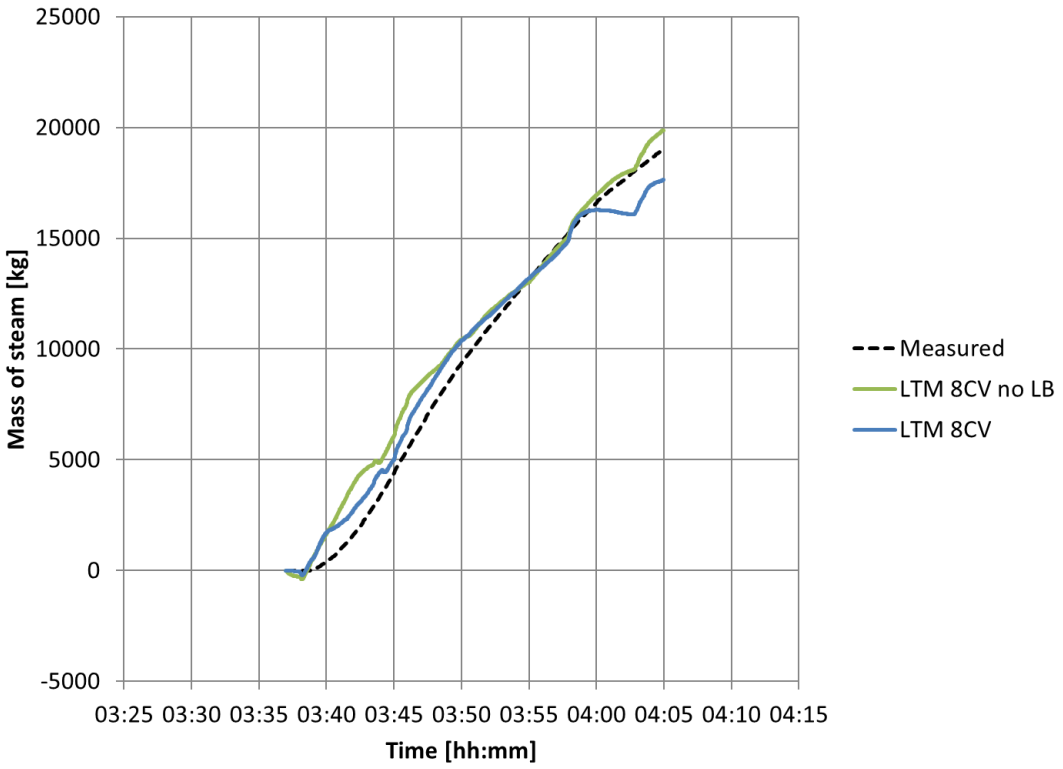


*Figure 85. Integrated steam exit flow results – 8CV with localised boiling model and without*

The liquid level tracking performance of the model with localised boiling was similar to the model without as shown in Figure 86. The liquid level determines how much metal has been quenched, Thus the height at which control volume three overflows was set to 0.1. This effectively assumes that 10% of the metal was quenched before the liquid flowed down to the next stage.

Another implication of this assumption is that 10% of the liquid volume was retained in the tubes of that stage. Although this is unlikely to occur in practice, for continuous separator overflow, the liquid has a residence time in the Superheater 1 as it flows through which can be accounted for by a certain retained level in the model. On the real plant, the actual quantity of liquid in a tube bundle during a flow-through situation is unknown.

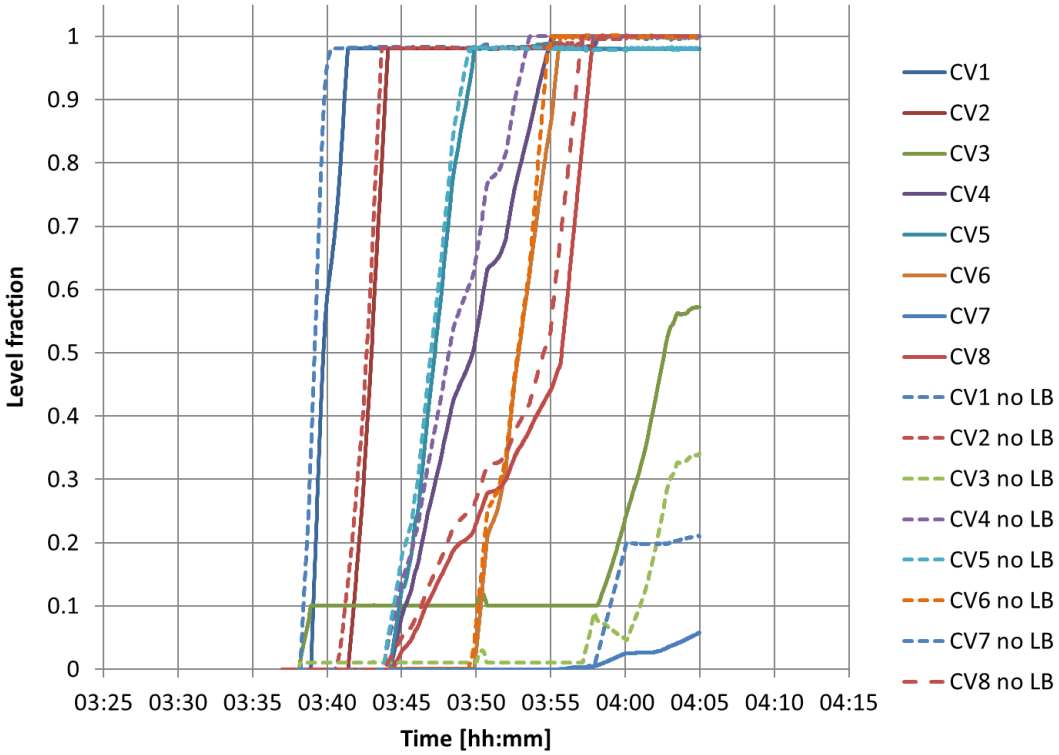


*Figure 86. Liquid levels with localised boiling model and without*

The steam temperatures calculated by the models with and without localised boiling provide similar results to each other as shown in Figure 87 and they correlate with the measured values although tending to drop to saturation sooner than the measured values do.

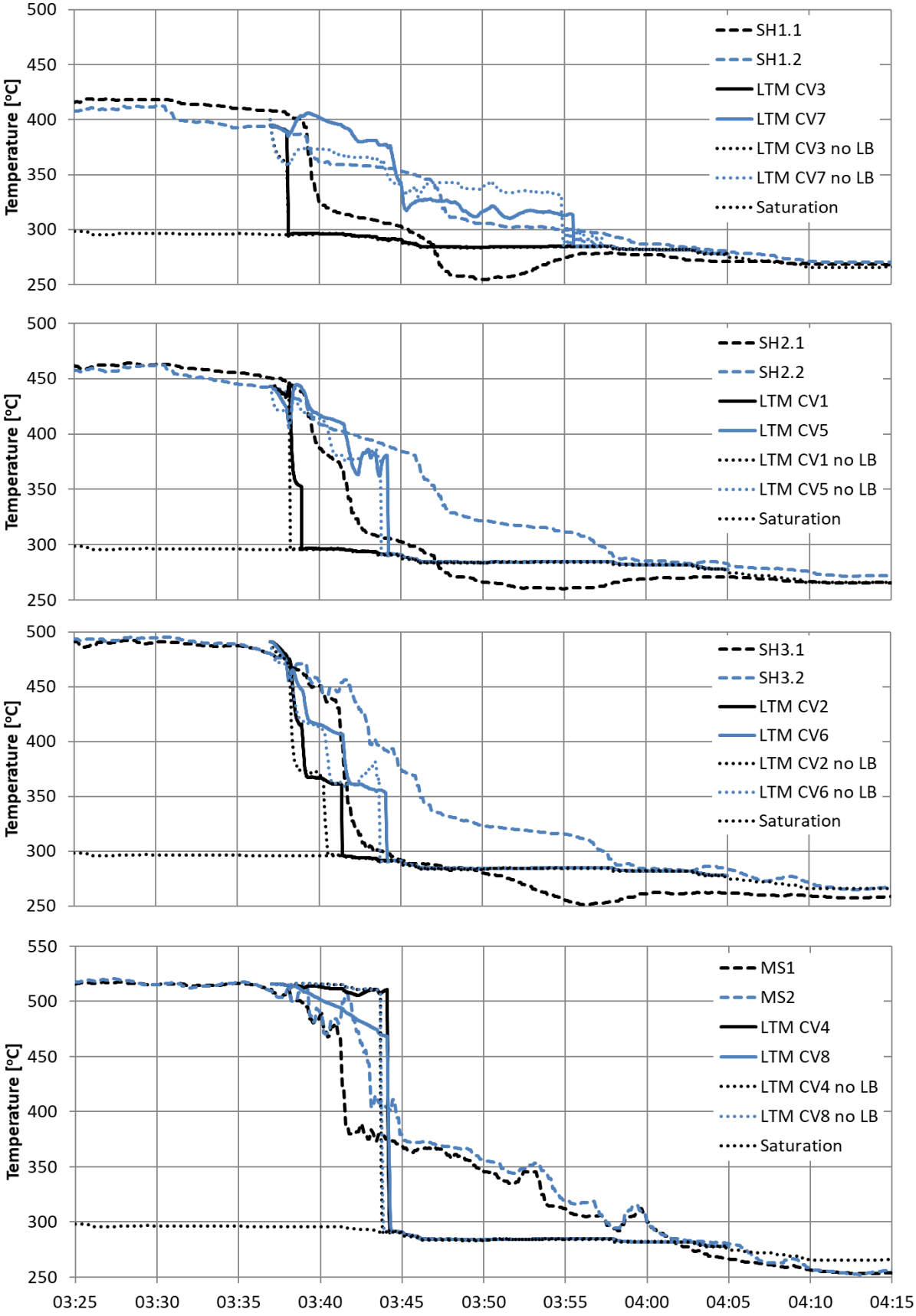


*Figure 87. Fluid temperature results – 8CV with localised boiling model and without*

In order to compare the metal temperatures of the localised boiling model with the lumped model, the matrix of metal temperatures for the headers and tube bundles associated with each control volume were averaged. The results are shown in Figure 88 and Figure 89 for the tube bundle temperatures and header temperatures respectively.

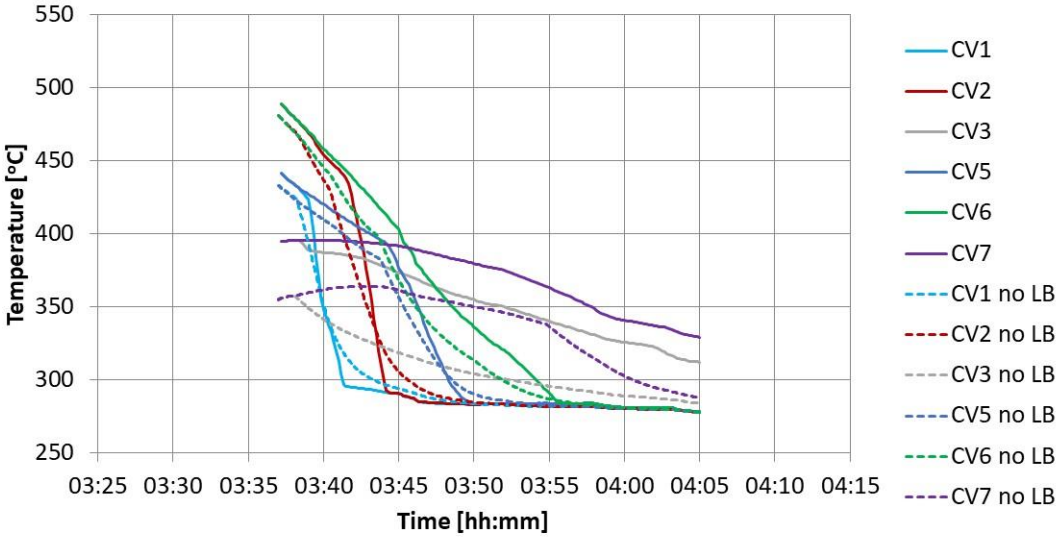


*Figure 88. Tube bundle average temperature results – 8CV with localised boiling model and without*

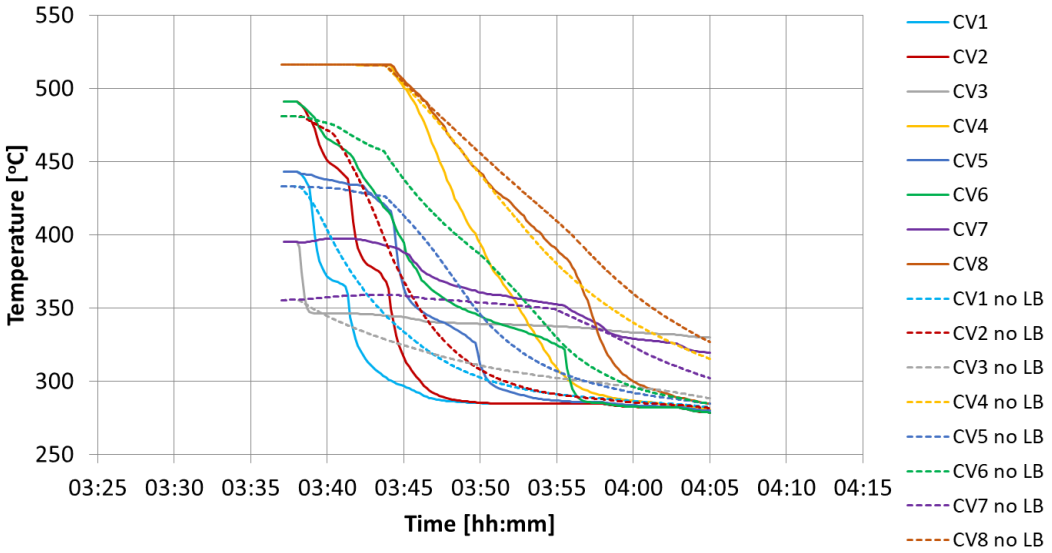


*Figure 89. Header average temperature results – 8CV with localised boiling model and without*

The rate of change of average metal temperature drop in the model with localised boiling is higher than the lumped model for most cases. This is due to the higher heat transfer rates. It is also evident that the initial value for control volumes three and seven was not the same in the runs with localised

boiling and without. The initial temperature of the header and tube bundle was assumed to be 395°C for the run with localised boiling compared to 355°C for the run without localised boiling.

The change was intended to improve the fluid temperature alignment with measured temperatures in the early stages of the simulation as seen for Superheater 1 in Figure 87. It was also intended to reduce the heating of Superheater 1 in the initial stages of the simulation as seen by the purple lines in Figure 88.

In reality, the temperature of the headers and tube bundle is not known at the start of the run. The conditions are transient at that point because the firing and steam flow has recently been shut down and there are only steam inlet and outlet temperature measurements available from which to estimate the initial temperature.

The change had an adverse effect on the gas outlet temperatures (Figure 90). Although the slope of the line was marginally improved to match the measured values, the additional initial temperature caused an offset of about 25°C which persisted for the duration of the simulation. This aligns with the metal temperature for control volume three and control volume seven which also sustained an offset for the duration of the simulation (Figure 88).

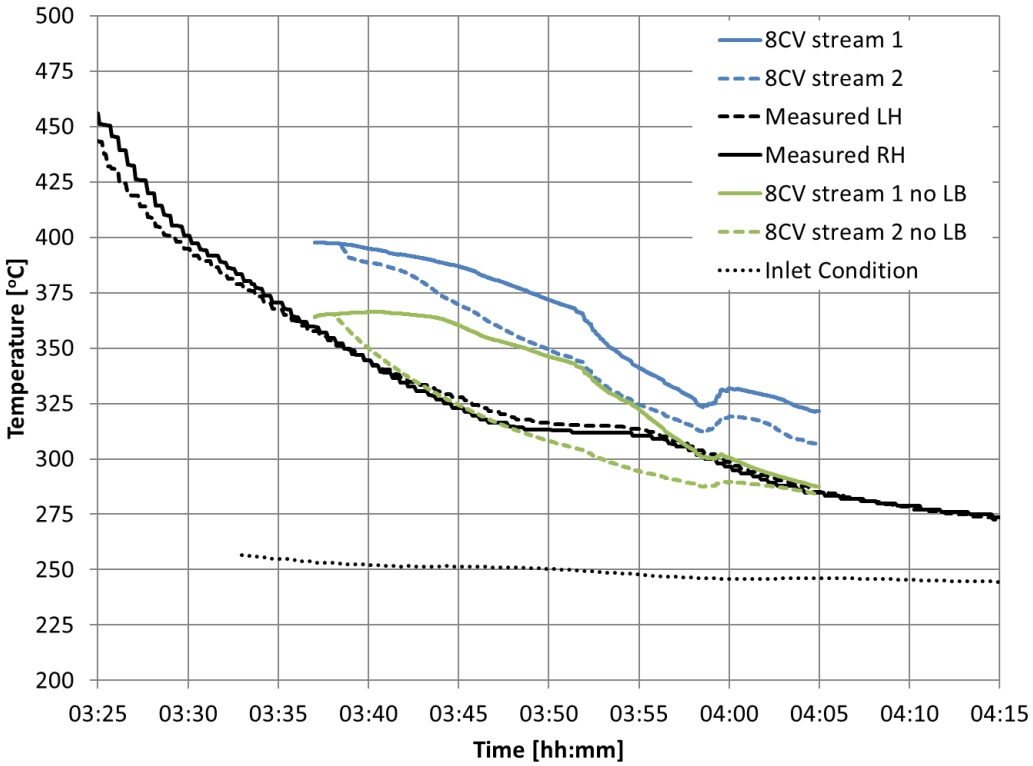


*Figure 90. Gas outlet temperature results – 8CV with localised boiling model and without*

The LTM with localised boiling does not provide significant improvement in the results. The outcome is similar to the LTM using the Morcos and Bergles correlation and the lumped metal temperature approach.

The duration for running the LTM with localised boiling case presented in the results above on a single processor was 33hours. This is largely due to the number of iterations required to find a uniform pressure in all the control volumes. The running time of the same case calculated using the LTM without localised boiling took 8hours. Thus the localised boiling LTM has a significant disadvantage in the processing effort required.

Although the LTM provides an overall analysis of the event, the results do not exactly match the plant data. However, the LTM enables the behaviour of the plant to be explained and the liquid level to be estimated.

In order to achieve better accuracy of the LTM it would be necessary to delve deeper into the detail of the superheater and the quenching event. The following areas could be considered to improve the accuracy:

- Model and calculate the flow of liquid in to the various control volumes. Such details would only be available from detailed three-dimensional geometry and computational fluid dynamics of the open channel type liquid flow. The flow path of the water needs to be accurately predicted in order to capture the detail of the metal quenched at any point in time.
- Discretise further – the superheater can be discretised into more control volumes with associated tube bundles and headers. This only makes sense once the path of liquid is known. Most likely parts of the tube bundles that are similarly quenched should be grouped together in the larger control volumes.
- Include subcooled conditions – The existing LTM steam control volumes are unable to become subcooled. In reality, the subcooled liquid overflowing from the separator does cause cooling of the superheater tubes to subcooled temperatures in certain areas. This enables the release of additional energy from the metal in the real system.

## 7.8 Localised liquid levels during quenching

The LTM considers the global level in the superheater. This enables identification of the components that were quenched. However, it does not determine the localised liquid levels which should be investigated especially after repeat quench events.

This section describes how to obtain estimates of the local liquid levels and is part of the methodology discussed in chapter 3 to determine the through-wall temperature gradients. At this point in the methodology, the root cause of quenching has already been identified and the focus has shifted to finding the damage that may have been caused.

In the case of quenching caused by condensation or quenching caused by separator overflow, some information from the modelling of the liquid level in the control volume representing the superheater steam space will be available. In other cases, such as an attemperator valve that leaked water, an overall level in the superheater will not be known, unless an estimate from plant measurements is available or modelling has been done. The LTM can be applied in these cases.

The flow of liquid during quenching is a gravity driven flow. Water will flow from the source to lower lying pipes and headers and will accumulate at the low points of the superheater. Depending on the path, the water will come into contact with various headers, tubes and pipes at different orientations. Two main categories of flow exist – namely flow-through and flooding. These are considered below in sections 7.8.1 and 7.8.2.

### 7.8.1 Liquid level in flooding situations

In order to determine the extent of quenching in flooding situations, it is necessary to have an estimate of the level as a function of time and the detailed geometry of the superheater system. The liquid tracking model (Refer chapter 7) can be used to determine the level fraction history. This level fraction must then be interpreted as a liquid level in the detailed plant geometry.

By studying drawings of the superheater, the distribution of volume as a function of height measured from the lowest point is determined. The level fraction history can then be interpreted as an actual height of liquid in the superheater over time. All the components below this height would have been affected by quenching. By analysing the rate of increase of the level fraction, it may be possible to determine which components were affected by a rapidly increasing level and which components experienced a slower level increase.

The quenched components may be orientated horizontally or vertically. The quenching of horizontal components by flooding and the subsequent temperature gradients can be calculated by the methods described in section 8.4. For vertical components, the quench would proceed upwards

along the axis of the pipe and the full circumference would be quenched at the same time. The two dimensional analysis presented in chapter 8 cannot be used because of the steep temperature gradient along the axis of the pipe. In this case, it is recommended to perform a separate study using finite element analysis of the pipe wall with the appropriate thermal boundary conditions.

## 7.8.2 Liquid level in flow-through situations

When liquid flows from one height to a lower height under the action of gravity, it can either fill the pipe or only partially fill the pipe and maintain a free surface. In order to fill the pipe, the entrance must be flooded and in order to fill the length of the pipe, the vapour must be allowed to escape.

### 7.8.2.1 Pipes running full

Assuming that a pipe runs full, the mass flow rate can be determined using the Bernoulli equation with an additional term for the head loss due to friction [130]. It is assumed that the upstream velocity is negligible and that upstream and downstream pressure is equal due to the interconnection of the legs of the superheater. Thus, the equation can be simplified to give:

$$v^2 = \sqrt{\frac{2g(z_2 - z_1)}{1 + f\frac{L}{D}}} \tag{133}$$

The friction factor, $f$, can be obtained from the Colebrook equation or the Moody chart [130]. By multiplying the velocity with the area of the pipe and the density of the fluid, the mass flow is determined:

$$\dot{m} = \rho A v \tag{134}$$

In the case of the separator overflow that occurred at Power Station A, tubes of the Superheater 1 are likely to have run full of water when the water made its way down to the Superheater 2 (refer Figure 72). Only some tubes would have been affected and we can estimate how many would have been affected if we knew the mass flow that each tube could carry. Assuming a pressure of 8MPa in the superheater and a tube diameter of 33mm, surface roughness of 30µm, length of 81m and an elevation drop of 5m, the mass flow per tube would be 0.87kg/s. Thus, if we expect a total mass flow of 120kg/s, we can estimate that about 140 tubes of Superheater 1 were affected by quenching. These tubes would have been the first ones that the water encountered as it flowed into the Superheater 1 inlet header.

#### 7.8.2.2 Partially filled pipe flow

For horizontal pipes and headers where the liquid flows along the bottom of the pipe without filling it, open channel flow analysis is appropriate. The frictional losses at the free surface of the liquid are assumed to be negligible and are ignored. The Manning equation is derived based on the assumption of uniform flow and gives the volume flow rate in terms of the slope of the channel as follows [130]:

$$Q = \frac{A\, R_h^{\frac{2}{3}}\, S_0^{\frac{1}{2}}}{n} \tag{135}$$

$$A = \frac{D^2}{8}(\theta - sin\theta) \tag{136}$$

$$P = \frac{D\,\theta}{2} \tag{137}$$

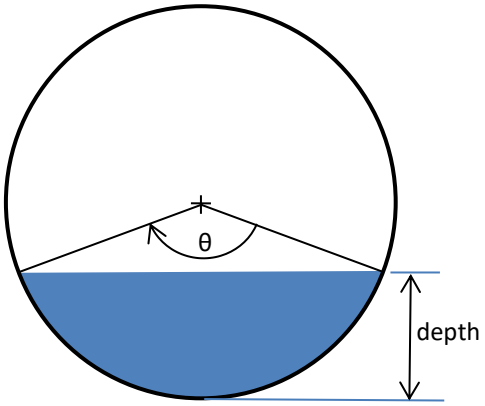


Where $R_h$ is the hydraulic radius of the flow equal to the area divided by the wetted perimeter ignoring the free surface, $S_0$ is the slope of the channel and $n$ is the Manning resistance coefficient which is taken to be 0.012 for steel surfaces. The derivation of the Manning equation assumes the depth of the flow is constant which means that the velocity is constant and the head loss of the flow is equal to the slope of the channel.

If the channel has no slope, then the depth will decrease along the length of the flow and the velocity will increase. This will cause an increase in the losses and the Manning equation is not valid in that situation. Thus, we assume that the pipe has a slope. Generally the pipes in the boiler are sloped to allow for drainage and typically a slope of 2% is used. Slopes can be obtained from drawings. However, it should be noted that the slope in the hot condition may not be the same as in the cold condition due to thermal expansion of the entire boiler. This affects the overall accuracy of the calculation.

In order to calculate a level inside a horizontal pipe, it is assumed that an estimate of the flow rate of water that quenched the pipe is known. The Manning equation can then be used together with the pipe geometry to determine the level inside the pipe.

By assuming a pipe inner diameter of 248mm and a density of the liquid of 722kg/m$^3$, the mass flow rate for open channel flow could be determined for various level fractions and pipe slopes as plotted in Figure 91. This graph highlights the significant dependence on pipe slope and as mentioned above, this parameter is unlikely to be accurate, assuming it is available. In absence of better pipe slope information, the graph can be used to find a range of values.

As an example, assume that it is suspected that 30 to 40kg/s of liquid flowed along a horizontal pipe with an internal diameter of 248mm. If the slope of the pipe is 2%, then from Figure 91 the level fraction of liquid in the pipe would have been between 0.48 to 0.57 or a depth of between 119mm and 141mm. If the slope of the pipe was 3%, it would reduce the required level to between 0.43 and 0.51. A lower slope of 1% would require between 0.59 and 0.73 to drive the flow.

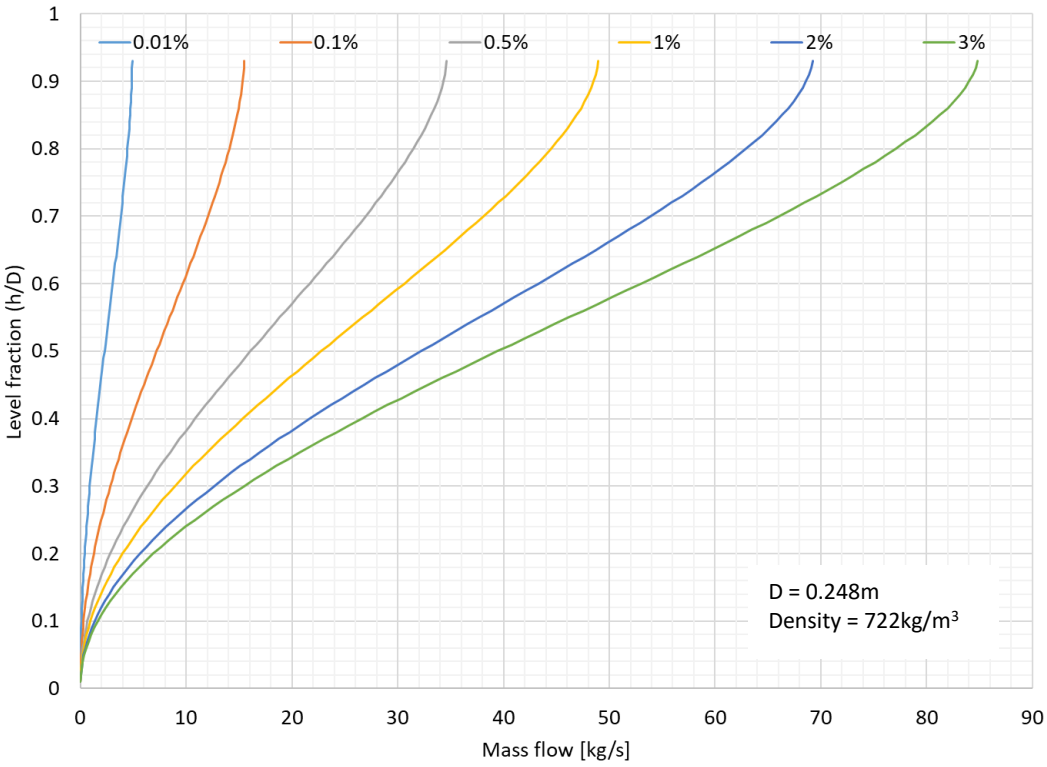


*Figure 91. Open channel pipe flow rate vs depth for uniform flow at various slopes*

The mass flows in Figure 91 are proportional to density and proportional to diameter to the power of 8/3. Thus, the results can be adapted to other pipe diameters and superheater pressures. Once

the approximate level for a particular horizontal pipe is determined, the temperature gradients in the pipe wall can be calculated (see section 8.4).

For vertical pipes that are not running full, it is difficult to determine the amount of surface area wetted by water. The conditions in the horizontal upstream pipe can be used to estimate the level turning into the vertical section. This level can be assumed to be constant for the length of pipe and the duration of the quench event in order to give a conservative estimate of the temperature gradients.

## 7.9 Summary

This chapter describes the development of the LTM which was created to enable better accuracy to be achieved in calculating the level of liquid in the superheater over time during a separator overflow event. The LTM was verified by comparison with the Flownex model and it was applied to a quenching event at Power Station A. It is evident that this type of high level modelling suffers from a lack of detail. The more control volumes that are used improve the accuracy but require more detail that is not available.

The LTM is a method of modelling to determine the liquid level in the superheater as a function of time as described in the methodology in section 3.7. Furthermore, if the results show that the behaviour of the variables in the model are consistent with plant data, then the existence of a separator overflow can be confirmed. This was demonstrated in the journal paper written on the subject which compared the results of the LTM and the Flownex model when applied to a quench incident [91].

The LTM provides a liquid level that is used in the steps required for repeat quench events as discussed in section 3.7. Repeated quenching leads to an accumulation of damage and it is important to identify the potential location of such damage for further investigation. The accurate determination of liquid levels in individual components in the complex superheater system without detailed information is not possible. At best, estimates can be made based on some basic calculations and good engineering judgement of where and how the water may have flowed. Once the liquid level has been determined, the through-wall temperature gradients can be calculated as discussed in the next chapter.

# 8. Through-wall temperature gradients

This chapter considers the measurement and calculation of through-wall temperature gradients of a horizontal pipe during quenching in support of activity 3.8 in the proposed methodology, as shown in Figure 92.

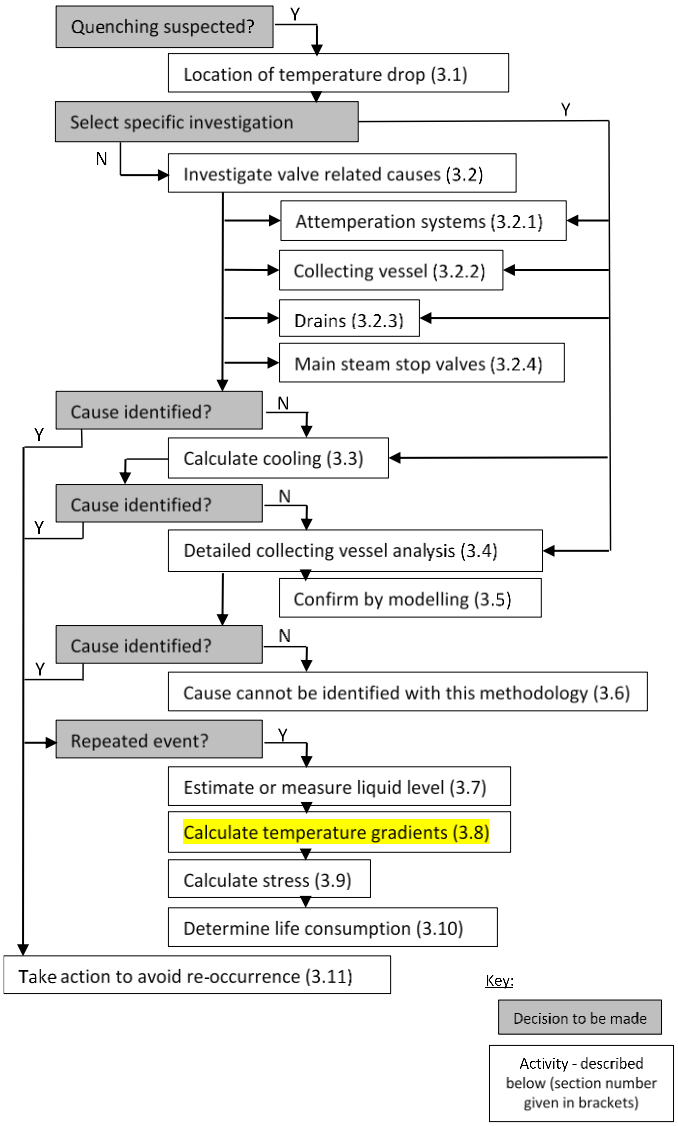


*Figure 92. Activity 3.8 in the methodology*

The temperature gradients enable the stresses in the wall to be calculated. The temperature gradients can be obtained through measurement by thermocouples installed on the outer surface of the pipe wall. This was done at Power Station A and the results are presented in section 8.3.

Alternatively, the gradients can be calculated. However, in that case it is necessary to assume a liquid level over time as well as the heat transfer coefficients. An experiment was conducted (Refer

section 8.2) to measure heat transfer coefficients to assist in determining what values to use in the calculation and to test the level finding methodology developed in this chapter.

In both cases, a transient conduction model of the pipe wall is required for reconstruction of the two dimensional through-wall temperature gradients. The derivation of the model is given below in section 8.1.

## 8.1 Transient conduction model of the pipe wall

A two dimensional transient heat conduction model of a pipe wall by Rousseau [131] was adapted for this work. The model considers the radial and circumferential temperature distributions within the pipe wall as a result of the applied boundary conditions. The model is based on a two dimensional control volume as shown in Figure 93.

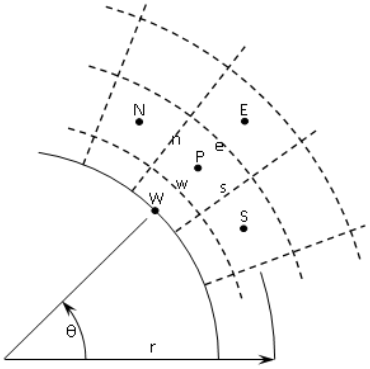


*Figure 93. Control volume used in the transient heat conduction model of the pipe wall*

It is assumed that there is no significant heat transfer along the pipe in the axial direction. Practically this means that local temperature variations along the pipe length are small in comparison to the temperature variations and heat transfer in the radial (r) and circumferential (θ) directions.

The heat conduction equation in polar co-ordinates for the generic elemental control volume is:

$$\rho c \frac{\partial T}{\partial t} = -\frac{1}{r}\frac{\partial}{\partial r}(r\varphi_r) - \frac{1}{r}\frac{\partial \varphi_\theta}{\partial \theta} - \frac{\partial \varphi_z}{\partial z} \qquad (138)$$

It is assumed that there is no internal heat generation in the solid. Now, by assuming $\frac{\partial \varphi_z}{\partial z} = 0$ and ρ and c are constant, the finite volume method can be applied to get:

$$\rho c \frac{\partial T}{\partial t} = -\frac{2}{r_e^2 - r_w^2}(r_e\varphi_{re} - r_w\varphi_{rw}) - \frac{2(r_e - r_w)}{(\theta_n - \theta_s)(r_e^2 - r_w^2)}(\varphi_{\theta n} - \varphi_{\theta s}) \qquad (139)$$

For a control volume bounded by solid control volumes only, conduction heat transfer exists at each of the boundaries. The temperature gradients, $\frac{\partial T}{\partial r}$ and $\frac{\partial T}{\partial \theta}$, are approximated by the temperature differences between the control volume under consideration and its neighbours and the material thermal properties are expressed in terms of the thermal diffusivity, α, as follows:

$$\frac{\partial T}{\partial t} = a_E T_E + a_W T_W + a_N T_N + a_S T_S - (a_E + a_W + a_N + a_S) T_P \qquad (140)$$

$$a_E = \frac{2\alpha r_e}{(r_e^2 - r_w^2)(r_E - r_P)}$$

$$a_W = \frac{2\alpha r_w}{(r_e^2 - r_w^2)(r_P - r_W)}$$

$$a_N = \frac{2\alpha (r_e - r_w)}{(\theta_n - \theta_s)(r_e^2 - r_w^2)(\theta_N - \theta_P)}$$

$$a_S = \frac{2\alpha (r_e - r_w)}{(\theta_n - \theta_s)(r_e^2 - r_w^2)(\theta_P - \theta_S)}$$

The control volumes at the inner and outer surfaces of the pipe are exposed to convection heat transfer. By arranging the resulting equations for those control volumes into the same form and expressing the heat transfer coefficient in terms of the Biot number, *Bi*. For the inner surface we get:

$$\frac{\partial T}{\partial t} = a_E T_E + a_{w,inner} T_{fluid} + a_N T_N + a_S T_S - (a_E + a_{W,inner} + a_N + a_S) T_P \qquad (141)$$

Where

$$a_{W,inner} = \frac{2\alpha r_w}{(r_e^2 - r_w^2)} \frac{h_{inner}}{k} = \frac{2\alpha Bi_{inner}}{(r_e^2 - r_w^2)}$$

The boundary elements along the walls of the pipe are assumed to be half the thickness of the other elements. However, the spacing of the temperature nodes is assumed to stay constant. Thus, the location of the temperature node at the boundary lies on the surface. This enables direct calculation of the wall temperature.

The temperature distribution in the pipe cross section is assumed to be symmetrical about the vertical axis. Hence only one half of the pipe is considered in the calculation. For the boundaries along the plane of symmetry at the top and bottom of the section, the surface is assumed to be adiabatic i.e. the coefficients for those directions in the above equations 140 and 141 are assumed to be zero.

Using the set of equations 140 and 141, it is now possible to perform time wise integration to solve the change in temperature with respect to time. A fully explicit solution scheme is used so that by assuming a discrete time step, Δt, the temperature at the point P can be expressed in terms of the known temperatures from the previous time step:

$$T_P = (T_P)_0 + [a_E T_E + a_W T_W + a_N T_N + a_S T_S - (a_E + a_W + a_N + a_S) T_P]_0 . \Delta t \qquad (142)$$

The model was verified by comparison to an analytic solution by Gwebu [132]. The analytical solution uses Bessel functions to calculate the transient one dimensional temperature profile in the wall of an infinitely long tube subjected to a step change in temperature. Initially the tube is at a uniform temperature of 30°C. At t=0s, the inner wall temperature is instantaneously set to 50°C and the outer wall temperature is set to 200°C.

As shown in Figure 94, the numerical model used in this work matches the analytical solution, except for when fewer elements are used and there are steep gradients (refer t=0.5s).

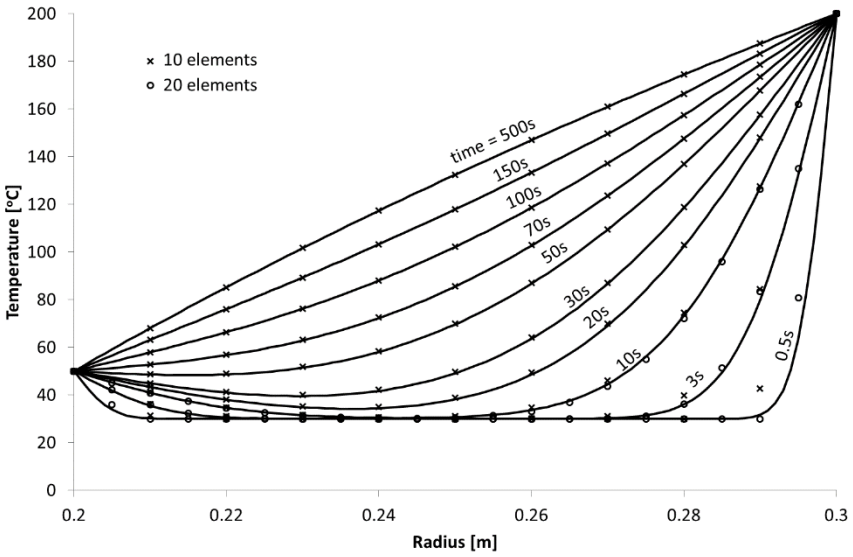


*Figure 94. Verification of the numerical pipe wall conduction model compared to an analytical solution from [132]*

### 8.1.1 Application to a steam pipe partly filled with liquid

Consider the situation shown in Figure 95, which shows the half cross section of the pipe with an arbitrary liquid level *L* and a layer of insulation around the outside of the pipe.

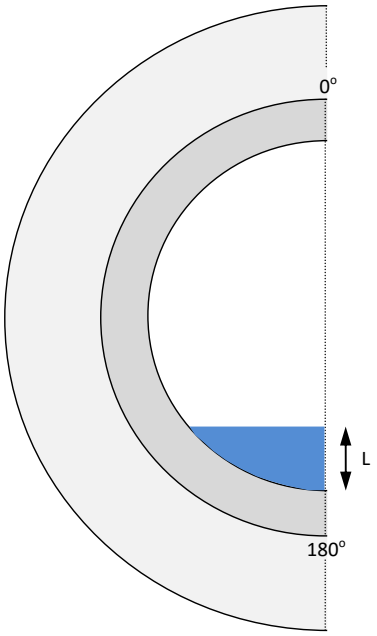


*Figure 95. Diagram of a thick-walled steam pipe partly filled with condensate*

For a saturated steam vapour/liquid mixture in equilibrium inside the pipe, the temperature of the fluid within the pipe would be uniform. However, the heat transfer coefficients at the interface between the vapour and the pipe and between the liquid and the pipe would be significantly different. Even when there is a moderate temperature difference between the metal and the liquid, Sobota [33] notes that where condensate is present, different heat transfer coefficients in the steam space and the liquid space can lead to significant temperature differences between the top and bottom of horizontal vessels such as steam drums, superheater headers and steam pipelines.

Under transient conditions such as cooling of the pipe, these different heat transfer coefficients would give rise to temperature gradients in the pipe wall in the circumferential direction. Thus, the method considers two regions on the inside surface of the pipe, each with a separate heat transfer coefficient, and if necessary, a different fluid temperature.

The pipe wall and insulation layer are separately discretized in the radial direction with a specified contact resistance between them. An outer heat transfer coefficient for convective heat transfer to the ambient is also allowed for.

An initial uniform temperature is assumed in the pipe wall. Owing to the time it takes for the temperatures in the insulation to approach steady state values, it is necessary to initialize the temperatures in the insulation with a steady state solution.

### 8.1.2 Forward and inverse calculations

The pipe wall transient conduction model can be used in the forward direction to calculate temperature gradients from known initial conditions and inner heat flux or it can be used in the inverse direction. In the inverse direction, the model is used to determine the through wall temperatures and the inner heat flux based on measured temperatures on the outside surface of the pipe or through the wall of the pipe.

The inverse calculation procedure relies on finding an inner heat transfer coefficient that produces the same temperature that was measured at the outer surface of the pipe at the end of the time step. The solution procedure is iterative. The results of the calculation provide both an estimated temperature distribution through the pipe wall and the inner surface heat flux.

## 8.2 Quenching heat transfer test rig

In order to provide data for testing the transient heat conduction model and to measure the heat transfer coefficients during quenching, an experiment was devised. The concept was to install thermocouples on a section of pipe and then heat the pipe and quench it with water at atmospheric pressure.

### 8.2.1 Apparatus and methodology

A test rig was constructed for the purposes of measuring temperatures through a pipe wall during quenching. The rig consisted of a 250mm long section of steam pipe with end plates welded onto each end (Figure 96). The circular end plates were cut to provide large openings at the top of the pipe for venting steam.

The steam pipe section was cut from a piece of scrap pipe that had previously been used in a boiler. The pipe material was confirmed to be X20 CrMoV 12-1 (1.4922) by analysing a sample of the material in a scanning electron microscope (SEM) with an energy-dispersive (EDS) detector. The analysis indicated a chrome content of 12.16% by weight which is above the 12% upper limit of the material specification, but the relatively small margin was not expected to affect the thermal characteristics of the material.

*Figure 96. Steam pipe section during fabrication showing endplate, support and water admission pipe*

An electric resistance heater contained within a band of ceramic blocks was used to heat the steam pipe section. A specialist company manufactured the ceramic band heater to their specifications that included a stainless steel outer plate. The 3kW heating element was fitted around the outside diameter of the steam pipe (See Figure 97). Mineral wool insulation was then used to insulate the outside of the heating element and over any exposed areas of the steam pipe and end plates.

Water for quenching the steam pipe was supplied from a hot water urn. The water was admitted into the lowest elevation possible inside the steam pipe via a 1” galvanised steel pipe and a ball valve (See Figure 97).

By keeping the ball valve open during a quench, the water level in the system could be monitored by means of the level indicator on the side of the urn. With the valve open, the urn continued to feed the steam pipe and thus slow down the drop in level due to evaporation during the quenching process. Prior to opening the valve, the initial level in the urn had to be set to obtain a desired level in the steam pipe.

*Figure 97. Ceramic band heating element fitted over the steam pipe (left) and water supply from Urn (right)*

Thermocouples were installed in the middle of the pipe length at various positions around the circumference and through the pipe wall (as shown in Figure 98). Encapsulated Type K thermocouples with a 1.5mm diameter were used.

Prior to installation of the thermocouples, 1mm deep slots were machined along the surface of the pipe to allow space for the thermocouples to run between the steam pipe and the ceramic band heating element.

The mid-wall thermocouples were installed into holes drilled from the outside diameter of the steam pipe to the required depth using a 2mm drill bit. The thermocouples were inserted into the holes and secured with spot-welded tabs to ensure good contact at the bottom of the hole. The thermocouples had to be bent through 90$^{o}$ at the exit of the holes to route axially along the steam pipe between the pipe and the ceramic heating band.

Prior to installation of the measurement points on the outer surface of the steam pipe, the locations were cleaned using a grinding disk to remove the oxide layer. The thermocouples were then placed on the surface and given a slight bend before securing with spot-welded tabs to ensure the tip made good contact with the outer surface of the steam pipe. An insulating paste (Holts Gun Gum) was then applied over the thermocouple to separate the measurement point from the ceramic heating band.

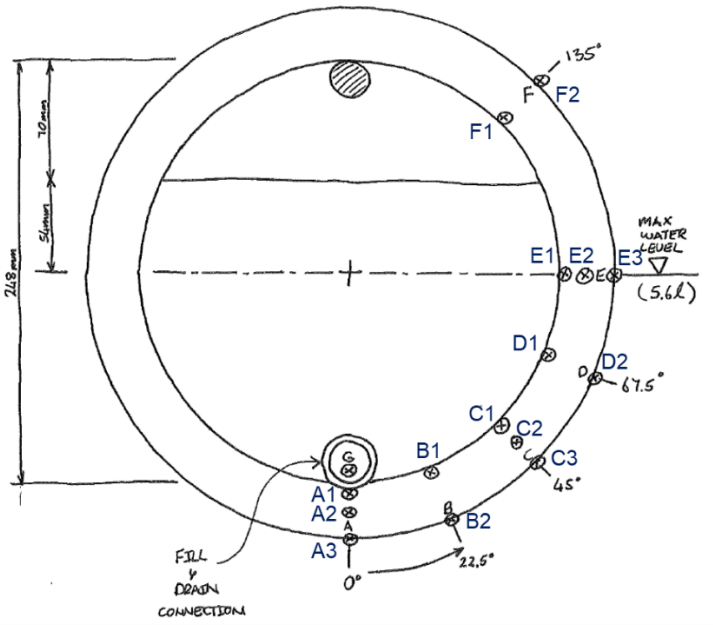


*Figure 98. Thermocouple locations, approximately in the middle of the pipe length*

*Figure 99. Thermocouple installation - Position A and B*

*Table 7 : Dimensions of the test pipe section and thermocouple locations*

| Nominal inside diameter and minimum wall thickness | | | | 248mm ID x 25.7mm |
|---|---|---|---|---|
| Length | | | | 250mm |
| **Position** | **Wall Thickness** | **Depth TC1*** | **Depth TC2** | **Depth TC3** |
| A | 29.3mm | 25.5mm (27.8mm) | 14.5mm | 0mm |
| B | 27.7mm | 25.5mm (26.3mm) | 0mm | N/A |
| C | 25.7mm | 23mm (24.6mm) | 15mm | 0mm |
| D | 28.0mm | 27mm | 0mm | N/A |
| E | 28.5mm | 23.5mm (27.2mm) | 14mm | 0mm |
| F | 28.2mm | 27mm | 0mm | N/A |

* Depths in brackets are for holes drilled deeper after test 11

A data logger was used to record the temperatures at an interval of one second. The accuracy of the data logger and amplifier circuitry was determined by injecting a known voltage into a single channel and comparing that to the value that was logged. This calibration of the logger and the manufacturer's certificate for the thermocouple wire was used to correct the measured data as per the calibration curve in Figure 100. The thermocouples were not individually calibrated.

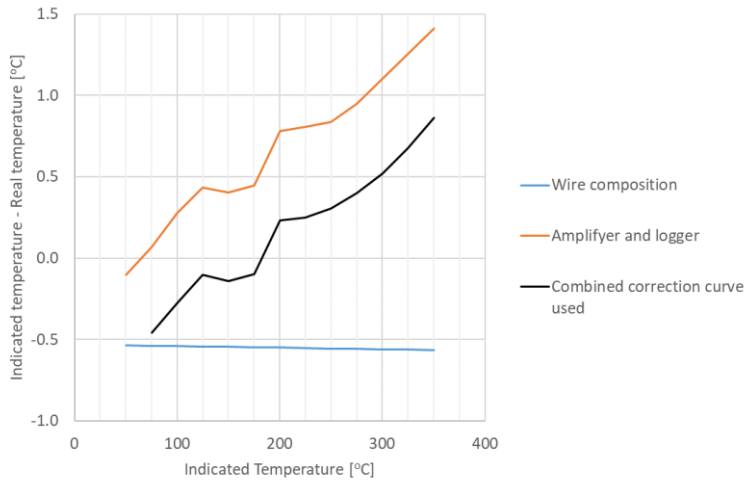


*Figure 100. Measurement system calibration applied to all points*

The testing procedure involved switching on the heating element and raising the metal temperature until all the temperature measurements showed values approximately 20°C higher than the target temperature. The heating cycle typically took 40 minutes for an initial temperature of 100°C and a target temperature of 250°C. The heating element was then switched off and the temperature gradients were allowed to settle. The settling phase required more than an hour for the metal temperature measurement values to be within 10°C of each other. The average cooling rate of the metal ranged from 1°C to 2°C per minute and could be manipulated by opening or closing the insulation pieces that covered the steam escape gaps. In some cases the metal temperature dropped below the target temperature and the element was then briefly energised to regain temperature.

After test 11, a different philosophy was applied for the remaining tests. The heating element was removed from the steam pipe after the heating phase and the steam pipe was then insulated and allowed to settle. Thus when the quench took place, the outer surface of the pipe was insulated and almost adiabatic.

The water level in the pre-heated urn was adjusted to the desired level. The maximum level prior to opening the valve was 179mm which equated to 94mm in the steam pipe after the valve was opened. It was intended to be able to fill the steam pipe up to the centreline with water (h = 124mm) however this was not achieved in practice due to splashing and overflow from the steam vents at high levels.

The urn thermostat was turned up and once the sounds of bubbling could be heard from within the urn, the valve was opened to quench the steam pipe. After approximately 10 minutes, the boiling inside the steam pipe had ceased and the valve was closed. The drain valve was then opened to empty the water from the steam pipe. The final level in the urn was measured.

A similar procedure was repeated for each test. Two sets of tests were carried out. The first set was to measure the heat transfer at various different initial metal temperatures. Tests were carried out at 105°C, 120 °C, 135 °C, 180 °C, 195°C, 200°C, 240°C,250°C and 300°C each with an initial water level of 94mm.

The second set of testing was to investigate the temperature profiles at different water levels. For these cases, the initial metal temperature was set to 250°C in each case and tests were carried out at initial water levels of 94mm, 68mm, 44mm, 34mm and 24mm.

*Table 8 : Schedule of tests*

| Test number | Initial metal temperature | Level | Comment |
|---|---|---|---|
| Test 1 | 300°C | N/A, Initial test | Temperature data lost |
| Test 2 | 300 °C | N/A, Initial test | Valve was closed prematurely |
| Test 3 | 250 °C | 94mm | Successful |
| Test 4 | 250 °C | 44mm | Successful |
| Test 5 | 300 °C | 94mm | Successful |
| Test 6 | 200 °C | 94mm | Successful |
| Test 7 | 105 °C | 94mm | Successful |
| Test 8 | 195 °C | 94mm | Successful |
| Test 9 | 250 °C | 68mm | Successful |
| Test 10 | 250 °C | 34mm | Successful |
| Test 11 | 250 °C | 24mm | Successful |
| Test 12 | 20 °C | N/A | Heating by hot water in two stages |
| Test 13 | 135 °C | 94mm | Element removed, outer re-insulated, successful |
| Test 14 | 120 °C | 94mm | Element removed, outer re-insulated, successful |
| Test 15 | 180 °C | 94mm | Element removed, outer re-insulated, successful |
| Test 16 | 240 °C | 94mm | Element removed, outer re-insulated, successful |

### 8.2.2 Data processing

The transient heat conduction model described in section 8.1 above was adapted to perform the data processing for the quenching experiment. A copy of the Scilab code is provided in Appendix J.

The variable steam pipe wall thickness (refer Table 7) necessitated that the calculation procedure refer to a matrix of radii to obtain the radius and element width for each control volume. This also allowed for exact positioning of control volumes to align with the physical location of the measurement points.

The calculation procedure performs the conduction calculation in the forward direction. This is accomplished by constructing an initial temperature field in the metal and then assuming a value for the heat flux at the boundary. The forward heat conduction calculation is run at small time steps (typically 0.1s) to the end of the time interval (typically 2s). The temperatures at the end of the time interval are compared to the measured temperatures. A new value of heat flux at the boundary is calculated based on minimising the square of the errors in calculated temperature compared to measured temperature.

The number of new heat flux values that can be calculated is limited to the number of temperature measurements. However; the boundary where the heat flux is applied consists of many control volumes. Thus the calculated values are applied along the same radius as the measurement point and the heat flux for the remaining boundary control volumes is estimated by linear interpolation.

Once the values are updated, the initial temperatures are reset and the calculation repeated. This process continues until convergence has been achieved for the time interval and then the calculation moves on to the next interval.

The measured temperatures were logged at an interval of one second. When running the calculation to find the required heat flux to produce the measured temperature change, it was found that a one second calculation interval was too short and that the calculation routine became unstable. This is because the speed of the heat conduction to the depth of the thermocouples was slower than the sampling rate, thus the calculation routine was unable to find reasonable estimates of the heat flux in the one second time interval. It was found that a time interval of two seconds was slow enough for the heat flux to influence the measurement points and hence provide stable results.

The material properties are an important consideration for the accuracy of the calculation. Data from two sources, namely Taler et al [83] and the DIN data sheet [133] were considered. The variation with temperature of the thermal conductivity and specific heat capacity of the material were taken into account. The equations provided in Figure 101 were used for producing the results. Density is considered to be constant because the model does not consider the change in dimensions of the steam pipe with change in temperature.

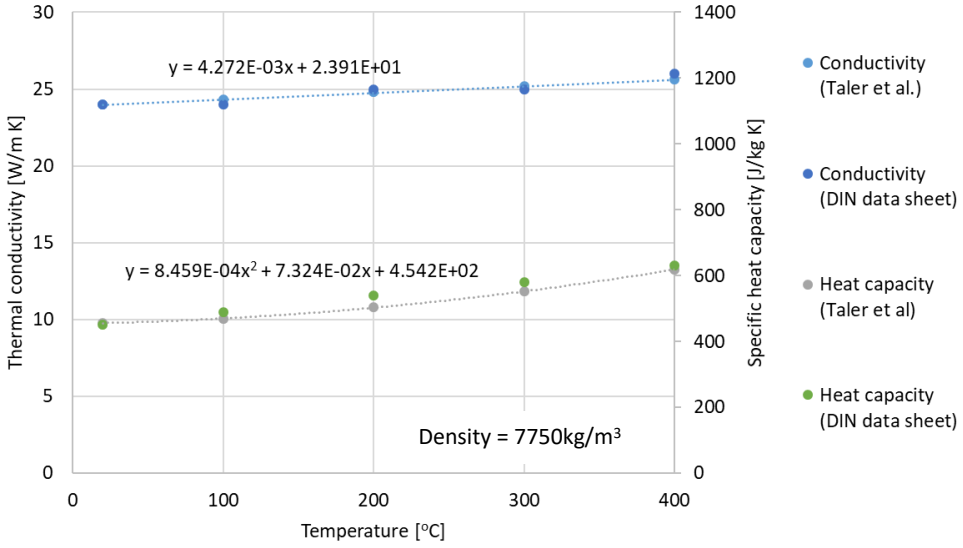


*Figure 101. Thermal properties of X20 CrMoV 12-1 (1.4922)*

The dependence of the results on the level of discretisation or number of control volumes used was studied by using the same input data and varying the number of divisions in the radial and circumferential directions. The results in Figure 102 show that gains in accuracy are not significant above 600 control volumes.

The calculation is less sensitive to time step as shown in Figure 103. The time step refers to the small increments over which the calculation runs and the metal temperatures are updated while the

larger time interval of the measured data (two seconds in this case) is the duration for which the boundary conditions remain constant.

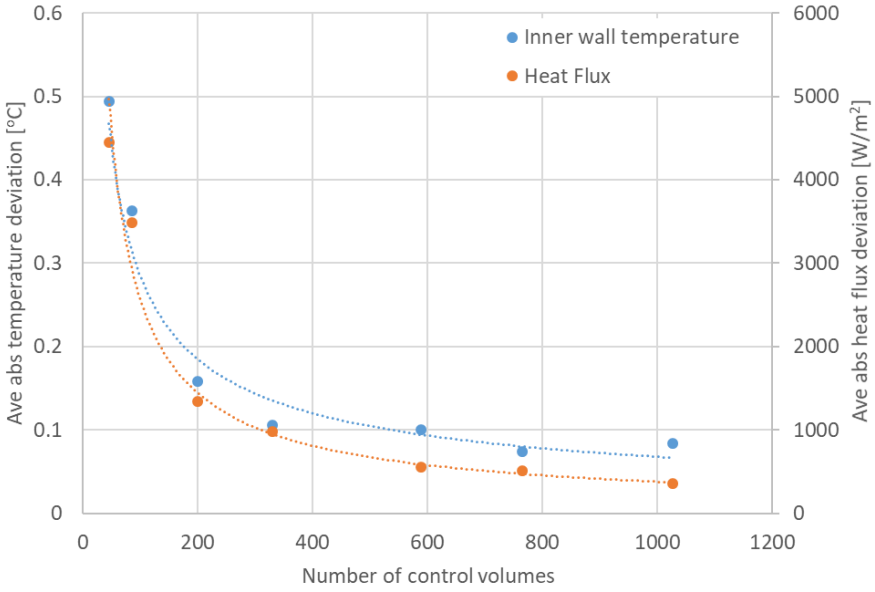


*Figure 102. Grid dependence of the results (Test 3, time step = 0.1s)*

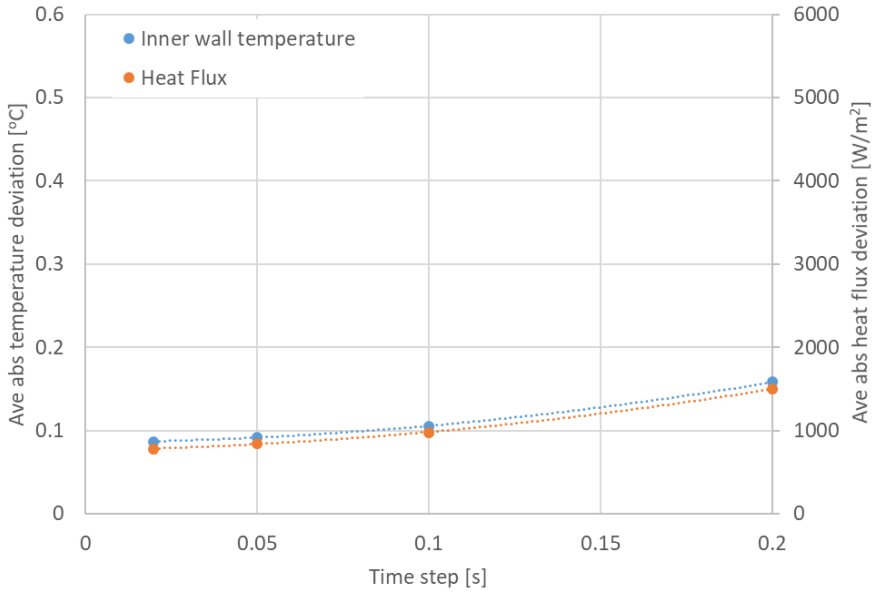


*Figure 103. Time step dependence of the results (Test 3, grid = 10 x 33)*

The results of the quenching experiment presented below were produced with 15 divisions in the radial and 51 divisions in the circumferential directions (765 control volumes). A time step of 0.1 seconds was used with a time interval of two seconds.

## 8.2.3 Results and discussion

The temperature data recorded for a typical test is shown in Figure 104.

Position E is initially wetted and quenched when the violent boiling phase occurs, but actually the water level of 94mm is lower than the height of position E which is at 124mm. Hence there is a dry-out at position E and recovery of the through-wall temperature gradient at around 14:35.

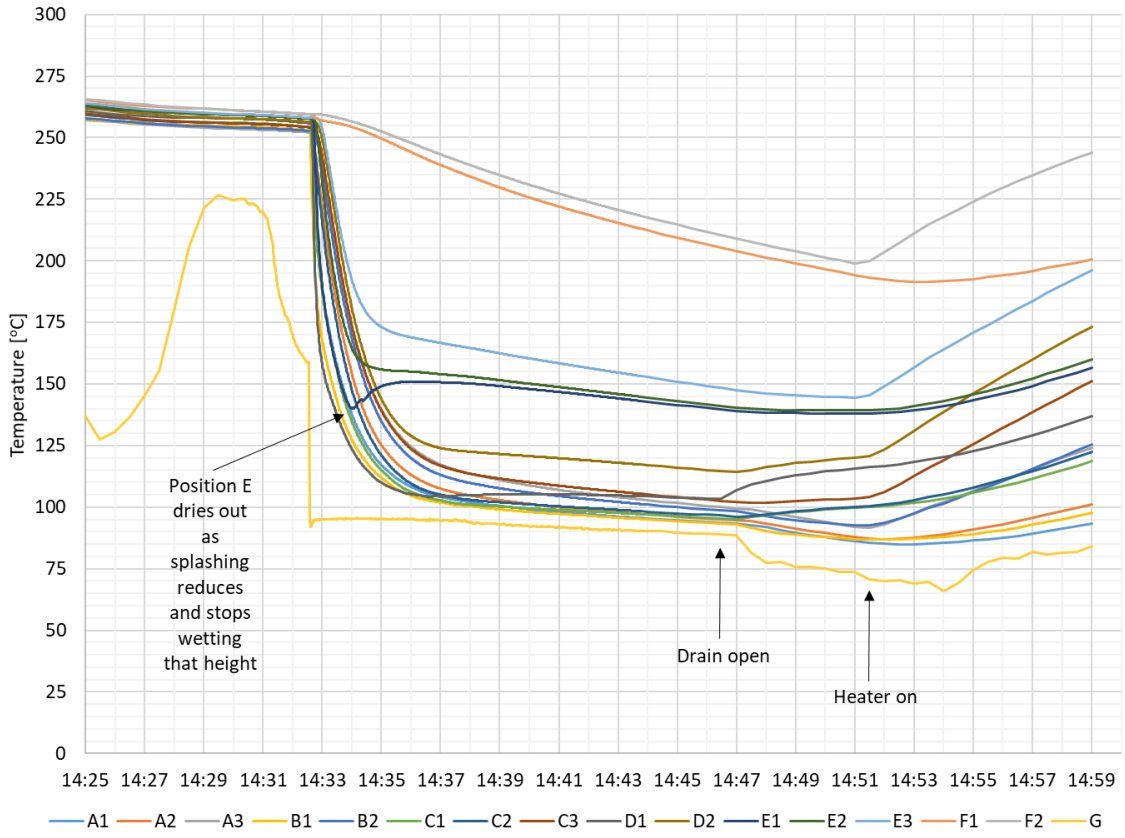


*Figure 104. Corrected temperature measurements - Test 3, Level = 94mm reducing to 89mm*

Thermocouple D1 has the fastest response to the quenching. This makes sense because D1 is located closest to the inner surface of the thermocouples under the water level. At around 14:36, position D1 deviates from the other measurements indicating a change in heat flow. Point D is well below the water level at 76mm and thus the change cannot be due to dry-out. The change is due to conduction heat transfer from the top section of the pipe providing heat to position D. This highlights the need to model the quenching in two dimensions to obtain the temperature gradients in the pipe cross section.

The calculated temperature profiles at selected times for Test 3 are shown in Figure 105. The steep temperature gradients through the wall as well as around the circumference of the pipe are evident. The water enters the pipe at 25 seconds into the simulation. At 30 seconds, the level may have

reached the final height but due to the thermal capacity, there is not a rapid drop in temperatures at all locations. At 30 seconds, 60 seconds and 90 seconds, blue lines mark an approximation of the water level. At 60 seconds, the level is not accurate because of the boiling and splashing that took place and significantly wetted the surface a few tens of millimetres above the actual water level.

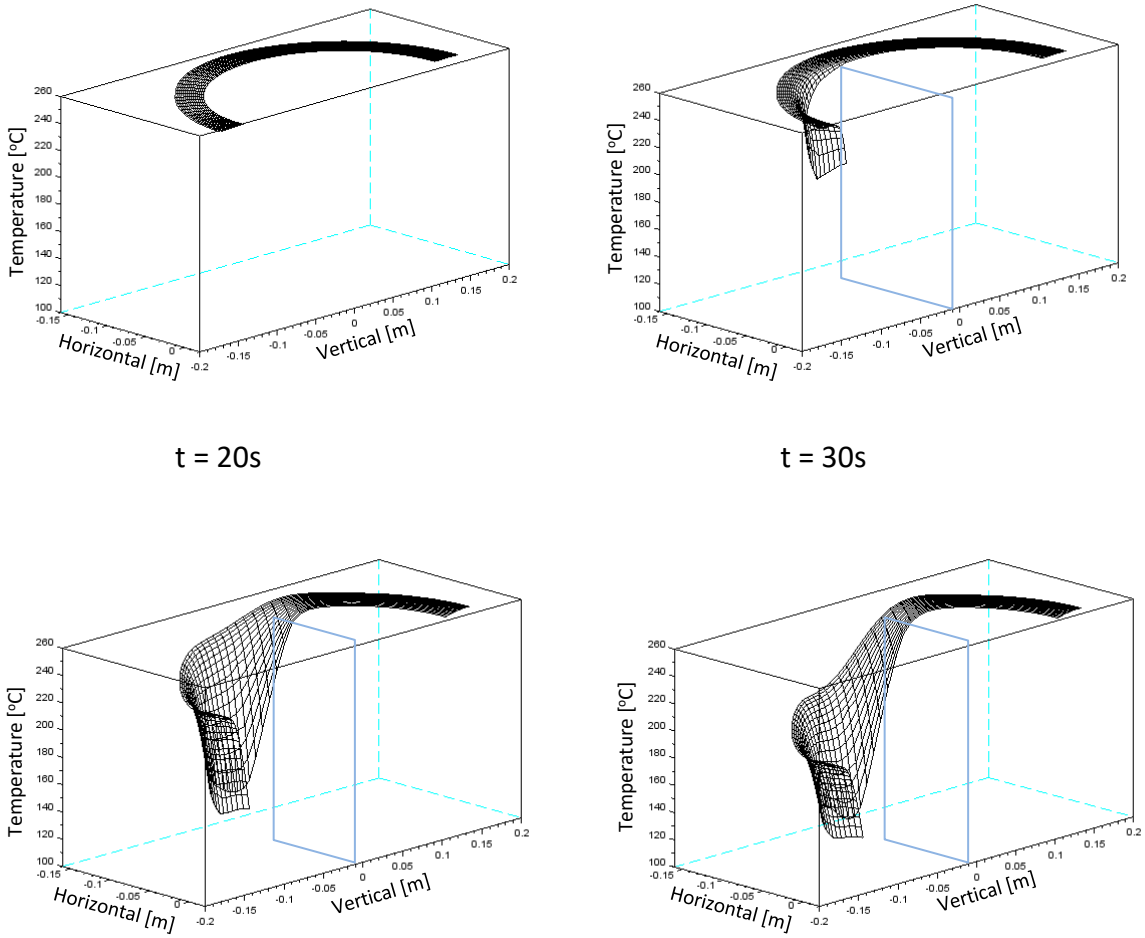


*Figure 105. Calculated temperature profiles - Test 3, Level = 94mm reducing to 89mm*

The calculated inner heat flux shown in Figure 106 confirms the relatively high heat flux experienced at all measured locations, except for position F which is above the water level. The highest heat flux is indicated at position E and there is some instability in the value. This is a real effect due to the splashing occurring at that height. After 100 seconds, the dry-out occurs and the heat flux drops.

As shown in the inset in Figure 106, the fluid temperature starts dropping at 24 seconds. Position B is first to respond with increased heat flux at the inner surface followed by position A and C and then later by D and finally E. At 30 seconds the level has most likely reached the final height.

The order of heat flux increase approximately agrees with the direction of the pipe filling with water except for position B which shows increased heat flux before position A and C. This is due to the installation depth of thermocouple B1 which is only 2.2mm from the inner surface compared to the depths of thermocouple A1 and C1 at 3.8mm and 2.7mm respectively. Ideally all thermocouples should have been located 1mm away from the inner surface to improve the response time of the measurement system. Further testing was carried out (Test 12 to Test 16) after modifying the depths of the thermocouples (See Table 8).

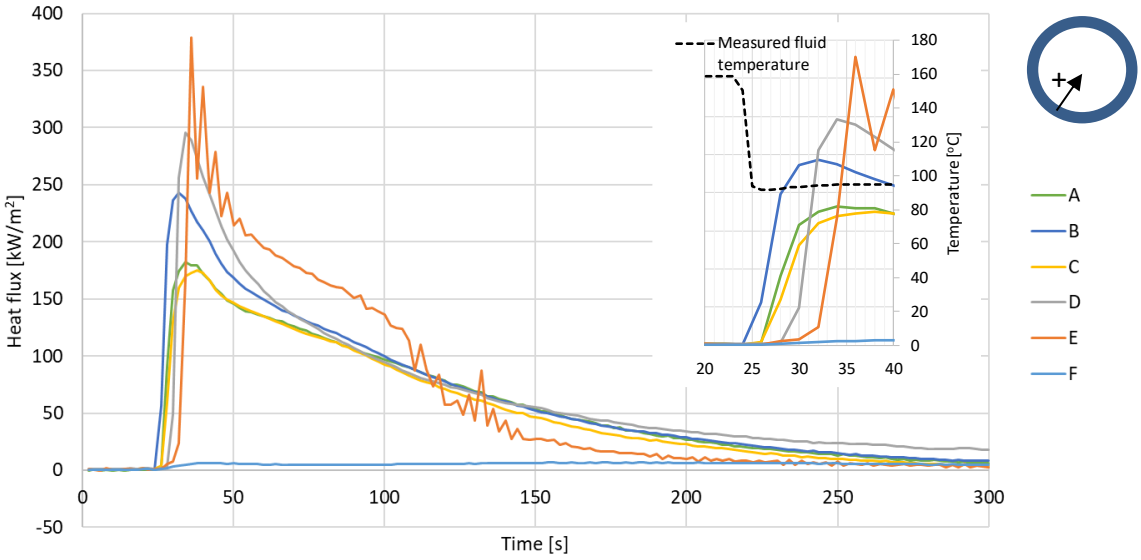


*Figure 106. Calculated heat flux at the inner surface (Test 3)*

The through-wall temperature profiles over time at positions A, C and E are plotted in Figure 107 with the temperature profiles at each location shown on a separate graph. The inner heat flux is determined by matching the calculated temperature at the inner thermocouples to the measured value and thus the plots of A1, C1 and E1 match the measured temperatures exactly.

The calculated mid-wall and outer temperatures do not match the measured values. At the outer measurement points, especially after 200 seconds, the measured temperature remains significantly above the calculated values. This is due to non-negligible heat flux at the outside of the pipe. The calculation assumes an ideally insulated adiabatic surface at the outside boundary of the pipe. In reality the surface is partially in contact with the ceramic blocks of the heating element. Where the blocks do not touch the pipe there is an air gap or the putty that was placed over the thermocouples.

The whole system is insulated and thus the ceramic heating band is at approximately the temperature of the metal when the quench is initiated. Thus, as the metal temperature drops, the temperature difference between the metal and the heating band sets up heat flow.

A similar situation exists for heat flow from the insulation of an insulated pipe, however the thermal conductivity of insulation is of the order of 0.05W/m K which is much lower than that of ceramic which can be 30W/m K or higher, especially the type of ceramics used in heating elements.

After test 11, the test procedure was changed to remove the heating element and replace the insulation prior to allowing the temperature gradients to settle before the quench. This greatly reduced the influence of the outer surface heat transfer on the temperature measurements as seen in Figure 108.

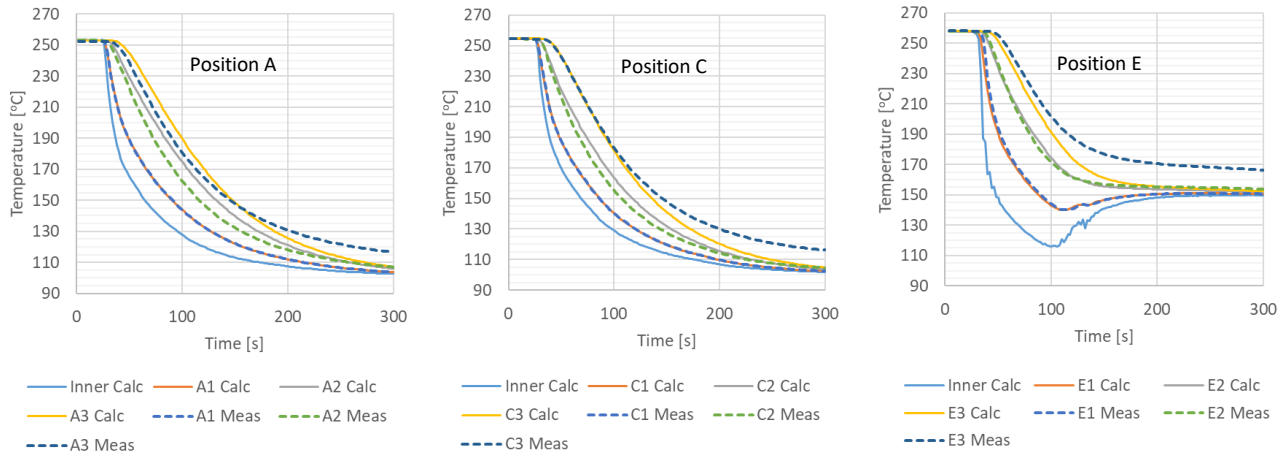


*Figure 107. Through wall temperature profiles – Calculated vs measured (Test 3)*

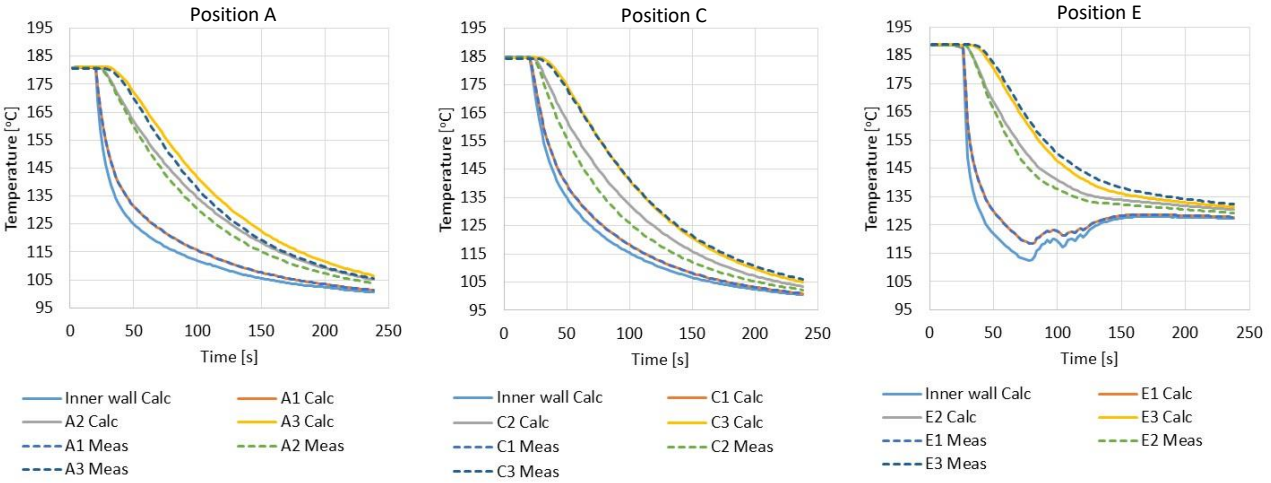


*Figure 108. Through wall temperature profiles – Calculated vs measured (Test 15)*

In order to overcome the limitation of the non-adiabatic outer wall for Tests 3 to 11, an outer heat flux was included in the heat transfer calculation. The outer heat flux was determined by matching the calculated outer temperatures at the positions of the thermocouples to the measured temperatures. The results are plotted Figure 109 and can be compared to Figure 110 that shows a test at a similar initial temperature but with the heating element removed for the quench.

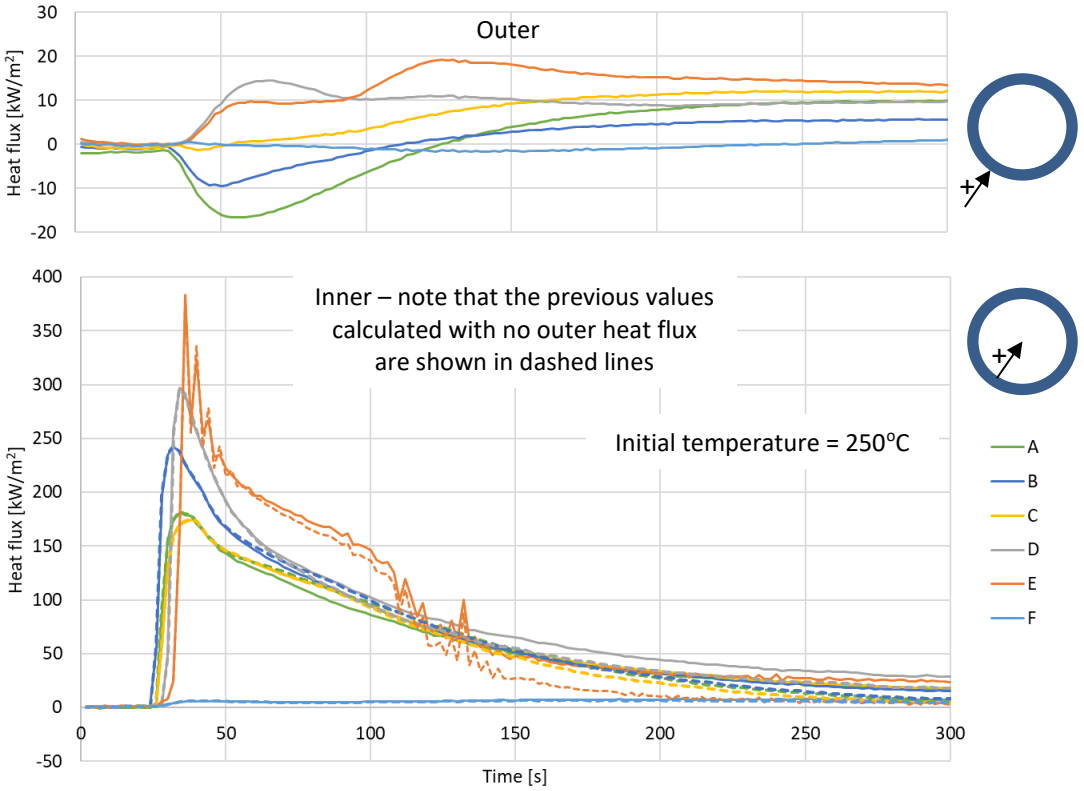


*Figure 109. Revised heat flux – Outer (top) and Inner (bottom), Test 3*

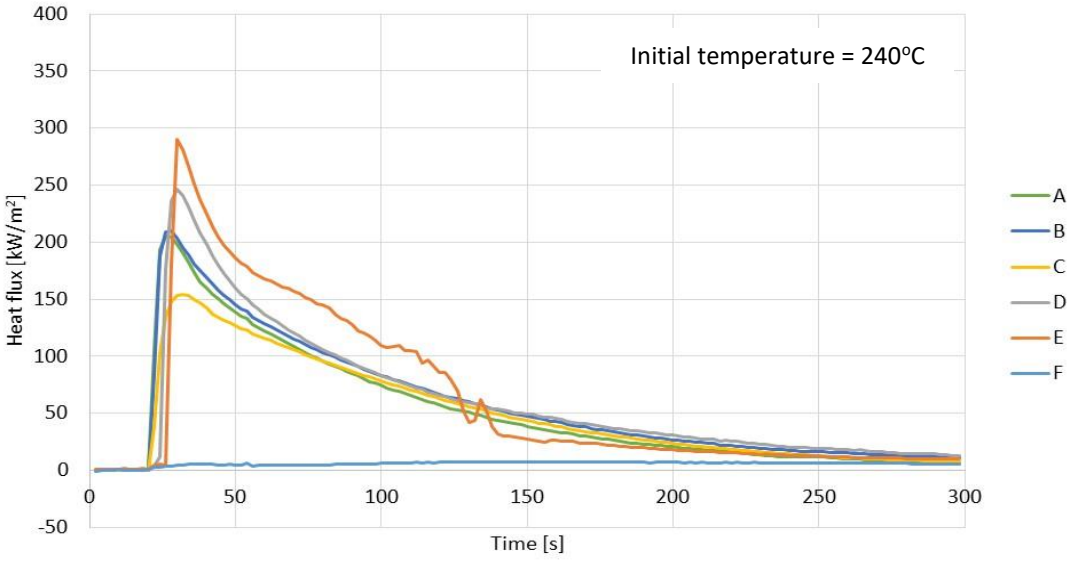


*Figure 110. Calculated Inner heat flux (Test 16 – heating element removed)*

The heat flux results of all the tests are plotted against temperature difference in Figure 111 and Figure 112. At the start of the test, the temperature difference is high and as the test progresses the temperature difference reduces and the points move across the graph from right to left.

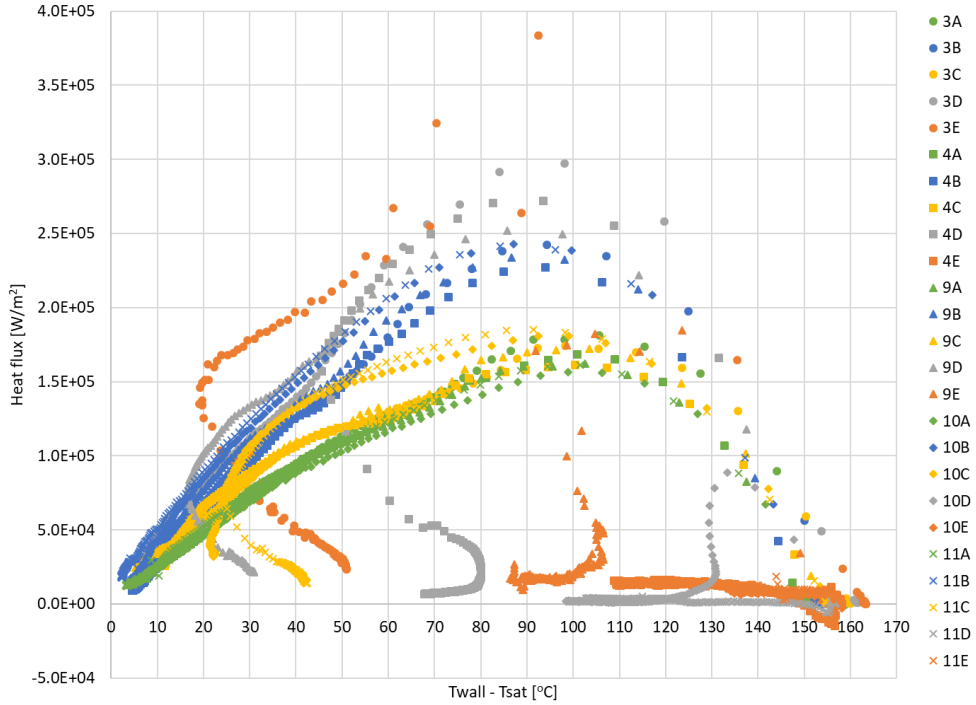


*Figure 111. Heat flux vs temperature difference – tests with varying water levels*

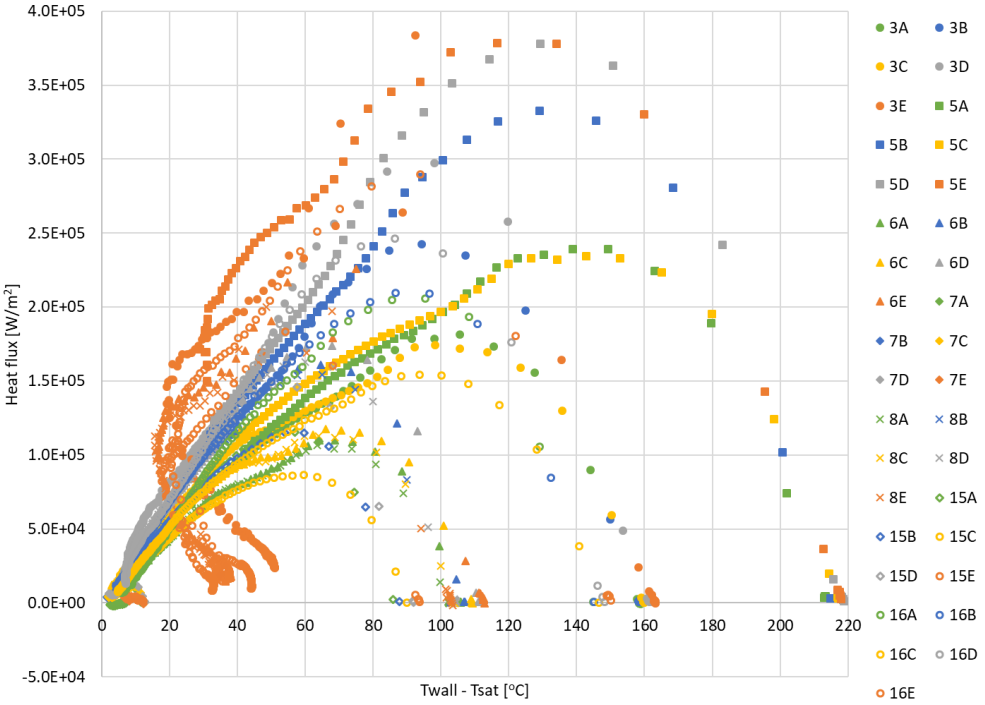


*Figure 112. Heat flux vs temperature difference for tests with varying initial metal temperature*

In Figure 111, it can be seen that the heat flux is affected by drying out at various positions depending on the fill level of the test. Drying out can be identified where the temperature difference starts increasing again for a lower heat flux. There are also some positions which are unaffected by boiling where the heat flux remains relatively low during the whole test.

The water level does not affect the relationship of heat flux to temperature difference but the initial temperature does (Figure 112). When looking at different initial temperature cases, we see there was a build-up of heat flux from the starting temperature on the right to a maximum heat flux which is below the trend of the other tests at the same temperature difference. To the left of the peaks, the results merge into a similar line towards the origin.

In Figure 113, the experimental results are compared to the pool boiling correlations discussed in section 6.3.4. The non-boiling results from the experiment were excluded from the plot. There is a significant deviation of maximum heat flux and the temperature difference at which it occurs. Although it cannot be stated for certain, there are two main differences between this experiment and the data from where the pool boiling correlations were developed. Firstly, the surface of the pipe in this experiment was not cleaned. It had an oxide layer on the inner surface of unknown thickness but with most likely poor thermal conductivity. Secondly, the boiling correlations were developed from steady state data whereas the above experiment is transient.

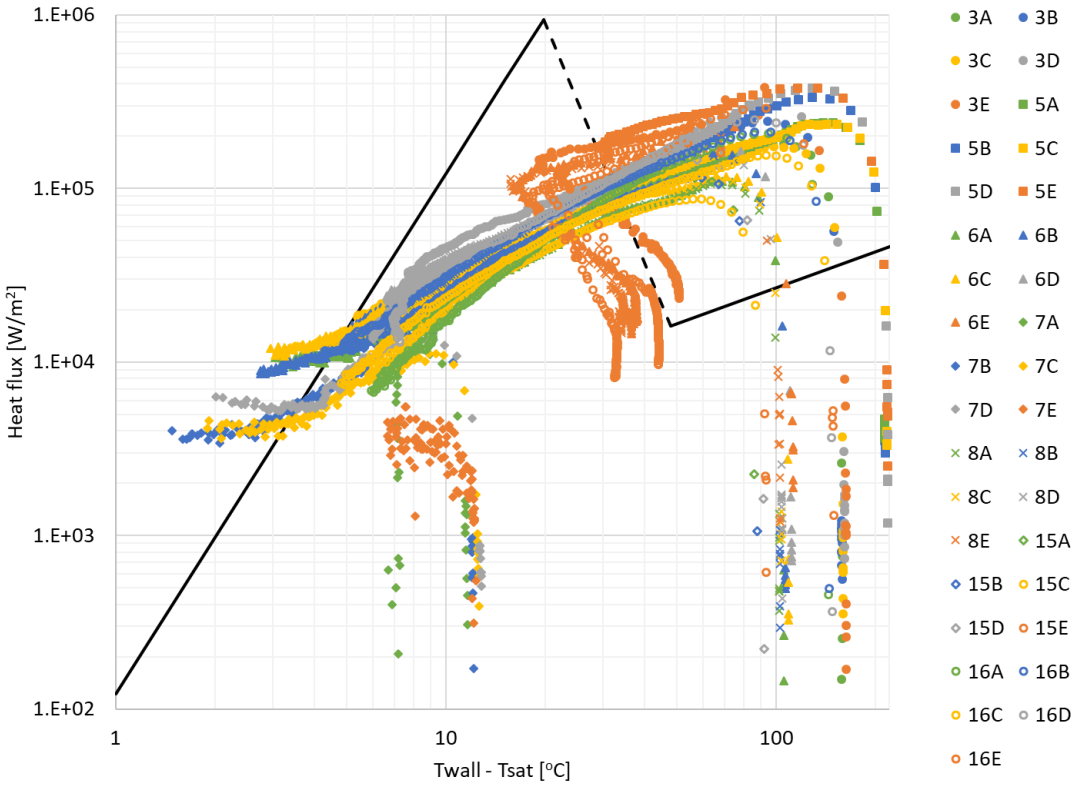


*Figure 113. Comparison of the test results against theoretical pool boiling correlations*

It is interesting to note that the slope of the results match the slope of the film boiling correlation, however the experiment measured much higher heat flux than would be predicted by film boiling by a factor of 8. The boiling in the experiment may be transition boiling, but there is no peak heat flux at the temperature associated with nucleate boiling as the surface temperature drops. Thus it would appear that nucleate boiling was present throughout, but at lower heat flux than would be predicted by the Rohsenow correlation [121].

The experiment was carried out under atmospheric air pressure. Extrapolating the limited results to higher pressures for use in power plant quenching problems is not possible with the limited data set available.

The calculated heat transfer coefficients at the inner surface of the pipe are relatively stable except for cases where the surface is splashed and later dries out at the measuring point location (point E). A typical result from the experiment is shown in Figure 114.

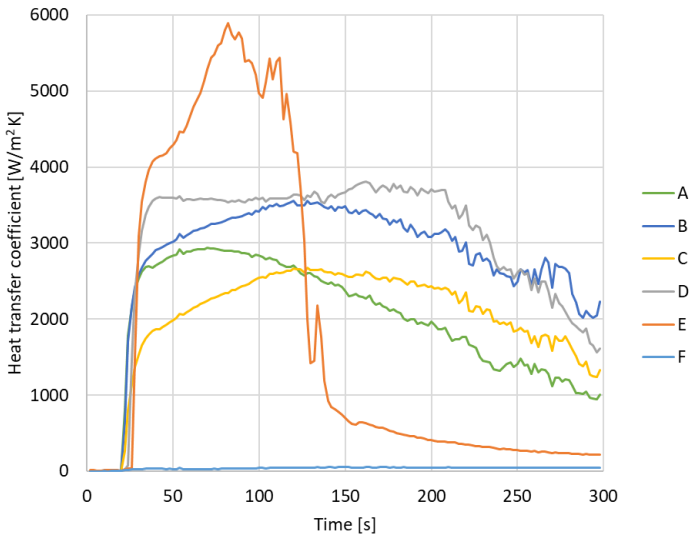


*Figure 114. Calculated inner heat transfer coefficients (Test 16)*

## 8.2.4 Conclusions of the experiment

The two-dimensional transient heat conduction model of the pipe wall successfully predicted the heat flux from the measured temperatures. The calculated mid-wall temperatures were within 5°C of the measured values during the steep transients caused by quenching.

The experiment highlighted the practical problems associated with the measurement of this type of quenching heat transfer and it provided an estimate of the internal heat transfer coefficient that

occurs at atmospheric pressure. While the surface is flooded, the heat transfer coefficient is relatively constant and does not show dependence on the temperature difference between the wall and the fluid. The quenching heat transfer coefficient is less than what is predicted from the commonly used nucleate pool boiling correlation but greater than what is predicted by the film boiling correlation. Transition boiling was not observed.

## 8.3 Plant measurements of pipe outer wall temperatures

Two sets of outer pipe temperature measurements were installed on the main steam system at Power Plant A. The temperature measurements were located on a horizontal section of pipe downstream from the boiler outlet as shown in Figure 6. The initial experiment consisted of only top and bottom thermocouples at three locations.

As discussed in section 1.3, a number of events were recorded where the bottom temperature suddenly dropped below the top temperature and a significant differential temperature between the top and bottom of the pipe persisted for some time. This led to the installation of a further set of thermocouples on the piping system. The intention was to install the thermocouples around the circumference of the pipe at a single cross section in order to detect the liquid level. Prior to deciding the exact positioning of each thermocouple, a numerical study was undertaken to determine the minimum number of measurement points needed around the circumference of the pipe to detect level. The study is described in section 8.3.1 below.

### 8.3.1 Selection of the number of measurements to detect level

The transient pipe wall conduction model was used in the forward direction to generate input data for testing the ability of the inverse calculation to measure level with different numbers of outer temperature measurement points. The same pipe material and geometry as the plant main steam pipe were assumed in the model. The outer wall measurement points were assumed to be equally spaced around half the circumference of the pipe from top ($0^o$) to bottom ($180^o$).

In the first step of the inverse calculation, the inner heat transfer coefficients for water and steam were specified. The calculation was then performed using different numbers of measurement points to determine the accuracy of each configuration to predict the level of condensate in the pipe. The results for a step change level profile and for a ramping level profile are shown in Figure 115 a) and b) respectively. In Figure 115 b), the sampling rate of 30s of the data used as input to the inverse heat transfer problem is not sufficient to accurately follow the input level change. The dashed line shows the best result that was obtained even with higher numbers of measurement points.

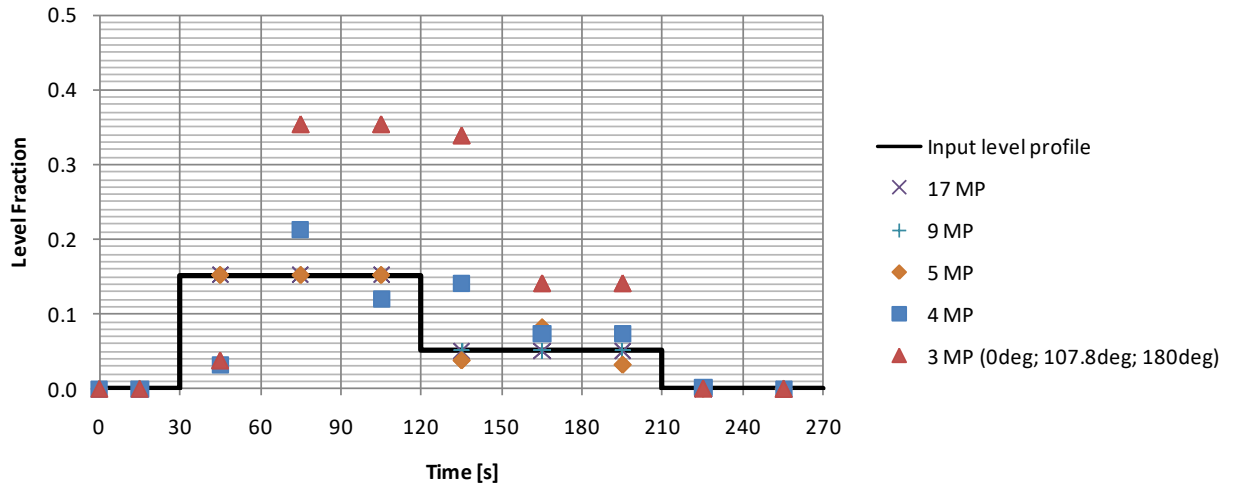


a) Step

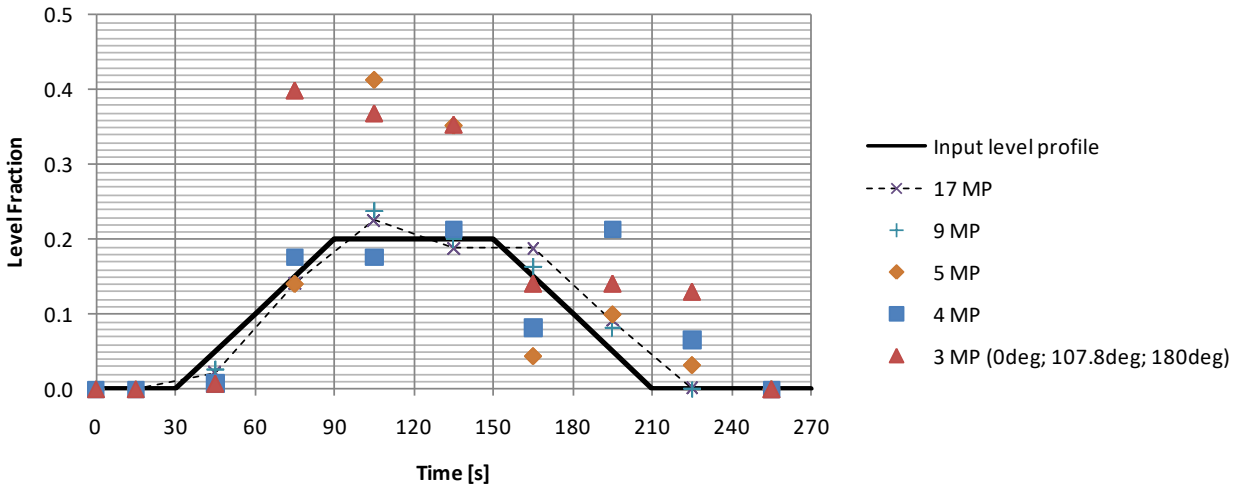


b) Ramp

*Figure 115. Calculated level profile for various numbers of measurement points (inner heat transfer coefficient for vapour and liquid given)*

The heat transfer coefficients for water and steam during quenching are not known nor constant. Potentially they could be estimated from temperatures, fluid properties and flow conditions within the pipe, or the inverse heat transfer problem can be solved to estimate the inner heat transfer coefficients.

A method of solving for inner heat transfer coefficient using the top (0°) and bottom (180°) pipe outer metal temperature measurement history was developed. The through-wall temperature profiles are calculated iteratively by minimizing the square of the error between the calculated and measured outer surface temperatures. It was found that the calculation was sensitive to the

temperature profile through the metal at each time step and that the calculation became unstable (as reported in [134], [135] and [136] amongst others).

A simple solution of limiting the heat transfer coefficient was applied based on the assumption that enough would be known about the conditions in the pipe to provide a limit for the separate vapour and liquid heat transfer coefficients.

Once the top and bottom heat transfer coefficients were estimated, a simple test was applied to decide if it was necessary to enter the level finding routine or not. If the liquid heat transfer coefficient was within 10% of the vapour coefficient, then the level was assumed to be zero.

To estimate level, the temperature profiles on the outer surface of the pipe were iteratively calculated while minimizing the square of the error between those profiles and measured outer surface temperature data. The results are shown in Figure 116.

The error in level estimated for each point of the graphs in Figure 116 relative to the input level was calculated. The standard deviation of the error (refer Figure 117) was calculated as a method to compare the accuracy of the different numbers of measuring points. The error is influenced by both the stability of the calculation routine in determining level and heat transfer coefficient and also the sampling interval.

With shorter sampling intervals, the delay in detecting changes in level is improved, however, the inverse calculation requires a period of time to allow changes on the inside of the pipe to travel through the wall to the outer surface and thus in this case the time interval could not be reduced to less than 30 seconds. Smaller time intervals than 30 seconds resulted in instability.

The sampling interval for the inverse calculation used in the quenching experiment (section 8.2.2) was much smaller because the measured temperatures were located closer to the unknown boundary.

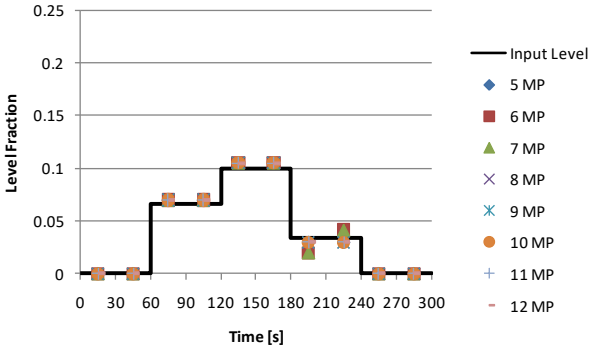


a) Step level profile, amplitude L=0.1

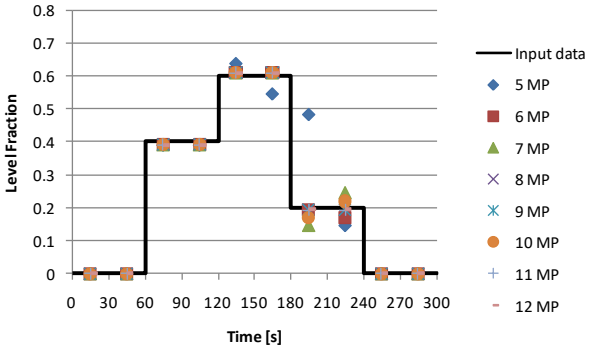


b) Step level profile, amplitude L=0.6

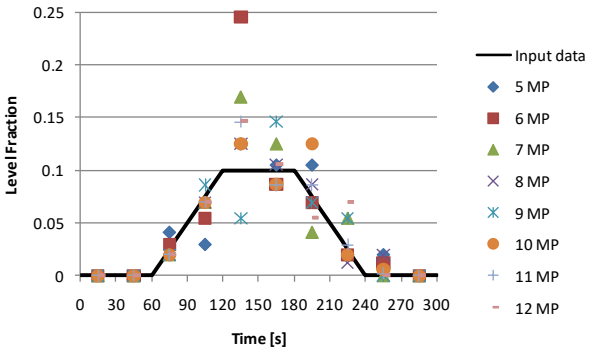


c) Ramp level profile, amplitude L=0.1

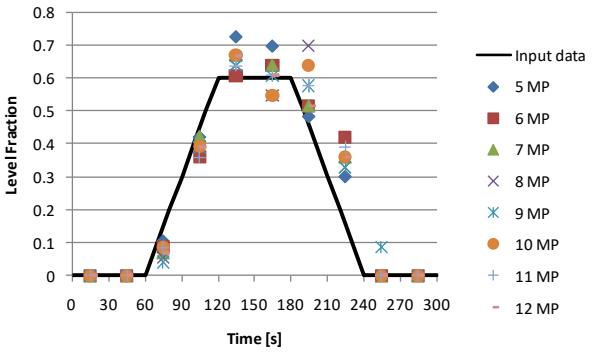


d) Ramp level profile, amplitude L=0.6

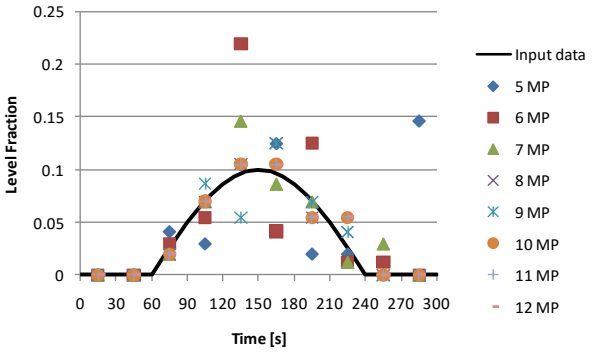


e) Sine level profile, amplitude L=0.1

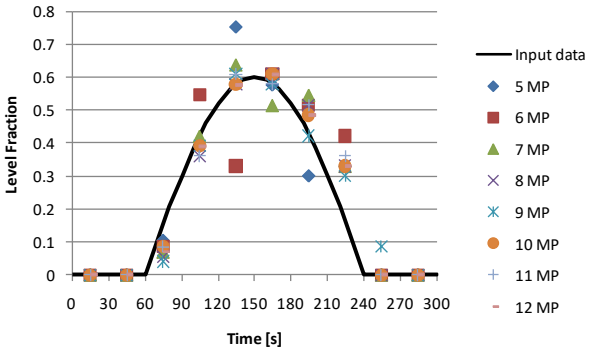


f) Sine level profile, amplitude L=0.6

*Figure 116. Calculated level profile for various numbers of measurement points (inner heat transfer coefficient for vapour and liquid estimated by inverse method)*

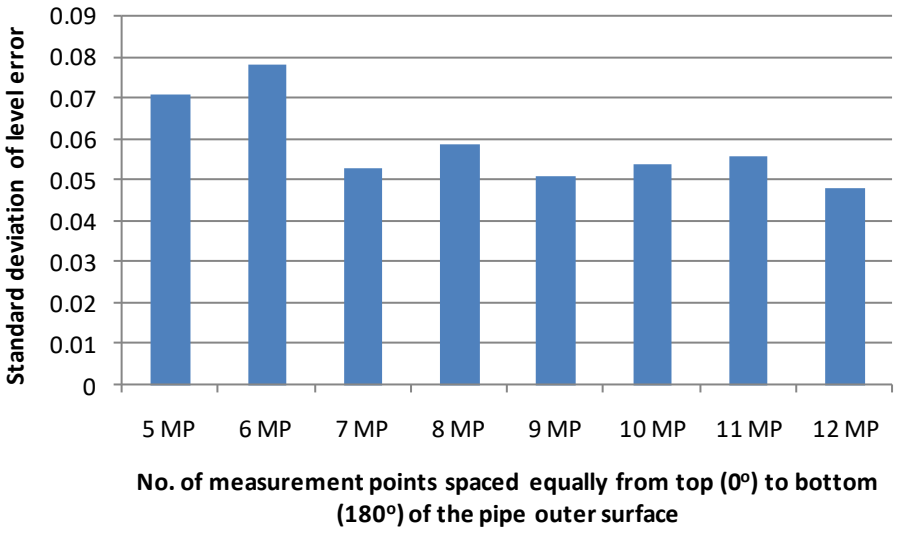


*Figure 117.Standard deviation of the errors incurred in the results presented in Figure 116.*

It was concluded that for this particular pipe geometry and material properties, nine measurement points around half the circumference would be the minimum number of measurements required to detect the level.

## 8.3.2 Installation details

The thermocouples were installed on the same section of pipe that had been previously instrumented with only top and bottom thermocouples (location 1 on Figure 6). A set of 15 thermocouples were installed around the circumference of the pipe as shown in Figure 118.

Type K thermocouples with a diameter of 3mm were used. The ends of the thermocouples were bent towards the pipe prior to the securing tabs being spot welded to the pipe. Thus the tabs firmly held the tip of the thermocouple against the pipe. After installation of the thermocouples, the pipe insulation and cladding were replaced with only the thermocouple leads protruding from the cladding.

A data logger was installed to continuously record the temperatures from the 15 thermocouples at fixed time intervals. Due to the unpredictable nature of the quenching events, the logger had to run for months at a time and thus the storage space constraints limited the sampling interval that could be logged. Hence, the majority of the data was captured at 2 minute intervals.

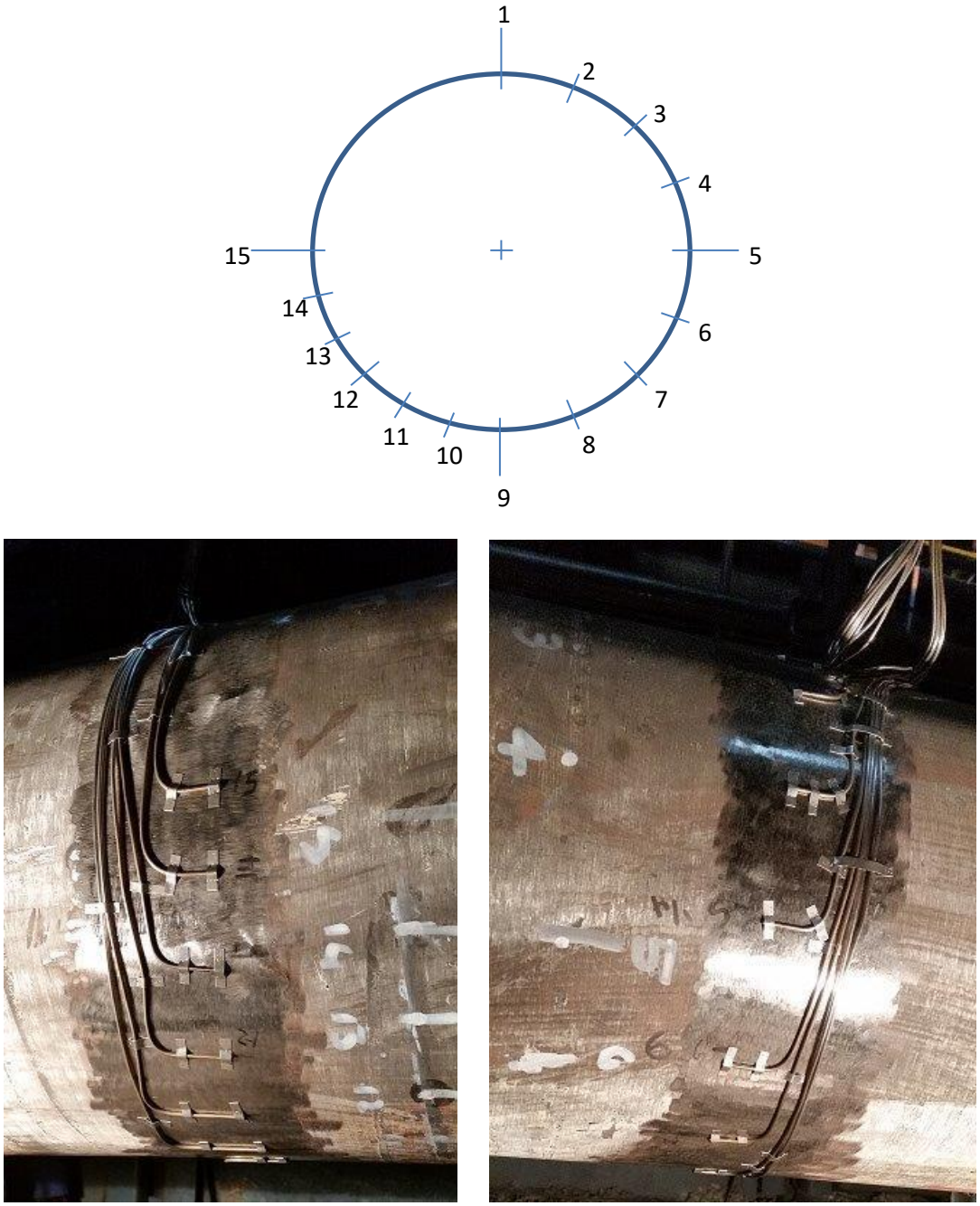


*Figure 118. Thermocouples installed around the circumference of the pipe*

## 8.3.3 Results from plant measurements

During the period from February 2017 to January 2018, the 15 thermocouples recorded the outer pipe temperatures. Most of the time, the difference between the temperature measurements was negligible and within the accuracy of the measurement system. However, 14 separate events were identified where quenching took place. The extent of the quench varied per event with the maximum differential temperature between the measurements at a point in time during each event

varying from 12°C to 70°C. A single event was selected for further evaluation based on the severity of the quench which was judged by selecting the highest initial temperature and a significant temperature drop. The measured temperatures for the selected event are given in Figure 119. The temperatures are corrected for the initial offset. The maximum initial offset was 2.89°C.

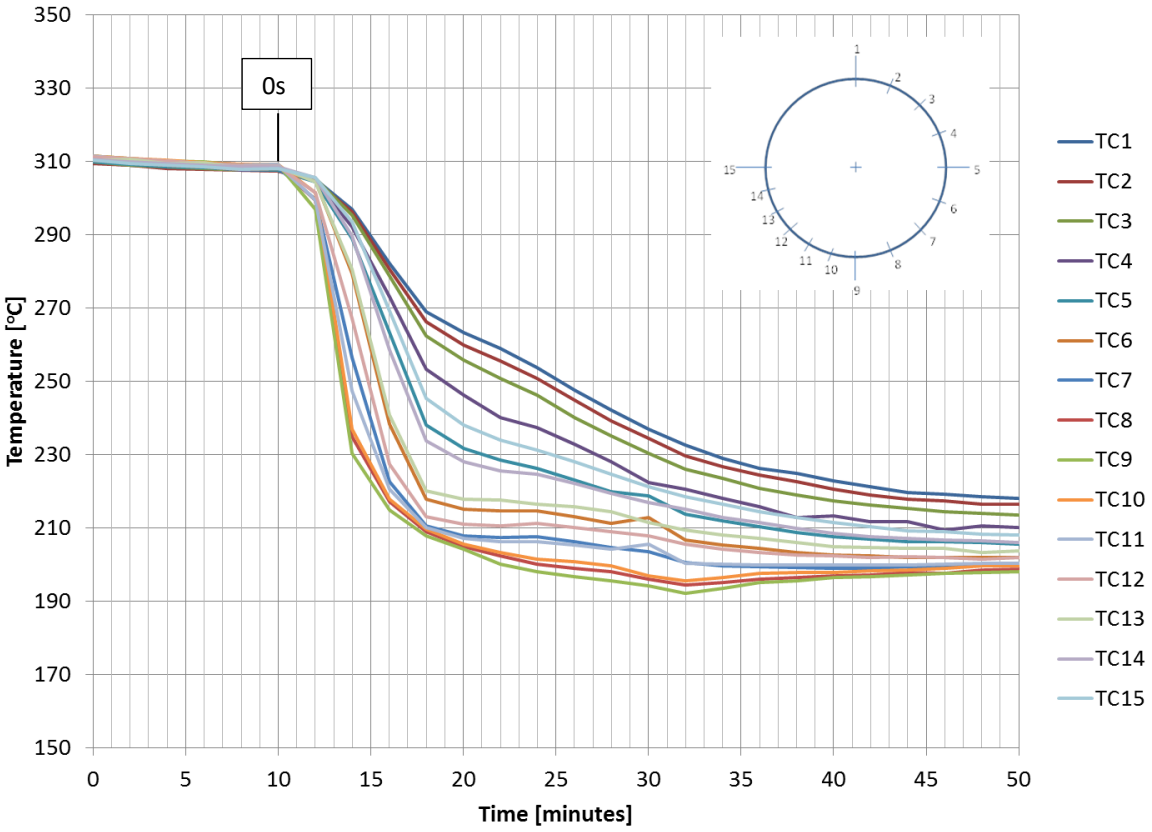


*Figure 119. Measured outer metal temperatures after correction for initial offset – main steam pipe (U1 17-09-2017)*

The temperature measurements for the event shown in Figure 119 were evaluated using the transient conduction model and the inverse calculation procedure. Two separate evaluations were done, one for each half of the pipe (TC1 to TC9 and TC15 to TC9 including TC1).

Owing to the assumption of one heat transfer coefficient for the gas side and one for the liquid side, it is not possible to match the outer temperatures around the circumference of the pipe exactly. In Figure 120 and Figure 121 the calculated outer pipe temperatures are plotted at various times and compared to the values measured. The error in calculated temperatures at 480 seconds, 600 seconds and 720 seconds are evident. The graphs highlight that the heat transfer coefficient in the liquid and gas space is not constant, both in time and in angular position. The data available and the model significantly simplifies the real situation.

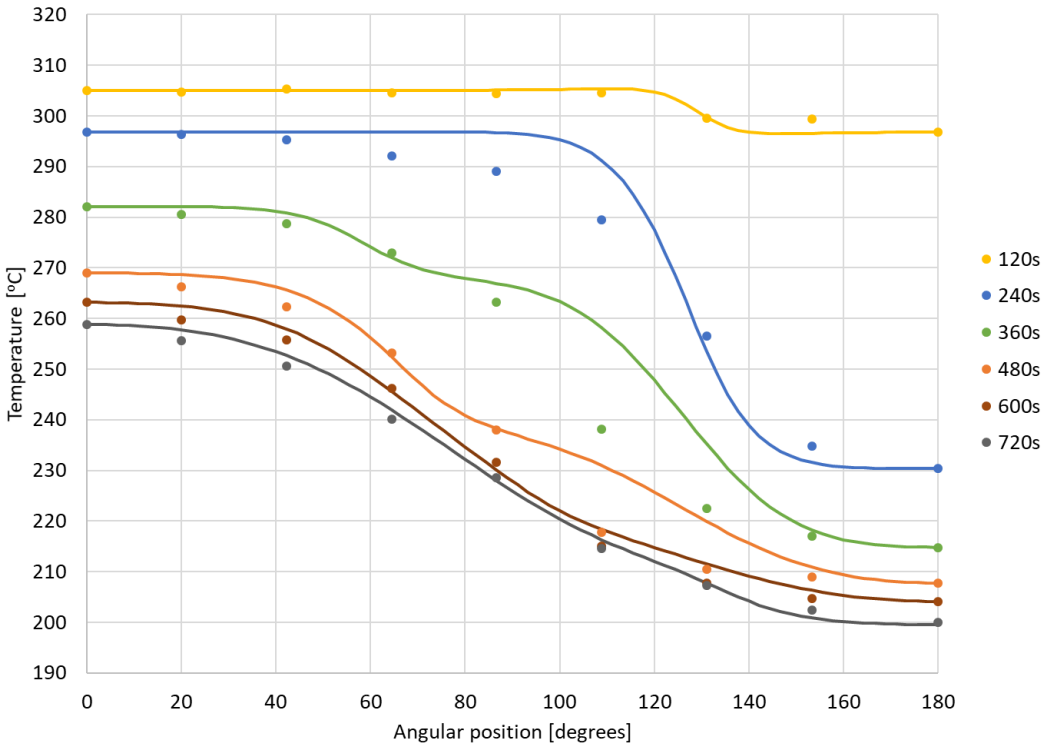


*Figure 120. Calculated outer temperatures using TC1 to TC9 compared to measured values*

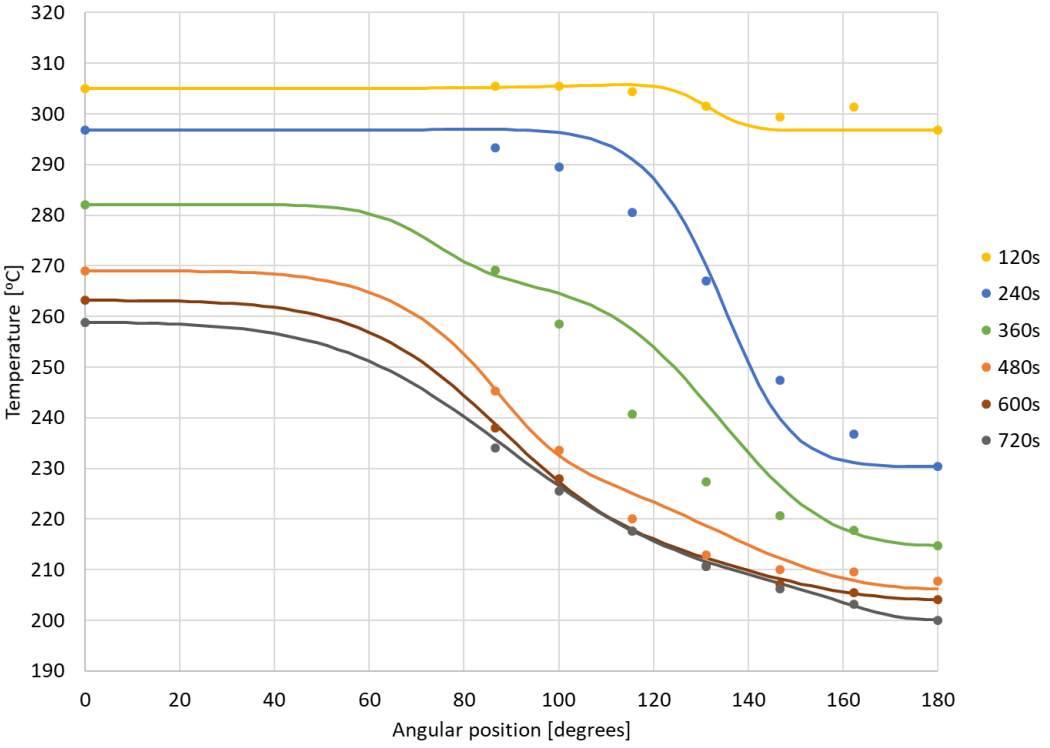


*Figure 121. Calculated outer temperatures using TC15 to TC9 compared to measured values*

The calculated levels are presented in Figure 122. Both sets of thermocouples give a similar overall level behaviour despite the closer spacing of the thermocouples 15 to 9. The level results appear to be plausible, although they cannot be confirmed by any other means. It would seem that for a period of time, the pipe ran more than half full of water. Depending on the slope of the pipe, this high level may be the result of a significant mass flow of water as discussed in 7.8.2.2.

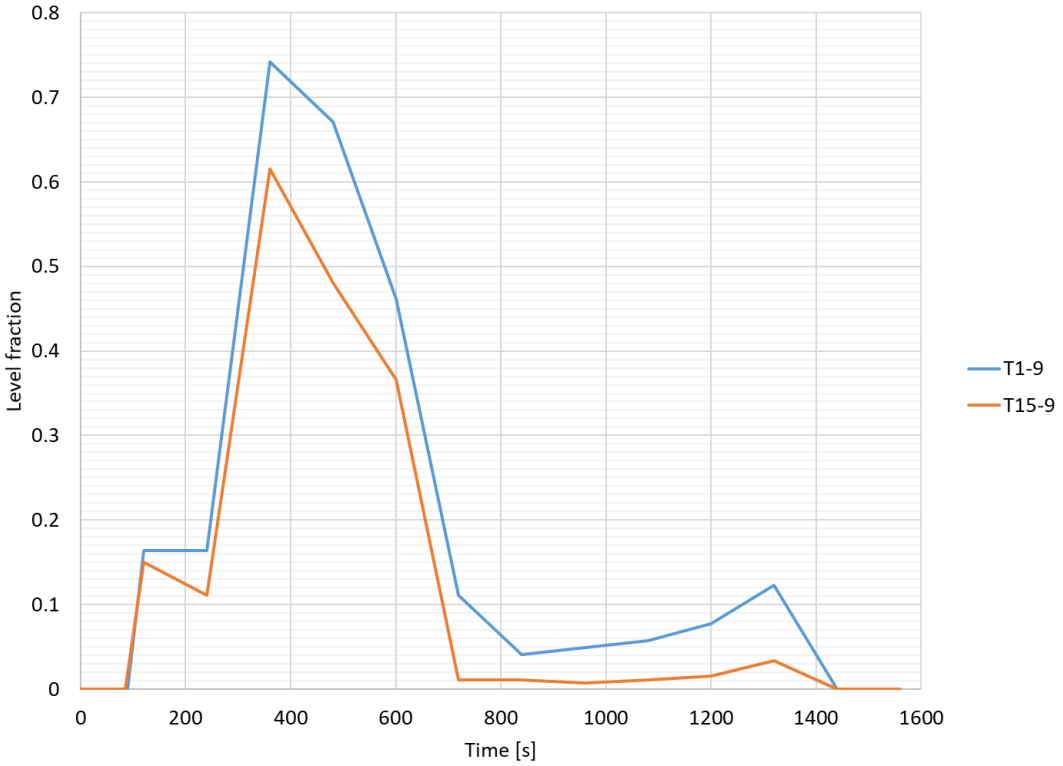


*Figure 122. Calculated levels (U1 17-09-2017)*

Another separate calculation and set of results was produced for the same event to more accurately determine the temperature profiles through the pipe wall and the heat flux at the inner surface. The liquid level was not considered in this second calculation and only the heat flux at the inner surface was determined. An inner heat transfer coefficient value that minimised the error between measured and simulated outer temperature was determined at each thermocouple location for each time interval.

The temperature profile results are plotted in Figure 123. The profiles are shown with a blue rectangle placed at the estimated level as calculated above and shown in Figure 122. At 120s and 240s, the temperature profiles and the liquid level appear to match. At 360s, it appears that the estimated level is greater than the real level as shown by the kink in the temperature profile which is closer to an effective level of 0.5. The real liquid level is transient and, as mentioned above, there is no method to measure or confirm the real value. Thus, the observation at 360s in Figure 123 highlights the expected uncertainty in this technique for level measurement.

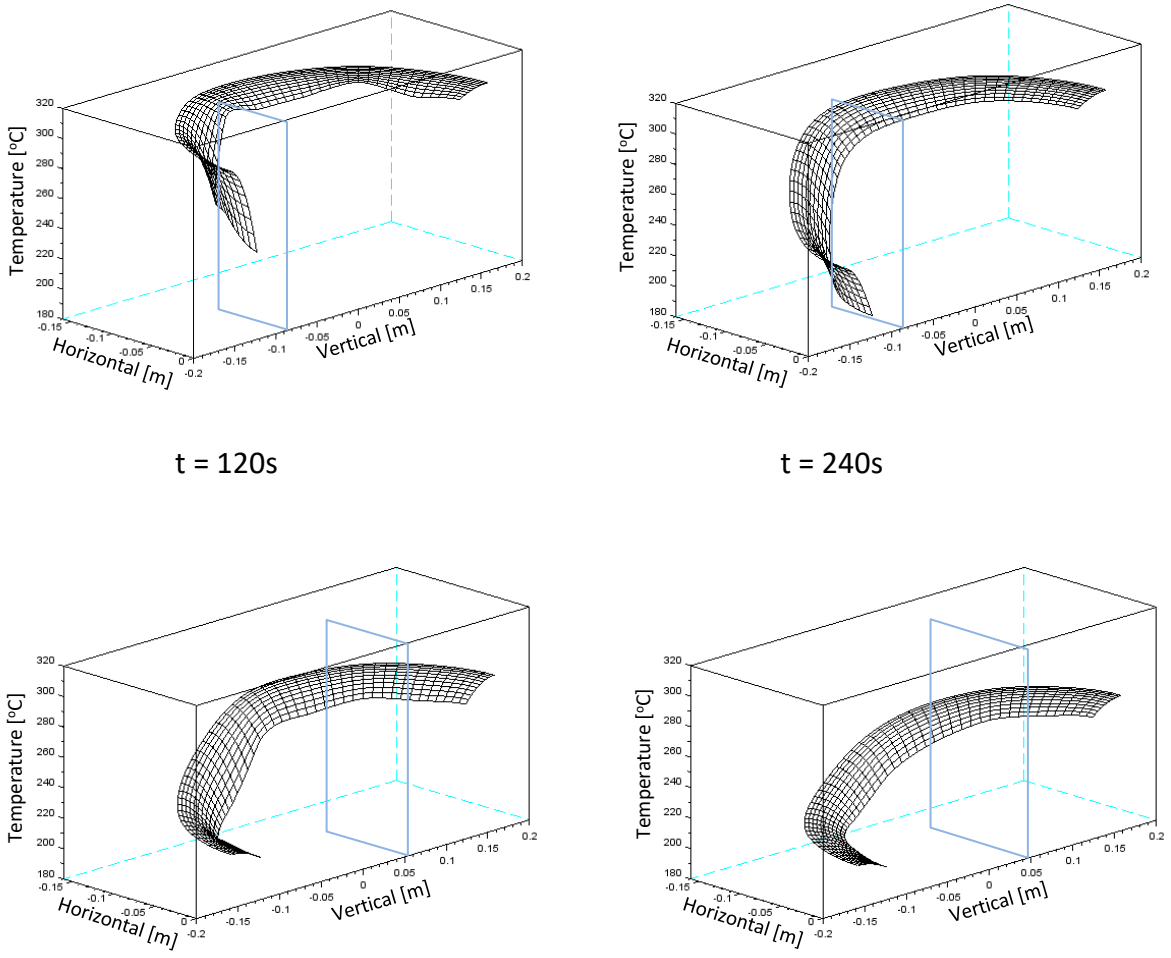


*Figure 123. Calculated temperature profiles (U1 17-09-2017)*

In Figure 124, the calculated inner heat flux is compared to the pool boiling correlations discussed in section 6.3.4. In this graph, the non-boiling data was not removed from the data set. It can be seen that heat transfer of the same magnitude as film boiling occurred at the top of the pipe in contact with the gas phase only. For the bottom part of the pipe in contact with liquid (TC9 to TC6), relatively high heat flux occurred but not as high as predicted by the theoretical nucleate boiling correlation. This result and the results from the quenching experiment (Refer Figure 113) both show that the peak nucleate heat flux did not occur at the temperature difference nor the magnitude expected.

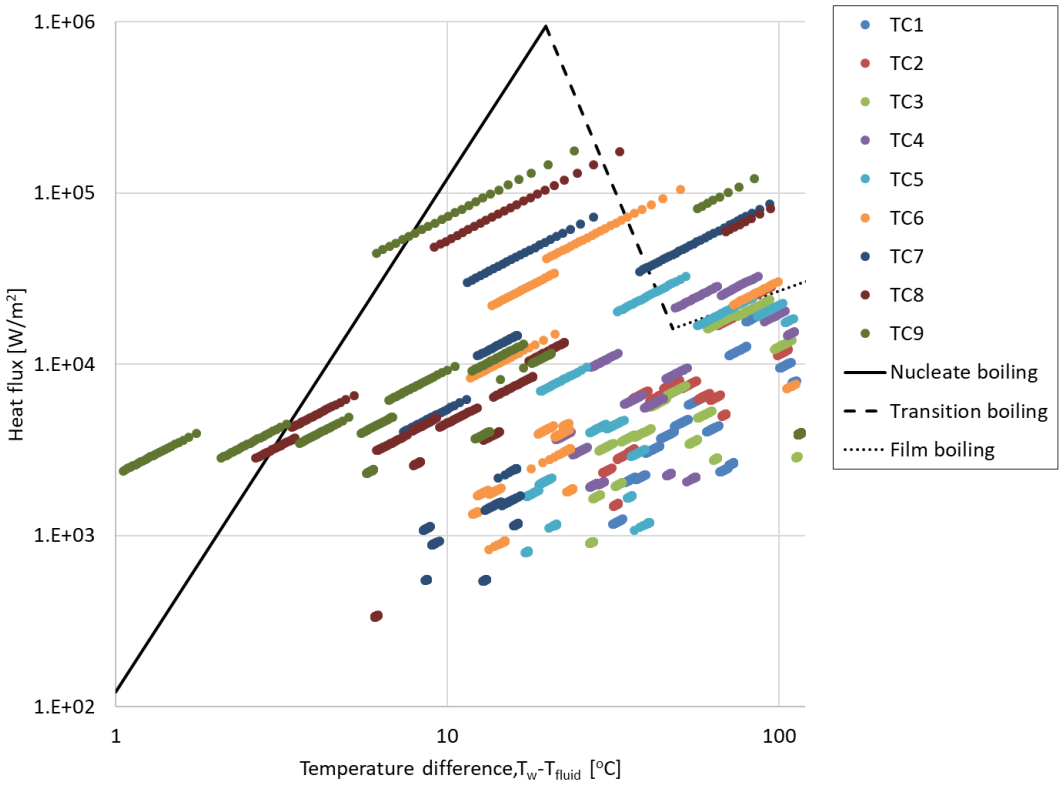


*Figure 124. Calculated heat flux compared to theoretical pool boiling correlations (U1 17-09-2017)*

## 8.3.4 Level results from quench experiment measurements

In order to further test and verify the ability to measure level by thermocouples positioned on the outer surface of the pipe, the model was applied to the quenching experiment data presented in section 8.2. Only the outer surface temperatures were used and the data was sampled at 60 second intervals to provide a stable input to the inverse calculation. Although the outer surface of the pipe was not adiabatic, it was found that the results were still reasonably accurate. In Figure 125 the actual level in the test pipe is plotted in dotted lines with each test shifted in time to enable the graphs to fit without overlapping. The level found by calculation is plotted in solid lines and shows that initially the calculated level jumps well above the actual level in each case. This is due to the splashing that occurred and wetted the pipe wall much higher than the actual level.

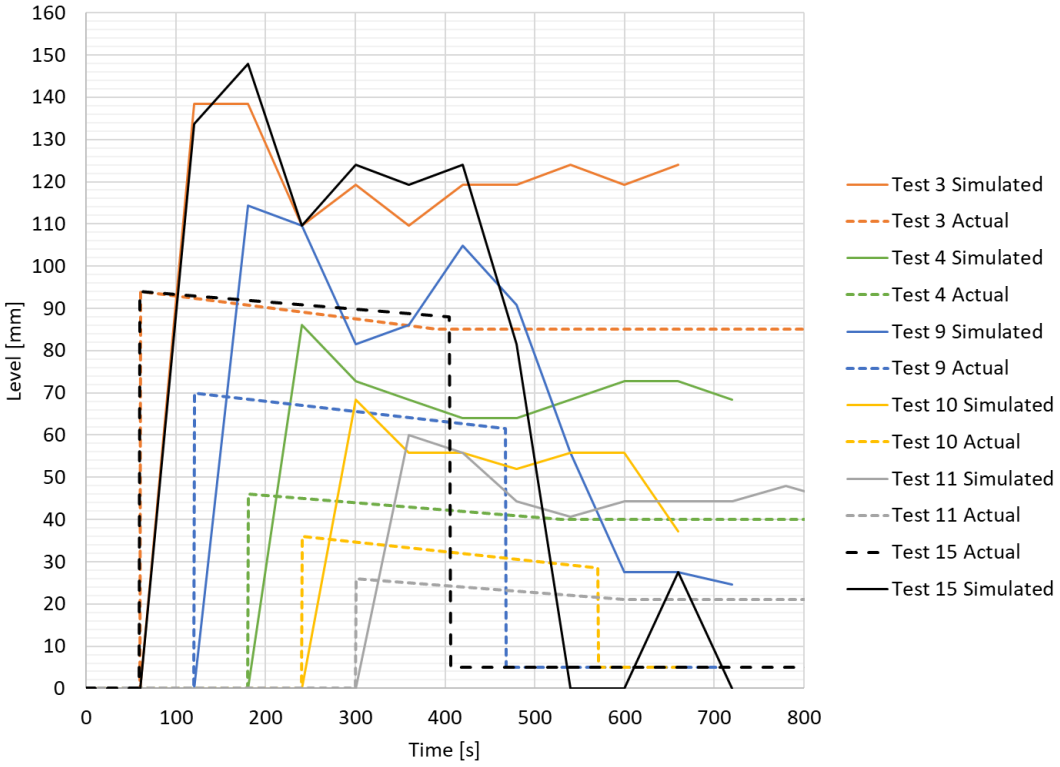


*Figure 125. Calculated levels of steam pipe quench experiment compared to actual levels*

As part of the level finding routine, the boiling heat transfer coefficients were also determined. They are plotted in Figure 126. The values calculated by the 60 second outer surface temperature measurements (dashed lines) are compared to the values calculated using the inner thermocouple data at a 2 second interval (solid lines). The inner heat transfer measurement was averaged over the number of locations under the liquid level during the test.

The inverse method using the outer measurements does surprisingly well at estimating the heat transfer coefficients over the first 120 seconds after the quench began. Thereafter, the heat transfer from the heating element influences the outer measurements and thus they predict a much reduced heat transfer coefficient.

Test 15 and test 16 were performed with adiabatic outer surface conditions and the results from those tests were less stable. However, test 15 and test 16 indicate higher transfer values at around 200 seconds which agrees with the inner thermocouple results.

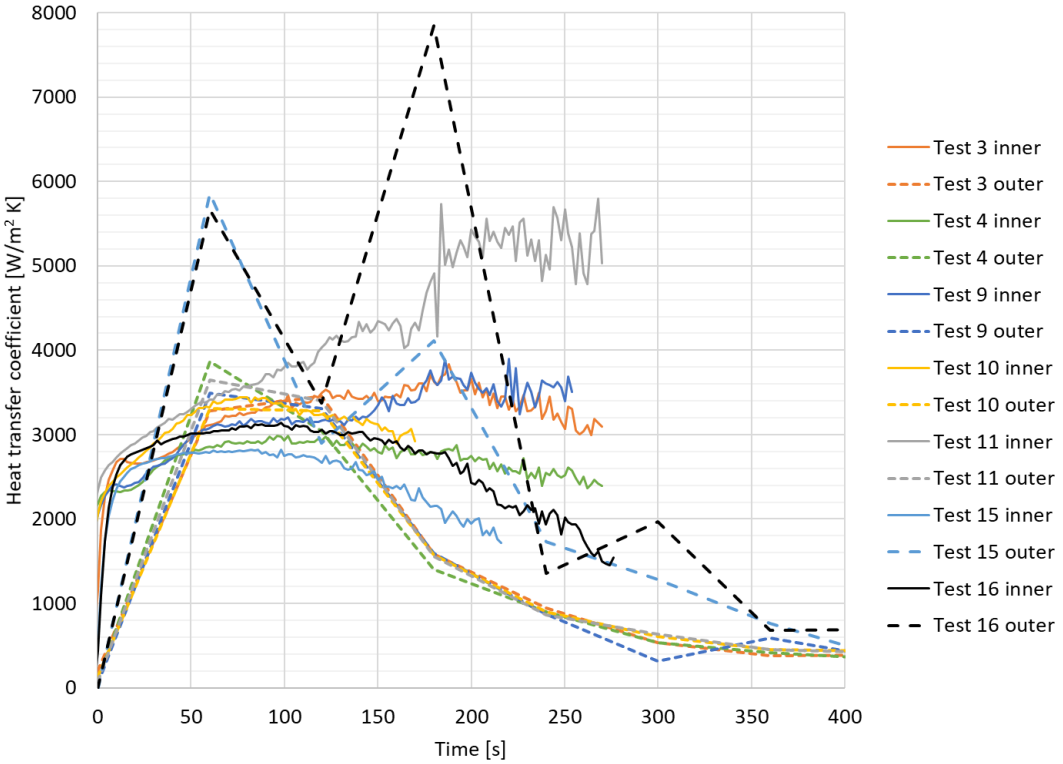


*Figure 126. Calculated boiling heat transfer coefficients using inner and outer thermocouples – quench experiment data*

## 8.4 Summary

In this chapter a transient two dimensional heat conduction model of a pipe cross section is developed. The model runs in the forward direction to determine the heat transfer through the pipe wall as a function of the boundary conditions that are imposed at the wall and the initial temperatures of the metal. The model can also be used in the inverse direction by iteratively applying guess values of a particular boundary condition in order to achieve a desired temperature at a particular point in the pipe wall.

The inverse calculation was used to analyse data from a quenching experiment that was specifically set up to test the methodology and the level finding capability of various thermocouples located around the circumference of a pipe. It was found that the level estimating capability of the outer temperature measurements was reasonably accurate, however, the measured boiling heat transfer coefficients were significantly lower than those predicted by the theory.

Data from plant measurements were also evaluated using the inverse method and it was found that similar values of heat flux existed during an actual quench event that occurred. The model was also able to find estimated liquid levels in the pipe, although these cannot be further verified.

The reason for the interest in measuring liquid level is to enable relatively accurate reconstruction of the temperature profile in the pipe wall. The minimum number of temperature measurements located around the circumference of the pipe was studied and for the case of a typical main steam pipe geometry, it was found that nine measurements equally spaced around half the pipe circumference would be required. These would need to be logged at 30 second intervals to provide good data for further analysis. Although it is technically feasible to install this equipment at every header and pipe in the plant, it is not justifiable.

Alternatively, the effects of quenching can be estimated by using the transient heat conduction model in the forward direction. In this case a liquid level must be estimated as well as the heat transfer coefficients in the liquid and gas space. These boundary conditions are imposed on the pipe and the resulting temperature gradients can be calculated.

The uncertainty in the level estimate over time is likely to be significant. In this case it is recommended to consider a constant liquid level and calculate the resulting temperature gradients. This approach is more conservative when estimating the stresses in the pipe wall.

The estimation of pipe through-wall temperature gradients is necessary for the calculation of stresses which can then be used to assess the damage caused by quenching. The next chapter briefly considers the calculation of stress from temperature gradients.

# 9. Stresses caused by quenching

Quenching causes significant through-wall temperature gradients in the superheater and main steam piping components. The preceding chapters discussed ways to estimate local liquid levels and local through-wall temperature gradients. The next step of the methodology is to determine the magnitude of stress in support of activity 3.9 in the methodology, as shown in Figure 127.

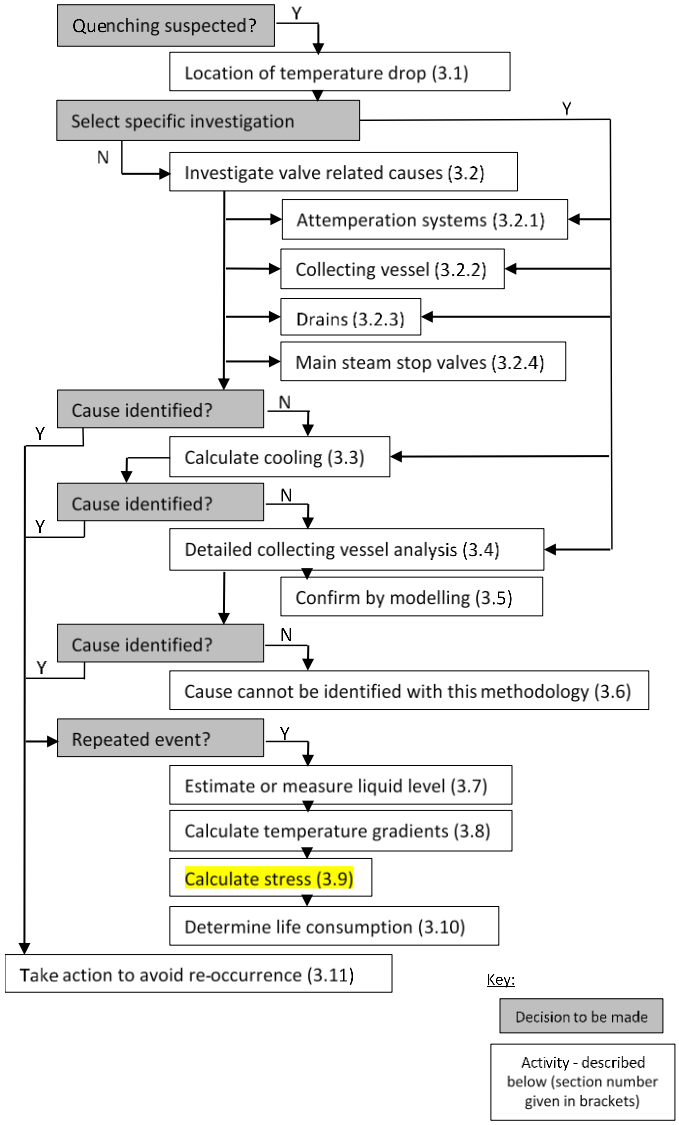


*Figure 127. Activity 3.9 in the methodology*

Once the stresses have been obtained, they are interpreted as the stress cycle in a fatigue calculation linked to a material damage model that can predict the life consumption or damage sustained by specific components due to quenching. The fatigue calculation is outside the scope of this project and is not presented here.

Equation 1 in chapter 2 provides a simple estimate of the maximum stress that can be caused due to thermal shock or quenching. This value is expected to be conservative but can be used as an indicator to decide if further analysis is warranted. For the case measured at Power Station A and shown in Figure 119, a maximum temperature difference of the fluid of 100$^{o}$C is assumed. Using the material properties of the pipe and a stress concentration factor of unity, the maximum thermal shock stress is found to be 164MPa. A stress cycle of this magnitude would cause fatigue damage of the component and thus a more detailed calculation is warranted.

For the event measured at Power Station A, the stresses caused by quenching were estimated with the aid of a two-dimensional finite element analysis (FEA) of the pipe cross section. A static structural analysis in ANSYS coupled to a transient thermal analysis was used. The pipe was modelled by using symmetry boundary conditions along the vertical edges of the half pipe cross section. A mesh of quadratic elements was used with five elements through the pipe wall and 48 elements around the circumference of the half circle. A mesh independency analysis showed that the chosen mesh size with 240 elements introduces an error in maximum equivalent stress of approximately 1.5%. The error is acceptable considering the goal of determining an order of magnitude of the stresses during quenching.

The initial temperature was set to the temperature of the pipe before the quenching event. Thus the model assumed the pipe had zero thermal stress prior to quenching.

The quench on 17 September 2017 that was measured by the outer thermocouples installed at the plant was evaluated (Refer section 8.3.3). In ANSYS, an adiabatic outer surface of the pipe was assumed and a heat transfer boundary condition was applied at the inner surface. The boundary conditions were defined based on the heat transfer coefficients calculated in section 8.3.3 together with the fluid temperature. The ANSYS transient thermal analysis was used to calculate the temperatures through the pipe wall and agreement with the pipe wall conduction model described in chapter 8 was achieved. The temperature profiles at various points in time are shown in Figure 128.

The calculated equivalent stress is shown in Figure 129. The development of the stress pattern over time shows that the inner surface experiences the highest stress. The stresses increase over time with the greatest stress of 81MPa experienced at the inner surface at the bottom of the pipe at 240s. The yield strength of the material is more than 300MPa at these temperatures and thus the

quenching would not cause any deformation. However, the high localized stress at the inner surface would cause crack initiation and growth, making it necessary to pursue this further with a fatigue calculation.

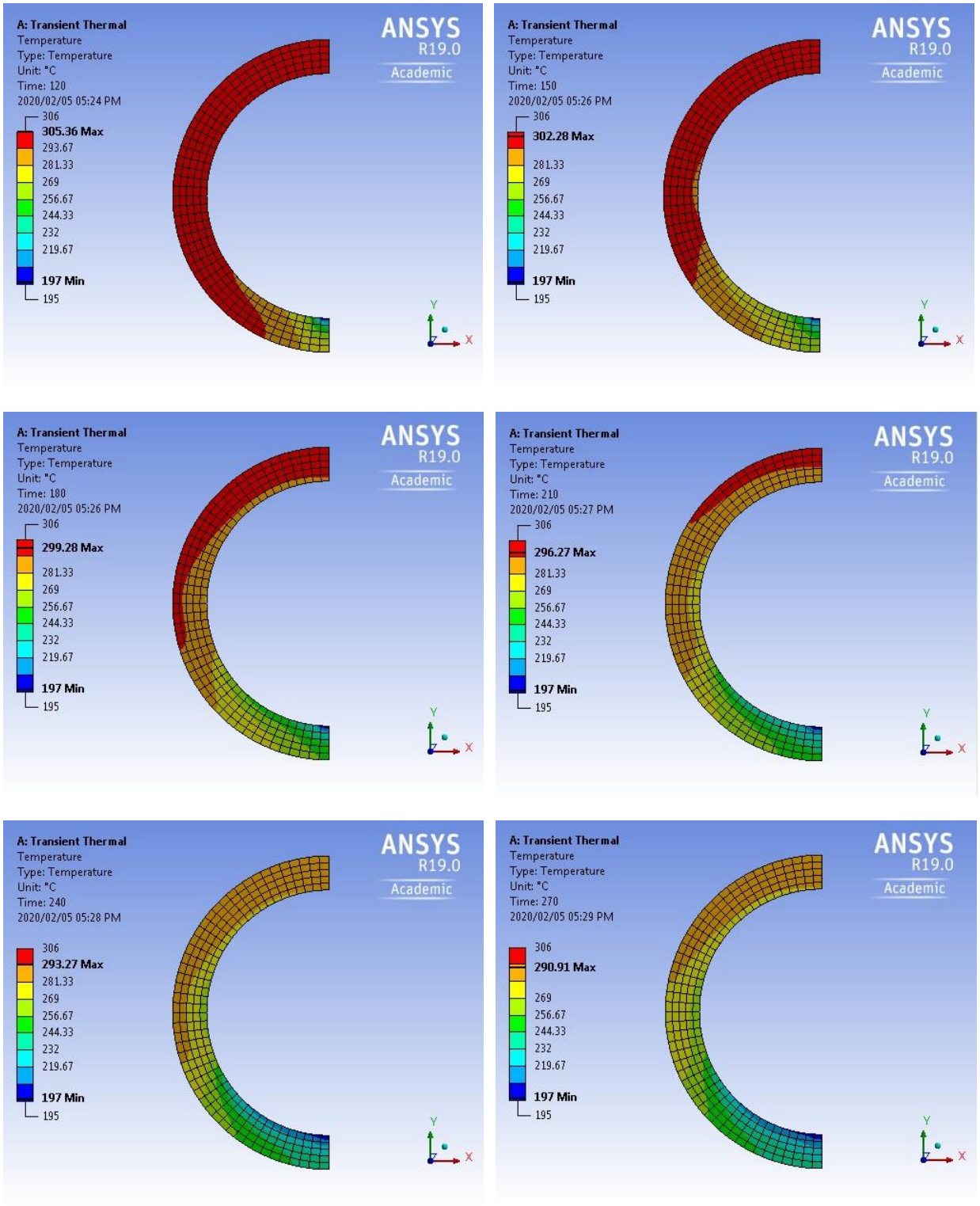


*Figure 128. Temperature distribution calculated in the main steam pipe during quenching (U1 17-09-2017)*

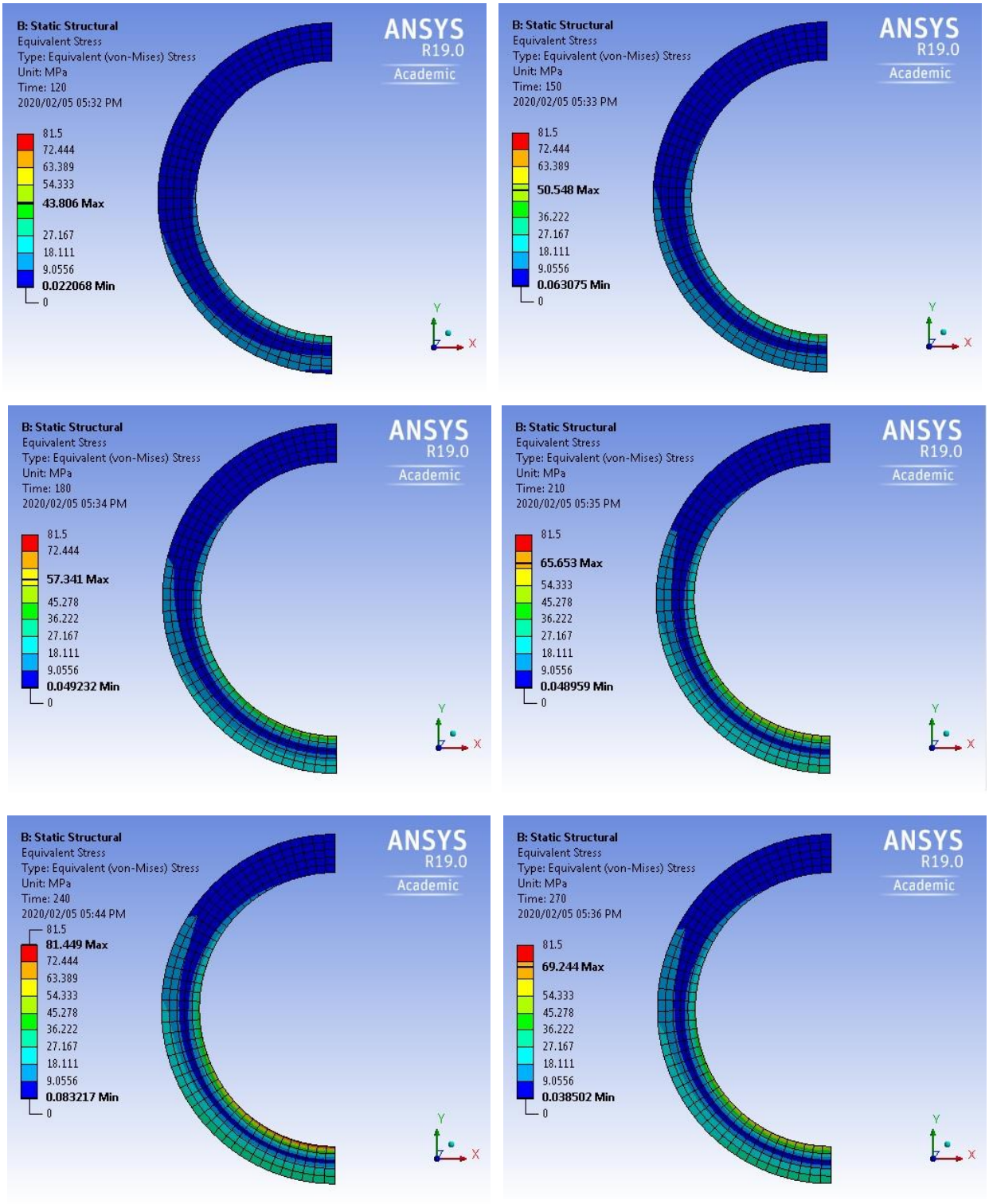


*Figure 129. Estimated stresses in the main steam pipe during quenching (U1 17-09-2017)*

The above event that occurred at Power Station A is not the worst case in terms of temperature gradients that have occurred. During other events, the main steam pipes were at temperatures above 500°C when they were quenched with water at 300°C. These temperature profiles and stresses were investigated and the results are given below (Figure 130 and Figure 131).

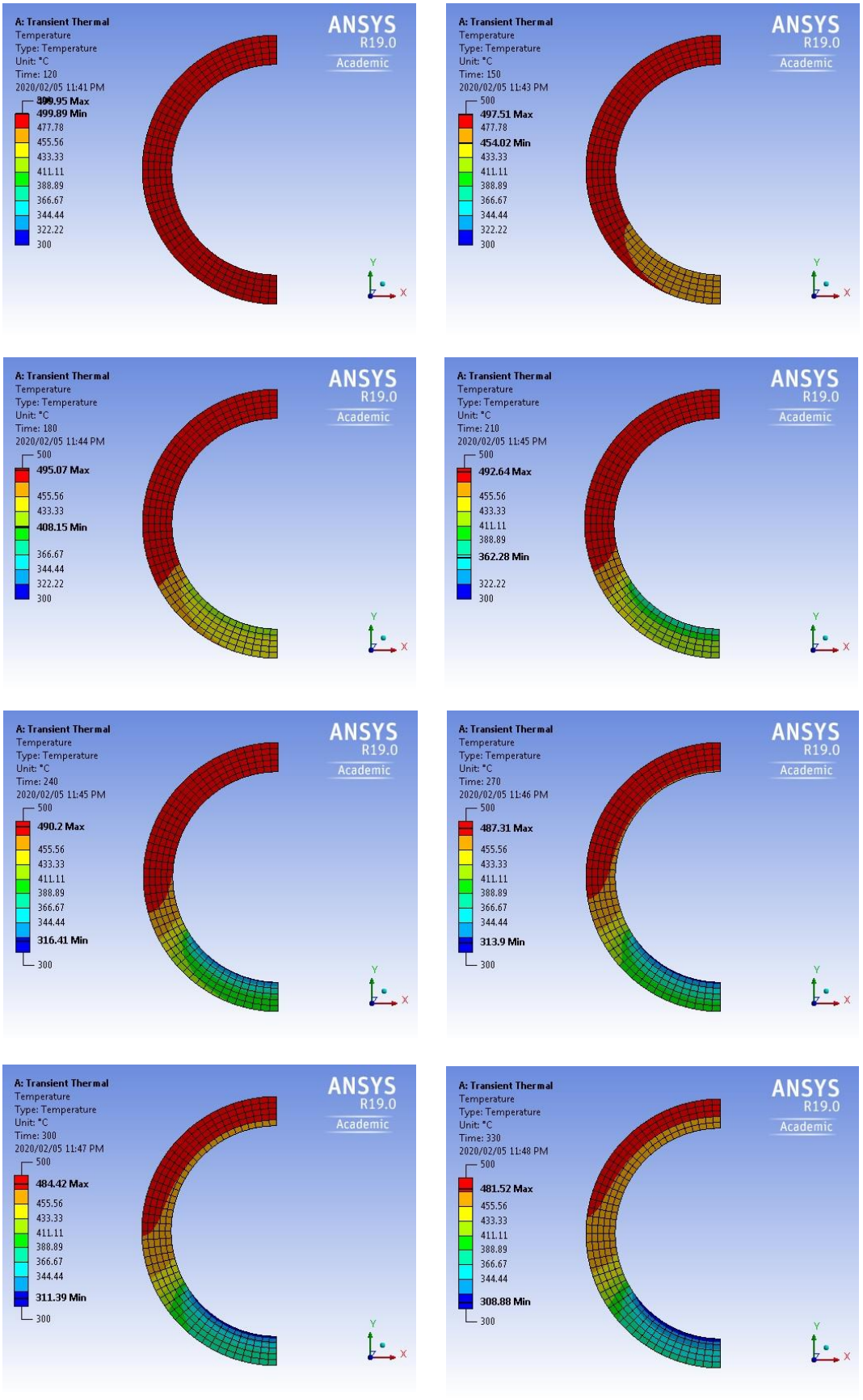


*Figure 130. Estimated temperatures in the main steam pipe during quenching*

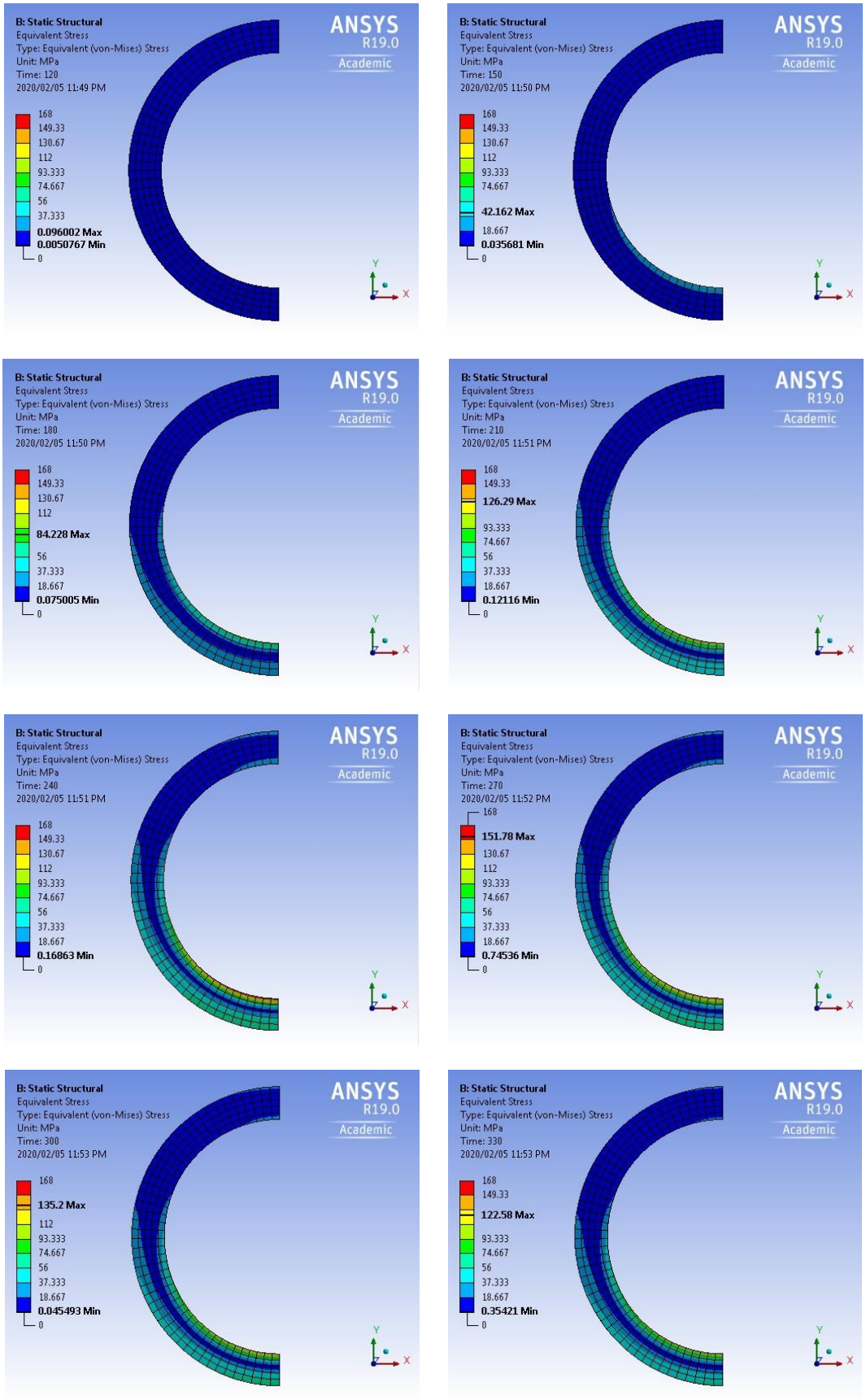


*Figure 131. Estimated stresses in the main steam pipe during quenching*

Besides the high initial temperature difference of nearly 200°C between the pipe wall and the water, the cases were calculated with a constant water level of 55mm (height fraction of 0.22) and a constant boiling heat transfer coefficient of 10 kW/m$^2$ K. The heat transfer coefficient is higher than the highest value of 7.3kW/m$^2$ measured in chapter 8.

The initial phase of the simulation up until 120 seconds had no water level as seen in the temperature and stress profiles (Figure 130 and Figure 131 top left). The water was then introduced over 10 seconds and the level was kept constant until the end of the simulation. The intention was to create a steep temperature gradient at the height of the water level. This effect can be seen in the temperature profiles in Figure 130.

The results show that the quench causes tensile stresses of the order of 168MPa at the bottom surface of the pipe wall. This is a significant stress cycle which would be superimposed on any other loading on the pipe at the time. The high stresses are only observed close to the flooded inside surface of the pipe. The bottom outer portion of the pipe is in compression to balance the inner tensile stresses.

The stress analysis above provides the order of magnitude of the stresses caused by quenching. The analysis shows that the stresses are not negligible, but it also highlights that for this case, the level of liquid does not play a major role in determining the highest stress that occurs. The level determines the height of internal surface of the pipe that is affected by high stresses and it also determines the through-wall stress pattern around the pipe circumference. This stress pattern could be important when considering headers with holes for tube connections.

Besides stresses in the two dimensional pipe cross section, the stresses in the axial direction along the pipe may also be important. A pipe quenched by liquid flowing along the bottom will tend to deflect upwards in the centre due to the non-uniform temperature profile and the effect of the thermal coefficient of expansion along the length of the pipe. This upwards bending of the pipe may cause damage to pipe supports.

# 10. Summary and conclusions

A number of quenching events took place over a number of years at Power Station A. Evidence in the form of early replacement of components and a series of high differential temperatures measured between the top and bottom outer surface of a steam pipe led to the initiation of this study into the causes and analysis of quenching. A review of available literature showed that a consolidated methodology to determine the cause of quenching did not exist. There were also no modelling techniques readily available to model the boiler in a shut down state in order to provide information that could be used to find the cause of quenching or potentially track the level of liquid as it accumulated in the superheater.

In this work, a methodology to determine the root cause of quenching in a once-through tower type boiler was developed and demonstrated. The methodology consists of a series of activities that includes three modelling elements (Refer Chapter 3).

The first activity involves the investigation of plant steam temperature drops and determining the location and path of the water. Potentially the cause of quenching will be determined after this first activity and then it is not necessary to continue with the methodology other than to take action and ensure that the failure that caused quenching is addressed.

The second activity requires the evaluation of valve related causes, namely attemperator spray valves, the valves used for collecting vessel level control and drain valves. The main steam stop valves, if fitted, can be used to isolate the main steam system and knowing their position is useful, but the valves are not a root cause of quenching.

The next activity in the methodology requires investigation of the potential for condensation in the superheater by cooling. This is accomplished by a heat transfer model of the superheater which is the first modelling element in the methodology. The model is presented in Chapter 4 and considers heat transfer on the inside and outside of the tubes. The tube wall temperature is represented by a lumped parameter for each of the tube bundles and headers. The model incorporates convection and radiation heat loss on the outside of the tube bundles of the superheater and either natural convection or condensation on the inside of the tubes.

The heat transfer model was applied to Power Station A and verified by comparison with plant data. The verification was difficult owing to the wide spread of measured steam temperatures and a lack of agreement of the calculated and measured superheater pressure. However, the cooling rate of the measured superheater tube metal temperatures matched the simulated value and it was also found that the real superheater pressure had been affected by leaking valves. Thus, the heat transfer model was considered to be sufficiently accurate for the intended purpose.

It was originally thought that the quenching at Power Station A was caused by cooling of the superheater. However, after application of the heat transfer model to the quenching cases, the results proved that this was not the case. The time taken to cool the superheater sufficiently to initiate condensation was beyond the time period when quenching typically occurred and the rate of condensate production would not be able to fill the superheater.

In the event that valve related causes and condensation by heat transfer fail to explain the quenching observed, then further detailed analysis of the collecting vessel and separator vessel system is warranted. This step was described in Chapter 5. It was found that the cause of quenching at Power Station A is separator vessel overflow. The particular configuration with a drop of 16m from the outlet of the separator vessels to the Superheater 1 inlet headers, without any interconnection between the separator steam outlets, promotes the formation of a siphon. The siphon initiates by poor collecting vessel level control which allows the separator vessels to fill and start to overflow. The first of the four separator vessels to overflow and cool the downstream pipe sufficiently initiates the siphon. The siphon is strengthened when subcooled liquid reaches the separator vessels. Once the siphon has been initiated, it draws down the other separator and collecting vessel levels. When the collecting vessel level drops, the controls react by reducing the circulation flow and the siphon is then fed by feed water which is added to the boiler to make up the difference between the minimum economiser inlet flow and the circulation flow. The operator is unaware of the situation because the plant instruments cannot detect a siphon. Thus, the siphon is able to continue and draw a significant amount of water into the superheater until the superheater and main steam system are flooded.

The progression of temperature drops in the superheater as well as the behaviour of the collecting vessel level and other systems such as the feed water, circulation and drains system were analysed in detail. Four cases studies are presented in the appendices and each case is consistent with the root cause described above.

The separator and collecting vessel system were modelled in Flownex and shown to perpetuate the siphon and match the behaviour seen in the plant measurements. The same model was applied to the similar configuration at another power station and it was found that a siphon could also be initiated, but the siphon was weaker and unable to reduce the level in the collecting vessel. Thus, the siphon could not be sustained because the plant controls would react and reduce the amount of water fed to the boiler.

Additional information about the exact location of some of the evaporator outlet temperature measurements at Power Station A were obtained. This information was not available before and led to further confirmation of the siphon effect and the reversal of flow in the distribution pipes to the

non-overflowing separators. Using the methodology, the root cause of quenching was successfully identified to be the siphon effect caused by the specific configuration at Power Station A.

Modelling the separator overflow is the second modelling element of the overall methodology and can be used to identify or confirm the presence of a separator overflow. Separator overflow modelling was undertaken using three different approaches namely: a simplified model programmed in Microsoft Excel, a Flownex model and the Liquid Tracking Model or LTM. The simplified model and the Flownex model are described in Chapter 6 while the LTM is discussed in Chapter 7.

The models consider the superheater as one or more control volumes containing a two phase fluid with the phases separated to create a level. The liquid phase exists at the bottom part of the control volume and the gas phase at the top part. The phases are in thermal equilibrium. The walls of the tubes and headers exchange heat with the steam in the control volume and inventory can be added or subtracted from the control volume. The transient mass and energy balance equations are solved for each control volume in order to determine the state of the fluid at the end of the time step.

In the case of Flownex, the transient momentum equation is also solved. However, the liquid mass flows are calculated by other means and then used as boundary conditions in the model. Thus, the momentum equation is not fully utilised and this is due to the lack of detail available for the modelling of the superheater during quenching.

The Flownex model consisted of two control volumes modelled using the two phase tank component. The model was used in an inverse manner to find the required separator overflow to minimise the error between measured and simulated superheater pressure. A reasonable match with plant data was achieved.

The LTM makes use of various simplifying assumptions to determine the flows of liquid and gas between control volumes without the detail required to enable the momentum equation to be solved. This approach is the correct level of modelling to apply to a large complex system such as the superheater at the limited level of detail that is available.

It was found that the superheater pressure is a useful indicator of events occurring on the plant. Any attempt to model the separator overflow must aim to reproduce the measured superheater pressure in the simulation. The superheater is generally isolated on the steam side but still pressurised. Any mass flow of steam or water into or out of the superheater affects the pressure and must be taken into account in the model.

The subcooled liquid interface that exists at the separator vessels causes condensation of steam. This creates a flow of steam in the reverse direction out of the superheater to the subcooled interface where the steam is condensed and increases the water temperature. The increase in water

temperature together with the water flowrate can be used to estimate the condensing steam flow. This condensing steam flow is considered in the models.

During the separator overflow, hot metal is quenched by water which evaporates. This evaporation increases the overall pressure in the superheater and the magnitude of the effect is dependent upon the amount of metal quenched as a function of time. Thus, the assumptions made in accounting for the quenching are important, but are difficult to do accurately because of the lack of detailed information about exactly where the water flowed and how fast it accumulated and filled the superheater.

The LTM attempts to address this problem with more detail than what was used in the simple model and the Flownex model. However, it was found that the additional detail and effort did not improve the LTM results significantly. The LTM achieved the best balance of accuracy of results and ease of implementation when the superheater was divided into eight control volumes. The eight control volumes split the superheater into two halves which matched the configuration at Power Station A considering the interconnections of the superheater legs. Thus, the most suitable number of control volumes to use when modelling other plants will be dependent on the plant configuration.

The minimum required level of detail was included in the models to replicate the real processes seen on the plant as verified by plant data. It is acknowledged that the models were not able to accurately predict the measured parameters. However, the overall characteristic of the transient steam pressure and temperature could be determined and this is an important positive result of the separator overflow modelling. On the gas side, the calculated transient outlet temperature behaviour did not match the measured data, but the temperature was of the same order of magnitude. The relative inaccuracy of the results is due to the philosophy of applying the least level of detail to the problem. However, this is appropriate for the intended purpose of the models which are to identify behaviour of especially steam side pressure and temperature during quenching.

The modelling of the separator overflow can be undertaken by means of any of the three methods described above. If only used for confirmation of the root cause of quenching, then the simple model may be adequate. For calculation of liquid level as it accumulates in the superheater, the LTM is recommended.

Following successful identification of the root cause of quenching and estimating the overall path of water and/or liquid level, the methodology in Chapter 3 suggests further evaluation of the through-wall temperature gradients, especially for repeat events. The overall liquid level in the superheater will be available from the modelling carried out in previous steps of the methodology. Local liquid levels can then be estimated.

In flow through situations, components affected by quenching are determined by visual inspection to determine the flow path. Where the flow was carried by multiple tubes, estimates of the flow rate per tube can be made to determine how many tubes were affected (Refer Chapter 7). In horizontal pipes and headers, the local levels can be estimated by an open channel type of flow analysis. However, the relationship of flow rate and water depth in the pipe is dependent on the pipe slope, which may not readily available. Ultimately, the prediction of water levels is a rough estimate and this should be considered before further action is taken, such as deciding which components to physically inspect for damage.

The third modelling element of the methodology is a two-dimensional transient pipe wall conduction model that can be used at selected localities to evaluate the temperature gradients within the pipe wall. The model can be used to perform an inverse calculation to find the boundary conditions that produce measured temperatures at particular locations. This method can be used to determine the heat flux at the inner wall of the pipe as well as the temperature gradients through the pipe wall.

At particular locations on the superheater piping and headers, it is possible to install thermocouples around the outer diameter to measure quenching and the water level. It was determined that nine measurement points at a pipe cross section around half the pipe circumference is required to detect level assuming piping of a similar thickness and diameter as the pipes considered in this study. An experiment of installing thermocouples around a pipe at Power Station A was carried out and quenching events were measured. It was found that significant temperature gradients occurred through the pipe wall and also that it was possible to estimate the liquid level in the pipe during quenching.

Thermocouples were also installed on a test section of pipe and quenching experiments were carried out to measure the heat transfer coefficients and provide data to test the level measurement capability of the outer wall temperature measurement points. It was found that the non-adiabatic outer surface of the pipe influenced the temperature measurements. Even with this unknown, it was demonstrated that the level measurement capability of the outer temperature measurement points and the calculation routine was relatively accurate. The measured heat transfer coefficients deviated significantly from the expected boiling correlations and the reasons for this deviation could not be fully explained. It may be due to the transient nature of the experiment compared to the steady state experiments used to create the correlations, or potentially the oxide layer on the surface of the pipe.

The stresses caused by quenching were briefly considered. The highest temperature gradients in the pipe wall occur at the inner surface of the pipe where water boils on the surface. Thus, quenching causes significant stresses on the inner surface of components which initiates cracks or

promotes crack growth. Maximum tensile stresses in non-uniform cross sections, such as holes in headers, will be worse affected and need to be modelled on a case-by-case basis.

The stresses during quenching are used in a material damage model to determine the accumulation of fatigue damage and reduction in life of a particular component. The fatigue calculation is outside of the scope of this project.

The project aimed to establish a methodology to find the root cause of quenching with particular application to Power Station A and to provide local temperature gradients that could be used for further stress analysis. These objectives were achieved and included the development of three modelling elements namely the superheater heat transfer model, the liquid tracking model and the transient heat conduction model of the pipe wall. The first two elements are applicable to a boiler after shut down, while the third element can be applied more widely.

The proposed methodology and associated models can be applied to other existing power plants and units that may experience quenching events from time to time. The methodology can be used to determine the cause of quenching and estimate liquid levels to assist in determining which components have been affected. In order to apply the liquid tracking model, basic information about the superheater and interconnecting piping is required. The information must enable the elevations, internal steam volumes and the metal masses to be determined. The heat transfer model requires the configuration of the tubes in the superheater, the tube dimensions and the material properties.

Once liquid levels have been determined, the local temperature gradients and stresses in those components can be estimated using the transient conduction model of the pipe wall. The two-dimensional model is applied at selected points where quenching is known to have occurred.

The design of new boilers may also benefit from parts of this study. Firstly, the piping configuration of the proposed new design can be evaluated for the possibility of a siphon forming. Where parallel circuits exist from the exit of the separator vessels and the superheater inlet is lower than the separators, it is advisable to interconnect the high point of the piping system. This balances the pressure of the parallel circuits and eliminates the possibility of a siphon.

Secondly, during the analysis of purging the gas side of a proposed new boiler design, the heat transfer model from this study can be used to calculate the cooling of the convection pass. The cooling effect and potential for condensation caused by the purge air flow rate can be evaluated.

The work also enabled better understanding of the complex and coupled physical transient phenomena occurring simultaneously during a boiler cooling down period. This will assist in devising improved operation of the boiler and enhanced control and instrumentation strategies to reduce the number of quenching events and prevent damage to the power plants.

# 11. List of References


[1] "World energy outlook 2018," International Energy Agency.

[2] J. Rudolph, S. Bergholz, B. Heinz and B. Jouan, AREVA Fatigue Concept - A Three Stage Approach to the Fatigue Assessment of Power Plant Components, Nuclear Power Plants, InTech, 2012.

[3] M. Bezuidenhout, P. Doubell, A. Downes, F. Havinga, A. Naidoo, M. Mkhize, M. Newby, R. Scheepers, W. Smit and P. van der Meer, "Risk management of plant with Finite Life design in Eskom," in *The Southern African Institute of Mining and Metallurgy, Ferrous and Base Metals Development Network Conference*, 2012.

[4] Eskom Research Testing and Development, "Life Assessment Results, Various," Eskom Internal Documentation, https://hyperwave.eskom.co.za/Eskom/Sustainability Division/Research Testing and Development/Plant Performance and Optimisation PP O/PPO COE FOLDERS/Physical Metallurgy/HP Pipework, 2008 - 2014.

[5] Eskom Engineering, "Summary of quenching incidents.xls," Eskom Internal Documentation, 2018.

[6] C. van Wyk, "Fossil fuel firing regulations standard," Eskom Internal Document, 240-105453648, 2016.

[7] J. Mandke, H. Burghard, G. Lamping and W. Campbell, "Industry survey on experience with main steam line thermal quenching," in *Proceedings of the American Power Conference (Vol. 53)*, 1991.

[8] R. Rosario, "Managing Thermal Quench Damage at Power Plants," *Power (https://www.powermag.com),* 04 01 2019.

[9] J. P. King, "Current experience in typical problems and failures with boiler piping components and supports," in *ASME Pressure Vessels and Piping Conference*, San Diego, California, 1998.

[10] R. Viswnathan, "An overview of failure mechanisms in high temperature components in power plants," in *ICF10*, Honolulu (USA), 2001.

[11] "Damage to Power Plants due to Cycling," EPRI, Palo Alto, CA, 2001, 1001507.

[12] J. Ford, J. Fernandes and A. Shibli, "Damage to Power Plant due to cyclic operation and guidelines for best practices," ETD Report No: 1096-gsp-81, 2009.

[13] S. Hesler, "Mitigating the Effects of Flexible Operation on Coal-Fired Power Plants".

[14] "Steam cooled spacer tube related cracking of secondary superheater outlet headers," Babcock and Wilcox power generation group, Plant service bulletin, Ohio, 1994.

[15] J. Delong, J. Bynum, F. Ellis, M. Rafiee, W. Siddall, T. Daikoku and H. Haneda, "Failure investigation of Eddystone main steam piping," *Welding Journal (Miami, United States),* vol. 64, no. 10, pp. 271-280, 1985.

[16] J. W. Price, "Thermal Shock Cracking: Design and Assessment Guidelines," *ASME Journal of Pressure Vessel Technology,* vol. 129, pp. 125 - 132, 2007.

[17] J. Taler, D. Taler, K. Kaczmarski, P. Dzierwa, M. Trojan and M. Jaremkiewicz, "Allowable Rates of Fluid Temperature Variations and Thermal Stress Monitoring in Pressure Elements of Supercritical Boilers," *Heat Transfer Engineering,* pp. 1-12, 2018.

[18] P. Hirschberg, A. P. Deardorff and J. Carey, "Operating experience regarding thermal fatigue of unisolable piping connected to PWR reactor coolant systems," in *International Conference on Fatigue of Reactor Components*, Napa, CA, 2000.

[19] X. Schuler and K. H. Herter, "Thermal fatigue due to stratification and thermal shock loading of piping," in *30th MPA Seminar in conjunction with the 9th German Japanese Seminar*, Stuttgart, 2004.

[20] L. L. da Silva, T. R. Mansur and C. A. Cimini Junior, "Thermal fatigue damage evaluation of a PWR NPP steam generator injection nozzle model subjected to thermal stratification phenomenon," *Nuclear Engineering and Design,* pp. 672-680, 2011.

[21] ASME Code, Boiler and pressure vessel code, Section II and III, New York, USA, 2001.

[22] BS EN12952-3, Water-tube boilers and auxiliary installations - Part 3: Design and calculation of pressure parts, 2001.

[23] British Energy, R5, assessment procedure for the high temperature response of structures; Issue 3, Gloucester, UK, 2003.

[24] A. Stoppato, A. Mirandola, G. Meneghetti and E. Lo Casto, "On the operation strategy of steam power plants working at variable load: Technical and Economic Issues," *Energy,* no. 37, pp. 228-236, 2012.

[25] A. Mirandola, A. Stoppato and E. Lo Casto, "Evaluation of the effects of the operation strategy of a steam power plant," *Energy,* vol. 35, pp. 1024-1032, 2010.

[26] J. Varley, "Dealing with Cycling: TRD 301 and Euro Norm compared," *Modern Power Systems 27,* pp. 33-38, 2007.

[27] R. Viswanathan, Damage Mechanisms and Life Assessment of High Temperature Components, ISBN 0871703580, 9780871703583: ASM International, 1989, pp. 209-125.

[28] J. King, "Recent experience in condition assessment of boiler header components and supports," in *1996 ASME Pressure Vessels and Piping Conference*, Montreal, Quebec, Canada, 1996.

[29] O. Kwon, M. Myers, A. Karstensen and D. Knowles, "The effect of the steam temperature fluctuations during steady state operation on the remnant life of the superheater header," *International Journal of Pressure Vessels and Piping,* vol. 83, p. 349, 2006.

[30] J. Taler, W. Zima and M. Jaremkiewicz, "Simple method for monitoring transient thermal streses in pipelines," *Journal of Thermal Stresses,* vol. 39, no. 4, pp. 386-397, 2016.

[31] EPRI, "Operational flexibility case study #6: Shutdown management of a once-through subcritical coal-fired plant," EPRI, Palo Alto, CA: 3002007024, 2015.

[32] EPRI, "Operational flexibility Implementation: case study #2," EPRI, Palo Alto, CA: 3002002103, 2013.

[33] T. Sobota, "Increasing the performance and reliability of a power boiler by monitoring thermal and strength parameters," *E3S Web Conf. 13, 04004,* 2017.

[34] N. Basson, "Studying water-wedging as a cause for short term overheating in the boiler of a coal-fired power plant," Thesis, Department of Mechanical Engineering, University of Cape Town, 2017.

[35] F. Gabrielli and H. Schwevers, “Design factors and water chemistry practices - supercritical power cycles,” in *15th International Conference on the Properties of Water and Steam. VDI-The Association of German Engineers, pp. 1-15*, 2008.

[36] K. Trangbaek, “Constrained control of a once-through boiler with recirculation,” in *Proceedings of the 17th World Congress, The International Federation of Automatic Control*, Seoul, Korea, 2008.

[37] E. Boje, “Control and Operability of Economiser Bypass in Once-through Steam Generators,” in *Proceedings of the 18th World Congress, The International Federation of Automatic Control*, Milano, Italy, 2011.

[38] E. Eitelberg and E. Boje, “Water circulation control during once-through boiler start-up,” *Control Engineering Practice,* vol. 12, pp. 677-685, 2004.

[39] T. Sobota, “Computer monitoring and optimization of the steam boiler performance,” *E3S Web of Conferences, Energy and Fuels,* vol. 14, 2016.

[40] A. Mills, Heat Transfer, Irwin, ISBN: 0-256-12817-0, 1992.

[41] H. Hajebzadeh, A. N. Ansari and S. Niazi, “Mathematical modeling and validation of a 320MW tangentially fired boiler: A case study,” *Applied Thermal Engineering,* vol. 146, pp. 232-242, 2019.

[42] C. Cantrell and S. Idem, “On-Line performance model of the convection passes of a pulverized coal boiler,” *Heat Tranfer Engineering,* vol. 31, no. 14, pp. 1173-1183, 2010.

[43] M. Trojan and D. Taler, “Thermal simulation of superheaters taking into account the processes occurring on the side of the steam and flue gas,” *Fuel,* vol. 150, pp. 75-87, 2015.

[44] P. Drosatos, N. Nikolopoulos, M. Agraniotis and G. Itskos, “Decoupled CFD simulation of furnace and heat exchangers in a lignite utility boiler,” *Fuel,* vol. 117, pp. 633-648, 2014.

[45] T. Kim, S. Choi and J.-S. Hyun, “Performance prediction of a large-scale circulating fluidized bed boiler by heat exchangers block simulation,” *Proceedings of the Institution of Mechanical Engineers, Part A: Journal of Power and Energy,* vol. 232, no. 4, pp. 416-424, 2015.

[46] P. Rousseau and L. Jestin, Fundamentals of thermal-fluid sciences, University of Cape Town, 2014.

[47] F. Alobaid, N. Mertens, R. Starkloff, T. Lanz, C. Heinze and B. Epple, “Progress in dynamic simulation of thermal power plants,” *Progress in Energy and Combustion Science,* vol. 59, pp. 79-162, 2016.

[48] R. Starkloff, F. Alobaid, K. Karner, B. Epple, M. Schmitz and F. Boehm, “Development and validation of a dynamic simulation model for a large coal-fired power plant,” *Applied Thermal Engineering,* vol. 91, pp. 496-506, 2015.

[49] J. Kuronen, M. Hotti and S. Tuuri, ““Modelling and dynamic simulation of cyclically operated pulverized coal-fired power plant,” in *9th EUROSIM Congress on Modelling and Simulation*, Oulu, Finland, 2016.

[50] P. Sarda, E. Hedrick, K. Reynolds, D. Bhattacharyya, S. Zitney and B. Omell, “Development of a dynamic model and control system for load-following studies of supercritical pulverised coal power plants,” *Processes,* vol. 6, no. 11, p. 226, 2018.

[51] K. Deng, C. Yang, H. Chen, N. Zhou and S. Huang, "Start-up and dynamic processes simulation of supercritical once-through boiler," *Applied Thermal Engineering,* vol. 115, pp. 937-946, 2017.

[52] G. Tang, M. Zhang, J. Gu, Y. Wu, H. Yang, Y. Zhang, G. Wei and J. Lyu, "Thermal-hydraulic calculation and analysis on evaporator system of a 660MWe ultra-supercritical CFB boiler," *Applied Thermal Engineering,* vol. 151, pp. 385-393, 2019.

[53] W. Zima, "Simulation of rapid increase in the steam mass flow rate at a supercritical power boiler outlet," *Energy,* vol. 173, pp. 995-1005, 2019.

[54] E. Adam and J. Marchetti, "Dynamic simulation of large boilers with natural recirculation," *Computers & chemical engineering,* vol. 23, no. 8, pp. 1031-1040, 1999.

[55] G. Lazaroiu, "Dynamic modelling of steam boiler drum," *Revue Roumaine des Sciences Techniques Serie Electrotechnique et Energetique,* vol. 44, no. 1, pp. 101-109, 1999.

[56] H. Walter, "Dynamic simulation of natural circulation steam generators with the use of finite volume algorithms – A comparison of four algorithms," *Simulation Modelling Practice and Theory,* vol. 15, no. 5, pp. 565-588, 2007.

[57] J. Taler, P. Dzierwa, D. Taler and P. Harchut, "Optimization of the boiler start-up taking into account thermal stresses," *Energy,* vol. 92, pp. 160-170, 2015.

[58] P. Sunil, J. Barve and P. Nataraj, "Mathematical modeling, simulation and validation of a boiler drum: Some investigations," *Energy,* vol. 126, pp. 312-325, 2017.

[59] N. Mertens, F. Alobaid, T. Lanz, B. Epple and H.-G. Kim, "Dynamic simulation of a triple-pressure combined-cycle plant: Hot start-up and shutdown," *Fuel,* vol. 167, pp. 135-148, 2016.

[60] F. Alobaid, K. Karner, J. Belz, B. Epple and H.-G. Kim, "Numerical and experimental study of a heat recovery steam generator during start-up procedure," *Energy,* no. 64, pp. 1057-1070, 2014.

[61] F. Alobaid, J. Strohle, B. Epple and H.-G. Kim, "Dynamic simulation of a supercritical once-through heat recovery steam generator during load changes and start-up procedures," *Applied Energy,* vol. 86, pp. 1274-1282, 2009.

[62] A. Benato, A. Stoppato and S. Bracco, "Combined cycle power plants: A comparison between two different dynamic models to evaluate transient behaviour and residual life," *Energy Convers Manage,* 2014.

[63] T. K. Ray, R. Ganguly and A. Gupta, "Optimal control strategy for minimization of exergy destruction," *Energy Conversion and Management,* no. 66, pp. 234-245, 2013.

[64] M. Botha and M. Hindley, "1-Way Fluid Structure Interaction Modelling Methodology for Boiler Tube Fatigue Failure," *Engineering Failure Analysis,* 2014.

[65] P. G. Rousseau and E. Z. Gwebu, "Modelling of a Superheater Heat Exchanger with Complex Flow Arrangement Including Flow and Temperature Maldistribution," *Heat Transfer Engineering,* 2018.

[66] S. Levy, Two-phase flow in complex systems, John Wiley & Sons, 1999.

[67] RELAP5-3D Code Manual, Volume I: Code Structure, System Models and Solution Methods, INEEL-EXT-98-00834, Revision 4.0, June 2012.

[68] A. Guelfi, D. Bestion, M. Boucker, P. Boudier, P. Fillion, M. Grandotto, J.-M. Hérard, E. Hervieu and P. Péturaud, "NEPTUNE: A New Software Platform for Advanced Nuclear Thermal Hydraulics," *Nuclear Science and Engineering,* no. 156, pp. 281-324, 2007.

[69] L. Pierobon, E. Casati, F. Casella, F. Haglind and P. Colonna, "Design methodology for flexible energy conversion systems accounting for dynamic performance," *Energy,* vol. 68, pp. 667-679, 2014.

[70] R. Terdalkar, D. Doupis, M. Clark, A. Joshi and C. Wang, "Transient simulation of high temperature high pressure solar tower receiver," *Energy Procedia,* vol. 69, pp. 1451-1460, 2015.

[71] C. Schuhbauer, M. Angerer, H. Spliethoff, F. Kluger and H. Tschaffon, "Coupled simulation of a tangentially hard coal fired 700C boiler," *Fuel,* vol. 122, pp. 149-163, 2014.

[72] H. Park, M. Faulkner, M. Turrell, P. Stopford and D. Kang, "Coupled fluid dynamics and whole plant simulation of coal combustion in a tangentially-fired boiler," *Fuel,* no. 89, pp. 2001-2010, 2010.

[73] M. Angerer, S. Kahlert and H. Spliethoff, "Transient simulation and fatigue evaluation of fast gas turbine startups and shutdowns in a combined cycle plant with an innovative thermal buffer storage," *Energy,* vol. 130, pp. 246-257, 2017.

[74] M. Trojan, "Computer modeling of a convective steam superheater," *archives of thermodynamics,* vol. 36, no. 1, pp. 125-137, 2015.

[75] J. H. Kruger and C. G. du Toit, "The simulation of a thermal-fluid system using an integrated systems CFD approach," in *Fifth International Conference on CFD in the Process Industries*, CSIRO, Melbourne, Australia, 2006.

[76] L. I. Diez, C. Cortes and A. Campo, "Modelling of pulverized coal boilers: review and validation of on-line simulation techniques," *Applied Thermal Engineering,* vol. 25, pp. 1516-1533, 2005.

[77] K. He, J. Li, Y. Xin, F. Zhenping, F. Yizhi and S. Xianyou, "Investigations on water condensation in the main steam pipe of a pressurized water reactor nuclear power station: Part II—Theoretical studies," *Proc IMechE Part A: J Power and Energy,* vol. 228, no. 4, pp. 391-401, 2014.

[78] Y. Zhang and T. Lu, "Study of the quantitative assessment method for high-cycle thermal fatigue of a T-pipe under turbulent fluid mixing based on the couled CFD-FEM method and the rainflow counting method," *Nuclear Engineering and Design,* vol. 309, pp. 175-196, 2016.

[79] R. Jethra, "Improving temperature measurement in power plants," *Power Engineering, Vol 117, Issue 3,* January 2013.

[80] P. Duda, "Numerical and experimental verification of two methods for solving an inverse heat conduction problem," *International Journal of Heat and Mass Transfer,* vol. 84, pp. 1101-1112, 2015.

[81] H. Yapıcı and B. Albayrak, "Numerical solutions of conjugate heat transfer and thermal stresses in a circular pipe externally heated with non-uniform heat flux," *Energy Conversion and Management,* vol. 45, no. 6, pp. 927-937, 2004.

[82] J. Taler, B. Weglowski, W. Zima, S. Gradziel and M. Zborowski, "Monitoring of transient temperature and thermal stresses in pressure components of steam boilers," *Int. J. Pres. Ves. & Piping,* vol. 72, pp. 231-241, 1997.

[83] J. Taler and P. Duda, Solving direct and inverse heat conduction problems, Springer Science and Business Media, 2010.

[84] J. Taler, B. Weglowski and M. Pilarczyk, "Monitoring of thermal stress in pressure components using inverse heat conduction methods," *International Journal of Numerical Methods for Heat & Fluid Flow,* vol. 27, no. 3, pp. 740-756, 2017.

[85] P. Duda, J. Taler and E. Roos, "Inverse method for temperature and stress monitoring in complex-shaped bodies," *Nuclear Engineering and Design,* vol. 227, pp. 331-347, 2004.

[86] M. Jaremkiewicz, "Accurate measurement of unsteady state fluid temperature," *Heat Mass Transfer,* vol. 53, pp. 887-897, 2017.

[87] J. Argaud, B. Bouriquet, M. Courtois and J. Le Roux, "Reconstruction by Data Assimilation of the Inner Temperature Field From Outer Measurement in Thick Pipe," in *ASME 2016 Pressure Vessels and Piping Conference*, American Society of Mechanical Engineers, 2016.

[88] T. Lu, B. Liu and P. X. Jiang, "Inverse estimation of the inner wall temperature fluctuations in a pipe elbow," *Applied Thermal Engineering,* vol. 31, pp. 1976-1982, 2011.

[89] R. Courant, K. Friedrichs and H. Lewy, "On the partial difference equations of mathematical physics," *IBM journal of Research and Development,* vol. 11, no. 2, pp. 215-234, 1967 (Originally published 1923).

[90] G. B. De Klerk and P. G. Rousseau, "Dynamic modelling of once-through boiler heat exchangers during shutdown with level tracking as a tool to investigate quenching," in *Eleventh South African Conference on Computational and Applied Mechanics, SACAM2018, ISBN978-1-77012-143-0*, Vanderbijlpark, South Africa, 2018.

[91] G. De Klerk, P. Rousseau and L. Jestin, "A dynamic modelling methodology to estimate the magnitude of unwanted liquid flows in high temperature boiler components," *ASME Journal of Thermal Science and Engineering Applications,* vol. 12, no. 5, 2020.

[92] W. M. Payten, T. Wei, K. U. Snowden, P. Bendeich, M. Law and D. Charman, "Crack initiation and crack growth assessment of a high pressure steam chest," *International Journal of Pressure Vessels and Piping,* vol. 88, pp. 34-44, 2011.

[93] A. Rossouw, "Boiler system modelling using Flownex," Diss. University of Cape Town, 2016.

[94] R. Hilpert, "Wärmeabgabe von geheizten drähten und rohren im luftstrom," *Forschung auf dem Gebiet des Ingenieurwesens A,* vol. 4, no. 5, pp. 215-224, 1933.

[95] M. Krishpersad and K. Ramroop, "A comparison of correlations for heat transfer from inclined pipes," *International Journal of Engineering (IJE),* vol. 4, no. 4, pp. 268-278, 2010.

[96] A. Žkauskas, "Heat transfer from tubes in crossflow," *Advances in heat transfer,* vol. 18. Elsevier, pp. 87-159, 1987.

[97] S. Churchill and M. Bernstein, "A correlating equation for forced convection from gases and liquids to a circular cylinder in crossflow," *J. Heat Transfer, Trans. ASME,* vol. 99, no. DOI:10.1115/1.3450685, pp. 300-306, 1977.

[98] V. Gnielinski, "Heat transfer in cross-flow around single rows of tubes and through tube bundles," in *VDI Heat Atlas, 2nd ed, Vol G7,*, Berlin, Heidelberg, Springer, 2010, pp. 725-730.

[99] N. W. Kuznetsov, W. W. Mitor, I. E. Dubovski, E. S. Karasina and editors, Thermal calculations of steam boilers (standard method), Moscow, Russia: Energia, 1973.

[100] W. O. Monnaemang, "A zonal model for radiation heat transfer in coal fired boiler furnaces," Dissertation, University of Cape Town, 2015.

[101] D. Taler and J. Taler, "Simplified analysis of radiation heat exchange in boiler superheaters," *Heat transfer engineering,* vol. 30, no. 8, pp. 1-9, 2009.

[102] Y. Zhang, Q. Li and H. Zhou, Theory and calculation of heat transfer in furnaces, Amsterdam: Academic Press, 2016.

[103] E. Z. Gwebu, A methodology for integrated thermofluid modelling of radiant superheaters in steady state and transient operations, University of Cape Town, PhD Thesis, 2018.

[104] H. Brummel, Thermal radiation of gas-solids-dispersions, Berlin Heidelberg: VDI Heat Atlas, 2nd Edition, Springer-Verlag, 2010.

[105] P. Biermann and D. Vortmeyer, "Wa¨rmestrahlung staubhaltiger Gase. (Radiation of gases containing dust particles.)," *Wärme-und Stoffübertragung,* vol. 2, no. 4, pp. 193-202, 1969.

[106] P. Furmanski, "Thermal and radiative properties of ash deposits on heat transfer surfaces of boilers," *Journal of Power Technologies,* vol. 79, 1995.

[107] F. P. Incropera and D. P. DeWitt, Fundamentals of heat and mass transfer (6th ed), New York: Wiley, 2007.

[108] V. Gnielinski, "Neue Gleichungen für den Wärme- und den Stoffübergang in turbulent durchströmten Rohren und Kanälen," *Forsch. Ing.-Wes.,* vol. 41, no. 1, pp. 8-16, 1975.

[109] Churchill, *Chem. Eng.,* vol. 84, no. 24, pp. 91-92, 1977.

[110] S. M. Morcos and A. E. Bergles, "Experimental Investigation of Combined Forced and Free Laminar Convection in Horizontal Tubes," *ASME Journal of Heat Transfer,* vol. 97, no. 2, DOI:10.1115/1.3450343, pp. 212-219, 1975.

[111] R. H. Perry and D. W. Green, Perry's chemical engineers handbook, Seventh Edition, McGraw-Hill, 1999.

[112] J. C. Chato, "Laminar condensation inside horizontal and inclined tubes," *ASHRAE Journal,* vol. 4, no. 252, 1962.

[113] M. Dobson, J. Chato, J. Wattelet, J. Gaibel, M. Ponchner, P. Kenney, R. Shimon, T. Villaneuva, N. Rhines, K. Sweeney, D. Allen and T. Hershberger, "Heat transfer and flow regimes during condensation in horizontal tubes," ACRC TR-57, Air conditioning and refrigeration centre, University of Illinois, 1994.

[114] D. Traviss, W. Rohsenow and A. Baron, "Forced-convection condensation inside tubes: A heat transfer equation for condenser design," *ASHRAE Transactions,* vol. 79 part 1, pp. 157-165, 1973.

[115] M. Holmgrem, "X Steam Tables, v2.6".

[116] "Engineering Toolbox," 2001. [Online]. Available: https://www.engineeringtoolbox.com/dry-air-properties-d_973.html. [Accessed 08 12 2018].

[117] Flownex, "Flownex simulation environment, Theory manual," www.flownex.com, 2016.

[118] G. Greyvenstein, "An implicit method for the analysis of transient flows in pipe networks," *Int. J. Numer. Methods Eng.,* Vols. 53, no.5, pp. 1127-1143, 2002.

[119] H. Wang, H. Wang, T. Zhu and W. Deng, "A novel model for steam transportation considering drainage loss in pipeline networks," *Applied Energy,* vol. 188, pp. 178-189, 2017.

[120] J. G. Leidenfrost, "Translation: On the fixation of water in diverse fire (1756)," *Int. J. Heat Mass Transfer,* vol. 9, p. 1153, 1966.

[121] W. M. Rohsenow, "A method of correlating heat transfer data for surface boiling of liquids," *Trans. ASME,* vol. 74, pp. 969-976, 1952.

[122] S. S. Kutateladze, "On the transition to film boiling under natural convection," *Kotloturbostroenie,* vol. 3, no. 10, 1948.

[123] N. Zuber, "Hydrodynamic aspects of nucleate boiling," Ph.D. dissertation, Department of Engineering, University of California, Los Angeles, 1959.

[124] T. H. K. Frederking and J. A. Clark, "Natural convection film boiling on a sphere," *Advances in Cryogenic Engineering,* vol. 8, pp. 501-506, 1962.

[125] N. Zuber, "On the stability of boiling heat transfer," *Trans. ASME,* vol. 80, pp. 711-720, 1958.

[126] K. Takrouri, J. Luxat and M. Hamed, "Measurement and analysis of the re-wetting front velocity during quench cooling of hot horizontal tubes," *Nuclear Engineering and Design,* vol. 311, pp. 184-198, 2017.

[127] J. Liao, R. Mei and J. F. Klausner, "A film boiling model for cryogenic chilldown at low mass flux inside a horizontal pipeline," *Heat and Mass Transfer,* vol. 42, pp. 891-900, 2006.

[128] J. Johnson and S. R. Shine, "Transient cryogenic chill down process in horizontal and inclined pipes," *Cryogenics,* vol. 71, pp. 7-17, 2015.

[129] L. Fick, "Application of the rate form of the equation of state for the dynamic simulation of thermal-hydraulic systems," Masters Dissertation, North-West University, South Africa, 2014.

[130] B. R. Munson, D. F. Young and T. H. Okiishi, Fundamentals of Fluid Mechanics, John Wiley & Sons, Inc., 1994.

[131] P. G. Rousseau, "Numerical solution of transient pipe heat transfer problem - RevF," UCT internal document, 2014.

[132] E. Z. Gwebu, "Transient boiler heat exchanger thermal behaviour analysis," Dissertation, University of Cape Town, 2014.

[133] Mannesmannrohren-Werke AG, "X20 CrMoV 12 1 Data Sheet," 1989.

[134] F. Mohebbi and M. Sellier, "Estimation of thermal conductivity, heat transfer coefficient, and heat flux using a three dimensional inverse analysis," *International Journal of Thermal Sciences,* vol. 99, pp. 258-270, 2016.

[135] A. Fernandes, M. dos Santos and G. Guimaraes, "An analytical transfer function method to solve inverse heat conduction problems," *Applied Mathematical Modelling,* vol. 39, no. 22, pp. 6897-6914, 2015.

[136] P. Duda, "A general method for solving transient multidimensional inverse heat transfer problems," *International Journal of Heat and Mass Transfer,* vol. 93, pp. 665-673, 2016.

# Appendix A. Collecting vessel level measurement

At Power Station A, the collecting vessel level is measured by two sets of differential pressure measurements. Each differential pressure transducer has a separate set of tapping points, one at the bottom of the vessel and one at the top of the vessel.

Where the impulse lines from the upper tapping points exit the lagging, there is an isolation valve and a condensing pot as shown in Figure 132 a). The condensing pot is not insulated and thus heat transfer to the ambient condenses steam inside the pot. This ensures that the impulse line from the upper tapping point down to the differential pressure transmitter is filled with a column of water. This column is the reference against which the height of water inside the vessel is measured.

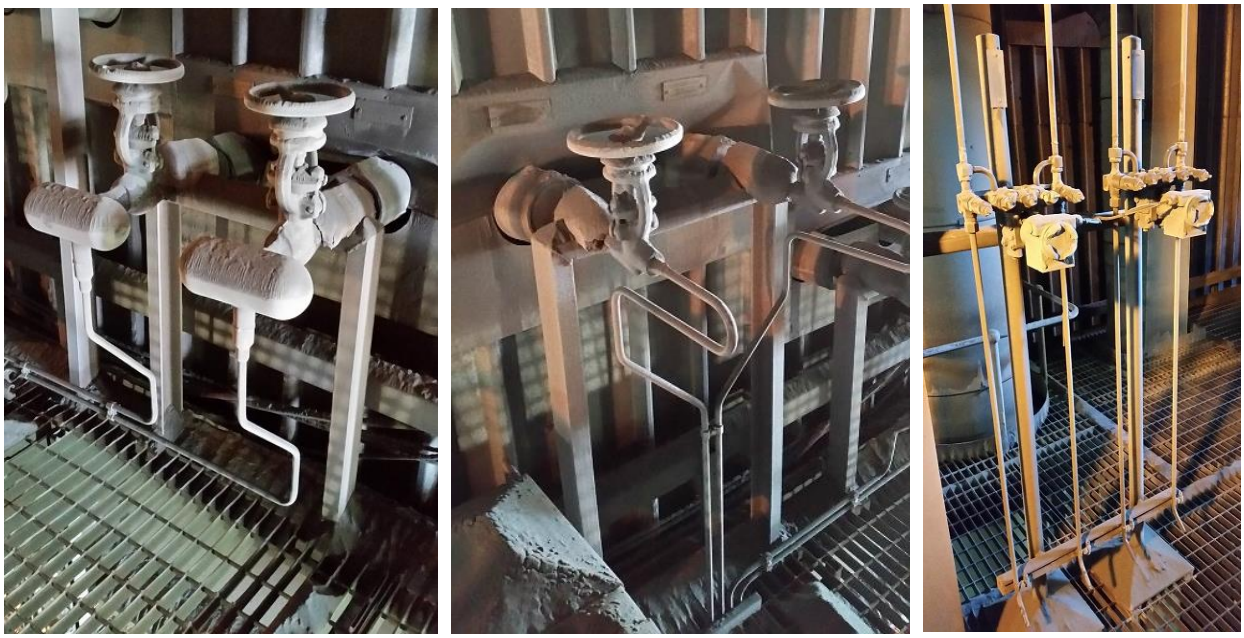

*a)* *b)* *c)*

*Figure 132. Collecting vessel level measurement a) Upper tapping points b) Lower tapping points c) Pressure transmitters*

The differential pressure between the two tapping points is measured by a pressure transmitter that gives an output signal from 4 to 20mA. This signal is received by the DCS and corrected to give a level at the present operating condition. A correction is required due to calibration of the instrument done at ambient conditions and due to the change in density of the fluid with pressure and temperature. The correction is done using a standard Siemens function block in the Teleperm XP AS 620 automation system.

Consider the system shown in Figure 133 a) which could occur during calibration of the transmitter when the plant is shut down. For the sake of this discussion, the vessel has a sight glass and the actual liquid level can be seen in order to perform the calibration. When the level is the lowest in

the sight glass the output of the transmitter is at its maximum. As the level rises, the transmitter output signal decreases. The reversal of the signal is either accounted for at the transmitter (if the model allows) or in the DCS. Now the water level can be physically altered from 0m to 8m and the output signal can be adjusted such that the 4 to 20mA signal is interpreted in the DCS as a height, h, from 0m to 8m respectively.

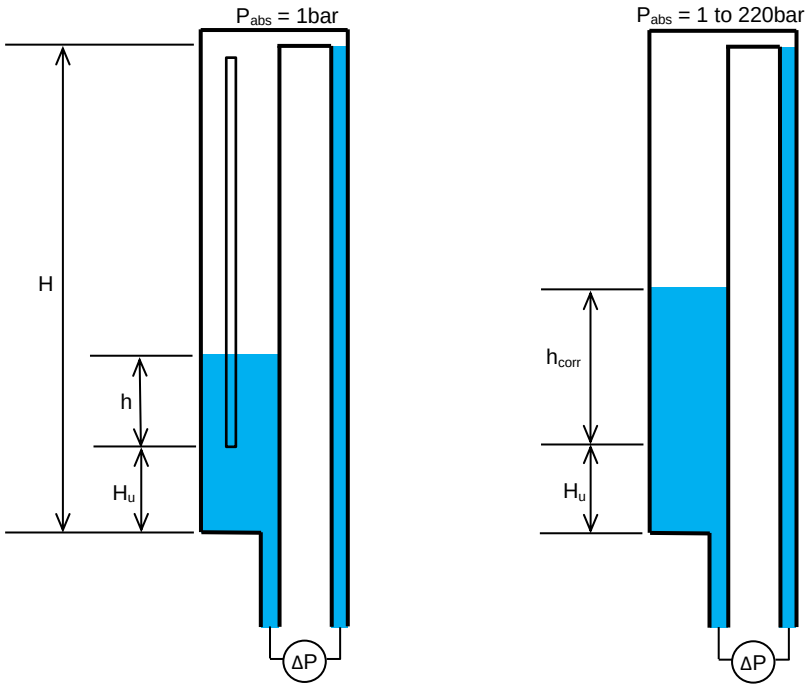


*Figure 133. Level transmitter a) Calibration (assumed) b) In operation*

The differential pressure during calibration (Figure 133a) can be expressed as follows:

$$\Delta P = g\left(\rho_{m1}H - \left(\rho_{L1}(H_U + h) + \rho_{G1}(H - H_U - h)\right)\right) \quad (143)$$

Where:

ΔP - Differential pressure
g - Gravitational constant [9.81m/s$^2$]
$\rho_{m1}$ - Density of the reference column at 1bar and at the specified reference temperature
$\rho_{L1}$ - Density of saturated liquid at 1bar
$\rho_{G1}$ - Density of saturated steam at 1bar
H - Distance between tapping points
$H_u$ – Distance from bottom tapping point up to bottom of sight glass
h – Height of liquid measured in the sight glass

Note that the function block assumes that the calibration is done at saturation conditions in the vessel i.e. the vessel is assumed to be at a pressure of 1 bar absolute and would need to be at a temperature of 99.6°C during calibration. The block also assumes that the reference column is at the specified reference temperature.

During operation, as shown in Figure 133 b), the pressure in the system is at the pressure of the boiler with saturated conditions in the vessel. Thus, the differential pressure measured by the transmitter can be expressed as:

$$\Delta P = g\left(\rho_m H - \left(\rho_L(H_U + h_{corr}) + \rho_G(H - H_U - h_{corr})\right)\right) \qquad (144)$$

Where:

$\rho_m$ - Density of the reference column at operating pressure and specified reference temperature
$\rho_L$ - Density of saturated liquid at operating pressure
$\rho_G$ - Density of saturated steam at operating pressure
$h_{corr}$ – Corrected or actual height of liquid measured in the sight glass at operating conditions

The differential pressure measured during operation is expressed in terms of the calibration equation 143 above. Thus equation 143 can be substituted into equation 144 and rewritten to give:

$$h_{corr} = \frac{(\rho_m - \rho_{m1}) - (\rho_G - \rho_{G1})}{\rho_L - \rho_G} H + \frac{\rho_{L1} - \rho_{G1}}{\rho_L - \rho_G}(H_U + h) - H_U \qquad (145)$$

The function block uses equation 145 above to correct the measured level to an actual level. The function block has built-in tables to determine the densities of water and steam and uses linear interpolation to obtain the required values. The function block is configured with the values of H and $H_u$. In operation, the measured h signal, the measured absolute pressure and the reference temperature are required as inputs to the function block. The temperature of the reference column is not measured so a constant value is used. This is set at 40°C.

In practice, the calibration is not performed as assumed in the derivation of the function block correction above. The collecting vessel does not have a sight glass to witness the level and calibration at 99.6°C is near impossible. Thus, the calibration is performed using a water column at ambient temperature or by applying a known pressure to the transmitter. In the latter case, a level of 0m would correspond to a pressure of 78.4kPa and a level of 8m to 0kPa.

Using this calibration method, the actual differential pressure can be calculated and used to estimate the error in indicated level. The results are shown in Figure 134. The uncorrected signals have a large error at operating pressure and high level. The corrected signals have much reduced error but still under read by 250mm at operating pressure and high levels.

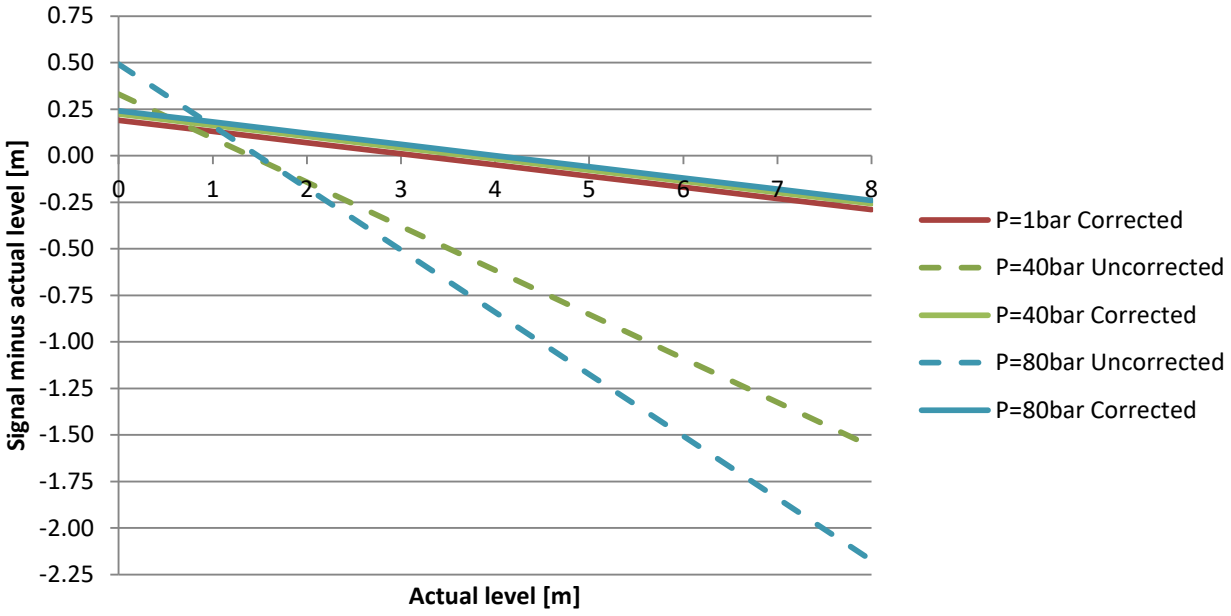


*Figure 134. Collecting vessel measured level error before and after correction*

The effect of the reference temperature was also considered. If the temperature of the reference column was actually 30°C instead of 40°C, it makes a 38mm difference in the indicated level. In general the method used to convert the differential pressure measured by the transmitter into the indicated level for control purposes is adequate. The error from this conversion can be up to 0.3m or 3.75% of full scale.

The physical arrangement of the level measuring equipment can also play a role in the accuracy. The location of the tapping points on the collecting vessel and the slope of the impulse lines may affect the measurement. The exact slopes of the impulse lines from the vessels to outside of the lagging could not be determined due to difficult access to inspect the actual collecting vessel. The upper tapping point on the vessel is on the hemispherical head as shown in Figure 135 (This and the length of the stub was confirmed from a drawing). From there it is assumed that the slope of the impulse line is towards the collecting vessel, but it may not be so. In the photograph in Figure 132 a), it can be seen that the part of the impulse line between the isolation valve and the condensing pot is downwards. The slopes of the impulse lines are to allow drainage and prevent a water plug in the line from affecting the level measurement. Assuming a minimum slope of 2% for the horizontal impulse lines, it is estimated that the top of the reference column is approximately 200mm above the highest possible level in the collecting vessel. However, in practice, it is only possible to measure a level up to the height of the tapping point – once the level exceeds the top tapping point, the reference column is then also affected by the level in the vessel and the pressure difference at the pressure transmitter no longer changes. The difference between the highest level in the vessel and

the tapping point is 50mm. Thus the height of the reference column above the tapping point is approximately 250mm.

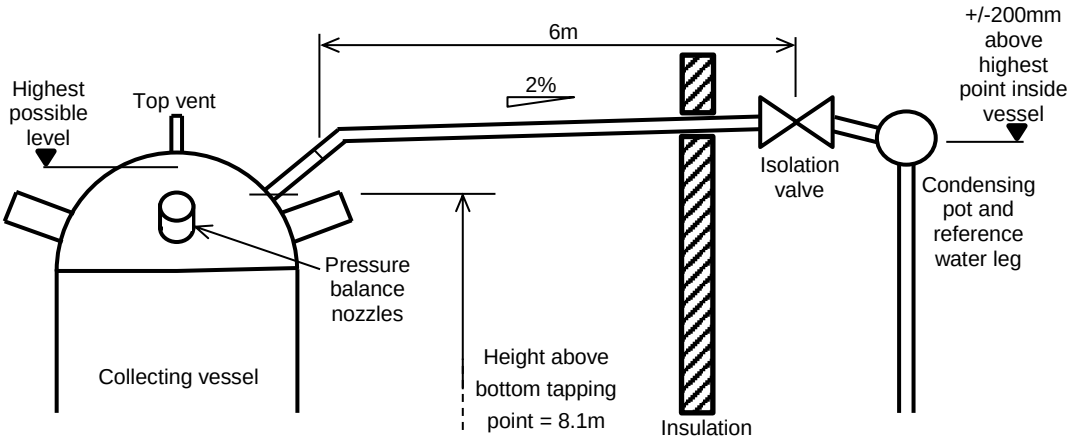


*Figure 135. Collecting vessel level measurement upper tapping point*

Now because the level measurement is referenced from the top of the reference water column, the measurement signal has an offset equal to the difference in physical height of the upper tapping point and the top of the reference water column. Thus the level measurement under- reads by approximately 250mm.

Furthermore, the height difference between the top and bottom tapping points on the collecting vessel is approximately 8.1m and not exactly 8m as per the range used in the treatment of the measurement signal. This is not a problem if the measurement signal is interpreted to be level referenced from the height of the top tapping point (and not height from the bottom of the vessel which is a more common way to think of level).

The information provided above can be used to interpret the measurement signals from the plant data system to approximate the true level that was measured. The density correction offset, true height of the reference column and the real range can be accounted for. Generally in the data there are periods where the collecting vessel level is high but remains constant for a time period. This is when the true level has exceeded the top tapping point.

During operation, the bottom tapping points for level measurement experience turbulent conditions due to the flow of liquid in the vessel. To stabilise the pressure in the impulse line, the entrance to the tapping points inside the vessel, are fitted with devices as shown in Figure 136. These devices are not expected to interfere with the accuracy of the level measurement system.

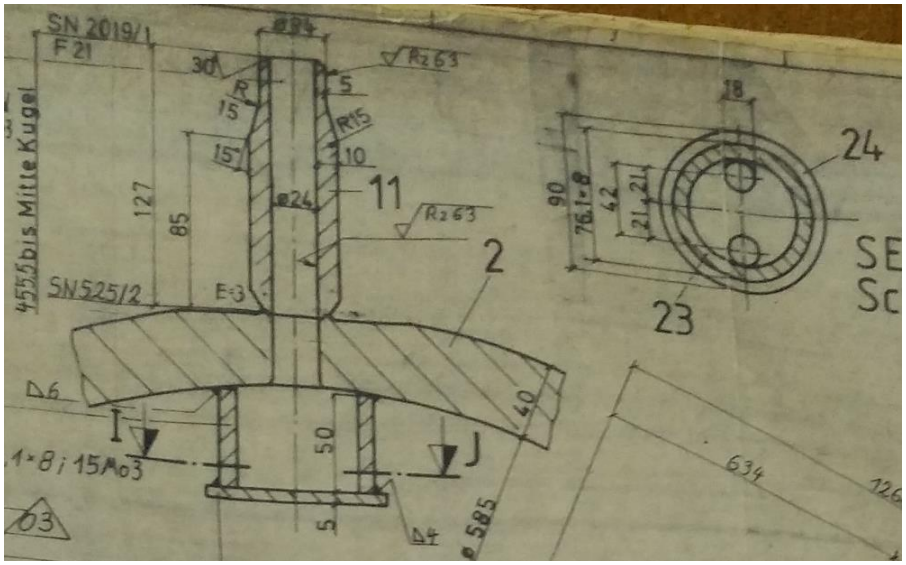


*Figure 136. Devices installed at entrance to lower tapping points*

# Appendix B. Inputs of the Flownex model of the separator and collecting vessel system

| | | |
|---|---|---|
| **1** | **Evaporator outlet header** | |
| 1.1 | Nodes – elevation | 97.95 m |
| 1.2 | Flow resistance – Flow admittance | 0.1 |
| **2** | **Distribution pipes from evaporator outlet to separator inlet** | |
| 2.1 | Pipe inner diameter | 145.8 mm |
| 2.2 | Pipe roughness | 30 µm |
| 2.3 | Number in parallel | 4 |
| 2.4 | Number of increments | 10 |
| 2.5 | Length (Pipes to separator 1 and 4: average of the estimated distribution pipe lengths) | 14.091 m |
| 2.6 | Length (Pipes to separator 2 and 3: average of the estimated distribution pipe lengths) | 12.74 m |
| 2.7 | Secondary loss factor (Pipes to separator 1 and 4: 5 x 90$^o$ smooth bends (r/D=3); Entrance loss for rounded flush (r/D=0.02); Exit loss) | 2.196 |
| 2.8 | Secondary loss factor (Pipes to separator 2 and 3: 3 x 90$^o$ smooth bends (r/D=3); 2 x 45$^o$ smooth bends (r/D=3); Entrance loss for rounded flush (r/D=0.02); Exit loss) | 2.068 |
| **3** | **Separator vessel two phase tanks** | |
| 3.1 | Elevation (bottom of tank) | 92.82 m |
| 3.2 | Tank diameter (Cylindrical vertical) | 585 mm |
| 3.3 | Tank height (Cylindrical vertical – specified as no end caps but in reality there are hemispherical heads so height is adjusted for the additional volume) | 8.78 m |
| 3.4 | Connection fraction of steam outlet | 1 |
| 3.5 | Connection fraction of distributer pipes from evaporator outlet | 0.904 |
| 3.6 | Connection fraction of collecting vessel vent pipe | 0.694 |
| 3.7 | Connection fraction of liquid drain to collecting vessel | 0 |
| **4** | **Collecting vessel two phase tank** | |
| 4.1 | Elevation (bottom of tank) | 89.96 m |
| 4.2 | Tank diameter (Cylindrical vertical) | 585 mm |
| 4.3 | Tank height (Cylindrical vertical – specified as no end caps but in reality there are hemispherical heads so height is adjusted for the additional volume) | 8.78 m |
| 4.4 | Connection fraction of vents to separator vessels | 1 |
| 4.5 | Connection fraction of liquid drains from separator vessels 1 and 4 | 0.122 |
| 4.6 | Connection fraction of liquid drains from separator vessels 2 and 3 | 0.164 |
| 4.7 | Connection fraction of liquid outlet | 0 |
| **5** | **Liquid drains from separator vessels to collecting vessel** | |
| 5.1 | Pipe inner diameter | 145 mm |
| 5.2 | Pipe roughness | 30 µm |
| 5.3 | Number in parallel | 4 |
| 5.4 | Number of increments | 10 |
| 5.5 | Length (Pipes from separator 1 and 4: average of the estimated distribution pipe lengths) | 11 m |
| 5.6 | Length (Pipes from separator 2 and 3: average of the estimated distribution pipe lengths) | 5 m |
| 5.7 | Secondary loss factor (1 x 90$^o$ smooth bend (r/D=1.5); 4 x 45$^o$ smooth bends (r/D=1.5); Entrance loss for rounded flush (r/D=0.02); Exit loss) | 2.1 |
| 5.8 | Secondary loss factor (Pipes from separator 2 and 3: 1 x 90$^o$ smooth bend (r/D=1.5); 2 x 45$^o$ smooth bends (r/D=1.5); Entrance loss for rounded flush (r/D=0.02); Exit loss) | 1.797 |
| **6** | **Vents from collecting vessel to separator vessels** | |
| 6.1 | Pipe inner diameter | 54 mm |
| 6.2 | Pipe roughness | 30 µm |
| 6.3 | Number in parallel | 1 |
| 6.4 | Number of increments | 5 |

| | | |
|---|---|---|
| 6.5 | Length (Pipes to separator 1 and 4: average of the estimated distribution pipe lengths) | 9 m |
| 6.6 | Length (Pipes to separator 2 and 3: average of the estimated distribution pipe lengths) | 4 m |
| 6.7 | Secondary loss factor (1 x 90$^o$ smooth bends (r/D=1.5); Entrance loss for rounded flush (r/D=0.02); Exit loss) | 1.542 |
| **7** | **Separator steam outlet pipes** | |
| 7.1 | Pipe inner diameter | 285 mm |
| 7.2 | Pipe roughness | 30 µm |
| 7.3 | Number in parallel | 1 |
| 7.4 | Number of increments | 10 |
| 7.5 | Length (Pipes to separator 1 and 4: average of the estimated distribution pipe lengths) | 3.2 m |
| 7.6 | Length (Pipes to separator 2 and 3: average of the estimated distribution pipe lengths) | 7.7 m |
| 7.7 | Secondary loss factor (Pipes from separator 1 and 4: 1 x 90$^o$ smooth bend (r/D=4); Entrance loss for rounded flush (r/D=0.02)) | 0.441 |
| 7.8 | Secondary loss factor (Pipes from separator 2 and 3: 1 x 90$^o$ smooth bend (r/D=4); 2 x 30$^o$ smooth bends (r/D=4); Entrance loss for rounded flush (r/D=0.02)) | 0.627 |
| **8** | **Steam pipes down to superheater 1 inlet headers** | |
| 8.1 | Pipe inner diameter | 285 mm |
| 8.2 | Pipe roughness | 30 µm |
| 8.3 | Number in parallel | 1 |
| 8.4 | Number of increments | 10 |
| 8.5 | Length (Pipes to separator 1 and 4: average of the estimated distribution pipe lengths) | 26 m |
| 8.6 | Length (Pipes to separator 2 and 3: average of the estimated distribution pipe lengths) | 21 m |
| 8.7 | Secondary loss factor (2 x 90$^o$ smooth bend (r/D=4)) | 0.321 |
| **9** | **Collecting vessel level controller** | |
| 9.1 | Proportional gain (only proportional control) | 93.33 (kg/s) /m |
| 9.2 | Level set point | 2.5 m |
| 9.3 | Output high limit | 310 kg/s |
| 9.4 | Output low limit | 0 |
| 9.5 | Linear rate of change limiter (increase or decrease) | 6 (kg/s) /s |
| 9.6 | Time delay | 1 s |

# Appendix C. Case Study A (U3 19-06-2012)

A quenching incident occurred shortly after a controlled shutdown at Unit 3, on 19 June 2012. The data from the plant instruments were used to analyse the incident. A summary of the incident is given below in Table 9.

*Table 9. Summary of main events that occurred at Unit 3 on 19 June 2012*

| Ref | Description | Time |
|---|---|---|
| 1 | Controlled shut down, load at 50% | 03:00:00 |
| 2 | Collecting vessel level starts rising | 03:23:06 |
| 3 | Mill fire out, collecting vessel drains opened to manage level | 03:25:06 |
| 4 | Circulation pump system starts | 03:26:00 |
| 5 | Oil fire out | 03:32:53 |
| 6 | HP bypasses close, Feed water flow has reduced to approx. 60kg/s, but continues on average at that rate, Fans are running at approx. 140kg/s. Regenerative air heater outlet temperature approx.250$^{o}$C | 03:33:06 |
| 7 | Subcooled conditions at evaporator outlet | 03:37:20 |
| 8 | 1 out of 4 separator vessels steam temperature drops below saturation | 03:38:13 |
| 9 | 2 out of 4 of the superheater 2 inlet header steam temperatures drop from 435$^{o}$C to saturation temperature | 03:39:20 |
| 10 | 1 out of 4 of the superheater 3 inlet header steam temperatures drop from 430$^{o}$C to saturation temperature | 03:42:00 |
| 11 | 2 out of 4 main steam temperatures drop from 460$^{o}$C to saturation temperature | 03:46:26 |
| 12 | Fans ramp up to 290kg/s for the purge | 03:54:00 |
| 13 | Fans decrease back to 140kg/s | 04:00:00 |
| 14 | Feed water flow to 0kg/s | 04:03:33 |

In Figure 137, it can be seen that the evaporator outlet temperature drops below the saturation temperature at 03:37. Shortly afterwards, the steam outlet temperature of separator 4 also drops below saturation. This indicates the presence of liquid at the separator 4 steam outlet at approximately 03:38.

Temperature measurements at various locations in the superheater show a drop to saturation temperature at different times. The superheater stages each have four separate parallel legs and the steam temperatures for each are measured at various locations.

The superheater leg one and leg four temperatures at the Superheater 2 inlet are first to drop to saturation as seen in Figure 138 at 03:39. At 03:45, these temperatures drop below the saturation temperature, clearly indicating liquid at those points.

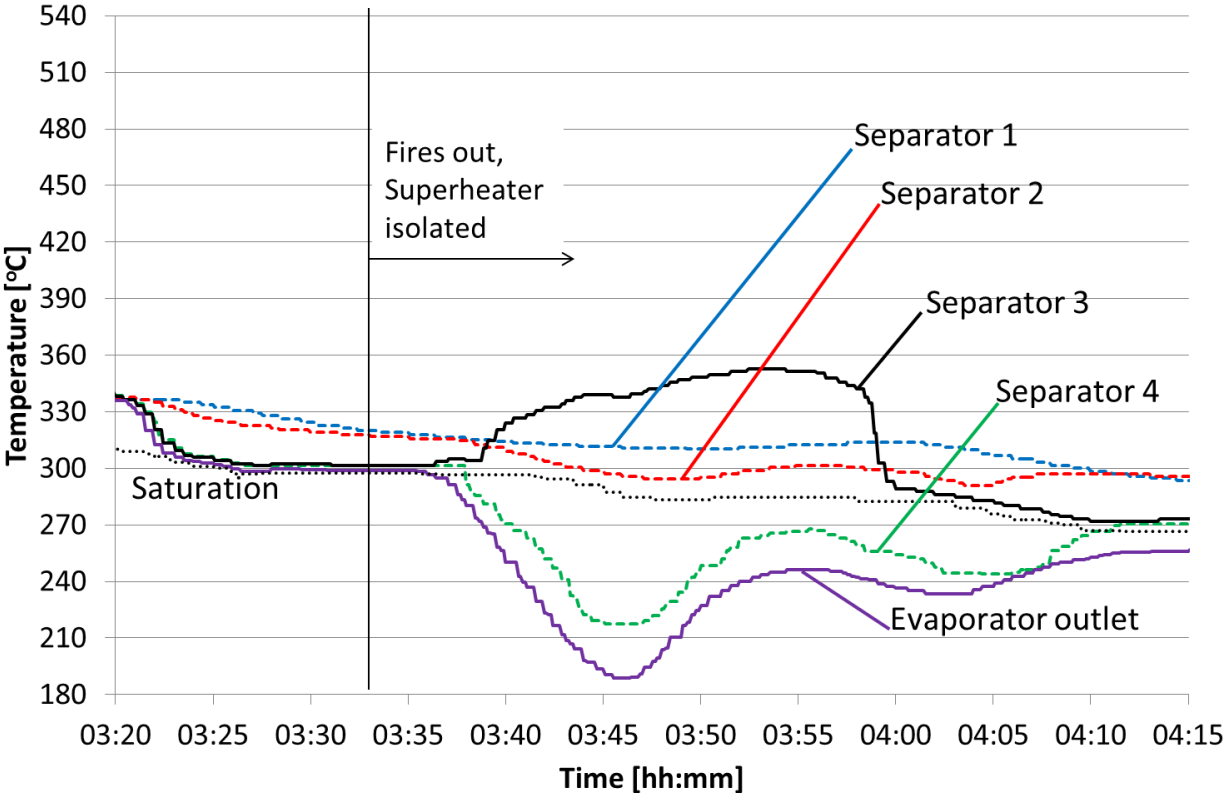


*Figure 137. Measured data from plant instruments – Separator steam outlet temperature (U3 19-06-2012)*

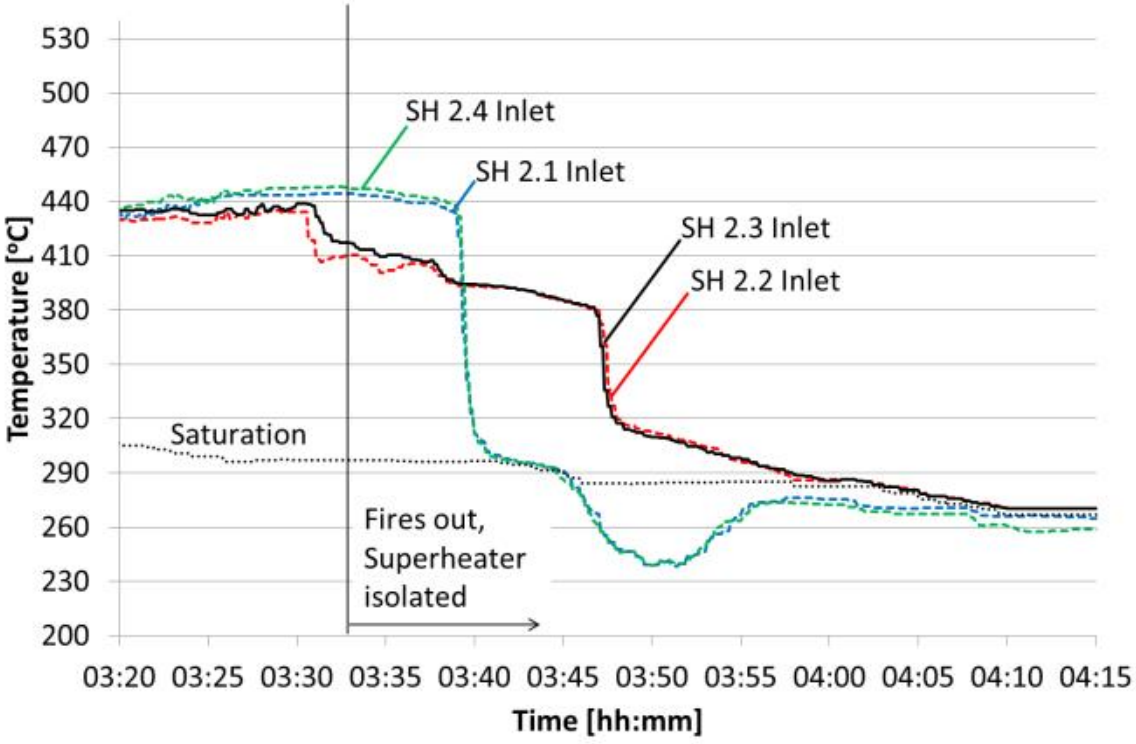


*Figure 138. Measured data from plant instruments - Superheater 2 inlet temperature (U3 19-06-2012)*

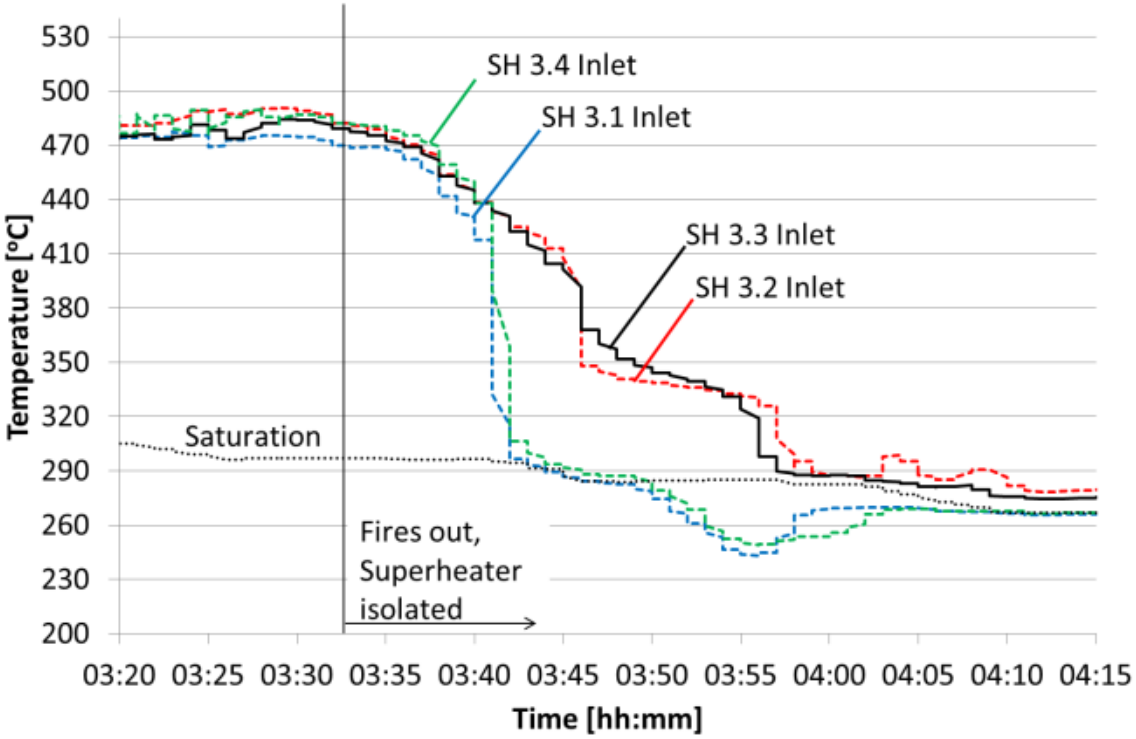


*Figure 139. Measured data from plant instruments- Superheater 3 inlet temperatures (U3 19-06-2012)*

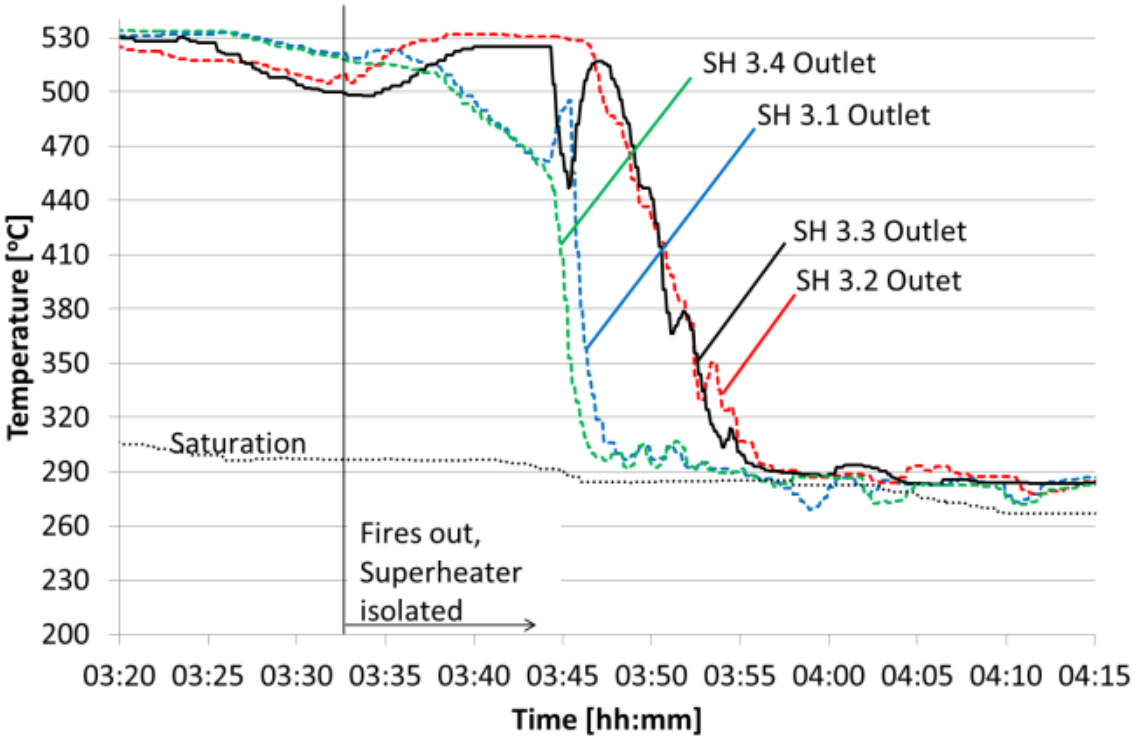


*Figure 140. Measured data from plant instruments - Superheater 3 outlet temperatures (U3 19-06-2012)*

In Figure 139, the progression of liquid to Superheater 3 inlet can be observed. The leg one and leg four Superheater 3 inlet temperatures drop to saturation at 03:42 (3 minutes after the superheater 2 inlet temperatures dropped.) Again the temperatures drop below saturation a few minutes later at 03:50.

The superheater outlet is affected at 03:45 with the leg 1 and leg 4 Superheater 3 outlet temperatures dropping to saturation as seen in Figure 140. This series of leg 1 and leg 4 temperature drops shows the progression of liquid as it flows through the superheater. In the case of the Superheater 3 outlet, there is almost no drop below saturation. This is because the Superheater 3 outlet temperature measurements are beyond the Superheater 3 outlet headers where the superheater legs are interconnected.

Concerning leg 2 and leg 3, note that the temperature drops occur at Superheater 3 inlet (Figure 139) approximately a minute before they occur at the Superheater 2 inlet (Figure 138). This indicates reverse flow and because the temperatures remain above saturation temperature, it is the reverse flow of colder steam from Superheater 3 inlet to Superheater 2 inlet.

Evidence of reverse flow can also be seen in the separator steam temperature measurements in Figure 137. The temperature of separator 3 becomes significantly superheated from 03:39 onwards.

It was observed that the superheater pressure measurements at three different locations were reading almost the same value over the time period and followed a particular trend. The average of the measured superheater pressure is shown in Figure 141. It can be seen that the pressure remains almost constant until 03:42 even though the fires are out. Then, the pressure suddenly drops from 8.1MPa to 6.8MPa by 03:46.

The collecting vessel level data was analysed to determine if high levels occurred. On three occasions, the level had exceeded seven metres. After rectifying the density correction, it was found that on all three occasions, the level had most likely exceeded the top tapping point height (Figure 142).

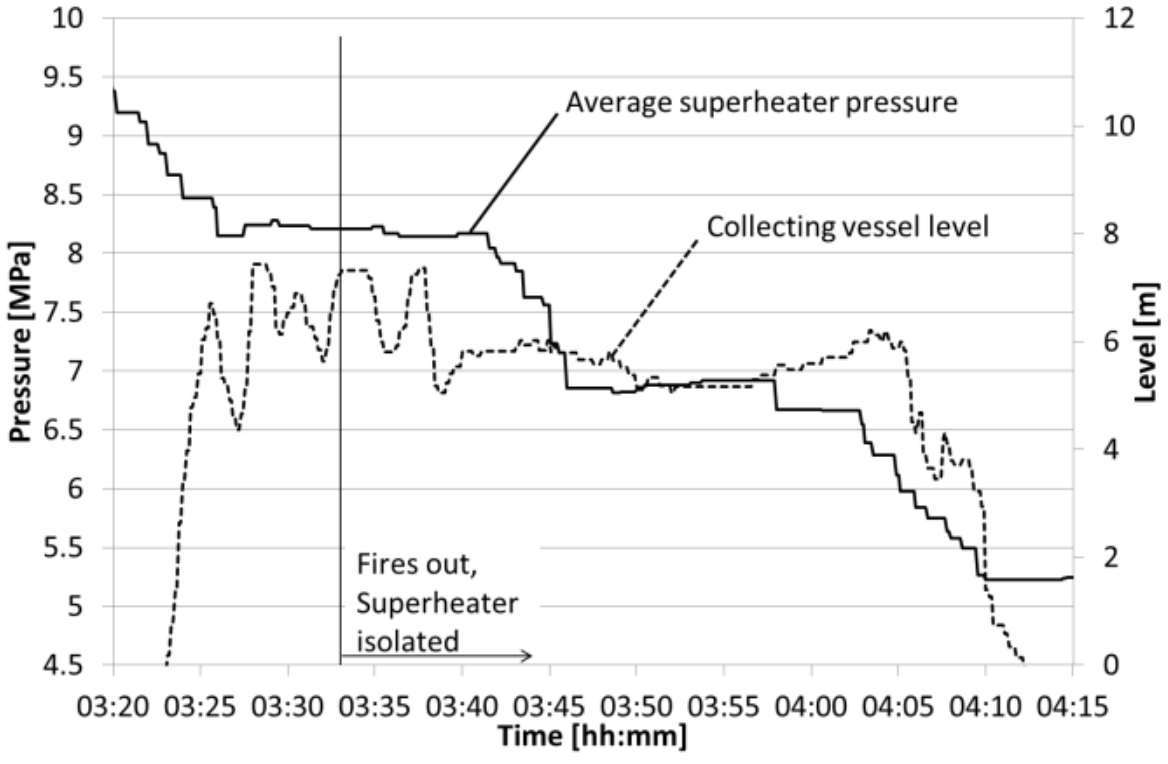


d)

*Figure 141. Measured data from plant instruments - Superheater pressure and collecting vessel level (U3 19-06-2012)*

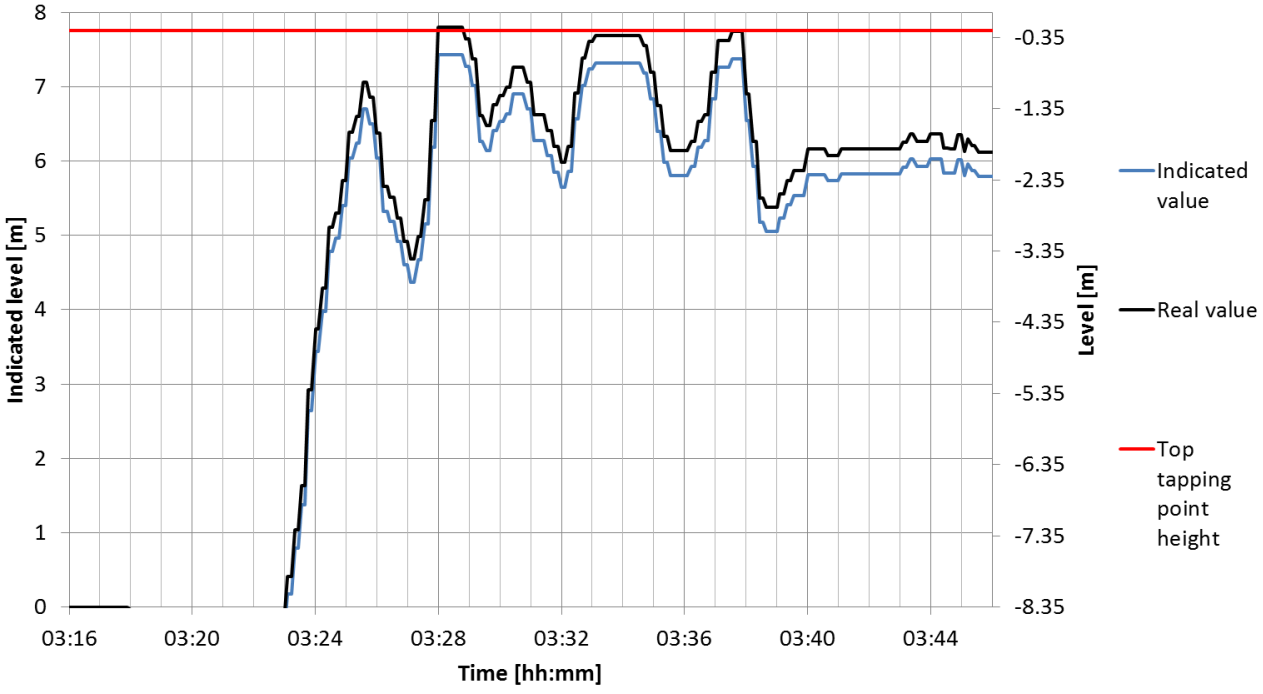


*Figure 142. Collecting vessel level - Indicated and re-calculated collecting vessel level (U3 19-06-2012)*

If the collecting vessel level exceeds the top tapping point height, there is still capacity in the separating vessels to accommodate additional liquid before an overflow into the superheater can occur. If the separators fill equally, then this volume is 3.8m$^3$.

To determine if a separator overflow occurred, the separator outlet steam temperature and other downstream temperature measurements can be interrogated. It was found that the separator outlet steam temperatures of separator 3 and separator 4 had gradually become saturated before there was any collecting vessel level. At that point in time, there was still saturated steam being generated in the evaporator and so this steam temperature was measured by the separator outlet measurements as it flowed into the superheater. It is interesting to note that separator 1 and 2 were not affected by the steam flow (Refer Figure 137).

Later at 03:30:30, a sudden drop of temperature by 25°C occurred at the SH2.2 inlet (Refer arrow A in Figure 143). The temperature did not drop to saturation, but is indicative of the arrival of colder steam at that point. Potentially, the high collecting vessel level that occurred two minutes earlier had caused some saturated liquid to overflow into the superheater.

Three minutes later, another high collecting vessel level occurred. The effects of this particular high collecting vessel level at 03:33 are almost negligible and perhaps it did not result in any overflow into the superheater.

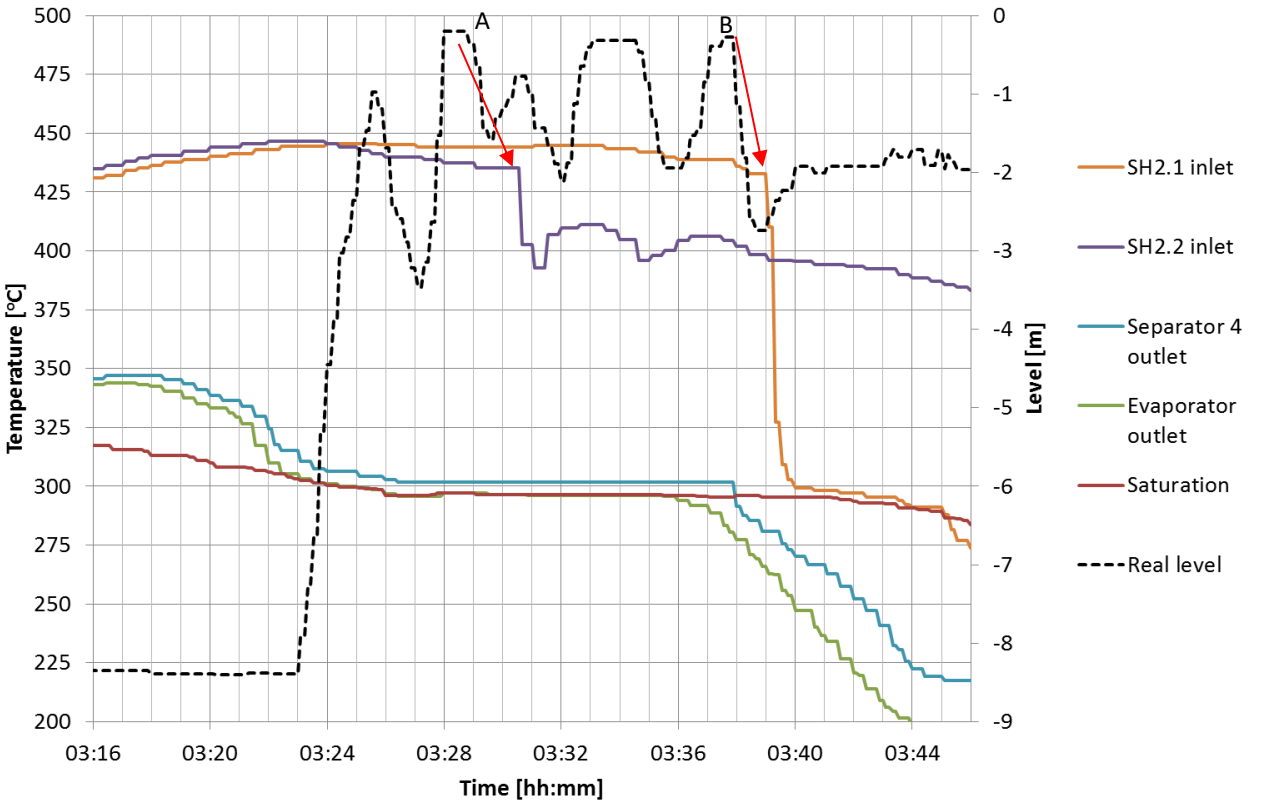


*Figure 143. Selected steam temperatures and re-calculated collecting vessel level (U3 19-06-2012)*

The third high level occurs at 03:37. In Figure 143 (arrow B), it can be seen that subcooled liquid arrives at the evaporator outlet at 03:36. Two minutes later at 03:38, the separator 4 outlet steam

temperature drops below saturation. This is a clear indication of liquid at the separator 4 steam outlet and thus the liquid must be overflowing into the superheater at that point.

At 03:39, the superheater 2.1 inlet temperature rapidly drops to saturation temperature. SH1.1 and SH1.4 share a common inlet and outlet header, hence the liquid flowing from separator 4 into the superheater can reach the superheater 2.1 inlet. The high collecting vessel level at 03:37 indicates that the separator and collecting vessel system level was out of control and it overflowed into the superheater and caused the temperature drop at the superheater 2.1 inlet.

Figure 144 shows the feed water flow, economiser inlet flow and the flow leaving the collecting vessel which is the sum of the drain and recirculation flows. The drain flow is estimated from the openings of the quick drain valves. The other flows are measured by permanently installed flow measurement devices (nozzles and orifice plates). Initially the feed water flow exceeds the economiser inlet flow. This is due to the HP bypasses being open at that stage and thus the difference in feed water flow and economiser inlet flow is due to the HP bypass spray flow. The HP bypasses close at 03:33.

The feed water flow reduces as it tries to control a constant economiser inlet flow while there is an increase in the recirculation flow. The recirculation flow joins the feed water flow upstream of the economiser inlet flow measurement. The increase in recirculation flow influences the required feed water flow. The control aim to maintain a constant economiser inlet flow and eventually, the feed water flow is zero at 03:33:30.

During the process of establishing the recirculation flow, two high collecting vessel level events had occurred at 03:28 and 03:33. In those instances, the quick drain valves and the recirculation flow had not reacted fast enough to prevent high levels and the evidence suggests that some separator overflow to the superheater had occurred.

At 03:36 it appears that the feed water was given a signal to increase the economiser inlet flow to 320kg/s. The sudden injection of feed water achieved an increased economiser inlet flow but caused a high level in the collecting vessel which reached the top tapping point of the level measurement by 03:37. The circulation pump responded, but the response was insufficient. The quick drain valves failed to respond with only one of the valves opening to 4%.

The surplus flow into the separator and collecting vessels at 03:37 is estimated at 75kg/s. This rate would fill the remaining volume in the separator vessels up to the highest point in 37 seconds. Then the water would overflow into the superheater.

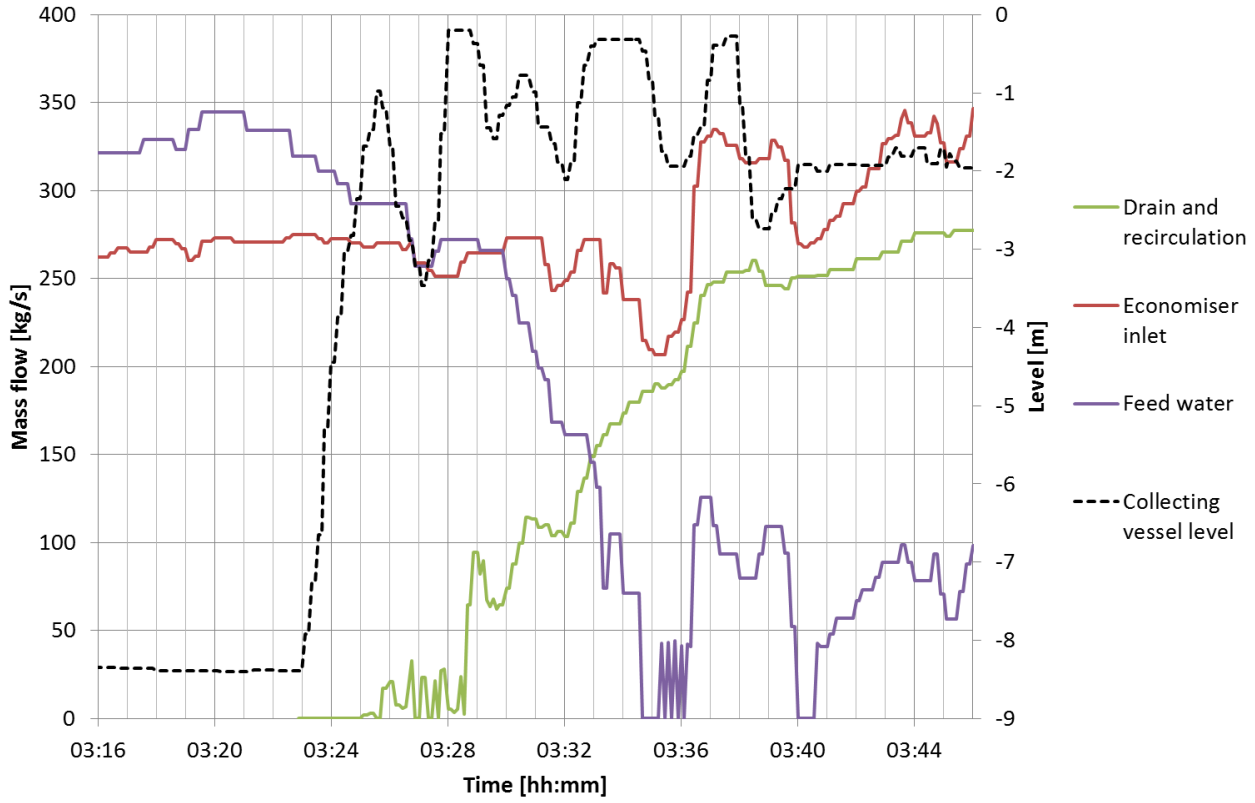


*Figure 144. Flows and re-calculated collecting vessel level (U3 19-06-2012)*

It should be noted that the temperature of the evaporator outlet is subcooled at 03:37 as seen in Figure 143. This subcooled liquid has been flowing in at the feed water inlet and has made its way through the economiser and evaporator until it reached the evaporator outlet. It has cooled the metal surfaces to the extent that the entire circuit is now filled with incompressible subcooled liquid. Thus at 03:37 there existed a direct relationship between inlet flow and outlet flow of the economiser / evaporator circuit. Any feed water flow added to circuit must be balanced by leakage flow or dump flow to prevent the separators from overflowing into the superheater.

As a result of the sudden increase in economiser flow set point, an increase in feed water flow occurred. This increase should increase level in the collecting vessel to allow the recirculation system to increase flow to the new economiser inlet flow set point. However, the collecting vessel level increase is too rapid and the circulation system response is too slow, most likely because the flow is still ramping up. Thus the collecting vessel level goes high and the liquid fills the separator vessels. There was no rapid response from the quick drain valves at this point. If they had opened, they may have prevented liquid overflowing from the separators and into the superheater.

It is assumed that due to pressure differences at the separator outlets, the separators fill at different rates and overflow at different times. In this case, separator 4 overflowed first. The other consequence of the subcooled liquid overflowing from the separators is that the falling liquid

column that overflows towards the superheater creates a siphon. The siphon rapidly decreases the pressure in separator 4 and causes water from the other separator vessels and the collecting vessel to flow towards separator 4. Hence the collecting vessel level reduces at 03:38.

While the separator 4 overflows into the superheater, there is a physical reduction in collecting vessel level. This causes a malfunction of the level control philosophy. The circulation system reduces flow because it appears that the collecting vessel level is under control. However, in reality the low pressure in separator 4 is causing water to flow out of the evaporator into separator 4 and overflow into the superheater. Thus the water bypasses the collecting vessel and the high level is not reflected in the collecting vessel.

This situation causes a mismatch between circulation flow and economiser inlet flow. Hence feed water is added to the boiler to make-up the economiser inlet flow rate set point. A significant amount of water is added to the system and most of it over flows into the superheater. In Figure 144, the difference in economiser inlet flow and recirculation flow persists from 03:38 onwards because the control setup is unaware that flow is siphoned into the superheater.

In summary, the cause of liquid in the superheater is overflow of the separator vessels. The overflow is caused by adding feed water to an already full economiser/evaporator circuit. The feed water is added by the control system because it receives false information about the level in the separator and collecting vessel system. The control system is unaware that a siphon can be formed to bypass liquid flow directly from a separator into the superheater without showing a high level in the collecting vessel.

# Appendix D. Case Study B (U5 02-01-2013)

A quenching event occurred shortly after a controlled shutdown at Unit 5 on 2 January 2013. A summary of the incident is given below in Table 10.

*Table 10. Summary of main events that occurred at Unit 5 on 2 January 2013*

| Ref | Description | Time |
|---|---|---|
| 1 | Controlled shut down, turbine inlet valves closed, boiler load 48% | 16:08:20 |
| 2 | Collecting vessel level starts rising, boiler load 31% | 16:26:12 |
| 3 | Collecting vessel drains opened to manage level | 16:28:28 |
| 4 | Circulation pump system starts | 16:30:44 |
| | Coal fire out, Fans reduce air flow to approx. 210kg/s | 16:31:52 |
| 6 | HP bypasses close for the first time (subsequently they open again on four separate occasions to control the superheater pressure before finally closing at 16:42:39) | 16:35:16 |
| 7 | Subcooled conditions at evaporator outlet and Separator 1 steam outlet temperature drops below saturation.<br>Feed water flow has reduced to approx. 60kg/s, but continues on average at that rate. | 16:38:06 |
| | Superheater 2 inlet steam temperatures in leg one and four drop from 400°C to saturation temperature | 16:39:48 |
| 8 | Oil fire out, Fans reduce air flow to 140kg/s and it remains approximately at that value for the remainder of the incident | 16:40:22 |
| 9 | Superheater 3 inlet steam temperatures in leg 1 and 4 drop to saturation temperature | 16:42:39 |
| 11 | 2 out of 4 main steam temperatures drop to saturation temperature | 16:45:00 |
| 12 | Boiler outlet main steam stop valves stayed open | N/A |
| 13 | Superheater drains did not open. | N/A |
| 14 | Main steam leg drains did not open. | N/A |

The behaviour of the steam temperatures in the superheater follows a similar pattern in case study B as it did for case study A. In Figure 145, the separator outlet temperatures indicate that subcooled liquid overflowed from separator 1 into the superheater.

The separator 1 outlet steam temperature follows the evaporator outlet temperature as subcooled liquid arrives at the separating vessels at 16h38. At 16h42, the separator 1 outlet temperature departs from the evaporator outlet temperature. The separator 1 outlet temperature is heated above the evaporator outlet temperature, but remains subcooled. At the same time, the steam outlet temperatures of Separator 2 and three become superheated, indicating the reverse flow of steam coming out of the superheater and into those separating vessels. This steam would readily condense as it comes into contact with the subcooled liquid in the separator vessels. The steam would heat the liquid.

This provides an explanation for the increase in Separator 1 outlet liquid temperature relative to the evaporator outlet temperature that occurs at 16h42. The water overflowing from separator 1 was

heated by steam condensing in the other separator vessels and flowing to separator 1. The heating effect is confirmed by the temperature at the circulation pump inlet.

The mass flow of water at the evaporator outlet is known because it is measured at the economiser inlet. Using this flow together with the measured temperature rise, the amount of energy gained by the water can be determined. By equating this to the flow of steam being condensed, the steam flow rate can be determined. This methodology is used further for analysing the quenching events in section 6.1.

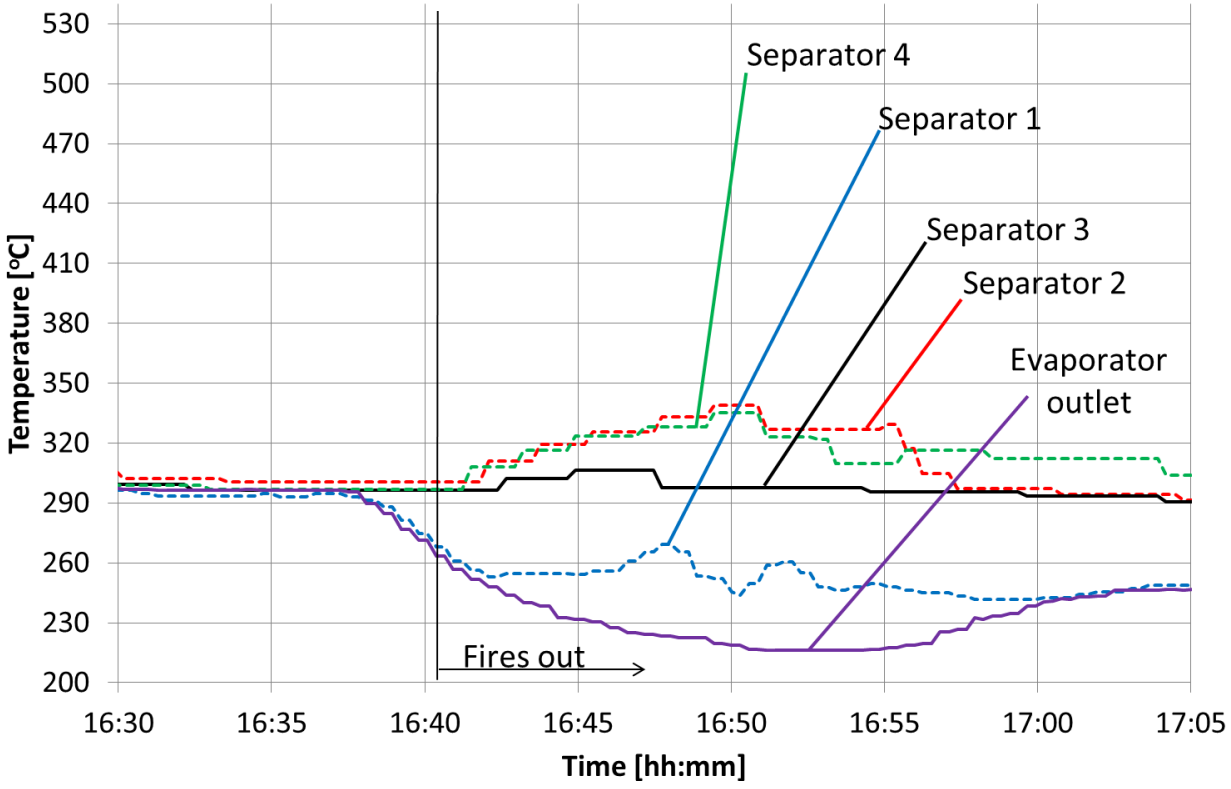


*Figure 145. Measured data from plant instruments- Separator outlet steam temperatures (U5 02-01-2013)*

The progression of liquid through the superheater can be identified in Figure 146, Figure 147 and Figure 148. The temperature drop of leg one and leg four temperatures occurs in the direction of flow.

Superheater leg one and four share a common inlet and outlet header of Superheater 1. Hence the liquid flows equally through both those legs, even though the separator overflow occurs from separator 1 only.

The reverse flow of steam back to the separators is also evident in Figure 147 and Figure 146. The leg 2 and 3 temperatures drop first at the superheater 3 inlet before they drop at the superheater 2 inlet.

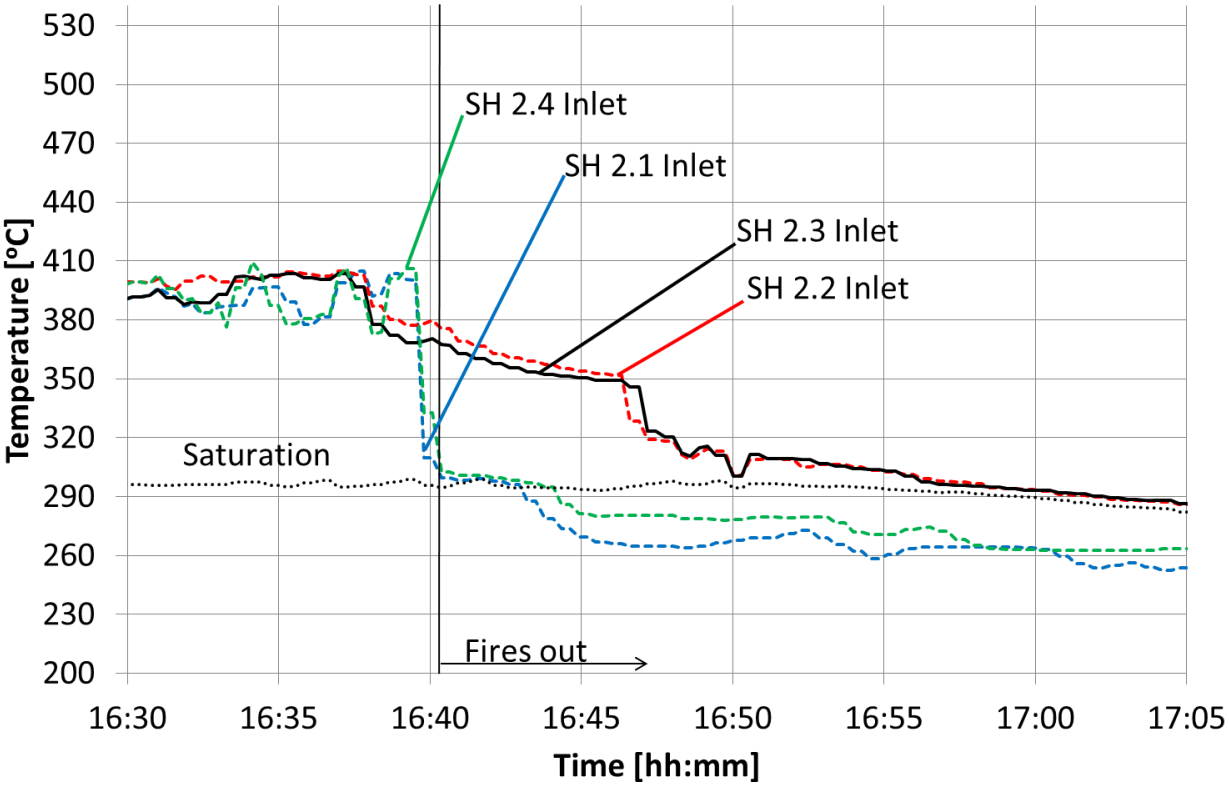


*Figure 146. Measured data from plant instruments- Superheater 2 inlet temperatures (U5 02-01-2013)*

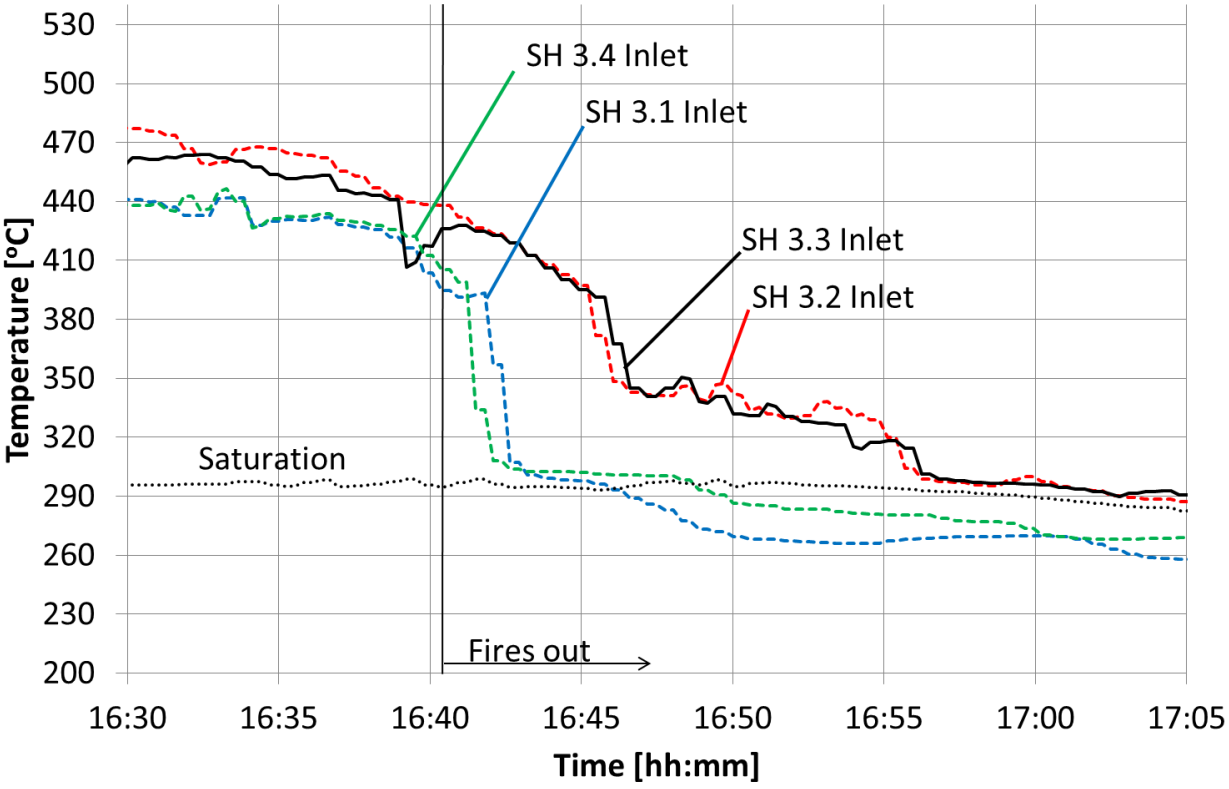


*Figure 147. Measured data from plant instruments- Superheater 3 inlet temperatures (U5 02-01-2013)*

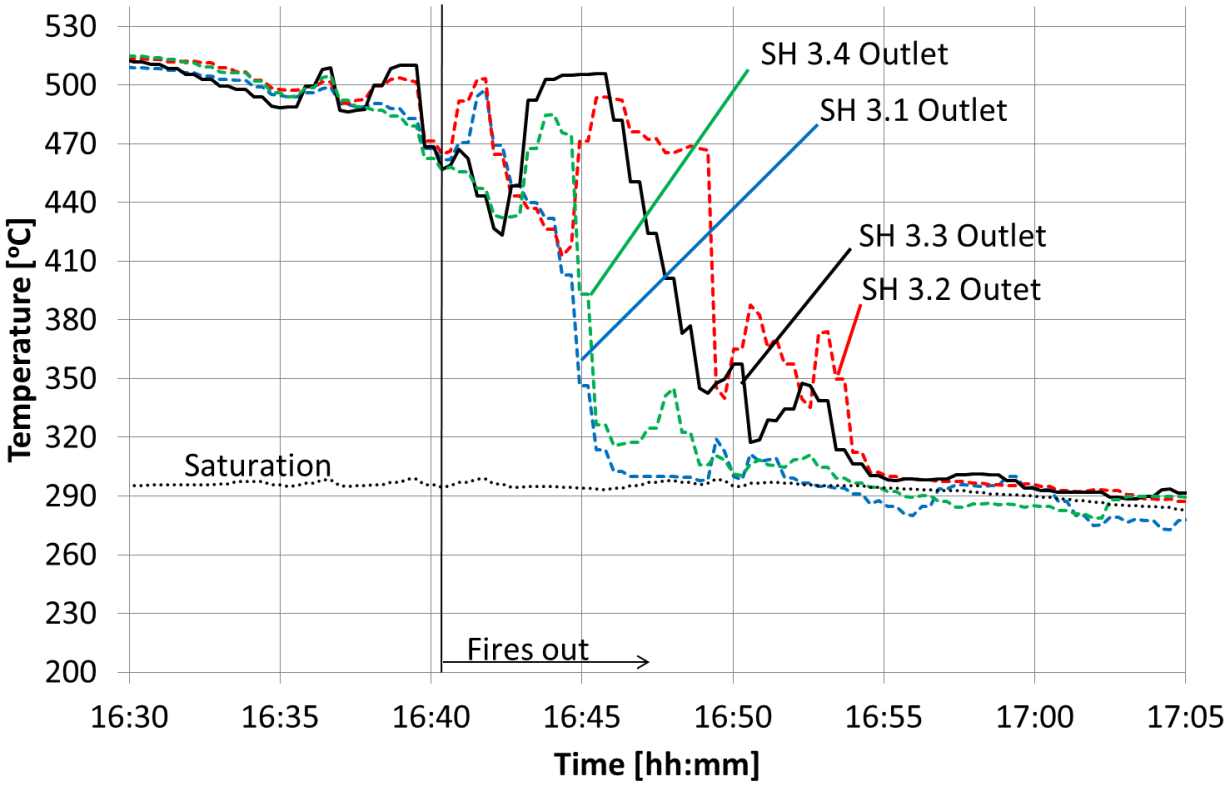


*Figure 148. Measured data from plant instruments- Superheater 3 outlet temperatures (U5 02-01-2013)*

At the boiler outlet, the leg one and four temperatures drop at 16h45 indicating the arrival of liquid at those points. The leg two and leg three headers are common with the leg one and leg four headers respectively. Thus, liquid emanating from superheater stage 3, leg 1 or 4 would most likely flow into the horizontal outlet header and then left or right in approximately equal proportions towards the ends. The closer end of the header leads directly into the main steam system where the thermocouples are located. Hence the immediate quenching of leg one and leg four.

Liquid flowing in the opposite direction, first encounters the portion of header where leg 2 or 3 connects. Some liquid most likely flows in reverse into the leg 2 or 3 superheater 3. The leg 2 and 3 steam measurements at the boiler exit thus measure a mixture of steam returning from the main steam system and eventually liquid that flows out of the header. Hence the delayed drop of leg 2 and 3 boiler outlet temperatures.

Concerning the cause of the separator overflow, the collecting vessel level is again interrogated. The collecting vessel level measurement was re-calculated and found to vary only marginally from the indicated value (Figure 149). Levels above 7m were recorded, but even after re-calculation, these high levels appear to still have margin before reaching the top tapping point.

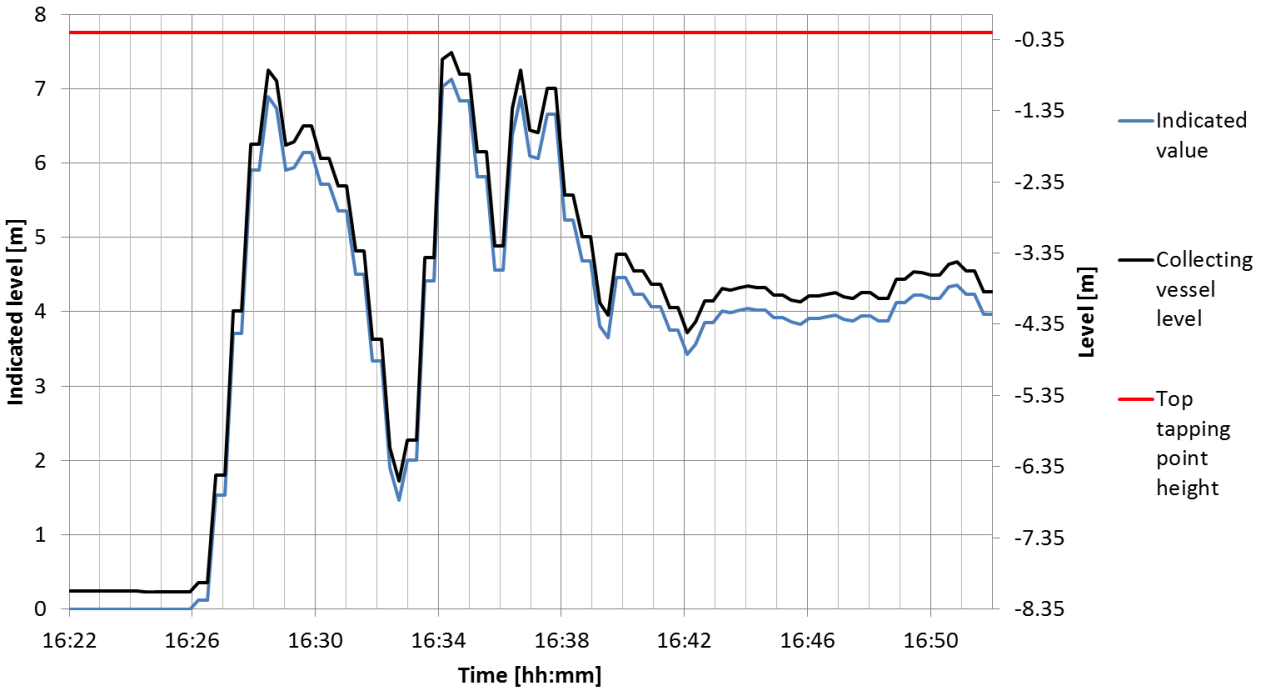


*Figure 149. Collecting vessel level - Indicated and re-calculated level (U5 02-01-2013)*

Thus the collecting vessel level appears to be in control, but from the information above, it is clear that a separator overflow did occur. It is difficult to know the exact moment when the separator overflow started to occur. Considering that the separator 1 outlet temperature immediately became

subcooled when the evaporator outlet become subcooled indicates that liquid was most likely overflowing already at that point in time (Figure 145).

In Figure 150, there is evidence from the SH2.4 inlet temperature measurement that colder steam was flowing past the temperature measurement point. The black arrows on Figure 150 show how each high collecting vessel level incident is followed by a rise and fall of the SH2.4 inlet temperature. Potentially the temperature behaviour is due to saturated liquid overflowing from the separators. As the liquid flows, through superheater 1, it is heated by the hot metal and evaporates to steam and thus the temperature at SH2.4 inlet does not drop to saturation temperature.

The SH2.4 measurement is potentially affected by the HP bypass opening, but this was investigated and no clear pattern could be seen. Thus the behaviour of the SH2.4 inlet temperature most likely indicates that each time the collecting vessel level went high there was separator overflow. This overflow cannot be identified at the separator outlet because the temperature was saturated.

At 16:38, with the arrival of sub cooled liquid at the evaporator outlet and the separators, a siphon is created from separator 1 into the superheater and it causes the collecting vessel level to drop (Figure 150). Once the level has dropped, the controls reduce the recirculation flow (Figure 151 at 16:39:30) and it is apparent that the economiser inlet flow set point was reduced at this time as well because the feed water flow did not respond to maintain the minimum value.

Although the economiser inlet flow drops to accommodate the reduced recirculation flow, it does not stop the feed water flow. Feed water continues to be added at a rate of approximately 50kg/s. This can also be seen in the difference between economiser inlet flow and recirculation flow from 16:40 to 16:51. Integrating the feed water flow over this period gives approximately 35t of water that overflowed into the superheater.

Again, as in case study A, the main failure of the system is the formation of a siphon which enables large amounts of water to overflow into the superheater from the separators without the control system being aware of it happening. The formation of a siphon requires a separator overflow to initiate the flow. If the initiator was removed, the siphon would not occur. In this case, the initiator is difficult to identify. The collecting vessel level appeared to remain in control but the evidence suggests an overflow occurred as early as 16:31.

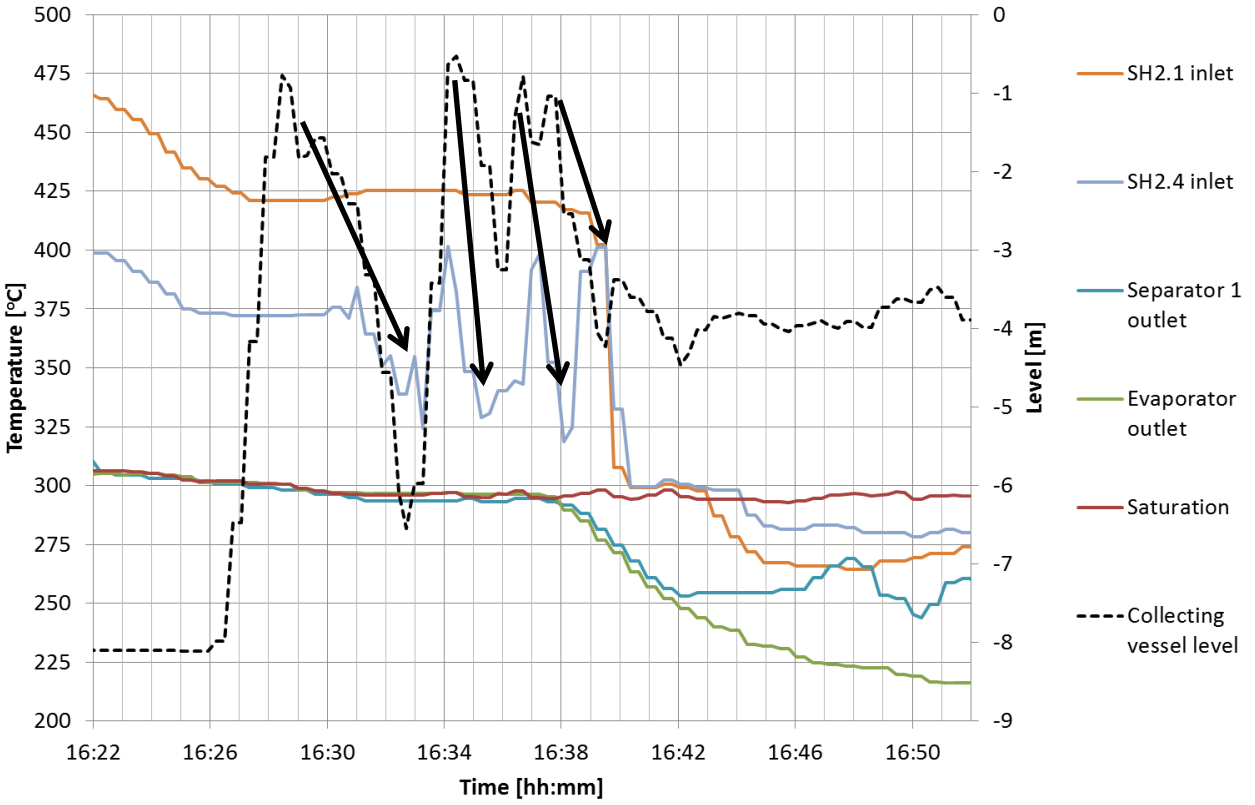


*Figure 150. Selected steam temperatures and recalculated collecting vessel level (U5 02-01-2013)*

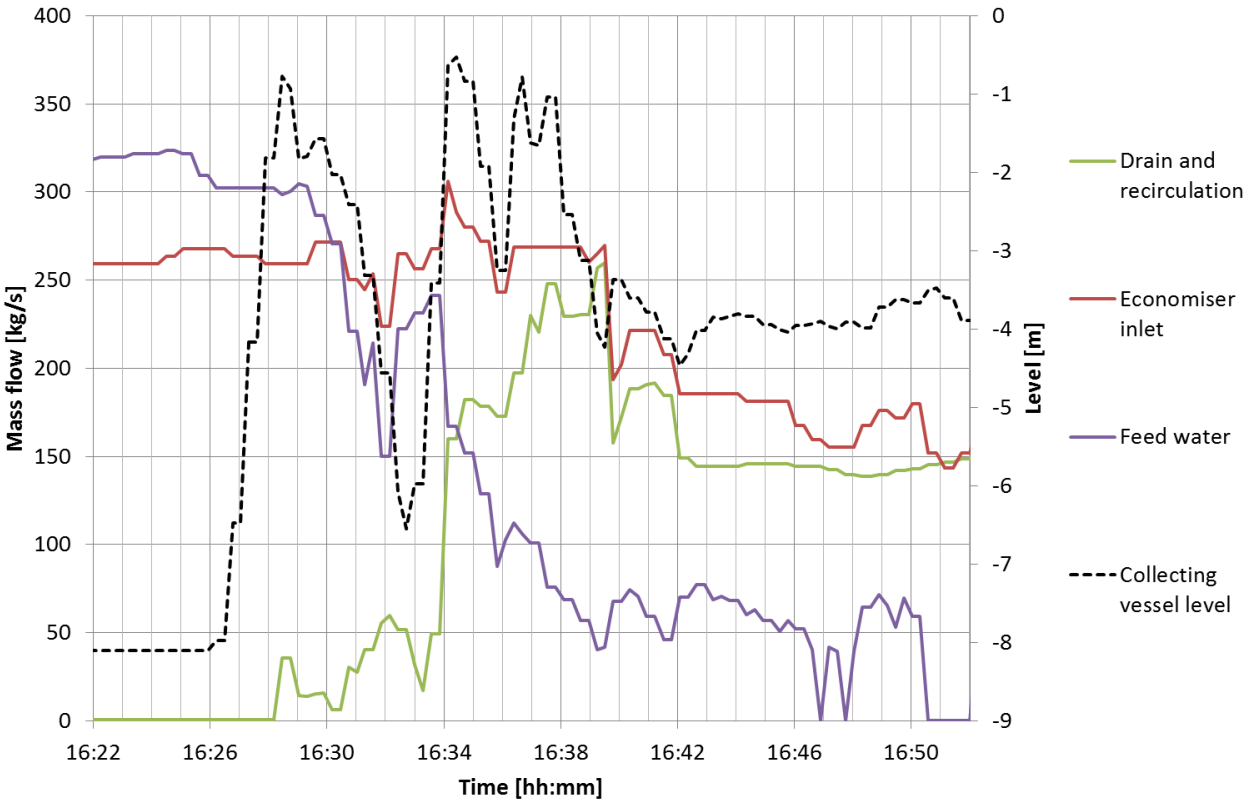


*Figure 151. Flows and re-calculated collecting vessel level (U5 02-01-2013)*

This anomaly can potentially stem from the level measurement being incorrect or the flow is physically not reaching the collecting vessel by it overflowing out the top of the separator, rather than draining out the bottom of the separators.

The pressure in the superheater was controlled by the HP bypasses until 16:42:39. The HP bypass opening can be compared with the measured pressures in Figure 152 – each time the Superheater 3 outlet pressure exceeded the set point at the time, the HP bypass opened and relieved the pressure. The source of pressure rise after 16:35 is unlikely to be from the fire side in the boiler. By 16:40, the fires were out and the temperature gradients that drive the heat flow to steam in the superheater would have levelled out and may even have reversed. Liquid evaporating on hot metal surfaces most likely causes the rapid temperature rises that are seen at 16:36, 16:39, 16:42 and 16:49.

Figure 152 also shows the difference between the superheater pressure measured at the inlet (at the collecting vessel) and at the outlet of superheater 3. Under zero flow conditions, the difference in pressures at these two points is only the static pressure as a result of the steam density and the height difference. Thus under zero flow conditions, the outlet pressure is approximately 10kPa higher than the inlet pressure.

In Figure 152, the zero flow condition can be identified from 16:35 to 16:42 where the collecting vessel pressure and outlet pressure are within 10kPa of each other (besides at times when the HP bypass opened). From 16:42 onwards, the outlet pressure is higher than the inlet pressure by an average of 125kPa. Considering that superheater 2 and 3 are not flooded with liquid, this pressure difference can only occur as a result of flow from the superheater outlet in reverse to the collecting vessel.

In the Figure 152 second part, it can be seen that the pressure difference suddenly disappears at 17:40. This is when the reverse steam flow comes to an end. The cause of the termination of reverse steam flow is the evaporator outlet condition which becomes saturated again at 17:40. (The evaporator outlet was subcooled from 16:38 to 17:40).

The difference in pressures potentially show that reverse steam flow existed from the superheater outlet back to the separators and collecting vessel. This flow of steam was condensed at the subcooled liquid interface.

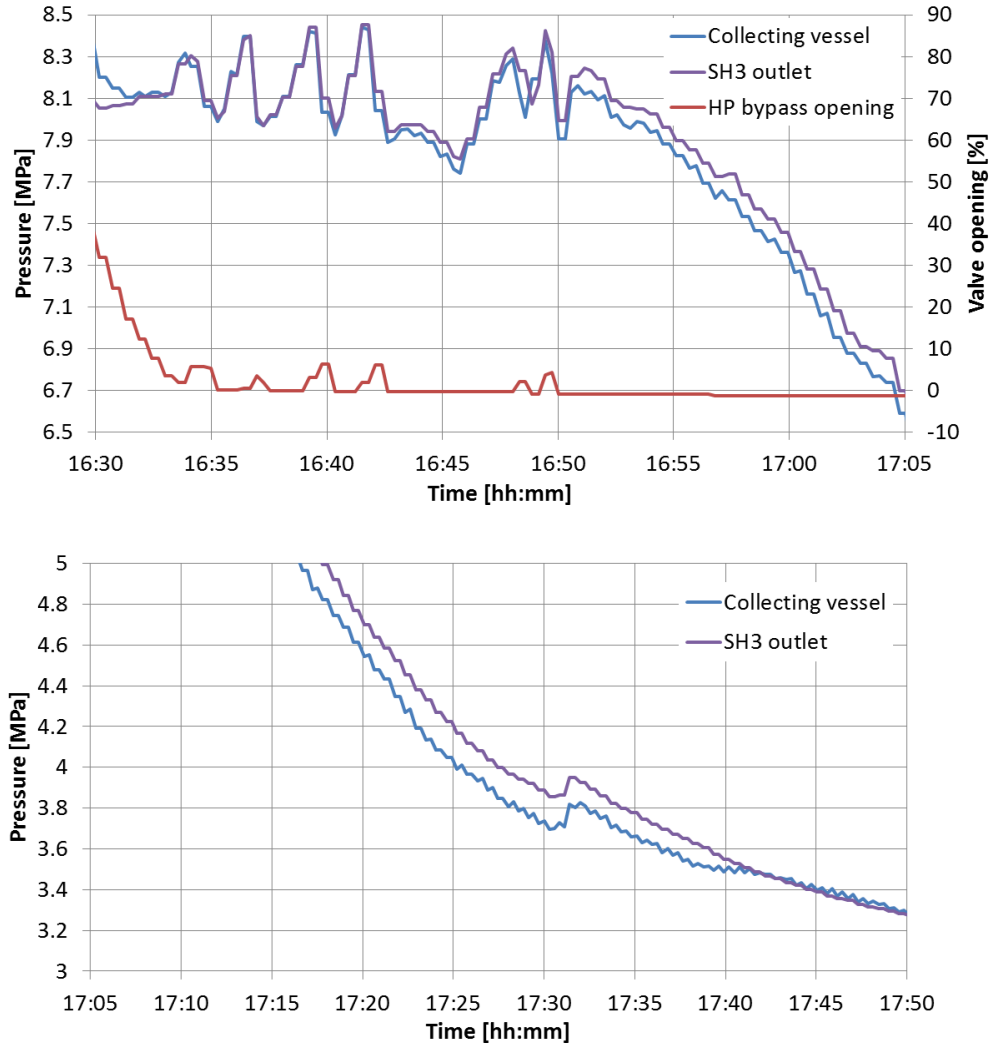


*Figure 152. Measured data from plant instruments- Superheater and collecting vessel pressure (U5 02-01-2013)*

In summary, case study B has demonstrated that the separator overflow occurs even if the corrected collecting vessel does not show level above the upper tapping point. Again a siphon occurred and caused a large overflow of water into the superheater because the control system is not designed to deal with it. Secondly, this case study provides further evidence of reverse steam flow to the subcooled liquid interface.

# Appendix E. Case Study C (U6 08-10-2018)

A quenching event occurred shortly after the boiler tripped at Unit 6 on 08 October 2018. A summary of the incident is given below in Table 11.

*Table 11. Summary of main events that occurred at Unit 6 on 8 October 2018*

| Ref | Description | Time |
|---|---|---|
| 1 | Boiler trip from a load of 500MWe, HP bypasses open to 100% immediately and control boiler pressure | 02:40:40 |
| 2 | Collecting vessel level starts rising | 02:51:40 |
| 3 | Collecting vessel drains opened to manage level | 02:56:00 |
| 4 | Feed water flow starts increasing in response to increased eco inlet flow set point. (Feed water flow had been around 60kg/s since the trip) | 02:58:00 |
| 5 | Circulation flow starts | 02:59:00 |
| 6 | Peak feed water flow of 200kg/s, Circulation flow reaches 100kg/s | 03:00:20 |
| 7 | Subcooled conditions at evaporator outlet | 03:01:40 |
| 8 | HP bypasses close, boiler pressure at 13.8MPa | 03:03:20 |
| 9 | 3 out of 4 of the superheater 2 inlet header steam temperatures drop from 410$^{o}$C to saturation temperature | 03:03:20 |
| 10 | Superheater drains open | 03:03:40 |
| 11 | 1 out of 4 separator vessels steam temperature drops below saturation | 03:04:00 |
| 12 | Collecting vessel quick drains start opening to assist in controlling level | 03:07:20 |
| 13 | Fans ramp up from zero flow to 140kg/s | 03:10:00 |
| 14 | 2 out of 4 main steam temperatures drop from 440$^{o}$C to saturation temperature | 03:10:00 |
| 15 | Circulation flow peaks at 330kg/s, Feed water flow reduces to zero | 03:11:30 |
| 16 | Main steam leg drains open | 03:19:20 |
| 17 | Fans ramp up to 300kg/s for the purge | 03:21:00 |
| 18 | Main steam stop valves close | 03:26:20 |

The separator outlet temperatures (Figure 153) show that an overflow of separator 1 occurred. (Note that there is an offset in the measured value which can be corrected by subtracting a bias of approximately 7$^{o}$C). As seen in the previous case studies, we again see superheated separator outlet temperatures at separators 2 and 3 and also separator 4 in this case.

The temperatures at the superheater 2 inlet (Figure 154) drop to saturation at 03:03:30. This is prior to the overflow of subcooled liquid from separator 1 at 03:04:00 and may indicate that saturated liquid overflowed from separator 1 until the system had cooled enough for subcooled conditions to prevail.

The leg one and leg four Superheater 2 inlets eventually drop below saturation at 3:09 and 3:12 respectively confirming the presence of liquid at that stage. The Superheater 3 inlet temperatures

are less definitive and do not show sudden temperature drops associated with liquid passing the measurement points. Leg one and leg four are potentially quenched by steam from 03:05 (Figure 155). The Superheater 3 outlets show definite quenching occurred on legs one and four (Figure 156).

Considering that the superheater drains opened at 03:03:40, it is likely that they drained a substantial amount of water from the superheater and prevented the water from getting further and causing more quenching damage.

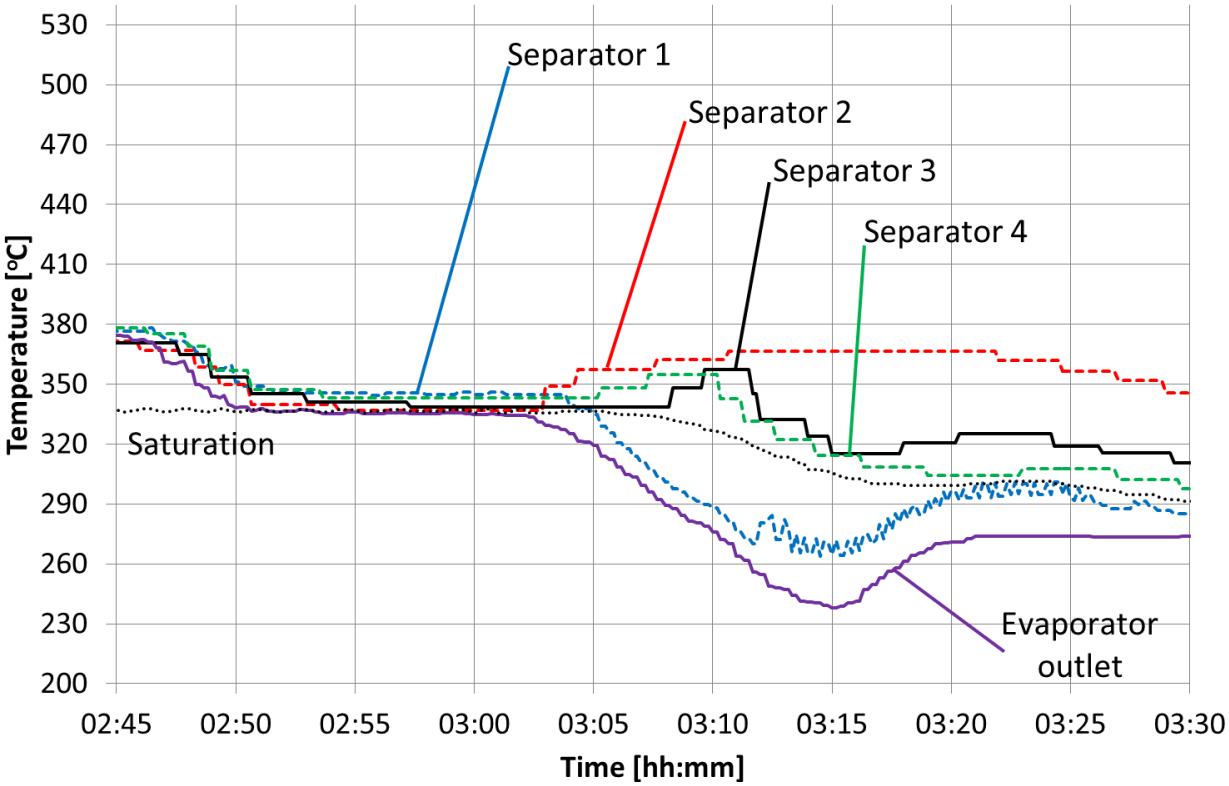


*Figure 153. Measured data from plant instruments- Separator outlet steam temperatures (U6 08-10-2018)*

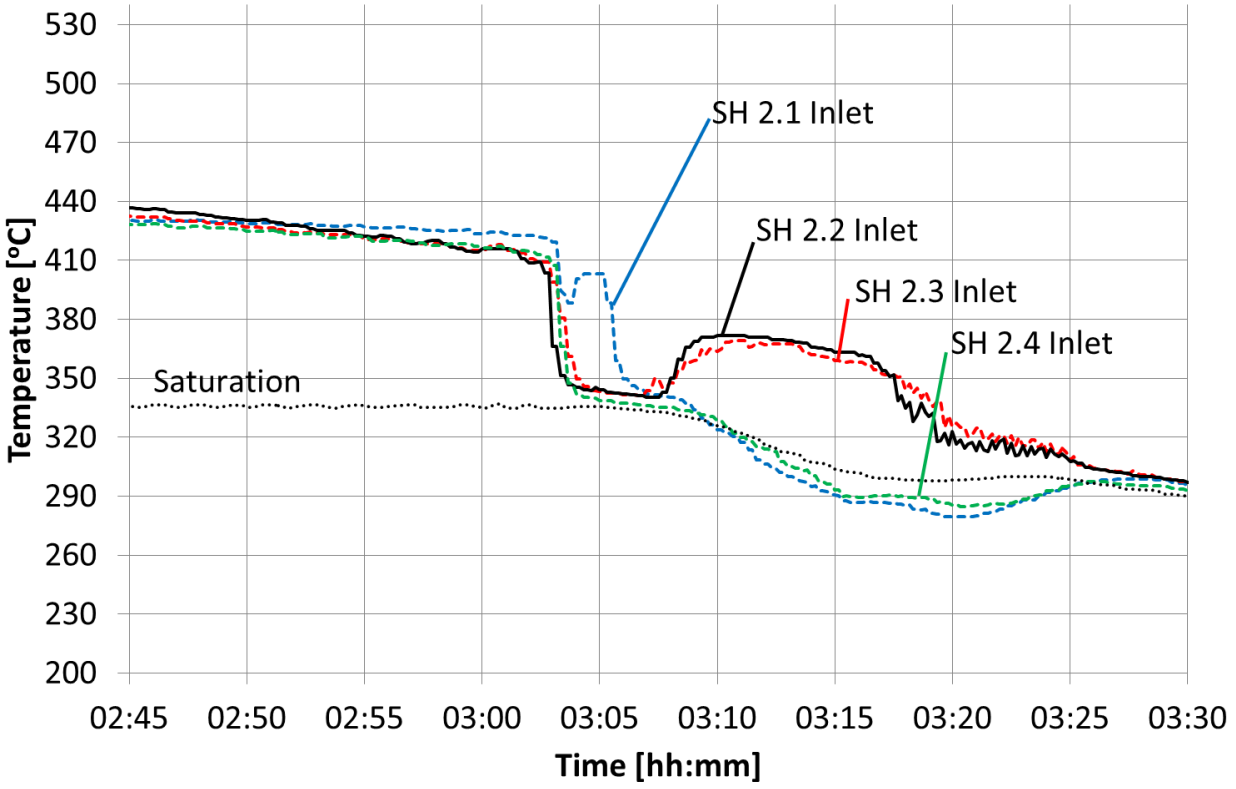


*Figure 154. Measured data from plant instruments- Superheater 2 inlet temperatures (U6 08-10-2018)*

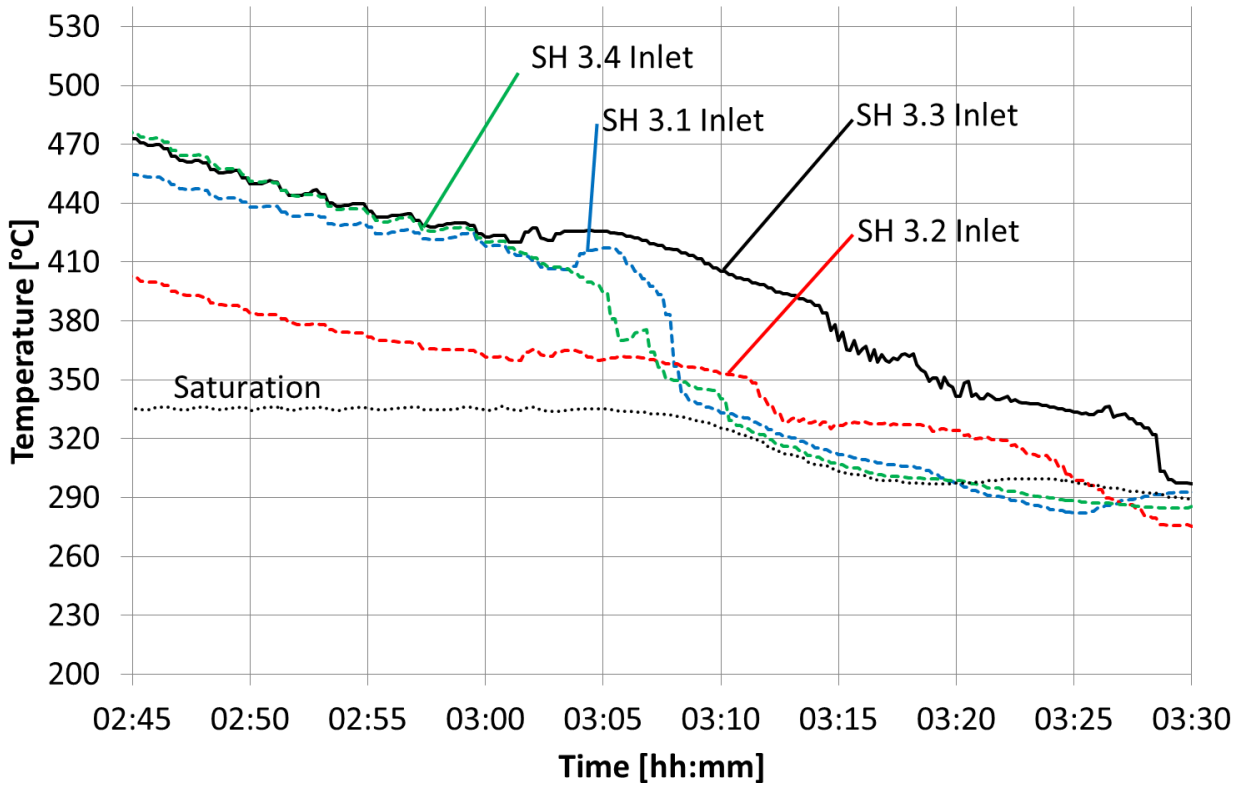


*Figure 155. Measured data from plant instruments- Superheater 3 inlet temperatures (U6 08-10-2018)*

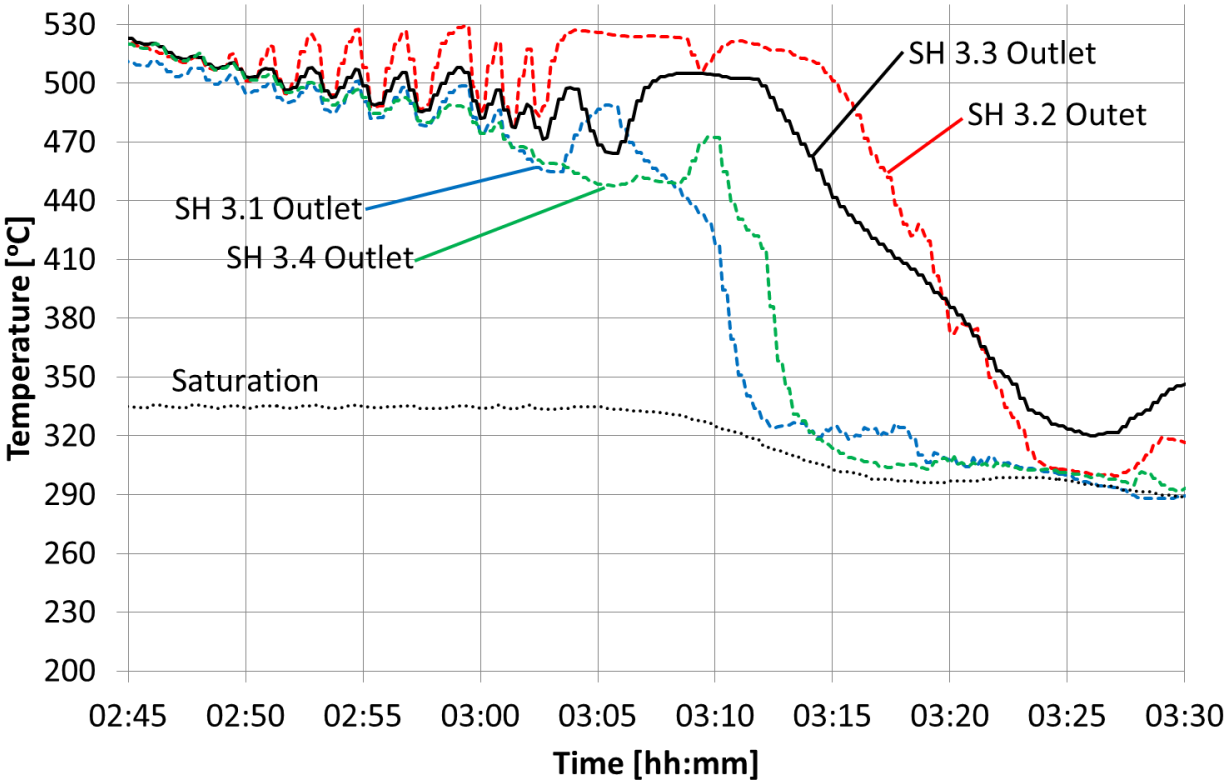


*Figure 156. Measured data from plant instruments- Superheater 3 outlet temperatures (U6 08-10-2018)*

The above information shows that a quenching event did occur and the progression of liquid and/or saturated steam can be followed through the superheater. The most likely source of water is a separator overflow, especially because the fans were not driving air flow through the boiler until after 3:10.

The collecting vessel level indicates that high levels were evident at 02:57:40 (Refer Figure 157) After re-calculating the level correction, this level may have exceeded the top tapping height of the collecting vessel level measurement. If the collecting vessel level is compared to the temperature drops seen at the superheater 2 inlet, the high collecting vessel level does not appear to be related to the temperature drops because they occur five minutes apart (Figure 158).

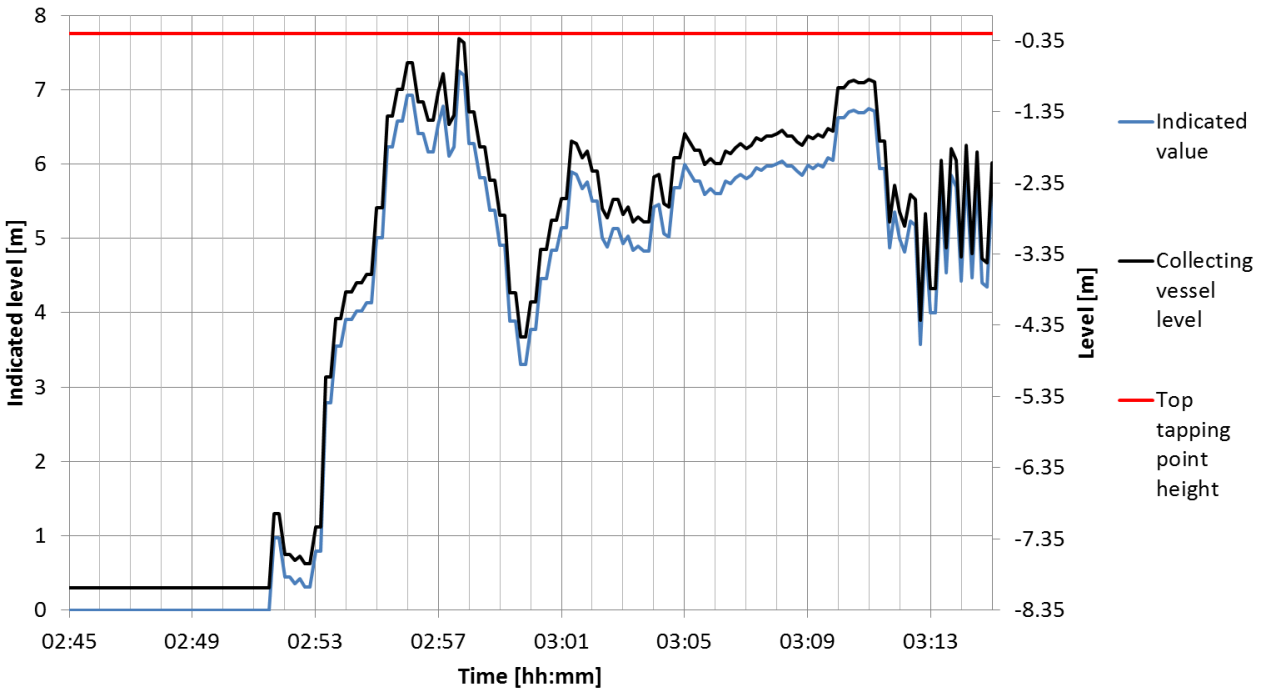


*Figure 157. Collecting vessel level - Indicated and re-calculated level (U6 08-10-2018)*

The collecting vessel level behaviour from 02:58 is difficult to correlate with flows at that time. The feed water flow and the economiser inlet flow both increased rapidly, but the collecting vessel level drops (Figure 159). The evaporator outlet temperature was still saturated at that time, so potentially the evaporator was still steaming and thus the increase in water flow caused more steam to be pushed out of the evaporator than water. However, potentially the evaporator outlet quality just continued to reduce and rather another mechanism was responsible for the apparent reduction in collecting vessel level.

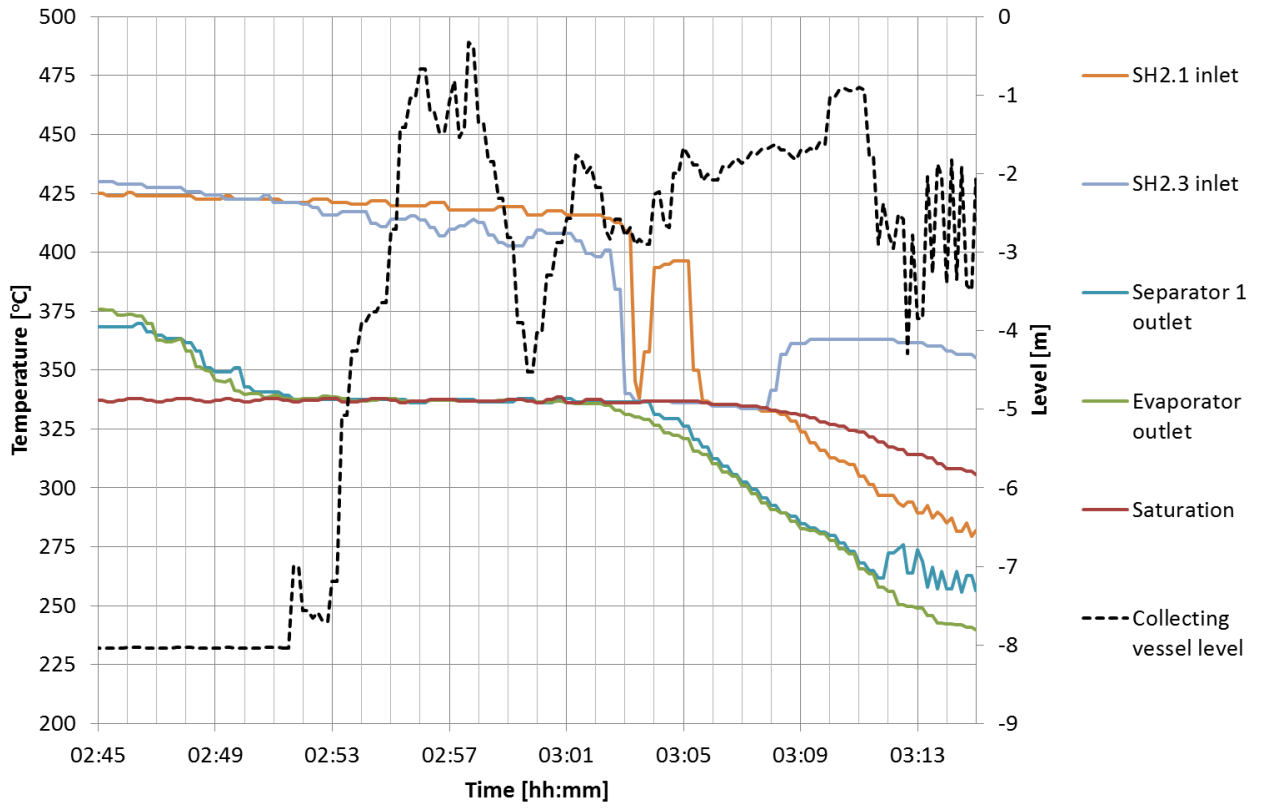


*Figure 158. Selected steam temperatures (adjusted to match saturation temperature) and recalculated collecting vessel level (U6 08-10-2018)*

Once the evaporator outlet becomes subcooled, there is a direct relationship between the economiser inlet flow and the evaporator outlet flow. This occurs at 03:01:40 when the economiser inlet flow rate was measured to be 260kg/s (Figure 159). At that time, the recirculation flow was 133kg/s and the feed water flow was 140kg/s. By mass balance, the economiser inlet flow should equal the sum of the feed water flow and the recirculation flow and it approximately does.

Since the economiser / evaporator circuit is filled with liquid, any feed water flow added should cause a rise in collecting vessel level. At 140kg/s, the rate of increase of collecting vessel level is 0.14m/s (considering that one collecting vessel and four separating vessels are filled simultaneously). As seen in Figure 159, the collecting vessel level does not increase at 03:01:40. Thus, the liquid is overflowing into the superheater at that time. This separator overflow managed to occur without increasing the collecting vessel level to maximum.

It is difficult to confirm when the separator overflow started. The collecting vessel level response from 02:59:30 until 03:01:30 is consistent with the economiser inlet, feed water flow and recirculation flow balance, but the exact quality of the saturated evaporator outlet flow is unknown, and thus the mass balance cannot be done with certainty. By integrating the feed water flow from

03:01:40 until 03:11:30, it amounts to 50 tons of water that potentially overflowed to the superheater in that period.

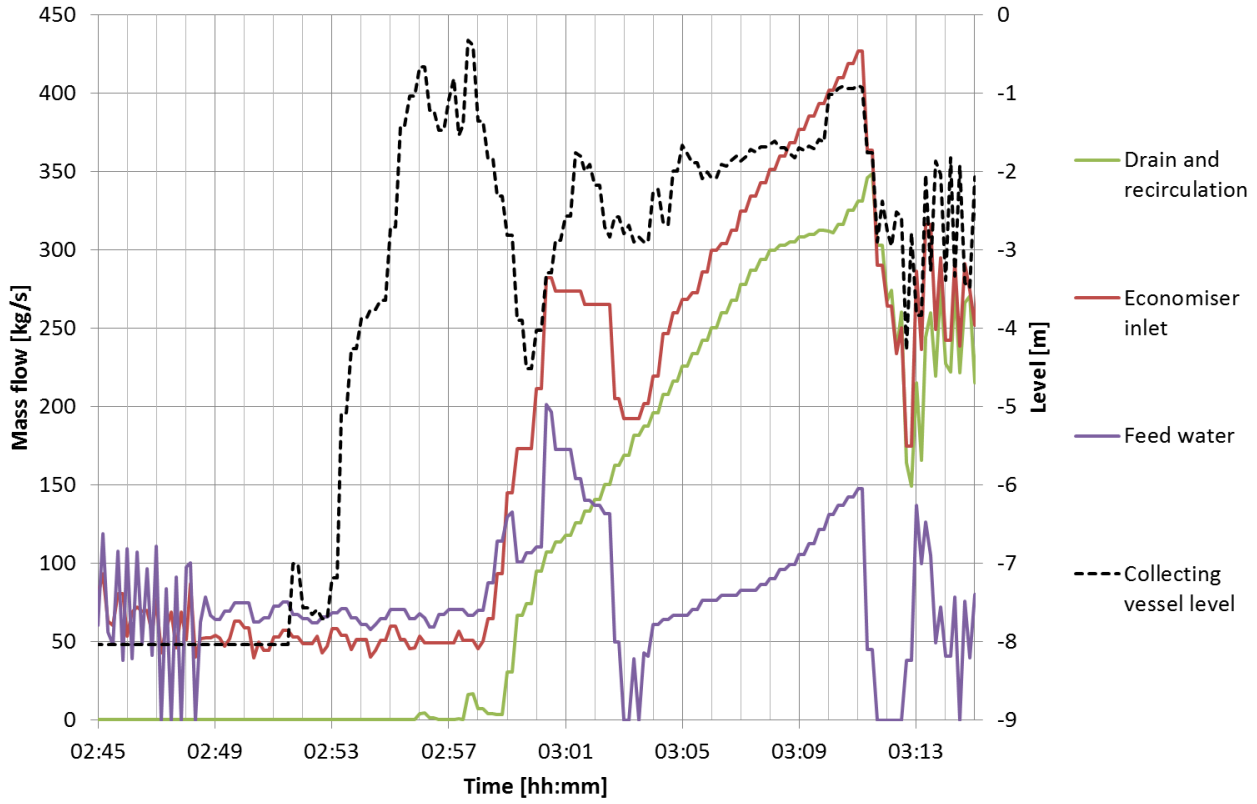


*Figure 159. Flows and re-calculated collecting vessel level (U6 08-10-2018)*

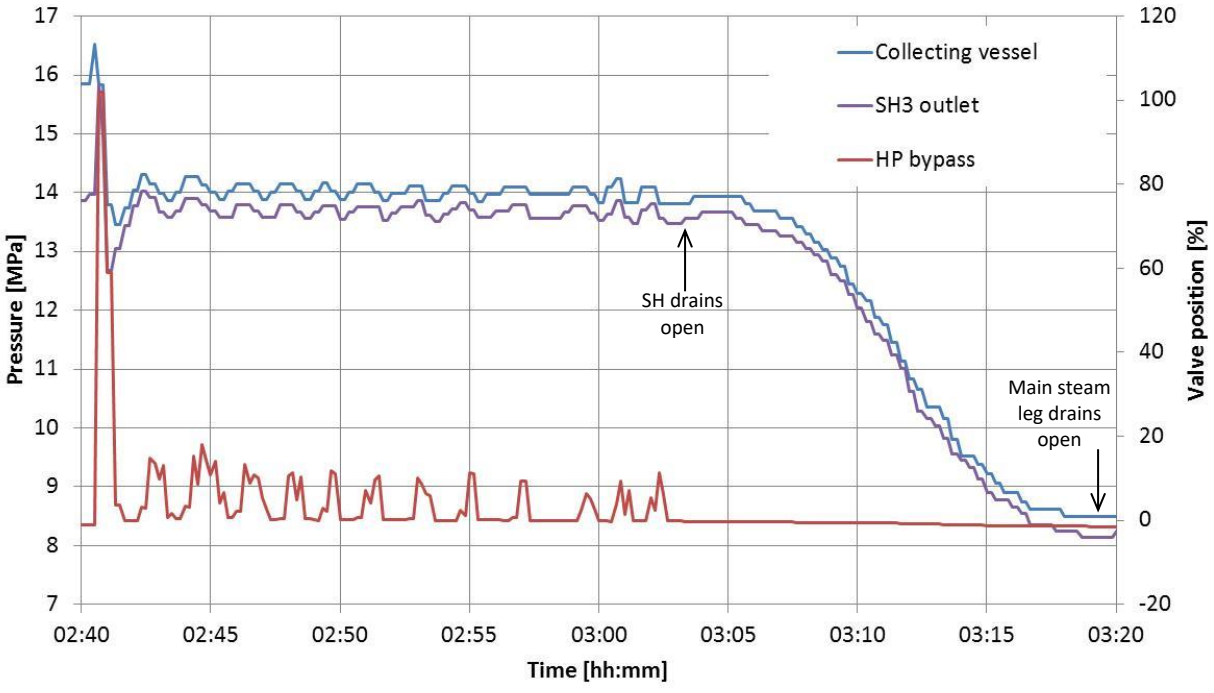

*Figure 160. Pressures and HP bypass valve opening (U6 08-10-2018)*

The pressure in the superheater is controlled at approximately 14MPa by the HP bypasses as shown in Figure 160. It is not clear if this amount of HP bypass opening is normally required for controlling boiler pressure after a trip. However, potentially the pressure build-up is caused by liquid overflow from the separator that is entering the superheater and evaporating into steam as it comes into contact with hot metal surfaces.

The difference in inlet pressure measured at the collecting vessel and the outlet pressure measured at the Superheater 3 outlet header indicates net positive flow through the superheater throughout the period. The outlet pressure is lower than the inlet pressure indicating pressure drop in the normal direction of flow.

In summary, a separator overflow did occur and most likely a siphon was created that caused the collecting vessel level not to show the true situation that a separator overflow was occurring. This was coupled with high feed water flow rates and the relatively slow ramp up of the circulation flow which took ten minutes to ramp up from 100kg/s to the rate corresponding with the collecting vessel level.

# Appendix F. Case Study D (U1 25-05-2012)

A quenching event occurred shortly after a controlled shutdown at Unit 1 on 25 May 2012. A summary of the incident is given in Table 12.

*Table 12. Summary of main events that occurred at Unit 1 on 25 May 2012*

| Ref | Description | Time |
|---|---|---|
| 1 | Turbine shutdown and breaker opened, Firing at 40% with two mills and oil fire. HP bypasses controlling boiler steam pressure | 14:34:00 |
| 2 | Collecting vessel level starts rising | 14:45:20 |
| 3 | Collecting vessel drains opened to manage level | 14:49:19 |
| 4 | Fires out, Fans ramp down but continue to run at nominal air flow | 14:53:03 |
| 5 | Circulation flow starts | 14:55:53 |
| 6 | Feed water flow starts decreasing from 300kg/s at 14:51:37 and reaches zero. | 14:56:37 |
| 7 | HP bypasses close, but open again intermittently to control boiler pressure at 8.5MPa | 14:56:48 |
| 8 | Feed water flow restarts and continues at an average of 100kg/s, Circulation flow still around 20kg/s | 14:57:32 |
| 9 | Collecting vessel level saturates at 7.49 m and remains at that value for 55 seconds until 15:01:22 | 15:00:27 |
| 10 | Subcooled conditions at evaporator outlet | 15:01:11 |
| 11 | 1 out of 4 separator vessels steam temperature drops below saturation | 15:02:39 |
| 12 | 2 out of 4 of the superheater 2 inlet header steam temperatures drop from 420$^{o}$C to saturation temperature | 15:03:06 |
| 13 | Collecting vessel quick drain valve closes | 15:03:36 |
| 14 | Superheater drains and main steam leg drains remain closed | - |

The separator outlet temperatures for this event display a similar pattern as the other cases (Figure 161). The evaporator outlet temperature drops below saturation temperature and so does the separator 4 steam outlet temperature. Separator 1 and separator 3 steam outlet temperatures become mildly superheated while separator 2 steam outlet temperature appears to be close to saturation temperature but with an offset.

In this case, there is no heating of the liquid overflowing from separator 4 which remains close to the evaporator outlet temperature (Figure 161).

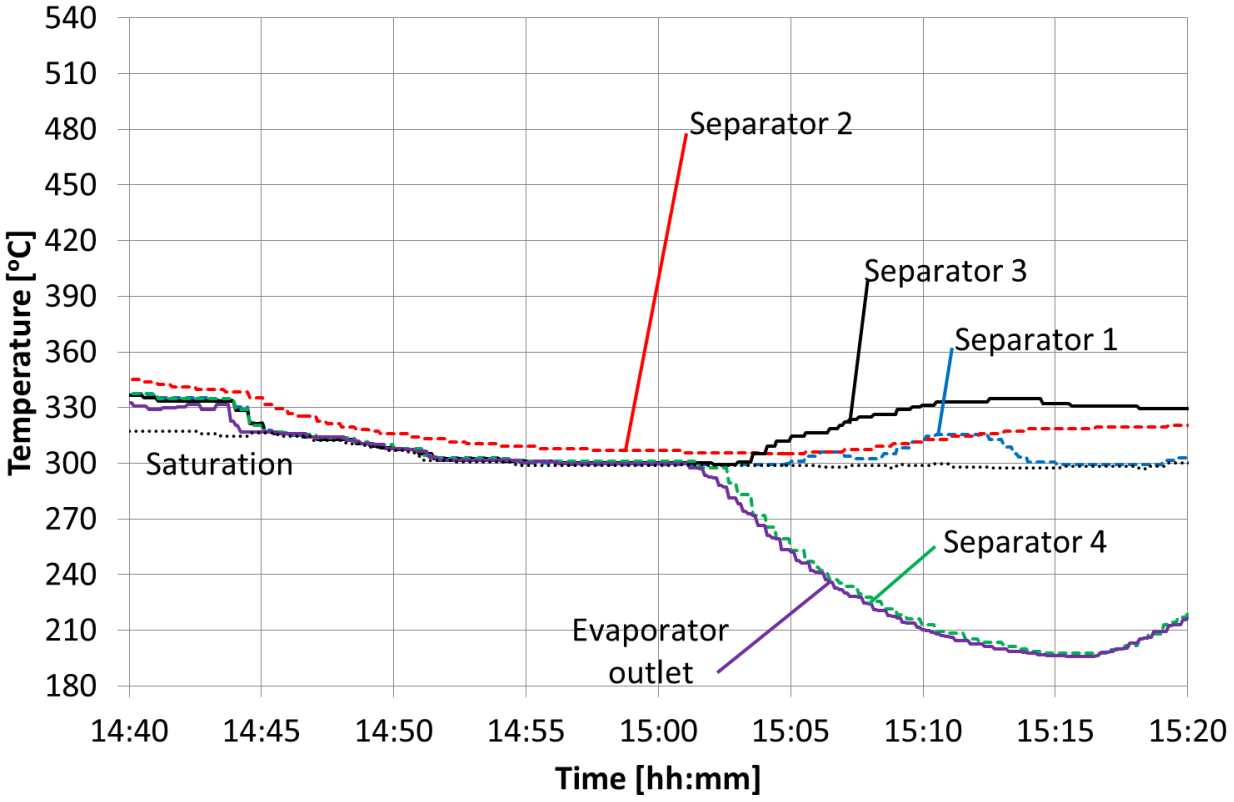


*Figure 161. Measured data from plant instruments- Separator outlet steam temperatures (U1 25-05-2012)*

The superheater steam temperatures again show the progression of liquid along leg one and leg four by the sudden drops to saturation temperature in the direction of flow (Figure 162, Figure 163 and Figure 164). There is also evidence of reverse flow of colder steam from SH3.2 and SH3.3 to SH2.2 and SH2.3 respectively.

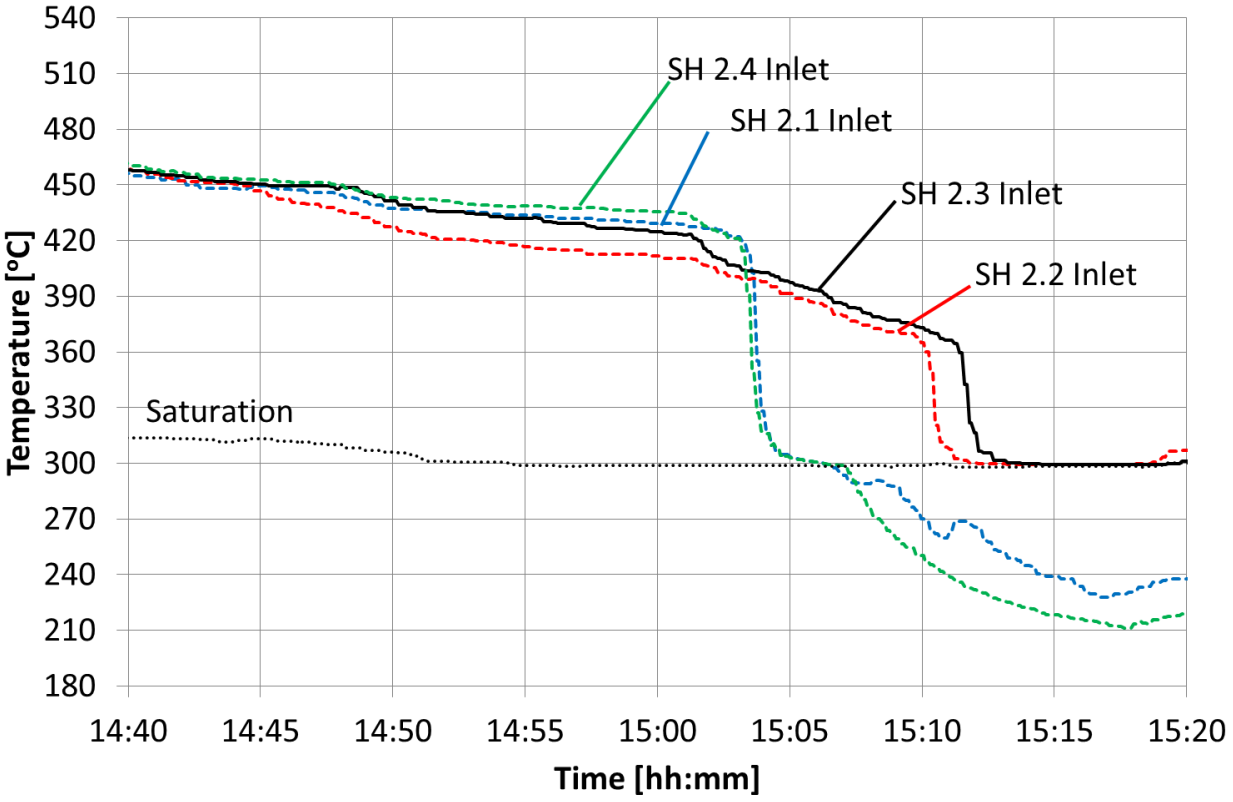


*Figure 162. Measured data from plant instruments- Superheater 2 inlet temperatures (U1 25-05-2012)*

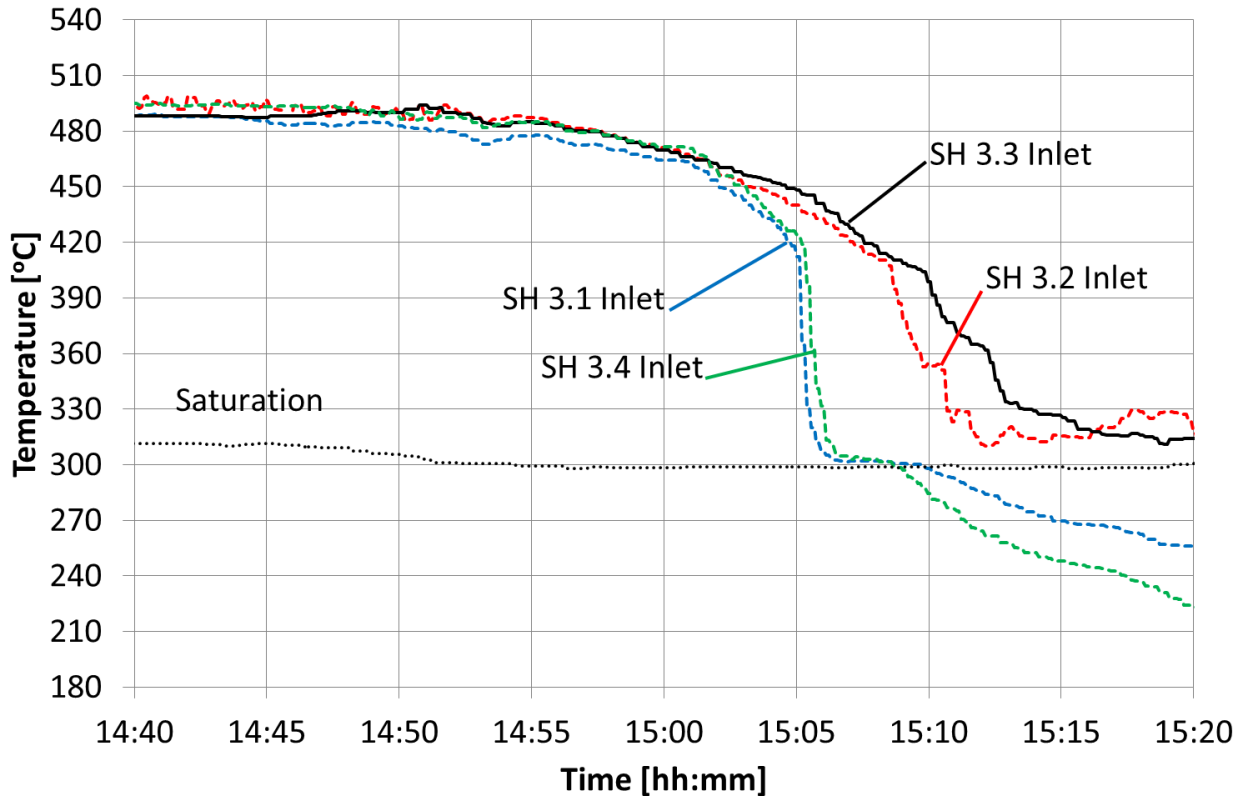


*Figure 163. Measured data from plant instruments- Superheater 3 inlet temperatures (U1 25-05-2012)*

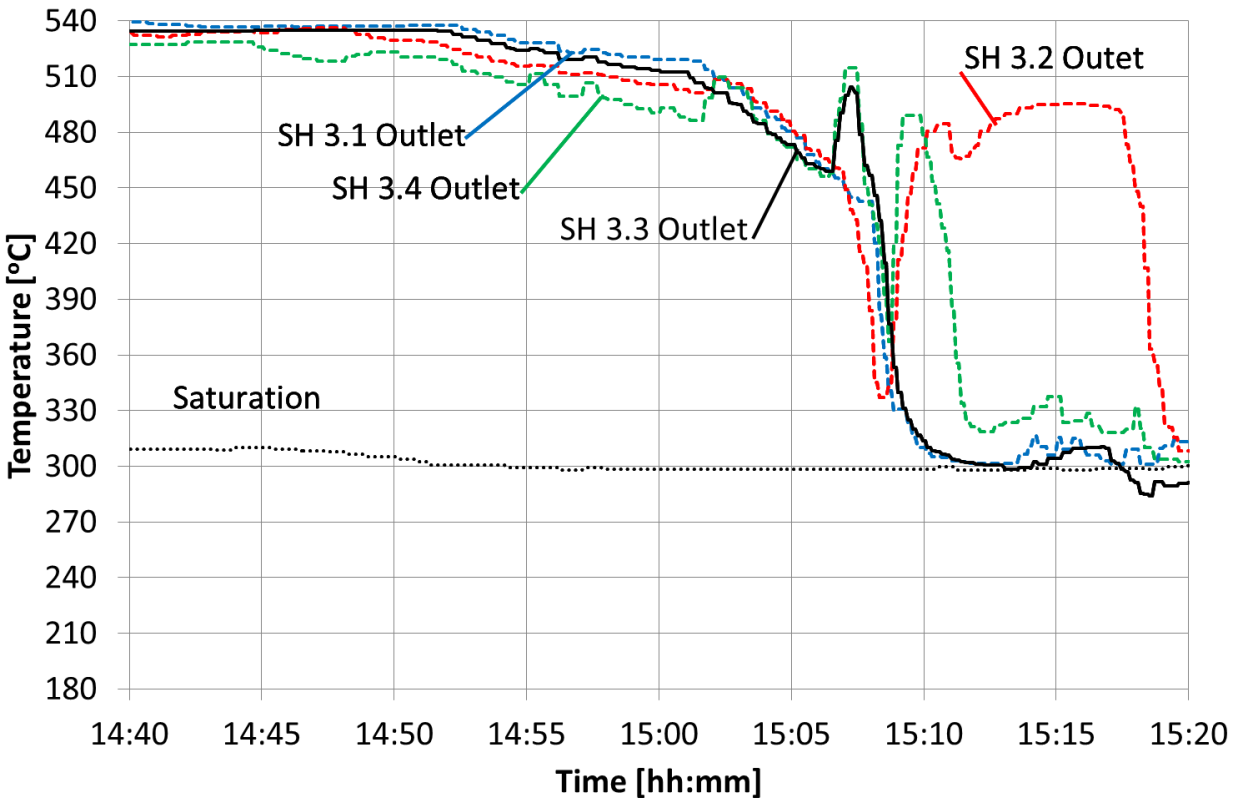


*Figure 164. Measured data from plant instruments- Superheater 3 outlet temperatures (U1 25-05-2012)*

At the boiler outlet (Figure 164) there are significant changes in temperature over relatively short periods of time with both cooling and heating taking place. The SH3.1 and SH3.3 outlets most likely have liquid flowing in them. The SH3.1 and SH3.4 show steam temperatures of the flow passing the measurement points. Initially at 15:08, the temperatures drop most likely with the arrival of liquid at the boiler outlet. Then the temperatures rise again as reverse flow is set up flowing out of the main steam system and back to the superheater.

Analysis of the collecting vessel level after correction of the measurement shows that the level went high above the top tapping point for approximately one minute just after 15:00 (Figure 165). By 15:04, the collecting vessel level appears to be back in control. However, in Figure 166, it can be seen that the SH2.4 inlet temperature drops to saturation at that time. This and the separator 4 steam outlet temperature show that liquid was overflowing from the separator into the superheater.

By 15:02, the evaporator outlet was subcooled. At that point in time, the evaporator and economiser circuit was full of liquid and any additional feed water added would result in separator overflow. In Figure 167, it can be seen that the feed water flow continues at an average of approximately 100kg/s after the evaporator is full.

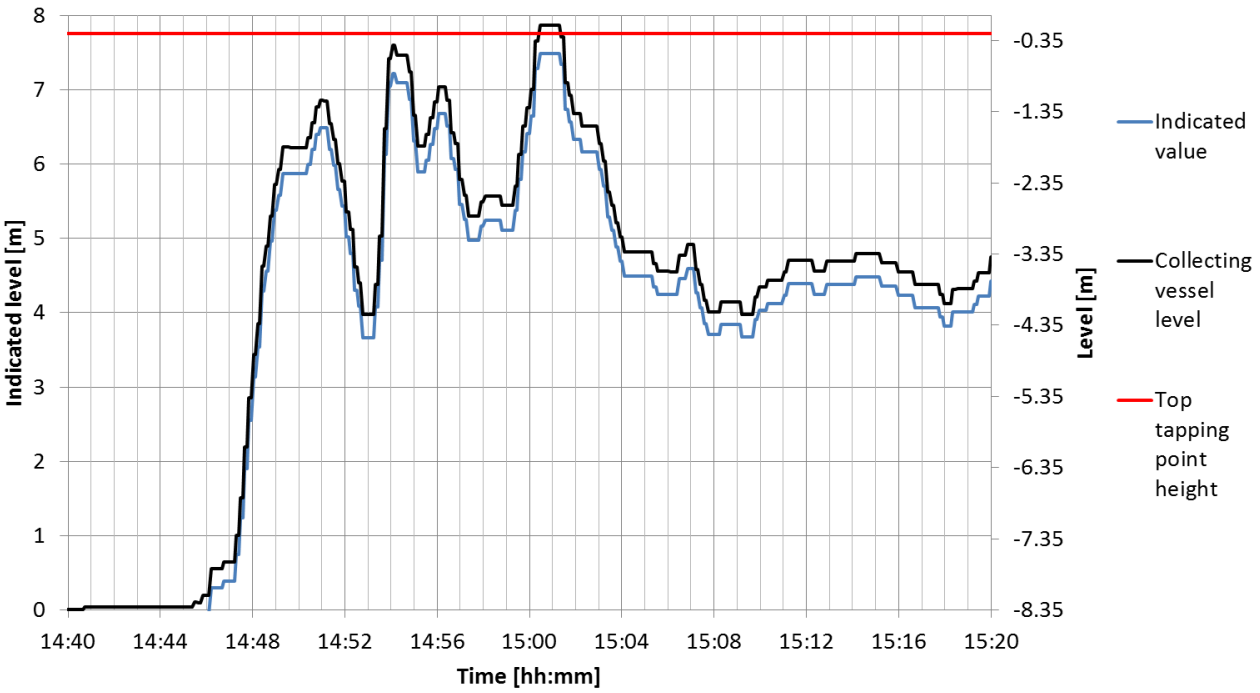


*Figure 165. Collecting vessel level - Indicated and re-calculated level (U1 25-05-2012)*

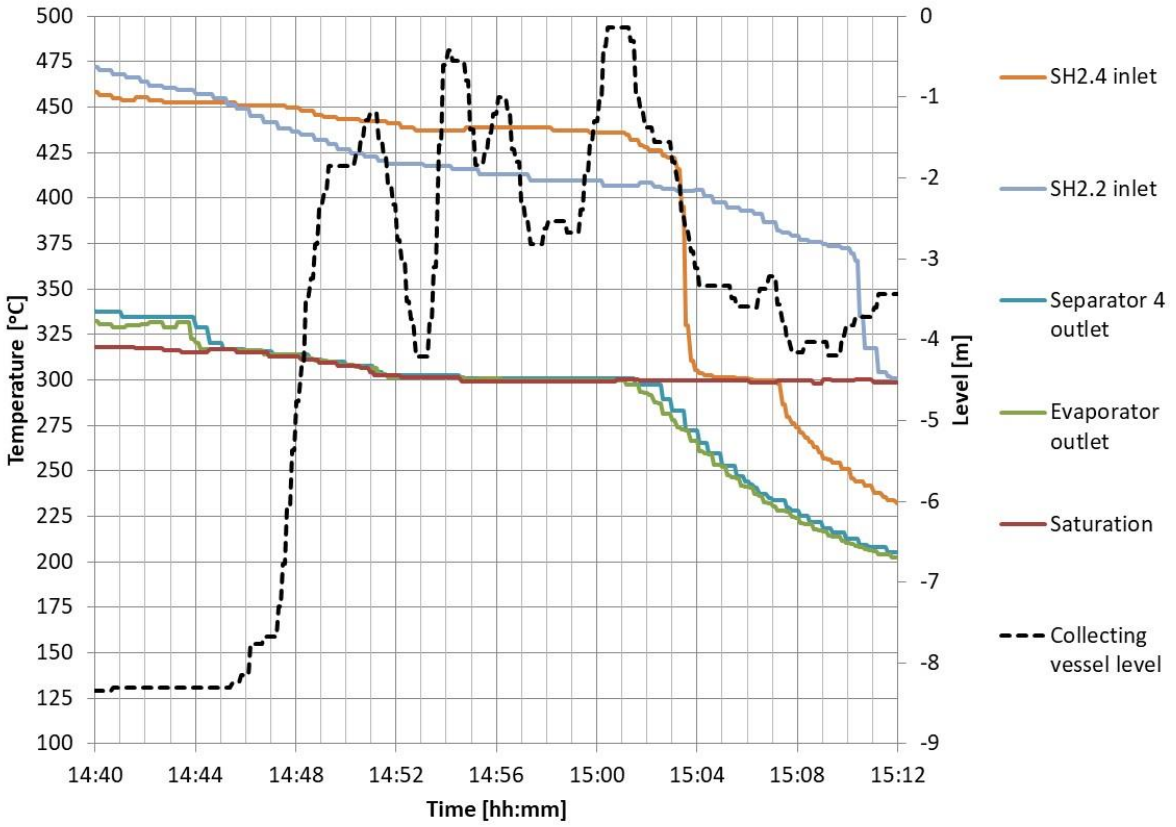


*Figure 166. Selected steam temperatures and re-calculated level (U1 25-05-2012)*

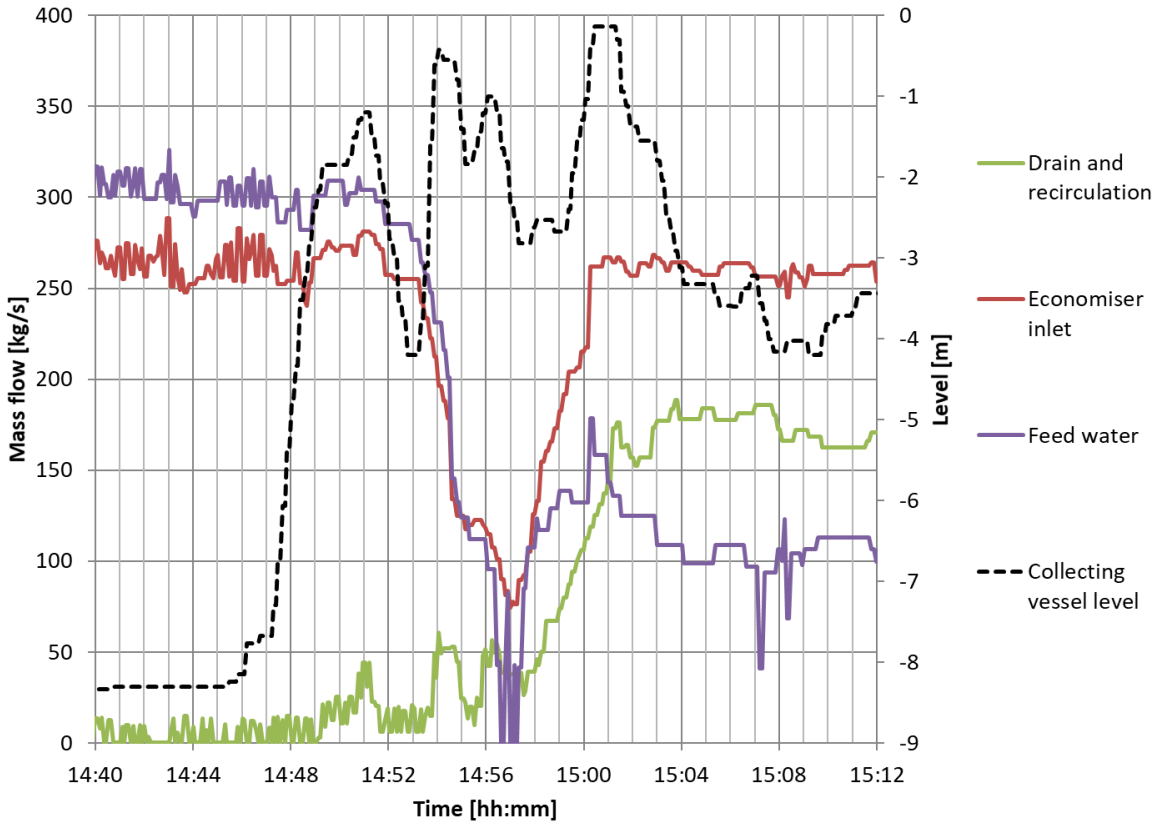


*Figure 167. Flows and re-calculated collecting vessel level (U1 25-05-2012)*

The behaviour of the collecting vessel level matches the previous cases. The high collecting vessel level with subcooled liquid at the evaporator outlet led to a siphon being created at separator 4. The siphon drained the other separating vessels and the collecting vessel. Thus the collecting vessel level appeared to be in control. Due to the depressed collecting vessel level, the circulation flow which is proportional to the level, failed to reach the 260kg/s economiser inlet flow set point. Thus the controls continued to add feed water to the evaporator circuit.

# Appendix G. Liquid tracking model - Scilab code

```
//Liquid level tracking model
//---------------------------

//Version 9 Date 19 Oct 2019
//By Gary de Klerk

//This program applies conservation of mass and conservation of energy to track
//the level of liquid in a boiler superheater system.

//Steam flow to subcooled liquid interface specified, 8 Control volume

//Load steam tables
exec('C:\Users\dklerkgb\Dropbox\PhD\LTM\XSteam.sci', -1);
exec('C:\Users\dklerkgb\Dropbox\PhD\LTM\RF EOS.sci', -1);

//Calculation variables
t=0.1;                //Timestep [s]
alpha_c=0.7;          //Alpha parameter for time integration (0 = explicit, 1 = fully implicit, 0.5 = Crank Nicolson solution)
relax=1;              //Relaxation parameter for the vapour massflow solver
criteria=(0.1)^2;     //Convergence criteria for the state in each control volume solver
criteria2=(0.1)^2;    //Convergence criteria for the vapour massflow solver
T_criteria=(0.1)^2;   //Convergence criteria for metal temperature
max_iter=50;          //Maximum number of iterations before accepting the answer and exiting the loop
criteria3=(0.1)^2;    //Convergence criteria for pressure found from enthalpy and density
m_criteria=(0.1)^2    //Convergence criteria for pressure for the main loop
relax3=1;             //Relaxation parameter for separator liquid overflow solver
sample_rate=1;        //sample rate for data storage in seconds
sample_rate2=10;      //sample rate for metal temperatures
k_p3=0.2;             //Controller gain for vapour flow control
time_stop_cond=1670;  //Time when vapour flow control switches off
n_tb_x=100;           //Number of increments along the tube bundle for conduction in the wall
n_h_x=20;             //Number of increments along the header for conduction in the wall
n_tb_s=3;             //Number of increments through the tube walls (min 3)
n_h_s=6;              //Number of increments though the header walls (min 3)

//Geometry (for each control volume in order of control volume number)
//Order of control volumes in this variable determines the order in all other variables, except T_g
geom=[
9.15   12.3   38.35   17.5   9.15   12.3   38.35   17.5
13538.5   9774   26281.5   72269   13538.5   9774   26281.5   72269
580   580   580   600   580   580   580   600
89   81.5   319.5   259.5   89   81.5   319.5   259.5
0.0466   0.0418   0.0375   0.303   0.0466   0.0418   0.0375   0.3025
0.0246   0.0239   0.0141   0.0321   0.0246   0.0239   0.0141   0.0321
43867   58046.5   183419   0   43867   58046.5   183419   0
580   580   574   0   580   580   574   0
877   1239.5   3990   0   877   1239.5   3990   0
1165   1617.5   5176.5   0   1165   1617.5   5176.5   0
150   163.5   161.5   0   150   163.5   161.5   0
0.0445   0.0445   0.0445   0   0.0445   0.0445   0.0445   0
0.0335   0.0341   0.0343   0   0.0335   0.0341   0.0343   0
0.0055   0.0052   0.0051   0   0.0055   0.0052   0.0051   0
0.96   0.48   0.12   0   0.96   0.48   0.12   0
0.07   0.07   0.085   0   0.07   0.07   0.085   0
185.97   185.97   185.97   0.00   185.97   185.97   185.97   0
0.98   0.98   0.1   0   0.98   0.98   0.1   0
0   0   0   0   0   0   0   0
34   32   35   25   34   32   35   25
41   25   42   0   41   25   42   0
10   10   20   80   10   10   20   80
38   38   76   0   38   38   76   0
];
```

```
no_of_cv=size(geom,2);
no_of_nodes = 10;
//Number of columns should be one less than number of nodes
//Row 1 = vapour flow from node
//Row 2 = vapour flow to node
v_flow_unknowns = [
1   2   4   5   6   8   9   10   9
3   1   9   7   5   10   2   6   10
];
unknowns=9;

//Reheater parameters (Area, Mass and Spec heat cap) in order of RH101, RH102, RH103 etc
RH_geom=[
2800.5   2800.5
82381.5   82381.5
577   577.0
185.975   185.975
0.24   0.240
0.11   0.110
0.057   0.057
];

//Gas flow through the control volumes, each column is a separate flow path of air/gas flow = total gas flow divided by number of
paths
//Flow starts at row 1. Element numbers are given in order down the column. Reheater elements are numbere 101, 102, 103 etc
gas_conn=[
1   5
6   2
101   102
7   3
];

no_of_gas_streams=size(gas_conn,2);

//Connection of control volumes for fluid flows
//Control volumes are numbered as per their position in the geom matrix above
//row to column defines liquid flow
//column to row defines vapour flow
//n+1 refers to connection of the separator vessels (a boundary condition)
//n+2 refers to connection of the downstream system i.e. to the HP turbine (also a boundary condition)
//The sum of values in any row (excl row and colomn n+1 and n+2) should add up to 1

conn=  [
0   1   0   0   0   0   0   0   0   0
0   0   0   0.4   0   0.4   0   0.2   0   0
1   0   0   0   0   0   0   0   0   0
0   0   0   0   0   0   0   0   0   1
0   0   0   0   0   1   0   0   0   0
0   0.4   0   0.2   0   0   0   0.4   0   0
0   0   0   0   1   0   0   0   1   0
0   0   0   0   0   0   0   0   0   1
0   0   1   0   0   0   0   0   0   0
0   0   0   0   0   0   0   0   0   0
]

//Constants
sigma=5.67E-8;  //Stefan Boltzmann constant [W/m^2 K^4]
e_ash=0.1;      //Emissivity of ash in the gas flow
e_wall=0.8;     //Emmissivity of the walls
g=9.81;         //Gravitational constant [m/s^2]

//Initial conditions
T_f=[443   491   395   516   443   491   395   516];
//Initial steam temperatures per control volume [degC]
x=[1   1   1   1   1   1   1   1];
//Initial steam quality
```

```
T_h_init=[443   491   395   516   443   491   395   516];
//Initial header metal temperature per control volume [degC]
T_tb_init=[443   491   395   0   443   491   395   0];
//Initial tube bundle metal temperature per control volume [degC]
T_RHtb=[452   452];
//Initial RH tube bundle temperature per reheater element [degC]

//Boundary conditions
//Time [s]  Pressure [kPa]  Separator overflow temp [degC]  Air flow inlet temp [degC]  Air mass flow rate [kg/s]   Vapour outflow at separator [kg/s]  Evaporator wall temp [degC] Separator liquid overflow rate [kg/s]
BC_in=[
0   8063.8   294.8   253.4   132.4   0.0   300.0   402.85   0.00
6   8063.8   291.3   253.3   132.4   0.0   300.0   402.46   0.00
13   8063.8   291.3   253.3   132.4   0.0   300.0   402.46   0.00
20   8063.8   291.3   253.3   132.4   0.0   300.0   402.46   0.00
26   8063.8   291.3   253.3   132.4   0.0   300.0   402.46   0.00
33   8063.8   286.0   253.2   132.4   0.7   300.0   402.12   0.00
40   8063.8   286.0   253.2   132.4   0.7   300.0   402.12   0.00
46   8063.8   282.9   253.2   132.4   2.9   300.0   401.46   0.00
53   8063.8   282.9   253.2   132.4   2.9   300.0   401.46   0.00
60   8063.8   280.1   253.1   128.8   1.3   300.0   398.92   0.00
];

function h_inner_mb=find_h_inner_mb(T_fluid, T_wall, id_pipe, t_pipe, k_pipe, nu_fluid, k_fluid, Pr_fluid, guess)
   Beta=1/(T_fluid+273.15);
   deltaT=abs(T_wall-T_fluid);
   Gr=g*Beta*id_pipe^3*deltaT/nu_fluid^2;
   h_inner_mb=guess;
   temp=guess+1;
   while abs(h_inner_mb-temp)>0.05
      temp=h_inner_mb;
      Pw=h_inner_mb*id_pipe/k_pipe*(id_pipe/t_pipe);
      Nu=(19.0096+(0.055*(Gr*Pr_fluid^1.35/Pw^0.25)^0.4)^2)^0.5;
      h_inner_mb=Nu*k_fluid/id_pipe;
   end;
endfunction

function h_inner_db=find_h_inner_db(mass_flow, id_pipe, rho_fluid, nu_fluid, k_fluid, Pr_fluid)
   velocity=mass_flow/rho_fluid/(%pi/4*id_pipe^2)
   Re=velocity*id_pipe/nu_fluid
   Nu=0.023*Re^0.8*Pr_fluid^0.4;
   h_inner_db=Nu*k_fluid/id_pipe;
endfunction

function h_outer=find_h_outer(A_duct, s_t, s_l, od_tube, rho_fluid, dyn_visc_fluid, Pr_fluid, k_fluid, mdot_fluid)
   free_v=abs(mdot_fluid)/(rho_fluid*A_duct)
   v_bar=free_v*s_t/(s_t-%pi/4*(od_tube))
   Re_gas=v_bar*od_tube*rho_fluid/dyn_visc_fluid;
   Nu_gas=0.3+(0.62*Re_gas^0.5*Pr_fluid^(1/3))/(1+0.4/Pr_fluid^(2/3))^0.25*(1+(Re_gas/282000)^(5/8))^(4/5);   //Churchill and Bernstein correlation
   fact=1+0.7/(1-%pi/(4*s_t/od_tube))^(1.5)*(s_l/s_t-0.3)/(s_l/s_t+0.7)^2;    //bundle factor for aligned tubes
   Nu_10_gas=fact*Nu_gas;                          //Nusselt number for a tube bundle of more than 10 tubes
   h_outer=Nu_10_gas*k_fluid/od_tube;
endfunction

function out=Get_pressures(v_m)
      //initialise the pressures and enthalpies
      for a=1:no_of_cv
         press(a)=P(i+1,a);
         enthalpy(a)=h(i+1,a);
      end

      count=0;
      continu=%T;
      while continu
         count=count+1;
```

```
 //initialise the i+1 summed mass flow values per control volume
for a=1:no_of_nodes;
   s_mdot_v(a)=0;
   s_mdot_v_h(a)=0;
end

//determine vapour enthalpies at all control volumes
for a=1:no_of_cv
   if T_f(i+1,a)>(XSteam('Tsat_p',press(a)/100)+0.01) then
      vap_enth(a) = XSteam('h_pT',press(a)/100,T_f(i+1,a));
   else
      vap_enth(a) = XSteam('hV_p',press(a)/100);
   end
end

//determine vapour enthalpies at nodes
for a=no_of_cv+1:no_of_nodes
   vap_enth(a) = 0;
end
for q=1:2
   for a=1:no_of_nodes;
      mass_in(a)=0;
      energy_in(a)=0;
   end
   for a=no_of_cv+1:no_of_nodes
     for b=1:unknowns
         if v_flow_unknowns(1,b)==a then
            if v_m(b)<0 then
               mass_in(a) = mass_in(a) - v_m(b);
               energy_in(a) = energy_in(a) - v_m(b)*vap_enth(v_flow_unknowns(2,b));
            end
         end
         if v_flow_unknowns(2,b)==a then
           if v_m(b)>=0 then
               mass_in(a) = mass_in(a) + v_m(b);
               energy_in(a) = energy_in(a) + v_m(b)*vap_enth(v_flow_unknowns(1,b));
           end
         end
      end
   end
   for a=no_of_cv+1:no_of_nodes
      if mass_in(a)~=0 then
         vap_enth(a) = energy_in(a)/mass_in(a);
      end
   end
end

//step through the connectivity matrix and sum the vapour mass flows and energy flows for each control volume
for a=1:unknowns
   from = v_flow_unknowns(1,a)
   to = v_flow_unknowns(2,a)
   s_mdot_v(from) = s_mdot_v(from) - v_m(a);
   s_mdot_v(to) = s_mdot_v(to) + v_m(a);
   if v_m(a)>=0 then
      s_mdot_v_h(from) = s_mdot_v_h(from) - v_m(a)*vap_enth(from);
      s_mdot_v_h(to) = s_mdot_v_h(to) + v_m(a)*vap_enth(from);
   else
      s_mdot_v_h(from) = s_mdot_v_h(from) - v_m(a)*vap_enth(to);
      s_mdot_v_h(to) = s_mdot_v_h(to) + v_m(a)*vap_enth(to);
   end
end

//Add in the separator vapour outflow flow boundary condition
for a=1:no_of_cv
   s_mdot_v(a) = s_mdot_v(a) - conn(a,no_of_cv+1)*BC(1,6);
   s_mdot_v_h(a)=s_mdot_v_h(a) - conn(a,no_of_cv+1)*BC(1,6)*vap_enth(a);
```

```
            out(9,a)=conn(a,no_of_cv+1)*BC(1,6);
            out(10,a)= vap_enth(a);
        end
        for a=no_of_cv+1:no_of_nodes
            out(10,a)= vap_enth(a);
        end
        //Calculate pressure in each control volume
        continu=%F
        for a=1:no_of_cv

            //Calculate the density at i+1 for the control volume
            density(a)=rho(i,a)+((1-
alpha_c)*(sum_mdot_L(i,a)+sum_mdot_v(i,a))+alpha_c*(sum_mdot_L(i+1,a)+s_mdot_v(a)))*t/geom(1,a);

            //Calculate the enthalpy at i+1 for the control volume
            du_at_i = sum_mdot_L_h(i,a) + sum_mdot_v_h(i,a) + Q_h(i,a) - Q_tbi(i,a);
            du_at_i_plus_1 = sum_mdot_L_h(i+1,a) + s_mdot_v_h(a) + Q_h(i+1,a) - Q_tbi(i+1,a);
            u2(a) = ((h(i,a)-P(i,a)/rho(i,a))*rho(i,a)*geom(1,a) + ((1-alpha_c)*du_at_i +
alpha_c*du_at_i_plus_1)*t)/(density(a)*geom(1,a));
            enthalpy(a) = u2(a) + press(a)/density(a);

            quality(a)=(enthalpy(a)-satL_h(press(a)/1000))/(satV_h(press(a)/1000)-satL_h(press(a)/1000));

            //Check if conditions in the control volume are saturated
            if quality(a)<=1 then
                //If saturated, use rate formulation to obtain the pressure at (i+1)
                G_0=Get_G(P(i,a),x(i,a));
                G_1=Get_G(press(a),quality(a));
                new_press(count,a)=P(i,a)+((1-alpha_c)*(G_0(1)*drho_dt(i,a)+G_0(2)*dh_dt(i,a))+alpha_c*(G_1(1)*(density(a)-
rho(i,a))/t + G_0(2)*(enthalpy(a)-h(i,a))/t))*t;
            else
                //If superheated, use steam tables to look up pressure at i+1
                new_press(count,a)=XSteam('P_hrho',enthalpy(a),density(a))*100;
            end
            out(8,a)=new_press(count,a)-press(a);
            if count<2 | ((new_press(count,a)-press(a))^2 > criteria3) then
                continu=%T;
            end

            press(a)=new_press(count,a);
            enthalpy(a) = u2(a) + press(a)/density(a);
        end

        //Update x to best value after final pressure is calculated
        for a=1:no_of_cv
            quality(a)=(enthalpy(a)-satL_h(press(a)/1000))/(satV_h(press(a)/1000)-satL_h(press(a)/1000));
        end

        if (count>max_iter) then
            continu=%F;
            out(7,1)=1;
        end
    end

    for a=1:no_of_cv
        out(2,a)=density(a);
        out(3,a)=enthalpy(a);
        out(4,a)=quality(a);
        out(1,a)=press(a);
        out(5,a)=s_mdot_v(a);
        out(6,a)=s_mdot_v_h(a);
    end
endfunction

//Initialising
```

```
Mtot(1)=0;
Etot(1)=0;

for j=1:no_of_cv
   P(1,j)=BC_in(1,2);
   dp_dt(1,j)=0;
   drho_dt(1,j)=0;
   dh_dt(1,j)=0;
   if x(1,j)>=1 then
      rho(1,j)=XSteam('rho_pT',P(1,j)/100,T_f(1,j));                    // [kg/m^3]
      h(1,j)=XSteam('h_pT',P(1,j)/100,T_f(1,j));
      level(1,j)=0;                                          //Volume fraction of liquid [0=empty to 1=full]
   else
      rho(1,j)=1/(x(1,j)*XSteam('vV_p',P(1,j)/100)+(1-x(1,j))*XSteam('vL_p',P(1,j)/100));
      h(1,j)=(1-x(1,j))*XSteam('hL_p',P(1,j)/100) + x(1,j)*XSteam('hV_p',P(1,j)/100);
      level(1,j)=((1-x(1,j))/XSteam('rhoL_P',P(1,j)/100))*rho(1,j);        //Volume fraction of liquid [0=empty to 1=full]
   end

   for k = 1:n_h_x
      h_hd(1,j,k)=0;       //Initial guess value of header inner h [W/m^2 K]
   end
   for k = 1:n_tb_x
      h_tbi(1,j,k)=0;      //Initial guess value of tube bundle inner h [W/m^2 K]
   end

   sum_mdot_L(1,j)=0;
   sum_mdot_L_h(1,j)=0;

   mdot_v(1,j)=0;
   sum_mdot_v(1,j)=0;
   sum_mdot_v_h(1,j)=0;

   Q_h(1,j)=0;
   Q_tbi(1,j)=0;
   Q_tbo(1,j)=0;
   Q_tbr(1,j)=0;

   Mtot = Mtot + geom(1,j)*rho(1,j);
   Etot = Etot + geom(1,j)*rho(1,j)*(h(1,j)-P(1,j)/rho(1,j));
end

for j = 1:(size(gas_conn,1)*size(gas_conn,2))
   T_g(1,1+(j-1)*2)=BC_in(1,4);
   T_g(1,2+(j-1)*2)=BC_in(1,4);
end

for j=no_of_cv+1:unknowns
   mdot_v(1,j)=0;
end

for j=1:unknowns
   x_guess(j,1)=0; //initial guess value
end

for j=1:no_of_gas_streams
   Q_RHtbo(j)=0;
end

BC(1,6)=0;
mdot_L_tot=0;
mdot_overflow=0;
V_out_iplus1=0;
E_out_iplus1=0;
y=1;
z=1;
```

```
sum_mdot_L(2)=mdot_overflow;
sum_mdot_L_h(2)=mdot_overflow*XSteam('h_pT',BC_in(1,2)/100,BC_in(1,3));
h_overflow = XSteam('h_pT',BC_in(1,2)/100,BC_in(1,3));
mdot_overflow_minus1=0;

for j = 1:no_of_cv
   for i = 1:2
      for k = 1:n_tb_x
         for s = 1:n_tb_s
            T_tb(s+(j-1)*n_tb_s,k+(i-1)*n_tb_x) = T_tb_init(1,j);
         end
         T_steam(j,k,i) = T_f(1,j);
      end
      for k = 1:n_h_x
         for s = 1:n_h_s
            T_h(s+(j-1)*n_h_s,k+(i-1)*n_h_x) = T_h_init(1,j);
         end
         T_steam(j,k+n_tb_x,i) = T_f(1,j);
      end
   end
   T_tb_outer(1,j) = T_tb_init(1,j);
end


for j = 1:no_of_cv
   if geom(7,j)~= 0 then
      geom(27,j) = geom(9,j) / (%pi * geom(13,j) * geom(23,j));
      thick = geom(12,j) - geom(13,j);
      for s = 1:n_tb_s
         if s==1 then
            r1 = geom(13,j)/2;
            r2 = r1 + thick/(n_tb_s-1)/2;
         else
            r1 = geom(13,j)/2 + (2*(s-1)-1)*thick/(n_tb_s-1)/2;
            if s==n_tb_s then
               r2 = r1 + thick/(n_tb_s-1)/2;
            else
               r2 = r1 + thick/(n_tb_s-1);
            end
         end
         cond_tb_k(j,s) = geom(21,j) * geom(27,j)*%pi*(r2^2-r1^2) / (geom(23,j)/n_tb_x);
         heat_cap_tb(j,s) = geom(7,j)/(%pi/4*((geom(13,j)+2*thick)^2-geom(13,j)^2)*geom(27,j)*geom(23,j)) * %pi*(r2^2-
r1^2)*geom(23,j)/n_tb_x*geom(27,j) * geom(8,j);
      end
      for s = 1:n_tb_s-1
         r1 = geom(13,j)/2 + (s-1)*thick/(n_tb_s-1);
         r2 = geom(13,j)/2 + s*thick/(n_tb_s-1);
         cond_tb_s(j,s) = 2*%pi*geom(21,j)*(geom(23,j)/n_tb_x)*geom(27,j) / log((r2/r1));
      end
   else
      for s = 1:n_tb_s
         cond_tb_k(j,s) = 0;
         heat_cap_tb(j,s) = 0;
      end
      for s = 1:n_tb_s-1
         cond_tb_s(j,s) = 0;
      end
   end

   if geom(2,j)~= 0 then
      geom(26,j) = geom(4,j) / (%pi * geom(5,j) * geom(22,j));
      for s = 1:n_h_s
         if s==1 then
            r1 = geom(5,j)/2;
            r2 = r1 + geom(6,j)/(n_h_s-1)/2;
         else
```

```
            r1 = geom(5,j)/2 + (2*(s-1)-1)*geom(6,j)/(n_h_s-1)/2;
            if s==n_h_s then
               r2 = r1 + geom(6,j)/(n_h_s-1)/2;
            else
               r2 = r1 + geom(6,j)/(n_h_s-1);
            end
         end
         cond_h_k(j,s) = geom(20,j) * geom(26,j)*%pi*(r2^2-r1^2) / (geom(22,j)/n_h_x);
         heat_cap_h(j,s) = geom(2,j)/(%pi/4*((geom(5,j)+2*geom(6,j))^2-geom(5,j)^2)*geom(26,j)*geom(22,j)) * %pi*(r2^2-
r1^2)*geom(22,j)/n_h_x*geom(26,j) * geom(3,j);
      end
      for s = 1:n_h_s-1
         r1 = geom(5,j)/2 + (s-1)*geom(6,j)/(n_h_s-1);
         r2 = geom(5,j)/2 + s*geom(6,j)/(n_h_s-1);
         cond_h_s(j,s) = 2*%pi*geom(20,j)*(geom(22,j)/n_h_x)*geom(26,j) / log((r2/r1));
      end
   else
      for s = 1:n_h_s
         cond_h_k(j,s) = 0;
         heat_cap_h(j,s) = 0;
      end
      for s = 1:n_h_s-1
         cond_h_s(j,s) = 0;
      end
   end

   //Assume control volume is configured with half the header volume at the lower part, then the tube increments in order up to the
upper part and the other half header at the top
   if geom(7,j)~= 0 then
      geom(25,j) = geom(1,j) - geom(4,j)*geom(5,j)/4
   end
   geom(24,j) = geom(1,j) - geom(25,j)
end

BC(2,6)=0;

for j = 1:no_of_cv
   r_P(y,j)=P(1,j);
   r_mdot_v(y,j)=mdot_v(1,j);
   r_T_f(y,j)=T_f(1,j);
   r_rho(y,j) = rho(1,j);
   r_h(y,j) = h(1,j);
   r_x(y,j) = x(1,j);
   r_level(y,j) = level(1,j);
   r_Q_h(y,j) = Q_h(1,j);
   r_Q_tbi(y,j) = Q_tbi(1,j);
   r_Q_tbo(y,j) = Q_tbo(1,j);
   r_Q_tbr(y,j) = Q_tbr(1,j);
end

for j = 1:(size(gas_conn,1)*size(gas_conn,2))
   r_T_g(y,j+1) = T_g(2+(j-1)*2);
end

for j=no_of_cv+1:unknowns
   r_mdot_v(y,j)=mdot_v(1,j);
end
r_mdot_overflow(y) = mdot_overflow;
r_mdot_L_tot(y) = mdot_L_tot;
r_T_g(y,1) = T_g(1,1);
r_Mtot(y) = Mtot;
r_Etot(y) = Etot;

//Calculating
i=1;
//Initialise i+1 variables
```

```
for j=1:no_of_cv
   T_f(i+1,j)=T_f(i,j);
   rho(i+1,j)=rho(i,j);
   h(i+1,j)=h(i,j);
   P(i+1,j)=P(i,j)
   level(i+1,j)=level(i,j);
   for k = 1:n_h_x
      h_hd(i+1,j,k)=h_hd(i,j,k);
   end
   for k = 1:n_tb_x
      h_tbi(i+1,j,k)=h_tbi(i,j,k);
   end
end

for j=1:no_of_gas_streams
   T_RHtb(i+1,j) = T_RHtb(i,j);
end

//Start main loop
for mi=1:round((BC_in(size(BC_in,1),1))/t)

   //Interpolation of the boundary condition matrix BC_in to find the boundary conditions for the timestep number mi
   for k=1:size(BC_in,1)
      if (mi*t)==BC_in(k,1) then
         BC(1,:)=BC_in(k,:)
      end
      if (mi*t>BC_in(k,1) & mi*t<BC_in(k+1,1)) then
         for j=1:size(BC_in,2)
            BC(1,j)=(BC_in(k+1,j)-BC_in(k,j))/(BC_in(k+1,1)-BC_in(k,1))*(mi*t-BC_in(k,1))+BC_in(k,j)
         end
      end
   end

         //Controller to determine liquid overflow and vapour flow to the subcooled liquid interface for next iteration
         control_errorP=P(i,1)-BC(1,2);

         //Vapour flow to subcooled liquid interface calculated by pressure controller
         if (mi*t)<time_stop_cond then
            BC(1,6)=k_p3*control_errorP;
         end
         mdot_overflow=BC(1,9);


         disp(mdot_overflow,BC(1,6));

      //Solve the heat transfer and metal temperatures
      count=0;
      cont=%T;
      while cont     //Repeat until tube bundle temperature and gas outlet temperatures at the new time step have converged
         count=count+1;

         //Calculate average outer tube bundle temperatures
         for j=1:no_of_cv
            if geom(7,j)~= 0 then
               T_tb_outer(i+1,j) = 0;
               for k = 1:n_tb_x
                  T_tb_outer(i+1,j) = T_tb_outer(i+1,j) + T_tb(1+(j-1)*n_tb_s,k+n_tb_x);
               end
               T_tb_outer(i+1,j) = T_tb_outer(i+1,j)/n_tb_x;
               //Calculate radiation to the walls
               Q_tbr(i+1,j) = e_wall*sigma*geom(11,j)/1000*((T_tb_outer(i+1,j)+273.15)^4 - (BC(1,7)+273.15)^4);
            else
               T_tb_outer(i+1,j) = 0;
               Q_tbr(i+1,j) = 0;
               h_c(i+1,j)=0;
               h_r(i+1,j)=0;
```

```
            Ntu(j)=0;
            eff(j)=0;
        end
    end

    //Calculate tube bundle outer heat transfer and gas temperatures
    posi=0;
    for flow=1:no_of_gas_streams;
        for k=1:size(gas_conn,1)
            j=gas_conn(k,flow)
            posi=posi+1;
            if k == 1 then
                T_g(i+1,posi)=BC(1,4);
            else
                T_g(i+1,posi)=T_g(i+1,posi-1);
            end
            posi=posi+1;

            //Gas side fluid properties
            rho_gas = -0.31743*log((T_g(i,posi-1)+T_g(i,posi))/2)+2.427;                    //Average gas
density [kg/m^3]
            mu_gas = -1.4357E-11*((T_g(i,posi-1)+T_g(i,posi))/2)^2 + 4.2503E-8*((T_g(i,posi-1)+T_g(i,posi))/2) + 1.7807E-
5;  //Average gas dynamic viscosity [Pas or Ns/m^2]
            k_gas = -2.1643E-8*((T_g(i,posi-1)+T_g(i,posi))/2)^2 + 7.3916E-5*((T_g(i,posi-1)+T_g(i,posi))/2) + 0.02476;
//Average conductivity of the gas [W/m K]
            cp_gas = 8.3571E-5*((T_g(i,posi-1)+T_g(i,posi))/2)^2 + 0.17256*((T_g(i,posi-1)+T_g(i,posi))/2) + 985.88;
//Specific heat of the gas [J/kg K]
            Pr_gas = cp_gas*mu_gas/k_gas;                                                  //Average Prandtl number of
the gas

            if j>100 then
                j=j-100;

h_c(i+1,no_of_cv+j)=find_h_outer(RH_geom(4,j),RH_geom(5,j),RH_geom(6,j),RH_geom(7,j),rho_gas,mu_gas,Pr_gas,k_gas,BC(1,
5)/no_of_gas_streams);
                h_r(i+1,no_of_cv+j)=e_ash*sigma*((T_RHtb(i,j)+273.15)^4-((T_g(i,posi-
1)+T_g(i,posi))/2+273.15)^4)/(T_RHtb(i,j)-(T_g(i,posi-1)+T_g(i,posi))/2);

Ntu(no_of_cv+j)=(h_c(i+1,no_of_cv+j)+h_r(i+1,no_of_cv+j))*RH_geom(1,j)/((BC(1,5)/no_of_gas_streams)*cp_gas);  //eff-Ntu
method for the air side of the tube bundle
                eff(no_of_cv+j)=1-exp(-Ntu(no_of_cv+j));                                   //eff for a single stream
heat exchanger
                T_g(i+1,posi) = eff(no_of_cv+j)*(T_RHtb(i+1,j) - T_g(i+1,posi-1)) + T_g(i+1,posi-1);
                Q_RHtbo(i+1,j) = BC(1,5)/no_of_gas_streams*cp_gas/1000*(T_g(i+1,posi) - T_g(i+1,posi-1));
                T_RHtb(i+1,j)=T_RHtb(i,j) - ((1-alpha_c)*Q_RHtbo(i,j) +
alpha_c*Q_RHtbo(i+1,j))*1000/(RH_geom(2,j)*RH_geom(3,j))*t;
            else

h_c(i+1,j)=find_h_outer(geom(17,j),geom(15,j),geom(16,j),geom(12,j),rho_gas,mu_gas,Pr_gas,k_gas,BC(1,5)/no_of_gas_streams);
                h_r(i+1,j)=e_ash*sigma*((T_tb_outer(i+1,j)+273.15)^4-((T_g(i,posi-
1)+T_g(i,posi))/2+273.15)^4)/(T_tb_outer(i+1,j)-(T_g(i,posi-1)+T_g(i,posi))/2);
                Ntu(j)=(h_c(i+1,j)+h_r(i+1,j))*geom(10,j)/(BC(1,5)/no_of_gas_streams*cp_gas);                  //eff-Ntu
method for the air side of the tube bundle
                eff(j)=1-exp(-Ntu(j));                                                 //eff for a single stream heat
exchanger
                T_g(i+1,posi) = eff(j)*(T_tb_outer(i+1,j) - T_g(i+1,posi-1)) + T_g(i+1,posi-1);
                cp_gas = 8.3571E-5*((T_g(i,posi-1)+T_g(i,posi))/2)^2 + 0.17256*((T_g(i,posi-1)+T_g(i,posi))/2) + 985.88;
//Specific heat of the gas [J/kg K]
                Q_tbo(i+1,j) = BC(1,5)/no_of_gas_streams*cp_gas/1000*(T_g(i+1,posi) - T_g(i+1,posi-1));
            end
        end
    end

    for j=1:no_of_cv

        //Determine the steam massflow to use in the heat transfer correlations for the control volume
```

```
                //Use values from previous time step (i.e. mdot_v at i)
                massflow = abs(conn(j,no_of_cv+1)*BC(2,6));
                for k = 1:unknowns
                    if v_flow_unknowns(1,k)==j then
                        if abs(mdot_v(i,k))>massflow then
                            massflow = abs(mdot_v(k));
                        end
                    end
                    if v_flow_unknowns(2,k)==j then
                        if abs(mdot_v(i,k))>massflow then
                            massflow = abs(mdot_v(k));
                        end
                    end
                end

                //Calculate steam temperatures
                dry = %F;
                if T_f(i,j)>XSteam('Tsat_p',P(i,j)/100) then
                    T_steam(j,1,i+1) = T_f(i,j)
                else
                    T_steam(j,1,i+1) = XSteam('Tsat_p',P(i,j)/100)
                end
                //Calculate steam temperatures in half the header
                for k = 2:round(n_h_x/2)
                    if (k*geom(24,j)/n_h_x)>(geom(1,j)*level(i,j)) then
                        dry = %T
                    end
                    if dry then
                        q_dot = h_hd(i+1,j,k)/1000*geom(4,j)/n_h_x*(T_h(1+(j-1)*n_h_s,k+n_h_x) - T_steam(j,k,i+1))
                        u1_pv = XSteam('u_pT',P(i,j)/100,T_steam(j,k,i)+0.01) +
P(i,j)/XSteam('rho_pT',P(i,j)/100,T_steam(j,k,i+1)+0.01)
                        Mt = geom(24,j)/n_h_x * XSteam('rho_pT',P(i,j)/100,T_steam(j,k,i+1)+0.01)      //geom(24,j) is the header
steam volume in m3 and geom(25,j) is the tube bundle steam volume
                        h1 = XSteam('h_pT',P(i,j)/100,T_steam(j,k-1,i+1)+0.01)
                        h2 = (q_dot*t/Mt + massflow*h1*t/Mt + u1_pv)/(1 + massflow*t/Mt)
                        if isnan(XSteam('T_ph',P(i,j)/100,h2)) then
                            T_steam(j,k,i+1) = T_steam(j,k-1,i+1)
                        else
                            if XSteam('T_ph',P(i,j)/100,h2) < XSteam('Tsat_p',P(i,j)/100) then
                                T_steam(j,k,i+1) = XSteam('Tsat_p',P(i,j)/100)
                            else
                                T_steam(j,k,i+1) = XSteam('T_ph',P(i,j)/100,h2)
                            end
                        end
                    else
                        T_steam(j,k,i+1) = T_steam(j,k-1,i+1);
                    end
                end
                //Calculate steam temperatures in the tube bundle
                for k = 1:n_tb_x
                    if geom(7,j)~=0 then
                        if (geom(24,j)/2+k*geom(25,j)/n_tb_x)>(geom(1,j)*level(i,j)) then
                            dry = %T;
                        end
                        if dry then
                            q_dot = h_tbi(i+1,j,k)/1000*geom(9,j)/n_tb_x*(T_tb(1+(j-1)*n_tb_s,k+n_tb_x) -
T_steam(j,round(n_h_x/2)+k,i+1))
                            u1_pv = XSteam('u_pT',P(i,j)/100,T_steam(j,round(n_h_x/2)+k,i)+0.01) +
P(i,j)/XSteam('rho_pT',P(i,j)/100,T_steam(j,round(n_h_x/2)+k,i+1)+0.01);
                            Mt = geom(25,j)/n_tb_x * XSteam('rho_pT',P(i,j)/100,T_steam(j,round(n_h_x/2)+k,i+1)+0.01);    //geom(25,j)
is the tube bundle steam volume
                            h1 = XSteam('h_pT',P(i,j)/100,T_steam(j,round(n_h_x/2)+k-1,i+1)+0.01);
                            h2 = (q_dot*t/Mt + massflow*h1*t/Mt + u1_pv)/(1 + massflow*t/Mt);
                            if isnan(XSteam('T_ph',P(i,j)/100,h2)) then
                                T_steam(j,round(n_h_x/2)+k,i+1) = T_steam(j,round(n_h_x/2)+k-1,i+1)
                            else
```

```
                        if XSteam('T_ph',P(i,j)/100,h2) < XSteam('Tsat_p',P(i,j)/100) then
                            T_steam(j,round(n_h_x/2)+k,i+1) = XSteam('Tsat_p',P(i,j)/100)
                        else
                            T_steam(j,round(n_h_x/2)+k,i+1) = XSteam('T_ph',P(i,j)/100,h2)
                        end
                    end
                else
                    T_steam(j,round(n_h_x/2)+k,i+1) = T_steam(j,round(n_h_x/2)+k-1,i+1);
                end
            else
                T_steam(j,round(n_h_x/2)+k,i+1) = 0;
            end
        end
        //Calculate steam temperatures in the other half of the header
        for k = round(n_h_x/2)+1:n_h_x

            if (geom(25,j)+k*geom(24,j)/n_h_x)>(geom(1,j)*level(i,j)) then
                dry = %T;
            end
            if dry then
                q_dot = h_hd(i+1,j,k)/1000*geom(4,j)/n_h_x*(T_h(1+(j-1)*n_h_s,k+n_h_x) - T_steam(j,n_tb_x+k,i+1));
                u1_pv = XSteam('u_pT',P(i,j)/100,T_steam(j,n_tb_x+k,i)+0.01) +
P(i,j)/XSteam('rho_pT',P(i,j)/100,T_steam(j,n_tb_x+k,i+1)+0.01);
                Mt = geom(24,j)/n_h_x * XSteam('rho_pT',P(i,j)/100,T_steam(j,n_tb_x+k,i+1)+0.01);    //geom(24,j) is the
header steam volume in m3
                if (geom(7,j)==0 & k==round(n_h_x/2)+1) then
                    h1 = XSteam('h_pT',P(i,j)/100,T_steam(j,k-1,i+1)+0.01);
                else
                    h1 = XSteam('h_pT',P(i,j)/100,T_steam(j,n_tb_x+k-1,i+1)+0.01);
                end
                h2 = (q_dot*t/Mt + massflow*h1*t/Mt + u1_pv)/(1 + massflow*t/Mt);
                if isnan(XSteam('T_ph',P(i,j)/100,h2)) then
                    T_steam(j,n_tb_x+k,i+1) = T_steam(j,n_tb_x+k-1,i+1)
                else
                    if XSteam('T_ph',P(i,j)/100,h2) < XSteam('Tsat_p',P(i,j)/100) then
                        T_steam(j,n_tb_x+k,i+1) = XSteam('Tsat_p',P(i,j)/100)
                    else
                        T_steam(j,n_tb_x+k,i+1) = XSteam('T_ph',P(i,j)/100,h2)
                    end
                end
            else
                if (geom(7,j)==0 & k==round(n_h_x/2)+1) then
                    T_steam(j,n_tb_x+k,i+1) = T_steam(j,k-1,i+1);
                else
                    T_steam(j,n_tb_x+k,i+1) = T_steam(j,n_tb_x+k-1,i+1);
                end
            end
        end


        //Calculate local heat transfer coefficients
        for posi = 1:n_h_x+n_tb_x
            //Check if steam is dry, then use superheated steam properties and Morcos and Bergles or Dittus Boelter
            if T_steam(j,posi,i+1)>XSteam('Tsat_p',P(i,j)/100) then
                rho_steam=XSteam('rho_pT',P(i,j)/100,T_steam(j,posi,i+1)+0.01);                    // Steam density [kg/m^3]
                nu_steam=XSteam('my_pT',P(i,j)/100,T_steam(j,posi,i+1)+0.01)/rho_steam;            // Dynamic viscsity [Pa s]
                k_steam=XSteam('tc_pT',P(i,j)/100,T_steam(j,posi,i+1)+0.01);                       // Thermal conductivity [W/m K]
                Pr_steam=XSteam('Cp_pT',P(i,j)/100,T_steam(j,posi,i+1)+0.01)*1000*nu_steam*rho_steam/k_steam;    //
Prandtl number

                if posi<=round(n_h_x/2) then
                    k = posi
                    h_mb=find_h_inner_mb(T_steam(j,posi,i+1),T_h(1+(j-
1)*n_h_s,k),geom(5,j),geom(6,j),geom(20,j),nu_steam,k_steam,Pr_steam,h_hd(i,j,k));
                    h_db=find_h_inner_db(massflow/geom(26,j),geom(5,j),rho_steam,nu_steam,k_steam,Pr_steam);
                    if h_mb>h_db then
```

```
                h_hd(i+1,j,k)=h_mb
            else
                h_hd(i+1,j,k)=h_db
            end
        else
            if posi<=(round(n_h_x/2)+n_tb_x) then
                if geom(7,j)~=0 then
                    k = posi-round(n_h_x/2)
                    h_mb=find_h_inner_mb(T_steam(j,posi,i+1),T_tb(1+(j-
1)*n_tb_s,k),geom(13,j),geom(14,j),geom(21,j),nu_steam,k_steam,Pr_steam,h_tbi(i,j,k));
                    h_db=find_h_inner_db(massflow/geom(27,j),geom(13,j),rho_steam,nu_steam,k_steam,Pr_steam);
                    if h_mb>h_db then
                        h_tbi(i+1,j,k)=h_mb
                    else
                        h_tbi(i+1,j,k)=h_db
                    end
                else
                    h_tbi(i+1,j,k)=0;
                end
            else
                k = posi-n_tb_x
                h_mb=find_h_inner_mb(T_steam(j,posi,i+1),T_h(1+(j-
1)*n_h_s,k),geom(5,j),geom(6,j),geom(20,j),nu_steam,k_steam,Pr_steam,h_hd(i,j,k));
                h_db=find_h_inner_db(massflow/geom(26,j),geom(5,j),rho_steam,nu_steam,k_steam,Pr_steam);
                if h_mb>h_db then
                    h_hd(i+1,j,k)=h_mb
                else
                    h_hd(i+1,j,k)=h_db
                end
            end
        end
    else
        //Else the steam in the control volume is wet or at saturation and boiling may be occurring

        if (geom(7,j)==0 & posi>round(n_h_x/2) & posi<=(round(n_h_x/2)+n_tb_x)) then //Check for control volumes
with no header
            k = posi-round(n_h_x/2)
            h_tbi(i+1,j,k) = 0;
        else

            //Fluid properties required for nucleate boiling correlations
            Tsat = XSteam('Tsat_p',P(i,j)/100);                    //degrees C
            rho_steam = XSteam('rhoV_p',P(i,j)/100);                //kg/m3
            rho_liq = XSteam('rhoL_p',P(i,j)/100);                  //kg/m3
            cp_liq = XSteam('CpL_p',P(i,j)/100,);                   //kJ/kg K
            h_fg = XSteam('hV_p',P(i,j)/100) - XSteam('hL_p',P(i,j)/100);   //kJ/kg K
            surf_ten = XSteam('st_p',P(i,j)/100,);                  //N/m
            mu_liq=XSteam('my_pT',P(i,j)/100,Tsat-0.01);            //Pa s
            cond_liq=XSteam('tcL_p',P(i,j)/100);                    //W/m K
            Pr_liq = cp_liq*1000*mu_liq/cond_liq;

            //Find the wall temperature
            if posi<=round(n_h_x/2) then
                k = posi
                Twall=T_h(1+(j-1)*n_h_s,n_h_x+k)
            else
                if posi<=(round(n_h_x/2)+n_tb_x) then
                    if geom(7,j)~=0 then
                        k = posi-round(n_h_x/2)
                        Twall=T_tb(1+(j-1)*n_tb_s,n_tb_x+k)
                    end
                else
                    k = posi-n_tb_x
                    Twall=T_h(1+(j-1)*n_h_s,n_h_x+k)
                end
            end
```

```
                        //Rohsenow nucleate boiling correlation
                        Ja = cp_liq*(Twall - Tsat)/h_fg              //Jacob number
                        NU = Ja^2/((0.013^3)*Pr_liq^2)               //Nusselt number
                        Lc = (surf_ten/((rho_liq-rho_steam)*9.81))^0.5          //equivalent length m
                        q_nuc = (NU*cond_liq/Lc)*(Twall - Tsat)/1000;   //kW/m^2

                        //Check max heat flux by nucleate boiling
                        q_max = 0.12*h_fg*(surf_ten*(rho_steam^2)*(rho_liq-rho_steam)*9.81)^0.25; //kW/m^2

                        if (q_nuc < q_max) then //nucleate boiling applies if nucleate heat flux is less than maximum
                           h_boil = NU*cond_liq/Lc; //W/m^2 K
                        else //Transition or film boiling applies
                           //Vapour properties required for film boiling correlations - Evaluate at average of wall temperature and
saturation temperature
                           rho_vapour = XSteam('rho_PT',P(i,j)/100,(Twall+Tsat)/2+0.01)          //kg/m^3
                           nu_vapour = XSteam('my_pT',P(i,j)/100,(Twall+Tsat)/2+0.01)/rho_vapour    //m^2 s
                           cp_vapour = XSteam('cp_pT',P(i,j)/100,(Twall+Tsat)/2+0.01)            //kJ/kg K
                           cond_vapour = XSteam('tc_pT',P(i,j)/100,(Twall+Tsat)/2+0.01)          //W/m K

                           //Calculation of the minimum film boiling heat flux
                           T_min = Tsat + 50;
                           T_min_guess = T_min + 1;
                           h_fg1 = h_fg+0.5*cp_vapour*(T_min_guess-Tsat);
                           q_min = 0.09*rho_vapour*h_fg*(surf_ten*9.81*(rho_liq-rho_vapour)/(rho_liq+rho_vapour)^2)^0.25
//kW/m^2
                           while abs(T_min-T_min_guess) > 0.01
                              T_min_guess = T_min;
                              h_fg1 = h_fg+0.5*cp_vapour*(T_min_guess-Tsat);
                              T_min = ((q_min/0.15)^(3/2))*(nu_vapour/(rho_liq-rho_vapour)/9.81/h_fg1/(cond_vapour/1000)^2)^0.5
+ Tsat;
                           end

                           if (Twall < T_min)//Transition boiling applies and the heat flux is linearly interpolated bewteen q_min and
q_max

                              T_max = 0.013*(Pr_liq^2*h_fg^2*q_max*Lc/cp_liq^2/(cond_liq/1000))^0.333 + Tsat;
                              q_trans = (Twall-T_max)/(T_min-T_max)*(q_min-q_max) + q_max;
                              h_boil = q_trans*1000/(Twall - Tsat);

                           else //Film boiling

                              h_fg1 = h_fg+0.5*cp_vapour*(Twall - Tsat);
                              h_boil = (0.15*((rho_liq-rho_vapour)*9.81*h_fg1*(cond_vapour/1000)^2/nu_vapour/(Twall-
Tsat))^0.333)*1000;
                           end
                        end
                        if posi<=round(n_h_x/2) then
                           if h_boil<(0.5*heat_cap_h(j,1)/((geom(4,j)/n_h_x)*t)) then
                              h_hd(i+1,j,k) = h_boil
                           else
                              h_hd(i+1,j,k) = (0.5*heat_cap_h(j,1)/((geom(4,j)/n_h_x)*t))
                           end
                        else
                           if posi<=(round(n_h_x/2)+n_tb_x) then
                              if geom(7,j)~=0 then
                                 if h_boil<(0.5*heat_cap_tb(j,1)/((geom(9,j)/n_tb_x)*t)) then
                                    h_tbi(i+1,j,k) = h_boil
                                 else
                                    h_tbi(i+1,j,k) = (0.5*heat_cap_tb(j,1)/((geom(9,j)/n_tb_x)*t))
                                 end
                              end
                           else
                              if h_boil<(0.5*heat_cap_h(j,1)/((geom(4,j)/n_h_x)*t)) then
                                 h_hd(i+1,j,k) = h_boil
                              else
```

```
                    h_hd(i+1,j,k) = (0.5*heat_cap_h(j,1)/((geom(4,j)/n_h_x)*t))
                end
            end
        end
    end
end
end


    //Calculate local metal temperatures and overall inner heat transfer
    for j=1:no_of_cv

        if geom(2,j)~= 0 then
            Q_h(i+1,j) = 0;
            for k = 1:n_h_x
                for s = 1:n_h_s
                    if s == n_h_s then
                        Q_n(i) = 0;
                        Q_n(i+1) = 0;
                    else
                        Q_n(i) = cond_h_s(j,s) * (T_h((s+1)+(j-1)*n_h_s , k)  -  T_h(s+(j-1)*n_h_s , k));
                        Q_n(i+1) = cond_h_s(j,s) * (T_h((s+1)+(j-1)*n_h_s , k+n_h_x)  -  T_h(s+(j-1)*n_h_s , k+n_h_x));
                    end
                    if s == 1 then
                        if k<=round(n_h_x/2) then
                            posi=k
                        else
                            posi=k+n_tb_x
                        end
                        Q_s(i) = h_hd(i,j,k)*geom(4,j)/n_h_x* (T_h(s+(j-1)*n_h_s , k)  -  T_steam(j,posi,i));
                        Q_s(i+1) = h_hd(i+1,j,k)*geom(4,j)/n_h_x* (T_h(s+(j-1)*n_h_s , k+n_h_x)  -  T_steam(j,posi,i+1));
                        Q_h(i+1,j) = Q_h(i+1,j) + Q_s(i+1)/1000;
                    else
                        Q_s(i) = cond_h_s(j,s-1) * (T_h(s+(j-1)*n_h_s , k)  -  T_h((s-1)+(j-1)*n_h_s , k));
                        Q_s(i+1) = cond_h_s(j,s-1) * (T_h(s+(j-1)*n_h_s , k+n_h_x)  -  T_h((s-1)+(j-1)*n_h_s , k+n_h_x));
                    end
                    if k == 1 then
                        Q_e(i) = 0;
                        Q_e(i+1) = 0;
                    else
                        Q_e(i) = cond_h_k(j,s) * (T_h(s+(j-1)*n_h_s , k)  -  T_h(s+(j-1)*n_h_s , k-1));
                        Q_e(i+1) = cond_h_k(j,s) * (T_h(s+(j-1)*n_h_s , k+n_h_x)  -  T_h(s+(j-1)*n_h_s , (k-1)+n_h_x));
                    end
                    if k == n_h_x then
                        Q_w(i) = 0;
                        Q_w(i+1) = 0;
                    else
                        Q_w(i) = cond_h_k(j,s) * (T_h(s+(j-1)*n_h_s , k+1)  -  T_h(s+(j-1)*n_h_s , k));
                        Q_w(i+1) = cond_h_k(j,s) * (T_h(s+(j-1)*n_h_s , (k+1)+n_h_x)  -  T_h(s+(j-1)*n_h_s , k+n_h_x));
                    end
                    new_T_h(j,k,s) = T_h(s+(j-1)*n_h_s,k) + ((1-alpha_c)*(Q_n(i)-Q_s(i)+Q_e(i)-Q_w(i)) +
alpha_c*(Q_n(i+1)-Q_s(i+1)+Q_e(i+1)-Q_w(i+1)))*t/heat_cap_h(j,s);
                end
            end
        else
            Q_h(i+1,j) = 0;
        end

        if geom(7,j)~=0 then

            Q_tbi(i+1,j) = 0;
            for k = 1:n_tb_x
                for s = 1:n_tb_s
                    if s == 1 then
                        Q_n(i) = h_tbi(i,j,k)*geom(9,j)/n_tb_x*(T_steam(j,k+round(n_h_x/2),i) - T_tb(1+(j-1)*n_tb_s,k));
```

```
                    Q_n(i+1) = h_tbi(i+1,j,k)*geom(9,j)/n_tb_x*(T_steam(j,k+round(n_h_x/2),i+1) - T_tb(1+(j-
1)*n_tb_s,k+n_tb_x));
                    Q_tbi(i+1,j) = Q_tbi(i+1,j) + Q_n(i+1)/1000;
                  else
                    Q_n(i) = cond_tb_s(j,s-1) * (T_tb((s-1)+(j-1)*n_tb_s , k) - T_tb(s+(j-1)*n_tb_s , k));
                    Q_n(i+1) = cond_tb_s(j,s-1) * (T_tb((s-1)+(j-1)*n_tb_s , k+n_tb_x) - T_tb(s+(j-1)*n_tb_s , k+n_tb_x));
                  end
                  if s == n_tb_s then
                    Q_s(i) = (Q_tbo(i,j)+Q_tbr(i,j))*1000/n_tb_x;
                    Q_s(i+1) = (Q_tbo(i+1,j)+Q_tbr(i+1,j))*1000/n_tb_x;
                  else
                    Q_s(i) = cond_tb_s(j,s) * (T_tb(s+(j-1)*n_tb_s , k) - T_tb((s+1)+(j-1)*n_tb_s , k));
                    Q_s(i+1) = cond_tb_s(j,s) * (T_tb(s+(j-1)*n_tb_s , k+n_tb_x) - T_tb((s+1)+(j-1)*n_tb_s , k+n_tb_x));
                  end
                  if k == 1 then
                    Q_e(i) = 0;
                    Q_e(i+1) = 0;
                  else
                    Q_e(i) = cond_tb_k(j,s) * (T_tb(s+(j-1)*n_tb_s , k)  -  T_tb(s+(j-1)*n_tb_s , k-1));
                    Q_e(i+1) = cond_tb_k(j,s) * (T_tb(s+(j-1)*n_tb_s , k+n_tb_x)  -  T_tb(s+(j-1)*n_tb_s , (k-1)+n_tb_x));
                  end
                  if k == n_tb_x then
                    Q_w(i) = 0;
                    Q_w(i+1) = 0;
                  else
                    Q_w(i) = cond_tb_k(j,s) * (T_tb(s+(j-1)*n_tb_s , k+1)  -  T_tb(s+(j-1)*n_tb_s , k));
                    Q_w(i+1) = cond_tb_k(j,s) * (T_tb(s+(j-1)*n_tb_s , (k+1)+n_tb_x)  -  T_tb(s+(j-1)*n_tb_s , k+n_tb_x));
                  end
                  new_T_tb(j,k,s) = T_tb(s+(j-1)*n_tb_s,k) + ((1-alpha_c)*(Q_n(i)-Q_s(i)+Q_e(i)-Q_w(i)) +
alpha_c*(Q_n(i+1)-Q_s(i+1)+Q_e(i+1)-Q_w(i+1)))*t/heat_cap_tb(j,s);
                end

              end
            else
              Q_tbi(i+1,j) = 0;
              Q_tbo(i+1,j) = 0;
              Q_tbr(i+1,j) = 0;
              for k = 1:n_tb_x
                for s = 1:n_tb_s
                  new_T_tb(j,k,s)=0;
                end
              end

            end

          end

          //Check convergence
          cont=%F;
          for j=1:no_of_cv
            for k = 1:n_h_x
              for s = 1:n_h_s
                //Test individual metal temp convergence
                if (T_h(s+(j-1)*n_h_s,k+n_h_x)-new_T_h(j,k,s))^2 > T_criteria then
                  cont=%T
                end
                //Update metal temperatures
                T_h(s+(j-1)*n_h_s,k+n_h_x) = new_T_h(j,k,s);
              end
            end
            for k = 1:n_tb_x
              for s = 1:n_tb_s
                //Test individual metal temp convergence
                if (T_tb(s+(j-1)*n_tb_s,k+n_tb_x)-new_T_tb(j,k,s))^2 > T_criteria then
                  cont=%T
                end
```

```
            //Update metal temperatures
            T_tb(s+(j-1)*n_tb_s,k+n_tb_x) = new_T_tb(j,k,s);
          end
        end
      end

      //Break the loop and display error message if maximum number of iterations exceeded
      if (count>max_iter) then
        cont=%F
        disp("Metal temperature solver - Max iterations reached",i);
      end

    end


  //Calculate the liquid mass flow and energy flow due to liquid exchange from one control volume to the next

    m=1;
    continues=%T;
    while m<=2 | continues
      m=m+1;
      continues=%F;



      //initialise the i+1 values
      for j=1:no_of_cv+2
        sum_mdot_L(i+1,j)=0;
        sum_mdot_L_h(i+1,j)=0;
      end
      //step through the connectivity matrix and sum the liquid mass flows and energy flows for each control volume
      for j=1:4//no_of_cv
        for k=1:no_of_cv
          if level(i+1,k)<1 then
            if (level(i+1,j)-geom(18,j))>0 then
              m_from_j_to_k = conn(j,k)*(level(i+1,j)-geom(18,j))*geom(1,j)*XSteam('rhoL_p',P(i+1,j)/100);
              if (level(i+1,k)+m_from_j_to_k/XSteam('rhoL_p',P(i+1,k)/100)/geom(1,k))>1 then
                m_from_j_to_k = (1-level(i+1,k))*geom(1,k)*XSteam('rhoL_p',P(i+1,k)/100);
              end
            else
              m_from_j_to_k=0;
            end
            if m_from_j_to_k/t > 100 then
              m_from_j_to_k = 100*t;
            end
            sum_mdot_L(i+1,j) = sum_mdot_L(i+1,j) - m_from_j_to_k/t;
            sum_mdot_L(i+1,k) = sum_mdot_L(i+1,k) + m_from_j_to_k/t;

            sum_mdot_L_h(i+1,j) = sum_mdot_L_h(i+1,j) - m_from_j_to_k/t*XSteam('hL_p',P(i+1,j)/100);
            sum_mdot_L_h(i+1,k) = sum_mdot_L_h(i+1,k) + m_from_j_to_k/t*XSteam('hL_p',P(i+1,j)/100);
          end
        end
      end

      //Add in the separator overflow boundary condition
      for j=1:no_of_cv
        mdot_from_sep_to_j = conn(no_of_cv+1,j)*mdot_overflow;
        sum_mdot_L(i+1,j) = sum_mdot_L(i+1,j) + mdot_from_sep_to_j;
        if (BC(1,3)+0.01)>XSteam('Tsat_p',P(i+1,j)/100) then
          //to avoid inadvertently adding steam to the cv if the temperature boundary condition is greater than saturation
temp
          sum_mdot_L_h(i+1,j) = sum_mdot_L_h(i+1,j) + mdot_from_sep_to_j*XSteam('hL_p',P(i+1,j)/100);
          h_overflow_plus1=XSteam('hL_p',P(i+1,j)/100);
        else
          sum_mdot_L_h(i+1,j) = sum_mdot_L_h(i+1,j) + mdot_from_sep_to_j*XSteam('h_pT',P(i+1,j)/100,BC(1,3));
          h_overflow_plus1=XSteam('h_pT',P(i+1,j)/100,BC(1,3));
```

```
    end
end

//Calculate flow in reverse from CV6 back to CV5, this because CV6 is actually higher in elevation than CV5
if (level(i+1,6) > 0) & (level(i+1,5) < geom(18,5)) then
    m_from_j_to_k = level(i+1,6)*geom(1,6)*XSteam('rhoL_p',P(i+1,6)/100);
    if (level(i+1,5)+m_from_j_to_k/XSteam('rhoL_p',P(i+1,5)/100)/geom(1,5))>1 then
        m_from_j_to_k = (1-level(i+1,5))*geom(1,5)*XSteam('rhoL_p',P(i+1,5)/100);
    end
    if m_from_j_to_k/t > 100 then
        m_from_j_to_k = 100*t;
    end
    sum_mdot_L(i+1,6) = sum_mdot_L(i+1,6) - m_from_j_to_k/t;
    sum_mdot_L(i+1,5) = sum_mdot_L(i+1,5) + m_from_j_to_k/t;

    sum_mdot_L_h(i+1,6) = sum_mdot_L_h(i+1,6) - m_from_j_to_k/t*XSteam('hL_p',P(i+1,6)/100);
    sum_mdot_L_h(i+1,5) = sum_mdot_L_h(i+1,5) + m_from_j_to_k/t*XSteam('hL_p',P(i+1,6)/100);
end

//Calculate flow in reverse from CV5 back to CV7 that can occur when 5 and 6 are full
if (level(i+1,6) > geom(18,6)) & (level(i+1,5) > geom(18,5)) then
    m_from_j_to_k = (level(i+1,5)-geom(18,5))*geom(1,5)*XSteam('rhoL_p',P(i+1,5)/100);
    if m_from_j_to_k/t > 100 then
        m_from_j_to_k = 100*t;
    end
    sum_mdot_L(i+1,5) = sum_mdot_L(i+1,5) - m_from_j_to_k/t;
    sum_mdot_L(i+1,7) = sum_mdot_L(i+1,7) + m_from_j_to_k/t;

    sum_mdot_L_h(i+1,5) = sum_mdot_L_h(i+1,5) - m_from_j_to_k/t*XSteam('hL_p',P(i+1,5)/100);
    sum_mdot_L_h(i+1,7) = sum_mdot_L_h(i+1,7) + m_from_j_to_k/t*XSteam('hL_p',P(i+1,5)/100);
end


//Solve for the required vapour massflows to achieve the same pressure in all of the control volumes

//Use the Newton Raphson method to iterate and find a solution of vapour flow rates such that the pressure in each
control volume is equal
count=0
cont=%T
deviation=0

while cont

   Pressure=Get_pressures(x_guess);

   C = zeros(unknowns,unknowns);
   for j=1:unknowns
      x_guess(j,1)=x_guess(j,1)+0.01;
      Pressure1=Get_pressures(x_guess);

      for k=1:no_of_cv-1;
         C(k,j) = ((Pressure1(1,k) - Pressure1(1,k+1)) - (Pressure(1,k)-Pressure(1,k+1)))/(0.01);
      end
      x_guess(j,1)=x_guess(j,1)-0.01;

      if j <= no_of_cv-1 then
         D(j,1)=-(Pressure(1,j)-Pressure(1,j+1));
      else
         n=j+1 //n=node number
         D(j,1)=0;
         for k = 1:unknowns // k = posn in x_guess and v_flow_unknowns
            if v_flow_unknowns(1,k) == n then
               C(j,k) = -1;
               D(j,1) = D(j,1) - x_guess(k);
            end
            if v_flow_unknowns(2,k) == n then
```

```
            C(j,k) = 1;
            D(j,1) = D(j,1) + x_guess(k);
          end
        end
        D(j,1) = -D(j,1);
      end
    end

    delta_x=C\D;
    x_new=x_guess+relax*delta_x;
    cont=%F
    count=count+1;
    deviation(count)=0;
    for j=1:no_of_cv-1
      V_flows(count,j)=x_guess(j);
      deviation(count)=deviation(count)+(Pressure(1,j)-Pressure(1,j+1))^2;
      if (x_new(j)-x_guess(j))^2 > criteria2 then
        cont=%T
      end
    end
    for j=no_of_cv:unknowns
      V_flows(count,j)=x_guess(j);
      n=j+1 //n=node number
      sum_V_flow=0;
      for k = 1:unknowns // k = posn in x_guess and v_flow_unknowns
        if v_flow_unknowns(1,k) == n then
          sum_V_flow = sum_V_flow - x_guess(k);
        end
        if v_flow_unknowns(2,k) == n then
          sum_V_flow = sum_V_flow + x_guess(k);

        end
      end

      deviation(count)=deviation(count)+(sum_V_flow)^2;

      if (x_new(j)-x_guess(j))^2 > criteria2 then
        cont=%T
      end
    end

    x_guess=x_new;

    if (count>max_iter) then
      cont=%F
      converged=%F
    else
      converged=%T
    end
  end

  for j=1:no_of_cv
    if Pressure(1,j)==10000 then
      disp("Pressure=10000, paused")
      pause
    end
  end

  if ~converged then
    best_deviation=deviation(count);
    for runs=1:count
      if deviation(runs)<best_deviation then
        best_deviation=deviation(runs);
        for j=1:no_of_cv-1
          x_new(j)=V_flows(runs,j);
        end
```

```
            end
        end
    end

    Pressure=Get_pressures(x_new);

    if Pressure(7,1)==1 then
        disp(Pressure(8,:),"Get Pressure function - Max iterations reached",mi);
    end

    //Write results of the iteration into the output matrices

    for j=1:no_of_cv
        if j<=unknowns
            mdot_v(i+1,j)=x_new(j,1);
        end
        P(i+1,j)=Pressure(1,j);
        rho(i+1,j)=Pressure(2,j);
        h(i+1,j)=Pressure(3,j);
        x(i+1,j)=Pressure(4,j);
        sum_mdot_v(i+1,j)=Pressure(5,j);
        sum_mdot_v_h(i+1,j)=Pressure(6,j);

        dp_dt(i+1,j)=(P(i+1,j)-P(i,j))/t;
        drho_dt(i+1,j)=(rho(i+1,j)-rho(i,j))/t;
        dh_dt(i+1,j)=(h(i+1,j)-h(i,j))/t;

        if x(i+1,j)<=1 then
            T_f(i+1,j)=XSteam('Tsat_P',P(i+1,j)/100);
            level(i+1,j)=((1-x(i+1,j))/XSteam('rhoL_P',P(i+1,j)/100))*rho(i+1,j);      //Volume fraction of liquid [0=empty to
1=full]
        else
            level(i+1,j)=0;
            T_f(i+1,j)=XSteam('T_Ph',P(i+1,j)/100,h(i+1,j));
        end
    end
    for j=no_of_cv+1:unknowns
        mdot_v(i+1,j)=x_new(j,1);
    end

    for j=1:no_of_cv
        check_P(m,j) = P(i+1,j)
        if (check_P(m,j) - check_P(m-1,j))^2 > m_criteria then
            continues=%T;
        end
    end

    if (m>max_iter) then
        continues=%F;
    end

end

if ~converged then
    disp(best_deviation,"Vapour mass flow solver - Max iterations reached",mi);
end


mdot_L_tot = mdot_L_tot + mdot_overflow*t                    //Total mass of overflow in kg
Mtot(i+1)=0;
Etot(i+1)=0;
V_out_i=V_out_iplus1;
E_out_i=E_out_iplus1;
V_out_iplus1=0;
E_out_iplus1=0;
```

```
            Q_in = 0;
            for j=1:no_of_cv
               Mtot(i+1) = Mtot(i+1) + geom(1,j)*rho(i+1,j);
               V_out_iplus1 = V_out_iplus1 + Pressure(9,j);
               Etot(i+1) = Etot(i+1) + geom(1,j)*rho(i+1,j)*(h(i+1,j)-P(i+1,j)/rho(i+1,j));
               E_out_iplus1 = E_out_iplus1 + Pressure(9,j)*Pressure(10,j);
               Q_in = Q_in + (1-alpha_c)*(Q_h(i,j)-Q_tbi(i,j)) + alpha_c*(Q_h(i+1,j)-Q_tbi(i+1,j))
            end
            Mbal(mi)=(Mtot(i+1)-Mtot(i)) - ((1-alpha_c)*mdot_overflow_minus1 + alpha_c*mdot_overflow - (1-alpha_c)*V_out_i
- alpha_c*V_out_iplus1)*t;
            Ebal(mi)=(Etot(i+1)-Etot(i)) - ((1-alpha_c)*mdot_overflow_minus1*h_overflow +
alpha_c*mdot_overflow*h_overflow_plus1 - (1-alpha_c)*E_out_i - alpha_c*E_out_iplus1 + Q_in)*t;

            h_overflow=h_overflow_plus1;
            mdot_overflow_minus1=mdot_overflow;
         disp("------","Complete",mi,"------");



//Store data at the specified sampling rate
      if (mi*t)/sample_rate == round((mi*t)/sample_rate) then
         y=y+1;
         for j = 1:no_of_cv
            r_P(y,j)=P(i+1,j);
            r_mdot_v(y,j)=mdot_v(i+1,j);
            r_T_f(y,j)=T_f(i+1,j);
            r_rho(y,j) = rho(i+1,j);
            r_h(y,j) = h(i+1,j);
            r_x(y,j) = x(i+1,j);
            r_level(y,j) = level(i+1,j);
            r_hc(y,j)=h_c(i+1,j);
            r_hr(y,j)=h_r(i+1,j);
            r_Q_h(y,j) = Q_h(i+1,j);
            r_Q_tbi(y,j) = Q_tbi(i+1,j);
            r_Q_tbo(y,j) = Q_tbo(i+1,j);
            r_Q_tbr(y,j) = Q_tbr(i+1,j);
            r_sum_mdot_L(y,j) = sum_mdot_L(i+1,j);
            r_sum_mdot_v(y,j) = sum_mdot_v(i+1,j);
         end
         for j=no_of_cv+1:unknowns
            r_mdot_v(y,j)=mdot_v(i+1,j);
         end
         for j=1:no_of_gas_streams
            r_T_RHtb(y,j) = T_RHtb(i+1,j);
            r_Q_RHtbo(y,j) = Q_RHtbo(i+1,j);

         end
         for j = 1:size(T_g,2)
            r_T_g(y,j) = T_g(i+1,j);
         end

         r_mdot_overflow(y) = mdot_overflow;
         r_condense_flow(y) = BC(1,6);
         r_mdot_L_tot(y) = mdot_L_tot;
         r_T_g(y,1) = T_g(i+1,1);
         r_Mtot(y) = Mtot(i+1);
         r_Etot(y) = Etot(i+1);
      end
      if (mi*t)/sample_rate2 == round((mi*t)/sample_rate2) then
         r_T_steam(1+(z-1)*(no_of_cv+1),1) = z
         r_T_h(1+(z-1)*(no_of_cv*n_h_s+1),1)=z
         r_h_hd(1+(z-1)*(no_of_cv+1),1) = z
         r_T_tb(1+(z-1)*(no_of_cv*n_tb_s+1),1)=z
         r_h_tbi(1+(z-1)*(no_of_cv+1),1) = z
         for j = 1:no_of_cv
            for k=1:n_h_x+n_tb_x
```

```
            r_T_steam(j+1+(z-1)*(no_of_cv+1),k) = T_steam(j,k,i+1)
        end
        for k=1:n_h_x
            for s=1:n_h_s
                r_T_h((j-1)*n_h_s+s+1+(z-1)*(no_of_cv*n_h_s+1),k) = T_h(s+(j-1)*n_h_s,k+n_h_x)
            end
            r_h_hd(j+1+(z-1)*(no_of_cv+1),k) = h_hd(i+1,j,k)
        end
        for k=1:n_tb_x
            for s=1:n_tb_s
                r_T_tb((j-1)*n_tb_s+s+1+(z-1)*(no_of_cv*n_tb_s+1),k) = T_tb(s+(j-1)*n_tb_s,k+n_tb_x)
            end
            r_h_tbi(j+1+(z-1)*(no_of_cv+1),k) = h_tbi(i+1,j,k)
        end
    end
    z=z+1;
end

//Transfer all the values at i+1 to position i to prepare for calculation of the next timestep
for j = 1:no_of_cv
    P(i,j) = P(i+1,j);
    mdot_v(i,j) = mdot_v(i+1,j);
    T_f(i,j) = T_f(i+1,j);

    for k = 1:n_tb_x
        for s = 1:n_tb_s
            T_tb(s+(j-1)*n_tb_s,k) = T_tb(s+(j-1)*n_tb_s,k+n_tb_x);
        end
        T_steam(j,k,i) = T_steam(j,k,i+1)
        h_tbi(i,j,k) = h_tbi(i+1,j,k);
    end
    for k = 1:n_h_x
        for s = 1:n_h_s
            T_h(s+(j-1)*n_h_s,k) = T_h(s+(j-1)*n_h_s,k+n_h_x);
        end
        T_steam(j,k+n_tb_x,i) = T_steam(j,k+n_tb_x,i+1)
        h_hd(i,j,k) = h_hd(i+1,j,k);
    end

    T_tb_outer(i,j)=T_tb_outer(i+1,j);
    rho(i,j) = rho(i+1,j);
    h(i,j) = h(i+1,j);
    x(i,j) = x(i+1,j);
    level(i,j) = level(i+1,j);
    hc(i,j)=h_c(i+1,j);
    hr(i,j)=h_r(i+1,j);
    Q_h(i,j) = Q_h(i+1,j);
    Q_tbi(i,j) = Q_tbi(i+1,j);
    Q_tbo(i,j) = Q_tbo(i+1,j);
    Q_tbr(i,j) = Q_tbr(i+1,j);
    sum_mdot_v(i,j)=sum_mdot_v(i+1,j);
    sum_mdot_v_h(i,j)=sum_mdot_v_h(i+1,j);
    dp_dt(i,j)=dp_dt(i+1,j);
    drho_dt(i,j)=drho_dt(i+1,j);
    dh_dt(i,j)=dh_dt(i+1,j);
end
for j=1:no_of_cv+2
    sum_mdot_L(i,j)=sum_mdot_L(i+1,j);
    sum_mdot_L_h(i,j)=sum_mdot_L_h(i+1,j);
end
for j=no_of_cv+1:unknowns
    mdot_v(i,j) = mdot_v(i+1,j);
end
for j=1:no_of_gas_streams
    T_RHtb(i,j) = T_RHtb(i+1,j);
    Q_RHtbo(i,j) = Q_RHtbo(i+1,j);
```

```
        end
        for j = 1:size(T_g,2)
            T_g(i,j) = T_g(i+1,j);
        end
        Mtot(i) = Mtot(i+1);
        Etot(i) = Etot(i+1);
        BC(2,6)=BC(1,6);
    end

//Create output matrix and write to file
no_of_lines = size(r_P,1);
Output(1,1) = 1;
Output(1,no_of_cv+1) = 2;
Output(1,2*no_of_cv+1) = 3;
Output(1,3*no_of_cv+1) = 4;
Output(1,4*no_of_cv+1) = 5;
Output(1,5*no_of_cv+1) = 6;
Output(1,6*no_of_cv+1) = 7;
Output(1,7*no_of_cv+1) = 8;
Output(1,8*no_of_cv+1) = 9;
Output(1,9*no_of_cv+1) = 10;
Output(1,10*no_of_cv+1) = 11;
Output(1,11*no_of_cv+1) = 12;
Output(1,12*no_of_cv+1) = 13;
Output(1,13*no_of_cv+1) = 14;
Output(1,14*no_of_cv+1) = 15;
Output(1,15*no_of_cv+1) = 16;
Output(1,16*no_of_cv+1) = 17;
Output(1,16*no_of_cv+1+size(T_g,2)) = 18;
for y=1:no_of_lines
    for j = 1:no_of_cv
        Output(y+1,j) = r_P(y,j);
        Output(y+1,no_of_cv+j) = r_T_f(y,j);
        Output(y+1,4*no_of_cv+j) = r_rho(y,j);
        Output(y+1,5*no_of_cv+j) = r_h(y,j);
        Output(y+1,6*no_of_cv+j) = r_x(y,j);
        Output(y+1,7*no_of_cv+j) = r_level(y,j);
        Output(y+1,8*no_of_cv+j) = r_Q_h(y,j);
        Output(y+1,9*no_of_cv+j) = r_Q_tbi(y,j);
        Output(y+1,10*no_of_cv+j) = r_Q_tbo(y,j);
        Output(y+1,11*no_of_cv+j) = r_Q_tbr(y,j);
        Output(y+1,12*no_of_cv+j) = r_sum_mdot_L(y,j);
        Output(y+1,13*no_of_cv+j) = r_sum_mdot_v(y,j);
    end
    for j = 1:size(T_g,2)
        Output(y+1,16*no_of_cv+j) = r_T_g(y,j);
    end
    for j=1:unknowns
        Output(y+1,(16*no_of_cv+size(T_g,2))+j) = r_mdot_v(y,j);
    end
    Output(y+1,(16*no_of_cv+size(T_g,2))+unknowns+1) = r_mdot_overflow(y);
    Output(y+1,(16*no_of_cv+size(T_g,2))+unknowns+2) = r_condense_flow(y);
end
Now=datevec(now())
fprintfMat(string(Now(1))+string(Now(2))+string(Now(3))+string(Now(4))+string(Now(5))+'.txt',Output);
fprintfMat(string(Now(1))+string(Now(2))+string(Now(3))+string(Now(4))+string(Now(5))+' T_steam.txt',r_T_steam);
fprintfMat(string(Now(1))+string(Now(2))+string(Now(3))+string(Now(4))+string(Now(5))+' T_h.txt',r_T_h);
fprintfMat(string(Now(1))+string(Now(2))+string(Now(3))+string(Now(4))+string(Now(5))+' T_tb.txt',r_T_tb);
fprintfMat(string(Now(1))+string(Now(2))+string(Now(3))+string(Now(4))+string(Now(5))+' h_hd.txt',r_h_hd);
fprintfMat(string(Now(1))+string(Now(2))+string(Now(3))+string(Now(4))+string(Now(5))+' h_tb.txt',r_h_tbi);
```

# Appendix H. Liquid tracking model – Basic verification by Flownex comparison

A Flownex model was configured to test that the results of the liquid tracking model were reasonable. The model did not include heat transfer. The intention was to investigate the effects of adding liquid (separator overflow) to two interconnected tanks (the superheater). A constant liquid flow rate was added to a tank. Initially the tank pressure was specified and then the boundary condition was removed to allow the tank pressure to vary. The tank was configured to overflow to the second tank if it exceeded a level fraction of 0.001.

The Flownex model and the results are shown in Figure 168. The same geometry and boundary conditions were used in both models. The results show that Flownex and the LTM agree. Following the successful verification without heat transfer, another model was configured to test the LTM against Flownex with heat transfer. The model and results are shown in Figure 169. Again the LTM results agree with the Flownex results, except at 50 seconds where the Flownex model predicts that tank two becomes saturated and starts showing level sooner than the LTM model predicts.

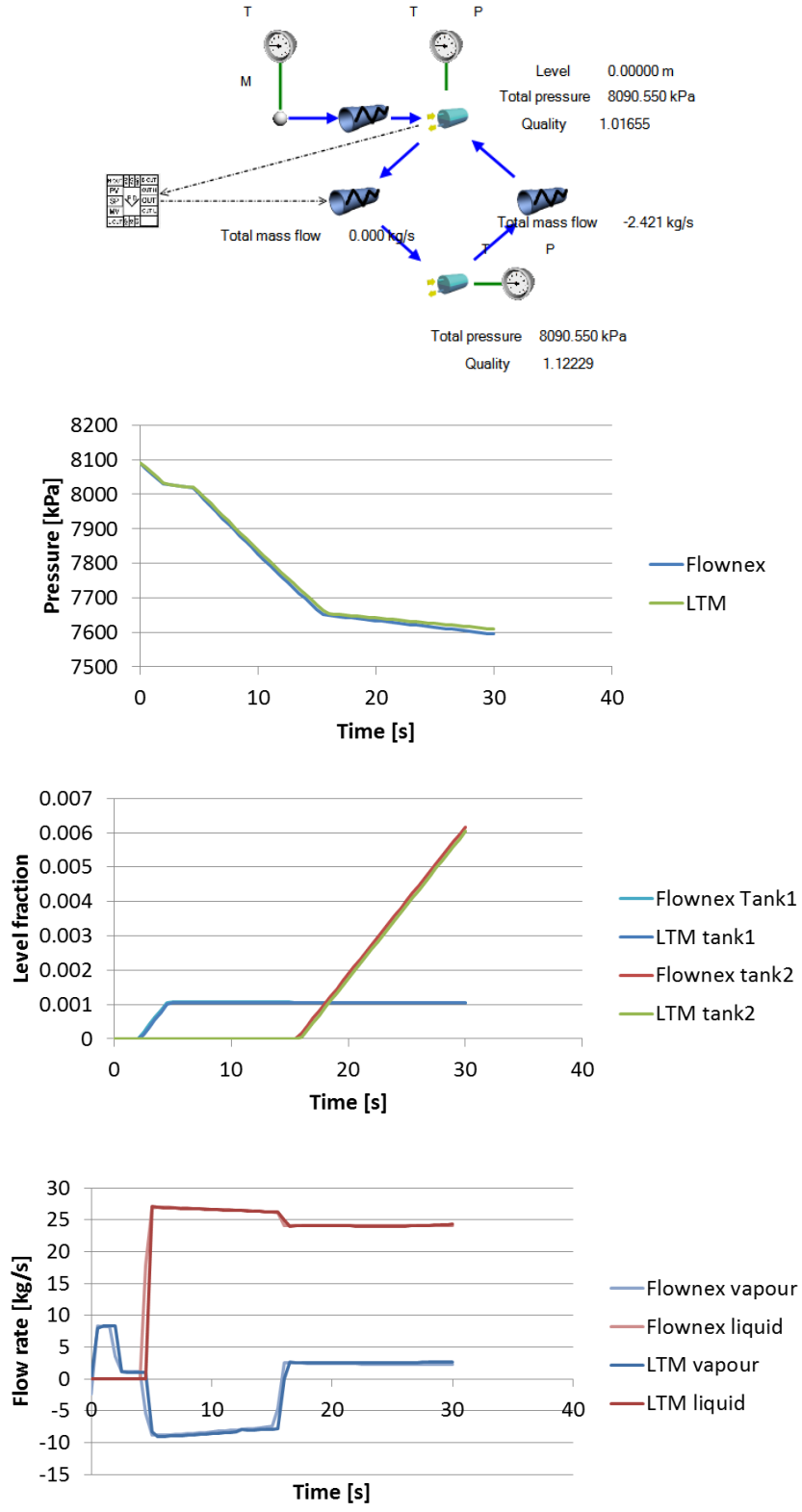


*Figure 168. Flownex simple model and results of LTM verification – no heat transfer*

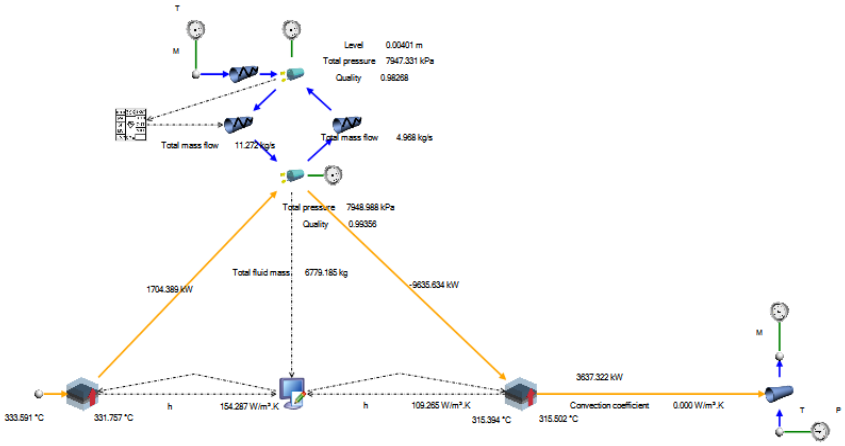


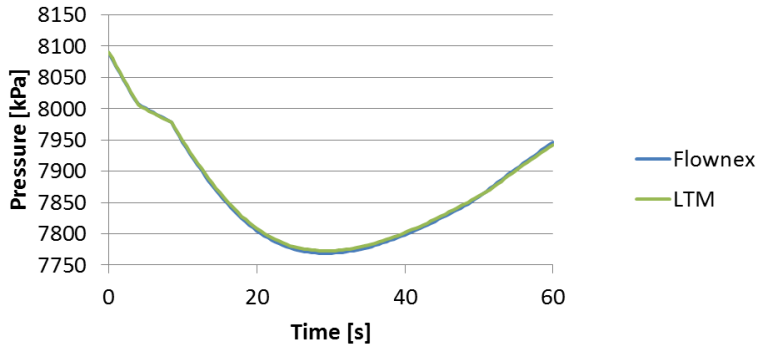


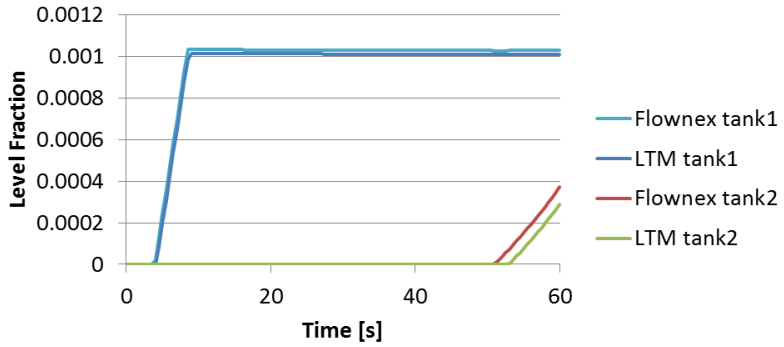


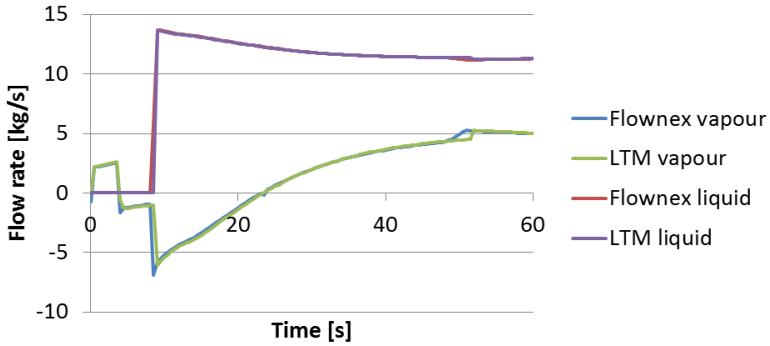


*Figure 169. Flownex simple model and results of LTM verification – with heat transfer*

# Appendix I. Liquid tracking model - Grid independence study

In this section, three levels of discretisation of the superheater were considered, namely, four, eight and sixteen control volumes. The tube and header internal heat transfer for this comparison did not include the localised boiling effects. Rather, the same approach as the Flownex model was used (Refer section 6.3.4). A lumped mass approach was applied for the header and tube bundle metal temperatures and the inner heat transfer coefficient was calculated by the area weighted formula based on the combined free and forced convection correlation of Morcos and Bergles [110].

In the four control volume model, the separate legs of the superheater were not considered and thus there were no parallel flows. Each stage of the superheater was considered as a single control volume as shown in Figure 170. The interconnection of the control volumes on the liquid side and on the vapour side are also shown together with the overflow heights that were used.

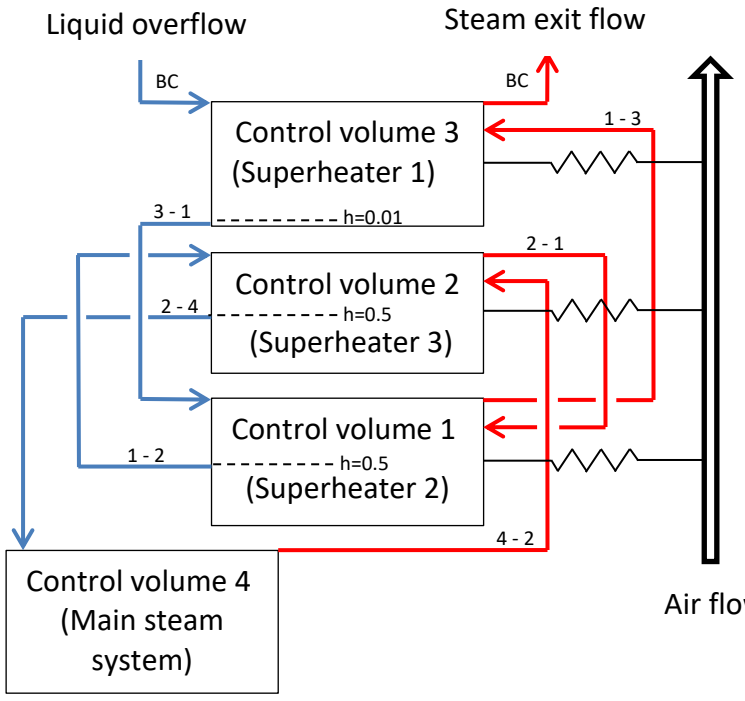


*Figure 170. Application of the LTM to a 4 control volume approximation of the superheater*

The eight control volume approximation considers two parallel streams of heat exchangers in the boiler. The configuration is shown in Figure 171. In this case there are two additional nodes to allow

for vapour flow to cross between the streams at the boiler outlet header as is the case in the real plant.

The liquid flows are also able to cross at the boiler outlet header. In the case of the real plant, two horizontal outlet headers extend the width of the boiler. The tubes for each of the four parallel legs of Superheater 3 connect to these two headers. When two of the four legs emit water into the headers, the water flows both left and right along the outlet headers. Potentially it could be assumed that the flow splits half left and half right, however an added complication is that the tubes of the other dry superheater legs are connected at the bottom of the headers. Thus the water in the header tends to drain into the dry superheater legs and flow in the reverse direction into those parts of the superheater. Hence, it is difficult to predict the flowrates of water in the respective directions. An assumption of a fixed liquid flow split ratio of 40:40:20 was used to account for the unknown flow distribution. This assumes that 40% of the flow from control volume two continues along the normal path to main steam control volume four. Part of the flow (20%) crosses over to main steam control volume eight and 40% crosses over into the heat exchanger tube bundle of the opposite side (control volume six). The numbers alongside the respective blue arrowheads in Figure 171 show the flow split fractions where applicable.

Owing to the configuration of the model, the liquid flows can only flow in the direction of the blue arrows shown in Figure 170 and Figure 171. There is a special case for the eight control volume model and that is when control volume two flows to control volume six. In the real plant, control volume six (which represents two legs of Superheater 3) is higher in elevation than control volume five (which represents two legs of Superheater 2) and thus control volume six drains to control volume five. To account for this in the model, a separate routine was written that transferred the level in control volume six back to control volume five if control volume five did not have a level above its overflow height at that point in time. Thus reverse flow of liquid was accounted for. A similar arrangement was programmed for the case where control volumes five and six were full and the liquid would be fills up the superheater into control volume seven.

On the gas side, the eight control volume model considers two separate gas streams that are roughly configured to match the real plant. The first stream interacts with control volumes one, six and seven including a heat transfer from the reheater between control volumes six and seven. The second gas stream interacts with control volumes five, two and three and includes heat transfer from the reheater between control volumes two and three.

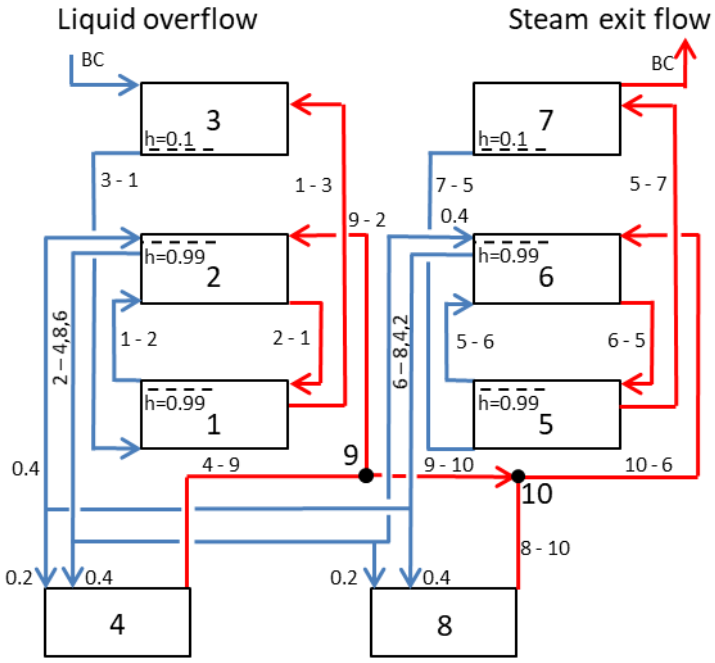


*Figure 171. Application of the LTM to an 8 control volume approximation of the superheater*

The sixteen control volume approximation is shown in Figure 172. As can be seen in Figure 174, this level of discretisation is the closest to the actual plant configuration. The four parallel legs of the superheater and the interconnection points are represented.

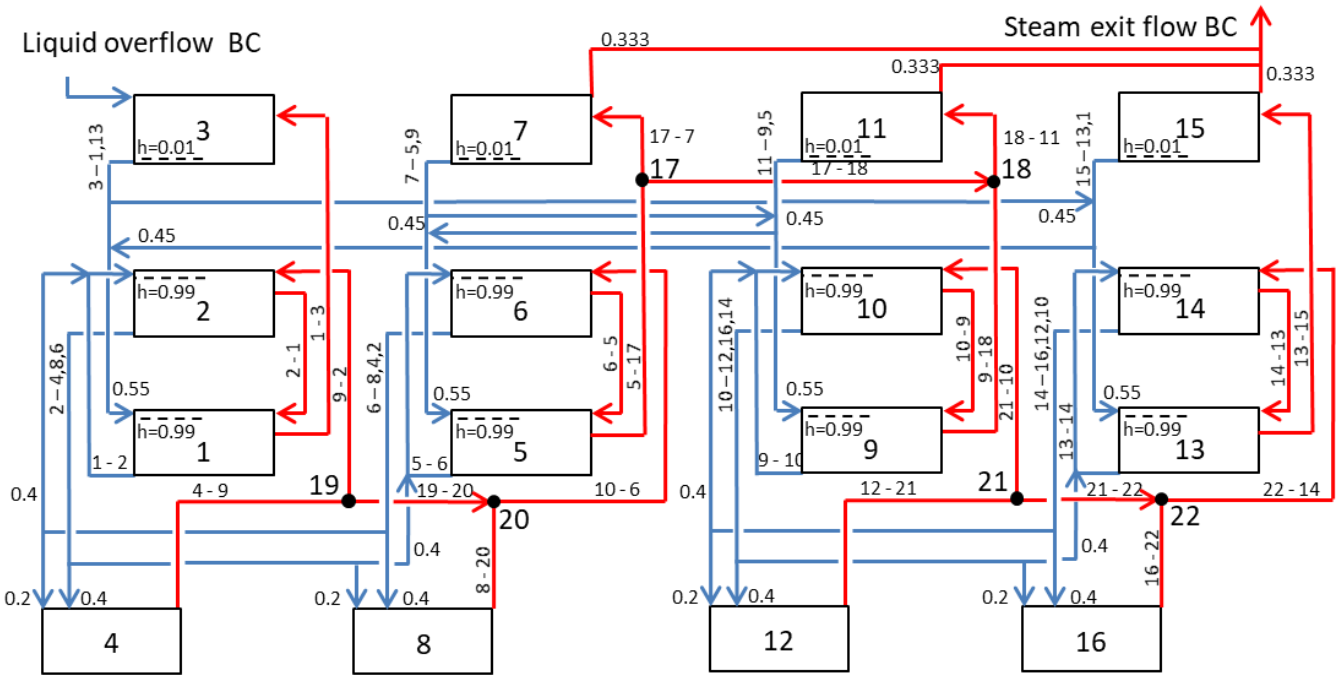


*Figure 172. Application of the LTM to a 16 control volume approximation of the superheater*

The vapour flows shown in red are positive in the direction of the arrows shown in Figure 172. The magnitude of the vapour flows are calculated at each time step and may be positive or negative.

The liquid flows occur mainly in the direction of the blue arrows with the assumed flow ratio fractions for split overflows of liquid shown close to their respective arrows in Figure 172. As with the eight control volume model above, the liquid flow split between downstream control volumes is difficult to predict. Assumptions have been made based on the perceived flow path of liquid when the liquid flows under the action of gravity through partly filled pipes and headers.

The potential for reverse liquid flow is increased in the sixteen control volume model compared to the eight volume model. Thus a specific overflow scheme as shown in Figure 173 was programmed into the LTM to deal with the flows. Although based on the blue arrows shown in Figure 172, the actual overflows in the model for a number of the control volumes were in the opposite direction.

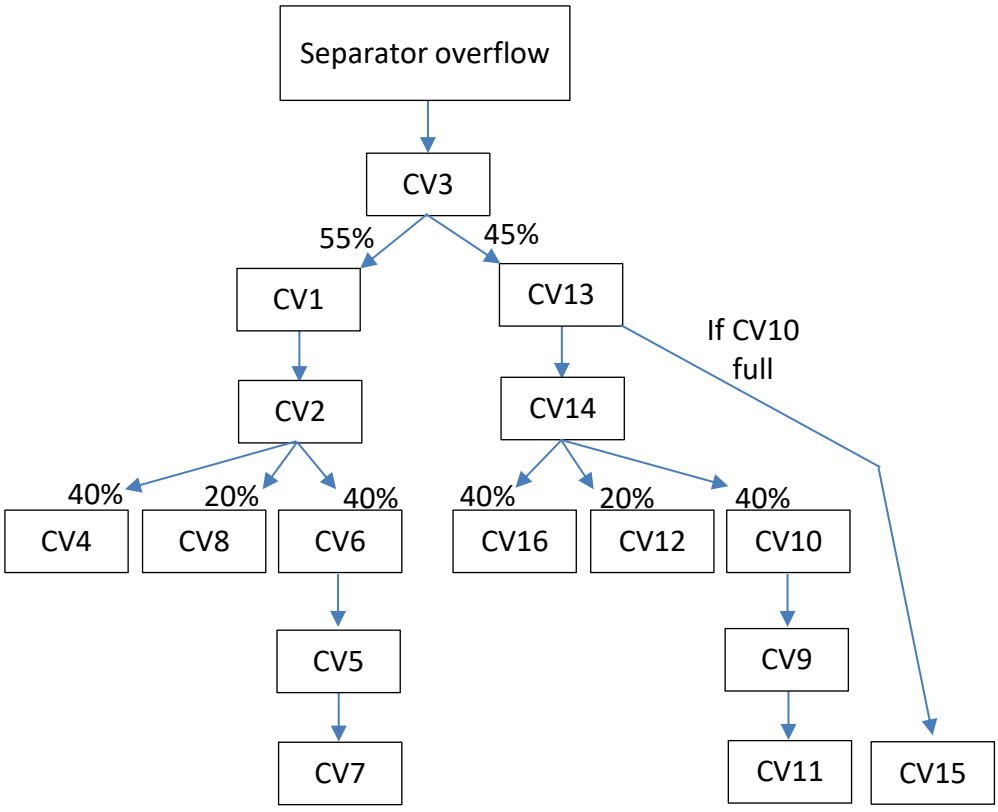


*Figure 173. LTM 16 control volume model liquid flow scheme*

The gas streams are configured as shown in Figure 174. The reheater interaction with the gas flow between stage one and stage three is not shown. Note that the order of control volumes in the direction of gas flow is not accurately shown here. The gas first interacts with stage two and then stage three in the model which is the same as it is in the real plant.

In Figure 174 also shows the actual interconnection on the various legs of the superheater. The normal direction of steam flow is downwards in the diagram. The headers are shown at inlet and

outlet of the grey blocks which represent the tube bundles. Thus the common headers can be identified – these are the locations where liquid overflow can cross from one leg to another. Physically on the plant, the lowest point is the stage 2 inlet header.

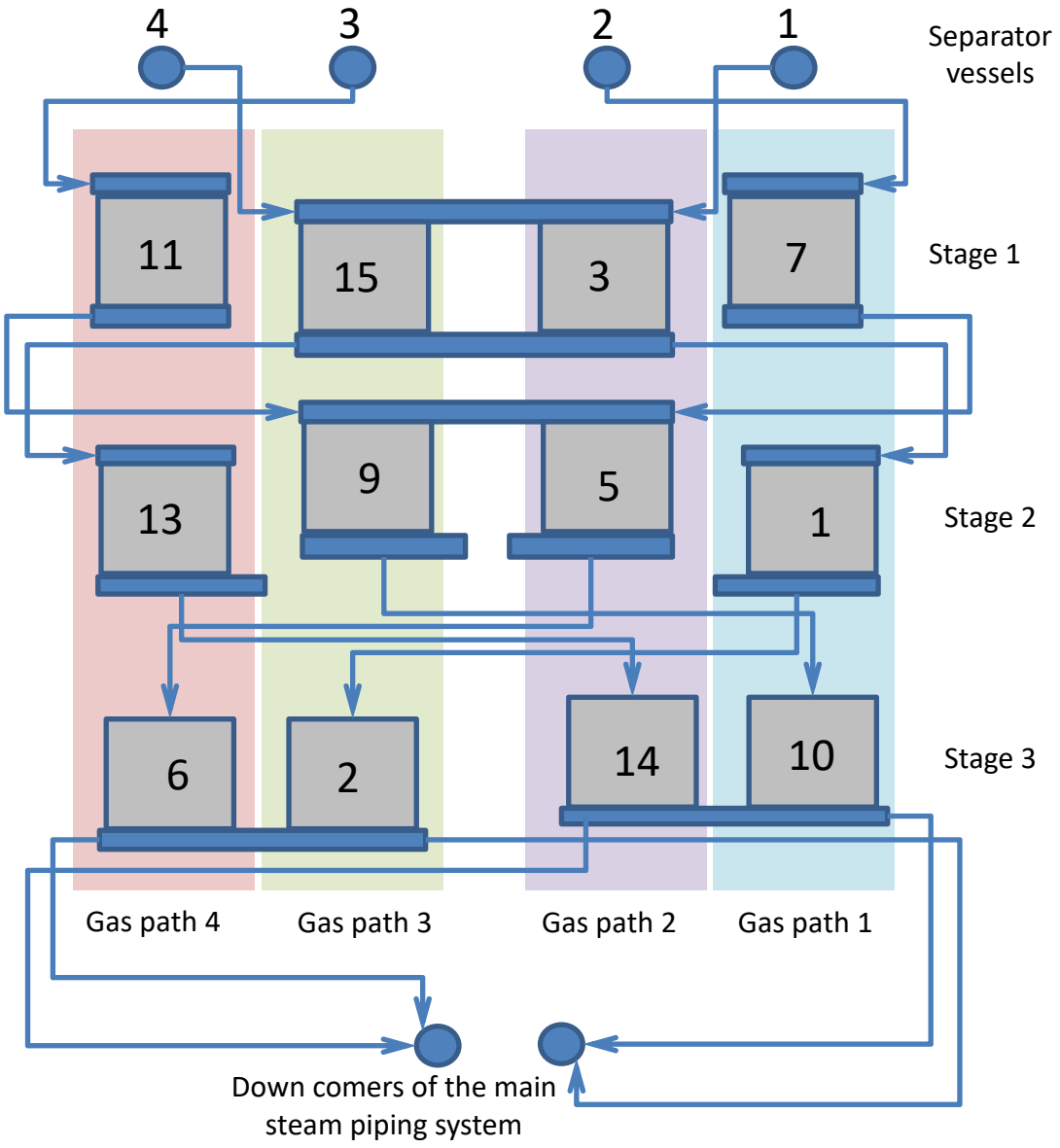


*Figure 174. Configuration of the superheater showing control volume numbers and gas path allocation*

The three different levels of discretisation were all able to solve successfully. The models each used a separator overflow rate boundary condition and calculated the necessary steam exit flow to maintain the superheater pressure close to the measured value. The superheater pressures for each of the runs are shown in Figure 175. Due to the method of using proportional control to adjust the steam exit flow according to the error between measured and simulated pressure, a deviation in measured and simulated pressure is expected when vapour exit flows become larger. The vapour exit flows become larger when steam is generated as water encounters the hot metal surfaces. This occurs at different times for the different control volume configurations in each level of discretisation and thus the marginally different pressure behaviours.

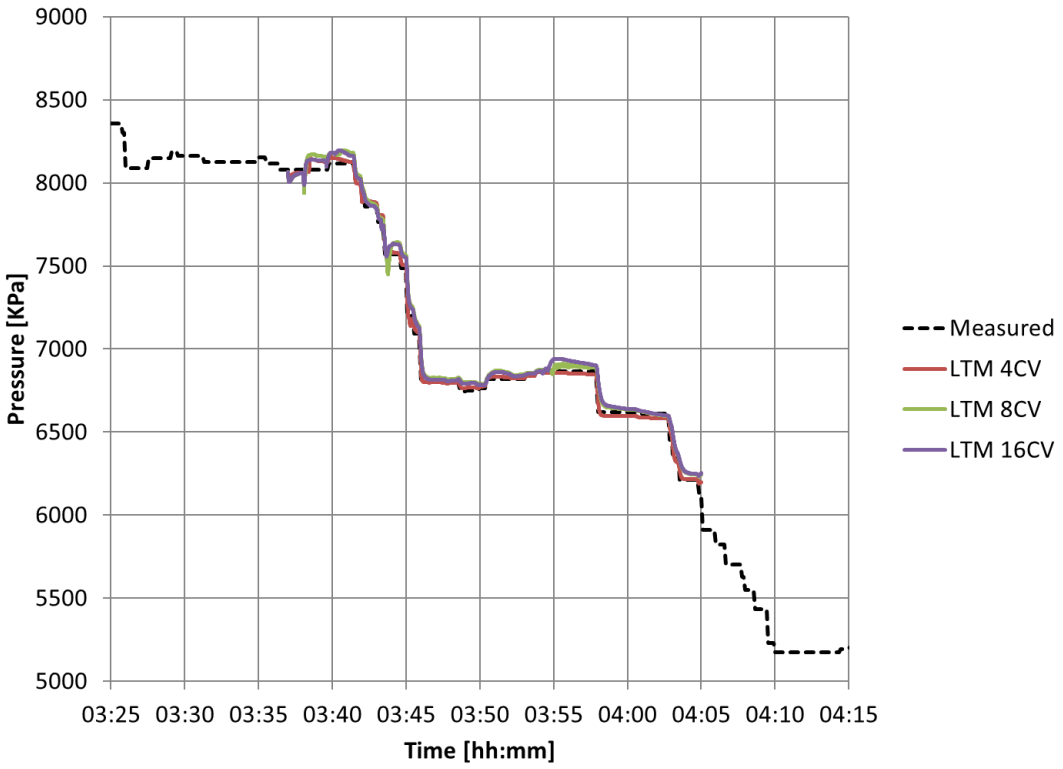


*Figure 175. Pressure results – 4CV, 8CV and 16CV LTM*

The constant gains were 0.2 for the eight and sixteen control volume models and 0.5 for the four control volume model. The gain determines a steam exit flow in kg/s from a pressure error signal in kPa. The four control volume model required a higher gain to improve the pressure behaviour in the initial stages up to 03:42.

The steam exit flow from the superheater to the sub cooled liquid interface for each level of discretisation is shown In Figure 176. The simulated values are compared to the 'measured' value calculated by the method described in section 6.1. The LTM values are erratic compared to the smooth 'measured' value.

The spikes in calculated steam exit flow are caused by the unsmoothed measured pressure data which exhibits steps in value and this in turn causes high separator overflow at each step.

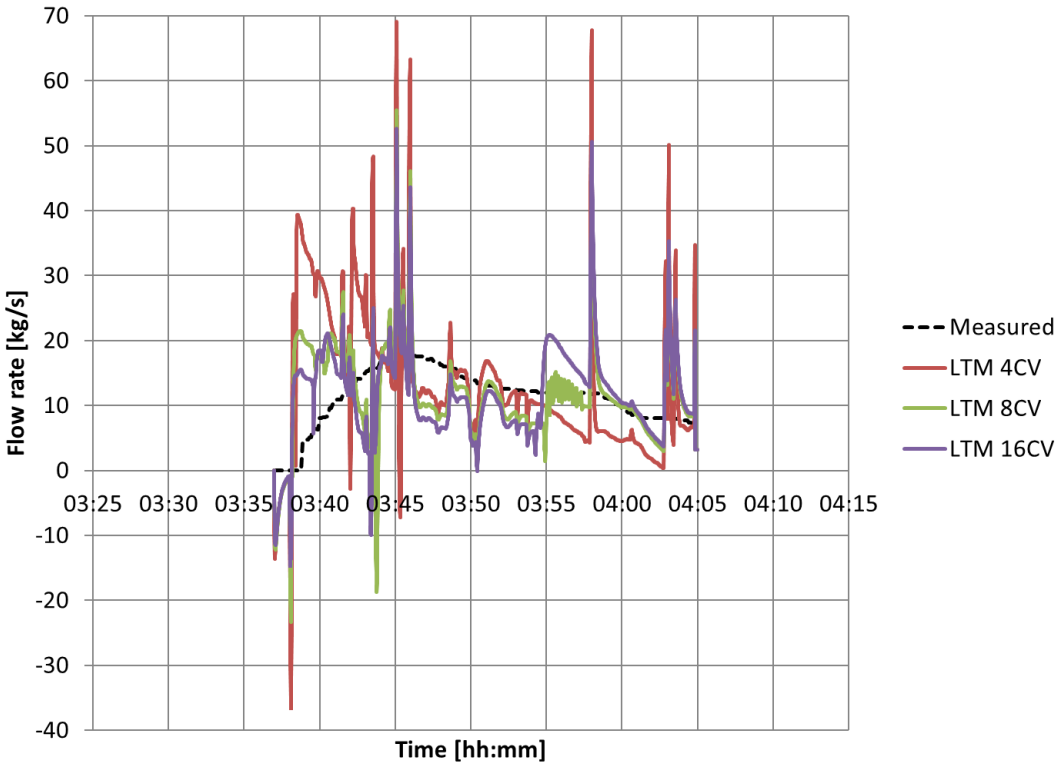


*Figure 176. Steam flow to sub cooled liquid interface – 4CV, 8CV and 16CV LTM*

In order to smooth the LTM results to provide a better comparison to the measured steam exit flow, the data was integrated with respect to time to give the accumulated mass of steam that exited the superheater via the sub-cooled liquid interface. The outcome in Figure 177 again shows that the LTM initially requires more steam exit flow to control pressure. This is because the LTM model reacts rapidly to the addition of water to any of the control volumes due to the homogeneous fluid in equilibrium assumption and the lumped metal masses. In reality it takes time for the liquid to flow into the superheater and reach all parts of the metal. Hence the LTM reacts faster than the real system.

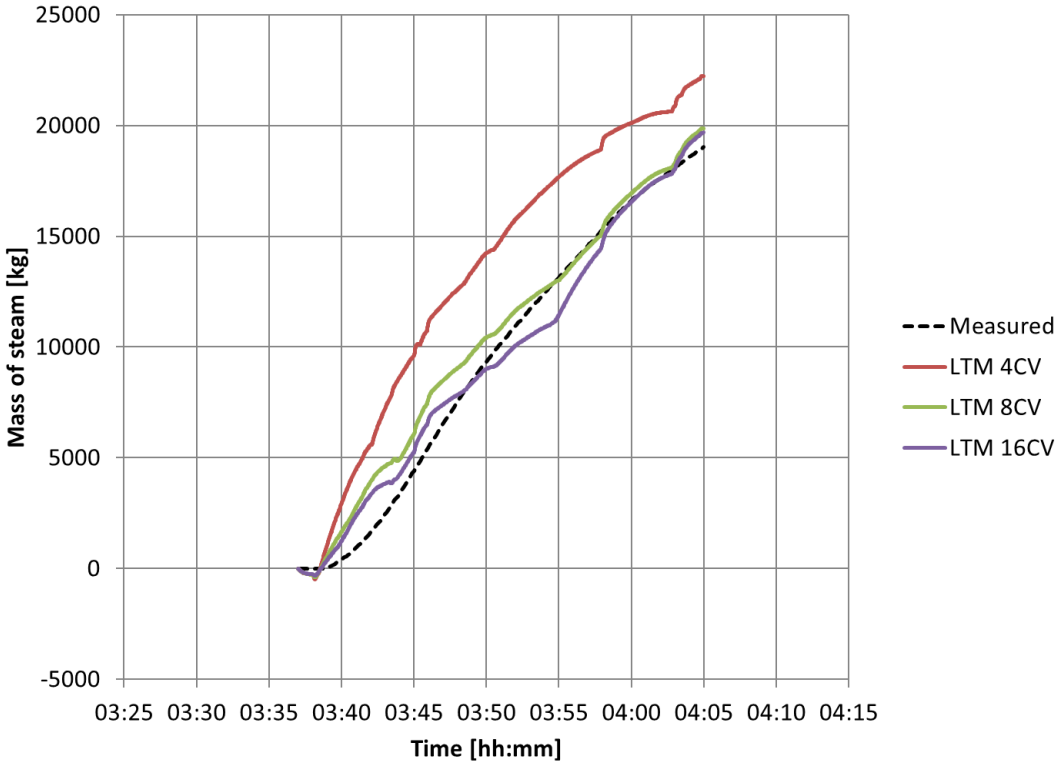


*Figure 177. Integrated steam flow or accumulative steam mass that flowed to the sub cooled liquid interface*

The LTM steam exit flows approximately matches the 'measured' vapour flow. Overall the four control volume LTM requires more exit flow than the measured exit flow. There are a limited number of lumped masses of metal in the four control volume model which are cooled simultaneously and release heat by generating steam in the superheater. This causes the rate of heat release in the four control volume model to be more than the real situation.

The eight and sixteen control volume LTM shows good agreement with the measured data indicating that the heat release more closely matched the real heat release that occurred. The heat release from the metal in the LTM is a function of the temperature difference between the fluid and the metal as well as the heat transfer coefficient. The liquid that flows into the LTM affects the heat transfer coefficient and the temperature difference in a control volume. Thus different liquid levels in the control volumes cause different heat release behaviour. This is true of the real system as well – heat is only rapidly released from the metal when liquid flows over it.

The comparative liquid levels for the three models are shown in Figure 178, Figure 179 and Figure 180. The reduced amount of detail is evident in the four control volume results. The four control volume has distinct steps in level where the overflow to the next control volume occurred and then once control volume four (the main steam control volume) was full, the other control volumes could continue filling.

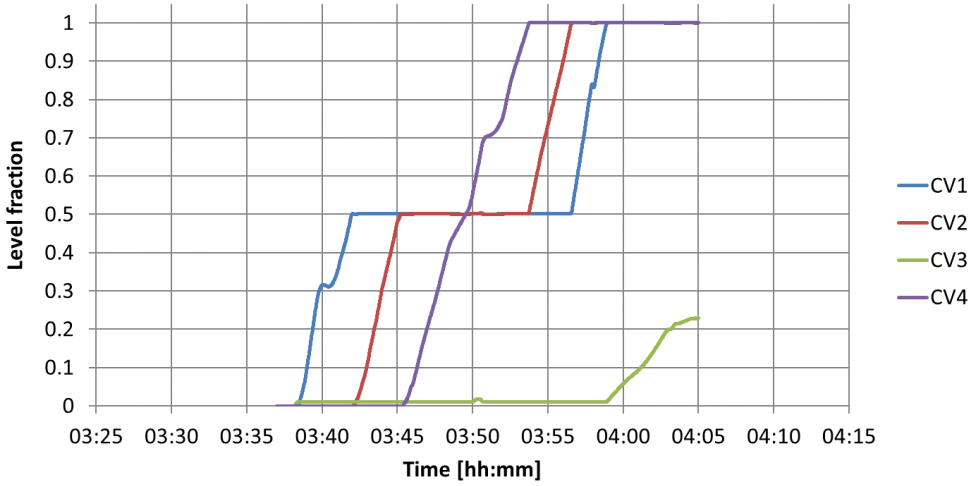


*Figure 178. Liquid levels 4CV LTM*

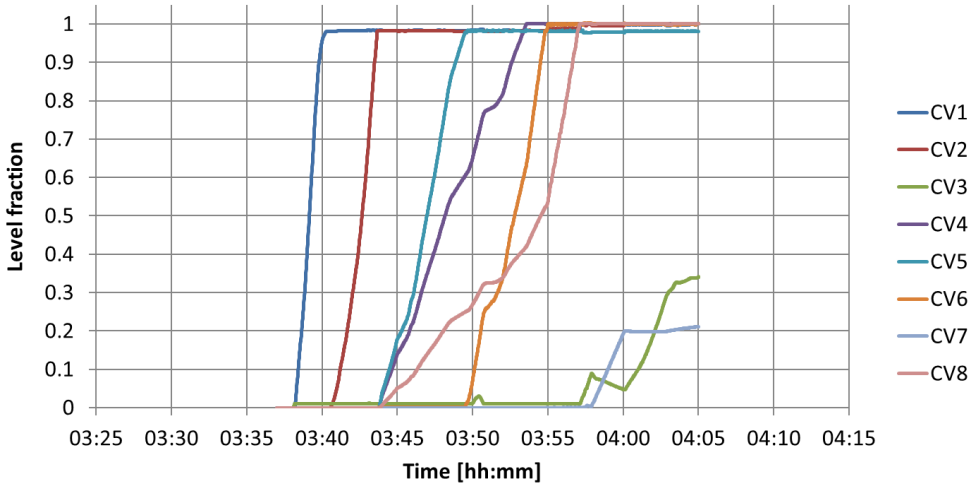


*Figure 179. Liquid levels 8CV LTM*

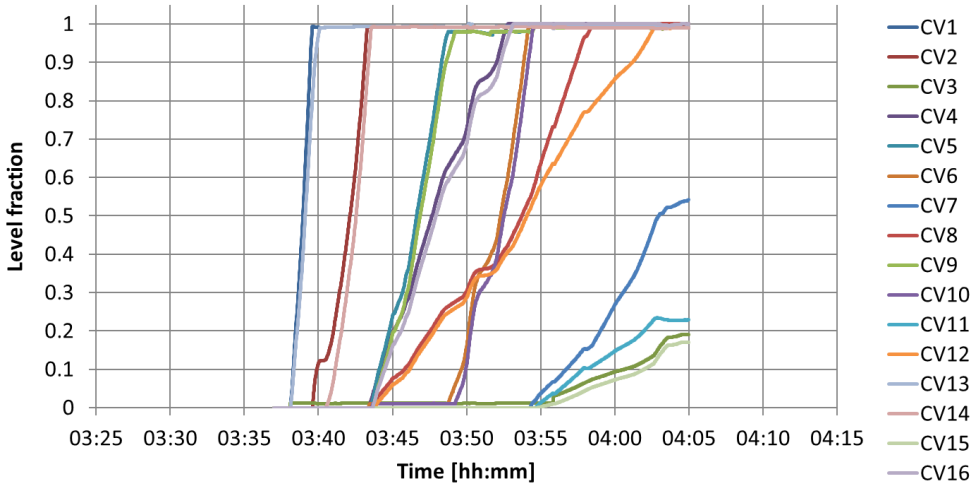


*Figure 180. Liquid levels 16CV LTM*

The eight and sixteen control volume models show similar results to each other. This explains the similar behaviour of the steam exit flow seen in Figure 177. The additional effort of the 16 control volume model is not warranted based on the quality of results up to this point.

The calculated superheater temperature history is compared to the averages of inlet and outlet temperature of the superheater sections in Figure 181, Figure 182 and Figure 183 for the four, eight and sixteen control volume results respectively.

The four legs of the superheater were grouped into two groups for averaging the respective measured temperatures in order to compare to the four and eight control volume results. The sixteen control volume results were directly compared to the measured steam temperatures.

The effect of the liquid entering a control volume is that the steam temperature rapidly drops to saturation temperature. This depends on the rate of water being added but in this case the rate is sufficient to cause rapid cooling of the steam.

The LTM temperatures show sudden drops to saturation temperature which mostly occur earlier than the drop in measured temperatures. Although earlier, the calculated temperatures reduce to saturation in the correct order and in some cases they exhibit the same behaviour of the temperature over time. The eight and sixteen control volumes results are similar to each other but better than the four control volume results.

The lumped tube bundle metal temperatures over time are shown in Figure 184, Figure 185 and Figure 186 for the four, eight and sixteen control volume models respectively. The lumped header temperatures are shown in Figure 187, Figure 188 and Figure 189. The additional detail afforded by the eight control volume model is evident when compared to the four control volume model.

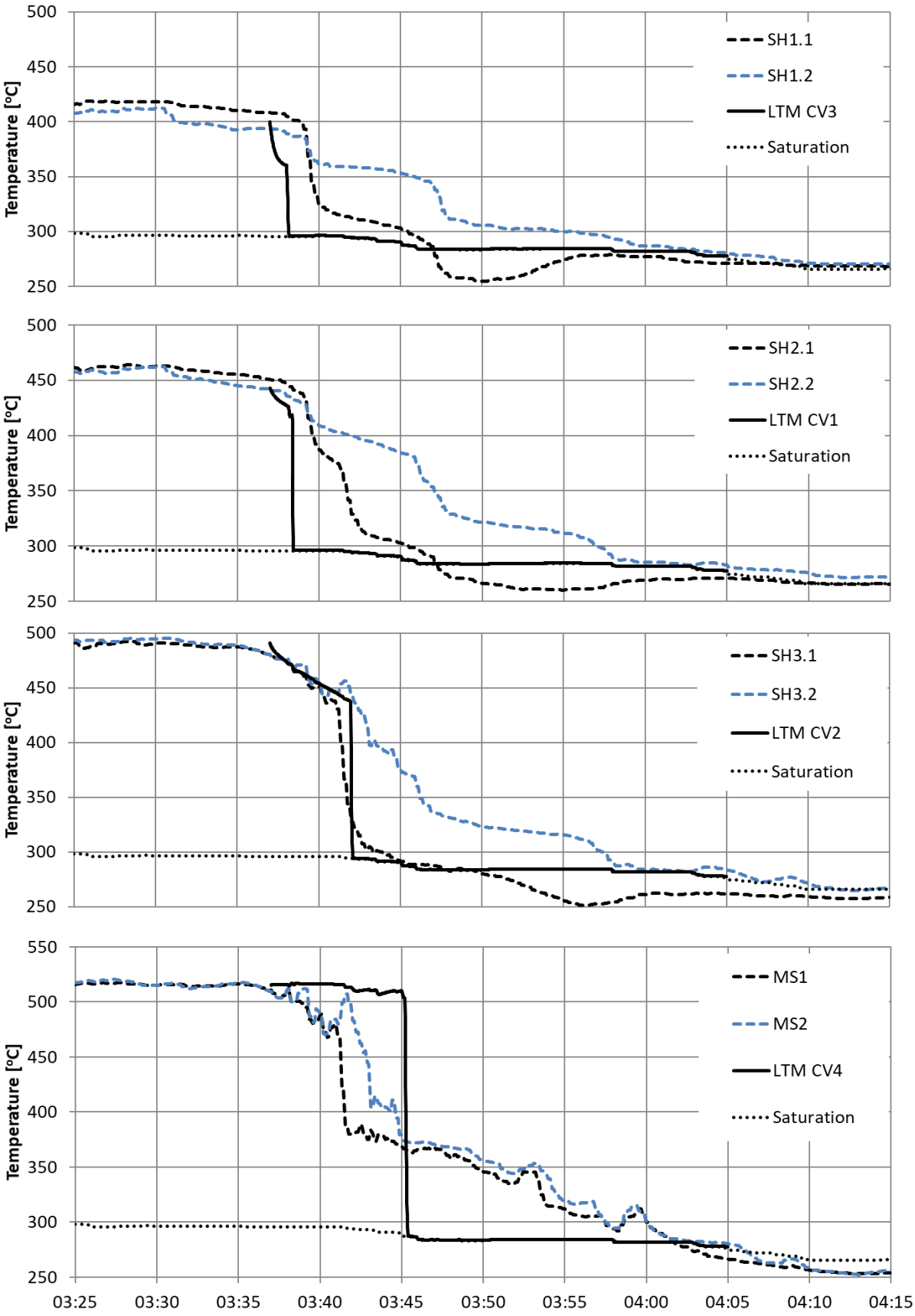


*Figure 181. Fluid temperature results – 4CV LTM*

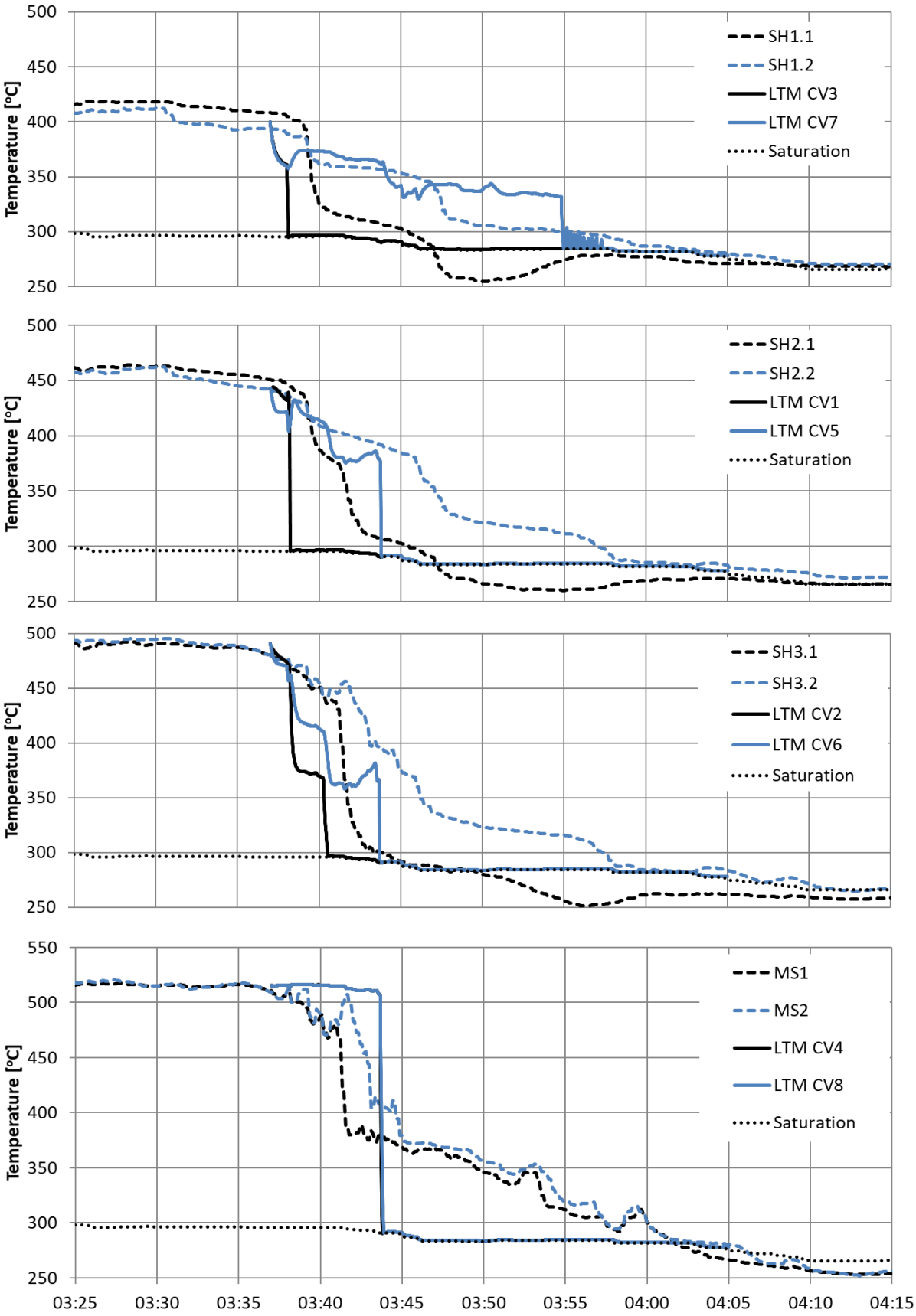


*Figure 182. Fluid temperature results – 8CV LTM*

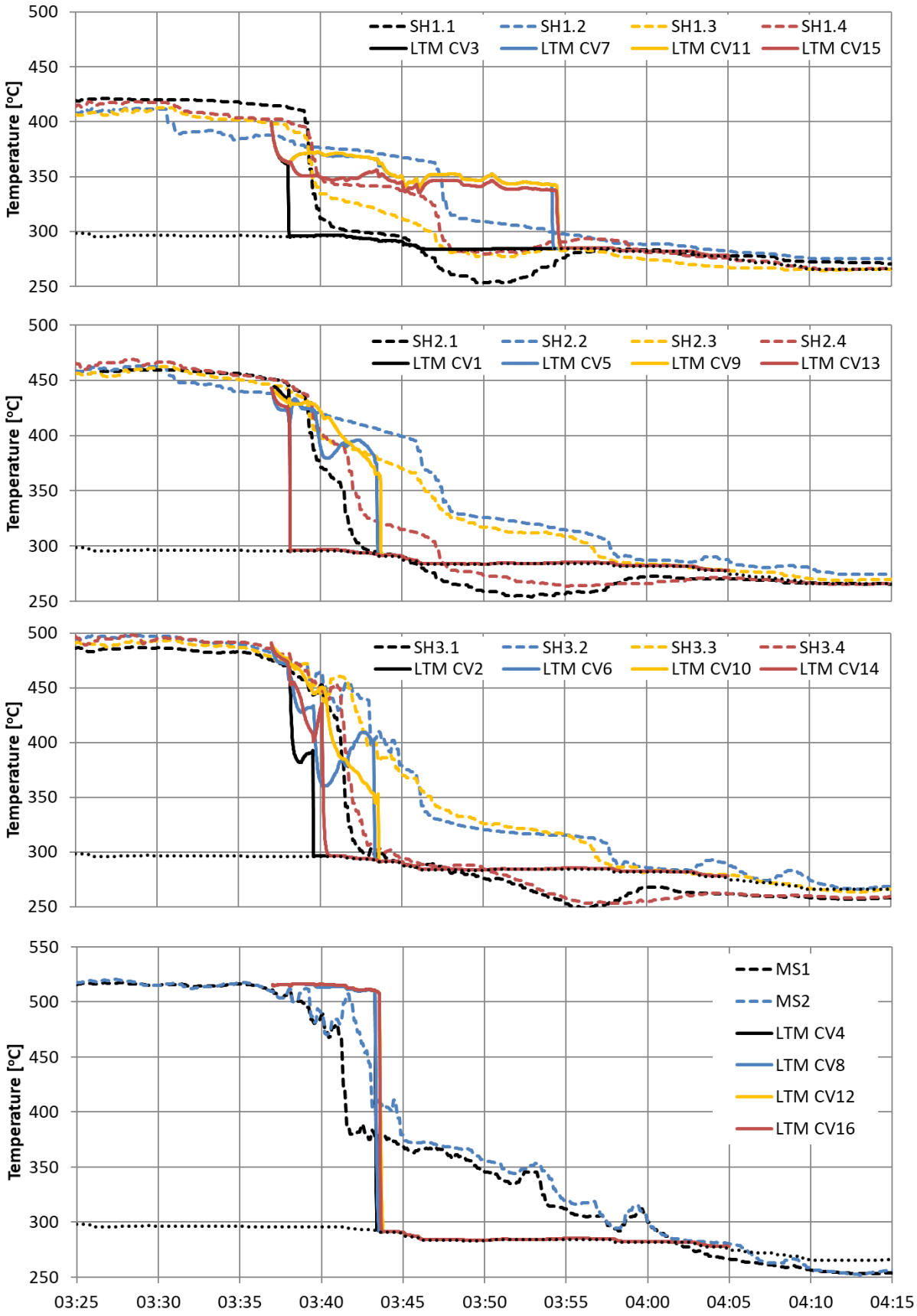


*Figure 183. Fluid temperature results – 16CV LTM*

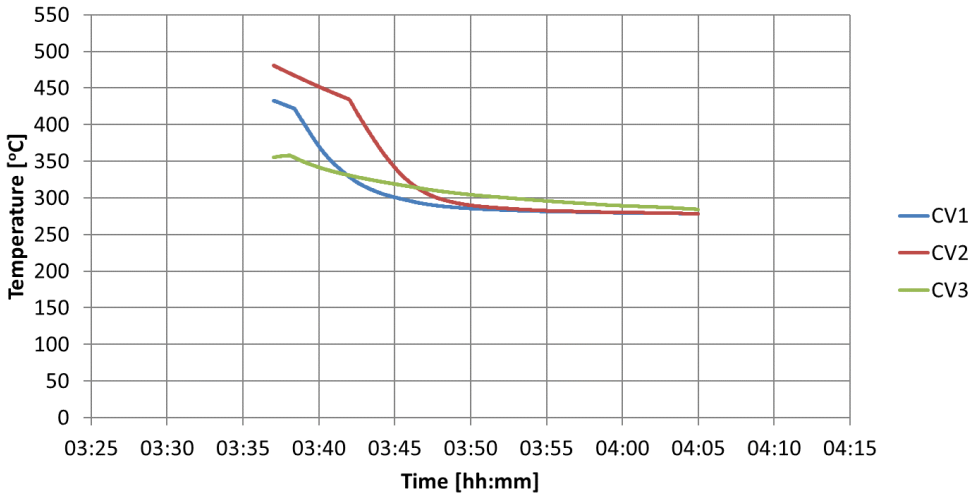


*Figure 184. Tube bundle temperatures 4CV LTM*

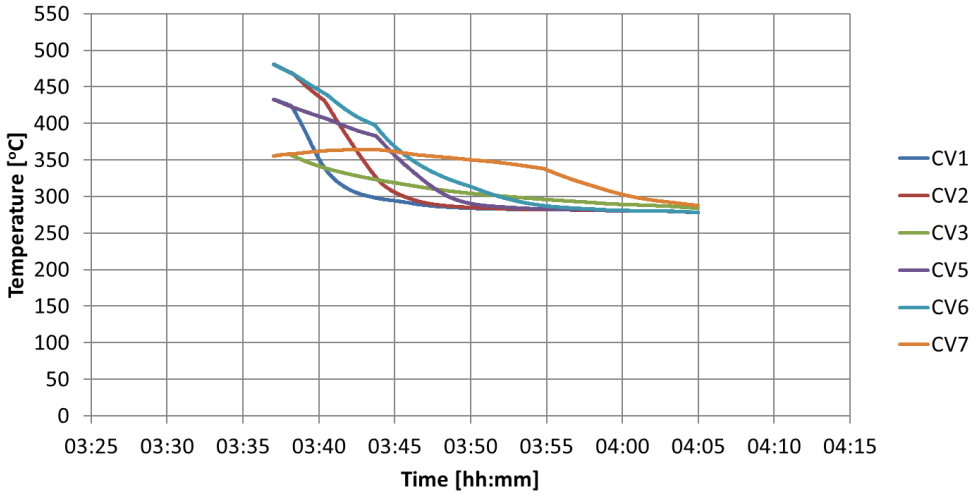


*Figure 185. Tube bundle temperatures 8CV LTM*

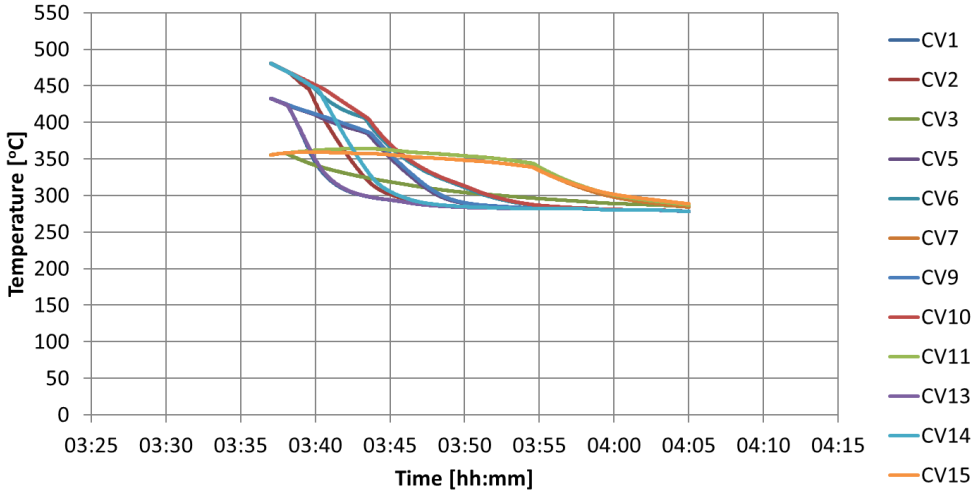


*Figure 186. Tube bundle temperatures 16CV LTM*

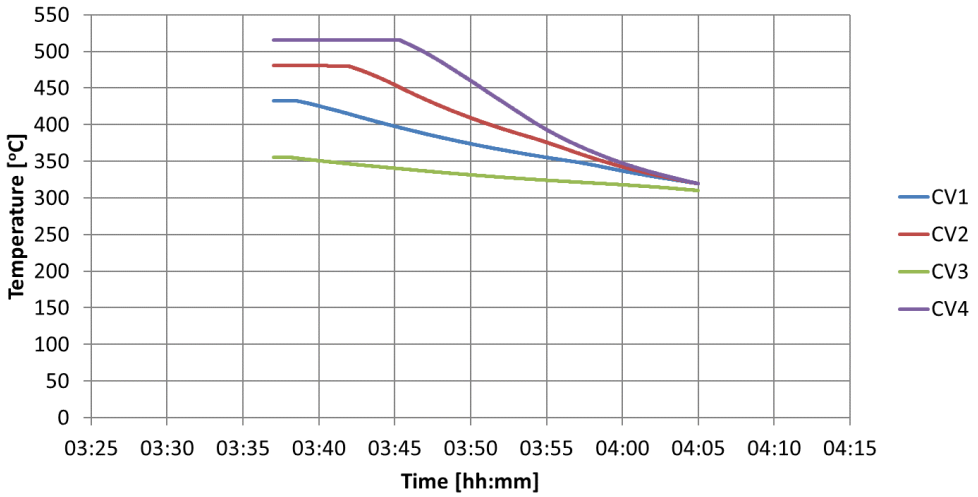


*Figure 187. Header temperatures 4CV LTM*

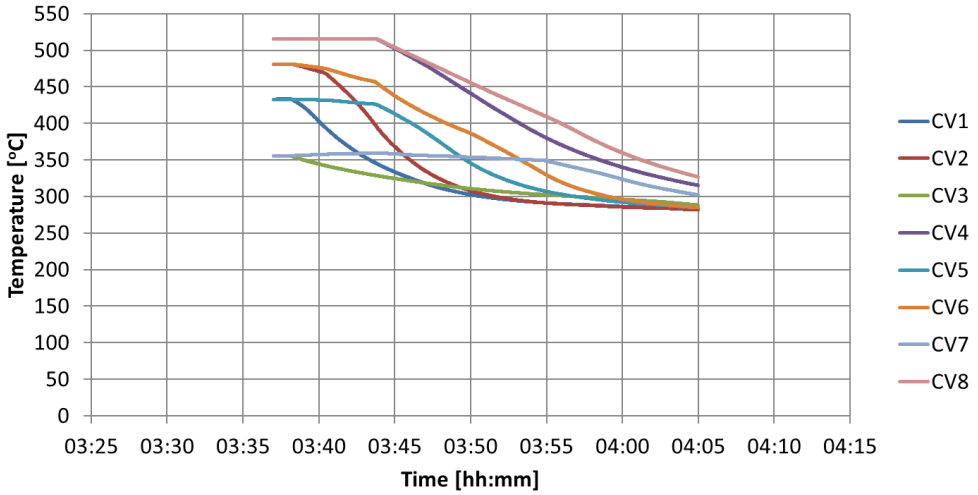


*Figure 188. Header temperatures 8CV LTM*

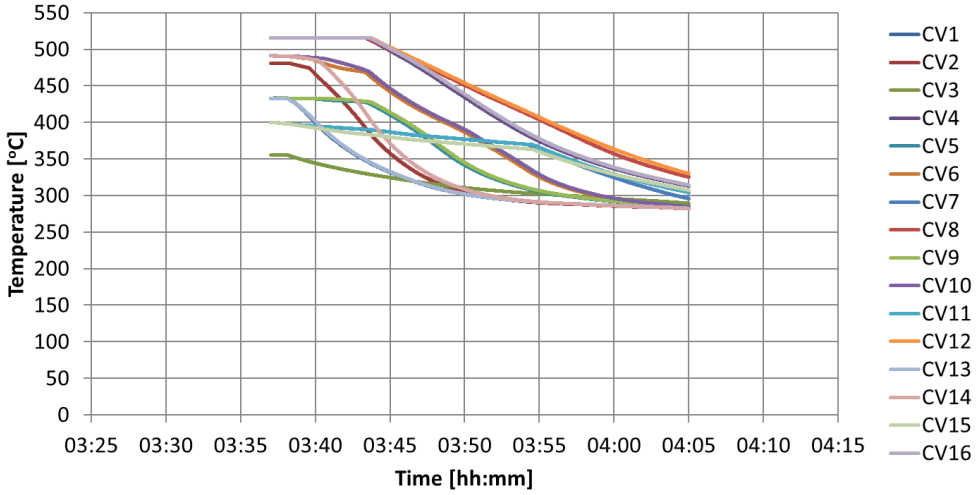


*Figure 189. Header temperatures 16CV LTM*

The measured gas outlet temperature is compared to the results of the four, eight and sixteen control volume models in Figure 190. The four control volume model achieves a reasonable result and the eight and sixteen control volume results are split between the same result as the four control volume model and a hotter result for most of the event.

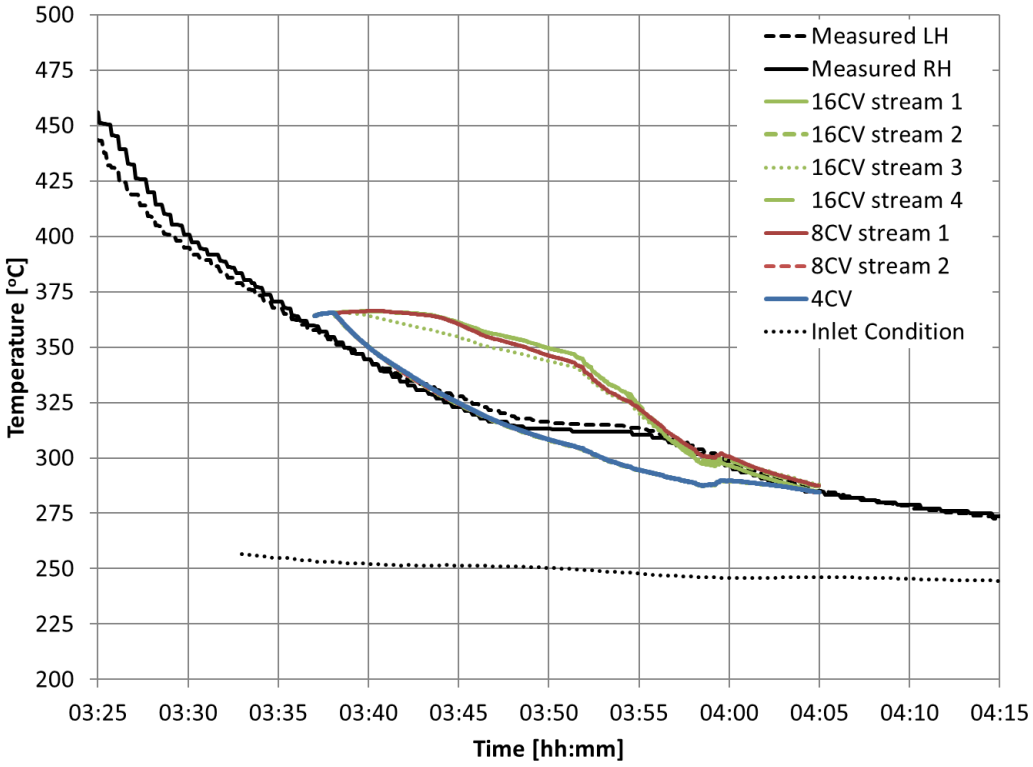


*Figure 190. Gas outlet temperatures – Measured values compared to 4CV, 8CV and 16CV LTM results*

In conclusion of the comparison of the different levels of discretisation, the eight control volume model provides better results that the four control volume model and requires less effort than the sixteen control volume model to configure and run. The increase in discretisation from eight to sixteen control volumes does not improve the results because the phenomenon of reverse flow of liquid in the superheater is already captured in the eight control volume model.

# Appendix J. Quench experiment data processing - Scilab code

```
//Transient pipe cross section calculation to analyse data from test rig
//Revision 4
//Date 27 December 2019
//Based on Rev5.1

//Inputs
//---------------------------------------------------
//Geometric input parameters
Di=0.25; //Inner diameter of the pipe in m
s=[0.0293   0.0277  0.02565 0.028   0.02852    0.02823  0.0298] //wall thickness in m for positions A, B, C, D, E, F

posn=[1 7/8 3/4 5/8 1/2 1/4 0]
depth=[
0.0273   0.014   0
0.0258   0       0
0.0241  0.0145  0
0.0265  0       0
0.0267   0.0135  0
0.0265  0       0
0       0       0
]; //depths of the thermocouple points measured from outer surface of the pipe, deepest first, Row 1=A, 2=B, 3=C, 4=D, 5=E, 6=F

//Material properties
rho_m=7750; //Metal density in kg/m^3

T_init=[0   239.790   239.790   239.471   240.089   239.900   241.446   241.376   240.987   243.221   243.102   245.216
245.485   245.565   249.693   249.623   175.238]

T_history=[
//  A1     A2     A3     B1     B2     C1     C2     C3     D1     D2     E1     E2     E3     F1     F2     G
2   239.760   239.770   239.441   240.089   239.880   241.426   241.346   240.977   243.211   243.082   245.176   245.485
245.565   249.683   249.613   175.636
4   239.750   239.750   239.431   240.069   239.860   241.406   241.336   240.957   243.191   243.072   245.156   245.475
245.525   249.663   249.584   175.209
6   239.750   239.760   239.431   240.069   239.860   241.426   241.326   240.947   243.181   243.062   245.146   245.455
245.525   249.653   249.584   174.125
8   239.730   239.740   239.411   240.039   239.840   241.386   241.316   240.927   243.171   243.032   245.116   245.425
245.495   249.613   249.544   173.230
10   239.700   239.730   239.381   240.029   239.810   241.366   241.286   240.917   243.141   243.032   245.096   245.405
245.465   249.584   249.524   171.837
];

index_inner=[15 12 10 7 5 2]
index_outer=[16 14 11 9 6 4]
index_mid=[0 13 0 8 0 3]

//Calculation variables
m=15; //number of elements in the pipe wall thickness direction
j=51; //number of elements around the circumference
relax=1; //relaxation parameter for the solver
t=0.05; //Setting the timestep in s
conv_tol=1^2; //Convergence tolerance
alpha_c=0.5 //Euler parameter
criteria=(0.01)^2//Convergence tolerance for the temperature calculator
criteria1=(0.001)^2
//---------------------------------------------------

//Function definitions
//---------------------------------------------------
```

```
function [E, W, N, S]=create_coeff_matrices(d_theta)
r=1;//Coefficients for temperatures along the inside of the pipe
theta=1;//Coefficients for temperature at inside top point
    T_m=(T_1(r,theta)+T_0(r,theta))/2
    alpha=(4.272E-03*T_m + 2.391E+01)/rho_m/(8.459E-04*T_m^2 + 7.324E-02*T_m + 4.542E+02)
    c_m=8.459E-04*T_m^2 + 7.324E-02*T_m + 4.542E+02
    rP=pos_r(r,theta)
    rE=pos_r(r+1,theta)
    r1=rP
    r2=(rP+rE)/2
    rS=pos_r(r,theta+1)
    drS=((r2-r1)+((rS+pos_r(r+1,theta+1))/2-rS))/2
    E(r,theta)=2*alpha/((r2^2-r1^2)*log(rE/rP))
    W(r,theta)=2*r1/(rho_m*(r2^2-r1^2)*c_m)
    N(r,theta)=0
    S(r,theta)=2*alpha*(drS)/((r2^2-r1^2)*(d_theta^2)/2*(rP+rS)/2)

for theta=2:j-1//Coefficients for temperatures along inside from top to bottom
    T_m=(T_1(r,theta)+T_0(r,theta))/2
    alpha=(4.272E-03*T_m + 2.391E+01)/rho_m/(8.459E-04*T_m^2 + 7.324E-02*T_m + 4.542E+02)
    c_m=8.459E-04*T_m^2 + 7.324E-02*T_m + 4.542E+02
    rP=pos_r(r,theta)
    rE=pos_r(r+1,theta)
    r1=rP
    r2=(rP+rE)/2
    rN=pos_r(r,theta-1)
    rS=pos_r(r,theta+1)
    drN=((r2-r1)+((rN+pos_r(r+1,theta-1))/2-rN))/2
    drS=((r2-r1)+((rS+pos_r(r+1,theta+1))/2-rS))/2
    E(r,theta)=2*alpha/((r2^2-r1^2)*log(rE/rP))
    W(r,theta)=2*r1/(rho_m*(r2^2-r1^2)*c_m)
    N(r,theta)=2*alpha*(drN)/((r2^2-r1^2)*d_theta^2*(rP+rN)/2)
    S(r,theta)=2*alpha*(drS)/((r2^2-r1^2)*d_theta^2*(rP+rS)/2)
end

theta=j;//Coefficients for temperatures at bottom inside point
    T_m=(T_1(r,theta)+T_0(r,theta))/2
    alpha=(4.272E-03*T_m + 2.391E+01)/rho_m/(8.459E-04*T_m^2 + 7.324E-02*T_m + 4.542E+02)
    c_m=8.459E-04*T_m^2 + 7.324E-02*T_m + 4.542E+02
    rP=pos_r(r,theta)
    rE=pos_r(r+1,theta)
    r1=rP
    r2=(rP+rE)/2
    rN=pos_r(r,theta-1)
    drN=((r2-r1)+((rN+pos_r(r+1,theta-1))/2-rN))/2
    E(r,theta)=2*alpha/((r2^2-r1^2)*log(rE/rP))
    W(r,theta)=2*r1/(rho_m*(r2^2-r1^2)*c_m)
    N(r,theta)=2*alpha*(drN)/((r2^2-r1^2)*(d_theta^2)/2*(rP+rN)/2)
    S(r,theta)=0

r=m;//Coefficients for temperatures along the outside of the pipe
theta=1;//Coefficients for temperature at outside top point
    T_m=(T_1(r,theta)+T_0(r,theta))/2
    alpha=(4.272E-03*T_m + 2.391E+01)/rho_m/(8.459E-04*T_m^2 + 7.324E-02*T_m + 4.542E+02)
    c_m=8.459E-04*T_m^2 + 7.324E-02*T_m + 4.542E+02
    rW=pos_r(r-1,theta)
    rP=pos_r(r,theta)
    r1=(rW+rP)/2
    r2=rP
    rS=pos_r(r,theta+1)
    drS=((r2-r1)+(rS-(pos_r(r-1,theta+1)+rS)/2))/2
    E(r,theta)=2*r2/(rho_m*(r2^2-r1^2)*c_m)
    W(r,theta)=2*alpha/((r2^2-r1^2)*log(rP/rW))
    N(r,theta)=0
    S(r,theta)=2*alpha*(drS)/((r2^2-r1^2)*(d_theta^2)/2*(rP+rS)/2)
```

```
for theta=2:j-1
    T_m=(T_1(r,theta)+T_0(r,theta))/2
    alpha=(4.272E-03*T_m + 2.391E+01)/rho_m/(8.459E-04*T_m^2 + 7.324E-02*T_m + 4.542E+02)
    c_m=8.459E-04*T_m^2 + 7.324E-02*T_m + 4.542E+02
    rW=pos_r(r-1,theta)
    rP=pos_r(r,theta)
    r1=(rW+rP)/2
    r2=rP
    rN=pos_r(r,theta-1)
    rS=pos_r(r,theta+1)
    drN=((r2-r1)+(rN-(pos_r(r-1,theta-1)+rN)/2))/2
    drS=((r2-r1)+(rS-(pos_r(r-1,theta+1)+rS)/2))/2
    E(r,theta)=2*r2/(rho_m*(r2^2-r1^2)*c_m)
    W(r,theta)=2*alpha/((r2^2-r1^2)*log(rP/rW))
    N(r,theta)=2*alpha*(drN)/((r2^2-r1^2)*d_theta^2*(rP+rN)/2)
    S(r,theta)=2*alpha*(drS)/((r2^2-r1^2)*d_theta^2*(rP+rS)/2)
end

theta=j;//Coefficients for temperatures at bottom outside point
    T_m=(T_1(r,theta)+T_0(r,theta))/2
    alpha=(4.272E-03*T_m + 2.391E+01)/rho_m/(8.459E-04*T_m^2 + 7.324E-02*T_m + 4.542E+02)
    c_m=8.459E-04*T_m^2 + 7.324E-02*T_m + 4.542E+02
    rW=pos_r(r-1,theta)
    rP=pos_r(r,theta)
    r1=(rW+rP)/2
    r2=rP
    rN=pos_r(r,theta-1)
    drN=((r2-r1)+(rN-(pos_r(r-1,theta-1)+rN)/2))/2
    E(r,theta)=2*r2/(rho_m*(r2^2-r1^2)*c_m)
    W(r,theta)=2*alpha/((r2^2-r1^2)*log(rP/rW))
    N(r,theta)=2*alpha*(drN)/((r2^2-r1^2)*(d_theta^2)/2*(rP+rN)/2)
    S(r,theta)=0

theta=1;//Coefficients for temperatures along edge radially outward at the top of the pipe
for r=2:m-1
    T_m=(T_1(r,theta)+T_0(r,theta))/2
    alpha=(4.272E-03*T_m + 2.391E+01)/rho_m/(8.459E-04*T_m^2 + 7.324E-02*T_m + 4.542E+02)
    rW=pos_r(r-1,theta)
    rP=pos_r(r,theta)
    rE=pos_r(r+1,theta)
    r1=(rW+rP)/2
    r2=(rP+rE)/2
    rS=pos_r(r,theta+1)
    drS=((r2-r1)+((rS+pos_r(r+1,theta+1))/2-(pos_r(r-1,theta+1)+rS)/2))/2
    E(r,theta)=2*alpha/((r2^2-r1^2)*log(rE/rP))
    W(r,theta)=2*alpha/((r2^2-r1^2)*log(rP/rW))
    N(r,theta)=0
    S(r,theta)=2*alpha*(drS)/((r2^2-r1^2)*(d_theta^2)/2*(rP+rS)/2)
end
theta=j;//Coefficients for temperatures along edge radially outward at the bottom of the pipe
for r=2:m-1
    T_m=(T_1(r,theta)+T_0(r,theta))/2
    alpha=(4.272E-03*T_m + 2.391E+01)/rho_m/(8.459E-04*T_m^2 + 7.324E-02*T_m + 4.542E+02)
    rW=pos_r(r-1,theta)
    rP=pos_r(r,theta)
    rE=pos_r(r+1,theta)
    r1=(rW+rP)/2
    r2=(rP+rE)/2
    rN=pos_r(r,theta-1)
    drN=((r2-r1)+((rN+pos_r(r+1,theta-1))/2-(pos_r(r-1,theta-1)+rN)/2))/2
    E(r,theta)=2*alpha/((r2^2-r1^2)*log(rE/rP))
    W(r,theta)=2*alpha/((r2^2-r1^2)*log(rP/rW))
    N(r,theta)=2*alpha*(drN)/((r2^2-r1^2)*(d_theta^2)/2*(rP+rN)/2)
    S(r,theta)=0
end
```

```
for r=2:m-1//Coefficients for temperatures at all internal points
   for theta=2:j-1
      T_m=(T_1(r,theta)+T_0(r,theta))/2
      alpha=(4.272E-03*T_m + 2.391E+01)/rho_m/(8.459E-04*T_m^2 + 7.324E-02*T_m + 4.542E+02)
      rW=pos_r(r-1,theta)
      rP=pos_r(r,theta)
      rE=pos_r(r+1,theta)
      r1=(rW+rP)/2
      r2=(rP+rE)/2
      rN=pos_r(r,theta-1)
      rS=pos_r(r,theta+1)
      drN=((r2-r1)+((rN+pos_r(r+1,theta-1))/2-(pos_r(r-1,theta-1)+rN)/2))/2
      drS=((r2-r1)+((rS+pos_r(r+1,theta+1))/2-(pos_r(r-1,theta+1)+rS)/2))/2
      E(r,theta)=2*alpha/((r2^2-r1^2)*log(rE/rP))
      W(r,theta)=2*alpha/((r2^2-r1^2)*log(rP/rW))
      N(r,theta)=2*alpha*(drN)/((r2^2-r1^2)*d_theta^2*(rP+rN)/2)
      S(r,theta)=2*alpha*(drS)/((r2^2-r1^2)*d_theta^2*(rP+rS)/2)
   end
end
endfunction

function [T1, q1]=calculate_temperature(T0, q0)
for r=1:m
   for theta=1:j
      T1(r,theta)=T0(r,theta)
   end
end
kount=0
converged=%F
while ~converged
   kount=kount+1
   r=1;
   theta=1;
   q1(r,theta)=a_S(r,theta)*T1(r,theta+1)-a_W(r,theta)*q_inner(theta)+a_E(r,theta)*T1(r+1,theta)-
(a_S(r,theta)+a_E(r,theta))*T1(r,theta)
   for theta=2:j-1
      q1(r,theta)=a_N(r,theta)*T1(r,theta-1)+a_S(r,theta)*T1(r,theta+1)-a_W(r,theta)*q_inner(theta)+a_E(r,theta)*T1(r+1,theta)-
(a_N(r,theta)+a_S(r,theta)+a_E(r,theta))*T1(r,theta)
   end
   theta=j;
   q1(r,theta)=a_N(r,theta)*T1(r,theta-1)-a_W(r,theta)*q_inner(theta)+a_E(r,theta)*T1(r+1,theta)-
(a_N(r,theta)+a_E(r,theta))*T1(r,theta)
   r=m;
   theta=1;
   q1(r,theta)=a_S(r,theta)*T1(r,theta+1)+a_W(r,theta)*T1(r-1,theta)+a_E(r,theta)*q_outer(theta)-
(a_S(r,theta)+a_W(r,theta))*T1(r,theta)
   for theta=2:j-1
      q1(r,theta)=a_N(r,theta)*T1(r,theta-1)+a_S(r,theta)*T1(r,theta+1)+a_W(r,theta)*T1(r-1,theta)+a_E(r,theta)*q_outer(theta)-
(a_N(r,theta)+a_S(r,theta)+a_W(r,theta))*T1(r,theta)
   end
   theta=j;
   q1(r,theta)=a_N(r,theta)*T1(r,theta-1)+a_W(r,theta)*T1(r-1,theta)+a_E(r,theta)*q_outer(theta)-
(a_N(r,theta)+a_W(r,theta))*T1(r,theta)
   theta=1;
   for r=2:m-1
      q1(r,theta)=a_S(r,theta)*T1(r,theta+1)+a_W(r,theta)*T1(r-1,theta)+a_E(r,theta)*T1(r+1,theta)-
(a_S(r,theta)+a_E(r,theta)+a_W(r,theta))*T1(r,theta)
   end
   theta=j;
   for r=2:m-1
      q1(r,theta)=a_N(r,theta)*T1(r,theta-1)+a_W(r,theta)*T1(r-1,theta)+a_E(r,theta)*T1(r+1,theta)-
(a_N(r,theta)+a_E(r,theta)+a_W(r,theta))*T1(r,theta)
   end
   for r=2:m-1
      for theta=2:j-1
```

```
        q1(r,theta)=a_N(r,theta)*T1(r,theta-1)+a_S(r,theta)*T1(r,theta+1)+a_W(r,theta)*T1(r-1,theta)+a_E(r,theta)*T1(r+1,theta)-
(a_N(r,theta)+a_S(r,theta)+a_E(r,theta)+a_W(r,theta))*T1(r,theta)
      end
    end
    converged=%T
    for r=1:m
      for theta=1:j
        Tnew(r,theta)=T0(r,theta)+t*(alpha_c*q1(r,theta) + (1-alpha_c)*q0(r,theta))
        if (Tnew(r,theta)-T1(r,theta))^2>=criteria1 then
          converged=%F
        end
        T1(r,theta)=Tnew(r,theta)
      end
    end
    if kount>50 then
      converged=%T
    end
end
endfunction

//Setting up position variables
location=7;
i=1
for theta=1:j
    x1=round(j*posn(location))
    x2=round(j*posn(location-1))
    y1=s(location)
    y2=s(location-1)
    dr=(y1+(theta-x1)/(x2-x1)*(y2-y1))/(m-1) //nominal thickness of an element

    pos_r(1,theta)=Di/2
    for r = 2 : m
      pos_r(r,theta) = Di/2 + dr*(r-1)
    end

    if theta==round(j*posn(location-1)) then
      location = location -1
      tc_theta_pos(i)=theta
      i=i+1
      for r = 1 : m
        depths(r)= Di/2+dr*(m-1) - pos_r(r,theta)
      end

      n=1
      for r = 2 : m
        if r==2 then
          if (depth(location,n)<(depths(r-1)) & depth(location,n)>=(depths(r)-dr/2)) then
            depths(r)=depth(location,n)
            tc_pos(n,theta)=r
            n=n+1
          end
        else
          if (depth(location,n)<(depths(r)+dr/2) & depth(location,n)>=(depths(r)-dr/2)) then
            depths(r)=depth(location,n)
            tc_pos(n,theta)=r
            n=n+1
          end
        end
      end
      for r = 1 : m
        pos_r(r,theta) = Di/2+dr*(m-1) - depths(r)
      end
    end
end

theta_j=%pi/(j-1);//size of single elment in the circumference direction
```

```
for theta=1:j
   pos_theta(theta)=(theta-1)*theta_j; //creating element position matrix in the circumferential direction
end

duration=0

x1=pos_r(tc_pos(1,tc_theta_pos(1)))
x2=pos_r(tc_pos(2,tc_theta_pos(1)))
y1=T_init(1,index_inner(1))
y2=T_init(1,index_outer(1))
grad=(y2-y1)/(x2-x1)
intercept=y1-grad*x1
for theta=1:tc_theta_pos(1)
   for r=1:m
      T_1(r,theta) = grad*pos_r(r,tc_theta_pos(1))+intercept
   end
end
for i=2:6
   theta = tc_theta_pos(i)
   if round(i/2)==i/2 then
      x1=pos_r(tc_pos(1,theta))
      x2=pos_r(tc_pos(2,theta))
      x3=pos_r(tc_pos(3,theta))
      y1=T_init(1,index_inner(i))
      y2=T_init(1,index_mid(i))
      y3=T_init(1,index_outer(i))
      a=((y1-y2)/(x1^2-x2^2) - (x1-x2)/(x1^2-x2^2)*(y3-y2)/(x3-x2))/(1-(x1-x2)/(x1^2-x2^2)*(x3^2-x2^2)/(x3-x2))
      b=(y3-y2)/(x3-x2) - a*(x3^2-x2^2)/(x3-x2)
      c=y1-a*x1^2-b*x1
      for r=1:m
         T_1(r,theta) = a*pos_r(r,theta)^2+b*pos_r(r,theta)+c
      end
   else
      x1=pos_r(tc_pos(1,theta))
      x2=pos_r(tc_pos(2,theta))
      y1=T_init(1,index_inner(i))
      y2=T_init(1,index_outer(i))
      grad=(y2-y1)/(x2-x1)
      intercept=y1-grad*x1
      for r=1:m
         T_1(r,theta) = grad*pos_r(r,theta)+intercept
      end
   end
end

for i=2:6
   for theta = tc_theta_pos(i-1)+1:tc_theta_pos(i)-1
      x1=tc_theta_pos(i-1)
      x2=tc_theta_pos(i)
      for r=1:m
         y1=T_1(r,tc_theta_pos(i-1))
         y2=T_1(r,tc_theta_pos(i))
         T_1(r,theta)=y1+(theta-x1)/(x2-x1)*(y2-y1)
      end
   end
end

for r=1:m
   for theta=1:j
      posx(r,theta)=pos_r(r,theta)*cos(pos_theta(theta)+%pi/2)//x positions for plotting
      posy(r,theta)=pos_r(r,theta)*sin(pos_theta(theta)+%pi/2)//y positions for plotting
      circ(r,theta)=1;
   end
end

//result matrix: col1 time col2 onwards gives heat flux per element in W/m^2, taken as constant over the time period
```

```
results(1,13)=0;
phase=1;
cont=%T;

for theta=1:j
   q_inner(theta)=0; //Initialise heat flux
   q_outer(theta)=0;
   for r=1:m
      s_1(r,theta)=0
   end
end

while phase<size(T_history,1)
   count=0
   T_0=T_1
   s_0=s_1
   start=duration
   while cont
      count=count+1
      [a_E, a_W, a_N, a_S]=create_coeff_matrices(theta_j)

      T_1=T_0
      s_1=s_0
      duration=start
      while round(duration*1000)/1000 <round(T_history(phase,1))
         [T_2, s_2]=calculate_temperature(T_1, s_1)
         T_1=T_2
         s_1=s_2
         duration=duration+t
      end

      //Routine for calculating the errors from the measured data
      for i=1:6

         error_inner(1,i)=(T_1(tc_pos(1,tc_theta_pos(i)),tc_theta_pos(i))-T_history(phase,index_inner(i)))^2

         error_outer(1,i)=(T_1(m,tc_theta_pos(i))-T_history(phase,index_outer(i)))^2

      end

      cont=%F
      for theta=1:j
         if error_inner(1,i)>=criteria then
            cont=%T
         end
         if error_outer(1,i)>=criteria then
            cont=%T
         end
      end

      //if convergence not achieved, then update q dot and repeat
      if cont
         //increment q dot to measure the gradient
         for theta=1:j
            q_inner(theta)=q_inner(theta)+1;
            q_outer(theta)=q_outer(theta)+1;
         end

         T_1=T_0
         s_1=s_0
         duration=start
         while round(duration*1000)/1000<round(T_history(phase,1))
            [T_2, s_2]=calculate_temperature(T_1, s_1)
            T_1=T_2
            s_1=s_2
            duration=duration+t
```

```
end

//Routine for calculating the errors from the measured data
for i=1:6

    error_inner(2,i)=(T_1(tc_pos(1,tc_theta_pos(i)),tc_theta_pos(i))-T_history(phase,index_inner(i)))^2

    error_outer(2,i)=(T_1(m,tc_theta_pos(i))-T_history(phase,index_outer(i)))^2

end

//increment q dot to find another point
for theta=1:j
    q_inner(theta)=q_inner(theta)-1+10;
    q_outer(theta)=q_outer(theta)-1+10;
end

T_1=T_0
s_1=s_0
duration=start
while round(duration*1000)/1000<round(T_history(phase,1))
    [T_2, s_2]=calculate_temperature(T_1, s_1)
    T_1=T_2
    s_1=s_2
    duration=duration+t
end

//Routine for calculating the errors from the measured data
for i=1:6

    error_inner(3,i)=(T_1(tc_pos(1,tc_theta_pos(i)),tc_theta_pos(i))-T_history(phase,index_inner(i)))^2

    error_outer(3,i)=(T_1(m,tc_theta_pos(i))-T_history(phase,index_outer(i)))^2

end

//increment q dot to measure the gradient
for theta=1:j
    q_inner(theta)=q_inner(theta)+1;
    q_outer(theta)=q_outer(theta)+1;
end

T_1=T_0
s_1=s_0
duration=start
while round(duration*1000)/1000<round(T_history(phase,1))
    [T_2, s_2]=calculate_temperature(T_1, s_1)
    T_1=T_2
    s_1=s_2
    duration=duration+t
end

//Routine for calculating the errors from the measured data
for i=1:6

    error_inner(4,i)=(T_1(tc_pos(1,tc_theta_pos(i)),tc_theta_pos(i))-T_history(phase,index_inner(i)))^2


    error_outer(4,i)=(T_1(m,tc_theta_pos(i))-T_history(phase,index_outer(i)))^2

end

//Reset q dot values
for theta=1:j
    q_inner(theta)=q_inner(theta)-1-10;
    q_outer(theta)=q_outer(theta)-1-10;
```

```
        q_outer_guess_values(count,theta)=q_outer(theta);
        q_inner_guess_values(count,theta)=q_inner(theta);
      end

      //calculate new guess values of q dot
      for i=1:6
        x1=q_inner(tc_theta_pos(i))
        x2=x1+10
        y1=(error_inner(2,i)-error_inner(1,i))/1
        y2=(error_inner(4,i)-error_inner(3,i))/1
        q_inner(tc_theta_pos(i))=x1+relax*y1/(y1-y2)*(x2-x1)

        x1=q_outer(tc_theta_pos(i))
        x2=x1+10
        y1=(error_outer(2,i)-error_outer(1,i))/1
        y2=(error_outer(4,i)-error_outer(3,i))/1
        q_outer(tc_theta_pos(i))=x1+relax*y1/(y1-y2)*(x2-x1)
      end

      for theta=1:(tc_theta_pos(2)-round(j/8))
        q_inner(theta)=q_inner(tc_theta_pos(1))
        q_outer(theta)=q_outer(tc_theta_pos(1))
      end

      for theta=(tc_theta_pos(2)-round(j/8))+1:tc_theta_pos(2)
        x1=(tc_theta_pos(2)-round(j/8))
        y1=q_inner(tc_theta_pos(1))
        x2=tc_theta_pos(2)
        y2=q_inner(tc_theta_pos(2))
        q_inner(theta)=y1+(theta-x1)/(x2-x1)*(y2-y1)
      end

      for i=3:6
        for theta = tc_theta_pos(i-1)+1:tc_theta_pos(i)-1
          x1=tc_theta_pos(i-1)
          y1=q_inner(tc_theta_pos(i-1))
          x2=tc_theta_pos(i)
          y2=q_inner(tc_theta_pos(i))
          q_inner(theta)=y1+(theta-x1)/(x2-x1)*(y2-y1)
        end
      end
      for i=2:6
        for theta = tc_theta_pos(i-1)+1:tc_theta_pos(i)-1
          x1=tc_theta_pos(i-1)
          x2=tc_theta_pos(i)
          y1=q_outer(tc_theta_pos(i-1))
          y2=q_outer(tc_theta_pos(i))
          q_outer(theta)=y1+(theta-x1)/(x2-x1)*(y2-y1)
        end
      end

    end
    cont=%F
    for theta=1:j
      if error_inner(1,i)>=criteria & (q_outer_guess_values(count,theta)-q_outer(theta))^2 >= conv_tol then
        cont=%T
      end
      if error_outer(1,i)>=criteria & (q_inner_guess_values(count,theta)-q_inner(theta))^2 >= conv_tol then
        cont=%T
      end
    end
  end

  disp("----------",duration,count,phase,"Solved phase, number of iterations, up to time")

  //plotting the results and writing to the output matrix
```

```
    for i=1:6
        error_result_inner(phase,i)=error_inner(1,i)
        error_result_outer(phase,i)=error_outer(1,i)
    end

    results(phase,1)=T_history(phase,1)
    T_results(phase,1)=T_history(phase,1)
    wall_T_results(phase,1)=T_history(phase,1)

    for i=1:6
        results(phase,1+i)=q_inner(tc_theta_pos(i))
        results(phase,6+1+i)=q_outer(tc_theta_pos(i))
    end

    count=2
    for i=6:-1:1
        theta=tc_theta_pos(i)
        wall_T_results(phase,i+1)=T_1(1,theta)
        for r=1:3
            if tc_pos(r,theta) <> 0 then
                T_results(phase,count)=T_1(tc_pos(r,theta),theta)
                count=count+1
            end
        end
    end

    if phase/5==round(phase/5) then
        show_window(phase)
        param3d1(posx,posy,T_1)
        param3d1(posx',posy',T_1',-45,1.5)
    end

    phase=phase+1;
    cont=%T;
end
```

# Appendix K. Inverse transient heat conduction model - Scilab code

```
//Transient pipe cross section calculation to determine level of condensate
//Revision 1
//Date 7 January 2020
//
//Goal is to solve for level using discrete temperature measurements from the outside surface of the pipe

//Inputs
//---------------------------------------------------
//Geometric input parameters
Di=0.246; //Inner diameter of the pipe in m
s=0.0343; //wall thickness in m
s_ins=0.16; //insulation thickness in m

//Material properties
rho_m=7750; //Metal density in kg/m^3
c_m=560; //Metal specific heat capacity in J/kg K
k_m=25; //Metal conductivity in W/m K
rho_ins=160; //Insulation density in kg/m^3
c_ins=850; //Insulation specific heat capacity in J/kg K
k_ins=0.1; //Insulation conductivity in W/m K
Int_cond=500; //Interfacial conductance in W/m^2 K

//Process input parameters
T_ambient=30; //Ambient air temperature where the pipe is situated
h_out=4; //Natural convection heat xfer coefficient on the outside of insulation to ambient air in W/m^2 K
h_gas=100; //Heat transfer coefficient in the gas region in W/m^2 K
h_liq=3000; //Heat transfer coefficient in the liquid region in W/m^2 K
fluid_T=[
120   208.9   208.9
240   217.9   217.9
325   217.9   217.9
360   196.0   196.0
480   196.0   196.0
600   196.0   196.0
720   195.9   195.9
840   195.9   195.9
960   195.9   195.9
1080   195.5   195.5
1200   194.9   194.9
1320   194.1   194.1
1440   192.8   192.8
1560   191.1   191.1
1680   190.8   190.8
1800   192.2   192.2
]

//The first row of this matrix is a header row giving the element position number of each thermocouple from top to bottom
//and 180deg being at the bottom. The first column in the matrix gives the time of the readings in s relative to the initial temperature
//which applies at t=0. The value in (1,1) is used as the initial temperature and applied over the whole pipe wall metal temp.
T_history=[
308.58   1   10   20   30   40   50   60   70   82
120   307.67   307.54   307.53   307.50   307.67   307.81   308.30   309.09   308.92
240   307.37   307.38   307.59   307.59   307.58   307.99   308.29   308.71   309.03
330   307.17   307.18   307.39   307.39   307.38   307.79   308.09   308.51   308.83
360   305.04   304.67   305.36   304.61   304.35   304.53   299.53   299.32   296.80
480   296.80   296.28   295.33   292.06   289.02   279.41   256.48   234.78   230.36
600   282.10   280.47   278.77   273.02   263.21   238.18   222.50   217.09   214.81
]
```

```
//Calculation variables
m=8; //number of elements in the pipe wall thickness direction
n=6; //number of elements in the insulation in the thickness direction
j=81; //number of elements around the circumference
time_step=0.05; //Setting the timestep NOTE POSSIBLE INSTABILITY, SHOULD CHECK BIOT NUMBER
criteria=(1)^2
relax=1
//-------------------------------------------------

//Derived parameters
dr=s/m; //size of single element in the wall thickness direction in m
dr_ins=s_ins/n; //size of single element in the insulation in the wall thickness direction in m
alpha_m=k_m/rho_m/c_m; //thermal diffusivity of the metal
alpha_ins=k_ins/rho_ins/c_ins;//thermal diffusivity of the insulation
theta_j=%pi/j;//size of single elment in the circumference direction
//-------------------------------------------------

function [coefficients]=populate_sparse_A(noz, r1, theta1, htc, k1, dr1, alpha, radius, E, W, N, S)
   coefficients=zeros(noz,noz)
   row=(r1-1)*(j+1)+theta1+2;
   select E
      case 1 then
         coefficients(row,(r1-2)*(j+1)+theta1+2)=2*alpha*(pos_r(r1)-dr1/2)/(((pos_r(r1)-dr1/2)^2-
(pos_r(r1)+dr1/2)^2)*(pos_r(r1-1)-pos_r(r1)))
      case 2 then
         coefficients(row,1)=2*alpha*htc*radius/k1/((pos_r(r1)+dr1/2)^2-(pos_r(r1))^2)
      case 3 then
         coefficients(row,(r1-2)*(j+1)+theta1+2)=2*alpha*(pos_r(r1)-dr1/2)/(((pos_r(r1))^2-(pos_r(r1)-dr1/2)^2)*(pos_r(r1)-
pos_r(r1-1)))
      case 4 then
         coefficients(row,(r1-2)*(j+1)+theta1+2)=2*alpha*htc*radius/k1/((pos_r(r1)+dr1/2)^2-(pos_r(r1))^2)
      case 5 then
         coefficients(row,2)=2*alpha*htc*radius/k1/((pos_r(r1)+dr1/2)^2-(pos_r(r1))^2)
   end
   select W
      case 1 then
         coefficients(row,r1*(j+1)+theta1+2)=2*alpha*(pos_r(r1)+dr1/2)/(((pos_r(r1)-dr1/2)^2-(pos_r(r1)+dr1/2)^2)*(pos_r(r1)-
pos_r(r1+1)))
      case 2 then
         coefficients(row,r1*(j+1)+theta1+2)=2*alpha*(pos_r(r1)+dr1/2)/(((pos_r(r1)+dr1/2)^2-(pos_r(r1))^2)*(pos_r(r1+1)-
pos_r(r1)))
      case 3 then
         coefficients(row,r1*(j+1)+theta1+2)=2*alpha*htc*radius/k1/((pos_r(r1))^2-(pos_r(r1)-dr1/2)^2)
      case 4 then
         coefficients(row,noz)=2*alpha*htc*radius/k1/((pos_r(r1))^2-(pos_r(r1)-dr1/2)^2)
   end
   select N
      case 1 then
         coefficients(row,(r1-1)*(j+1)+theta1-1+2)=2*alpha*((pos_r(r1)-dr1/2)-(pos_r(r1)+dr1/2))/(pos_r(r1)*((pos_r(r1)-
dr1/2)^2-(pos_r(r1)+dr1/2)^2)*(pos_e_th(theta1-1)-pos_e_th(theta1))*(pos_theta(theta1-1)-pos_theta(theta1)))
      case 2 then
         //0
      case 3 then
         coefficients(row,(r1-1)*(j+1)+theta1-1+2)=2*alpha*(pos_r(r1)-(pos_r(r1)+dr1/2))/(pos_r(r1)*((pos_r(r1))^2-
(pos_r(r1)+dr1/2)^2)*(pos_e_th(theta1-1)-pos_e_th(theta1))*(pos_theta(theta1-1)-pos_theta(theta1)))
      case 4 then
         coefficients(row,(r1-1)*(j+1)+theta1-1+2)=2*alpha*(pos_r(r1)-(pos_r(r1)+dr1/2))/(pos_r(r1)*((pos_r(r1))^2-
(pos_r(r1)+dr1/2)^2)*(pos_e_th(theta1-1)-pos_theta(theta1))*(pos_theta(theta1-1)-pos_theta(theta1)))
      case 5 then
         coefficients(row,(r1-1)*(j+1)+theta1-1+2)=2*alpha*((pos_r(r1)-dr1/2)-pos_r(r1))/(pos_r(r1)*((pos_r(r1)-dr1/2)^2-
(pos_r(r1))^2)*(pos_e_th(theta1-1)-pos_e_th(theta1))*(pos_theta(theta1-1)-pos_theta(theta1)))
      case 6 then
         coefficients(row,(r1-1)*(j+1)+theta1-1+2)=2*alpha*((pos_r(r1)-dr1/2)-pos_r(r1))/(pos_r(r1)*((pos_r(r1)-dr1/2)^2-
(pos_r(r1))^2)*(pos_e_th(theta1-1)-pos_theta(theta1))*(pos_theta(theta1-1)-pos_theta(theta1)))
      case 7 then
```

```
        coefficients(row,(r1-1)*(j+1)+theta1-1+2)=2*alpha*((pos_r(r1)-dr1/2)-(pos_r(r1)+dr1/2))/(pos_r(r1)*((pos_r(r1)-
dr1/2)^2-(pos_r(r1)+dr1/2)^2)*(pos_e_th(theta1-1)-pos_theta(theta1))*(pos_theta(theta1-1)-pos_theta(theta1)))
    end
    select S
        case 1 then
        coefficients(row,(r1-1)*(j+1)+theta1+1+2)=2*alpha*((pos_r(r1)-dr1/2)-(pos_r(r1)+dr1/2))/(pos_r(r1)*((pos_r(r1)-
dr1/2)^2-(pos_r(r1)+dr1/2)^2)*(pos_e_th(theta1-1)-pos_e_th(theta1))*(pos_theta(theta1)-pos_theta(theta1+1)))
        case 2 then
        coefficients(row,(r1-1)*(j+1)+theta1+1+2)=2*alpha*(pos_r(r1)-(pos_r(r1)+dr1/2))/(pos_r(r1)*((pos_r(r1))^2-
(pos_r(r1)+dr1/2)^2)*(pos_theta(theta1)-pos_e_th(theta1))*(pos_theta(theta1)-pos_theta(theta1+1)))
        case 3 then
        coefficients(row,(r1-1)*(j+1)+theta1+1+2)=2*alpha*(pos_r(r1)-(pos_r(r1)+dr1/2))/(pos_r(r1)*((pos_r(r1))^2-
(pos_r(r1)+dr1/2)^2)*(pos_e_th(theta1-1)-pos_e_th(theta1))*(pos_theta(theta1)-pos_theta(theta1+1)))
        case 4 then
            //0
        case 5 then
        coefficients(row,(r1-1)*(j+1)+theta1+1+2)=2*alpha*((pos_r(r1)-dr1/2)-pos_r(r1))/(pos_r(r1)*((pos_r(r1)-dr1/2)^2-
(pos_r(r1))^2)*(pos_theta(theta1)-pos_e_th(theta1))*(pos_theta(theta1)-pos_theta(theta1+1)))
        case 6 then
        coefficients(row,(r1-1)*(j+1)+theta1+1+2)=2*alpha*((pos_r(r1)-dr1/2)-pos_r(r1))/(pos_r(r1)*((pos_r(r1)-dr1/2)^2-
(pos_r(r1))^2)*(pos_e_th(theta1-1)-pos_e_th(theta1))*(pos_theta(theta1)-pos_theta(theta1+1)))
        case 7 then
        coefficients(row,(r1-1)*(j+1)+theta1+1+2)=2*alpha*((pos_r(r1)-dr1/2)-(pos_r(r1)+dr1/2))/(pos_r(r1)*((pos_r(r1)-
dr1/2)^2-(pos_r(r1)+dr1/2)^2)*(pos_theta(theta1)-pos_e_th(theta1))*(pos_theta(theta1)-pos_theta(theta1+1)))
    end
endfunction

//Calculation
for r=1:m+1
    pos_r(r)=Di/2+(r-1)*dr; //creating position matrix in the r direction in m
end
for r=(m+2):(m+2+n)
    pos_r(r)=Di/2+s+(r-(m+2))*dr_ins
end
for theta=1:j+1
    pos_theta(theta)=(theta-1)*theta_j; //creating element position matrix in the circumferential direction
    pos_e_th(theta)=(theta-1+0.5)*theta_j; //creating element boundary matrix in the circumferential direction
end
pos_e_th(j+1)=0

duration=0;

R_total=1/(2*%pi*pos_r(m+2)*Int_cond)+log(pos_r(m+1+n+1)/pos_r(m+2))/(2*%pi*k_ins)+1/(2*%pi*pos_r(m+1+n+1)*h_out)
Q_steady=(T_history(1,1)-T_ambient)/R_total

for r=1:m+2+n
    for theta=1:j+1
        if r<=m+1 then
            T_1((r-1)*(j+1)+theta+2)=T_history(1,1); //Set initial metal and insulation temperature for calculation
            posx(r,theta)=pos_r(r)*cos(pos_theta(theta)+%pi/2)//x positions for plotting
            posy(r,theta)=pos_r(r)*sin(pos_theta(theta)+%pi/2)//y positions for plotting
            circ(r,theta)=1;
        else
            T_1((r-1)*(j+1)+theta+2)=T_history(1,1)-
Q_steady*(1/(2*%pi*pos_r(m+2)*Int_cond)+log(pos_r(r)/pos_r(m+2))/(2*%pi*k_ins));
        end
    end
end
for theta=2:size(T_history,2)
    posx_history(1,theta-1)=posx(m+1,T_history(1,theta))
    posy_history(1,theta-1)=posy(m+1,T_history(1,theta))
end

T_1(1)=fluid_T(1,2)
T_1(2)=fluid_T(1,3)
T_1((m+1)*(j+1)+(n+1)*(j+1)+3)=T_ambient;
```

```
//Construct the sparse matrix
rows=(m+1)*(j+1)+(n+1)*(j+1)+3
sparse_A(rows,rows)=0
level_e=0

r=1;//Coefficients for temperatures along the inside of the pipe
theta=1;//Coefficients for temperature at inside top point
sparse_A=sparse_A+populate_sparse_A(rows,r,theta,h_gas,k_m,dr,alpha_m,Di/2,2,2,2,2)
for theta=2:j-level_e //Coefficients for temperature at inside points in gas area
   sparse_A=sparse_A+populate_sparse_A(rows,r,theta,h_gas,k_m,dr,alpha_m,Di/2,2,2,3,3)
end
for theta=(j-level_e)+1:j //Coefficients for temperature at inside points in liquid area
   if level_e==0 then
      sparse_A=sparse_A+populate_sparse_A(rows,r,theta,h_gas,k_m,dr,alpha_m,Di/2,5,2,3,3)
   else
      sparse_A=sparse_A+populate_sparse_A(rows,r,theta,h_liq,k_m,dr,alpha_m,Di/2,5,2,3,3)
   end
end
theta=j+1;//Coefficients for temperature at inside bottom point
sparse_A=sparse_A+populate_sparse_A(rows,r,theta,h_liq,k_m,dr,alpha_m,Di/2,5,2,4,4)

for r=2:m //Coefficients for temperatures at all internal points of the pipe wall
   for theta=2:j
      sparse_A=sparse_A+populate_sparse_A(rows,r,theta,0,0,dr,alpha_m,0,1,1,1,1)
   end
end

r=m+1;//Coefficients for temperatures along the outside of the pipe
theta=1;//Coefficients for temperature at outside top point
sparse_A=sparse_A+populate_sparse_A(rows,r,theta,Int_cond,k_m,dr,alpha_m,(Di+2*s)/2,3,3,2,5)
for theta=2:j
   sparse_A=sparse_A+populate_sparse_A(rows,r,theta,Int_cond,k_m,dr,alpha_m,(Di+2*s)/2,3,3,5,6)
end
theta=j+1;//Coefficients for temperatures at bottom outside point
sparse_A=sparse_A+populate_sparse_A(rows,r,theta,Int_cond,k_m,dr,alpha_m,(Di+2*s)/2,3,3,6,4)

theta=1;//Coefficients for temperatures along edge radially outward at the top of the pipe
for r=2:m
   sparse_A=sparse_A+populate_sparse_A(rows,r,theta,0,0,dr,alpha_m,0,1,1,2,7)
end
theta=j+1;//Coefficients for temperatures along edge radially outward at the bottom of the pipe
for r=2:m
   sparse_A=sparse_A+populate_sparse_A(rows,r,theta,0,0,dr,alpha_m,0,1,1,7,4)
end

r=m+2;//Coefficients for temperatures along the inside of the insulation
theta=1;//Coefficients for temperature at inside top point
sparse_A=sparse_A+populate_sparse_A(rows,r,theta,Int_cond,k_ins,dr_ins,alpha_ins,(Di+2*s)/2,4,2,2,2)
for theta=2:j //Coefficients for temperatures along iside
   sparse_A=sparse_A+populate_sparse_A(rows,r,theta,Int_cond,k_ins,dr_ins,alpha_ins,(Di+2*s)/2,4,2,3,3)
end
theta=j+1;//Coefficients for temperature at inside bottom point
sparse_A=sparse_A+populate_sparse_A(rows,r,theta,Int_cond,k_ins,dr_ins,alpha_ins,(Di+2*s)/2,4,2,4,4)

for r=m+3:m+n+1 //Coefficients for temperatures at all internal points of the insulation
   for theta=2:j
      sparse_A=sparse_A+populate_sparse_A(rows,r,theta,0,0,dr_ins,alpha_ins,0,1,1,1,1)
   end
end

r=m+n+2;//Coefficients for temperatures along the outside of the pipe
theta=1;//Coefficients for temperature at outside top point
sparse_A=sparse_A+populate_sparse_A(rows,r,theta,h_out,k_ins,dr_ins,alpha_ins,(Di+2*s+2*s_ins)/2,3,4,2,5)
for theta=2:j
   sparse_A=sparse_A+populate_sparse_A(rows,r,theta,h_out,k_ins,dr_ins,alpha_ins,(Di+2*s+2*s_ins)/2,3,4,5,6)
```

```
end
theta=j+1;//Coefficients for temperatures at bottom outside point
sparse_A=sparse_A+populate_sparse_A(rows,r,theta,h_out,k_ins,dr_ins,alpha_ins,(Di+2*s+2*s_ins)/2,3,4,6,4)

theta=1;//Coefficients for temperatures along edge radially outward at the top of the pipe
for r=m+3:m+n+1
   sparse_A=sparse_A+populate_sparse_A(rows,r,theta,0,0,dr_ins,alpha_ins,0,1,1,2,7)
end
theta=j+1;//Coefficients for temperatures along edge radially outward at the bottom of the pipe
for r=m+3:m+n+1
   sparse_A=sparse_A+populate_sparse_A(rows,r,theta,0,0,dr_ins,alpha_ins,0,1,1,7,4)
end
for a1=3:rows-1
   sparse_A(a1,a1)=0
   coeff_sum=0
   for a2=1:rows
      coeff_sum=coeff_sum+sparse_A(a1,a2)
   end
   sparse_A(a1,a1)=-coeff_sum
end

//initialise result matrix: col1 time col2 level in fraction col3 level in elem no
phase=1;
h_gas(phase)=100; //Heat transfer coefficient in the gas region in W/m^2 K
h_liq(phase)=3000; //Heat transfer coefficient in the liquid region in W/m^2 K
level_e=5;

while round(duration*1000)/1000<T_history(size(T_history,1),1)
   T_1(1)=fluid_T(phase,2)
   T_1(2)=fluid_T(phase,3)
   T_0=T_1;
   start=duration;
   counter=1;
   cont=%T
   h_gas(phase)=50; //Heat transfer coefficient in the gas region in W/m^2 K
   h_liq(phase)=500; //Heat transfer coefficient in the liquid region in W/m^2 K
   level_e=5
   repeated =%F
   error_levels=[0]

   while cont
      count=1
      continues=%T
      guess_values_gas=[0]
      guess_values_liq=[0]

      while continues

         for theta=1:j-level_e //Coefficients for temperature at inside points in gas area
            sparse_A(theta+2,theta+2)=sparse_A(theta+2,theta+2)+sparse_A(theta+2,1)+sparse_A(theta+2,2)
            sparse_A(theta+2,1)=0
            sparse_A(theta+2,2)=0
            sparse_A(theta+2,1)=2*alpha_m*h_gas(phase)*Di/2/k_m/((pos_r(1)+dr/2)^2-(pos_r(1))^2)
            sparse_A(theta+2,theta+2)=sparse_A(theta+2,theta+2)-sparse_A(theta+2,1)
         end
         for theta=(j-level_e)+1:j+1 //Coefficients for temperature at inside points in liquid area
            if level_e==0 then
               sparse_A(theta+2,theta+2)=sparse_A(theta+2,theta+2)+sparse_A(theta+2,2)+sparse_A(theta+2,1)
               sparse_A(theta+2,1)=0
               sparse_A(theta+2,2)=0
               sparse_A(theta+2,2)=2*alpha_m*h_gas(phase)*Di/2/k_m/((pos_r(1)+dr/2)^2-(pos_r(1))^2)
               sparse_A(theta+2,theta+2)=sparse_A(theta+2,theta+2)-sparse_A(theta+2,2)
            else
               sparse_A(theta+2,theta+2)=sparse_A(theta+2,theta+2)+sparse_A(theta+2,2)+sparse_A(theta+2,1)
               sparse_A(theta+2,1)=0
               sparse_A(theta+2,2)=0
```

```
        sparse_A(theta+2,2)=2*alpha_m*h_liq(phase)*Di/2/k_m/((pos_r(1)+dr/2)^2-(pos_r(1))^2)
        sparse_A(theta+2,theta+2)=sparse_A(theta+2,theta+2)-sparse_A(theta+2,2)
    end
end
T_1=T_0
duration=start
while round(duration*1000)/1000<round(T_history(phase+1,1))
    T_2=T_1+(sparse_A*T_1)*time_step
    T_1=T_2
    duration=duration+time_step
end

//Routine for calculating the errors from the measured data
        error_gas(1,count)=(T_1((m+1-1)*(j+1)+T_history(1,2)+2)-T_history(phase+1,2))^2
        error_liq(1,count)=(T_1((m+1-1)*(j+1)+T_history(1,size(T_history,2))+2)-T_history(phase+1,size(T_history,2)))^2

h_gas(phase)=h_gas(phase)+1;
h_liq(phase)=h_liq(phase)+1;

for theta=1:j-level_e //Coefficients for temperature at inside points in gas area
    sparse_A(theta+2,theta+2)=sparse_A(theta+2,theta+2)+sparse_A(theta+2,1)+sparse_A(theta+2,2)
    sparse_A(theta+2,1)=0
    sparse_A(theta+2,2)=0
    sparse_A(theta+2,1)=2*alpha_m*h_gas(phase)*Di/2/k_m/((pos_r(1)+dr/2)^2-(pos_r(1))^2)
    sparse_A(theta+2,theta+2)=sparse_A(theta+2,theta+2)-sparse_A(theta+2,1)
end
for theta=(j-level_e)+1:j+1 //Coefficients for temperature at inside points in liquid area
    if level_e==0 then
        sparse_A(theta+2,theta+2)=sparse_A(theta+2,theta+2)+sparse_A(theta+2,2)+sparse_A(theta+2,1)
        sparse_A(theta+2,1)=0
        sparse_A(theta+2,2)=0
        sparse_A(theta+2,2)=2*alpha_m*h_gas(phase)*Di/2/k_m/((pos_r(1)+dr/2)^2-(pos_r(1))^2)
        sparse_A(theta+2,theta+2)=sparse_A(theta+2,theta+2)-sparse_A(theta+2,2)
    else
        sparse_A(theta+2,theta+2)=sparse_A(theta+2,theta+2)+sparse_A(theta+2,2)+sparse_A(theta+2,1)
        sparse_A(theta+2,1)=0
        sparse_A(theta+2,2)=0
        sparse_A(theta+2,2)=2*alpha_m*h_liq(phase)*Di/2/k_m/((pos_r(1)+dr/2)^2-(pos_r(1))^2)
        sparse_A(theta+2,theta+2)=sparse_A(theta+2,theta+2)-sparse_A(theta+2,2)
    end
end
T_1=T_0
duration=start
while round(duration*1000)/1000<round(T_history(phase+1,1))
    T_2=T_1+(sparse_A*T_1)*time_step
    T_1=T_2
    duration=duration+time_step
end

//Routine for calculating the errors from the measured data
        error_gas(2,count)=(T_1((m+1-1)*(j+1)+T_history(1,2)+2)-T_history(phase+1,2))^2
        error_liq(2,count)=(T_1((m+1-1)*(j+1)+T_history(1,size(T_history,2))+2)-T_history(phase+1,size(T_history,2)))^2

h_gas(phase)=h_gas(phase)-1+10;
h_liq(phase)=h_liq(phase)-1+10;

for theta=1:j-level_e //Coefficients for temperature at inside points in gas area
    sparse_A(theta+2,theta+2)=sparse_A(theta+2,theta+2)+sparse_A(theta+2,1)+sparse_A(theta+2,2)
    sparse_A(theta+2,1)=0
    sparse_A(theta+2,2)=0
    sparse_A(theta+2,1)=2*alpha_m*h_gas(phase)*Di/2/k_m/((pos_r(1)+dr/2)^2-(pos_r(1))^2)
    sparse_A(theta+2,theta+2)=sparse_A(theta+2,theta+2)-sparse_A(theta+2,1)
end
for theta=(j-level_e)+1:j+1 //Coefficients for temperature at inside points in liquid area
    if level_e==0 then
        sparse_A(theta+2,theta+2)=sparse_A(theta+2,theta+2)+sparse_A(theta+2,2)+sparse_A(theta+2,1)
```

```
        sparse_A(theta+2,1)=0
        sparse_A(theta+2,2)=0
        sparse_A(theta+2,2)=2*alpha_m*h_gas(phase)*Di/2/k_m/((pos_r(1)+dr/2)^2-(pos_r(1))^2)
        sparse_A(theta+2,theta+2)=sparse_A(theta+2,theta+2)-sparse_A(theta+2,2)
    else
        sparse_A(theta+2,theta+2)=sparse_A(theta+2,theta+2)+sparse_A(theta+2,2)+sparse_A(theta+2,1)
        sparse_A(theta+2,1)=0
        sparse_A(theta+2,2)=0
        sparse_A(theta+2,2)=2*alpha_m*h_liq(phase)*Di/2/k_m/((pos_r(1)+dr/2)^2-(pos_r(1))^2)
        sparse_A(theta+2,theta+2)=sparse_A(theta+2,theta+2)-sparse_A(theta+2,2)
    end
end
T_1=T_0
duration=start
while round(duration*1000)/1000<round(T_history(phase+1,1))
    T_2=T_1+(sparse_A*T_1)*time_step
    T_1=T_2
    duration=duration+time_step
end

//Routine for calculating the errors from the measured data
        error_gas(3,count)=(T_1((m+1-1)*(j+1)+T_history(1,2)+2)-T_history(phase+1,2))^2
        error_liq(3,count)=(T_1((m+1-1)*(j+1)+T_history(1,size(T_history,2))+2)-T_history(phase+1,size(T_history,2)))^2

h_gas(phase)=h_gas(phase)+1;
h_liq(phase)=h_liq(phase)+1;

for theta=1:j-level_e //Coefficients for temperature at inside points in gas area
    sparse_A(theta+2,theta+2)=sparse_A(theta+2,theta+2)+sparse_A(theta+2,1)+sparse_A(theta+2,2)
    sparse_A(theta+2,1)=0
    sparse_A(theta+2,2)=0
    sparse_A(theta+2,1)=2*alpha_m*h_gas(phase)*Di/2/k_m/((pos_r(1)+dr/2)^2-(pos_r(1))^2)
    sparse_A(theta+2,theta+2)=sparse_A(theta+2,theta+2)-sparse_A(theta+2,1)
end
for theta=(j-level_e)+1:j+1 //Coefficients for temperature at inside points in liquid area
    if level_e==0 then
        sparse_A(theta+2,theta+2)=sparse_A(theta+2,theta+2)+sparse_A(theta+2,2)+sparse_A(theta+2,1)
        sparse_A(theta+2,1)=0
        sparse_A(theta+2,2)=0
        sparse_A(theta+2,2)=2*alpha_m*h_gas(phase)*Di/2/k_m/((pos_r(1)+dr/2)^2-(pos_r(1))^2)
        sparse_A(theta+2,theta+2)=sparse_A(theta+2,theta+2)-sparse_A(theta+2,2)
    else
        sparse_A(theta+2,theta+2)=sparse_A(theta+2,theta+2)+sparse_A(theta+2,2)+sparse_A(theta+2,1)
        sparse_A(theta+2,1)=0
        sparse_A(theta+2,2)=0
        sparse_A(theta+2,2)=2*alpha_m*h_liq(phase)*Di/2/k_m/((pos_r(1)+dr/2)^2-(pos_r(1))^2)
        sparse_A(theta+2,theta+2)=sparse_A(theta+2,theta+2)-sparse_A(theta+2,2)
    end
end
T_1=T_0
duration=start
while round(duration*1000)/1000<round(T_history(phase+1,1))
    T_2=T_1+(sparse_A*T_1)*time_step
    T_1=T_2
    duration=duration+time_step
end

//Routine for calculating the errors from the measured data
        error_gas(4,count)=(T_1((m+1-1)*(j+1)+T_history(1,2)+2)-T_history(phase+1,2))^2
        error_liq(4,count)=(T_1((m+1-1)*(j+1)+T_history(1,size(T_history,2))+2)-T_history(phase+1,size(T_history,2)))^2

h_gas(phase)=h_gas(phase)-1-10
h_liq(phase)=h_liq(phase)-1-10
guess_values_gas(count)=h_gas(phase)
guess_values_liq(count)=h_liq(phase)
```

```
    x1=h_gas(phase)+0.5
    x2=x1+10
    y1=(error_gas(2,count)-error_gas(1,count))/1
    y2=(error_gas(4,count)-error_gas(3,count))/1
    if (y1-y2)<>0 then
       h_gas(phase)=x1+relax*y1/(y1-y2)*(x2-x1)
    end

    x1=h_liq(phase)+0.5
    x2=x1+10
    y1=(error_liq(2,count)-error_liq(1,count))/1
    y2=(error_liq(4,count)-error_liq(3,count))/1
    if (y1-y2)<>0 then
       h_liq(phase)=x1+relax*y1/(y1-y2)*(x2-x1)
    end

    //Test convergence
    continues=%F
    if (h_gas(phase)-guess_values_gas(count))^2>criteria then
       continues=%T
    end
    if (h_liq(phase)-guess_values_liq(count))^2>criteria & level_e>0 then
       continues=%T
    end

    if count==15 & continues then
       min_err=error_liq(1,1)
       for i=1:count
          if error_liq(1,i)<=min_err then
             min_err=error_liq(1,i)
             h_liq(phase)=guess_values_liq(i)
          end
       end
       min_err=error_gas(1,1)
       for i=1:count
          if error_gas(1,i)<=min_err then
             min_err=error_gas(1,i)
             h_gas(phase)=guess_values_gas(i)
          end
       end

       continues=%F
    end

    disp(count)
    count=count+1
end

disp(h_liq(phase),h_gas(phase),"For next iteration, heat transfer coefficients (gas/liquid):")

guess_values_level(phase,counter)=level_e


continues=%T
pos_e=1
while continues
    level_e=pos_e-1

    for theta=1:j-level_e //Coefficients for temperature at inside points in gas area
       sparse_A(theta+2,theta+2)=sparse_A(theta+2,theta+2)+sparse_A(theta+2,1)+sparse_A(theta+2,2)
       sparse_A(theta+2,1)=0
       sparse_A(theta+2,2)=0
       sparse_A(theta+2,1)=2*alpha_m*h_gas(phase)*Di/2/k_m/((pos_r(1)+dr/2)^2-(pos_r(1))^2)
       sparse_A(theta+2,theta+2)=sparse_A(theta+2,theta+2)-sparse_A(theta+2,1)
    end
    for theta=(j-level_e)+1:j+1 //Coefficients for temperature at inside points in liquid area
```

```
        if level_e==0 then
            sparse_A(theta+2,theta+2)=sparse_A(theta+2,theta+2)+sparse_A(theta+2,2)+sparse_A(theta+2,1)
            sparse_A(theta+2,1)=0
            sparse_A(theta+2,2)=0
            sparse_A(theta+2,2)=2*alpha_m*h_gas(phase)*Di/2/k_m/((pos_r(1)+dr/2)^2-(pos_r(1))^2)
            sparse_A(theta+2,theta+2)=sparse_A(theta+2,theta+2)-sparse_A(theta+2,2)
        else
            sparse_A(theta+2,theta+2)=sparse_A(theta+2,theta+2)+sparse_A(theta+2,2)+sparse_A(theta+2,1)
            sparse_A(theta+2,1)=0
            sparse_A(theta+2,2)=0
            sparse_A(theta+2,2)=2*alpha_m*h_liq(phase)*Di/2/k_m/((pos_r(1)+dr/2)^2-(pos_r(1))^2)
            sparse_A(theta+2,theta+2)=sparse_A(theta+2,theta+2)-sparse_A(theta+2,2)
        end
    end
    T_1=T_0
    duration=start
    while round(duration*1000)/1000<round(T_history(phase+1,1))
        T_2=T_1+(sparse_A*T_1)*time_step
        T_1=T_2
        duration=duration+time_step
    end

    //Routine for calculating the errors from the measured data
    error_level(pos_e,phase)=0;
    for i=2:size(T_history,2)
        error_level(pos_e,phase)=error_level(pos_e,phase)+(T_1((m+1-1)*(j+1)+T_history(1,i)+2)-T_history(phase+1,i))^2
    end

    if pos_e==1 then
        min_err=error_level(1,phase)
        count=pos_e
    end
    if error_level(pos_e,phase)<min_err then
        min_err=error_level(pos_e,phase)
        count=pos_e
    end

    if pos_e>=j | pos_e>20+count then
        continues=%F
    end

    if pos_e/10==round(pos_e/10) then
        disp(pos_e)
    end
    pos_e=pos_e+1
end

error_levels(counter)=error_level(count)
level_e=count-1

disp(level_e,"For next iteration, Level = ")

//Test convergence
if level_e==guess_values_level(phase,counter) | repeated then
    cont=%F
end

if cont then
    for i=1:counter-1
        if level_e==guess_values_level(phase,i) then
            repeated=%T
        end
    end

    if repeated then
        min_err=error_levels(1)
```

```
        for i=1:counter
            if error_levels(i)<=min_err then
                min_err=error_levels(i)
                level_e=guess_values_level(phase,i)
            end
        end
    end
end

//If converged then update values
if ~cont then
    for theta=1:j-level_e //Coefficients for temperature at inside points in gas area
        sparse_A(theta+2,theta+2)=sparse_A(theta+2,theta+2)+sparse_A(theta+2,1)+sparse_A(theta+2,2)
        sparse_A(theta+2,1)=0
        sparse_A(theta+2,2)=0
        sparse_A(theta+2,1)=2*alpha_m*h_gas(phase)*Di/2/k_m/((pos_r(1)+dr/2)^2-(pos_r(1))^2)
        sparse_A(theta+2,theta+2)=sparse_A(theta+2,theta+2)-sparse_A(theta+2,1)
    end
    for theta=(j-level_e)+1:j+1 //Coefficients for temperature at inside points in liquid area
        if level_e==0 then
            sparse_A(theta+2,theta+2)=sparse_A(theta+2,theta+2)+sparse_A(theta+2,2)+sparse_A(theta+2,1)
            sparse_A(theta+2,1)=0
            sparse_A(theta+2,2)=0
            sparse_A(theta+2,2)=2*alpha_m*h_gas(phase)*Di/2/k_m/((pos_r(1)+dr/2)^2-(pos_r(1))^2)
            sparse_A(theta+2,theta+2)=sparse_A(theta+2,theta+2)-sparse_A(theta+2,2)
        else
            sparse_A(theta+2,theta+2)=sparse_A(theta+2,theta+2)+sparse_A(theta+2,2)+sparse_A(theta+2,1)
            sparse_A(theta+2,1)=0
            sparse_A(theta+2,2)=0
            sparse_A(theta+2,2)=2*alpha_m*h_liq(phase)*Di/2/k_m/((pos_r(1)+dr/2)^2-(pos_r(1))^2)
            sparse_A(theta+2,theta+2)=sparse_A(theta+2,theta+2)-sparse_A(theta+2,2)
        end
    end
    T_1=T_0
    duration=start
    while round(duration*1000)/1000<round(T_history(phase+1,1))
        T_2=T_1+(sparse_A*T_1)*time_step
        T_1=T_2
        duration=duration+time_step
    end

    results(phase,4)=0;
    for i=2:size(T_history,2)
        results(phase,4)=results(phase,4)+(T_1((m+1-1)*(j+1)+T_history(1,i)+2)-T_history(phase+1,i))^2
    end

end

counter=counter+1
end

h_gas(phase+1)=h_gas(phase)
h_liq(phase+1)=h_liq(phase)
disp("--------------------")
disp("--------------------",h_liq(phase),h_gas(phase),level_e,"Solution found. level=    h_gas=    h_liq=")


//plotting the results and writing to the output matrix
for r=1:m+1
    for theta=1:j+1
        T_plot(r,theta)=T_1((r-1)*(j+1)+theta+2)
    end
end

for theta=2:size(T_history,2)
    Plot_history(1,theta-1)=T_history(phase+1,theta)
```

```
    end

    //circ=circ*0
    //circ=circ+floor(min(T_plot)-1)
    show_window(phase)
    param3d1(posx_history,posy_history,Plot_history)
    p=get("hdl")
    p.foreground=3
    p.thickness=1
    p.mark_style=2

    param3d1(posx,posy,T_plot)
    param3d1(posx',posy',T_plot',-45,1.5)
    //param3d1(posx,posy,circ)
    //param3d1(posx',posy',circ',-45,1.5,"Horizontal[m]@Vertical [m]@Temperature [degC]")
    p=gca(); //get current axes
    p.data_bounds=[-0.153,-0.153,195;0,0.153,305]

    results(phase,1)=duration
    results(phase,2)=(1-cos(theta_j*(level_e-0.5)))/2;
    results(phase,3)=level_e
    results(phase,5)=h_gas(phase)
    results(phase,6)=h_liq(phase)
    results(phase,7)=T_1(1+2)
    results(phase,8)=T_1(j+1+2)

    for theta=1:j+1
        results(phase,theta+8)=T_1((m+1-1)*(j+1)+theta+2)
    end
    phase=phase+1
end
```